

**A Study on the Stabilisation of Phosphorus (V) Stabilised
Lanthanide Carbenes and other di- $\lambda^5\sigma^4$ -Phosphorane
Lanthanide Complexes.**

A dissertation presented to the Faculty of Science in part fulfilment of the requirement
for the Doctor of Philosophy at the University of Malta

Supervisor: Prof. Ulrich Baisch Dr. rer. nat. (LMU-Munich)

Duncan Micallef

2021



L-Universit 
ta' Malta

University of Malta Library – Electronic Thesis & Dissertations (ETD) Repository

The copyright of this thesis/dissertation belongs to the author. The author's rights in respect of this work are as defined by the Copyright Act (Chapter 415) of the Laws of Malta or as modified by any successive legislation.

Users may access this full-text thesis/dissertation and can make use of the information contained in accordance with the Copyright Act provided that the author must be properly acknowledged. Further distribution or reproduction in any format is prohibited without the prior permission of the copyright holder.

Statement of Authenticity

The undersigned declare that this dissertation is based on work carried out by Duncan Micallef for the Ph.D under the supervision of Prof. Ulrich Baisch with the Department of Chemistry.

Duncan Micallef
Candidate

Prof. Ulrich Baisch
Supervisor



The research work disclosed in this publication is partially funded by the Endeavour Scholarship Scheme (Malta). Project part-financed by the European Social Fund - Operational Programme II – European Structural and Investment Funds 2014-2020
“Investing in human capital to create more opportunities and promote the well-being of society”.



Operational Programme II – European Structural and Investment Funds 2014-2020
“Investing in human capital to create more opportunities and promote the well-being of society”
Project part-financed by the European Social Fund
Co-financing rate: 80% European Union; 20% National Funds



ACKNOWLEDGEMENTS

The completion of this dissertation was only possible thanks to the help of a number of individuals.

First and foremost I would like to extend my sincerest appreciation to my supervisor Prof. Ulrich Baisch for his never ceasing assistance, sound guidance and encouragement. Without his help I would not have acquired the knowledge, skills and techniques required for the completion of this dissertation and for working in this field of Chemistry. I would also like to express my gratitude to Prof. Liana Vella Zarb for her help throughout the project, especially with regards to the interpretation of X-ray powder diffraction data. To both I would like to express my appreciation for their assistance in the collection of X-ray diffraction data at the CrEMa laboratories. Other X-ray diffraction work would not have been possible without the help of Dr. Dmitry Chernyshov, Dr. Diadkin Vadim and Dr. Harald Müller at ESRF and Dr. Micheal Probert at Newcastle University.

I would to like to mention and gratefully thank both Mr. Gabriel Gauci and Mr. Emanuel Joseph whose laboratory work was invaluable in the current work. My sincerest thanks also go out to Mr. Luke Frendo for his help and advice as a senior member of the joint research group of which I was a member of for these past years.

My gratitude is also extended to Prof. Robert M. Borg for his invaluable help in using the NMR spectrometer and to Dr. Godwin Sammut for his help in using the GC MS equipment, at the Department of Chemistry, University of Malta. Characterisation of many of the samples would not have been possible without the help of these two staff members. I would also like to extend my gratitude to Prof. Emmanuel Sinagra for his constant interest in my work, and his indispensable help and advice with regards to administrative issues. I am also most thankful for the help extended to me by the technical and administrative staff of the Department of Chemistry, especially the technical staff, mainly Mr. Jonathan Spiteri, Ms. Maria-Stella Grima and Mr. Mark Zerafa, for providing both material and technical support throughout the study.

I would also like to acknowledge the assistance of the Scholarships Unit at the Department of Education, without which this dissertation would not have been possible.

Last but not least I must also thank my family for their constant support for the duration of the work leading up to this dissertation and indeed throughout the course.

ABSTRACT

The synthesis, stabilisation and characterisation of various lanthanide complexes of isoelectronic di- $\lambda^5\sigma^4$ -phosphorane ligands was attempted. These isoelectronic di- $\lambda^5\sigma^4$ -phosphorane ligands are divided into the carbene and non-carbene groups where the central moieties of the ligands are C^{2-} for the former and N^- and O for the latter group. Lanthanide complexation proved difficult in most cases however the study did yield interesting novel results. Two novel crystal structures for the non-carbene precursor di- $\lambda^5\sigma^4$ -phosphorane ligands $HN(Ph_2PO)_2$ and $O((iPrNH)_2PO)_2$ have been structurally characterised through PXRD and SXRD respectively and chemically through IR, 1H and ^{31}P NMR and GC-MS. A novel complex for $O((Et_2N)_2PO)_2$ namely $Ca_2(O((Et_2N)_2PO)_2)_2(NO_3)_4(H_2O)_2$ was characterised by SXRD from serendipitously collected crystals. PXRD data for $K[HC(Ph_2PNiPr)_2]$, which has not been previously structurally characterised, was collected. IR, 1H NMR and PXRD data for an as of yet unknown complex of $HN(Ph_2PS)_2$ with hydrated $Eu(ClO_4)_3$ was also collected and characterisation is also being undertaken. Stabilisation studies were undertaken using co-crystallisation techniques. These co-crystallisation studies dealt mainly with amorphous products of the synthesis of $[Sm(C(Ph_2PNSiMe_3)_2)(NCy_2)(THF)]$ which were believed to principally contain methanide analogues of the desired carbene. The co-crystallisation studies indicated that co-crystallisation was difficult to achieve and that its use in stabilisation is limited.

TABLE OF CONTENTS

Statement of Authenticity	ii
ACKNOWLEDGEMENTS	iv
ABSTRACT	v
TABLE OF CONTENTS	vi
LIST OF ABBREVIATIONS	xvi
LIST OF FIGURES	xviii
LIST OF SCHEMES	xxxvi
LIST OF TABLES	xxxviii
1. INTRODUCTION	1
2. LITERATURE REVIEW	4
2.1. Chemistry of the lanthanide metals	4
2.2. Introduction to isoelectronic di- $\lambda^5\sigma^4$ -phosphorane ligand lanthanide complexes	6
2.3. Organometallic lanthanide compounds	7
2.3.1. Lanthanide cyclopentadienyl and anionic aromatic ligand complexes	7
2.3.2. Lanthanide arene complexes	10
2.3.3. Lanthanide allyls	11
2.3.4. Lanthanide – carbon σ bonds	11
2.3.5. Other Ln to C bonding	13
2.4. Introduction to carbenes	14
2.4.1. N-heterocyclic carbenes	17
2.4.2. Heteroatomic λ^5 -phosphane or phosphorane stabilised carbenes	18
2.4.3. Synthesis of $\lambda^5\sigma^4$ -phosphorus stabilised carbenes	22
2.4.3.1. Synthesis of iminophosphorane geminal dianions	22
2.4.3.1.1. Phospha-Staudinger method	22
2.4.3.1.2. Kirsanov method	23
2.4.3.2. Synthesis of thiophosphinoyl stabilised carbenes	25
2.5. Typical starting reagents for lanthanide carbenes	27
2.5.1. Lanthanide iodide reagents	28
2.5.1.1. The preparation of anhydrous lanthanide iodides ($\text{LnI}_3 \cdot x\text{H}_2\text{O}$, $x=0$)	29
2.5.1.2. Lanthanide triiodide THF solvates	29
2.5.2. Lanthanide benzyl complexes	32
2.5.3. Other lanthanide starting reagents for phosphorus (V) stabilised carbenes	34

TABLE OF CONTENTS (CONTINUED)

2.6. Lanthanide Carbenes.....	34
2.6.1. Lanthanide–NHCs or Arduengo carbenes.....	34
2.6.2. Lanthanide- λ^5 -phosphorane stabilised geminal dianion carbenes.....	35
2.6.2.1. Early non-NHC lanthanide carbenes	35
2.6.2.2. Lanthanide iminophosphorano geminal dianion carbenes	36
2.6.2.2.1. Lanthanide iminophosphorano carbenes synthesis and characterisation	36
2.6.2.2.1.1 Lanthanide iminophosphorano carbenes of non-trivalent lanthanides	44
2.6.2.2.2. Lanthanide iminophosphorano carbene reactivity and applications ..	45
2.6.2.3. Lanthanide thiophosphonyl geminal dianion carbenes	51
2.6.2.3.1. Lanthanide thiophosphonyl carbenes synthesis and characterisation	51
2.6.2.3.2. Lanthanide thiophosphonyl carbene reactivity	54
2.7. Metal-Organic lanthanide complexes of non-carbene di- $\lambda^5\sigma^4$ -phosphorane ligands.....	55
2.7.1. Pyrophosphoramidate analogues.....	56
2.7.2. Compounds with the structure $X(R_2PY)_2$, where $X = HN$, $Y = S$, and their complexes.....	60
2.7.3. Compounds with the structure $X(R_2PY)_2$, where $X = HN$, $Y = O$, and their complexes.....	63
2.8. Stabilisation of compounds by co-crystallisation	65
3. EXPERIMENTAL.....	68
3.1. Instrumentation and software used for product characterisation.....	68
3.2. Schlenk line techniques	69
3.2.1. Argon Purification	69
3.2.2. General conditions and procedures	70
3.2.3. Drying of solvents	70
3.3. Reaction procedures.....	71
3.3.1. Synthesis of Lanthanide carbene complexes.....	71
3.3.1.1. Ligand synthesis	71
3.3.1.1.1. Synthesis of $K[HC(Ph_2PNiPr)_2]$ through the Kirsanov method	71
3.3.1.1.1.1 Synthesis of $[H_2C(Ph_2PNH(iPr))_2]Br_2$	72

TABLE OF CONTENTS (CONTINUED)

3.3.1.1.1.1	Reagents used.....	72
3.3.1.1.1.2	[H ₂ C(Ph ₂ PNH(<i>i</i> Pr)) ₂]Br ₂ _1	72
3.3.1.1.1.3	Characterisation data	73
3.3.1.1.2	Synthesis of K[HC(Ph ₂ PN <i>i</i> Pr) ₂]	73
3.3.1.1.2.1	Reagents used.....	73
3.3.1.1.2.2	General procedure for K[HC(Ph ₂ PN <i>i</i> Pr) ₂]	74
3.3.1.1.2.3	K[HC(Ph ₂ PN <i>i</i> Pr) ₂]-1	74
3.3.1.1.2.4	K[HC(Ph ₂ PN <i>i</i> Pr) ₂]-2	74
3.3.1.1.2.5	Characterisation data	74
3.3.1.1.2.	Synthesis of H ₂ C(Ph ₂ PNSiMe ₃) ₂	75
3.3.1.1.2.1	Reagents used.....	75
3.3.1.1.2.2	General procedure	76
3.3.1.1.2.3	H ₂ C(Ph ₂ PNSiMe ₃) ₂ -1	76
3.3.1.1.2.4	H ₂ C(Ph ₂ PNSiMe ₃) ₂ -2	76
3.3.1.1.2.5	H ₂ C(Ph ₂ PNSiMe ₃) ₂ -3	77
3.3.1.1.2.6	Characterisation data	77
3.3.1.1.3.	Synthesis of H ₂ C(Ph ₂ PS) ₂	77
3.3.1.1.3.1	Reagents used.....	78
3.3.1.1.3.2	General procedure	78
3.3.1.1.3.3	H ₂ C(Ph ₂ PS) ₂ -1	78
3.3.1.1.3.4	H ₂ C(Ph ₂ PS) ₂ -2	78
3.3.1.1.3.5	H ₂ C(Ph ₂ PS) ₂ -3	79
3.3.1.1.3.6	Characterisation data	79
3.3.1.2.	Lanthanide starting reagents	79
3.3.1.2.1.	Synthesis of LnI ₃ (THF) _{3.5} complexes	80
3.3.1.2.1.1	Reagents used.....	81
3.3.1.2.1.2	NdI ₃ (THF) _{3.5} -1	81
3.3.1.2.1.3	SmI ₃ (THF) _{3.5} -1 and SmI ₃ (THF) _{3.5} -2	81
3.3.1.2.1.4	Characterisation data	83
3.3.1.2.2.	Synthesis of [Sm(NCy ₂) ₃ THF]·C ₆ H ₅ CH ₃	83
3.3.1.2.2.1	Reagents used.....	84
3.3.1.2.2.2	[Sm(NCy ₂) ₃ THF]·C ₆ H ₅ CH ₃ -1	84

TABLE OF CONTENTS (CONTINUED)

3.3.1.2.2.3	Characterisation data.....	85
3.3.1.3.	Complexation	85
3.3.1.3.1.	Synthesis of $[\text{Sm}(\text{C}(\text{Ph}_2\text{PNSiMe}_3)_2)(\text{NCy}_2)(\text{THF})] \cdot 0.5(\text{C}_6\text{H}_5\text{CH}_3)$..	85
3.3.1.3.1.1	Reagents used	86
3.3.1.3.1.2	General procedure.....	86
3.3.1.3.1.3	$[\text{Sm}(\text{C}(\text{Ph}_2\text{PNSiMe}_3)_2)(\text{NCy}_2)(\text{THF})]_1$	86
3.3.1.3.1.4	$[\text{Sm}(\text{C}(\text{Ph}_2\text{PNSiMe}_3)_2)(\text{NCy}_2)(\text{THF})]_2$	87
3.3.1.3.1.5	$[\text{Sm}(\text{C}(\text{Ph}_2\text{PNSiMe}_3)_2)(\text{NCy}_2)(\text{THF})]_3$	87
3.3.1.3.1.6	$[\text{Sm}(\text{C}(\text{Ph}_2\text{PNSiMe}_3)_2)(\text{NCy}_2)(\text{THF})]_4$	88
3.3.1.3.1.7	Characterisation data.....	88
3.3.1.3.2.	Synthesis of $[\text{Nd}(\text{C}(\text{Ph}_2\text{PNiPr})_2)(\text{HC}(\text{Ph}_2\text{PNiPr})_2)] \cdot 2\text{THF}$	89
3.3.1.3.2.1	Reagents used	90
3.3.1.3.2.2	$[\text{Nd}(\text{C}(\text{Ph}_2\text{PNiPr})_2)(\text{HC}(\text{Ph}_2\text{PNiPr})_2)] \cdot 2\text{THF}_1$	90
3.3.1.3.2.3	$[\text{Nd}(\text{C}(\text{Ph}_2\text{PNiPr})_2)(\text{HC}(\text{Ph}_2\text{PNiPr})_2)] \cdot 2\text{THF}_2$	91
3.3.1.3.2.4	Characterisation data.....	91
3.3.1.3.3.	Synthesis of $[\text{Sm}_2(\text{C}(\text{Ph}_2\text{PS})_2)_2\text{I}_2\text{THF}_4] \cdot 4(\text{C}_6\text{H}_5\text{CH}_3)$	92
3.3.1.3.3.1	Reagents used	92
3.3.1.3.3.2	General procedure.....	93
3.3.1.3.3.3	$[\text{Sm}_2(\text{C}(\text{Ph}_2\text{PS})_2)_2\text{I}_2\text{THF}_4] \cdot 4(\text{C}_6\text{H}_5\text{CH}_3)_1$	93
3.3.1.3.3.4	$[\text{Sm}_2(\text{C}(\text{Ph}_2\text{PS})_2)_2\text{I}_2\text{THF}_4] \cdot 4(\text{C}_6\text{H}_5\text{CH}_3)_2$	94
3.3.1.3.3.5	$[\text{Sm}_2(\text{C}(\text{Ph}_2\text{PS})_2)_2\text{I}_2\text{THF}_4] \cdot 4(\text{C}_6\text{H}_5\text{CH}_3)_3$	94
3.3.1.3.3.6	$[\text{Sm}_2(\text{C}(\text{Ph}_2\text{PS})_2)_2\text{I}_2\text{THF}_4] \cdot 4(\text{C}_6\text{H}_5\text{CH}_3)_4$	95
3.3.1.3.3.7	Characterisation data.....	95
3.3.2.	Synthesis of Lanthanide non-carbene di- $\lambda^5\sigma^4$ -phosphorane complexes	96
3.3.2.1.	Ligand synthesis	96
3.3.2.1.1.	Synthesis of $\text{HN}(\text{Ph}_2\text{PO})_2$	97
3.3.2.1.1.1	Reagents used	97
3.3.2.1.1.2	$\text{HN}(\text{Ph}_2\text{PO})_2_1$	98
3.3.2.1.1.3	Characterisation data.....	98
3.3.2.1.2.	Synthesis of $\text{HN}(\text{Ph}_2\text{PS})_2$	98
3.3.2.1.2.1	Reagents used	99
3.3.2.1.2.2	$\text{HN}(\text{Ph}_2\text{PS})_2_1$	99

TABLE OF CONTENTS (CONTINUED)

3.3.2.1.2.3	Characterisation data.....	99
3.3.2.1.3.	Synthesis of $O((Et_2N)_2PO)_2$	100
3.3.2.1.3.1	Reagents used.....	101
3.3.2.1.3.2	$(O((Et_2N)_2PO)_2)_1$	101
3.3.2.1.3.3	Characterisation data.....	103
3.3.2.1.4.	Synthesis of $O((iPrNH)_2PO)_2$	103
3.3.2.1.4.1	Reagents used.....	104
3.3.2.1.4.2	$O((iPrNH)_2PO)_2_1$	104
3.3.2.1.4.3	Characterisation data.....	106
3.3.2.2.	Complexation.....	107
3.3.2.2.1.	Synthesis of $[Eu(N(Ph_2PO)_2)_3]$	107
3.3.2.2.1.1	Reagents used.....	108
3.3.2.2.1.2	General procedure.....	108
3.3.2.2.1.3	$[Eu(N(Ph_2PO)_2)_3]_1$	108
3.3.2.2.1.4	$[Eu(N(Ph_2PO)_2)_3]_2$	108
3.3.2.2.1.5	Characterisation data.....	109
3.3.2.2.2.	Synthesis of $HN(Ph_2PS)_2+Eu(ClO_4)_3 \cdot n(H_2O)$	109
3.3.2.2.2.1	Reagents used.....	110
3.3.2.2.2.2	$HN(Ph_2PS)_2+Eu(ClO_4)_3 \cdot n(H_2O)_1$	110
3.3.2.2.2.3	Characterisation data.....	111
3.3.2.2.3.	Synthesis of $O((Et_2N)_2PO)_2+Nd(ClO_4)_3$ complex.....	111
3.3.2.2.3.1	Reagents used.....	112
3.3.2.2.3.2	$O((Et_2N)_2PO)_2+Nd(ClO_4)_3_1$	112
3.3.2.2.3.3	Characterisation data.....	113
3.3.3.	Co-Crystallisation.....	114
3.3.3.1.	Co-crystallisation attempts of $[Sm(C(Ph_2PNSiMe_3)_2)(NCy_2)(THF)]$ $\cdot 0.5(C_6H_5CH_3)$	114
3.3.3.1.1.	Reagents used.....	115
3.3.3.1.2.	General considerations.....	116
3.3.3.1.3.	Co-crystallisation procedures.....	116
3.3.3.1.4.	Single crystal preparation and collection.....	117
3.3.3.1.5.	Characterisation techniques used for co-crystal samples.....	118

TABLE OF CONTENTS (CONTINUED)

4. RESULTS AND DISCUSSION.....	119
4.1. Lanthanide carbene complexes.....	119
4.1.1. Ligands and ligand precursors.....	119
4.1.1.1. Characterisation of $[\text{H}_2\text{C}(\text{Ph}_2\text{PNH}(i\text{Pr}))_2]\text{Br}_2$ and $\text{K}[\text{HC}(\text{Ph}_2\text{PN}i\text{Pr})_2]$	119
4.1.1.1.1. Characterisation of $[\text{H}_2\text{C}(\text{Ph}_2\text{PNH}(i\text{Pr}))_2]\text{Br}_2$	119
4.1.1.1.1.1. Analysis by Infra-red spectroscopy	119
4.1.1.1.1.2. Analysis by ^1H NMR spectroscopy	122
4.1.1.1.1.3. Conclusion	127
4.1.1.1.2. Characterisation of $\text{K}[\text{HC}(\text{Ph}_2\text{PN}i\text{Pr})_2]$	127
4.1.1.1.2.1. Analysis by Infra-red spectroscopy	128
4.1.1.1.2.2. Analysis by ^1H NMR spectroscopy	131
4.1.1.1.2.3. Analysis by Powder X-ray diffraction.....	143
4.1.1.1.2.4. Conclusion	143
4.1.1.2. Characterisation of $\text{H}_2\text{C}(\text{Ph}_2\text{PNSiMe}_3)_2$	144
4.1.1.2.1. Analysis by Infra-red spectroscopy	144
4.1.1.2.2. Analysis by ^1H NMR spectroscopy	145
4.1.1.2.3. Conclusion	146
4.1.1.3. Characterisation of $\text{H}_2\text{C}(\text{Ph}_2\text{PS})_2$	146
4.1.1.3.1. Analysis by Infra-red spectroscopy	147
4.1.1.3.2. Analysis by ^1H NMR spectroscopy	148
4.1.1.3.3. Analysis by Microscopy	149
4.1.1.3.4. Analysis by Powder X-ray diffraction.....	149
4.1.1.3.5. $\text{H}_2\text{C}(\text{Ph}_2\text{PS})_2$ polymorphism	150
4.1.1.3.6. Conclusion	152
4.1.1.4. Summary.....	152
4.1.2. Lanthanide starting reagents.....	153
4.1.2.1. Characterisation of $\text{LnI}_3(\text{THF})_{3.5}$ complexes.....	153
4.1.2.1.1. Analysis by Infra-red spectroscopy	153
4.1.2.1.1.1. $\text{NdI}_3(\text{THF})_{3.5_1}$	154
4.1.2.1.1.2. $\text{SmI}_3(\text{THF})_{3.5_1}$ and $\text{SmI}_3(\text{THF})_{3.5_2}$	154
4.1.2.1.2. Analysis by UV-visible light spectroscopy	155
4.1.2.1.3. Analysis by Powder X-ray Diffraction	156

TABLE OF CONTENTS (CONTINUED)

4.1.2.1.4. Conclusion	156
4.1.2.2. Characterisation of [Sm(NCy ₂) ₃ THF]·C ₆ H ₅ CH ₃	157
4.1.2.2.1. Analysis by Infra-red spectroscopy	157
4.1.2.2.2. Analysis by Microscopy	161
4.1.2.2.3. Conclusion	161
4.1.2.3. Summary.....	162
4.1.3. Complexation products.....	163
4.1.3.1. Characterisation of [Sm(C(Ph ₂ PNSiMe ₃) ₂ (NCy ₂)(THF)] ·0.5(C ₆ H ₅ CH ₃)	163
4.1.3.1.1. Analysis by Infra-red spectroscopy	163
4.1.3.1.2. Analysis by Microscopy	176
4.1.3.1.3. Analysis by Single crystal X-ray diffraction	178
4.1.3.1.4. Decomposition of H ₂ C(Ph ₂ PNSiMe ₃) ₂	180
4.1.3.1.5. Analysis by Powder X-ray diffraction	183
4.1.3.1.6. Conclusion	185
4.1.3.2. Characterisation of [Nd(C(Ph ₂ PN <i>i</i> Pr) ₂ (HC(Ph ₂ PN <i>i</i> Pr) ₂)]·2THF.....	187
4.1.3.2.1. Analysis by Infra-red spectroscopy	188
4.1.3.2.2. Analysis by Microscopy	194
4.1.3.2.3. Conclusion	194
4.1.3.3. Characterisation of [Sm ₂ (C(Ph ₂ PS) ₂) ₂ I ₂ THF ₄]·4(C ₆ H ₅ CH ₃).....	195
4.1.3.3.1. Analysis by Infra-red spectroscopy	196
4.1.3.3.2. Analysis by ¹ H NMR spectroscopy	204
4.1.3.3.3. Analysis by Microscopy	206
4.1.3.3.4. Analysis by Powder X-ray diffraction	211
4.1.3.3.5. Conclusion.....	215
4.1.3.4. Summary.....	216
4.2. Lanthanide non-carbene di-λ ⁵ σ ⁴ -phosphorane complexes.....	218
4.2.1. Ligands and ligand precursors.....	218
4.2.1.1. Characterisation of HN(Ph ₂ PO) ₂	218
4.2.1.1.1. Analysis by Infra-red spectroscopy	218
4.2.1.1.2. Analysis by ¹ H NMR spectroscopy	222
4.2.1.1.3. Analysis by Melting point determination.	225

TABLE OF CONTENTS (CONTINUED)

4.2.1.1.4.	Analysis by Powder X-ray diffraction.....	225
4.2.1.1.5.	Conclusion	229
4.2.1.2.	Characterisation of $\text{HN}(\text{Ph}_2\text{PS})_2$	229
4.2.1.2.1.	Analysis by Infra-red spectroscopy	230
4.2.1.2.2.	Analysis by ^1H NMR spectroscopy	233
4.2.1.2.3.	Analysis by Powder X-ray diffraction	234
4.2.1.2.4.	Conclusion	235
4.2.1.3.	Characterisation of $\text{O}((\text{Et}_2\text{N})_2\text{PO})_2$	235
4.2.1.3.1.	Analysis by Infra-red spectroscopy	236
4.2.1.3.2.	Analysis by ^1H NMR spectroscopy	242
4.2.1.3.3.	Analysis by ^{31}P NMR spectroscopy.....	246
4.2.1.3.4.	Analysis by Gas Chromatography Mass Spectroscopy (GC-MS) ..	251
4.2.1.3.5.	Analysis by Single crystal X-ray diffraction	254
4.2.1.3.6.	Conclusion	257
4.2.1.4.	Characterisation of $\text{O}((i\text{PrNH})_2\text{PO})_2$	258
4.2.1.4.1.	Analysis by Infra-red spectroscopy	258
4.2.1.4.2.	Analysis by ^1H NMR spectroscopy	261
4.2.1.4.3.	Analysis by ^{31}P NMR spectroscopy	267
4.2.1.4.4.	Analysis by Gas chromatography Mass spectroscopy (GC-MS) ..	270
4.2.1.4.5.	Analysis by Microscopy	274
4.2.1.4.6.	Analysis by Single crystal X-ray diffraction	275
4.2.1.4.6.1	$\text{O}((i\text{PrNH})_2\text{PO})_2$ _1_b1	275
4.2.1.4.6.2	Structural Comparison of mono-N-substituted Pyrophosphoramides.....	278
4.2.1.4.7.	Conclusion	285
4.2.1.5.	Summary.....	286
4.2.2.	Complexation products.....	287
4.2.2.1.	Characterisation of $[\text{Eu}(\text{N}(\text{Ph}_2\text{PO})_2)_3]$	287
4.2.2.1.1.	Analysis by Infra-red spectroscopy	287
4.2.2.1.2.	Analysis by ^1H NMR spectroscopy	290
4.2.2.1.3.	Analysis by Powder X-ray diffraction	293
4.2.2.1.4.	Conclusion	295

TABLE OF CONTENTS (CONTINUED)

4.2.2.2. Characterisation of $\text{HN}(\text{Ph}_2\text{PS})_2+\text{Eu}(\text{ClO}_4)_3 \cdot n(\text{H}_2\text{O})$	296
4.2.2.2.1. Analysis by Infra-red spectroscopy	296
4.2.2.2.2. Analysis by ^1H NMR spectroscopy	298
4.2.2.2.3. Analysis by Microscopy and luminescence	299
4.2.2.2.4. Analysis by Powder X-ray diffraction	299
4.2.2.2.5. Conclusion	300
4.2.2.3. Characterisation of $\text{O}((\text{Et}_2\text{N})_2\text{PO})_2+\text{Nd}(\text{ClO}_4)_3$	300
4.2.2.3.1. Analysis by Infra-red spectroscopy	301
4.2.2.3.2. Analysis by ^1H NMR spectroscopy	303
4.2.2.3.3. Analysis by ^{31}P NMR spectroscopy	305
4.2.2.3.4. Analysis by Gas Chromatography Mass Spectroscopy (GC-MS) ..	306
4.2.2.3.5. Analysis by Hot stage microscopy	309
4.2.2.3.6. Analysis by Microscopy	309
4.2.2.3.7. Conclusion	310
4.2.2.4. Summary	311
4.3. Co-Crystallisation	311
4.3.1. Characterisation of co-crystallisation products of $[\text{Sm}(\text{C}(\text{Ph}_2\text{PNSiMe}_3)_2)(\text{NCy}_2)(\text{THF})] \cdot 0.5(\text{C}_6\text{H}_5\text{CH}_3)$	312
4.3.1.1. Analysis by Infra-red spectroscopy	313
4.3.1.2. Analysis by Powder X-ray diffraction	320
4.3.1.3. Analysis by Raman spectroscopy	325
4.3.1.4. Analysis by Single crystal X-ray diffraction	325
4.3.1.5. Conclusion	327
4.3.2. Summary	329
5. CONCLUSIONS AND FURTHER WORK	330
REFERENCES	335
APPENDICES	365
APPENDIX 1: SCHLENK LINE TECHNIQUES	366
APPENDIX 2: DRYING OF SOLVENTS	380
APPENDIX 3: PREPARATION OF LITHIUM DICYCLOHEXYLAMIDE	386
APPENDIX 4: PURIFICATION OF PYROPHOSPHORYL TETRACHLORIDE (PPTC)	389

TABLE OF CONTENTS (CONTINUED)

APPENDIX 5: CHARACTERISATION OF 1,1-BIS(DIPHENYLPHOSPHINO)METHANE (dppm).....	393
APPENDIX 6: EXPERIMENTAL DATA FOR $\text{H}_2\text{C}(\text{Ph}_2\text{PNSiMe}_3)_2$	398
APPENDIX 7: EXPERIMENTAL DATA FOR $\text{H}_2\text{C}(\text{Ph}_2\text{PS})_2$	404
APPENDIX 8: EXPERIMENTAL DATA FOR $\text{LnI}_3(\text{THF})_{3.5}$ STARTING REAGENTS.	410
APPENDIX 9: ADDITIONAL IR, NMR AND PXRD RESULTS FROM THE PREPARATION ATTEMPTS OF $[\text{Sm}_2(\text{C}(\text{Ph}_2\text{PS})_2)_2\text{I}_2\text{THF}_4] \cdot 4(\text{C}_6\text{H}_5\text{CH}_3)$	416
APPENDIX 10: EXPERIMENTAL DATA FOR $\text{Et}_2\text{NH}_2\text{Cl}$	421
APPENDIX 11: ADDITIONAL NMR RESULTS FOR $\text{O}((\text{Et}_2\text{N})_2\text{PO})_2_1$ AND $\text{O}((\text{Et}_2\text{N})_2\text{PO})_2_1_{f13}$	424
APPENDIX 12: CRYSTALLOGRAPHIC DATA FOR PRODUCT $\text{O}((\text{Et}_2\text{N})_2\text{PO})_2_1_{f13}$	428
APPENDIX 13: EXPERIMENTAL DATA FOR $(i\text{PrNH})_3\text{PO}$	436
APPENDIX 14: CRYSTALLOGRAPHIC DATA FOR PRODUCT $\text{O}((i\text{PrNH})_2\text{PO})_2_1_{b1}$	441
APPENDIX 15: SUMMARY OF THE STRUCTURE COMPARISON OF KNOWN MONO-N-SUBSTITUTED PYROPHOSPHORAMIDES.	447
APPENDIX 16: ORGANIC CO-FORMER PXRD ANALYSIS.....	451
APPENDIX 17: RAMAN SPECTROSCOPY OF CO-CRYSTALLISATION PRODUCTS.	453
APPENDIX 18: INITIAL CRYSTALLOGRAPHIC DATA FOR $[\text{N}(\text{Ph}_2\text{PCH}_3)(\text{Ph}_2\text{PNH}_2)][\text{Cl}] \cdot \text{Ph}_2\text{P}(\text{O})\text{NH}_2$	456

LIST OF ABBREVIATIONS

Z	Atomic number
EDTA	Ethylenediaminetetraacetic acid
CN	Coordination number
UV	Ultra violet
NMR	Nuclear magnetic resonance
MRI	Magnetic resonance imaging
n^*	Effective quantum number
n	Principle quantum number
Cp^-	Cyclopentadiene monovalent anion
Cp^*	Pentamethylcyclopentadiene
THF	Tetrahydrofuran
DME	Dimethoxyethane
nBu	n -Butyl ($-C_4H_9$) moiety
1,7-Me ₂ TACD	1,7-Dimethyl-1,4,7,10-tetraazacyclododecane
tmed	Tetramethylethylenediamine
tBu	<i>tert</i> -Butyl ($-C(CH_3)_3$) moiety
RE	Rare earth
dippform	2,6-Diisopropylphenylformamidinato ligand
CCPh	Deprotonated phenylacetylene
HOMO	Highest occupied molecular orbital
MO	Molecular orbital
LUMO	Lowest unoccupied molecular orbital
NHC	N-heterocyclic carbene
e^-	Electron
$p\pi$	p-p π bonding orbital
$p\pi^*$	p-p π antibonding orbital
P^+R_3	Phosphonio group
σ^*	Sigma antibonding orbital
dppm	1,1-Bis(diphenylphosphino)methane
Me	Methyl ($-CH_3$) moiety
iPr	<i>iso</i> -Propyl ($-CH(CH_3)_2$) moiety
DIPP	Diisopropylphenyl ($-2,6-iPr(C_6H_3)$) moiety

KHMDS	Potassium bis(trimethylsilylamide)
PPTC	Pyrophosphoryl tetrachloride
2,2-DMP	2,2-Dimethoxypropane
DMF	Dimethylformamide
SXRD	Single crystal X-ray diffraction
KO ^t Bu	Potassium <i>tert</i> -butoxide
TMEDA	Tetramethylethylenediamine
DMSO	Dimethyl sulfoxide
cif	Crystallographic information file
CSD	Cambridge structural database
XRD	X-Ray diffraction
HSAB	Hard-soft acid-base theory
NCy ₂	Dicyclohexylamide
¹ H NMR	Proton nuclear magnetic resonance
Et	Ethyl (-C ₂ H ₅) moiety
TMTAC	1,3,5-Trimethyl-1,3,5-triazacyclohexane
Tp ^{tBu,Me}	Hydrotris(3- <i>tert</i> -butyl-5-methylpyrazolyl)borate
BODDI	(2,6- <i>i</i> Pr ₂ Ph)NC(Me)CHCOCHC(Me)N(2,6- <i>i</i> Pr ₂ Ph)
DFT	Density functional theory
NBO	Natural bond orbital
Mes	2,4,6-Trimethylphenyl (-2,4,6-Me-C ₆ H ₂) moiety
Mn	Number average molar mass
³¹ P NMR	Phosphorus 31 nuclear magnetic resonance
API	Active pharmaceutical ingredient
CL-20	2,4,6,8,10,12-Hexanitro-2,4,6,8,10,12-hexaazaisowurtzitane
IR	Infra-red
PXRD	Powder X-ray diffraction
TNT	2,4,6-Trinitrotoluene
TGA	Thermogravimetric analysis
GC MS	Gas chromatography mass spectroscopy
ESRF	European Synchrotron Radiation Facility
DEE	Diethyl ether
Bz	Benzyl (-CH ₂ -C ₆ H ₅) moiety
CCDC	Cambridge Crystallographic Data Centre

LIST OF FIGURES

Figure 2.1: Periodic Table showing the Lanthanide Metals encapsulated in red.	4
Figure 2.2: General molecular diagram for di- $\lambda^5\sigma^4$ -phosphorane structure.....	6
Figure 2.3: Structure of $\text{Cp}^*_2\text{Ln}(\mu_2\text{-Cl}_2)\text{AL}_2$ complexes.	8
Figure 2.4: Basic structure of lanthanide arene bonding.	10
Figure 2.5: Structure of compounds $\text{Ln}(\text{o}-(\text{Me}_2\text{NCH}_2)\text{C}_6\text{H}_4)_3$. ¹⁵	12
Figure 2.6: Basic structure of the triphenylphosphine ylide derivatives, where R = H, alkyl of C 1-10, phenyl or trimethylsilyl.....	13
Figure 2.7: a. Basic structure of an organic carbene, b. Electron configuration of the non-bonding carbene electrons for the singlet and triplet states.....	14
Figure 2.8: MO diagrams of carbenes having a. σ -electron withdrawing substituents, b. σ -electron donating substituents. ⁸⁴	15
Figure 2.9: Section of a general MO diagram for a carbene having π -electron donating substituents.....	16
Figure 2.10: General structures of NHCs or Arduengo carbenes.	17
Figure 2.11: General structure of λ^5 -phosphane stabilised carbenes, where X = NR, O or S.	18
Figure 2.12: Phosphonium ylide resonance hybrid structures.	19
Figure 2.13: Electronic structure of the λ^5 -phosphorane stabilised geminal dianions. ⁹⁸	20
Figure 2.14: MO diagram for the bonding of the λ^5 -phosphane carbenes with transition metals. ⁹⁷	21
Figure 2.15: Two main carbene stabilisation structures for the bonding of p_π with transition metal centres. ¹⁰⁷	21
Figure 2.16: Aminophosphonium salt product of the Kirsanov reaction for dppm with RNH_2 . ³⁶	24
Figure 2.17: The preparation of the various neutral (4a-c), mono-anion (5a-c) and dianion (6a-c) derivatives of the bis(diphenyliminophosphorano)methanes synthesised by Demange and co-workers. ³⁶	25
Figure 2.18: Structure of bis(diphenylthiophosphinoyl)methane from SXRD data, 30% probability displacement ellipsoids. ³⁵	26

LIST OF FIGURES (continued)

Figure 2.19: The structures of the ions in the unit cell of [GdI ₂ (THF) ₅][GdI ₄ (THF) ₂] (built in VESTA from cif data obtained from the CSD). ¹³⁷	32
Figure 2.20: Lanthanide tri-benzyl series [Ln(CH ₂ C ₆ H ₅) ₃ (THF) ₃] a) tri-η ² (where Ln = Ce, Pr or Nd) b) mono-η ² (where Ln = Sm) c) η ¹ (where Ln = Gd, Dy or Er). ⁹	33
Figure 2.21: Structures of Sm(Cp*) ₂ (C(N(CH ₃)C(CH ₃)) ₂) and Sm(Cp*) ₂ (C(N(CH ₃)C(CH ₃)) ₂) ₂ . ⁸⁹	35
Figure 2.22: Structures of the samarium and yttrium complexes of bis(diphenyl-N- trimethylsilyl-iminophosphorano)methandiide. ^{7,163}	37
Figure 2.23: Charge distribution common in iminophosphorano carbene ligands complexed with lanthanides.....	38
Figure 2.24: Kohn-Sham orbitals for a) HOMO, b) HOMO-1 and c) HOMO-2 for [Y(C(Ph ₂ PNSiMe ₃) ₂)(CH ₂ C ₆ H ₅)(THF)]. ¹⁸⁸	39
Figure 2.25: Structure of [Y(C(PPh ₂ NSiMe ₃) ₂)(Ga(NArCH) ₂)(THF) ₂] (Ar=2,6- diiso-propylphenyl). ¹⁹⁰	42
Figure 2.26: Complex prepared by Gregson et al. of the formula [K(18-crown- 6)(THF) ₂][RE(C(Ph ₂ PNSiMe ₃) ₂) ₂] ⁺ (THF) ₂ . ⁴²	43
Figure 2.27: Structure for complexes of the formula [RE(Ag)(C(Ph ₂ PNSiMe ₃) ₂) ₂]. ¹⁹⁴	44
Figure 2.28: a) HOMO-2 and b) HOMO-3 of [Ce(C(Ph ₂ PNSiMe ₃) ₂)(O-2,6- <i>i</i> PrC ₆ H ₄) ₂]. ¹⁰	45
Figure 2.29: Reaction products of early Y carbenes with bulky ketones. ⁴³	46
Figure 2.30: Reactions published for [Y(C(Ph ₂ PNSiMe ₃) ₂)(CH ₂ C ₆ H ₅)(THF)]. ⁴⁴	47
Figure 2.31: Reactions published for [Y(C(Ph ₂ PNSiMe ₃) ₂)I(THF) ₂]. ⁴⁵	48
Figure 2.32: Further methandiide to methanide C=Y bond opening for [Y(C(Ph ₂ PNSiMe ₃) ₂)I(THF) ₂] on reaction with inorganic amides. ¹⁹³	49
Figure 2.33: [Li(THF) ₄][Sm(C(Ph ₂ PS) ₂) ₂] (left) and [(Sm ₂ (C(Ph ₂ PS) ₂) ₂ (THF) ₄ (μ-I) ₂] (right). ⁸	51
Figure 2.34: Structure change in the [Tm(C(Ph ₂ PS) ₂) ₂] ⁻ complex with temperature. ¹²³	52
Figure 2.35: Structure of [Li(THF) ₂ Sc(C(Ph ₂ PS) ₂) ₂] with displacement ellipsoids at 50% probability. ¹⁹⁸	53

LIST OF FIGURES (continued)

Figure 2.36: Structure of [Sc(C(Ph ₂ PS) ₂)(HC(Ph ₂ PS) ₂)(THF)]. ¹⁹⁸	53
Figure 2.37: Structure of [Li(THF)(Ln(C(Ph ₂ PS) ₂ (COPh ₂)) ₂), where Ln = Sm or Tm (built in VESTA from cif data obtained from CSD). ^{8,123}	54
Figure 2.38: Cluster product of the reaction of [(Sc(C(Ph ₂ PS) ₂)Cl(Py) ₂] ₂ ·Py with 0.5 equivalents of benzophenone (built in VESTA from cif data obtained from CSD). ¹⁹⁷	54
Figure 2.39: General molecular diagram of di-λ ⁵ σ ⁴ -phosphorane pyrophosphoryl amides.	56
Figure 2.40: Molecular structures of [Th(O((Me ₂ N) ₂ PO) ₂) ₂ Cl ₄] (left) and [U(O((Me ₂ N) ₂ PO) ₂) ₂ (NCS) ₄] (right).....	57
Figure 2.41: Molecular structures of [M(O((Me ₂ N) ₂ PO) ₂) ₃][ClO ₄] ₂ (left, only chlorine atoms of perchlorate are given) where M = Mg ²⁺ , Cu ²⁺ or Co ²⁺ and [Cu(O((Me ₂ N) ₂ PO) ₂) ₂ (ClO ₄) ₂] (right).	59
Figure 2.42: Molecular structure of [Mn(O(<i>t</i> Bu)N(H) ₂ PO) ₂) ₂ DMF ₂][Cl] ₂ ·2H ₂ O.	60
Figure 2.43: Molecular diagram of the fragment of the complex depicting the N-M bond of interest.....	61
Figure 2.44: Molecular diagrams of [Ti(N(Ph ₂ PS) ₂)(HN(Ph ₂ PS) ₂)Cl ₂][Ti ₂ Cl ₉] (left) and [Ti(N(Ph ₂ PS) ₂)(HN(Ph ₂ PS) ₂)Cl ₂][Ti ₂ Cl ₉] (right).....	61
Figure 2.45: Molecular structure of [Ru(N(Ph ₂ PS) ₂)(C ₆ (Me) ₆)], (built in VESTA).	61
Figure 2.46: Molecular structures of [M(N(Ph ₂ PS) ₂) ₃] (left) and [M(N(Ph ₂ PS) ₂)Cp ₂] (right) typical for the metals described in text.	62
Figure 2.47: Molecular diagram of tautomer structure for HN(Ph ₂ PO) ₂ published by Nöth in 1982. ²³⁶	63
Figure 2.48: Trigonal prismatic (left) and Octahedral [Tb(N(Ph ₂ PO) ₂) ₃] ₂ ·0.75H ₂ O.	64
Figure 2.49: Structure of Isoniazid	67
Figure 3.1: Molecular diagram of [H ₂ C(Ph ₂ PNH(<i>i</i> Pr)) ₂]Br ₂	71
Figure 3.2: Molecular diagram of K[HC(Ph ₂ PN <i>i</i> Pr) ₂].....	72
Figure 3.3: Molecular diagram of the ligand H ₂ C(Ph ₂ PNSiMe ₃) ₂	75
Figure 3.4: Molecular diagram of H ₂ C(Ph ₂ PS) ₂	77
Figure 3.5: Structure of [NdI ₂ (THF) ₅][NdI ₄ (THF) ₂] (built in VESTA from cif data obtained from CSD).....	80
Figure 3.6: Second set up used to remove iodine from crude SmI ₃ ·THF _{3.5}	82

LIST OF FIGURES (continued)

Figure 3.7: Molecular diagram of $[\text{Sm}(\text{NCy}_2)_3\text{THF}] \cdot \text{C}_6\text{H}_5\text{CH}_3$	84
Figure 3.8: Molecular diagram of $[\text{Nd}(\text{C}(\text{Ph}_2\text{PNiPr})_2)(\text{HC}(\text{Ph}_2\text{PNiPr})_2)]$	89
Figure 3.9: Molecular diagram of $[\text{Sm}_2(\text{C}(\text{Ph}_2\text{PS})_2)_2\text{I}_2\text{THF}_4] \cdot 4(\text{C}_6\text{H}_5\text{CH}_3)$	92
Figure 3.10: Molecular diagram of the ligand $\text{HN}(\text{Ph}_2\text{PO})_2$	97
Figure 3.11: Molecular diagram of $\text{HN}(\text{Ph}_2\text{PS})_2$	99
Figure 3.12: Molecular diagram of $\text{O}((\text{Et}_2\text{N})_2\text{PO})_2$	100
Figure 3.13: Molecular diagram of $\text{O}((i\text{PrNH})_2\text{PO})_2$	104
Figure 3.14: Molecular diagram $[\text{Eu}(\text{N}(\text{Ph}_2\text{PO})_2)_3]$	107
Figure 3.15: Molecular diagrams of co-formers, biphenyl (left), 4,4'-bipyridine (centre) and 4,4'-oxydianiline (right).....	115
Figure 4.1: Tentative band assignment for IR spectrum for product $[\text{H}_2\text{C}(\text{Ph}_2\text{PNH}(i\text{Pr}))_2]\text{Br}_2_1$	120
Figure 4.2: Full ^1H NMR spectrum of $[\text{H}_2\text{C}(\text{Ph}_2\text{PNH}(i\text{Pr}))_2]\text{Br}_2_1$ in CDCl_3	123
Figure 4.3: Detail of the spectrum for $[\text{H}_2\text{C}(\text{Ph}_2\text{PNH}(i\text{Pr}))_2]\text{Br}_2_1$ showing triplet at 6.56 ppm.	124
Figure 4.4: ^1H NMR peaks for $[\text{H}_2\text{C}(\text{Ph}_2\text{PNH}(i\text{Pr}))_2]\text{Br}_2_1$ believed to be due to phenyl protons.....	125
Figure 4.5: Doublet of triplets structure fit for the peaks around 7.61 ppm.	126
Figure 4.6: IR spectra of $\text{K}[\text{HC}(\text{Ph}_2\text{PN}(i\text{Pr}))_2]_1$ (blue) and $\text{K}[\text{HC}(\text{Ph}_2\text{PN}(i\text{Pr}))_2]_2$ (orange).	128
Figure 4.7: Tentative band assignment for IR spectrum of product $\text{K}[\text{HC}(\text{Ph}_2\text{PN}(i\text{Pr}))_2]_2$	130
Figure 4.8: Full ^1H NMR spectrum of $\text{K}[\text{HC}(\text{Ph}_2\text{PN}(i\text{Pr}))_2]_1$ in CDCl_3	132
Figure 4.9: Full ^1H NMR spectrum of $\text{K}[\text{HC}(\text{Ph}_2\text{PN}(i\text{Pr}))_2]_2$ in CDCl_3	132
Figure 4.10: ^1H NMR spectrum in the range of 4-0 ppm for $\text{K}[\text{HC}(\text{Ph}_2\text{PN}(i\text{Pr}))_2]_1$ in CDCl_3	133
Figure 4.11: ^1H NMR spectrum in the range of 4-0 ppm for $\text{K}[\text{HC}(\text{Ph}_2\text{PN}(i\text{Pr}))_2]_2$ in CDCl_3	134
Figure 4.12: Triplet attributed to the PCHP protons in the ^1H NMR spectrum of $\text{K}[\text{HC}(\text{Ph}_2\text{PN}(i\text{Pr}))_2]_2$	136
Figure 4.13: Doublet associated with the $\text{CH}_3(i\text{Pr})$ protons in the ^1H NMR spectrum of $\text{K}[\text{HC}(\text{Ph}_2\text{PN}(i\text{Pr}))_2]_2$	137

LIST OF FIGURES (continued)

Figure 4.14: Multiplet associated with the NCH(<i>i</i> Pr) protons in the ¹ H NMR spectrum of K[HC(Ph ₂ PN <i>i</i> Pr) ₂] ₂	138
Figure 4.15: Basic coupling observable for the multiplet associated with the NCH(<i>i</i> Pr) protons in the ¹ H NMR spectrum of K[HC(Ph ₂ PN <i>i</i> Pr) ₂] ₂	139
Figure 4.16: Peaks in the ¹ H NMR spectrum of K[HC(Ph ₂ PN <i>i</i> Pr) ₂] ₂ in CDCl ₃ found in the range typical of phenyl protons.	141
Figure 4.17: Structure of coupling for peaks around 7.90 ppm and 7.70 ppm for the ¹ H NMR spectrum of K[HC(Ph ₂ PN <i>i</i> Pr) ₂] ₂ in CDCl ₃	142
Figure 4.18: PXRD patterns of K[HC(Ph ₂ PN <i>i</i> Pr) ₂] ₂ (blue) and [H ₂ C(Ph ₂ PNH(<i>i</i> Pr)) ₂]Br ₂ REFCODE: WERRUH (orange).	143
Figure 4.19: IR spectra of dppm (black), H ₂ C(Ph ₂ PS) ₂ _2a (red) and H ₂ C(Ph ₂ PS) ₂ _2b (blue).	148
Figure 4.20: Unit cell of <i>P</i> 2 ₁ / <i>n</i> polymorph of H ₂ C(Ph ₂ PS) ₂ showing the P=S---H-C(phenyl) interactions.	151
Figure 4.21: Unit cell of <i>C</i> 2/ <i>c</i> polymorph of H ₂ C(Ph ₂ PS) ₂ showing the P=S---H-C(methylene) interactions.	151
Figure 4.22: IR spectrum of [Sm(NCy ₂) ₃ THF]·C ₆ H ₅ CH ₃ _1 in nujol.	158
Figure 4.23: Details of the IR spectra of [Sm(NCy ₂) ₃ THF]·C ₆ H ₅ CH ₃ _1 (blue), Cy ₂ NH (orange) and the data provided in literature for [Sm(NCy ₂) ₃ THF]·C ₆ H ₅ CH ₃ (black).	158
Figure 4.24: IR spectra of [Sm(NCy ₂) ₃ THF]·C ₆ H ₅ CH ₃ (blue) and [(Cy ₂ N) ₂ Sm(μ-Cl)(THF)] ₂ (orange).	160
Figure 4.25: Micrograph of [Sm(NCy ₂) ₃ THF]·C ₆ H ₅ CH ₃ _1.	161
Figure 4.26: Change in structure on deprotonation of H ₂ C(Ph ₂ PNSiMe ₃) ₂	164
Figure 4.27: IR spectra of [Sm(C(Ph ₂ PNSiMe ₃) ₂)(NCy ₂)(THF)]_1 in nujol (blue), H ₂ C(Ph ₂ PNSiMe ₃) ₂ (orange) and [Sm(C(Ph ₂ PNSiMe ₃) ₂)(NCy ₂)(THF)] literature data (black).	167
Figure 4.28: IR spectra of [Sm(C(Ph ₂ PNSiMe ₃) ₂)(NCy ₂)(THF)]_1 in nujol (blue), [Sm(NCy ₂) ₃ THF]·C ₆ H ₅ CH ₃ _1 (orange) and [Sm(NCy ₂) ₃ THF]·C ₆ H ₅ CH ₃ literature data (black).	168
Figure 4.29: IR spectra of [Sm(C(Ph ₂ PNSiMe ₃) ₂)(NCy ₂)(THF)]_2 (orange) and Ph ₂ P(O)NH ₂ (blue).	170

LIST OF FIGURES (continued)

Figure 4.30: IR spectra of the two precipitates constituting [Sm(C(Ph ₂ PNSiMe ₃) ₂)(NCy ₂)(THF)] ₃ (1 st precipitate in blue and 2 nd in orange).	171
Figure 4.31: IR spectra of [Sm(C(Ph ₂ PNSiMe ₃) ₂)(NCy ₂)(THF)] ₃ (1 st precipitate in blue and 2 nd in orange), [Sm(C(Ph ₂ PNSiMe ₃) ₂)(NCy ₂)(THF)] literature data (black), H ₂ C(Ph ₂ PNSiMe ₃) ₂ (red) and [Sm(NCy ₂) ₃ THF]·C ₆ H ₅ CH ₃ _1 (green).	171
Figure 4.32: IR spectrum of [Sm(C(Ph ₂ PNSiMe ₃) ₂)(NCy ₂)(THF)] ₄ in KBr	173
Figure 4.33: Micrograph of [Sm(C(Ph ₂ PNSiMe ₃) ₂)(NCy ₂)(THF)] ₁	177
Figure 4.34: Micrographs of [Sm(C(Ph ₂ PNSiMe ₃) ₂)(NCy ₂)(THF)] ₂ , top left shows the crystalline bed stored under mother liquor, while the ones on the top right and bottom show a crop of crystals and single crystals stored in the NMR tube above the mother liquor.	177
Figure 4.35: Two micrographs of the product [Sm(C(Ph ₂ PNSiMe ₃) ₂)(NCy ₂)(THF)] ₃	178
Figure 4.36: Crystal structure obtained from [Sm(C(Ph ₂ PNSiMe ₃) ₂)(NCy ₂)(THF)] ₂ showing clearly that the compound obtained was diphenylphosphinamide.	179
Figure 4.37: PXRD pattern of [Sm(C(Ph ₂ PNSiMe ₃) ₂)(NCy ₂)(THF)] ₄	183
Figure 4.38: PXRD patterns of [Sm(C(Ph ₂ PNSiMe ₃) ₂)(NCy ₂)(THF)] ₄ (blue) and literature [Sm(C(Ph ₂ PNSiMe ₃) ₂)(NCy ₂)(THF)] (orange).....	183
Figure 4.39: Experimental PXRD pattern of [Sm(C(Ph ₂ PNSiMe ₃) ₂)(NCy ₂)(THF)] ₄ (blue) and the calculated PXRD patterns of H ₂ C(Ph ₂ PNSiMe ₃) ₂ (orange), [Sm(NCy ₂) ₃ THF]·C ₆ H ₅ CH ₃ (green) and LiNCy ₂ (red).	184
Figure 4.40: Experimental PXRD pattern of [Sm(C(Ph ₂ PNSiMe ₃) ₂)(NCy ₂)(THF)] ₄ (blue) and the calculated PXRD patterns of Ph ₂ P(O)NH ₂ _P ₂ 1 ₂ 1 ₂ 1 (orange), Ph ₂ P(O)NH ₂ _P ₂ 1/ <i>c</i> (green) and [N(Ph ₂ PCH ₃)(Ph ₂ PNH ₂)] [Br]. Ph ₂ P(O)NH ₂ (red).	185
Figure 4.41: IR spectra of [Nd(C(Ph ₂ PN <i>i</i> Pr) ₂)(HC(Ph ₂ PN <i>i</i> Pr) ₂)]·2THF_1 (blue) and [Nd(C(Ph ₂ PN <i>i</i> Pr) ₂)(HC(Ph ₂ PN <i>i</i> Pr) ₂)]·2THF_2 (orange) and K(HC(Ph ₂ PN <i>i</i> Pr) ₂)_2 (black).	190

LIST OF FIGURES (continued)

Figure 4.42: Details of IR spectra of [Nd(C(Ph ₂ PNiPr) ₂)(HC(Ph ₂ PNiPr) ₂)]·2THF_1 (blue) and [Nd(C(Ph ₂ PNiPr) ₂)(HC(Ph ₂ PNiPr) ₂)]·2THF_2 (orange) and K(HC(Ph ₂ PNiPr) ₂)_2 (black), in the region 1600 cm ⁻¹ to 400 cm ⁻¹	192
Figure 4.43: IR spectra of [Sm ₂ (C(Ph ₂ PS) ₂) ₂ I ₂ THF ₄]·4(C ₆ H ₅ CH ₃)_2a_1 (blue) and H ₂ C(Ph ₂ PS) ₂ _C2/c polymorph (green) and H ₂ C(Ph ₂ PS) ₂ _P2 ₁ /c polymorph (orange) and SmI ₃ .THF _{3.5} _2 (black).....	197
Figure 4.44: IR spectrum of [Sm ₂ (C(Ph ₂ PS) ₂) ₂ I ₂ THF ₄]·4(C ₆ H ₅ CH ₃)_4a_2 (black), H ₂ C(Ph ₂ PS) ₂ P2 ₁ /c polymorph (orange) and H ₂ C(Ph ₂ PS) ₂ C2/c polymorph (blue).....	199
Figure 4.45: IR spectra of [Sm ₂ (C(Ph ₂ PS) ₂) ₂ I ₂ THF ₄]·4(C ₆ H ₅ CH ₃)_1b (blue) and H ₂ C(Ph ₂ PS) ₂ _1 (orange) and [Sm ₂ (C(Ph ₂ PS) ₂) ₂ I ₂ THF ₄]·4(C ₆ H ₅ CH ₃)_1a (green), in the region 1800 cm ⁻¹ to 400 cm ⁻¹	201
Figure 4.46: IR spectra of [Sm ₂ (C(Ph ₂ PS) ₂) ₂ I ₂ THF ₄]·4(C ₆ H ₅ CH ₃)_3b_2 (blue), H ₂ C(Ph ₂ PS) ₂ _C2/c polymorph (orange) and H ₂ C(Ph ₂ PS) ₂ _P2 ₁ /c polymorph (green) and SmI ₃ .THF _{3.5} _2 (black), in the region 1600 cm ⁻¹ to 400 cm ⁻¹	203
Figure 4.47: Micrograph of [Sm ₂ (C(Ph ₂ PS) ₂) ₂ I ₂ THF ₄]·4(C ₆ H ₅ CH ₃)_2a.	206
Figure 4.48: Micrograph of [Sm ₂ (C(Ph ₂ PS) ₂) ₂ I ₂ THF ₄]·4(C ₆ H ₅ CH ₃)_3a.	207
Figure 4.49: Micrograph of [Sm ₂ (C(Ph ₂ PS) ₂) ₂ I ₂ THF ₄]·4(C ₆ H ₅ CH ₃)_2a_2	207
Figure 4.50: Micrograph of [Sm ₂ (C(Ph ₂ PS) ₂) ₂ I ₂ THF ₄]·4(C ₆ H ₅ CH ₃)_4a_2	208
Figure 4.51: Micrograph of [Sm ₂ (C(Ph ₂ PS) ₂) ₂ I ₂ THF ₄]·4(C ₆ H ₅ CH ₃)_1b.	209
Figure 4.52: Micrograph of [Sm ₂ (C(Ph ₂ PS) ₂) ₂ I ₂ THF ₄]·4(C ₆ H ₅ CH ₃)_2b.	209
Figure 4.53: Micrograph of [Sm ₂ (C(Ph ₂ PS) ₂) ₂ I ₂ THF ₄]·4(C ₆ H ₅ CH ₃)_4b.	209
Figure 4.54: Micrograph of [Sm ₂ (C(Ph ₂ PS) ₂) ₂ I ₂ THF ₄]·4(C ₆ H ₅ CH ₃)_3b_1.	210
Figure 4.55: Micrographs for [Sm ₂ (C(Ph ₂ PS) ₂) ₂ I ₂ THF ₄]·4(C ₆ H ₅ CH ₃)_3b_2 and H ₂ C(Ph ₂ PS) ₂ _1	210
Figure 4.56: Micrograph for [Sm ₂ (C(Ph ₂ PS) ₂) ₂ I ₂ THF ₄]·4(C ₆ H ₅ CH ₃)_2a_1	211
Figure 4.57: PXRD pattern of [Sm ₂ (C(Ph ₂ PS) ₂) ₂ I ₂ THF ₄]·4(C ₆ H ₅ CH ₃)_2b with the range containing peaks most likely due to the major high symmetry phase noted in orange, while the range containing peaks most likely due to the minor lower symmetry phase noted in green.	213

LIST OF FIGURES (continued)

Figure 4.58: PXRD pattern of [Sm ₂ (C(Ph ₂ PS) ₂) ₂ I ₂ THF ₄]·4(C ₆ H ₅ CH ₃) ₂ b (blue) and the calculated PXRD pattern of LiI·H ₂ O (orange).....	213
Figure 4.59: IR spectra of the starting reagent HN(Ph ₂ P) ₂ (blue) and the product HN(Ph ₂ PO) ₂ (orange).....	218
Figure 4.60: Assignment of bands in the IR spectrum of HN(Ph ₂ PO) ₂ _1, as described for the proposed amine tautomer and for the spectrum of the starting reagent.	220
Figure 4.61: Molecular diagram of tautomer structure for HN(Ph ₂ PO) ₂ published by Nöth in 1982.	221
Figure 4.62: Assignment of bands in the HN(Ph ₂ PO) ₂ product, as described for the tautomer proposed by Nöth in 1982 and for the spectrum of the starting reagent.	222
Figure 4.63: ¹ H NMR spectrum of HN(Ph ₂ PO) ₂ _1.	223
Figure 4.64: ¹ H NMR spectrum of HN(Ph ₂ PO) ₂ _1 showing multiplet structures for the peaks believed to be due to the ortho and para protons.	224
Figure 4.65: Completed unit cell for the crystal structure obtained for HN(Ph ₂ PO) ₂ _1.	226
Figure 4.66: Packing structure for HN(Ph ₂ PO) ₂ _1 crystals, with major synthons shown in sections enclosed in green and red.	227
Figure 4.67: Newman Diagrams of a) staggered and b) eclipsed conformations typical of HN(R ₂ P(VI)) ₂ (where VI = O/S/Se), green X represents the position of the central nitrogen in the structure.	228
Figure 4.68: Example for crystalline structures in a) staggered and b) eclipsed conformations for polymorphs of HN(Ph ₂ PSe) ₂	228
Figure 4.69: Eclipsed conformation observed for the molecular structure of HN(Ph ₂ PO) ₂ _1.	229
Figure 4.70: IR spectra of HN(Ph ₂ PS) ₂ _1 (blue) and HN(Ph ₂ P) ₂ (orange).	230
Figure 4.71: Details of IR spectra of HN(Ph ₂ PS) ₂ _1 (blue) and HN(Ph ₂ P) ₂ (orange) in the range 1600-400 cm ⁻¹ with tentative assignments.	232
Figure 4.72: ¹ H NMR spectrum of HN(Ph ₂ PS) ₂ _1 showing the peaks in the aromatic region.	233

LIST OF FIGURES (continued)

Figure 4.73: PXRD patterns of HN(Ph ₂ PS) _{2_1} (blue) and the same product published in literature by Husebye and Maartmann-Moe (orange).	235
Figure 4.74: IR spectra of O(Cl ₂ PO) ₂ (blue), diethylamine (red) and O((Et ₂ N) ₂ PO) _{2_1} (black).....	236
Figure 4.75: IR spectra of O((Et ₂ N) ₂ PO) _{2_1} (black) and Et ₂ NH ₂ Cl (red), in the range 1900-400 cm ⁻¹	238
Figure 4.76: IR spectra of O((Et ₂ N) ₂ PO) _{2_1} (black) and O((Et ₂ N) ₂ PO) _{2_1_f13} (red).	238
Figure 4.77: ¹ H NMR spectrum of O((Et ₂ N) ₂ PO) _{2_1}	242
Figure 4.78: Detail of ¹ H NMR spectrum of O((Et ₂ N) ₂ PO) _{2_1_f13} showing peaks of main interest and integration values.	245
Figure 4.79: ³¹ P{ ¹ H} NMR spectrum of O((Et ₂ N) ₂ PO) _{2_1}	247
Figure 4.80: Expected structure change on formation of O((Et ₂ N) ₂ PO) _{2_1} from PPTC, pyrophosphoryl moiety (red) and the changed groups (green).....	248
Figure 4.81: ³¹ P{ ¹ H} NMR spectrum of O((Et ₂ N) ₂ PO) _{2_1_f13}	250
Figure 4.82: Gas chromatograph of O((Et ₂ N) ₂ PO) _{2_1}	251
Figure 4.83: Mass spectrum of the 10.89 minute fraction of O((Et ₂ N) ₂ PO) _{2_1}	252
Figure 4.84: Gas chromatograph of O((Et ₂ N) ₂ PO) _{2_1_f13}	253
Figure 4.85: Mass spectrum of the 10.56 minute fraction of O((Et ₂ N) ₂ PO) _{2_1_f13} (above) and the 10.89 minute fraction of O((Et ₂ N) ₂ PO) _{2_1} (below).....	253
Figure 4.86: Molecular structure obtained for O((Et ₂ N) ₂ PO) _{2_1_f13}	255
Figure 4.87: Unit cell for O((Et ₂ N) ₂ PO) _{2_1_f13} , as viewed along the <i>a</i> -axis.	255
Figure 4.88: Intermolecular (black) and intramolecular (blue) N–O---H–O hydrogen bonding that created the packing chains for O((Et ₂ N) ₂ PO) _{2_1_f13} along the <i>a</i> -axis, viewed along the <i>c</i> -axis.	257
Figure 4.89: IR spectra of O((<i>i</i> PrNH) ₂ PO) _{2_1_b} (black), O((<i>i</i> PrNH) ₂ PO) _{2_1_c1} (red) and O((<i>i</i> PrNH) ₂ PO) _{2_1_c2} (green) and O((<i>i</i> PrNH) ₂ PO) _{2_1_b1} (blue).	259
Figure 4.90: IR spectra of column chromatography fractions obtained from O((<i>i</i> PrNH) ₂ PO) _{2_1_c1}	261
Figure 4.91: ¹ H NMR spectra of O((<i>i</i> PrNH) ₂ PO) _{2_1_b} (blue) and <i>i</i> PrNH ₃ Cl (red)....	262
Figure 4.92: ¹ H NMR spectrum of O((<i>i</i> PrNH) ₂ PO) _{2_1_b1}	262

LIST OF FIGURES (continued)

Figure 4.93: ^1H NMR spectrum of $\text{O}((i\text{PrNH})_2\text{PO})_2_1_c2$	265
Figure 4.94: ^1H NMR of fractions f7, f9, f10 and f15 of $\text{O}((i\text{PrNH})_2\text{PO})_2_1_c1$	266
Figure 4.95: $^{31}\text{P}\{^1\text{H}\}$ NMR spectra of $\text{O}((i\text{PrNH})_2\text{PO})_2_1_b$ (red) and $\text{O}((i\text{PrNH})_2\text{PO})_2_1_b1$ (blue).....	268
Figure 4.96: $^{31}\text{P}\{^1\text{H}\}$ NMR spectrum of $\text{O}((i\text{PrNH})_2\text{PO})_2_1_c1$	269
Figure 4.97: Gas chromatograph of $\text{O}((i\text{PrNH})_2\text{PO})_2_1_c1_f10$	271
Figure 4.98: Mass spectrum of $\text{O}((i\text{PrNH})_2\text{PO})_2_1_c1_f10$	271
Figure 4.99: Gas chromatograph of $\text{O}((i\text{PrNH})_2\text{PO})_2_1_b1$	274
Figure 4.100: Micrographs of solids obtained for the $\text{O}((i\text{PrNH})_2\text{PO})_2_1$ reaction.	274
Figure 4.101: Molecular structure obtained for $\text{O}((i\text{PrNH})_2\text{PO})_2_1_b1$	276
Figure 4.102: Unit cell for $\text{O}((i\text{PrNH})_2\text{PO})_2_1_b1$	276
Figure 4.103: Hydrogen bonding synthons present in the structure of $\text{O}((i\text{PrNH})_2\text{PO})_2_1_b1$	277
Figure 4.104: Antiparallel columns of $\text{O}((i\text{PrNH})_2\text{PO})_2$ along the a axis.	278
Figure 4.105: Categorisation of pyrophosphoramides under discussion, including structures published from data obtained by SXR D for the solid products, along with the liquid $\text{O}((\text{Me}_2\text{N})_2\text{PO})_2$	279
Figure 4.106: The hydrogen bonding motif common to all crystals having a $P2_1/c$ space group as described in the published structures: (a) $\text{O}((t\text{BuNH})_2\text{PO})_2$; (b) $\text{O}((2\text{-MePhNH})_2\text{PO})_2$ published by Pourayoubi, M. et al.; (c) $\text{O}((2\text{-MePhNH})_2\text{PO})_2$ published by Cameron, S.T. et al.	281
Figure 4.107: Basic unit for the supramolecular H-bonding motif that is common to all three mono-N-substituted pyrophosphoramides that crystallise in a $P2_1/c$ space group, $\text{A} = (\text{R})\text{N-H}$	281
Figure 4.108: H-bonding synthons in $P2_1/c$ structures: (a) intermolecular ring synthon; (b) the two variants of the intramolecular synthon where A is the non-intermolecular bonding amine.	281
Figure 4.109: Hydrogen bonding motif for $\text{O}((4\text{-MePhNH})_2\text{PO})_2$ (a) as viewed along the a -axis, showing the complete repeatable moiety described for this structure (left) and offset to show the staggered conformation of the pyrophosphoramide (right); (b) The ring synthon that is the base for the motif given in a simplified diagram.	283

LIST OF FIGURES (continued)

Figure 4.110: Intermolecular and intramolecular non-hydrogen bonding interactions in the structure of $O((4\text{-MePhNH})_2\text{PO})_2$	283
Figure 4.111: IR spectra of $[\text{Eu}(\text{N}(\text{Ph}_2\text{PO})_2)_3]_1$ (blue) and $\text{HN}(\text{Ph}_2\text{PO})_2_1$ (orange).	287
Figure 4.112: IR spectra of $[\text{Eu}(\text{N}(\text{Ph}_2\text{PO})_2)_3]_2$ (blue) and $\text{HN}(\text{Ph}_2\text{PO})_2_1$ (orange), in the range 1800cm^{-1} to 400cm^{-1}	289
Figure 4.113: Detail of the aromatic region of the ^1H NMR spectra for $[\text{Eu}(\text{N}(\text{Ph}_2\text{PO})_2)_3]_1$ (blue) and $\text{HN}(\text{Ph}_2\text{PO})_2_1$ (red).	291
Figure 4.114: Detail of the aromatic region of the ^1H NMR spectra for $[\text{Eu}(\text{N}(\text{Ph}_2\text{PO})_2)_3]_2$ (blue) and $\text{HN}(\text{Ph}_2\text{PO})_2_1$ (red).	292
Figure 4.115: Powder patterns for $[\text{Eu}(\text{N}(\text{Ph}_2\text{PO})_2)_3]_1$ (blue) and BOLGIS (orange).	293
Figure 4.116: Powder patterns for $[\text{Eu}(\text{N}(\text{Ph}_2\text{PO})_2)_3]_2$ (black) and ZAXDIN (red) and HIWDUN (blue).	294
Figure 4.117: Powder patterns for $[\text{Eu}(\text{N}(\text{Ph}_2\text{PO})_2)_3]_2$ (blue) and $\alpha\text{-KNO}_3$ in a <i>Pmcn</i> space group (orange), the experimental peaks not attributable to this $\alpha\text{-KNO}_3$ are labelled in red.	295
Figure 4.118: Molecular representation of the theoretical sulphide analogue of $[\text{Eu}(\text{N}(\text{Ph}_2\text{PO})_2)_3] - [\text{Eu}(\text{N}(\text{Ph}_2\text{PS})_2)_3]$	296
Figure 4.119: IR spectra, in the region $1600\text{-}400\text{ cm}^{-1}$, for $\text{HN}(\text{Ph}_2\text{PS})_2+\text{Eu}(\text{ClO}_4)_3\cdot n(\text{H}_2\text{O})_1$ (blue) and $\text{HN}(\text{Ph}_2\text{PS})_2_1$ (orange). .	297
Figure 4.120: ^1H NMR spectra for $\text{HN}(\text{Ph}_2\text{PS})_2+\text{Eu}(\text{ClO}_4)_3\cdot n(\text{H}_2\text{O})_1$ (blue) and $\text{HN}(\text{Ph}_2\text{PS})_2_1$ (red).	298
Figure 4.121: Micrographs of $\text{HN}(\text{Ph}_2\text{PS})_2+\text{Eu}(\text{ClO}_4)_3\cdot n(\text{H}_2\text{O})_1$ showing (left) particles with clear habit and (right) the same product under 254 nm UV-Visible radiation.	299
Figure 4.122: PXRD patterns for $\text{HN}(\text{Ph}_2\text{PS})_2+\text{Eu}(\text{ClO}_4)_3\cdot n(\text{H}_2\text{O})_1$ (blue) and BOLGEO01 (orange).	300
Figure 4.123: IR spectra of $O((\text{Et}_2\text{N})_2\text{PO})_2+\text{Nd}(\text{ClO}_4)_3_1$ (black), $O((\text{Et}_2\text{N})_2\text{PO})_2_1$ (red) and $O((\text{Et}_2\text{N})_2\text{PO})_2_1_{f13}$ (green).	301

LIST OF FIGURES (continued)

Figure 4.124: IR spectra of $O((Et_2N)_2PO)_2+Nd(ClO_4)_3_1$ (black), $O((Et_2N)_2PO)_2_1_f13$ (red) and $Nd(ClO_4)_3$ dried using 2,2-DMP (green).	302
Figure 4.125: 1H NMR spectrum of $O((Et_2N)_2PO)_2+Nd(ClO_4)_3_1$ in $CDCl_3$	303
Figure 4.126: $^{31}P\{^1H\}$ NMR spectrum of $O((Et_2N)_2PO)_2+Nd(ClO_4)_3_1$ in $CDCl_3$	306
Figure 4.127: Gas chromatography of $O((Et_2N)_2PO)_2+Nd(ClO_4)_3_1$	307
Figure 4.128: Comparison of the Mass spectra of $O((Et_2N)_2PO)_2_1$ (GC peak at 10.90 min.), $O((Et_2N)_2PO)_2_1_f13$ (GC peak at 10.56 min.) and $O((Et_2N)_2PO)_2+Nd(ClO_4)_3_1$ (GC peak at 10.60 min.).	307
Figure 4.129: Mass spectra of the $O((Et_2N)_2PO)_2+Nd(ClO_4)_3_1$ (GC peak at 12.23 minutes).	309
Figure 4.130: Micrograph of crystals obtained from the viscous liquid $O((Et_2N)_2PO)_2+Nd(ClO_4)_3_1$	310
Figure 4.131: IR spectra of $Sm(C(Ph_2PNSiMe_3)_2)(NCy_2)(THF)]_3$:biphenyl (blue), $[Sm(C(Ph_2PNSiMe_3)_2)(NCy_2)(THF)]_3$:4,4'-bipyridine in nujol (orange), $[Sm(C(Ph_2PNSiMe_3)_2)(NCy_2)(THF)]_3$:4,4'-oxydianiline (green) and $[Sm(C(Ph_2PNSiMe_3)_2)(NCy_2)(THF)]_3$ (black).	312
Figure 4.132: IR spectra of $[Sm(C(Ph_2PNSiMe_3)_2)(NCy_2)(THF)]_4$:biphenyl (blue), $[Sm(C(Ph_2PNSiMe_3)_2)(NCy_2)(THF)]_4$:4,4'-bipyridine (orange) and $[Sm(C(Ph_2PNSiMe_3)_2)(NCy_2)(THF)]_4$:4,4'-oxydianiline (green).	313
Figure 4.133: IR spectra of $[Sm(C(Ph_2PNSiMe_3)_2)(NCy_2)(THF)]_4$:biphenyl (blue), $[Sm(C(Ph_2PNSiMe_3)_2)(NCy_2)(THF)]_4$ (orange) and biphenyl (green) in the region $1800-400\text{ cm}^{-1}$	314
Figure 4.134: IR spectra of $[Sm(C(Ph_2PNSiMe_3)_2)(NCy_2)(THF)]_4$:4,4'-bipyridine (blue), $[Sm(C(Ph_2PNSiMe_3)_2)(NCy_2)(THF)]_4$ (orange) and 4,4'- bipyridine (green) in the region $1800-400\text{ cm}^{-1}$	316
Figure 4.135: IR spectra of $[Sm(C(Ph_2PNSiMe_3)_2)(NCy_2)(THF)]_4$:4,4'- oxydianiline (blue), $[Sm(C(Ph_2PNSiMe_3)_2)(NCy_2)(THF)]_4$ (orange) and 4,4'-oxydianiline (green) in the region $1800-400\text{ cm}^{-1}$	317
Figure 4.136: PXRD patterns of $[Sm(C(Ph_2PNSiMe_3)_2)(NCy_2)(THF)]_4$ (blue) and $[Sm(C(Ph_2PNSiMe_3)_2)(NCy_2)(THF)]_4$:biphenyl (orange).	321

LIST OF FIGURES (continued)

Figure 4.137: PXRD patterns of [Sm(C(Ph ₂ PNSiMe ₃) ₂ (NCy ₂)(THF)] ₄ (blue), [Sm(C(Ph ₂ PNSiMe ₃) ₂ (NCy ₂)(THF)] ₄ :4,4'-bipyridine (orange) and [Sm(C(Ph ₂ PNSiMe ₃) ₂ (NCy ₂)(THF)] ₄ :4,4'-oxydianiline (green).....	321
Figure 4.138: Experimental PXRD pattern of [Sm(C(Ph ₂ PNSiMe ₃) ₂ (NCy ₂)(THF)] ₄ :biphenyl (blue) and calculated PXRD pattern of the biphenyl form, published in the CSD as BIPHEN04 (orange).....	322
Figure 4.139: Experimental PXRD pattern of [Sm(C(Ph ₂ PNSiMe ₃) ₂ (NCy ₂)(THF)] ₄ :4,4'-bipyridine (blue) and calculated PXRD pattern of 4,4'-bipyridine in <i>P</i> -1 unit cell (orange).....	323
Figure 4.140: Experimental PXRD pattern of [Sm(C(Ph ₂ PNSiMe ₃) ₂ (NCy ₂)(THF)] ₄ :4,4'-oxydianiline (blue) and calculated PXRD pattern of the <i>P</i> ₂ ₁ ₂ ₁ polymorph of 4,4'- oxydianiline, published in the CSD as SUCVER (orange).....	324
Figure 4.141: Structures of the iso-structural [N(Ph ₂ PCH ₃)(Ph ₂ PNH ₂)] [Cl] · Ph ₂ P(O)NH ₂ (left) and [N(Ph ₂ PCH ₃)(Ph ₂ PNH ₂)] [Br] · Ph ₂ P(O)NH ₂ (right).....	326
Figure A-1.1: Set up for the reduction of MnO ₂ to MnO oxygen scavenger, diagram (left, drawn using ACD/ChemSketch software) and photograph (right) .	369
Figure A-1.2: MnO column set in line in the path leading argon to the Schlenk line. .	370
Figure A-1.3: Diagram of Set up of moisture and oxygen scavenger columns using purchased inert gas purifiers (drawn using ACD/ChemSketch software).....	372
Figure A-1.4: Connection set up for connecting the gas purifiers to Nalgene tubing used throughout the set up.	373
Figure A-1.5: Liquid transfer via cannula (drawn using ACD/ChemSketch software).....	373
Figure A-1.6: Filtration using the filtration tube technique (drawn using ACD/ChemSketch software).....	375
Figure A-1.7: Cannula filtration set up (drawn using ACD/ChemSketch software)....	375
Figure A-1.8: Test tube formed for ampoule preparation.....	376
Figure A-1.9: Large tube-like flask set up used to purge and fill ampoule tubes.....	377

LIST OF FIGURES (continued)

Figure A-1.10: Filled ampoule.....	377
Figure A-1.11: Weighing set up used to weigh air and moisture sensitive compounds in inert conditions.	378
Figure A-2.1: Solvent drying still set up used throughout the study (drawn using ACD/ChemSketch software).....	380
Figure A-2.2: Toluene being dried in still showing typical deep purple colour of Na/Benzophenone indicator indicating dryness.....	384
Figure A-2.3: Dry Acetonitrile stored over 3Å molecular sieves.....	385
Figure A-3.1: Molecular diagram of LiNCy ₂	386
Figure A-3.2: IR spectra of LiNCy ₂ _1 (black), LiNCy ₂ _2 (red) and Cy ₂ NH (green)..	387
Figure A-4.1: Molecular diagram of pyrophosphoryl tetrachloride (PPTC).....	389
Figure A-4.2: General molecular diagram of organic pyrophosphoryl compounds derived from PPTC.	389
Figure A-4.3: Short path distillation used for the purification of PPTC.....	390
Figure A-4.4: Purging of amber glass bottle to be used for the storage of PPTC.	391
Figure A-4.5: IR Spectrum of the purified PPTC.....	391
Figure A-4.6: ³¹ P{ ¹ H} NMR spectrum of purified PPTC.	392
Figure A-5.1: Molecular diagram of dppm.....	393
Figure A-5.2: IR spectrum of purchased dppm, in KBr disc.....	393
Figure A-5.3: Full ¹ H NMR spectrum for dppm as purchased in CDCl ₃	395
Figure A-5.4: Detail of dppm spectrum showing triplet assigned to the ¹ H on PCH ₂ P.	397
Figure A-6.1: IR spectra of H ₂ C(Ph ₂ PNSiMe ₃) ₂ _1 (orange), H ₂ C(Ph ₂ PNSiMe ₃) ₂ _2 (blue), trimethylsilyl azide (red) and dppm (green).....	398
Figure A-6.2: IR spectra of H ₂ C(Ph ₂ PNSiMe ₃) ₂ _2 (blue) with the literature data (orange).	399
Figure A-6.3: IR spectra of H ₂ C(Ph ₂ PNSiMe ₃) ₂ _3 (blue) and H ₂ C(Ph ₂ PNSiMe ₃) ₂ _1 (orange).	400
Figure A-6.4: Full ¹ H NMR spectrum for H ₂ C(Ph ₂ PSiMe ₃) ₂ _1 in C ₆ D ₆	400
Figure A-6.5: Detail of triplet in ¹ H NMR spectrum of H ₂ C(Ph ₂ PSiMe ₃) ₂ _1 assigned to PCH ₂ P protons.	401

LIST OF FIGURES (continued)

Figure A-6.6: Detail showing the peaks attributed to the phenyl protons of $\text{H}_2\text{C}(\text{Ph}_2\text{PSiMe}_3)_2_1$	402
Figure A-6.7: Detail showing the peaks around 7.41 ppm for the spectrum of $\text{H}_2\text{C}(\text{Ph}_2\text{PSiMe}_3)_2_1$	402
Figure A-6.8: Detail showing the range 0.4 to 0.05 ppm for the spectrum of $\text{H}_2\text{C}(\text{Ph}_2\text{PSiMe}_3)_2_1$	403
Figure A-7.1: IR spectrum of the $\text{H}_2\text{C}(\text{Ph}_2\text{PS})_2_1$ (blue) and dppm (orange).	404
Figure A-7.2: Possible P=S vibration bands in the IR spectrum of $\text{H}_2\text{C}(\text{Ph}_2\text{PS})_2_1$...	404
Figure A-7.3: IR spectra of $\text{H}_2\text{C}(\text{Ph}_2\text{PS})_2_2\text{a}$ (blue) and $\text{H}_2\text{C}(\text{Ph}_2\text{PS})_2_2\text{b}$ (orange)....	405
Figure A-7.4: IR spectra of $\text{H}_2\text{C}(\text{Ph}_2\text{PS})_2_3\text{a}$ (blue) and $\text{H}_2\text{C}(\text{Ph}_2\text{PS})_2_3\text{b}$ (orange)....	405
Figure A-7.5: ^1H NMR spectrum for $\text{H}_2\text{C}(\text{Ph}_2\text{PS})_2_1$ in C_6D_6	406
Figure A-7.6: Triplet at 3.84 ppm attributed to the PCH_2P protons.	407
Figure A-7.7: ^1H NMR spectra of all the $\text{H}_2\text{C}(\text{Ph}_2\text{PS})_2$ solids obtained in the study. ...	407
Figure A-7.8: Crystals of $\text{H}_2\text{C}(\text{Ph}_2\text{PS})_2_1$ under polarised light.	408
Figure A-7.9: PXRD patterns of $\text{H}_2\text{C}(\text{Ph}_2\text{PS})_2_2\text{b}$ (blue), $P2_1/n$ (orange) and $C2/c$ (red).....	409
Figure A-8.1: IR spectra of $\text{NdI}_3(\text{THF})_{3.5_1}$ in Nujol (blue).	410
Figure A-8.2: IR spectra of $\text{NdI}_3(\text{THF})_{3.5_1}$ (blue), $\text{NdI}_3(\text{THF})_{3.5}$ (red), $\text{NdI}_3(\text{THF})_4$ (green) and THF (black).	411
Figure A-8.3: UV-vis spectra of $\text{NdI}_3(\text{THF})_{3.5_1}$ (blue) and $\text{NdCl}_3 \cdot n\text{H}_2\text{O}$ (orange) in the range 400-900 nm.	412
Figure A-8.4: UV-vis Spectra of $\text{NdI}_3(\text{THF})_{3.5_1\text{a}}$ (blue) and $\text{NdI}_3(\text{THF})_{3.5_1\text{b}}$ (orange).....	413
Figure A-8.5: IR Spectra of $\text{SmI}_3(\text{THF})_{3.5_1}$ (blue) and $\text{SmI}_3(\text{THF})_{3.5_2}$ (orange) in Nujol mull.	413
Figure A-8.6: IR spectra of $\text{SmI}_3(\text{THF})_{3.5_1}$ (blue) and $\text{SmI}_3(\text{THF})_{3.5_2}$ (orange), $\text{SmI}_3(\text{THF})_{3.5}$ in literature (black) and Nujol (green) in the region of $1800\text{-}400\text{ cm}^{-1}$	414
Figure A-8.7: Micrograph of $\text{SmI}_3(\text{THF})_{3.5_2}$	415
Figure A-8.8: PXRD patterns of $\text{SmI}_3(\text{THF})_{3.5_2}$ (blue) and calculated $\text{SmI}_3(\text{THF})_{3.5}$ literature data (orange).	415

LIST OF FIGURES (continued)

Figure A-9.1: IR spectra of [Sm ₂ (C(Ph ₂ PS) ₂) ₂ I ₂ THF ₄].4(C ₆ H ₅ CH ₃) ₁ a (blue) and H ₂ C(Ph ₂ PS) _{2_1} (orange).	416
Figure A-9.2: IR spectra of [Sm ₂ (C(Ph ₂ PS) ₂) ₂ I ₂ THF ₄].4(C ₆ H ₅ CH ₃) ₁ b (blue) and [Sm ₂ (C(Ph ₂ PS) ₂) ₂ I ₂ THF ₄].4(C ₆ H ₅ CH ₃) ₁ c (black) and H ₂ C(Ph ₂ PS) _{2_C2/c} polymorph (green) and H ₂ C(Ph ₂ PS) _{2_P21/c} polymorph (orange), in the region 2000 cm ⁻¹ to 400 cm ⁻¹	416
Figure A-9.3: IR spectra of [Sm ₂ (C(Ph ₂ PS) ₂) ₂ I ₂ THF ₄].4(C ₆ H ₅ CH ₃) ₂ a (blue) and H ₂ C(Ph ₂ PS) _{2_C2/c} polymorph (orange), in the region 1800 cm ⁻¹ to 400 cm ⁻¹	417
Figure A-9.4: IR spectra of [Sm ₂ (C(Ph ₂ PS) ₂) ₂ I ₂ THF ₄].4(C ₆ H ₅ CH ₃) ₂ a ₂ (black) and H ₂ C(Ph ₂ PS) _{2_C2/c} polymorph (green) and H ₂ C(Ph ₂ PS) _{2_P21/c} polymorph (red), in the region of 1600 to 400 cm ⁻¹	417
Figure A-9.5: IR spectra of [Sm ₂ (C(Ph ₂ PS) ₂) ₂ I ₂ THF ₄].4(C ₆ H ₅ CH ₃) ₂ b (blue) and H ₂ C(Ph ₂ PS) _{2_C2/c} polymorph (red) and H ₂ C(Ph ₂ PS) _{2_P21/c} polymorph (green) and SmI ₃ .THF _{3.5_2} (black), in the region 1600 cm ⁻¹ to 400 cm ⁻¹	417
Figure A-9.6: IR spectra of [Sm ₂ (C(Ph ₂ PS) ₂) ₂ I ₂ THF ₄].4(C ₆ H ₅ CH ₃) ₃ a (black) and H ₂ C(Ph ₂ PS) _{2_C2/c} polymorph (orange) and H ₂ C(Ph ₂ PS) _{2_P21/c} polymorph (blue).	418
Figure A-9.7: IR spectra of [Sm ₂ (C(Ph ₂ PS) ₂) ₂ I ₂ THF ₄].4(C ₆ H ₅ CH ₃) ₃ a (blue) and H ₂ C(Ph ₂ PS) _{2_C2/c} polymorph (green) and [Sm ₂ (C(Ph ₂ PS) ₂) ₂ I ₂ THF ₄].4(C ₆ H ₅ CH ₃) ₃ b ₁ (orange).	418
Figure A-9.8: IR spectra of [Sm ₂ (C(Ph ₂ PS) ₂) ₂ I ₂ THF ₄].4(C ₆ H ₅ CH ₃) ₄ a (blue) and H ₂ C(Ph ₂ PS) _{2_C2/c} polymorph (green) and H ₂ C(Ph ₂ PS) _{2_P21/c} polymorph (orange) in the region 1800 cm ⁻¹ to 400 cm ⁻¹	418
Figure A-9.9: IR spectra of [Sm ₂ (C(Ph ₂ PS) ₂) ₂ I ₂ THF ₄].4(C ₆ H ₅ CH ₃) ₄ a ₁ (blue) and [Sm ₂ (C(Ph ₂ PS) ₂) ₂ I ₂ THF ₄].4(C ₆ H ₅ CH ₃) ₄ a (orange).	419
Figure A-9.10: ¹ H NMR spectra of [Sm ₂ (C(Ph ₂ PS) ₂) ₂ I ₂ THF ₄].4(C ₆ H ₅ CH ₃) ₂ a (blue) and [Sm ₂ (C(Ph ₂ PS) ₂) ₂ I ₂ THF ₄].4(C ₆ H ₅ CH ₃) ₂ b (green) and H ₂ C(Ph ₂ PS) ₂ in CDCl ₃ (red).	419
Figure A-9.11: ¹ H NMR spectra of [Sm ₂ (C(Ph ₂ PS) ₂) ₂ I ₂ THF ₄].4(C ₆ H ₅ CH ₃) ₃ b ₂ (blue) and H ₂ C(Ph ₂ PS) ₂ in benzene-d ₆ (red).	420

LIST OF FIGURES (continued)

Figure A-9.12: PXRD pattern of $[\text{Sm}_2(\text{C}(\text{Ph}_2\text{PS})_2)_2\text{I}_2\text{THF}_4] \cdot 4(\text{C}_6\text{H}_5\text{CH}_3)_2$	420
Figure A-10.1: ^1H NMR spectrum of $\text{Et}_2\text{NH}_2\text{Cl}$	421
Figure A-10.2: IR spectra of diethylamine (blue) and diethylammonium chloride (orange).	423
Figure A-11.1: ^1H NMR spectrum of $\text{O}((\text{Et}_2\text{N})_2\text{PO})_2_1$	424
Figure A-11.2: ^1H NMR spectrum of $\text{O}((\text{Et}_2\text{N})_2\text{PO})_2_1_{\text{f13}}$	425
Figure A-11.3: $^{31}\text{P}\{^1\text{H}\}$ NMR spectra of PPTC (blue) and $\text{O}((\text{Et}_2\text{N})_2\text{PO})_2_1$ (light red).	426
Figure A-11.4: ^{31}P NMR spectrum of $\text{O}((\text{Et}_2\text{N})_2\text{PO})_2_1$ with detail of peak at 8.50 ppm given in inset.	426
Figure A-11.5: Detail of ^{31}P NMR spectrum of $\text{O}((\text{Et}_2\text{N})_2\text{PO})_2_1_{\text{f13}}$	427
Figure A-12.1: Crystal used in structure determination of $\text{O}((\text{Et}_2\text{N})_2\text{PO})_2_1_{\text{f13}}$	428
Figure A-13.1: Micrograph of $(i\text{PrNH})_3\text{PO}$	437
Figure A-13.2: $^{31}\text{P}\{^1\text{H}\}$ NMR spectra of $(i\text{PrNH})_3\text{PO}$	438
Figure A-13.3: Gas chromatograph of $(i\text{PrNH})_3\text{PO}$	438
Figure A-13.4: Mass spectrum of $(i\text{PrNH})_3\text{PO}$	439
Figure A-13.5: ^1H NMR spectrum of $(i\text{PrNH})_3\text{PO}$	440
Figure A-13.6: IR spectra of $(i\text{PrNH})_3\text{PO}$	440
Figure A-14.1: Crystal used in structure determination of $\text{O}((i\text{PrNH})_2\text{PO})_2_1_{\text{b1}}$	441
Figure A-16.1: Experimental PXRD patterns of biphenyl (blue) and calculated PXRD pattern of BIPHEN04 (orange).	451
Figure A-16.2: Experimental PXRD patterns of 4,4'-bipyridine (blue) and calculated PXRD pattern of anhydrous 4,4'-bipyridine in a spacegroup $P-1$ (orange).	452
Figure A-16.3: Experimental PXRD patterns of 4,4'-oxydianiline (blue) and calculated PXRD pattern of SUCVER (orange).	452
Figure A-17.1: Raman spectrum of biphenyl.	453
Figure A-17.2: Raman spectrum of 4,4'-bipyridine	453
Figure A-17.3: Raman spectrum of 4,4'-Oxydianiline.	454
Figure A-17.4: Raman spectra of $[\text{Sm}(\text{C}(\text{Ph}_2\text{PNSiMe}_3)_2)(\text{NCy}_2)(\text{THF})]_4$:biphenyl (blue) and biphenyl (orange).	454

LIST OF FIGURES (continued)

Figure A-17.5: Raman spectra of $[\text{Sm}(\text{C}(\text{Ph}_2\text{PNSiMe}_3)_2(\text{NCy}_2)(\text{THF})]_{-4:4,4^-}$ - bipyridine (orange) and 4,4'-bipyridine (blue).	454
Figure A-17.6: Raman spectrum of $[\text{Sm}(\text{C}(\text{Ph}_2\text{PNSiMe}_3)_2(\text{NCy}_2)(\text{THF})]_{-4:4,4^-}$ - oxydianiline.....	455

LIST OF SCHEMES

Scheme 2.1: Synthesis of bis(diphenyl-N-trimethylsilyliminodiphenylphosphorano)methane. ³⁴	22
Scheme 2.2: Mechanism for the formation of triphenyliminophosphoranes. ¹¹⁷	23
Scheme 2.3: Reaction of phosphorus (V) halides published by Kirsanov in 1954. ⁹⁹	23
Scheme 2.4: Preparation of triphenyliminophosphorane analogues through the modified Kirsanov route as first published by Horner and Oediger and expanded on by Zimmer and Singh. ^{117,119,120}	23
Scheme 2.5: Synthesis of bis(diphenylphosphino)methane disulphide by the oxidation of dppm with sulphur.	26
Scheme 2.6: Ortho-C-H bond activation mechanism proposed for the synthesis of compounds given in Figure 2.28. ⁴³	46
Scheme 2.7: Mechanisms for the initiation of lactide polymerisation by [Nd(C(Ph ₂ PN <i>i</i> Pr) ₂)(HC(Ph ₂ PN <i>i</i> Pr) ₂)] a) using KOEt b) using <i>i</i> PrOH. ¹²	50
Scheme 2.8: Dehydrating action of 2,2-DMP showing reaction with water to form acetone and methanol.	58
Scheme 2.9: Synthesis of [N ⁺ (Ph ₂ PO ⁻)(Ph ₂ POH)]	63
Scheme 3.1: Synthesis of [Sm(NC _y ₂) ₃ THF]	84
Scheme 3.2: Synthesis of [Sm(C(Ph ₂ PNSiMe ₃) ₂)(NC _y ₂)(THF)]	86
Scheme 3.3: Synthesis of [Nd(C(Ph ₂ PN <i>i</i> Pr) ₂)(HC(Ph ₂ PN <i>i</i> Pr) ₂)]	90
Scheme 3.4: Synthesis of [Sm ₂ (C(Ph ₂ PS) ₂) ₂ L ₂ THF ₄]	92
Scheme 3.5: Synthesis of HN(Ph ₂ PO) ₂	97
Scheme 3.6: Synthesis of HN(Ph ₂ PS) ₂	99
Scheme 3.7: General synthesis reaction for the preparation of O((R _{3-n} NH _{n-1}) ₂ PO) ₂ compounds.	100
Scheme 3.8: Synthesis of [Eu(N(Ph ₂ PO) ₂) ₃]	107
Scheme 3.9: Reaction expected in the current study to form a O((Et ₂ N) ₂ PO) ₂ +Nd(ClO ₄) ₃ complex.	112
Scheme 4.1: General moisture induced decomposition reaction of H ₂ C(Ph ₂ PNSiMe ₃) ₂	180
Scheme 4.2: Hydrolysis reaction for H ₂ C(Ph ₂ PNPh) ₂ proposed by Aguiar and Beisler. ²⁹⁵	180

LIST OF SCHEMES (continued)

Scheme 4.3: Overview of the hydrolysis decomposition mechanism of $\text{H}_2\text{C}(\text{Ph}_2\text{PNPh})_2$; products obtained highlighted in green.	181
Scheme 4.4: Nucleophilic substitution by silyl amine with organic acid chloride (top) and the nucleophilic substitution of $\text{Ph}_2\text{P}(\text{O})\text{NHSiMe}_3$ with H_2NSiMe_3 in an analogous mechanism (bottom).	182
Scheme 4.5: Full multi-step moisture induced decomposition reaction of $\text{H}_2\text{C}(\text{Ph}_2\text{PNSiMe}_3)_2$	182
Scheme A-1.1: Thermal decomposition of $\text{Mn}(\text{NO}_3)_2 \cdot 6\text{H}_2\text{O}$	368
Scheme A-1.2: Reduction of MnO_2 to MnO	368
Scheme A-3.1: Synthesis of LiNCy_2	386

LIST OF TABLES

Table 2.1: THF solvated Rare Earth triiodides.	30
Table 2.2: Bond lengths of N–M bonds given in literature.	62
Table 3.1: Details of the column chromatography fractions of O((Et ₂ N) ₂ PO) ₂ _1.	102
Table 3.2: Details of the column chromatography fractions of O((iPrNH) ₂ PO) ₂ _1_c1	105
Table 3.3: Synthesis attempts for Eu(N(Ph ₂ PS) ₂) ₃ through wet chemical methods. ...	110
Table 3.4: Hot Stage microscopy temperature profile used in the synthesis of HN(Ph ₂ PS) ₂ +Eu(ClO ₄) ₃ ·n(H ₂ O)_1.	111
Table 3.5: Intermolecular interactions believed to be available for co-formers used in this study.	115
Table 3.6: Details of co-crystallisation procedures undertaken.	116
Table 3.7: Details of crystallisation from toluene of [Sm(C(Ph ₂ PNSiMe ₃) ₂)(NCy ₂)(THF)]_4 co-crystallisation products.....	117
Table 4.1: ¹ H NMR spectroscopy data for [H ₂ C(Ph ₂ PNH(<i>i</i> Pr)) ₂]Br ₂ in CDCl ₃ as given in literature. ³⁶	122
Table 4.2: ¹ H NMR experimental data for [H ₂ C(Ph ₂ PNH(<i>i</i> Pr)) ₂]Br ₂ _1 in CDCl ₃	123
Table 4.3: Reaction data for the synthesis of K[HC(Ph ₂ PN(<i>i</i> Pr)) ₂] from [H ₂ C(Ph ₂ PNH(<i>i</i> Pr)) ₂]Br ₂ _1.	127
Table 4.4: ¹ H NMR literature data published for Li[HC(Ph ₂ PN <i>i</i> Pr) ₂] in THF-d ₈ . ³⁶	133
Table 4.5: Comparison of data for the literature Li salt (in THF-d ₈) and the two products K[HC(Ph ₂ PN <i>i</i> Pr) ₂]-1 (-1) and K[HC(Ph ₂ PN <i>i</i> Pr) ₂]-2 (-2) (both in CDCl ₃).	134
Table 4.6: Comparison of coupling constants for literature data and experimental data for K[HC(Ph ₂ PN <i>i</i> Pr) ₂]-2.	136
Table 4.7: Tentative assignment of characteristic IR bands of H ₂ C(Ph ₂ PNSiMe ₃) ₂ prepared in this study.	145
Table 4.8: Bands of interest in the IR spectra of all products of H ₂ C(Ph ₂ PS) ₂ in the range 805 to 590 cm ⁻¹	148
Table 4.9: Yields of LnI ₃ (THF) _{3.5} products.	153
Table 4.10: Published XRD bond length data for the P-C and P-N bonds in relevant H ₂ C(Ph ₂ PNR) ₂ derivatives.	188

LIST OF TABLES (continued)

Table 4.11: Products collected from initial solid and filtrate workup respectively, including yields in brackets.	196
Table 4.12: Cell parameters and statistics for unit cell obtained through indexing and Pawley refinement of $\text{HN}(\text{Ph}_2\text{PO})_2_1$	225
Table 4.13: Unit cell parameters for the structure solution of $\text{HN}(\text{Ph}_2\text{PO})_2_1$	226
Table 4.14: ^1H NMR experimental data for proton peaks of $\text{O}((\text{Et}_2\text{N})_2\text{PO})_2_1$ in CDCl_3	243
Table 4.15: Crystal data for $\text{O}((\text{Et}_2\text{N})_2\text{PO})_2_1_{\text{f13}}$	254
Table 4.16: ^1H NMR experimental data and assignment for proton peaks of $\text{O}((i\text{PrNH})_2\text{PO})_2_1_{\text{b1}}$ in CDCl_3	263
Table 4.17: ^1H NMR experimental data and assignment for proton peaks of $\text{O}((i\text{PrNH})_2\text{PO})_2_1_{\text{c1}}$ in CDCl_3	264
Table 4.18: Comparison of analogous peaks in the spectra of the chromatography fractions f7, f9, f10 and f15 of $\text{O}((i\text{PrNH})_2\text{PO})_2_1_{\text{c1}}$	267
Table 4.19: $^{31}\text{P}\{^1\text{H}\}$ NMR peak data for the various products obtained during the attempts to synthesise $\text{O}((i\text{PrNH})_2\text{PO})_2$, giving the analogous peaks for each row and the relative intensities of the peaks in brackets.	270
Table 4.20: Mass spectra peak data comparison for the $\text{O}((i\text{PrNH})_2\text{PO})_2_1_{\text{b1}}$ Gas chromatography peaks at 6.618 and 7.313 minutes and the peaks in the Mass spectra for $(i\text{PrNH})_3\text{PO}$ and $\text{O}((i\text{PrNH})_2\text{PO})_2_1_{\text{c1}}_{\text{f10}}$	273
Table 4.21: Crystal data for $\text{O}((i\text{PrNH})_2\text{PO})_2_1_{\text{b1}}$	275
Table A-1.1: Chemical composition of ZPure $\text{O}_2/\text{H}_2\text{O}$ purifiers.....	371
Table A-2.1: Drying procedure for THF.	381
Table A-2.2: Drying procedure for Diethyl ether.	382
Table A-2.3: Drying procedure for petroleum ether 30-40, 40-60 °C and n-hexane....	383
Table A-2.4: Drying procedure for Toluene.	383
Table A-2.5: Drying procedure for dichloromethane and chloroform.	384
Table A-2.6: Drying procedure for acetonitrile.	385
Table A-5.1: Assignment of IR bands of dppm from spectrum in Figure A-5.2.....	394
Table A-5.2: ^1H NMR experimental data for the purchased dppm.	396
Table A-5.3: ^1H NMR spectrum data for dppm obtained from literature. ²⁸⁰	396
Table A-6.1: Details of phenyl ring proton peaks for $\text{H}_2\text{C}(\text{Ph}_2\text{PNSiMe}_3)_2_1$	401

LIST OF TABLES (continued)

Table A-6.2: Integration data for singlets in the region 0.4 to 0.05 ppm in the spectrum of $\text{H}_2\text{C}(\text{Ph}_2\text{PSiMe}_3)_2_1$	403
Table A-7.1: Integration details for the peaks assigned to PCH_2P , o-H and m/p-H respectively.	406
Table A-7.2: Details of proton peaks in spectra for $\text{H}_2\text{C}(\text{Ph}_2\text{PS})_2_2\text{a}$, $_2\text{b}$, $_3\text{a}$ and $_3\text{b}$ in CDCl_3	408
Table A-10.1: ^1H NMR experimental data and assignment for proton peaks of $\text{Et}_2\text{NH}_2\text{Cl}$ in CDCl_3	422
Table A-12.1: Crystal data and structure refinement for $\text{O}((\text{Et}_2\text{N})_2\text{PO})_2_1_1\text{f13}$	428
Table A-12.2: Fractional Atomic Coordinates ($\times 10^4$) and Equivalent Isotropic Displacement Parameters ($\text{\AA}^2 \times 10^3$) for $\text{O}((\text{Et}_2\text{N})_2\text{PO})_2_1_1\text{f13}$. U_{eq} is defined as 1/3 of the trace of the orthogonalised U_{IJ} tensor.....	429
Table A-12.3: Anisotropic Displacement Parameters ($\text{\AA}^2 \times 10^3$) for $\text{O}((\text{Et}_2\text{N})_2\text{PO})_2_1_1\text{f13}$. The Anisotropic displacement factor exponent takes the form: $-2\pi^2[h^2a^*U_{11}+2hka^*b^*U_{12}+\dots]$	430
Table A-12.4: Bond Lengths for $\text{O}((\text{Et}_2\text{N})_2\text{PO})_2_1_1\text{f13}$	431
Table A-12.5: Bond Angles for $\text{O}((\text{Et}_2\text{N})_2\text{PO})_2_1_1\text{f13}$	431
Table A-12.6: Hydrogen Atom Coordinates ($\text{\AA} \times 10^4$) and Isotropic Displacement Parameters ($\text{\AA}^2 \times 10^3$) for $\text{O}((\text{Et}_2\text{N})_2\text{PO})_2_1_1\text{f13}$	433
Table A-13.1: ^1H NMR experimental data and assignment for proton peaks of $(i\text{PrNH})_3\text{PO}$ in CDCl_3 :	439
Table A-14.1: Crystal data and structure refinement for $\text{O}((i\text{PrNH})_2\text{PO})_2_1_1\text{b1}$	441
Table A-14.2: Fractional Atomic Coordinates ($\times 10^4$) and Equivalent Isotropic Displacement Parameters ($\text{\AA}^2 \times 10^3$) for $\text{O}((i\text{PrNH})_2\text{PO})_2_1_1\text{b1}$. U_{eq} is defined as 1/3 of the trace of the orthogonalised U_{IJ} tensor.....	442
Table A-14.3: Anisotropic Displacement Parameters ($\text{\AA}^2 \times 10^3$) for $\text{O}((i\text{PrNH})_2\text{PO})_2_1_1\text{b1}$. The Anisotropic displacement factor exponent takes the form: $-2\pi^2[h^2a^*U_{11}+2hka^*b^*U_{12}+\dots]$	443
Table A-14.4: Bond Lengths for $\text{O}((i\text{PrNH})_2\text{PO})_2_1_1\text{b1}$	443
Table A-14.5: Bond Angles for $\text{O}((i\text{PrNH})_2\text{PO})_2_1_1\text{b1}$	444
Table A-14.6: Hydrogen Atom Coordinates ($\text{\AA} \times 10^4$) and Isotropic Displacement Parameters ($\text{\AA}^2 \times 10^3$) for $\text{O}((i\text{PrNH})_2\text{PO})_2_1_1\text{b1}$	444

LIST OF TABLES (continued)

Table A-18.1: Crystal data and structure refinement for [N(Ph ₂ PCH ₃)(Ph ₂ PNH ₂)] [Cl] · Ph ₂ P(O)NH ₂	456
Table A-18.2: Fractional Atomic Coordinates ($\times 10^4$) and Equivalent Isotropic Displacement Parameters ($\text{\AA}^2 \times 10^3$) for [N(Ph ₂ PCH ₃)(Ph ₂ PNH ₂)] [Cl] · Ph ₂ P(O)NH ₂ . U _{eq} is defined as 1/3 of the trace of the orthogonalised U _{ij} tensor.	457
Table A-18.3: Anisotropic Displacement Parameters ($\text{\AA}^2 \times 10^3$) for [N(Ph ₂ PCH ₃)(Ph ₂ PNH ₂)] [Cl] · Ph ₂ P(O)NH ₂ . The Anisotropic displacement factor exponent takes the form: - $2\pi^2[h^2a^2U_{11}+2hka*b*U_{12}+\dots]$	458
Table A-18.4: Bond Lengths for [N(Ph ₂ PCH ₃)(Ph ₂ PNH ₂)] [Cl] · Ph ₂ P(O)NH ₂	458
Table A-18.5: Bond Angles for [N(Ph ₂ PCH ₃)(Ph ₂ PNH ₂)] [Cl] · Ph ₂ P(O)NH ₂	459
Table A-18.6: Hydrogen Atom Coordinates ($\text{\AA} \times 10^4$) and Isotropic Displacement Parameters ($\text{\AA}^2 \times 10^3$) for [N(Ph ₂ PCH ₃)(Ph ₂ PNH ₂)] [Cl] · Ph ₂ P(O)NH ₂	460

1. INTRODUCTION

Catalysis is frequently used in manufacturing processes especially in the chemical, pharmaceutical and materials industries. Given its widespread use, there is still scope for improvement in this field. A catalyst can be described as a substance which will increase the rate of a reaction without being consumed. Catalysis is therefore commonly used to simply increase the rate or decrease activation energy of the reaction and thereby reduce manufacturing time and costs. Other uses include aiding the initiation of reactions which do not occur under non-catalysed circumstances and the preferential preparation of one isomer of a substance over other isomers.¹ Transition metal organometallic compounds make up the largest family of compounds that are used as catalysts. Another group of metals used for organometallic catalysts are the lanthanide metals.

The lanthanides are a group of 15 metals found in Period 6 of the periodic table, from lanthanum to lutetium. They are bound by the 6sⁿ alkali and alkali earth metals, caesium and barium, and the third row of the transition metals. The lanthanides are technically defined by their orbital structure, with an electron configuration of [Xe]4fⁿ6s² or [Xe]4fⁿ5d^m6s² depending on the lanthanide.² Due to their orbital structure these elements behave in a fashion very similar to that of the alkali earth metals and in a different manner to the other group in the f-block, the actinides. Therefore one of their major features is the prominence of salt formation and the formation of highly ionic complexes, as for the chemistry of Group 2 metals. Given this the organometallic chemistry of the lanthanide metals is heavily influenced by principles regulating the formation and stability of ionic coordination complexes. Another similarity to the Group 2 metals is the relative non-toxicity of lanthanide compounds in comparison to the transition metals cations used in various fields.^{3,4}

Although the field of organometallic lanthanide chemistry has been growing since the earliest studies in 1954, it is still a unexplored area.^{5,6} Given the preference of the lanthanide metals towards the formation of ionic or chelated complexes, the formation of stable organometallic compounds has been challenging and the formation of higher order metal to carbon bonds, such as the double bond present in lanthanide carbenes, has only been published recently.⁷⁻¹⁰

Early studies of lanthanide carbenes dealt mainly with nitrogen heterocyclic carbene complexes with later studies dealing with the complexes of phosphorus (V) stabilised geminal dianions. Throughout these studies the main interest in these

lanthanide carbene complexes was in their application in catalysis.^{11,12} This is an important field given that the lanthanides are far less hazardous to living organisms than many of the heavy metals currently used in the field of catalysis, since they have LD₅₀ values in the ranges of 10 to 7650 mg/kg for mice, noted in various studies.^{3,4,13} This is of importance with regards to the synthesis of more environmentally friendly catalysts with their application being of interest in the expansion of green chemistry methods.¹⁴

Lanthanide carbenes are usually unstable in the presence of air and moisture and therefore have to be prepared under dry nitrogen or argon and using dried solvents. Therefore these complex catalysts had to be used *in situ* after their synthesis and the catalysed reactions had to be undertaken under conditions similar to the strict conditions adhered to during the synthesis of the catalysts. One of the main aims of the current research in this field is therefore the conversion of these highly air-sensitive metal carbenes into more manageable solids for use in catalysis on an industrial scale, where such demanding atmospheric and temperature conditions are not desirable. This process of stabilisation should be undergone using green chemical methods in an attempt to minimize or eliminate the use of environmentally hazardous solvents and reagents. Co-crystallisation as described in this study is one such method.¹⁵⁻¹⁷ Compounds are known to have different thermodynamic and kinetic stabilities in different solid states. Co-crystals which are more stable than the initial solid crystalline co-formers are known in literature and thus the interest in the stabilisation of these carbenes.¹⁵⁻¹⁷

Another main aim of this study is the synthesis of metal-organic lanthanide complexes of ligands which are isostructural and isoelectronic to the lanthanide carbenes described beforehand. These are of interest given that the limited known species are more air and moisture stable than the analogous lanthanide carbenes and their application in synthesis and catalysis has not been widely described.

In the current study the preparation and stabilisation of a number of known and novel solid state species of lanthanide di- $\lambda^5\sigma^4$ -phosphorane complexes which contain either carbene or its isoelectronic analogues are to be explored and described.

1.1. Statement of Scope

The main aim of the current study was to synthesise lanthanide carbene complexes and use methods to increase their stability towards air and moisture. The main method applied to stabilise these compounds was co-crystallisation.

The work therefore focuses on various steps leading to different intended outcomes. These steps can be delineated as:

- Preparation of lanthanide starting reagents.
- Synthesis of carbene and geminal dianion ligands.
- Synthesis of lanthanide carbenes containing Nd^{3+} and Sm^{3+} as described in literature, giving information for the early and middle lanthanide series.
- Stabilisation studies:
 - Co-crystallisation
- Analysis of compounds and crystals at all stages by X-ray diffraction techniques.

Thus, the scope was to find novel lanthanide carbene solids which are more air and moisture stable than those already published in literature. The field of lanthanide carbenes is relatively new and very little work has been undergone to enhance the use of these complexes in a practical setting. Therefore the work in stabilisation for these complexes in order to ease their use in other situations is novel.

Another main aim of the study was to synthesise and characterise both known and novel lanthanide compounds from ligands which are isostructural and more importantly isoelectronic to the carbene ligands. This was undergone to obtain air and moisture stable analogues of the lanthanide carbenes and thus compare trends in the structure and chemistry of these complexes with the analogous lanthanide carbenes with special reference to the formation of N–Ln or O–Ln bonds analogous to the C=Ln bond of the methandiides. The lanthanides used in these studies were Nd^{3+} and Eu^{3+} as representatives of the early to middle lanthanide series.

2. LITERATURE REVIEW

2.1. Chemistry of the lanthanide metals

The lanthanide metals are a group of 14 elements found after lanthanum in period 6 of the periodic table, as shown in Figure 2.1, and in which the 4f orbitals are consecutively filled. The lanthanides are usually characterised by the presence of one of two electron configurations, namely $[Xe]4f^n6s^2$ or $[Xe]4f^m5d^m6s^2$, where $1 > n > 14$ and $0 > m > 1$.¹ Lanthanide chemistry is a relatively recent field of study due to the fact that lanthanide ores typically contain a mixture of metal ions and that the separation of the ions is difficult because of their similar chemical and physical properties.¹⁸

Key:									
atomic number	Symbol								
name	name								
standard atomic weight	standard atomic weight								
1	H	hydrogen	1.008	1.008(1)	2	He	helium	4.0026	4.0026
3	Li	lithium	6.941	6.94(1)	4	Be	beryllium	9.0122	9.0122
11	Na	sodium	22.990	22.990	12	Mg	magnesium	24.305	24.304, 24.307
13	Al	aluminium	26.982	26.982	14	Si	silicon	28.086	28.086
15	P	phosphorus	30.974	30.974	16	S	sulfur	32.06	32.06
17	Cl	chlorine	35.45	35.45	18	Ar	argon	39.948	39.948
19	K	potassium	39.098	39.098	20	Ca	calcium	40.078(4)	40.078(4)
21	Sc	scandium	44.956	44.956	22	Ti	titanium	47.887	47.887
23	V	vanadium	50.942	50.942	24	Cr	chromium	51.996	51.996
25	Mn	manganese	54.938	54.938	26	Fe	iron	55.845(2)	55.845(2)
27	Co	cobalt	58.933	58.933	28	Ni	nickel	58.693	58.693
29	Cu	copper	63.546(3)	63.546(3)	30	Zn	zinc	65.38(2)	65.38(2)
31	Ga	gallium	69.723	69.723	32	Ge	germanium	72.630(8)	72.630(8)
33	As	arsenic	74.922	74.922	34	Se	selenium	78.971(8)	78.971(8)
35	Br	bromine	79.904	79.904	36	Kr	krypton	83.798(2)	83.798(2)
37	Rb	rubidium	85.468	85.468	38	Sr	strontium	87.62	87.62
39	Y	yttrium	88.906	88.906	40	Zr	zirconium	91.224(2)	91.224(2)
41	Nb	niobium	92.906	92.906	42	Mo	molybdenum	95.94	95.94
43	Tc	technetium	98	98	44	Ru	ruthenium	101.07(2)	101.07(2)
45	Rh	rhodium	102.91	102.91	46	Pd	palladium	106.42	106.42
47	Ag	silver	107.87	107.87	48	Cd	cadmium	112.41	112.41
49	In	indium	114.82	114.82	50	Sn	tin	118.71	118.71
51	Sb	antimony	121.76	121.76	52	Te	tellurium	127.6(2)	127.6(2)
53	I	iodine	126.90	126.90	54	Xe	xenon	131.29	131.29
55	Cs	caesium	132.91	132.91	56	Ba	barium	137.33	137.33
57-71	lanthanoids				72	Hf	hafnium	178.49(2)	178.49(2)
73	Ta	tantalum	180.95	180.95	74	W	tungsten	183.84	183.84
75	Re	rhenium	186.21	186.21	76	Os	osmium	190.23(2)	190.23(2)
77	Ir	iridium	192.22	192.22	78	Pt	platinum	195.08	195.08
79	Au	gold	196.97	196.97	80	Hg	mercury	200.59	200.59
81	Tl	thallium	204.38	204.38	82	Pb	lead	207.2	207.2
83	Bi	bismuth	208.98	208.98	84	Po	polonium		
85	At	astatine			86	Rn	radon		
87	Fr	francium			88	Ra	radium		
89-103	actinoids				104	Rf	rutherfordium		
105	Db	dubnium			106	Sg	seaborgium		
107	Bh	bohrium			108	Hs	hassium		
109	Mt	meitnerium			110	Ds	darmstadtium		
111	Rg	roentgenium			112	Cn	copernicium		
113	Nh	nihonium			114	Fl	flerovium		
115	Mc	moscovium			116	Lv	livermorium		
117	Ts	tennessine			118	Og	oganeson		
57	La	lanthanum	138.91	138.91	58	Ce	cerium	140.12	140.12
59	Pr	praseodymium	140.91	140.91	60	Nd	neodymium	144.24	144.24
61	Pm	promethium			62	Sm	samarium	150.36(2)	150.36(2)
63	Eu	europtium	151.96	151.96	64	Gd	gadolinium	157.25(2)	157.25(2)
65	Tb	terbium	158.93	158.93	66	Dy	dysprosium	162.50	162.50
67	Ho	holmium	164.93	164.93	68	Er	erbium	167.26	167.26
69	Tm	thulium	168.93	168.93	70	Yb	ytterbium	173.05	173.05
71	Lu	lutetium	174.97	174.97	89	Ac	actinium		
90	Th	thorium	232.04	232.04	91	Pa	protactinium		
92	U	uranium	238.03	238.03	93	Np	neptunium		
94	Pu	plutonium			95	Am	americium		
96	Cm	curium			97	Bk	berkelium		
98	Cf	californium			99	Es	einsteinium		
100	Fm	fermium			101	Md	meitnerium		
102	No	nobelium			103	Lr	lawrencium		

Figure 2.1: Periodic Table showing the Lanthanide Metals encapsulated in red.

From the earliest research it transpired that the most common influence on lanthanide chemistry was the formation of hard trivalent cations of the metals.² The trivalent cations usually have the electron configuration of $[Xe]4f^n$. A number of other oxidation states, mainly +2 and +4, are also known for some lanthanides and the formation of these states is dependent mainly on the total enthalpy change when considering all enthalpy changes as described through their respective Born-Haber cycles.¹ These hard cations are formed through the ionisation of the valance orbitals of the elemental lanthanides, namely the $6s^2$ and the 5d or 4f orbitals. Higher oxidation states are rarely observed given that for the atomic number, Z, of the lanthanides other electrons

in the 4f, 5s and 5p (the latter two being part of the Xe electron configuration) orbitals are too tightly bound to the ion. More influential on the hardness of the lanthanide cations is the fact that the 4f orbitals act as internal orbitals shielded from valence orbitals of possible ligands by the more expansive 5s² and 5p⁶ orbitals and therefore covalent or covalent-like bonding, as seen in the transition metals and the p block elements, is much less common than ionic bonding.

This has led to an extensive chemistry based on the hard cations formed, similar to that of the alkali and alkali earth metals, with particular reference to the latter.¹⁹ Lanthanides show a varied coordination chemistry following many of the rules set out for the coordination chemistry of the alkali and alkali earth metals, including the importance between the relation of the coordination number and the ionic radius, influence of steric hindrance on coordination, preferred bonding towards anionic ligands with donor atoms of high electronegativity (such as O, N and F) and the preference towards bonding with chelates.²

The preference to bond with hard anions such as oxygen and nitrogen tends to produce complexes with organic ligands which contain these atoms typically referred to as metal-organic lanthanide complexes. This preference however does not exclude organometallic chemistry for the lanthanides, again with the major comparisons being made with the organometallic compounds of Group 1 and 2 metals.^{2,20} The stability of organolanthanide compounds to air and moisture is less than that of compounds that these same metals form with hard ionic or Lewis base ligands.

Given the large ionic radii of the lanthanide cations, unlike the common Group 1 and 2 metal complexes, the co-ordination sphere of these cations usually has a coordination number (CN) ranging from 6 to 12, with a predominance of CN 8, 9, 10.²¹ Organometallic compounds of lanthanides on the other hand tend to show a lower predominant range, even as low as CN 3 and 4 which is found in numerous cyclopentadienyl lanthanide complexes,^{1,22} if bonding is considered to be ionic.

The internal-like 4f orbitals give the lanthanide atoms and cations a number of different physical properties, with particular reference to their spectral and magnetic properties. The spectral properties of lanthanides differ from those of the transition metals especially with the prominence of the f-f transitions in comparison to the d-d transitions, both of which are Laporte forbidden and therefore show weak absorptions.¹⁹ The limited orbital overlap of the 4f orbitals with the ligand valence orbitals decreases the number of vibrational and rotational modes available. Therefore, sharp absorption and emission

In all the complexes of ligands with the structure as given in Figure 2.2 chelation to the metal centre through the fragments on the Y site is always present.³⁹ This is typical of lanthanide complexes as chelation is favoured thermodynamically. The bonding nature of this chelation follows the preference for hard electron donors as described in Section 2.1 previously. The same is therefore expected for the central N⁻ and O fragments where these too are reasonably hard Lewis bases. Therefore the lanthanide complexes of the ligands X(R₂PY)₂, having X = N⁻ or O, are noted as being metal-organic complexes that should follow the typical lanthanide behaviour as outlined in Section 2.1.

Unlike these analogues, the ligands X(R₂PY)₂, with X = C²⁻, have been shown to form carbenes of the type, [C(R₂PY)₂]²⁻, where Y = NR or S.^{7,9,40-42} These carbene complexes have been established for the lanthanides with the central methandiide group forming an Ln=C bond with the coordinated carbon. Therefore not only is this group of ligands interesting in that they form organometallic lanthanide compounds, unlike the previously discussed analogues, but they also form one of only two major groups of lanthanide carbene complexes as yet published in literature. These complexes not only showed the consistent formation of these carbene species but have also been shown to be useful in synthesis, catalysis and reaction initiation.⁴³⁻⁴⁶ However, these lanthanide carbenes are known to be more air and moisture sensitive than the analogous compounds previously discussed thus making their synthesis and use difficult.^{30,31} Given that the synthesis of these carbene complexes require knowledge of organometallic lanthanide chemistry and that these are of interest in a greater number of fields than the two previous analogous groups the review of this chemistry and these compounds is given in greater detail.

2.3. Organometallic lanthanide compounds

2.3.1. Lanthanide cyclopentadienyl and anionic aromatic ligand complexes

Some of the earliest reported organometallic lanthanide complexes are the cyclopentadienyl (Cp⁻) lanthanide complexes with the formula Ln(C₅H₅)₃ or Ln(Cp)₃ as described by Wilkinson and Birmingham in 1954.⁵ These, apart from the cerium based complex, were found to be reasonably stable in air but all were moisture sensitive. Further work gave details into the physical and chemical properties of these complexes, such as

a sublimation temperature in the region of 150-260 °C at 10^{-4} mmHg and their reaction with FeCl_2 which produces ferrocene and the lanthanide chloride, as is the case with Group 1 and 2 cyclopentadienyl complexes.⁴⁷ From this early research of the chemical properties of these cyclopentadienyl complexes of the lanthanides it is clear that the bonding for the $\text{Ln}(\text{Cp})_3$ is mostly ionic, in the form cation- π interactions, as seen in various alkaline and alkaline earth metal complexes.⁴⁸ This is in contrast to the cyclopentadienyl complexes of the transition metals which are bonded covalently through the nd orbitals overlapping with the π orbitals of the anion ligand, Cp^- .²⁰

Unlike complexes of the cyclopentadienyl ligand most of the well-known pentamethylcyclopentadienyl (Cp^*) complexes do not have the $\text{Ln}(\text{Cp}^*)_3$ structure. This ligand was first used in the synthesis of lanthanide compounds by Schumann and colleagues for compounds with a structure of $\text{Cp}^*_2\text{Ln}(\mu_2\text{-Cl}_2)\text{AL}_2$, (as shown in Figure 2.3) where Ln indicates the entire lanthanide series, A = Li, Na or K and L = diethyl ether, THF or dimethoxyethane (DME).⁴⁹ These complexes have proven themselves as being some of the most versatile organolanthanide starting reagents. Through salt elimination a number of other adducts may replace the $[\text{AlCl}_2\text{L}_2]^-$ fragment with other ligands. This is commonly used in order to produce new reagents.⁵⁰ Unlike the $\text{Ln}(\text{Cp})_3$, the Cp^* ligand was initially thought to be too bulky to form the $\text{Ln}(\text{Cp}^*)_3$ compound group.⁵¹ However this structure is known for the early lanthanides, from lanthanum to samarium and gadolinium. These were synthesised from the reaction of the $[\text{Ln}(\text{Cp}^*)_2][\text{B}(\text{C}_6\text{H}_5)_4]$ with K^+Cp^{*-} in benzene.^{52,53} Apart from this, complexes containing the di(pentamethylcyclopentadienyl)lanthanide(III) moiety are most common with a third and possibly fourth ligand, as with the dichlorides mentioned earlier.⁵¹ These ligands become the main reaction centres of many of the compounds described, leaving the Cp^* ligands in a spectator role or controlling kinetic factors towards compound reactivity.

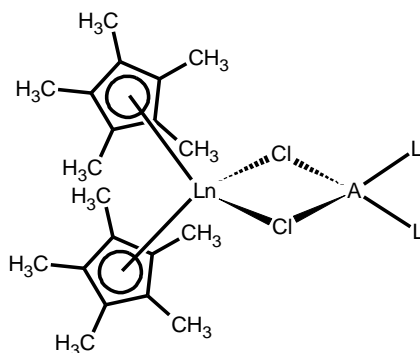


Figure 2.3: Structure of $\text{Cp}^*_2\text{Ln}(\mu_2\text{-Cl}_2)\text{AL}_2$ complexes.

Other substituted cyclopentadienyl ligands have been widely studied and comprise one of the major sections of organolanthanide chemistry.^{6,54} Studies range from the application of other sterically demanding substituents to substituents which increase the hapticity of the ligand. Sterically demanding substituents were used in numerous reactions, one example being that of trimethylsilyl-cyclopentadienyl ($\text{Me}_3\text{SiC}_5\text{H}_4^-$) which was used to isolate a number of Ln^{2+} (where $\text{Ln} = \text{Pr, Gd, Tb or Lu}$) cations through the reduction of the $\text{Ln}(\text{Me}_3\text{SiC}_5\text{H}_4)_3$ by potassium to form a potassium salt with the $[\text{Ln}(\text{Me}_3\text{SiC}_5\text{H}_4)_3]^-$ anionic complex.⁵⁵ Similarly trimethylsilyl-tetramethylcyclopentadienyl ($\text{Me}_3\text{SiC}_5\text{Me}_4^-$) has been used in a large number of precursors of the general formula $\text{Ln}(\text{Me}_3\text{SiC}_5\text{Me}_4)_2\text{L}_2$ in the synthesis of a number of lanthanide clusters.^{56,57} The very bulky ligand (4-*n*Bu-C₆H₄)₅-cyclopentadienyl was also used in a similar fashion, whereby truly sandwich-like cyclopentadienyl-lanthanide compounds were synthesised for the well-known divalent Sm^{2+} , Eu^{2+} and Yb^{2+} .⁵⁸

Research has also been published regarding cyclopentadienyl ligands of increased denticity, through independently coordinating substituents. Apart from numerous clusters prepared recently, the formation of the simple complexes of the structure $[(\text{Me}_2\text{NC}_6\text{H}_4\text{C}_5\text{H}_4)\text{LnY}_2]$, where $\text{Ln} = \text{Nd, Sm, Gd or Dy}$ and $\text{Y} = \text{BH}_4^-$ or C_3H_5^- have been described; these are of interest as catalysts.^{59,60} The borohydride derivative was shown to catalyse the polymerisation of methylmethacrylate,⁵⁹ while the allyl complex was shown to catalyse the polymerisation of isoprene discriminating in favour of the 1,4-*cis* structure of the polymer.⁶⁰

To the present day the synthesis and reactions of cyclopentadienyl and pentamethylcyclopentadienyl lanthanide complexes are a foundation block of organolanthanide chemistry.⁵⁰ These cyclic aromatic ligands are usually used as spectator ligands as they themselves are not known to react with many compounds.^{6,54} They also tend to act as protecting groups which allow the reaction of the lanthanides on other sites typically occupied by other reactive ligands. This therefore leads to their popularity in many organometallic lanthanide complexes which contain other ligands which are of greater chemical interest. However, they are also easily replaced by stronger Lewis base ligands such as amines, alkoxides and aryloxides.⁵⁰

2.3.2. Lanthanide arene complexes

Lanthanide arene complexes, wherein the complex contains a neutral arene derivative are known and these have a basic structure as shown in Figure 2.4. As with the cyclopentadienyl lanthanide complexes the bonding in lanthanide arene complexes is known to be mainly ionic cation- π interactions.⁵⁰

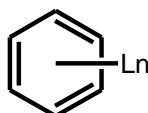


Figure 2.4: Basic structure of lanthanide arene bonding.

An early lanthanide arene was synthesised and characterised by Cotton and Schowtzer in 1986: this being the $[\text{Sm}(\eta^6\text{-C}_6(\text{CH}_3)_6)(\text{AlCl}_4)_3]$.⁶¹ This contained the Sm^{3+} cation bound to the neutral and electron rich hexamethylbenzene ($\text{C}_6(\text{CH}_3)_6$) in bonding similar to that of cyclopentadienyl complexes and AlCl_4^- which causes the formation of a Lewis acid electron deficient metal centre.⁵⁰ Other early examples of rare earth arenes are the $\text{Ln}(\eta^6\text{-}(t\text{Bu})_3\text{C}_6\text{H}_3)$, where $\text{Ln} = \text{Y}(0)$ or $\text{Gd}(0)$. These are more electron rich metal centres having a valency of 0.⁶² It is interesting to note that in the case of $\text{Gd}(0)$ the presence of the filled $6s^2$ and possibly $5d^1$ orbitals allows bonding with the weaker Lewis base $(t\text{Bu})_3\text{C}_6\text{H}_3$.

The latest work on lanthanide arene complexes deals mainly with complexes of trivalent and divalent lanthanide centres in which the arene ligand is not only bound by the cation- π interactions but by coordination through mainly N bonding moieties. Such ligands have been seen in the form of amidinate, guanidinate and triazenide compounds wherein the N moieties bind in a single bond to the metal centre while the arene moiety binds to the centre by cation- π interactions.⁶³⁻⁶⁵ In most cases the lanthanide centres are divalent, typically Eu^{2+} , Sm^{2+} and Yb^{2+} .⁶³⁻⁶⁵ Other later work saw the synthesis and characterisation of a number of arene compounds which lacked denticity through substituents, as with the ligands mentioned previously. A number of boratabenzene derivatives were found to form stable lanthanide arenes with trivalent Sm, Dy and Lu.⁶⁶ A complex with 1,3,5-trimethylbenzene in the form of $(1,3,5\text{-Me}_3\text{C}_6\text{H}_3)\text{Ce}(\text{N}(\text{C}_6\text{F}_5)_2)_3$ has also been published, having a metal centre (Ce^{3+}) with a primary coordination sphere which is saturated with bulky ligands, namely $\text{Ce}(\text{N}(\text{C}_6\text{F}_5)_2)_3$.⁶⁷

2.3.3. Lanthanide allyls

This is a well-known group of lanthanide organometallic compounds that contain ionic bonding to allyl groups. Like the cyclopentadienyl ligands these are mainly encountered as spectator ligands and act directly in reactions only on rare occasions.⁵⁴ Numerous lanthanide allyl complexes have been synthesised, from the early $[\text{Li}(1,4\text{-dioxane})_n]^+[\text{Ln}(\eta^3\text{-C}_3\text{H}_5)_4]^-$ (where Ln = Ce, Nd, Sm, Gd or Dy and $n = 2$)^{68,69} to the more recently synthesized compounds $[(1,7\text{-Me}_2\text{TACD})\text{RE}(\eta^3\text{-C}_3\text{H}_5)_2]$ and $[(1,7\text{-Me}_2\text{TACD})\text{RE}(\eta^3\text{-C}_3\text{H}_5)_2\text{K}(\text{THF})]_n$, where RE = Y or any lanthanide and 1,7-Me₂TACD is the chelating agent 1,7-dimethyl-1,4,7,10-tetraazacyclododecane:⁷⁰ the polymeric compound being used in the synthesis of a number of hydride clusters.⁷⁰ The hydride prepared from the lanthanum (III) complex showed catalytic activity in the dehydrogenation of $(\text{H}_3\text{C})_2\text{NH}\cdot\text{BH}_3$ to the cyclic dimer $((\text{H}_3\text{C})_2\text{NBH}_2)_2$.⁷¹ Catalytic activity of lanthanide allyl complexes is also known although not as widespread; such as in the case of the polymerisation of 1,3-butadiene by the complexes $[\text{Ln}(\eta^3\text{-C}_3\text{H}_5)_2(\text{THF})_3][\text{B}(\text{C}_6\text{X}_5)_4]$ and $[\text{Ln}(\eta^3\text{-C}_3\text{H}_5)(\text{THF})_6][\text{B}(\text{C}_6\text{H}_5)_4]_2$ (where Ln = La or Nd, while X = H or F) in the presence of trisisobutylaluminium.⁷²

2.3.4. Lanthanide – carbon σ bonds

$\text{Ln}-\text{C}$ σ bonds, although not as stable as the dispersed ionic bonding of the cyclopentadienyl, pentamethylcyclopentadienyl and allyl lanthanide compounds became known recently in the field of organometallic lanthanide chemistry. These bonds although considered to be σ single bonds have a high ionic character, as would be expected for lanthanide compounds. The simplest ligand that can form such a bond is the methyl ligand, which is mainly known in the compound group $[\text{Li}(\text{L})]_3[\text{Ln}(\text{CH}_3)_6]$, where L = tetramethylethylenediamine (tmed) or 1,2-dimethoxyethane and where Ln represents the majority of the lanthanides.^{73,74} In the same studies the $\text{Ln}-\text{C}$ σ bond was also established for the heavy lanthanides and the *tert*-butyl ligand in the compounds $[\text{Li}(\text{tmed})_2][\text{Ln}(\text{tBu})_4]$ (where Ln = Tb or Lu) and $[\text{Li}(\text{Et}_2\text{O})_4][\text{Er}(\text{tBu})_4]$.⁷³ These are all thermally unstable. It should be noted that the methyl anion also has a tendency to form clusters with lanthanides, a characteristic which is also common for other alkyls, both with the lanthanides and the Group 1 and 2 metals.²

The most common ligand that bonds to lanthanide centres in a σ bond is the bis(trimethylsilyl)methyl fragment; used mainly in starting reagents for organolanthanide reactions.^{2,50} The neutral tris(bis(trimethylsilyl)methyl)lanthanide(III) with a formula of $\text{Ln}(\text{CH}(\text{SiMe}_3)_2)_3$ is known for many of the lanthanides and has a pyramidal structure. These complexes are prepared mainly by the reaction of bis(trimethylsilyl)methyl lithium with the respective $[\text{Ln}(\text{OC}_6\text{H}_3(\text{tBu})_2\text{-2,6})_3]$, through a metathesis reaction.⁷⁵⁻⁷⁷ It should be noted that lanthanide compounds containing the bis(trimethylsilyl)methyl ligand are also well known in lanthanide complexes with other groups such as halides. The main interest of these compounds arises from their use as starting reagents, these being soluble in non-polar solvents.⁷⁵ These compounds are all air and moisture sensitive.

Phenyl and phenyl-based ligands are also well known. A recent addition to this group are the tribenzyl lanthanide(III) complexes of the structure $\text{Ln}(\text{CH}_2\text{C}_6\text{H}_5)_3(\text{THF})_3$ (where $\text{Ln} = \text{Y, La, Ce, Pr, Nd, Sm, Gd, Dy, or Er}$) which have also shown strong basicity of the ligands and acid-base reactivity of the said ligands to produce other organolanthanide compounds.⁹ Earlier phenyl ligands typically contained secondary substituent moieties which allowed the phenyl ligand to bind to the metal centres with greater denticity. One such example arises from the heavy lanthanide complexes of the ligand, $[\text{o}-(\text{Me}_2\text{NCH}_2)\text{C}_6\text{H}_4]^-$ with the simple composition of $\text{Ln}(\text{o}-(\text{Me}_2\text{NCH}_2)\text{C}_6\text{H}_4)_3$ for $\text{Ln} = \text{Er}^{3+}, \text{Yb}^{3+}$ or Lu^{3+} ,¹⁵ as given in Figure 2.5.

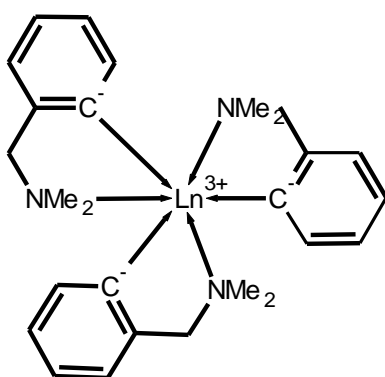


Figure 2.5: Structure of compounds $\text{Ln}(\text{o}-(\text{Me}_2\text{NCH}_2)\text{C}_6\text{H}_4)_3$.¹⁵

This phenyl ligand was attested recently as a starting reagent for the preparation of the lanthanide complexes of the cyclopentadienyl derivative ligand, cyclopentadienyl-N-silyl tri(*tert*-butyl)phosphazene, a cyclopentadienyl ring stabilised by a single $-\text{Si}(\text{Me})_2\text{N}=\text{P}(\text{tBu})_3$ fragment.¹⁶ A series of complexes similar in structure to the

aforementioned compound but that bond entirely by Ln–C σ bonds was prepared by using a series of triphenylphosphine ylide derivatives with the molecular structure given in Figure 2.6.⁷⁸ In this case the ligand bonds to the lanthanide centre via the two anionic carbons shown in Figure 2.6, namely the methylene carbon and the deprotonated phenyl carbon.

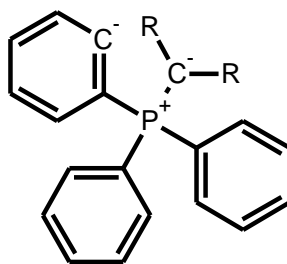


Figure 2.6: Basic structure of the triphenylphosphine ylide derivatives, where R = H, alkyl of C 1-10, phenyl or trimethylsilyl.

The molecular structure of the complexes, which is known for all the lanthanides, is homologous to that of the $\text{Ln}(\text{o}-(\text{Me}_2\text{NCH}_2)\text{C}_6\text{H}_4)_3$.⁷⁸ Although this increased denticity is common, Ln–C(phenyl) σ bonds are also known for the Yb(II) complexes of pentafluorophenyl (C_6F_5^-), namely the octahedral $\text{Yb}(\text{II})(\text{C}_6\text{F}_5)_2(\text{THF})_4$ and the distorted square pyramidal $[\text{Yb}(\text{C}_5\text{Me}_5)(\text{C}_6\text{F}_5)(\text{THF})_3]$.¹⁷ In both cases the presence of the fluorine atoms act to stabilise the bonding through electrostatic interactions between the lanthanide and fluorine.¹⁷

Ln–C σ bonds are also known for a number of deprotonated alkynes. One such case are the two analogous lanthanide compounds of the structure $\text{Ln}(\text{dippform})_2(\text{CCPh})(\text{THF})$, where Ln = Nd^{3+} or Sm^{3+} , dippform = 2,6-diisopropylphenylformamidinato ligand and CCPh = deprotonated phenylacetylene.⁷⁹ Otherwise the majority of alkyne compounds remain clusters.⁸⁰

2.3.5. Other Ln to C bonding

Other organolanthanide compounds having different bonding than that mentioned previously in Section 2.3 are also known but to a lesser extent. The group which is dealt with in the current study, the lanthanide carbenes, are one such group, with details given in Section 2.6. Other groups which are of interest are lanthanides π bonded to alkene and

alkyne ligands. The most interesting of these compounds are all ytterbium(II) complexes which are therefore electron rich as compared to other lanthanide ions. In the case of alkene bonding two compounds are known $(\text{Me}_5\text{C}_5)_2\text{Yb}(\mu_2\text{-C}_2\text{H}_4)\text{Pt}(\text{PPh}_3)_2$ and $[\text{Yb}[\text{C}(\text{SiMe}_3)_2(\text{SiMe}_2\text{CH}=\text{CH}_2)]\text{I}\cdot\text{OEt}_2]_2$.^{81,82} In the former case the bonding is preserved by electron donation to the olefin from the electron rich Pt(0).⁸¹ In the latter case the bonding of the alkene group is maintained by the Ln-C σ bond binding the ligand to the centre at the tris(trimethylsilyl)methyl C.⁸² A more stable complex was formed with the alkyne 2-butyne ($\text{MeC}\equiv\text{CMe}$) in the form $(\text{Me}_5\text{C}_5)_2\text{Yb}(\mu_2\text{-MeC}\equiv\text{CMe})$, wherein unlike the former two complexes no additional stabilisation was required.⁸³ The interest of these compounds is mainly due to the ability of cation- π interactions on such small and non-delocalised π donors and the conditions that facilitate such bonding.

2.4. Introduction to carbenes

Metal carbenes are organometallic complexes with at least 1 organic carbene ligand. Carbenes are neutral ligands with a central C atom having 6 outer electrons and two substituents as given in the structure shown in Figure 2.7(a). The non-bonding electrons localised on the central carbon define the nature and reactivity of these species. These electrons occupy the frontier orbitals of the molecule, which for the common bent C_{2v} symmetry, are the σ and p_π orbitals.⁸⁴ There are two categories of organic carbenes, namely those in the singlet and in the triplet ground state. The main difference between these two states lies in the configuration of the two non-bonding electrons in the σ and p_π orbitals. In the singlet state the non-bonding electrons are paired in the lower energy σ orbital. In the triplet state the two electrons are equally distributed between both orbitals and are not spin-paired.⁸⁴ These electron configurations are given in Figure 2.7(b).

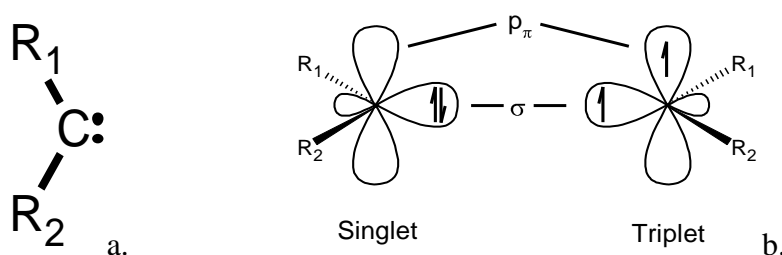


Figure 2.7: a. Basic structure of an organic carbene, b. Electron configuration of the non-bonding carbene electrons for the singlet and triplet states.

Commonly the state obtained is dependent on the electronegativity of the substituents R_1 and R_2 . When the substituents are σ -electron donating, as with alkyl groups, the triplet state is favoured while σ -electron withdrawing substituents, such as -OR and -NR₂ groups, favour the singlet state. Exemplar Molecular Orbital (MO) diagrams (in C_{2v} symmetry) for the singlet and triplet state carbenes, as shown in Figure 2.7(b), are given in Figure 2.8(a) and (b) respectively. In Figure 2.8 the substituents R_1 and R_2 are considered identical, thus given as X. The molecular orbitals a_1 and b_2 relate to the simple bonding orbitals between the substituents and the central carbene carbon and are not discussed further hereunder. The orbitals given in Figure 2.7(b) are clearly shown in both MO diagrams in Figure 2.8 as the $p_\pi(b_1)$ and the $\sigma(a_1)$ orbitals.

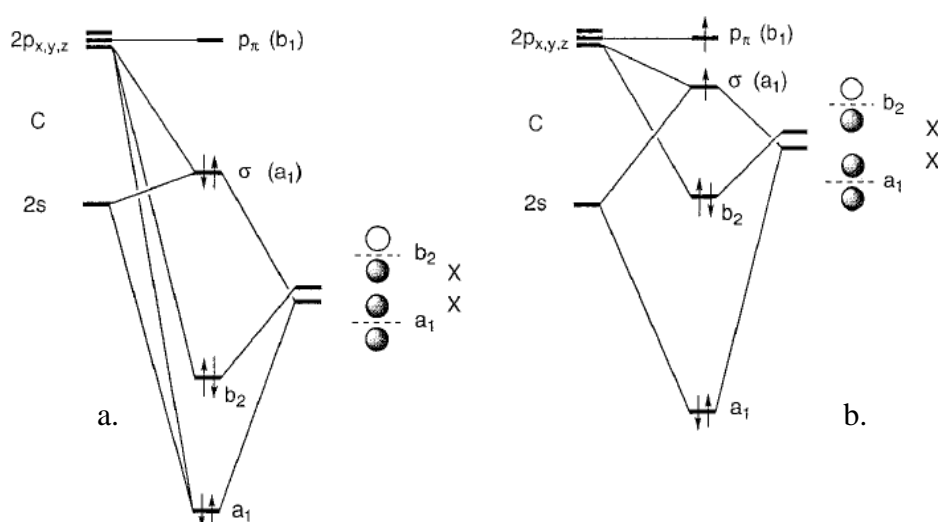


Figure 2.8: MO diagrams of carbenes having a. σ -electron withdrawing substituents, b. σ -electron donating substituents.⁸⁴

The orbital which contributes most towards the properties of the carbene is the $\sigma(a_1)$ orbital. It is clear in Figure 2.8 that the most important difference between singlet and triplet state carbenes lies in the energy level of this orbital. If there is no interaction between the substituent a_1 bonding orbitals and the C 2p orbitals not contributing to the molecular b_2 bonding orbital, a species where these two C 2p orbitals remain energetically degenerate is obtained. Due to the energetic degeneracy of these C 2p orbitals the two non-bonding electrons are distributed between both orbitals and are not spin-paired; forming a triplet ground state. However, most substituents show interaction of the substituent a_1 bonding orbitals with the symmetrically relevant C 2p orbital forming the $\sigma(a_1)$ orbital and leaving the remaining C 2p orbital as the $p_\pi(b_1)$ orbital. Typically,

electronegative species show a preference towards the increased perturbation between s (such as the substituent a_1 bonding orbitals) and p orbitals. Therefore, on transitioning from σ -electron donating to more electronegative σ -electron withdrawing substituents the $\sigma(a_1)$ orbital will contain a greater s character.

As the s character of the $\sigma(a_1)$ orbital increases this shifts to lower energy levels causing an increase in the energy difference between the $\sigma(a_1)$ and the $p_\pi(b_1)$ orbitals ($\Delta E_{\sigma-p}$) and therefore a loss of energetic degeneracy between these two orbitals. If $\Delta E_{\sigma-p}$ is greater than the pair repulsion energy a singlet state is favoured causing the $\sigma(a_1)$ orbital to become the new Highest Occupied Molecular Orbital (HOMO). In the presence of σ -electron donating substituents, where the perturbation is less intense, the $\Delta E_{\sigma-p}$ is smaller than the pair repulsion energy, as shown in Figure 2.8(b), and triplet states are favoured. For σ -electron donating groups a less bent geometry is also favoured.

Of greater interest in the current study is the effect of p orbitals and π bonding on bonding in the organic carbenes. Two types of substituents occur, π -electron donating and π -electron withdrawing, both of which are known to stabilise carbenes through the mesomeric effect.⁸⁵ π -electron donating substituents stabilise the p_π orbital through the mesomeric effect by bonding with the said orbital. From a MO perspective the relevant p or π orbitals of these π -electron donating substituents overlap with the p_π orbital to form an occupied b_1 bonding orbital of an energy level below that of the σ orbital. Simultaneously the anti-bonding $p_\pi(b_1)$ orbital is formed at a higher energy than the original unperturbed p_π orbital. The σ orbital remains the HOMO while the anti-bonding $p_\pi(b_1)$ orbital obtains a higher energy thus making it the Lowest Unoccupied Molecular Orbital (LUMO) as given in Figure 2.9. This system retains a singlet state, since the majority of substituents which are π -electron donating are also σ -electron withdrawing.

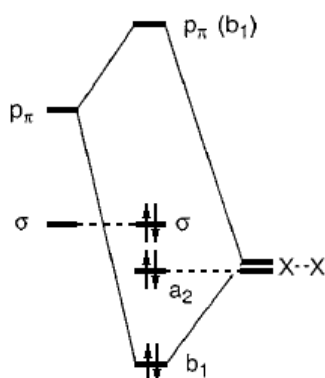


Figure 2.9: Section of a general MO diagram for a carbene having π -electron donating substituents.

On the other hand a smaller group of carbenes with π -electron withdrawing p orbitals, mostly of elements or their fragments which are more electropositive than carbon,⁸⁶ hold a linear geometry of triplet carbenes but the carbene is stabilised by the mesomeric affect with bonding between the σ orbital and the relevant unfilled substituents' p orbitals. This produces a singlet carbene by lowering the energy of the σ orbital without the increase in hybridisation with the C 2s and the substituent ns orbitals.⁸⁴

2.4.1. N-heterocyclic carbenes

N-heterocyclic carbenes (NHCs) have the general molecular structure as shown in Figure 2.10. NHCs are also known as Arduengo carbenes although these were first reported by Öfele in 1968.⁸⁷ Arduengo published the synthesis and characterisation of the first stable NHC, 1,3-di-1-adamantylimidazol-2-ylidene,⁸⁸ in 1991. Since this early work NHCs have been studied extensively with regards to their stability, structure, complexation, reactivity and catalytic behaviour. NHCs were in fact the first carbenes to form carbene complexes with lanthanides to be characterised and published.⁸⁹

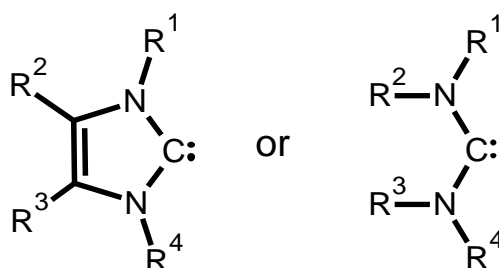


Figure 2.10: General structures of NHCs or Arduengo carbenes.

The two main factors that give rise to the stability of NHC compounds are the σ -withdrawing effect and π -donating effect of the N atoms.⁸⁸ The σ -withdrawing effect of N atoms has been shown to be the most important factor in numerous theoretical investigations.⁹⁰⁻⁹⁴ The overall stability of the many NHCs has been shown to be mainly due to the energy difference between the singlet carbene as opposed to the triplet carbene ($\Delta E_{\sigma-p}$).⁹⁵ The increase in $\Delta E_{\sigma-p}$ for NHCs arises from the bonding of the un-perturbed p_{π} orbital to the relevant occupied p or π orbitals of the π -electron donating substituents as described in Section 2.4 previously.

The synthesis and characterisation of the acyclic bis(di-isopropylamino)carbene by Alder and co-workers showed that the cyclic and unsaturated groups are not necessary for the preparation of thermodynamically stable NHCs.⁹⁶ This therefore indicates that it is indeed the presence of the heteroatoms that stabilises the carbenes through both σ -withdrawing effects and π -donating effects of N atoms.

2.4.2. Heteroatomic λ^5 -phosphane or phosphorane stabilised carbenes

In the case of the iminophosphorano, thiophosphinoyl and phosphonate compounds the carbenes are described as carbanions with the general molecular structure given in Figure 2.11.⁹⁷ Unlike the stabilisation of NHC compounds, the phosphorus moieties do not stabilise the carbene through σ -electron withdrawing and π -electron donating effects.⁹⁸ The latter effect is not noticeable due to the fact that the energetic barrier towards planarization in the three coordinated phosphorus is higher than that for the three coordinated nitrogen,^{99,100} and this does not allow for the conjugation of any lone pairs. It should be noted that planarization of the three coordinated phosphorus is possible under strict conditions.¹⁰⁰ The lack of stabilisation by σ -electron withdrawing and π -electron donating effects is true for both the three coordinated phosphorus compounds and the four coordinated phosphorus atoms.

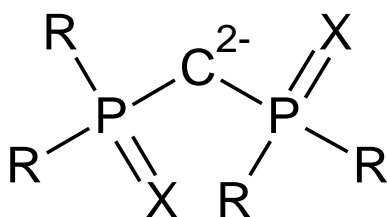


Figure 2.11: General structure of λ^5 -phosphane stabilised carbenes, where X = NR, O or S.

Although this is the molecular structure for most of the metal carbenes used in the current study, earlier studies were undertaken using single λ^3 -phosphane carbenes, with the earliest example being the carbene produced from the precursor [bis(diisopropylamino)phosphino](trimethylsilyl)diazo-methane.¹⁰¹ This compound and a number of phosphinosilyl analogues, have been shown to be only somewhat stable while their respective carbenes were found to be more stable. Later work saw the replacement of the silyl groups with phosphonio groups ($-P^+R_3$). However these showed

little difference from the activity of the silyl groups as both acted as π -withdrawing groups,¹⁰² in contrast to the π -donating phosphino groups. It is of interest to note that this withdrawal occurs from the carbene lone pair to the σ^* orbitals of the Si–C and P–C respectively, by the process of negative hyperconjugation.¹⁰³ This is an important feature in the stabilisation of λ^5 -phosphane carbenes which will be discussed further on. It should be noted that this early work indicated that the $\Delta E_{\sigma-p}$ was far smaller for the NHCs due to the energy barrier for planarization around the phosphorus atom as described earlier in this section.¹⁰⁴ Various reasons have been given in numerous studies for the stabilisation of λ^5 -phosphane carbenes, the main ones being listed below:¹⁰⁵

- Electrostatic interactions
- $d\pi$ - $p\pi$ interactions
- negative hyperconjugation
- high polarizability of the Y elements (where the Y heteroatoms are bonded to the phosphorus)

Today the stabilisation of these compounds has been linked mainly to the negative hyperconjugation of the phosphorus atom in the molecule and polarization effects.⁸⁴ This stabilisation can be interpreted by the resonance hybrid system typical of phosphonium ylides as given in Figure 2.12.¹⁰⁶

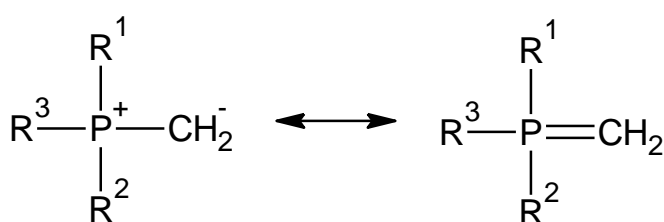


Figure 2.12: Phosphonium ylide resonance hybrid structures.

This resonance hybrid for the phosphonium ylides can also be applied for compounds with the same molecular structure for all elements in Groups 5 and 6.¹⁰⁶ If the phosphorus analogue has a greater electronegativity than carbon (nitrogen and oxygen) the compound is found to be electrostatically unstable. Otherwise the ylide structure is preferred to various degrees, stabilised by electrostatic and negative hyperconjugation effects.¹⁰⁶ This has led to studies on the stabilisation of simple anions

of the type $R^1R^2PCH_2^-$, wherein the two groups on the phosphorus act to increase the stability of the anion by decreasing the partial charge difference and increasing negative hyperconjugation.^{105,106}

This also applies for the stabilisation of carbanions and also for the stabilisation of the dianions from which various metal carbenes are prepared. In fact it has been shown that not only is it unnecessary for the carbene molecules to have two λ^5 -phosphane moieties but that it is possible to use different moieties to achieve differing chemical properties.⁹⁷ In general the dianions take on the molecular structure given in Figure 2.13 wherein the negative charge is distributed over the methylene carbon and the heteroatom linked to the phosphorus, while the phosphorus maintains a positive charge.

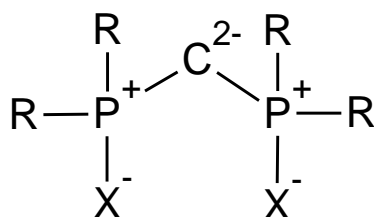


Figure 2.13: Electronic structure of the λ^5 -phosphorane stabilised geminal dianions.⁹⁸

Since the methylene dianion is stabilised in such a way, the formal bond number of the P=X bond decreases as the anti-bonding, σ^* , orbital is occupied, leading to an increase in the P–X distance and a localisation of electron density on the respective heteroatom, X.⁹⁸

In terms of bonding with transition metal centres, a simple description is depicted in Figure 2.14. In the free state the compounds are dianions and in theory the two carbene orbitals σ and p_π are fully filled and both act as donor orbitals with no back bonding.⁹⁷ For the transition metals the bonding of the p_π orbitals with metal centre orbitals acts against the stabilisation of the same orbital by negative hyperconjugation, this being both an interesting and problematic feature of these complexes. This can be better explained using Figure 2.15.¹⁰⁷ Therefore it is the balance of these features that provides the stability of the metal complexes in the case of the transition metals.

This molecular and orbital structure is however the main reason why such compounds are useful in the synthesis of non-transition metal carbenes, such as for Group 1 and 2 metals,^{108–110} the lanthanides, actinides and early heavy p-block elements.^{111–113} In the first four groups the double donor ability is necessary since all the metal centres

involved have a greatly diminished ability to donate electrons.² In the case of these groups the p_π donating capability must be enhanced in order to stabilise the $M=C$ bond but the stability of the dianion must not be diminished drastically so as to maintain ionic and chelating bonding with the metal centres. This is also a significant challenge to the synthesis of such carbenes.

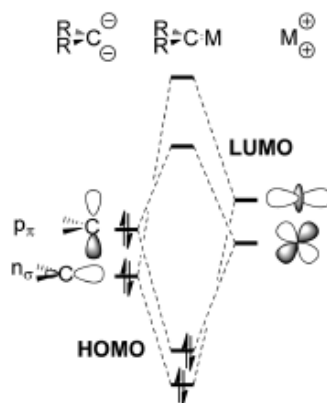


Figure 2.14: MO diagram for the bonding of the λ^5 -phospha carbenes with transition metals.⁹⁷

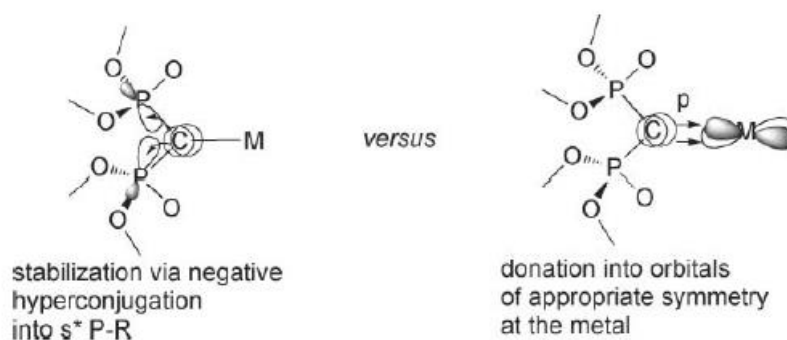


Figure 2.15: Two main carbene stabilisation structures for the bonding of p_π with transition metal centres.¹⁰⁷

Independent to all of this, it should always be kept in mind that these dianions, although frequently depicted as formally having $M=C$ bonds to metal or metalloid centres, have a π bond which is very polarised. Numerous studies for a number of centres have shown that the π bond orbitals are centred on the dianion carbon with relatively small contributions from the metal centres' orbitals.^{10,114,115} It should be noted that although these dianions are mainly used in the synthesis of compounds containing the $M=C$ bond,^{107,109,110,112} since the ligands are geminal dianions they have shown the capability of producing a number of clusters.¹⁰⁸⁻¹¹⁰

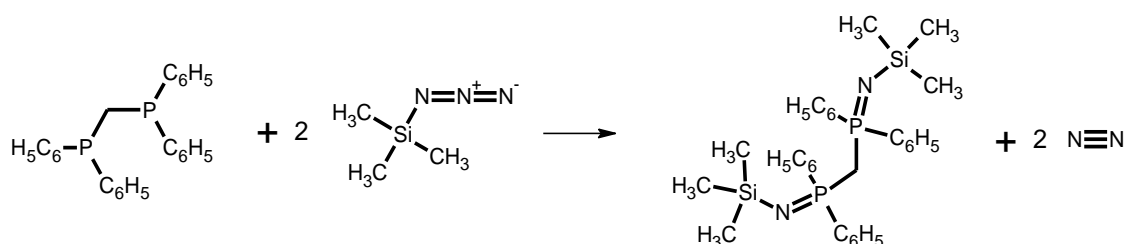
2.4.3. Synthesis of $\lambda^5\sigma^4$ -phosphorus stabilised carbenes

2.4.3.1. Synthesis of iminophosphorane geminal dianions

Two major synthesis routes are used for the preparation of the molecules of bis(diphenyliminophosphorano)methane analogues.³¹ These are the phospha-Staudinger and Kirsanov methods.³¹

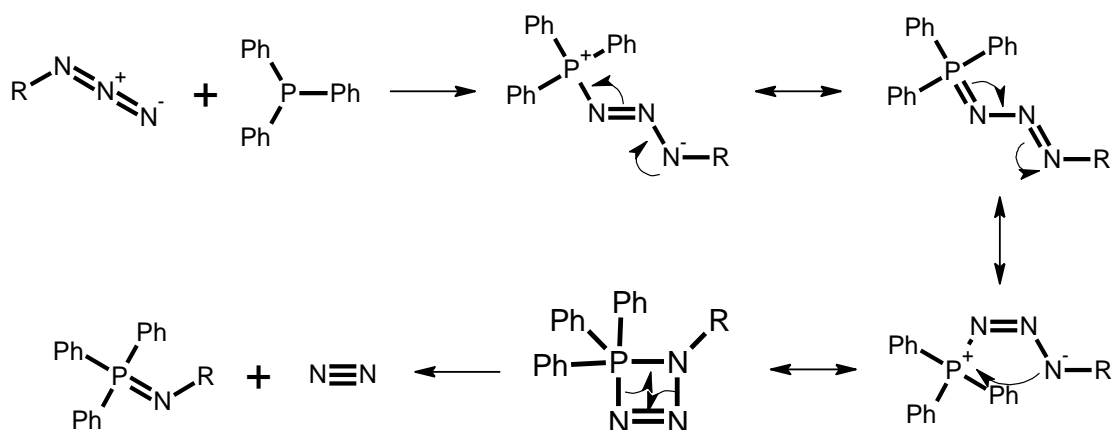
2.4.3.1.1. Phospha-Staudinger method

This is one of the earliest synthesis routes used for the production of iminophosphorane geminal dianions by the reaction of 1,1-diphenylphosphinomethane (dppm) with trimethylsilyl azide to form bis(diphenyl-N-trimethylsilyliminophosphorano)-methane, as published by Appel and Rupert in 1974.³⁴ This reaction was also applied to 1,2-diphenylphosphinoethane and 1,3-diphenylphosphinopropane and in general yielded positive results. The reaction is given in Scheme 2.1:



Scheme 2.1: Synthesis of bis(diphenyl-N-trimethylsilyliminodiphenylphosphorano)methane.³⁴

The reaction was undergone by reacting dppm and trimethylsilyl azide in a 1:2.5 ratio.³⁴ This method is transferable to a number of other organic azides, like 2,4,6-trimethylphenyl (2,4,6-Me₃C₆H₂), 2,6-diisopropylphenyl (2,6-(*i*Pr)₂C₆H₃ or DIPP) and the adamantyl azides.¹¹⁶ The main setback that this synthesis encounters is the stability of the azide reagents which can vary from stable to explosive.³¹ The mechanism for the formation of triphenyliminophosphoranes via this synthesis method is given in the Scheme 2.2:



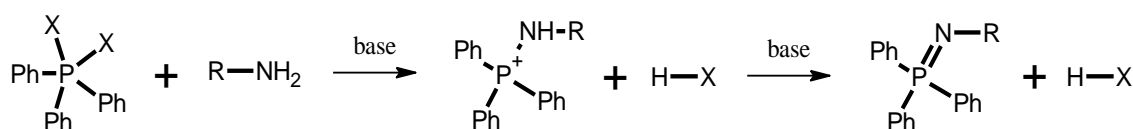
Scheme 2.2: Mechanism for the formation of triphenyliminophosphoranes.¹¹⁷

2.4.3.1.2. Kirsanov method

The Kirsanov method is another method used for the preparation of iminophosphorane geminal dianions, which was initially published as far back as 1950,^{36,118} with further work from the same author in 1954,⁹⁹ 1956 and 1957.¹¹⁹ The original synthesis and its numerous variations were expanded on in various publications.^{119,120} In all variations of this reaction a phosphorus(V)halide or a phosphorus(V)organohalide is reacted with an organic amine to prepare an iminophosphorane as the final product, as shown in Schemes 2.3 and 2.4.



Scheme 2.3: Reaction of phosphorus (V) halides published by Kirsanov in 1954.⁹⁹



Scheme 2.4: Preparation of triphenyliminophosphorane analogues through the modified Kirsanov route as first published by Horner and Oediger and expanded on by Zimmer and Singh.^{117,119,120}

The Kirsanov method was extended to the preparation of bis(diphenyliminophosphorano)methane analogues as a multiple step reaction pathway by Demange and co-workers.³⁶ It seems that although the preparation of these compounds requires multiple steps it is more versatile than other methods published prior, again mainly due to the stability, or lack thereof, of the organic azides required.

In this study dppm was used as the main phosphorus containing starting reagent. The first step was the bromination of dppm in dichloromethane in a 2:1 ratio, to prepare the necessary halide to continue through the Kirsanov route. The product $[\text{dppmBr}_2^+][\text{Br}^-]_2$ was then obtained as a white precipitate. The second step was the reaction with the relevant amine. For the aliphatic amines *iso*-propylamine and (S)-2-methyl-butylamine, reaction with $[\text{dppmBr}_2^+][\text{Br}^-]_2$ required tributylamine whereas for aniline tri-butyl amine was not required. In all cases the reaction of the $[\text{dppmBr}_2^+][\text{Br}^-]_2$ gives aminophosphonium salts as products, of the general formula $[\text{CH}_2(\text{P}^+-\text{NHR})_2][\text{Br}^-]_2$, with the structure shown in Figure 2.16.

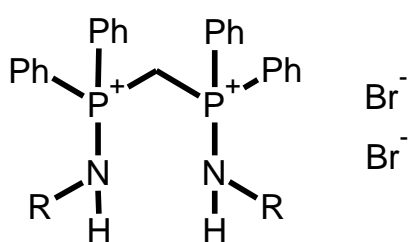


Figure 2.16: Aminophosphonium salt product of the Kirsanov reaction for dppm with RNH_2 .³⁶

The aminophosphonium salts were then used to easily synthesize a number of compounds, ranging from the bis(diphenyliminophosphorano)methane compounds to numerous anionic species of these compounds by reacting with methyl lithium at different stoichiometry.³⁶ The neutral bis(diphenyliminophosphorano)methane compounds were synthesised by the reaction with 2 equivalents of methyl lithium. 3 equivalents and 4 equivalents of methyl lithium with $[\text{dppmBr}_2^+][\text{Br}^-]_2$ gave the lithium stabilised mono-anion and dianion respectively. All of these reactions are shown in Figure 2.17.

These derivatives of the various bis(diphenyliminophosphorano)methane compounds can be used as the starting point for geminal dianion based lanthanide carbenes.³¹

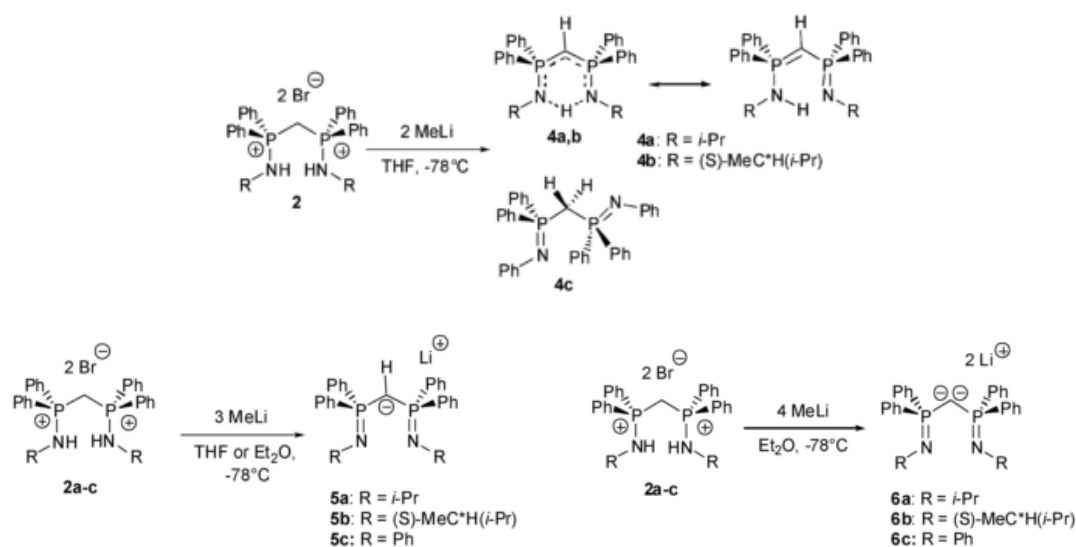


Figure 2.17: The preparation of the various neutral (4a-c), mono-anion (5a-c) and dianion (6a-c) derivatives of the bis(diphenyliminophosphorano)methanes synthesised by Demange and co-workers.³⁶

Buchard and co-workers used a bis(diphenyliminophosphorano)methandiide chloride for their work but did not release the synthesis method for the chloride, citing the synthesis by Demange.¹² The same group also dealt with the same reaction using the bromide salt.¹²¹ In each case the neutral compound, given in Figure 2.17 as 4a-c, was collected and stored but was not used to prepare the various charged compounds.³⁶ In this study the charged compounds were only prepared from the salts indicated by 2a-c in Figure 2.17.³⁶

The double deprotonation of the neutral compounds in this group requires a considerable amount of reaction time and is carried out in the presence of strong bases.⁹⁸ The deprotonation of these compounds has been undergone using strong bases such as methyl lithium,^{30,97} *n*-butyl lithium,^{97,122} potassium bis(trimethylsilylamide) (KHMDs)^{12,40} and respective lanthanide benzyls.^{9,41,115} All of the species mentioned above have been used in the synthesis of various organometallic complexes.

2.4.3.2. Synthesis of thiophosphinoyl stabilised carbenes

A common member of the thiophosphinoyl stabilised carbenes is bis(diphenylphosphino)methane disulphide or bis(diphenylthiophosphinoyl)methane, which is presented in Figure 2.18.

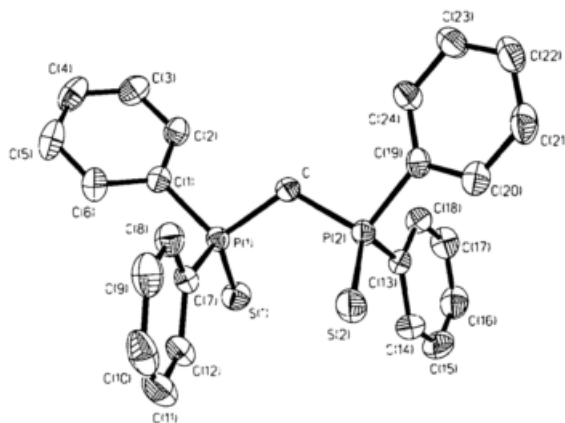
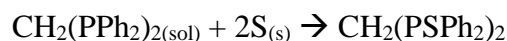


Figure 2.18: Structure of bis(diphenylthiophosphinoyl)methane from SXRD data, 30% probability displacement ellipsoids.³⁵

Since sulphur cannot bond with further organic moieties, substitutions like those noted in Section 2.4.3.1 for iminophosphanes cannot be undergone, limiting the tunability of the chemical properties of this compound and other members of this group in general.⁹⁷ The reaction is the reduction of sulphur in the presence of and by the bis(diphenylphosphino)methane or respective analogues.³¹ The synthesis of this compound was published very early on by Carmalt and co-workers in 1996.³⁵ The simple reaction is presented in Scheme 2.5:



Scheme 2.5: Synthesis of bis(diphenylphosphino)methane disulphide by the oxidation of dppm with sulphur.

The synthesis included the reaction of elemental sulphur with 1,1-diphenylphosphinomethane (dppm) in a toluene solution at a molar ratio of 2:1 at room temperature. The compound was obtained as a crystalline solid, in a quantitative yield.³⁵ It is in fact this compound that is most widely used in synthesising the M=C bond containing compounds dealt with in this field of study.^{8,98,123}

The dianion can easily be obtained by the reaction of the thiophosphinoyl with 2 equivalents of methyl lithium under the appropriate conditions.¹²⁴ It appears that detailed study in the phenyl substituted analogues of bis(diphenylthiophosphinoyl)methane in coordination compounds is much less explored.⁹⁸ The dianion and the monoanion can both be formed by the reaction of bis(diphenylthiophosphinoyl)methane with methyl lithium in either toluene or diethyl ether.³⁰

2.5. Typical starting reagents for lanthanide carbenes

Synthesis is a mainstay of all organometallic chemistry and as with the majority of reactions in synthetic chemistry, this is commonly undertaken in a liquid solution. Therefore, the solubility of the reagents and products of a reaction is important in any synthesis. A basic ideal of synthesis is that the reagents are soluble in the reaction solution since this will allow for the thorough mixture of the reagents at a molecular level, although this is not always the case.^{125,126} The solubility of the reagents in a solvent is mainly dependent on what moieties and synthons are available in the solution between the solute and the solvent. For ionic and very polar solutes the solvent of choice is likewise highly polar while for non-polar compounds, especially large organic compounds, non-polar solvents are more efficient.

Therefore, for organometallic synthesis the conundrum arises in the reaction of organic compounds with metal containing reagents. Although organic compounds come with a very large variety of moieties and polarities the most common starting reagents for many metals are indeed salts, since the electronegativity of many metals is low enough to ensure that salt formation with non-metals are very common.² Since transition metals commonly have a higher electronegativity than the Group 1 and 2 metals and the lanthanides, they can readily form compounds with soft basic ligands such as cyclopentadiene, alkyls and phosphines.¹⁹ Rare earth complexes of cyclopentadienes, alkyls and phosphines have been synthesised and characterised as well but are not as air or moisture stable as the hard ligand complexes.⁵⁰

In the case of the lanthanides the most widely available starting materials are the ionic oxides, Ln_2O_3 (where $\text{Ln} = \text{La}, \text{Nd-Lu}$), LnO_2 (where $\text{Ln} = \text{Ce}, \text{Pr or Tb}$) and Ln_6O_{11} (where $\text{Ln} = \text{Pr}$).¹⁹ The main issue with the use of these oxides is that they are insoluble in most solvents, including water. The halides are also available, although these are more easily prepared *in situ* from the oxides by the reaction with the relevant acid, especially for non-air or moisture sensitive reactions. The nitrates and carbonates can also be purchased. In aqueous or highly polar solvents, like alcohols, ethers and DMSO, the halides, nitrates and halates are the best starting reagents due to their greater solubility.¹²⁷⁻¹³³ DMSO is known to form a number of complexes with the lanthanides, of the stoichiometry $[\text{Ln}(\text{DMSO})_8]\text{I}_3$ (where $\text{Ln} = \text{La}, \text{Ce}, \text{Pr}, \text{Nd}, \text{Sm}, \text{Gd}, \text{Tb}, \text{Dy}, \text{Er}, \text{Lu}$ or the rare earth Y), $[\text{Ln}(\text{DMSO})_4(\text{NO}_3)_3]$ (where $\text{Ln} = \text{La-Sm or Gd}$) and $[\text{Ln}(\text{DMSO})_3(\text{NO}_3)_3]$ (where $\text{Ln} = \text{Ho}, \text{Yb and Y}$).^{134,135} The former most complexes are

prepared by the dissolution of anhydrous iodides in DMSO,¹³⁴ while the latter two groups are synthesised from the reaction of the nitrates in DMSO and crystallisation in a number of alcohols and acetonitrile.¹³⁵ The problem arises in the synthesis of organolanthanide compounds in which two restrictions are met, namely:

- 1) The common instability of the products to moisture, which eliminates the use of water as a solvent, solvents containing water and hydrated reagents.
- 2) The lack of solubility of many of the organic reagents in highly polar solvents, which decreases the homogeneity of the reaction mixture and therefore the rate of reaction.

Experimental work on the energetics of the bonding of lanthanide compounds was undertaken fairly early on.^{50,136} The bond disruption enthalpies of a number of samarium bonds with various ligands show that the iodides are thermodynamically more labile than the other halides and therefore more useful as a starting reagent.¹³⁶ THF is one of the most thermodynamically labile ligands studied and this is seen in a number of reactions especially for the sulphur based phosphoranes. Although not studied, the benzyl ligands seem to be more labile than the iodides.⁹ The instability and reactivity of many of the lanthanide ligand pairs is also due to the ionic nature of their bonding and therefore is undertaken through kinetically favourable paths rather than low disruptive enthalpies.^{50,136}

2.5.1. Lanthanide iodide reagents

This section deals with the approach used to mitigate the problems with reagents which are outlined above. In many of the studies relating to the synthesis of the lanthanide carbenes the iodides are the mostly used starting reagents and therefore will be looked into in greater detail.^{8,10,12,115,123} Along with the iodides, the benzyls and a number of other starting reagents have also been used.^{7,9,115}

2.5.1.1. The preparation of anhydrous lanthanide iodides ($\text{LnI}_3 \cdot x\text{H}_2\text{O}$, $x=0$)

The lanthanide iodides, like the chlorides, are very good starting reagents for any reaction introducing lanthanide cations into complexes and compounds. In the synthesis of air and moisture unstable lanthanide compounds it is important that the starting reagents are anhydrous. In the case of the iodides the anhydrous starting reagents are either unavailable commercially or very expensive in very small amounts. Therefore in most literature it is stated that the anhydrous iodides were prepared within the study.^{10,40,115,137} A number of procedures have been presented in literature for the preparation of anhydrous lanthanide iodides. These include the preparations of:

- Anhydrous un-solvated lanthanide iodides^{138–140}
- Lanthanide triiodide THF solvates
- Non-THF solvated lanthanide triiodides^{141–143}
- Lanthanide diiodides^{144–148}

In the current study the main iodide starting reagents used are the tetrahydrofuran (THF) solvated lanthanide iodides, which will be discussed in more detail below.

2.5.1.2. Lanthanide triiodide THF solvates

These are prepared from the oxidation of lanthanide metals with elemental iodine under an inert atmosphere.¹³⁷ For the now widely used THF solvated lanthanide triiodides there are two main chemical structures that divide the lanthanides into two distinct groups. These two structures are the neutral complex $\text{LnI}_3(\text{THF})_x$ (where $x = 3, 4$) and the salt complex $[\text{LnI}_2(\text{THF})_5][\text{LnI}_4(\text{THF})_2]$.^{10,137,149–157} The simple stoichiometry of the latter is usually given as $\text{LnI}_3(\text{THF})_{3.5}$. In both cases the iodide anions and the THF ligands are bonded in the inner coordination sphere of the lanthanide (III) cations.^{137,149–151,157,158} Other THF coordinate complexes are also known.¹⁵⁹ The various complexes are listed in Table 2.1:

Table 2.1: THF solvated Rare Earth triiodides.

Rare Earth	Complexes	Structure	Notes
Yttrium (Y)	$\text{YI}_3(\text{THF})_{3.5}$ ¹³⁷	$[\text{LnI}_2(\text{THF})_5][\text{LnI}_4(\text{THF})_2]$	Similar reactivity to lanthanides, often included as a member of the Rare Earths
Lanthanum (La)	$\text{LaI}_3(\text{THF})_4$, ^{137,150} $\text{LaI}_2(\text{THF})_5\text{I}_3$ ¹⁵⁹	$\text{LnI}_3(\text{THF})_4$, $[\text{LaI}_2(\text{THF})_5][\text{I}_3]$	
Cerium (Ce)	$\text{CeI}_3(\text{THF})_4$ ^{10,137}	$\text{LnI}_3(\text{THF})_4$	
Praseodymium (Pr)	$\text{PrI}_3(\text{THF})_4$ ¹³⁷	$\text{LnI}_3(\text{THF})_4$	
Neodymium (Nd)	$\text{NdI}_3(\text{THF})_4$, ¹⁵¹ $\text{NdI}_3(\text{THF})_{3.5}$ ^{137,152}	$\text{LnI}_3(\text{THF})_4$, $[\text{LnI}_2(\text{THF})_5][\text{LnI}_4(\text{THF})_2]$	
Promethium (Pm)	N/A	N/A	Common isotope radioactive
Samarium (Sm)	$\text{SmI}_3(\text{THF})_{3.5}$ ^{137,153}	$[\text{LnI}_2(\text{THF})_5][\text{LnI}_4(\text{THF})_2]$	
Europium (Eu)	N/A	N/A	Used mainly as the EuI_2
Gadolinium (Gd)	$\text{GdI}_3(\text{THF})_{3.5}$ ¹³⁷	$[\text{LnI}_2(\text{THF})_5][\text{LnI}_4(\text{THF})_2]$	
Terbium (Tb)	$\text{TbI}_3(\text{THF})_x$ ¹⁵⁴⁻¹⁵⁶	N/A	Studied mainly in solution, no XRD studies
Dysprosium (Dy)	$\text{DyI}_3(\text{THF})_{3.5}$ ¹³⁷	$[\text{LnI}_2(\text{THF})_5][\text{LnI}_4(\text{THF})_2]$	
Holmium (Ho)	$\text{HoI}_3(\text{THF})_x$	N/A	Studied mainly in solution
Erbium (Er)	$\text{ErI}_3(\text{THF})_{3.5}$ ¹³⁷	$[\text{LnI}_2(\text{THF})_5][\text{LnI}_4(\text{THF})_2]$	
Thulium (Tm)	$\text{TmI}_3(\text{THF})_{3.5}$ ¹³⁷	$[\text{LnI}_2(\text{THF})_5][\text{LnI}_4(\text{THF})_2]$	
Ytterbium (Yb)	$\text{YbI}_3(\text{THF})_{3.5}$, ¹⁵⁷ $\text{YbI}_3(\text{THF})_3$ ¹⁴⁹	$[\text{LnI}_2(\text{THF})_5][\text{LnI}_4(\text{THF})_2]$, $\text{LnI}_3(\text{THF})_3$	Both complexes known
Lutetium (Lu)	$\text{LuI}_3(\text{THF})_x$ ¹⁵⁸	N/A	not widely studied

As can be seen from Table 2.1 the total CN for the complexes ranges from 6 to 7, with the coordination of the trivalent cations with THF ranging between 2 and 5. The early lanthanides (La^{3+} , Ce^{3+} , Pr^{3+} and Nd^{3+}) have been shown to produce complexes having a CN of 7 with various ligand compositions.^{10,137,150–152,159} This is expected since they have the largest ionic radii.¹⁶⁰ Neodymium, unlike the first three lanthanides, is also known to form the salt structure $[\text{NdI}_2(\text{THF})_5][\text{NdI}_4(\text{THF})_2]$ with a stoichiometry of $\text{NdI}_3(\text{THF})_{3.5}$.^{137,152} This salt structure is also attested for the remainder of the lanthanides (from Sm^{3+} to Yb^{3+}) which have smaller ionic radii than those of the earlier lanthanides. In the case of the $\text{LnI}_3(\text{THF})_{3.5}$ structure two complex ions were found in compounds, with a 7 coordinated cation $[\text{LnI}_2(\text{THF})_5]^+$ and the 6 coordinated anion $[\text{LnI}_4(\text{THF})_2]^-$.^{137,153,157} The trivalent ytterbium also coordinates in the neutral 6 coordinate complex $\text{YbI}_3(\text{THF})_3$. This is as expected given that it has the smallest radius of the partially filled 4f orbital cations.¹⁴⁹ Therefore, as expected, the published structures of the THF solvated lanthanide triiodides follow the trend of decreased coordination due to the decrease in lanthanide cation radii. In the salt structure the number of the coordinated iodide and THF per complex center indicates that steric factors are also important.

Although one would assume that terbium and holmium follow the same trend and therefore have the structure $[\text{LnI}_2(\text{THF})_5][\text{LnI}_4(\text{THF})_2]$, structural studies such as Single Crystal X-Ray Diffraction (SXRD) have not been published.^{154–156} The THF solvate of lutetium triiodide has not been widely studied, with the solid attested as a white insoluble precipitate after the suspension of the anhydrous LuI_3 in THF being a possible candidate.¹⁵⁸ The structure is therefore unknown. The rare earth yttrium (Y^{3+}) has also shown coordination in the salt structure $[\text{YI}_2(\text{THF})_5][\text{YI}_4(\text{THF})_2]$, as expected given its radius.¹³⁷

There are various pathways to the synthesis of these complexes, with the most practical being published by Izod and co-workers in 2004.¹³⁷ This procedure was undertaken with La, Pr, Nd, Sm, Gd, Dy, Er, Tm and the rare earth Y. In the publication, elemental iodine was reacted with a lanthanide metal slurry in dry THF at 0 °C.¹³⁷ All these iodides were characterised using SXRD. One of the structures that was published was that of the gadolinium complex $[\text{GdI}_2(\text{THF})_5][\text{GdI}_4(\text{THF})_2]$, presented hereunder in Figure 2.19.

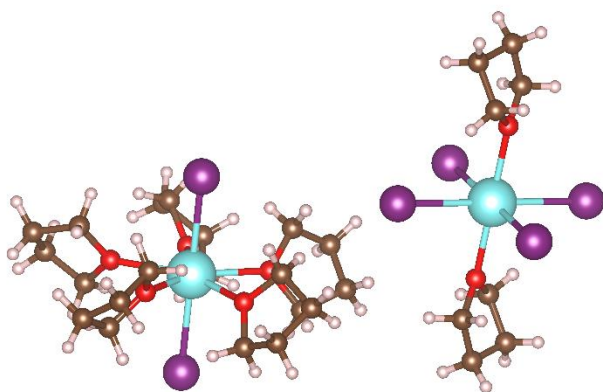


Figure 2.19: The structures of the ions in the unit cell of $[\text{GdI}_2(\text{THF})_5][\text{GdI}_4(\text{THF})_2]$ (built in VESTA from cif data obtained from the CSD).¹³⁷

These iodides are partially soluble in ethers and THF but remain insoluble in other hydrocarbon solvents, such as benzene, toluene and hexane; giving a suspension rather than a solution of the complex.

The salt $[\text{SmI}_2(\text{THF})_5][\text{SmI}_4(\text{THF})_2]$ was one of the earliest THF solvated lanthanide triiodides recorded, synthesised by the oxidation of SmI_2 in THF solution, using dry oxygen gas.¹⁵³ The salt produced was formed as a yellow crystalline precipitate.¹⁵³ An orange-yellow isomorphous complex was also synthesised for Yb^{3+} through an oxidation process, as an unintended product.¹⁵⁷

Apart from the method described by Izod and co-workers, another method for the preparation of $\text{LaI}_3(\text{THF})_4$ and $\text{CeI}_3(\text{THF})_x$ has been published. This was undertaken by the reaction of the respective metal with iodoethane in THF under reflux.¹⁵⁰ The preparation of $\text{LaI}_2(\text{THF})_5\text{I}_3$ as a red crystalline solid was published in 1997, with the reaction of the lanthanum powder with 1,2-diiodoethane in THF.¹⁵⁹ Terbium triiodide (TbI_3) has been used as a reagent in various publications but it is commonly employed as the anhydrous form in a THF solution, and crystallographic studies for the solvate have not been published.^{155,156}

2.5.2. Lanthanide benzyl complexes

Lately a series of lanthanide tri-benzyl complexes with a general formula of $[\text{Ln}(\text{CH}_2\text{C}_6\text{H}_5)_3(\text{THF})_3]$ (where Ln = La, Ce, Pr, Nd, Sm, Gd, Dy, Er or the rare earth Y) were synthesised from the above mentioned iodides by Wooles and co-workers,⁹ produced by reacting the THF solvated lanthanide triiodides, described in Section

2.5.1.2., with benzyl potassium ($\text{KCH}_2\text{C}_6\text{H}_5$). These complexes, although containing three benzyl rings, are still not fully soluble in toluene and are insoluble in benzene as shown in studies where they are used as starting materials for the lanthanide bis(diphenyl-N-trimethylsilyliminophosphorano)methandiides carbenes,⁹ $[\text{C}(\text{Ph}_2\text{PNSiMe}_3)_2]^{2-}$. Ytterbium, on the other hand, produces the salt $[\text{Yb}^{\text{II}}(\text{CH}_2\text{C}_6\text{H}_5)(\text{THF})_5][\text{Yb}^{\text{III}}(\text{CH}_2\text{C}_6\text{H}_5)_4(\text{THF})_2]$ on undertaking the same reaction using $\text{YbI}_3(\text{THF})_{3.5}$ with the partial reduction of Yb^{3+} to Yb^{2+} .

Structurally these compounds are of interest since the early lanthanide tri-benzyls (where Ln = Ce, Pr or Nd) show a hapticity of 2 (η^2) on all three benzyl ligands, while samarium has only one benzyl with a η^2 . The lighter lanthanides on the other hand do not show this η^2 hapticity with simple Ln–C bonds. The three structures are shown in Figure 2.20. In all cases the products have a *fac*-isomerism.

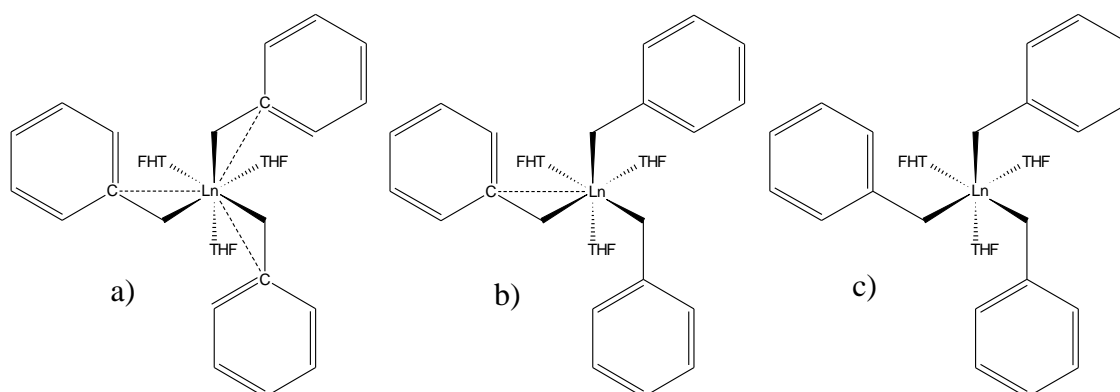


Figure 2.20: Lanthanide tri-benzyl series $[\text{Ln}(\text{CH}_2\text{C}_6\text{H}_5)_3(\text{THF})_3]$ a) tri- η^2 (where Ln = Ce, Pr or Nd) b) mono- η^2 (where Ln = Sm) c) η^1 (where Ln = Gd, Dy or Er).⁹

The advantage of these complexes over the triiodides is that during the preparation of the lanthanide carbenes toluene is formed as a by-product, rather than as a salt which may lead to ligand redistribution reactions and salt occlusion.¹⁶¹ Furthermore, it is easier to undertake reactions with the benzyl in that even weak acids, such as the protonated iminophosphorano compounds, can remove the ligand while the removal of the iodide ion must be undertaken by salt metathesis.⁴¹

In the various lanthanide synthesis with the triiodides and di-benzyl iodides, iodide ligands are known to remain in the product with the THF being the first to be replaced by the new ligands.^{41,45,115,123} In the case of the larger lanthanides, the carbene synthesis with the tri-benzyls leads to the formation of complexes without benzyl or THF ligands remaining in the final product.⁹ This therefore indicates that the benzyl is a better

leaving group than the iodide, although THF remains the primary leaving group. This can be explained by the Hard Soft Acid Base (HSAB) theory wherein the benzyl ligand is softer than the iodide and therefore the bonding with the hard lanthanide cations is better with the latter ligand than with the former.

A number of the rare earth metals were also found to produce the di-benzyl iodides $[\text{Ln}(\text{CH}_2\text{C}_6\text{H}_5)_2\text{I}(\text{THF})_3]$ (where Ln = Dy, Er or Y), which seem to be stable to ligand scrambling.^{41,115} For the latter two rare earth metals this was achieved by the reaction of benzyl potassium, $\text{KCH}_2\text{C}_6\text{H}_5$, with the relevant THF solvated lanthanide iodide in a 2:1 molar ratio.⁴¹ The same procedure was attempted for dysprosium but a powder could not be obtained, and further reactions were undergone using the oil produced.¹¹⁵ To the knowledge of the author analogous compounds for the larger lanthanides have not yet been synthesised and characterised.

2.5.3. Other lanthanide starting reagents for phosphorus (V) stabilised carbenes

Other complexes have been sporadically used as starting reagents for the synthesis of lanthanide carbenes. One of the earliest characterised lanthanide carbenes was $[\text{Sm}(\text{C}(\text{Ph}_2\text{PNSiMe}_3)_2)(\text{NCy}_2)(\text{THF})]$ which was synthesised from the reaction of $\text{H}_2\text{C}(\text{Ph}_2\text{PNSiMe}_3)_2$ with the samarium tris(dicyclohexylamide) $[\text{Sm}(\text{NCy}_2)_3(\text{THF})] \cdot \text{C}_6\text{H}_5\text{CH}_3$, where $\text{NCy}_2 = \text{N}(\text{C}_6\text{H}_{11})_2$.⁷ $[\text{Sm}(\text{NCy}_2)_3(\text{THF})] \cdot \text{C}_6\text{H}_5\text{CH}_3$ was synthesised from the reaction of $\text{SmCl}_3(\text{THF})_3$ and LiNCy_2 .¹⁶² The rare earth carbene $[\text{Y}(\text{C}(\text{Ph}_2\text{PNSiMe}_3)_2)(\text{CH}_2\text{SiMe}_3)(\text{THF})]$ was also an early rare earth carbene synthesised from $[\text{Y}(\text{CH}_2\text{SiMe}_3)_3(\text{THF})_2]$ as a starting reagent.^{163,164}

2.6. Lanthanide Carbenes

2.6.1. Lanthanide–NHCs or Arduengo carbenes

Lanthanide carbenes derived from the NHCs or Arduengo carbenes are some of the most widely studied carbenes and organolanthanide compounds. Numerous types of lanthanide-NHCs are known. These are synthesised through a variety of methods and are themselves used in various reactions. The earliest lanthanide-NHC complexes were published by Arduengo and co-workers as early as 1994.⁸⁹ These were the divalent

samarium complexes with 1,3,4,5-tetramethylimidazol-2-ylidene, namely $\text{Sm}(\text{Cp}^*)_2(\text{C}(\text{N}(\text{CH}_3)\text{C}(\text{CH}_3))_2)$ and $\text{Sm}(\text{Cp}^*)_2(\text{C}(\text{N}(\text{CH}_3)\text{C}(\text{CH}_3))_2)_2$ and having the molecular structures shown in Figure 2.21:⁸⁹

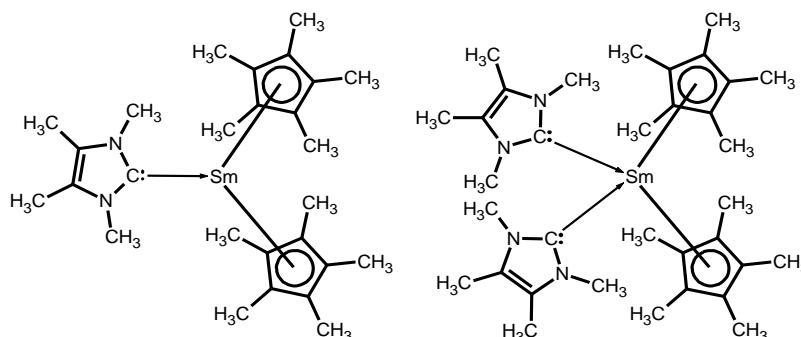


Figure 2.21: Structures of $\text{Sm}(\text{Cp}^*)_2(\text{C}(\text{N}(\text{CH}_3)\text{C}(\text{CH}_3))_2)$ and $\text{Sm}(\text{Cp}^*)_2(\text{C}(\text{N}(\text{CH}_3)\text{C}(\text{CH}_3))_2)_2$.⁸⁹

Since this early work the field has been expanded to include a numerous amount of lanthanide-NHC complexes,^{165–172} with work on new complexes being published as recently as 2019.¹⁷³ In some of the latest work novel lanthanide-NHC complexes of divalent Ce^{2+} and Yb^{2+} have also been characterised further expanding the chemistry of this class of compounds.¹⁷³ These complexes have found use mainly in the field of catalysis.^{174–176} An interesting example is the selective polymerisation of isoprene to 1,4-trans polyisoprene.¹¹ This family of carbenes will not be discussed further as it is not be used in the current study.

2.6.2. Lanthanide- λ^5 -phosphorane stabilised geminal dianion carbenes

As described in Sections 2.4.2 and 2.4.3, λ^5 -phosphorane stabilised geminal dianions are used in many publications to form various lanthanide carbene complexes, due to their coordination characteristics.

2.6.2.1. Early non-NHC lanthanide carbenes

The λ^5 -phosphorane stabilised geminal dianions are today well established as they form quite stable complexes through their chelating ability and the internal dianions stabilisation through charge distribution, as described in Section 2.4.2.^{97,98,107} Early studies in non-NHC carbene complexes of lanthanides and rare earths dealt primarily

with alkylidenes.^{50,177} The earliest tentative lanthanide-alkylidene carbenes were for the heavy lanthanides erbium(III) and lutetium(III), namely [Er(CHSiMe₃)(CH₂SiMe₃)] and Li[Lu(CHSiMe₃)(CH₂SiMe₃)₂] respectively.¹⁷⁸ The ligand CHSiMe₃ is known to act as a carbene in numerous transition metal complexes.¹⁷⁸ The complexes were produced from the decomposition of [Er(CH₂SiMe₃)·THF₂] and [Li(OEt)₂][Lu(CH₂SiMe₃)₄] respectively in solution; however in each case no structural data could be obtained.¹⁷⁸ Later attempts at preparing alkylidene carbene complexes led to the formation of clusters such as the [Cp*₃La₃(μ-Cl)₃(μ₃-Cl)(μ₃-CH₂)(THF)₃].¹⁷⁹ Clusters that have the methylene group in a bridging fashion and are stabilised by methylaluminate moieties include [(TMTACSm)(Smμ₂-CH₃)((μ₆-C)(Al(μ₂-CH₂)₂)(CH₃)₃((μ₃-CH₂)(μ₂-CH₃)Al(CH₃)₂)₂], where TMTAC = 1,3,5-trimethyl-1,3,5-triazacyclohexane, and [(Tp^{tBu,Me})AlMe][Y((μ-CH₂)(μ-Me)AlMe₂)₂((μ-CH₃)₂AlMe₂)(AlMe₂)], where Tp^{tBu,Me} = hydrotris(3-*tert*-butyl-5-methylpyrazolyl)borate.^{180,181} (BODDI)Lu₂(CH₂SiMe₃)₂(μ₂-CHSiMe₃)(THF)₂, where BODDI = (2,6-*i*Pr₂Ph)NC(Me)CHCOCHC(Me)N(2,6-*i*Pr₂Ph) is the only truly alkylidene cluster that has been synthesised and characterised fairly recently.¹⁸²

Non cluster methylaluminate stabilised alkylidene complexes of rare earth metals are known mainly for two compounds, [(Tp^{tBu,Me})La[(μ-CH₂)((μ-CH₃)Al(CH₃)₂)₂]] and [(1-N(C₆H₃-*o*-*i*Pr-*p*-Me)₂)Sc((μ-CH₂)((μ-CH₃)Al(CH₃)₂)₂)].^{183,184} Density functional theory (DFT) calculations regarding the latter complex indicate that the Sc–C bond is not a simple double bond but that the charge is distributed through delocalisation about the scandium, aluminium, methylene and methyl moieties, with the former two taking up positive charges while the latter two take on the majority of the electron density.¹⁸⁴ Other compounds which are somewhat similar are known for the early lanthanides lanthanum and praseodymium but have garnered less interest due to their cluster like forms.^{181,185}

2.6.2.2. Lanthanide iminophosphorano geminal dianion carbenes

2.6.2.2.1. Lanthanide iminophosphorano carbenes synthesis and characterisation

The first bis(iminophosphorano)carbene complex of a rare earth, specifically a lanthanide (III) ion, was characterised by Aparna *et al.* in 2000, the complex was [Sm(C(Ph₂PNSiMe₃)₂)(NCy₂)(THF)], where NCy₂ is dicyclohexylamide,⁷ with the structure given in Figure 2.22. This complex was synthesised by the reaction of the

[Sm(NCy₂)₃(THF)] with H₂C(Ph₂PNSiMe₃)₂ in toluene.⁷ The lanthanide carbene proved to be not only air-sensitive but also underwent thermolysis in toluene under argon at 120 °C.⁷ The synthesis and characterisation of this compound occurred after a number of years in which such carbene complexes were known only for transition and Group 4 metals.¹⁸⁶ In this case no studies into the reactivity of the complex have been published and work was more focused on the publication of more efficient ways to synthesise such complexes and on their workup.

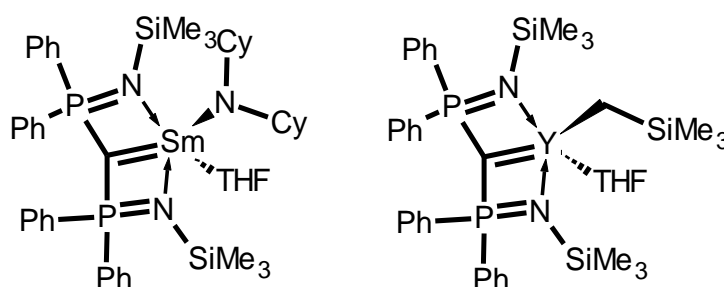


Figure 2.22: Structures of the samarium and yttrium complexes of bis(diphenyl-N-trimethylsilyliminophosphorano)methandiide.^{7,163}

The next rare earth bis(iminophosphorano)carbene complex was published only in 2008. This was [Y(C(Ph₂PNSiMe₃)₂)(CH₂SiMe₂)(THF)], showing the structure given in Figure 2.22.¹⁶³ In these early studies the main reaction methodology involved an acid-base reaction, reacting an acidic methane derivative, namely H₂C(Ph₂PNSiMe₃)₂, with a basic ligand containing lanthanide complex, namely [Sm(NCy₂)₃(THF)] and [Y(CH₂SiMe₂)₃(THF)₂].^{31,187} It was noted that the synthesis of the latter carbene was easier due to the stronger basicity of the CH₂SiMe₂⁻ ligands as compared to that of the NCy₂⁻ ligands in the starting reagents used in the respective synthesis.³¹

Natural bond orbital (NBO) analysis of the latter compound indicated that the bonding remains mainly ionic.¹⁶³ SXR analysis also showed that the charge on the ligand in the complex is not fully concentrated on the central C but distributed as given in Figure 2.23. However the NBO data also suggests that although delocalisation is present, the electron density remains concentrated on the central C with the C 2p contributions to the C–P (dominating the HOMO) and C–Y (dominating the HOMO-2) bonds being 53.5% and 49.0% respectively, with P 3p and Y only contributing 4.1% and 3.7% respectively.¹⁶³ This is a trend that has been seen in later studies of carbene complexes using SXR and NBO analysis.

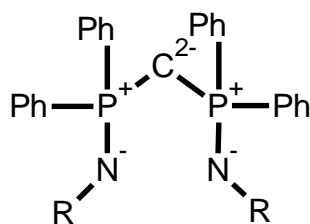


Figure 2.23: Charge distribution common in iminophosphorano carbene ligands complexed with lanthanides.

From the many iminophosphorano geminal dianion carbene ligands known and derived from the bis(iminophosphorano)methane compounds described in Section 2.4.3, the ligand bis(diphenyl-N-trimethylsilyl-iminophosphorano)methandiide used in the synthesis of the two aforementioned complexes [Sm(C(Ph₂PNSiMe₃)₂)(NCy₂)(THF)] and [Y(C(Ph₂PNSiMe₃)₂)(CH₂SiMe₂)(THF)] has found the most widespread use in the synthesis of lanthanide iminophosphorano carbenes.³¹ After the publication of the research on [Y(C(Ph₂PNSiMe₃)₂)(CH₂SiMe₂)(THF)] by Liddle and co-workers in 2008, work by the same group has expanded onto other bis(diphenyl-N-trimethylsilyl-iminophosphorano)methandiide rare earth and lanthanide complexes.³¹

An acid-base methodology as described for the two prior complexes was maintained for many of the later studies described hereunder. In a study by Mills *et al.* in 2009 an analogue of the yttrium (III) carbene complex mentioned prior, [Y(C(Ph₂PNSiMe₃)₂)(CH₂C₆H₅)(THF)], was prepared by the reaction of H₂C(Ph₂PNSiMe₃)₂ with the octahedral yttrium tri-benzyl Y(CH₂C₆H₅)₃(THF)₃, which was in turn prepared as described in Section 2.5.2.^{9,188}

DFT studies of this compound were undergone in the same study, indicating that the Y–C_(benzyl) bond is dominated by the HOMO while the C=Y bond is dominated by the HOMO-1 and HOMO-2 which relate to the π and σ bonds, as presented in Figure 2.24.¹⁸⁸ These calculations also indicate that the charge distribution on the ligand is similar to that given in Figure 2.23 above. Further calculations also gave bond orders of 0.66 (Y–C_(carbene)), 0.35 (Y–C_(benzyl)), 0.29(Y–N), and 1.27(C–P) and Mulliken charges of +1.63 (Y), -1.04 (C_(carbene)), -0.34 (C_(alkyl)), +1.31 (P), and -1.12 (N), thus giving further evidence supporting this electron density distribution.¹⁸⁸

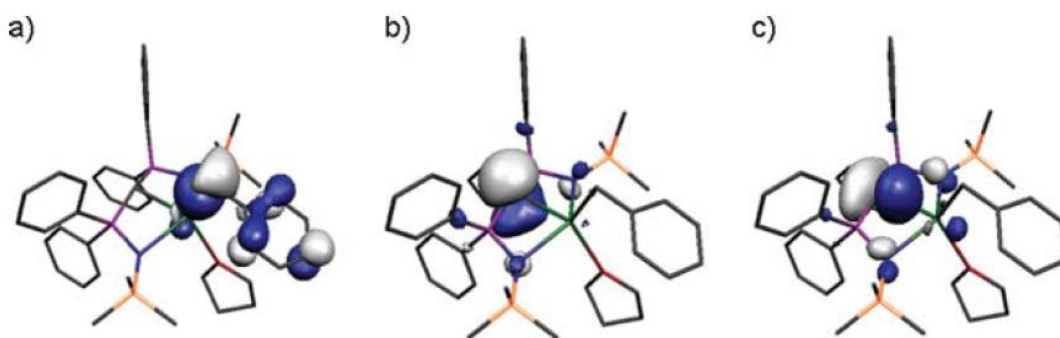


Figure 2.24: Kohn-Sham orbitals for a) HOMO, b) HOMO-1 and c) HOMO-2 for [Y(C(Ph₂PNSiMe₃)₂)(CH₂C₆H₅)(THF)].¹⁸⁸

This study proposed a very versatile reaction method which was used relatively unchanged to prepare a series of lanthanide bis(diphenyl-N-trimethylsilyliminophosphorano)methandiide complexes for the majority of the lanthanides, in another study by the same group.⁹ Molecular structural analogues with the formula [Ln(C(Ph₂PNSiMe₃)₂)(CH₂C₆H₅)(THF)] were prepared by the same procedure for the heavier lanthanides dysprosium and erbium.⁹ The same procedure applied to the larger or earlier lanthanides La³⁺, Ce³⁺, Pr³⁺, Nd³⁺, Sm³⁺, and Gd³⁺, on the other hand produced compounds with the formula [Ln(C(Ph₂PNSiMe₃)₂)(HC(Ph₂PNSiMe₃)₂)].⁹ In all cases the synthesis was undergone using the respective lanthanide tri-benzyl compounds Ln(CH₂C₆H₅)₃(THF)₃, which were found to be more easily prepared and stored than the other lanthanide and rare earth starting reagents described in Section 2.5.3. and furthermore they are greatly basic, yielding toluene as the conjugate acid.¹⁸⁸ Products were characterised using mainly SXRD and NMR with no DFT and NBO studies being undergone.⁹

Later work dealt with creating complexes with more adaptable spectator ligands to increase the versatility of the use of these complexes.³¹ Compounds of the structure [Ln(C(Ph₂PNR)₂)(HC(Ph₂PNR)₂)] are inherently less versatile in their use due to the secondary methanide occupying possible reaction sites and inhibiting the presence of reaction influencing secondary ligands.³¹ Therefore the synthesis and characterisation of lanthanide carbene complexes where a significant part of the primary coordination sphere was not occupied by non-useful spectator ligands has been the focus of much of the work in this field. An acid-base approach similar to that used in the synthesis of the early carbenes such as the [Ln(C(Ph₂PNSiMe₃)₂)(CH₂C₆H₅)(THF)] and the [Ln(C(Ph₂PNSiMe₃)₂)(HC(Ph₂PNSiMe₃)₂)] analogues was used.

Mills and co-workers worked on the smaller radii Y^{3+} and Er^{3+} rare earths, seeing that these already proved to form complexes without the methanide ligands.⁴¹ In the published work the starting reagent was changed from $Ln(CH_2C_6H_5)_3(THF)_3$ to $Ln(CH_2C_6H_5)_2I(THF)_3$ where $Ln = Er$ or Y , with the latter being prepared in a similar manner to the former but using a different stoichiometry. When the iodide was applied to the same synthetic procedure as the synthesis of $[Ln(C(Ph_2PNSiMe_3)_2)(CH_2C_6H_5)(THF)]$ from the tri-benzyl, the complex $[Ln(C(Ph_2PNSiMe_3)_2)(THF)_2I]$, where $Ln = Er$ or Y , was produced.⁴¹ A similar approach was used in an attempt to prepare $[Dy(C(Ph_2PNSiMe_3)_2)(THF)_2I]$ but this was thwarted by the inability to isolate $Dy(CH_2C_6H_5)_2I(THF)_3$.¹¹⁵ Instead of $Dy(CH_2C_6H_5)_2I(THF)_3$ an oil was formed which yielded only a number of methanides which could not be deprotonated to the methandiide carbene.¹¹⁵

Concurrently to the publication of the synthesis and characterisation of the $[Ln(C(Ph_2PNSiMe_3)_2)(HC(Ph_2PNSiMe_3)_2)]$ series mentioned beforehand, (where $Ln = La^{3+}, Ce^{3+}, Pr^{3+}, Nd^{3+}, Sm^{3+},$ or Gd^{3+}), separate work by Buchard and co-workers synthesised a single early lanthanide carbene complex with a similar molecular structure, namely $[Nd(C(Ph_2PNiPr)_2)(HC(Ph_2PNiPr)_2)]$.⁴⁰ A different approach was undertaken in the synthesis of this complex, wherein instead of an acid-base methodology salt elimination or metathesis to initially prepare the respective methanide complex was used. In this case this ligand was found to be more susceptible to deprotonation. The salt $K[HC(Ph_2PNiPr)_2]$ was used as the main starting reagent to produce the methanide complex $[Nd(HC(Ph_2PNiPr)_2)_2I]$ on reaction with $NdI_3 \cdot THF_{3.5}$.⁴⁰ This complex was then deprotonated with potassium bis(trimethylsilyl)amide (KHMDs) to produce the aforementioned neodymium carbene. Interestingly the deprotonation via KHMDs did not produce the synthesis of the bis(carbene) $[Nd(C(Ph_2PNiPr)_2)_2]$,⁴⁰ which could be due to the fact that KHMDs is not usually basic enough to deprotonate such methanides and that the initial deprotonation occurred only due to the activation of the C–H on coordination.^{31,40}

The synthesis of $[Nd(C(Ph_2PNiPr)_2)(HC(Ph_2PNiPr)_2)]$ described above increased the interest in the use of salt elimination as an alternative method to the acid-base methodology mainly used prior.^{40,187} The use of salt elimination introduced the far more numerous and diverse group of lanthanide bis(iminophosphorano)methanide complexes as starting reagents for the synthesis of novel lanthanide bis(iminophosphorano)methandiide carbenes, some of which have been characterised

beforehand.¹⁸⁹ Initially the main issue with this method was the particular difficulty in salt elimination on reaction of light alkali metal salts of $\text{H}_2\text{C}(\text{Ph}_2\text{PNSiMe}_3)_2$, that is salts having a composition of $\text{MHC}(\text{Ph}_2\text{PNSiMe}_3)_2$ where $\text{M} = \text{Li}^+$, Na^+ or K^+ , with early lanthanide salts, mainly iodides.¹¹⁵

The first salt metathesis reaction which yielded a rare earth bis(diphenyl-N-trimethylsilyl-iminophosphorano)methanide complex used in the preparation of a carbene was published for $[\text{Y}(\text{HC}(\text{Ph}_2\text{PNSiMe}_3)_2)_2(\text{THF})]$,¹⁹⁰ using $[\text{K}(\text{HC}(\text{Ph}_2\text{PNSiMe}_3)_2)(\text{THF})_2]$ and $\text{YI}_3(\text{THF})_{3.5}$.¹⁹⁰ This was then used to prepare $[\text{Y}(\text{C}(\text{Ph}_2\text{PNSiMe}_3)_2)\text{I}(\text{THF})_2]$ by reacting the yttrium methanide with benzyl potassium.¹⁹⁰ The synthesis of early lanthanide bis(diphenyl-N-trimethylsilyl-iminophosphorano)methanides from a similar method proved ineffective, with decomposition of the product on heating the reaction solution.¹¹⁵ This was however bypassed in later studies by the use of the heavier alkali metal compound $[\text{RbHC}(\text{Ph}_2\text{PNSiMe}_3)_2\text{THF}_2]$ to prepare the $[\text{Ln}(\text{HC}(\text{Ph}_2\text{PNSiMe}_3)_2)_2(\text{THF})]$, where $\text{Ln} = \text{La}^{3+}$ or Ce^{3+} .^{10,191} The greater electropositive nature of the rubidium seems to favour the elimination of the respective iodide.^{10,191} The complex $[\text{Ce}(\text{HC}(\text{Ph}_2\text{PNSiMe}_3)_2)_2(\text{THF})]$ was then reacted with benzyl potassium to prepare the carbene complex $[\text{Ce}(\text{C}(\text{Ph}_2\text{PNSiMe}_3)_2)\text{I}(\text{DME})]$.¹⁰ The series of $[\text{Ln}(\text{HC}(\text{Ph}_2\text{PNSiMe}_3)_2)_2(\text{THF})]$ complexes was expanded in the form of a number of toluene solvates for $\text{Ln} = \text{Nd}$, Gd or Tb but no published carbenes have been synthesised from these.¹⁸⁷

Like the initial complex prepared in such a manner, namely $[\text{Nd}(\text{C}(\text{Ph}_2\text{PN}i\text{Pr})_2)(\text{HC}(\text{Ph}_2\text{PN}i\text{Pr})_2)]$, this salt elimination methodology found better use in complexes of non trimethylsilyl derivatives of bis(iminophosphorano)methane. As noted earlier the failure of the deprotonation of the bis(diphenyl-N-isopropyl-iminophosphorano)methanide $[\text{Nd}(\text{HC}(\text{Ph}_2\text{PN}i\text{Pr})_2)_2(\text{THF})_2]$ on reaction with KHMDs , indicates a greater complexity in the deprotonation of such coordinated ligands.⁴⁰ The lanthanum methanide of bis(diphenyl-N-mesityl-iminophosphorano)methanide $[\text{La}(\text{HC}(\text{Ph}_2\text{PNMes})_2)_2(\text{THF})_2]$ (where $\text{Mes} = 2,4,6\text{-Me-C}_6\text{H}_2$) was easily synthesised through salt metathesis of the lanthanum iodide and $\text{KHC}(\text{Ph}_2\text{PNMes})_2$.¹¹⁵ From the complex $[\text{La}(\text{HC}(\text{Ph}_2\text{PNMes})_2)_2(\text{THF})_2]$, the carbene $[\text{La}(\text{C}(\text{Ph}_2\text{PNMes})_2)\text{I}(\text{THF})_3]$ was easily prepared by reacting the complex with benzyl potassium.¹¹⁵ DFT calculations regarding this complex again indicate the ionic nature of the bonding and a charge distribution with low bond orders.¹¹⁵

This success indicated that bulkier substituents may influence the ease of salt metathesis preparation of the initial methanide and the deprotonation of the complex. In later research the $[\text{Ln}(\text{HC}(\text{Ph}_2\text{PNMe}_3)_2)_2(\text{THF})_n]$ series was extended to other lanthanides, where $\text{Ln} = \text{Ce}, \text{Pr}, \text{Nd}, \text{Sm}$ or Gd for $n = 2$,¹⁹² and $\text{Ln} = \text{Yb}$ for $n = 1$, through similar synthesis.¹⁸⁷ The same procedure to prepare the dysprosium and erbium analogues yielded the salts $[\text{Ln}(\text{HC}(\text{Ph}_2\text{PNMe}_3)_2)_2][\text{HC}(\text{Ph}_2\text{PNMe}_3)_2]$ where $\text{Ln} = \text{Dy}$ or Er .¹⁸⁷ Unfortunately the attempt to synthesise analogues to $[\text{La}(\text{C}(\text{Ph}_2\text{PNMe}_3)_2)\text{I}(\text{THF})_3]$ from the aforementioned lanthanide methanides produced complexes of the formula $[\text{Ln}(\text{C}(\text{Ph}_2\text{PNMe}_3)_2)(\text{HC}(\text{Ph}_2\text{PNMe}_3)_2)]$, where $\text{Ln} = \text{Ce}, \text{Pr}$ or Gd .¹⁸⁷ However it should be noted that although still in the early stages of development the salt elimination or salt metathesis methodology has proven viable for the preparation of early lanthanide bis(iminophosphorano)methandiide complexes lacking methanide spectator ligands.

As many of the complexes lacking methanide spectator ligands contain the iodide and THF ligands, the exchange of these ligands with other ligands of greater chemical interest is important. One example of this was published in the synthesis and characterisation of the rare earth hetero bimetallic complex $[\text{Y}(\text{C}(\text{PPh}_2\text{NSiMe}_3)_2)(\text{Ga}(\text{NArCH})_2)(\text{THF})_2]$ ($\text{Ar} = 2,6\text{-diiso-propylphenyl}$) with the molecular structure given in Figure 2.25.¹⁹⁰ The complex was prepared by reacting the gallium NHC carbene analogue with the yttrium carbene $[\text{Y}(\text{C}(\text{Ph}_2\text{PNSiMe}_3)_2)\text{I}(\text{THF})_2]$.¹⁹⁰ $[\text{Y}(\text{C}(\text{Ph}_2\text{PNSiMe}_3)_2)\text{I}(\text{THF})_2]$ was also used to prepare two $[\text{Y}(\text{C}(\text{Ph}_2\text{PNSiMe}_3)_2)(\text{THF})(\text{NR}_2)]$ carbene species, where $\text{R} = \text{SiMe}_3$ or SiMe_2tBu , on reaction with the respective KNR_2 salts in toluene.¹⁹³

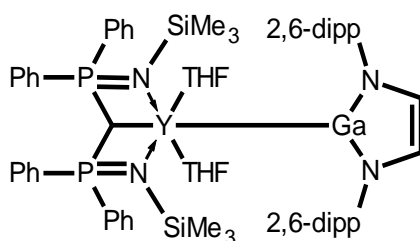


Figure 2.25: Structure of $[\text{Y}(\text{C}(\text{PPh}_2\text{NSiMe}_3)_2)(\text{Ga}(\text{NArCH})_2)(\text{THF})_2]$ ($\text{Ar} = 2,6\text{-diiso-propylphenyl}$).¹⁹⁰

The latest field of research in $\text{H}_2\text{C}(\text{Ph}_2\text{PNR})_2$ lanthanide carbene derivatives dealt with the publication of rare earth bis(carbene) complexes of the bis(diphenyliminophosphorano)methandiide species. The first complexes obtained for

this class of compounds had the formula $[\text{K}(18\text{-crown-}6)(\text{THF})_2][\text{RE}(\text{C}(\text{Ph}_2\text{PNSiMe}_3)_2)_2] \cdot (\text{THF})_2$, where $\text{RE} = \text{Y}^{3+}$ or Dy^{3+} , with the structure as shown in Figure 2.26.⁴² These were prepared by reacting the respective $[\text{RE}(\text{C}(\text{Ph}_2\text{PNSiMe}_3)_2)(\text{HC}(\text{Ph}_2\text{PNSiMe}_3)_2)]$ with 1 equivalent of benzyl potassium in the presence of 18-crown-6.⁴² Using the same technique, later work yielded both early lanthanide analogues of the structure $[\text{K}(18\text{-crown-}6)(\text{THF})_2][\text{RE}(\text{C}(\text{Ph}_2\text{PNSiMe}_3)_2)_2] \cdot \text{L}$, where $\text{RE} = \text{Ce}^{3+}$ and Pr^{3+} and $\text{L} = \text{Toluene}$ and the late lanthanide analogue of the same structure where $\text{RE} = \text{Tb}^{3+}$ and $\text{L} = \text{THF}$.¹⁹⁴ The latest member of this class of compounds was $[\text{Li}(\text{THF})_4][\text{Nd}(\text{C}(\text{Ph}_2\text{PNSiMe}_3)_2)_2] \cdot \text{DEE}$, having the same rare earth bis(carbene) complex structure described previously.¹⁹⁵ This was prepared via reaction of NdCl_3 with two equivalents of $\text{Li}_2(\text{C}(\text{Ph}_2\text{PNSiMe}_3)_2)$.¹⁹⁵

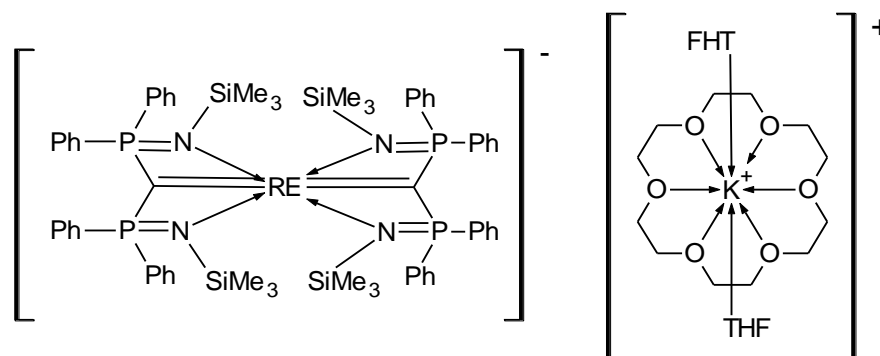


Figure 2.26: Complex prepared by Gregson et al. of the formula $[\text{K}(18\text{-crown-}6)(\text{THF})_2][\text{RE}(\text{C}(\text{Ph}_2\text{PNSiMe}_3)_2)_2] \cdot (\text{THF})_2$.⁴²

The $[\text{K}(18\text{-crown-}6)(\text{THF})_2][\text{RE}(\text{C}(\text{Ph}_2\text{PNSiMe}_3)_2)_2]$ species, where $\text{RE} = \text{Pr}^{3+}$ and Tb^{3+} , were also used in preparation of carbene species having the structure $[\text{RE}(\text{Ag})(\text{C}(\text{Ph}_2\text{PNSiMe}_3)_2)_2]$, as given in Figure 2.27.¹⁹⁴ In these species the $\text{M}=\text{C}$ bond remains for only one of the ligands as the other methandiide centre bonds with both the lanthanide and silver cations. The Ag^+ cation also coordinates with one of the iminophosphorane nitrogen centres of the remaining carbene ligand, replacing the previous $\text{RE}-\text{N}$ coordination. This indicated that the full chelation of the lanthanide through coordination with both iminophosphorane nitrogens noted throughout all the previous bis(diphenyliminophosphorano)methandiide carbene species may not be a strict requirement for the stability of these carbenes.¹⁹⁴

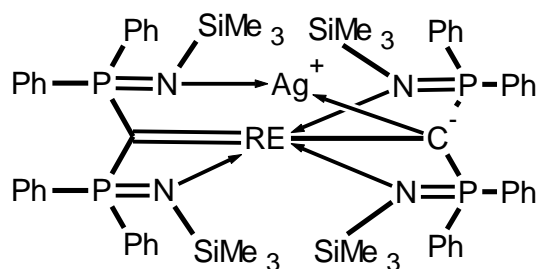


Figure 2.27: Structure for complexes of the formula $[\text{RE}(\text{Ag})(\text{C}(\text{Ph}_2\text{PNSiMe}_3)_2)_2]$.¹⁹⁴

2.6.2.2.1.1 Lanthanide iminophosphorano carbenes of non-trivalent lanthanides

Two main examples of non-trivalent lanthanide iminophosphorano carbene complexes are known, namely the cerium(IV) species $[\text{Ce}(\text{C}(\text{Ph}_2\text{PNSiMe}_3)_2)(\text{O}-2,6\text{-}i\text{PrC}_6\text{H}_4)_2]$ and $[\text{Ce}(\text{C}(\text{Ph}_2\text{PNSiMe}_3)_2)_2]$.^{10,194} The former was synthesised in a number of steps from the bis(iminophosphorano)methanide cerium(III) complex $[\text{Ce}(\text{CH}(\text{Ph}_2\text{PNSiMe}_3)_2)(\text{THF})_2\text{I}_2]$,¹⁰ while the latter was synthesised through the oxidation of the complex $[\text{K}(18\text{-crown-}6)(\text{THF})_2][\text{Ce}(\text{C}(\text{Ph}_2\text{PNSiMe}_3)_2)_2] \cdot \text{Toluene}$, discussed in the previous section, by $\text{Ag}[\text{BPh}_4]$.¹⁹⁴

As with most of the complexes discussed earlier orbital calculations indicate that the bonding is largely ionic in both. For $[\text{Ce}(\text{C}(\text{Ph}_2\text{PNSiMe}_3)_2)(\text{O}-2,6\text{-}i\text{PrC}_6\text{H}_4)_2]$, DFT calculations indicate that the HOMO and HOMO-1 are actually distributed along the phenyl rings, with the HOMO-2 and HOMO-3 comprising the $\text{C}=\text{Ce}^{4+}$ bond, as shown in Figure 2.28. In both complexes the $\text{C}=\text{Ce}^{4+}$ bond has a Nalewajski–Mrozek bond order of 1.1, as compared to that of $\text{C}=\text{Y}$ being 0.7, which indicates a significantly more covalent bond.^{10,194} NBO analyses for both compounds showed that the σ bond is composed of 13% Ce and 87% C character. The cerium component is constructed from 3% 6s, 21% 5d and 76% 4f character for the mono-carbene and 1% 6s, 48% 5d and 53% 4f character for the bis(carbene).^{10,194} The π bond is composed of 12% Ce character for the mono-carbene and 8% Ce character for the bis(carbene). Despite the difference in composition the orbital contribution in both cases of the π bond comprises of 1% 6p, 19% 5d and 80% 4f character.^{10,194} In each case, like the Ln(III) counterparts, the bonding is mainly attributed to the central carbon and the majority of the Ln contribution is still from the “internal” 4f orbitals, even though the 5d, 6s and 6p orbitals which are usually considered too energetic for bonding still contribute towards the bonding. However for the cerium(IV) bis(carbene) there is a significantly greater 5d contribution for the $\text{Ce}=\text{C}$

σ bond when compared to all the carbenes discussed previously.¹⁹⁴ In both complexes the cerium(IV) showed a greater input on bonding orbitals than what has been established before.^{10,163,188,190,194}

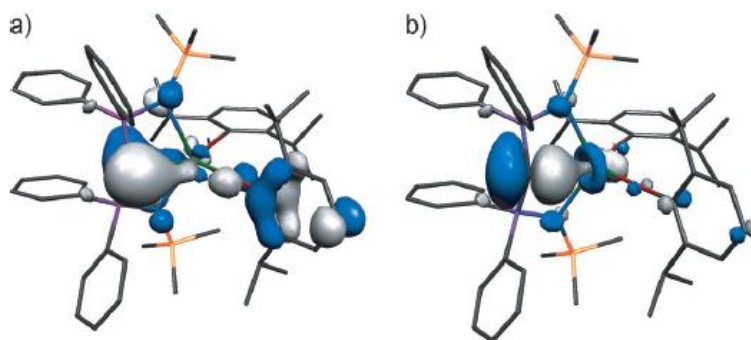


Figure 2.28: a) HOMO-2 and b) HOMO-3 of $[\text{Ce}(\text{C}(\text{Ph}_2\text{PNSiMe}_3)_2)(\text{O}-2,6\text{-}i\text{PrC}_6\text{H}_4)_2]$.¹⁰

2.6.2.2.2. Lanthanide iminophosphorano carbene reactivity and applications

Much of the work on the reactivity of such lanthanide carbenes was actually undergone for the rare earth yttrium (III) complexes. The earliest studies regarding the reactivity of such compounds dealt with $[\text{Y}(\text{C}(\text{Ph}_2\text{PNSiMe}_3)_2)(\text{CH}_2\text{SiMe}_2)(\text{THF})]$. Mills and co-workers published the capability of this complex to activate C–H bonds.⁴³ The complex was reacted with benzophenone to initially prepare the lanthanide carbene-alkoxide product $[\text{Y}(\text{C}(\text{Ph}_2\text{PNSiMe}_3)_2)(\text{OC}(\text{CH}_2\text{SiMe}_2)\text{Ph}_2)(\text{THF})]$ through 1,2-migratory insertion of the CH_2SiMe_2 ligand on the benzophenone carbonyl.⁴³ Further reaction with 2 equivalents of benzophenone in toluene led to the formation of the more interesting complex containing an *iso*-benzofuran derivative ligand, which is given in Figure 2.29 (a).⁴³ A similar product was obtained by reacting $[\text{Y}(\text{C}(\text{Ph}_2\text{PNSiMe}_3)_2)\text{I}(\text{THF})_2]$, in similar conditions, with *tert*-butyl phenyl ketone wherein the alkoxide was replaced by the iodide ligand, as given in Figure 2.29 (b).⁴³ However reaction of the iodide complex with benzophenone yielded the complex in Figure 2.29 (c), which on salt elimination with $\text{KOC}(\text{CH}_2\text{SiMe}_2)\text{Ph}_2$ yielded the product in Figure 2.29 (a). The latter reaction indicated that the 2-(diphenylmethoxide) benzophenone complex was an intermediate product in the formation of the initial *iso*-benzofuran complex.

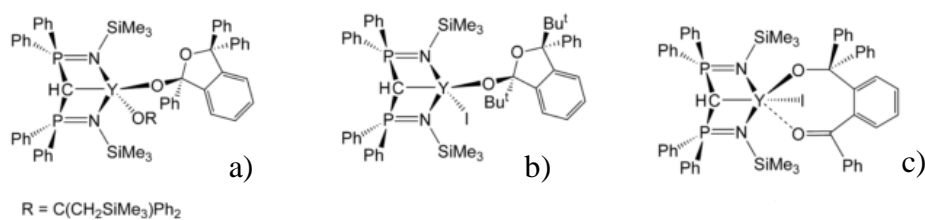
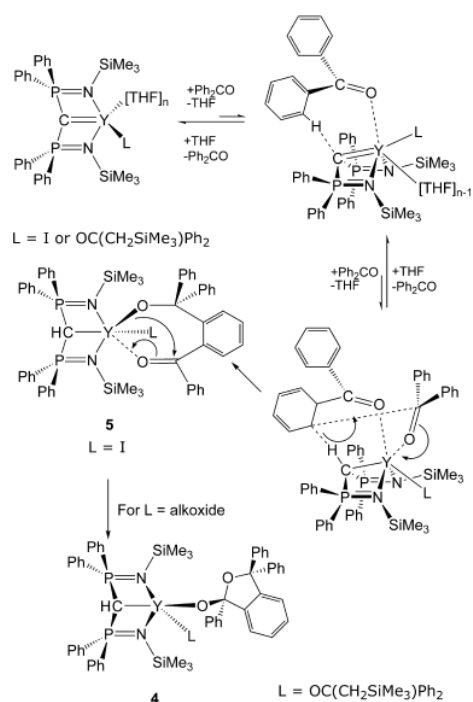


Figure 2.29: Reaction products of early Y carbenes with bulky ketones.⁴³

The two starting complexes therefore showed the propensity to activate the ortho-C–H bond of phenyl ketones, with the general mechanism proposed in the case of such yttrium carbenes given in the Scheme 2.6. It was however noted that on reaction with methyl phenyl ketone the C–H bond activation occurred preferentially on the α -C of the methyl. This in turn underwent a cyclotetramerization/dehydration reaction to give diastereomers of dynopinacol, along with the final decomposition of the reagent.⁴³



Scheme 2.6: Ortho-C-H bond activation mechanism proposed for the synthesis of compounds given in Figure 2.28.⁴³

Concurrent to this study, the reactivity of a similar yttrium (III) complex, namely [Y(C(Ph₂PNSiMe₃)₂)(CH₂C₆H₅)(THF)], to benzophenone was published. As with the [Y(C(Ph₂PNSiMe₃)₂)(CH₂SiMe₂)(THF)] complex, the initial reaction was the 1,2-migratory insertion of the benzyl onto the benzophenone to produce the carbene-alkoxide

$[Y(C(Ph_2PNSiMe_3)_2)(OC(CH_2C_6H_5)Ph_2)(THF)]$.¹⁸⁸ In an attempt to undergo Wittig reaction this complex was reacted in a 1:1 molar ratio with benzophenone in benzene but this only yielded the cluster product $[Y(\mu-C(Ph_2PNSiMe_3)_2)(OC(CH_2C_6H_5)Ph_2)_2]$.¹⁸⁸ In this study by Mills and co-workers another 1,2-migratory insertion was published. In this case the complex $[Y(C(Ph_2PNSiMe_3)_2)(CH_2C_6H_5)(THF)]$ was reacted with azobenzene yielding colourless crystals from a green oil found to be $[Y(C(Ph_2PNSiMe_3)_2)(Ph_2NNPh(CH_2C_6H_5))(THF)]$.¹⁸⁸ In all cases described above it seems that the reaction occurs firstly on the Y–C_{alkyl} bond, with the removal of other spectator ligands being secondary. The Y=C bond seems to react afterwards in secondary reactions.

Later work on the reactivity of these complexes was mainly undertaken by Mills and co-workers and dealt with the complexes $[Y(C(Ph_2PNSiMe_3)_2)(CH_2C_6H_5)(THF)]$ and $[Y(C(Ph_2PNSiMe_3)_2)I(THF)_2]$.^{44,45} The various reactions which these two compounds undertook in these initial studies are given in Figures 2.30 and 2.31.

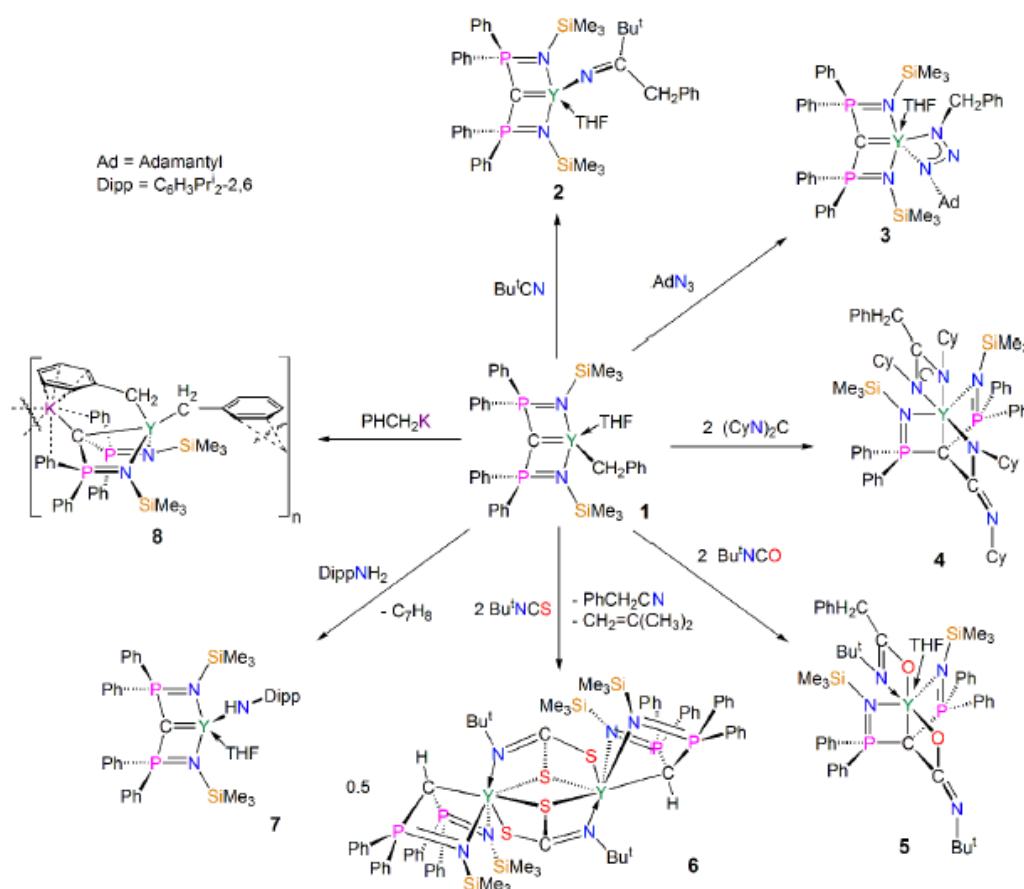


Figure 2.30: Reactions published for $[Y(C(Ph_2PNSiMe_3)_2)(CH_2C_6H_5)(THF)]$.⁴⁴

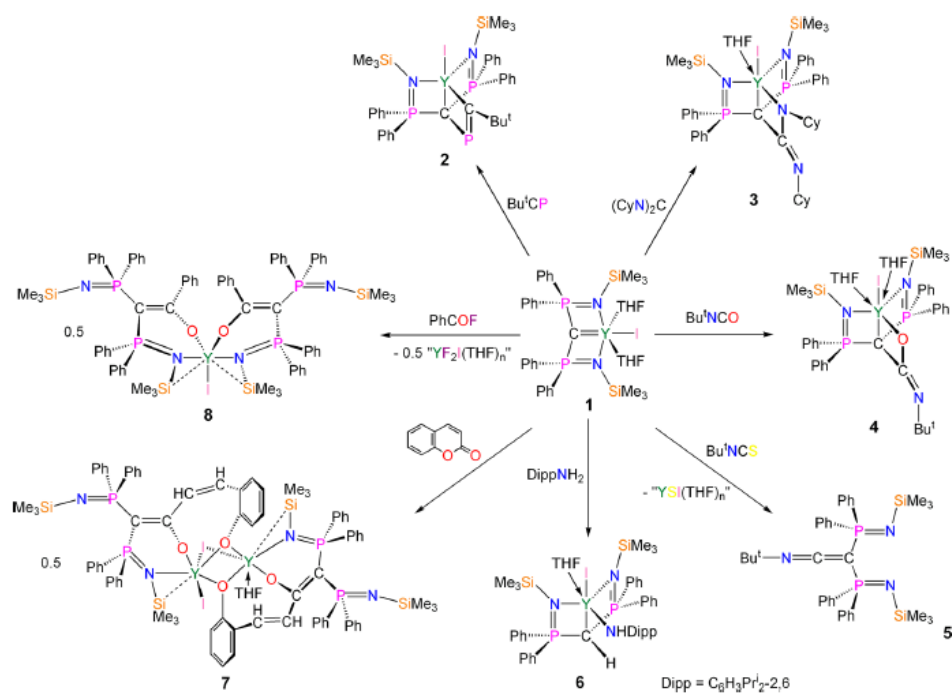


Figure 2.31: Reactions published for $[Y(C(Ph_2PNSiMe_3)_2)I(THF)_2]$.⁴⁵

In both species the reactions can be categorised into 4 groups. The first group consists of methandiide to methanide $C=Y$ bond opening reactions, producing compounds 4 and 5 for the benzyl and compounds 2, 3, 4 and 6 for the iodide and these reactions tend to replace the carbene by a tetra dentate chelating methanide derivative ligand.^{44,45} The second reaction group is the formation of clusters typically through a methandiide to methanide $C=Y$ bond opening reaction and these are typified by the synthesis of compounds 6 and 8 from the benzyl and compound 7 from the iodide.^{44,45} It should be noted that cluster formation on reaction is fairly expected as in many cases highly ionic metal organic bonding leads to cluster formation in order to maximise coulombic attraction.

The final two reaction groups seem to be specific to either complex; Wittig like reactions which were published for the iodide complex and which yield compounds such as 5, 7 and 8 in Figure 2.31 or ligand exchanges which were observed for the benzyl complex in the preparation of compounds 2, 3 and 7 in Figure 2.30.^{44,45} The only true Wittig reaction product is compound 5, formed from the reaction of the iodide complex with *tert*-butyl *iso*-thiocyanate.⁴⁵ The other compounds 7 and 8 in Figure 2.31 also show typical Wittig product morphology but the presence of Lewis basic oxygen maintains complexation with the metal centre.⁴⁵ In the case of ligand exchange this was only seen

for the benzyl ligand, leaving the THF uninvolved, as expected from the earlier work.^{43,188} Given the greater stability of rare earth to halogen bonds ligand exchange was rarely seen for the iodide. It is noteworthy to compare the reaction of the two carbene complexes with 2,6-diisopropylaniline (H_2NDIPP).^{44,45} In the presence of the benzyl ligand exchange occurred to give compound 7, while a methandiide to methanide C=Y bond opening reaction occurred with the iodide complex to give compound 6.⁴⁵ This could indicate some effect of spectator ligands on the reactivity of the carbene bond. This methandiide to methanide C=Y bond opening for $[Y(C(Ph_2PNSiMe_3)_2)I(THF)_2]$ was later described on reaction of this complex with $KN(Si-iPr_3)_2$, $KN(SiMe_2tBu)_2$ and $KN(Si-iPr_3)(SiMe_2tBu)$. The methandiide protonation occurred as either a silyl methyl or iso-propyl methyl group from the secondary ligand acted as the acid, as given in Figure 2.32.¹⁹³ These reactions occurred despite the fact that similar reactions have yielded secondary ligand exchange as described in Section 2.6.2.2.1.

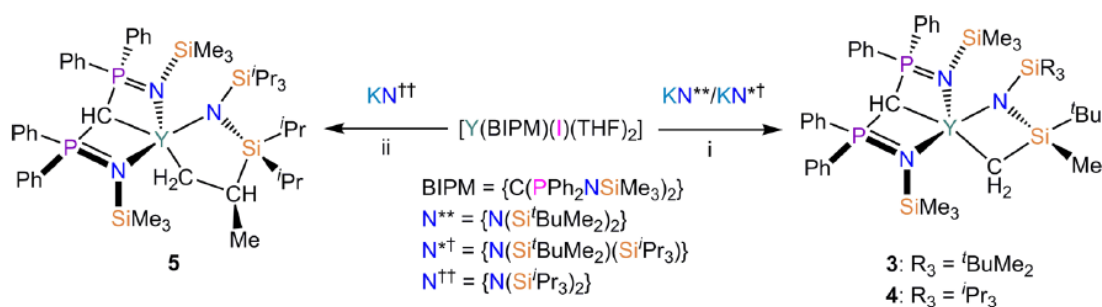
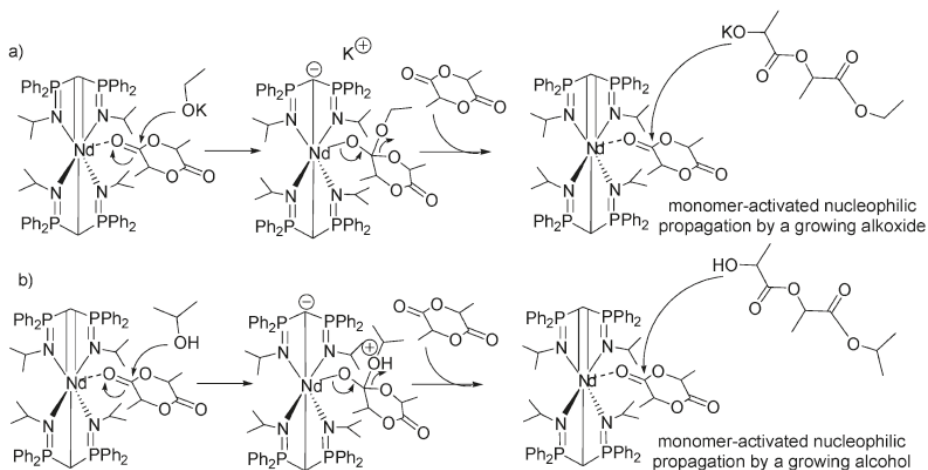


Figure 2.32: Further methandiide to methanide C=Y bond opening for $[Y(C(Ph_2PNSiMe_3)_2)I(THF)_2]$ on reaction with inorganic amides.¹⁹³

Clusters similar to products 6 and 8 obtained from $[Y(C(Ph_2PNSiMe_3)_2)(CH_2C_6H_5)(THF)]$ have also been produced for the thalium containing species $[NdTi(C(Ph_2PNSiMe_3)_2)(Cp)(LiCl_2THF_2)]$ and $[SmTi(C(Ph_2PNSiMe_3)_2)(LiCl_2THF_2)Cl]_2$ in work published by Ge, S *et al.* in 2020.¹⁹⁶

Buchard and co-workers dealt with the catalytic activity of the complex $[Nd(C(Ph_2PNiPr)_2)(HC(Ph_2PNiPr)_2)]$.¹² This compound has been found to act as a catalyst in the ring opening polymerisation of *rac*-lactide, in the presence of potassium ethoxide or *iso*-propanol as initiators.¹² The mechanism proposed for the initiation and propagation of lactide polymerisation in both cases is given in Scheme 2.7.



Scheme 2.7: Mechanisms for the initiation of lactide polymerisation by [Nd(C(Ph₂PNiPr)₂)(HC(Ph₂PNiPr)₂)] a) using KOEt b) using *i*PrOH.¹²

The complex was found to be non-catalytically active on its own and was only active in the presence of an initiator; in the case of the study either potassium ethoxide or *iso*-propanol. In the study the polymerisation was mainly undergone using a 200:1:1 molar ratio of the *rac*-lactide, [Nd(C(Ph₂PNiPr)₂)(HC(Ph₂PNiPr)₂)] and *iso*-propanol, wherein the *iso*-propanol was added slowly to the reaction mixture containing the lactide and the Nd carbene complex.¹² Under these conditions the number average molar mass (M_n) was found to range between 16000 and 31000, with polydispersity indices ranging from 1.05 to 1.11. The M_n and the yield were found to increase on increasing the reaction time, which indicates the controllability of the reaction.¹² The polydispersity indices remain fairly good, also indicating a good distribution of the molar mass, even when the change in reaction time changes the M_n drastically. This further indicates the good controllability of the reaction.

The polymerisation was also known to be undergone in the presence of potassium ethoxide (KOEt) alone but in a very chaotic way and with a polydispersity index of 1.66.¹² On repeating the experimental procedure using the Nd carbene and *iso*-propanol but replacing the alcohol with KOEt the reaction became more controllable than when using KOEt alone, giving an 85% yield, with a 20200 M_n and a polydispersity index of 1.05.¹² Similar results were obtained on repeating the reactions with (*S,S*)-lactide instead of *rac*-lactide, with no adverse effects noted on the M_n , yield and polydispersity index.¹² Interestingly polymerisation of (*S,S*)-lactide led to the synthesis of only isotactic polylactic acid with no epimerisation noted.¹² Reaction of the *rac*-lactide on the other hand always afforded atactic polylactic acid.¹²

2.6.2.3. Lanthanide thiophosphonyl geminal dianion carbenes

2.6.2.3.1. Lanthanide thiophosphonyl carbenes synthesis and characterisation

Unlike their iminophosphorano counterparts the rare earth complexes of bis(thiophosphonyl)methandiides are not well known, with only complexes of bis(diphenylthiophosphonyl)methandiide published. Much of the work into the complexation of this ligand was done by Le Floch and co-workers.³¹ Early work by this and other groups mainly dealt with Group 1, Group 2 and transition metal complexes of this ligand.^{98,124}

As with the iminophosphorano analogues the earliest published rare earth bis(diphenylthiophosphonyl)methandiide complex was for the early lanthanide samarium.⁸ Two complexes were published, namely the monomeric salt $[\text{Li}(\text{THF})_4][\text{Sm}(\text{C}(\text{Ph}_2\text{PS})_2)_2]$ and the dimeric $[(\text{Sm}_2(\text{C}(\text{Ph}_2\text{PS})_2)_2(\text{THF})_4(\mu\text{-I}))_2]$ complex, with the molecular structures given in Figure 2.33.

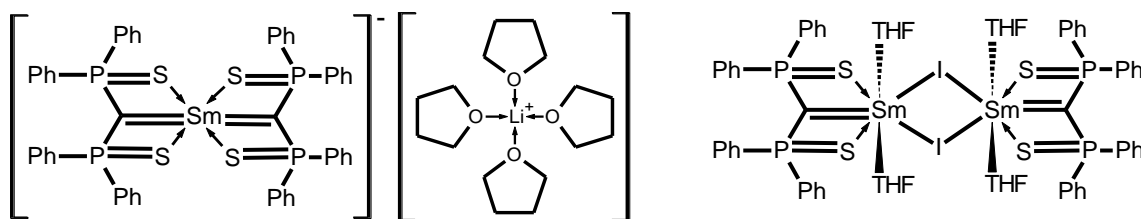


Figure 2.33: $[\text{Li}(\text{THF})_4][\text{Sm}(\text{C}(\text{Ph}_2\text{PS})_2)_2]$ (left) and $[(\text{Sm}_2(\text{C}(\text{Ph}_2\text{PS})_2)_2(\text{THF})_4(\mu\text{-I}))_2]$ (right).⁸

Bis(carbene) complexes like $[\text{Li}(\text{THF})_4][\text{Sm}(\text{C}(\text{Ph}_2\text{PS})_2)_2]$ have only been synthesised recently for the iminophosphorano lanthanide analogues, while compounds analogous to $[(\text{Sm}_2(\text{C}(\text{Ph}_2\text{PS})_2)_2(\text{THF})_4(\mu\text{-I}))_2]$ are still unknown.⁴² The synthesis of both complexes was easily undergone by salt metathesis of the iodide $\text{SmI}_3\text{THF}_{3.5}$ with the lithium methandiide salt $\text{Li}_2\text{C}(\text{Ph}_2\text{PS})_2$.⁸

For both complexes, the heavy lanthanide thulium (III) counterparts were also synthesised and characterised by the same group.¹²³ The reactions undertaken for these syntheses were the same as those for the samarium complexes.¹²³ In each case SXRD analysis also showed that the compounds were crystallographically isomorphous. Despite this, the study of the monomeric thulium anion $[\text{Tm}(\text{C}(\text{Ph}_2\text{PS})_2)_2]^-$ showed changes in the structure on changing temperature.¹²³ At temperatures <177 K the low temperature form

depicted in Figure 2.34 was formed, wherein only one of the methandiide ligands is planar with the second taking a trigonal pyramidal geometry with the carbenic electron pair occupying a non-bonding lone pair. This form changes at temperatures >177 K to the high temperature form wherein both ligands are planar with the charge distributed over all the complex. It was proposed that this may be possible through π overlap of the two C 2p and Tm 5d orbitals in line with each other.¹²³

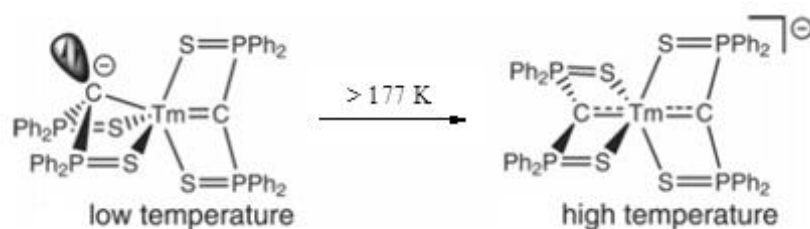


Figure 2.34: Structure change in the $[\text{Tm}(\text{C}(\text{Ph}_2\text{PS})_2)_2]^-$ complex with temperature.¹²³

Despite such an early success in the preparation of these two lanthanide (III) carbene complexes and the success in the synthesis and characterisation of transition metal carbenes of bis(diphenylthiophosphonyl)methandiides further work on expanding the series to the remainder of the lanthanides and on the synthesis of other lanthanide carbene species is lacking.^{31,50,98} However the successful use of salt metathesis from the $\text{Li}_2\text{C}(\text{Ph}_2\text{PS})_2$ salt is still of interest in the field of the bis(diphenyliminophosphorano)methandiide complexes of lanthanides.

Further work was only undergone for the rare earth complexes of scandium (III) by Fustier, M. and co-workers. The first scandium carbene, $[(\text{Sc}(\text{C}(\text{Ph}_2\text{PS})_2)\text{Cl}(\text{THF})_2)]$, was prepared by the reaction of the $\text{Li}_2\text{C}(\text{Ph}_2\text{PS})_2$ salt with $\text{ScCl}_3\text{THF}_3$ in a salt elimination reaction.¹⁹⁷ This complex was only attested through ^{31}P NMR. On dissolution of $[(\text{Sc}(\text{C}(\text{Ph}_2\text{PS})_2)\text{Cl}(\text{THF})_2)]$ in pyridine the THF ligand was replaced by pyridine and a solid with the molecular structure of $[(\text{Sc}(\text{C}(\text{Ph}_2\text{PS})_2)\text{Cl}(\text{Py})_2)]\cdot\text{Py}$, where Py = pyridine, was isolated.¹⁹⁷ This complex is unlike any of the lanthanide complexes of this ligand but shares structural features with the $[\text{Y}(\text{C}(\text{Ph}_2\text{PNSiMe}_3)_2)\text{I}(\text{THF})_2]$ and $[\text{La}(\text{C}(\text{Ph}_2\text{PNMe}_3)_2)\text{I}(\text{THF})_3]$ complexes described earlier in Section 2.6.2.2.1. The carbene $[\text{Li}][\text{Sc}(\text{C}(\text{Ph}_2\text{PS})_2)_2]$ also formed as a minor side product of this reaction having a proposed structure similar to that of $[\text{Li}(\text{THF})_4][\text{Sm}(\text{C}(\text{Ph}_2\text{PS})_2)_2]$, as is presented in Figure 2.33.¹⁹⁷ The study also conducted DFT studies of a theoretical structure for $[(\text{Sc}(\text{C}(\text{Ph}_2\text{PS})_2)\text{Cl}(\text{Py})_2)]\cdot\text{Py}$ in which, unlike the lanthanide and yttrium, the $\text{Sc}=\text{C}$, comprised of the HOMO and HOMO-1, seems to have a significant Sc 3d character.¹⁹⁷

The anionic species $[\text{Sc}(\text{C}(\text{Ph}_2\text{PS})_2)_2]^-$ which was first observed by Fustier and co-workers in 2010, was properly described by the same group in 2015 through SXRD, in the complex $[\text{Li}(\text{THF})_2\text{Sc}(\text{C}(\text{Ph}_2\text{PS})_2)_2]$, as having the structure given in Figure 2.35.¹⁹⁸ The ligands take up a planar conformation as in the $[\text{Li}(\text{THF})_4][\text{Tm}(\text{C}(\text{Ph}_2\text{PS})_2)_2]$ complex at temperatures >177 K.

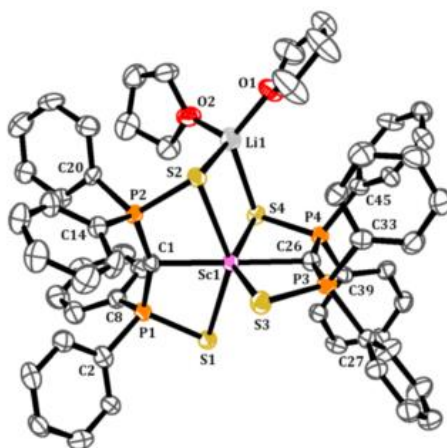


Figure 2.35: Structure of $[\text{Li}(\text{THF})_2\text{Sc}(\text{C}(\text{Ph}_2\text{PS})_2)_2]$ with displacement ellipsoids at 50% probability.¹⁹⁸

An interesting complex published in the same study was $[\text{Sc}(\text{C}(\text{Ph}_2\text{PS})_2)(\text{HC}(\text{Ph}_2\text{PS})_2)(\text{THF})]$, with the structure given in Figure 2.36.¹⁹⁸ This was produced by the reaction of $\text{H}_2\text{C}(\text{Ph}_2\text{PS})_2$ with the benzyl $\text{Sc}(\text{CH}_2\text{C}_6\text{H}_5)_3\text{THF}_3$ in toluene.¹⁹⁸ Both the structure and synthesis, using an acid-base methodology, of this compound mirror those of the complexes of formula $[\text{Ln}(\text{C}(\text{Ph}_2\text{PNSiMe}_3)_2)(\text{HC}(\text{Ph}_2\text{PNSiMe}_3)_2)]$ described in Section 2.6.2.2.1.^{9,198}

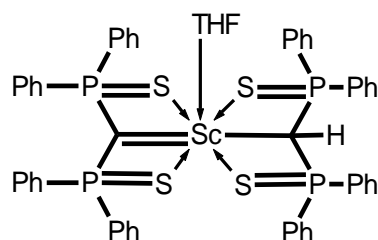


Figure 2.36: Structure of $[\text{Sc}(\text{C}(\text{Ph}_2\text{PS})_2)(\text{HC}(\text{Ph}_2\text{PS})_2)(\text{THF})]$.¹⁹⁸

Scandium carbenes were also prepared through ligand exchange from $[(\text{Sc}(\text{C}(\text{Ph}_2\text{PS})_2)\text{Cl})(\text{THF})_2]$ and $[(\text{Sc}(\text{C}(\text{Ph}_2\text{PS})_2)\text{Cl})(\text{Py})_2] \cdot \text{Py}$. The carbene complex $[(\text{Sc}(\text{C}(\text{Ph}_2\text{PS})_2)(\text{N}(\text{SiMe}_3)_2)(\text{THF})]$ was prepared from the reaction of $[(\text{Sc}(\text{C}(\text{Ph}_2\text{PS})_2)\text{Cl})(\text{THF})_2]$ and $\text{LiN}(\text{SiMe}_3)_2$,¹⁹⁸ while $[(\text{Sc}(\text{C}(\text{Ph}_2\text{PS})_2)(\text{P}(\text{SiMe}_3)_2)(\text{Py})_2)]$ was prepared from $[(\text{Sc}(\text{C}(\text{Ph}_2\text{PS})_2)\text{Cl})(\text{Py})_2] \cdot \text{Py}$ and $\text{Li}(\text{THF})_{1.5}\text{P}(\text{SiMe}_3)_2$.¹⁹⁸

2.6.2.3.2. Lanthanide thiophosphonyl carbene reactivity

Since so few lanthanide and rare earth carbene complexes of bis(diphenylthiophosphonyl)methandiide have been published the reactivity of these complexes is even less known in contrast to that of the iminophosphorano analogues. The main reaction feature of the dimer $[\text{Ln}_2(\text{C}(\text{Ph}_2\text{PS})_2)_2(\text{THF})_4(\mu\text{-I})_2]$ and the salt $[\text{Li}(\text{THF})_4][\text{Ln}(\text{C}(\text{Ph}_2\text{PS})_2)_2]$ was the synthesis of the alkene product $\text{Ph}_2\text{C}=\text{C}(\text{Ph}_2\text{PS})_2$ from a Wittig like reaction with benzophenone.^{8,123} The salt reacted with 2 equivalents of benzophenone to initially form the isolated cluster $[\text{Li}(\text{THF})(\text{Ln}(\text{C}(\text{Ph}_2\text{PS})_2(\text{COPh}_2))_2)]$, with the structure given in Figure 2.37.¹²³

A comparable cluster was formed in a similar attempt to react $[(\text{Sc}(\text{C}(\text{Ph}_2\text{PS})_2\text{Cl}(\text{Py})_2)]\cdot\text{Py}$ with benzophenone having the structure given in Figure 2.38.¹⁹⁷ On addition of excess $[(\text{Sc}(\text{C}(\text{Ph}_2\text{PS})_2\text{Cl}(\text{Py})_2)]\cdot\text{Py}$ to the cluster, $\text{Ph}_2\text{C}=\text{C}(\text{Ph}_2\text{PS})_2$ was produced. The alkene was also produced by direct reaction of $[(\text{Sc}(\text{C}(\text{Ph}_2\text{PS})_2\text{Cl}(\text{Py})_2)]\cdot\text{Py}$ with 1 equivalent of benzophenone.¹⁹⁷

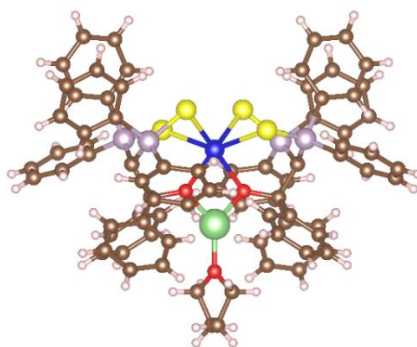


Figure 2.37: Structure of $[\text{Li}(\text{THF})(\text{Ln}(\text{C}(\text{Ph}_2\text{PS})_2(\text{COPh}_2))_2]$, where Ln = Sm or Tm (built in VESTA from cif data obtained from CSD).^{8,123}

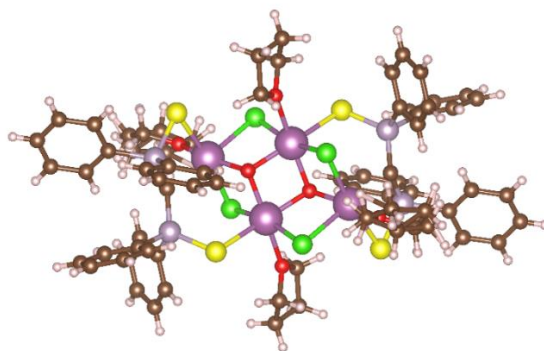


Figure 2.38: Cluster product of the reaction of $[(\text{Sc}(\text{C}(\text{Ph}_2\text{PS})_2\text{Cl}(\text{Py})_2)]\cdot\text{Py}$ with 0.5 equivalents of benzophenone (built in VESTA from cif data obtained from CSD).¹⁹⁷

2.7. Metal-Organic lanthanide complexes of non-carbene di- $\lambda^5\sigma^4$ -phosphorane ligands

Compounds with a di- $\lambda^5\sigma^4$ -phosphorane structure similar to the fully protonated carbene ligands are also known in literature. These have the generic structure noted in Figure 2.2 where X = HN or O while Y = NR, O or S. The synthesis and characterisation of many of these compounds has been reported in literature.^{34,199} Previous studies observed that the structure of these analogues enables chelation of these compounds with metal centres of various types through the electron donors on the Y substituent.³⁹

The current study focused more on the effect of the X group on complexation. The methylene analogues $\text{H}_2\text{C}(\text{Ph}_2\text{PNR})_2$ and $\text{H}_2\text{C}(\text{Ph}_2\text{PS})_2$ are known to form not only simple chelate complexes but also tridentate complexes of the mono-anionic methanides and di-anionic methandiides. The latter species are known to complex with numerous metals to form phosphorus (V) stabilised carbenes, as described in detail for lanthanides in Section 2.6.2.³¹ In the structure of the di- $\lambda^5\sigma^4$ -phosphorane given in Figure 2.2 when X is the mono-anionic derivative of HN, namely N^- or the neutral O it is isoelectronic to the carbon C^{2-} of the methandiides.²⁰⁰ Given the isoelectronic character of these groups, similarities and differences in any trends in the structure and chemistry of these isoelectronic compounds and their complexes with lanthanide metals, especially with regards to the formation of N–Ln or O–Ln bonds analogous to the C=Ln bond, are of great interest. One major difference noted in published literature for these non-carbene isoelectronic analogues and their complexes was the lack of X–M bonds analogous to the C=Ln bonds for most non-carbene complexes. Another difference noted in literature was the increased air and moisture stability for the complexes of these non-carbene isoelectronic analogues.

2.7.1. Pyrophosphoramidate analogues

The main focus of the current study with regards to compounds where $X = O$ was on pyrophosphoryl amide compounds with the structure given in Figure 2.39.

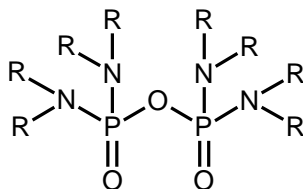


Figure 2.39: General molecular diagram of di- $\lambda^5\sigma^4$ -phosphorane pyrophosphoryl amides.

The earliest published compound of this type, which was studied intensively, was octamethylpyrophosphoramidate ($O((Me_2N)_2PO)_2$), also known with the common name of Schradan. This compound was used as an insecticide for sucking and chewing insects which are agricultural pests on crops.^{201,202} After oxidation Schradan acts in the body as an inhibitor to the Cholinesterase family of neurotransmitters, through both chemical and enzymatic routes.²⁰³ Unlike other chemicals used in the mid-twentieth century this compound was effective as an insecticide because it was a water soluble neutral molecule, whilst many other water soluble insecticides were salts and therefore they were not absorbed into the nervous system of the target pests.²⁰⁴ This compound was also found to be toxic to mammals, including humans, through ingestion. However it shows low levels of bio-concentration. Schradan has fallen out of use as better insecticides have become commercially available and nowadays its use is not approved in European countries.²⁰⁵

One of the earliest viable synthetic methods of Schradan was through the reaction of $POCl(NMe_2)_2$ with various alkali metal hydroxides.²⁰⁶ A second synthetic route for this compound was published a year later through the reaction of liquefied dimethylamine with the liquid pyrophosphoryl tetrachloride (PPTC).¹⁹⁹ Given that Schradan is a liquid at room temperature, to the knowledge of the author, structural studies through crystallographic techniques were not published.

Apart from its use as a pesticide, in the mid-twentieth century Schradan was also studied for its chelation ability with numerous metal centres. These studies mainly dealt with the complexation of Schradan with alkali earth, transition and actinide metals, as well as Sn^{4+} .^{33,207-210} The earliest studies dealt with the coordination of Schradan with tetravalent metal cations, namely the metalloid tin(IV) (Sn^{4+}), the transition metal cations,

Ti⁴⁺, Zr⁴⁺ and Hf⁴⁺ and the earlier actinide metals U⁴⁺ and Th⁴⁺, as synthesised and characterised by du Preez and Sadie in 1966.²⁰⁷ These complexes were prepared under inert conditions using a dry box since the complexes obtained were found to be hygroscopic. In all cases the complexes were prepared from chlorides in acetonitrile solutions. The complexes of tin and the transition metals were found to have the stoichiometry of MCl₄·O((Me₂N)₂PO)₂, while the complex obtained from thorium was noted to have the stoichiometry of ThCl₄·[O((Me₂N)₂PO)₂]₂. The complex obtained for uranium(IV) had the stoichiometry of UCl₄·[O((Me₂N)₂PO)₂]_{1.5} which could indicate a non-monomeric complex structure. Unfortunately, in this study structure solution from XRD data was not undertaken and the accurate structures of these compounds remain unknown.

Further work regarding the complexation of Schradan with the tetravalent actinides uranium(IV) and thorium(IV), using other starting reagents and reaction conditions, was undertaken. The complex ThCl₄·[O((Me₂N)₂PO)₂]₂, synthesised as described previously, was characterised using SXRD data by Kepert, D.L. *et al.* in 1983 and was observed to have the structure [Th(O((Me₂N)₂PO)₂)₂Cl₄], as given in Figure 2.40.²¹⁰ The same study also published the structure for the similar complex [U(O((Me₂N)₂PO)₂)₂(NCS)₄], which was synthesised through the reaction of the ligand with UCl₄ and KNCS in acetone.²¹⁰ The structure of this compound is also given in Figure 2.40. Both of the structures depicted in this figure have a distorted square anti-prismatic coordination. Unlike the complex [Th(O((Me₂N)₂PO)₂)₂Cl₄], the complex [U(O((Me₂N)₂PO)₂)₂(NCS)₄] which was also prepared under inert conditions was noted to be stable in normal laboratory conditions.²¹⁰

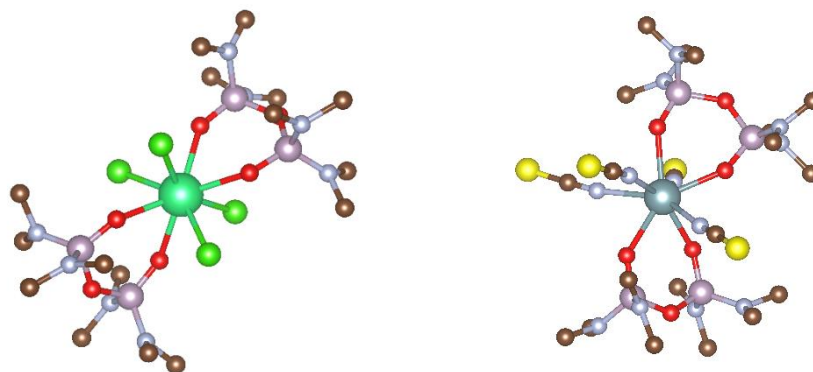
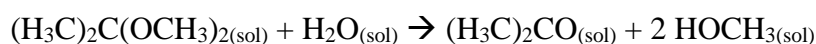


Figure 2.40: Molecular structures of [Th(O((Me₂N)₂PO)₂)₂Cl₄] (left) and [U(O((Me₂N)₂PO)₂)₂(NCS)₄] (right).

A study by Joesten, M.D. and co-workers in 1967 also prepared the complex $\text{Th}(\text{ClO}_4)_2 \cdot [\text{O}((\text{Me}_2\text{N})_2\text{PO})_2]_2$, synthesised under similar conditions to the chloride analogue, although structure solution was not undertaken.³³ Unlike the chloride analogue the dehydration of the reagents was undertaken prior to the reaction by means of 2,2-dimethoxypropane (2,2-DMP).³³ 2,2-DMP acts as a dehydrating agent wherein it reacts with water in solution to produce methanol and acetone as products, as given in Scheme 2.8. Therefore this is a good dehydrating agent for hydrated salts in an acetone solution where one of the products is actually the solvent itself.



Scheme 2.8: Dehydrating action of 2,2-DMP showing reaction with water to form acetone and methanol.

Other non-tetravalent complexes of Schradan were also published in literature. In the study by Joesten, M.D. and co-workers in 1967 the uranium(VI) complex $\text{UO}_2(\text{ClO}_4)_2 \cdot [\text{O}((\text{Me}_2\text{N})_2\text{PO})_2]_3$ and the molybdenum(V) complex $\text{MoOCl}_3 \cdot \text{O}((\text{Me}_2\text{N})_2\text{PO})_2$ were also synthesised.³³ The former was prepared in acetone using hydrated $\text{UO}_2(\text{ClO}_4)_2$ as the starting reagent and 2,2-DMP to dehydrate this reagent. Structure solution for the solids was not undertaken and in both cases the use of inert conditions was not noted, apart from use of the dehydrating agent 2,2-DMP. This indicated that the products were not air or moisture sensitive.

With regards to other lower valency metal centres, Joesten and co-workers in 1970 prepared complexes of magnesium(II), copper(II) and cobalt(II) all having the same octahedral *tris*- $(\text{O}((\text{Me}_2\text{N})_2\text{PO})_2)$ structure of $[\text{M}(\text{O}((\text{Me}_2\text{N})_2\text{PO})_2)_3][\text{ClO}_4]_2$, where $\text{M} = \text{Mg}^{2+}$, Cu^{2+} or Co^{2+} , as given in Figure 2.41.²⁰⁸ Hydrated perchlorates were used and dehydrated prior to the reaction using 2,2-DMP, however no other inert conditions were specified. In 1970 the same research group published the synthesis and characterisation of another copper(II) complex of the same ligand, namely $[\text{Cu}(\text{O}((\text{Me}_2\text{N})_2\text{PO})_2)_2(\text{ClO}_4)_2]$, with the structure also given in Figure 2.41.²⁰⁹ This structure was also obtained as an octahedral complex with the perchlorate anions occupying the axial positions. These were noted to show Jahn-Teller tetragonal elongation, which is known for such Cu^{2+} complexes. Again 2,2-DMP was used to dehydrate the reagents but no other inert conditions were used.

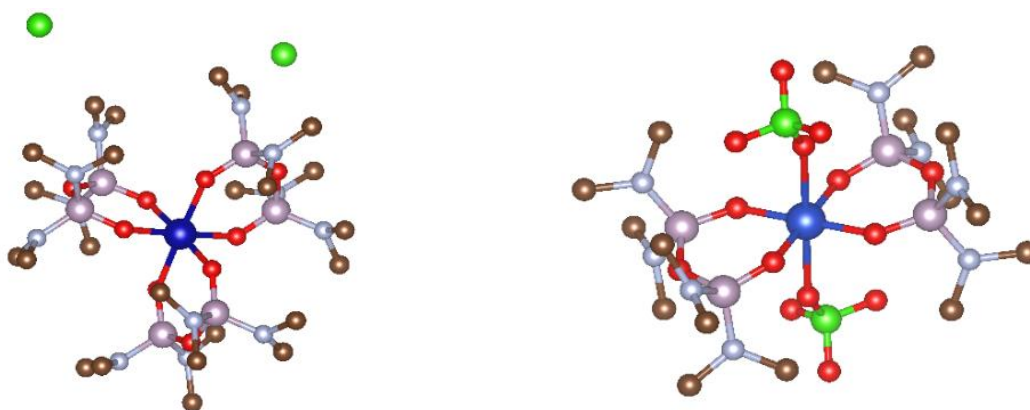


Figure 2.41: Molecular structures of $[M(O((Me_2N)_2PO)_2)_3][ClO_4]_2$ (left, only chlorine atoms of perchlorate are given) where $M = Mg^{2+}$, Cu^{2+} or Co^{2+} and $[Cu(O((Me_2N)_2PO)_2)_2(ClO_4)_2]$ (right).

Therefore in all the cases discussed in this section it was noted that the product complexes, except those synthesised from chlorides, were not air or moisture sensitive. However the preparations of these complexes were undertaken using either inert conditions or 2,2-DMP as a dehydrating agent within the reaction solution. Structural data also indicated that despite the fact that the isoelectronic structure of the Schradan was similar to that of the phosphorus (V) stabilised carbenes described earlier no central oxygen O–M bond was noted.

Other Schradan analogues have been synthesised although no common reaction methodology for these analogues has been published. The compounds $O((2\text{-MePh})N(H))_2PO_2$ and $O((t\text{Bu})N(H))_2PO_2$ were synthesised and structurally characterised.^{211,212} The latter compound was complexed with manganese(II) to give the complex $[Mn(O((t\text{Bu})N(H))_2PO_2)_2DMF_2][Cl]_2 \cdot 2H_2O$ and the octahedral coordination structure of this complex was published by Tarahhomi and co-workers in 2013,²¹³ as given in Figure 2.42, where the chelating ligands occupy the equatorial coordination positions. The compounds $O((4\text{-MePh})N(H))_2PO_2$ and $O((CH_2C_6H_5)N(CH_3))_2PO_2$ were also synthesised and characterised using single crystal X-ray diffraction (SXRD) as part of a Hirschfeld analysis of several phosphoramides.²¹⁴ The ligand $O((i\text{Pr})N(H))_2PO_2$ which is discussed in the current study is also available commercially, however no synthesis and structural data was noted in literature by the author.²¹⁵

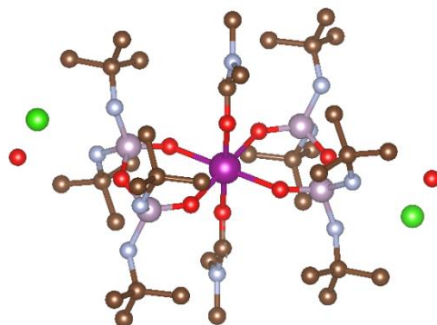


Figure 2.42: Molecular structure of $[\text{Mn}(\text{O}((t\text{Bu})\text{N}(\text{H}))_2\text{PO})_2]\text{DMF}_2[\text{Cl}]_2 \cdot 2\text{H}_2\text{O}$.

2.7.2. Compounds with the structure $\text{X}(\text{R}_2\text{PY})_2$, where $\text{X} = \text{HN}$, $\text{Y} = \text{S}$, and their complexes

Compounds with a $\text{di-}\lambda^5\sigma^4$ -phosphorane structure as given in Figure 2.2 where $\text{X} = \text{HN}$ and $\text{Y} = \text{S}$ have been well studied and various analogues containing various organic groups in the R positions have been synthesised. Methyl, *iso*-propyl, phenyl and *iso*-butyl analogues of $\text{HN}(\text{R}_2\text{PS})_2$ are all known in literature and are prepared by various methods.^{216–219} Preparations seem to have been undertaken under inert conditions due to the reactivity of the reagents used. Two prominent methods were noted for the synthesis of these analogues, the first was the reaction of $\text{R}_2\text{P}(\text{S})\text{NH}_2$ and $\text{R}_2\text{P}(\text{S})\text{Br}$ in the presence of $\text{KO}t\text{Bu}$,^{216,217} while the second method was the reaction of R_2PCl with $\text{HN}(\text{SiMe}_3)_2$ followed by sulphur.^{218–220} The structure of all these analogues contained the amine while the sulphur remained deprotonated with clear $\text{P}=\text{S}$ and $\text{P}-\text{N}$ bonds.^{218,220–222} The crystal symmetry of these compounds did not show any trends with space groups ranging from $P-1$ for the phenyl, $P2_1/n$ and $P2_1/a$ for the *iso*-butyl and *iso*-propyl derivatives and $Pbca$ for the methyl derivatives. In terms of starting reagents the anionic $[\text{N}(\text{R}_2\text{PS})_2]^-$ species has been synthesised and structurally characterised in the polymeric salt $\text{K}[\text{N}(\text{R}_2\text{PS})_2]$.²²³

In these early studies the salts of these analogues with the $[\text{N}(\text{R}_2\text{PS})_2]^-$ species were also studied with regards to their coordination ability, mainly with transition metals. Silvestru and co-workers synthesised and characterised the complex $[\text{Co}(\text{N}(\text{Me}_2\text{PS})_2)]$ while Husebye and Maartmann-Moe published the structure for the $[\text{Se}(\text{N}(\text{Ph}_2\text{PS})_2)]$.^{217,221} Cupertino and co-workers published the synthesis and structure of the tetrahedral di- $[\text{N}(i\text{Pr}_2\text{PS})_2]^-$ complexes of Zn^{2+} , Cd^{2+} and Ni^{2+} and the square planar di- $[\text{N}(i\text{Pr}_2\text{PS})_2]^-$ complexes of Pt^{2+} and Pd^{2+} , all of which showed chemistry typical of complexes of these transition metals.^{218,224} Further to this, extensive synthesis and

structural characterisation of transition metal complexes, typically forming either tetra coordinated complexes or clusters has been undertaken.²²⁵ Details on these complexes are not given here due to the fact that the main interest of the current study lies in complexes of these compounds with lanthanides and complexes having N–M bonds.

In most complexes characterised using XRD data no N–M bond was noted for the transition metals. Complexes with the moiety given in Figure 2.43 were only noted for the transition metals Ti and Ru. Two complexes have been structurally characterised for titanium, namely $[\text{Ti}(\text{N}(\text{Ph}_2\text{PS})_2)(\text{HN}(\text{Ph}_2\text{PS})_2)\text{Cl}_2][\text{Ti}_2\text{Cl}_9]$ and $[\text{Ti}_2(\text{N}(\text{Ph}_2\text{PS})_2)_2-\mu\text{-S}_2,\text{Cl}][\text{Ti}_2\text{Cl}_9]$, with the structures given in Figure 2.44.^{226,227} Only one ruthenium compound is known having the formula $[\text{Ru}(\text{N}(\text{Ph}_2\text{PS})_2)(\text{C}_6(\text{Me})_6)]$, and the structure given in Figure 2.45.²²⁸ Both were prepared under stringent inert conditions.

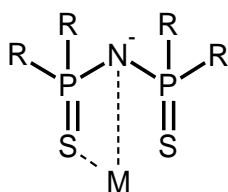


Figure 2.43: Molecular diagram of the fragment of the complex depicting the N–M bond of interest.

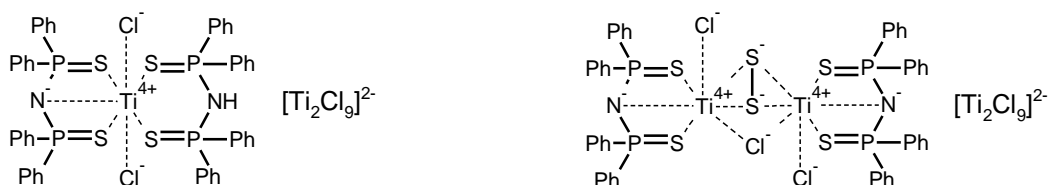


Figure 2.44: Molecular diagrams of $[\text{Ti}(\text{N}(\text{Ph}_2\text{PS})_2)(\text{HN}(\text{Ph}_2\text{PS})_2)\text{Cl}_2][\text{Ti}_2\text{Cl}_9]$ (left) and $[\text{Ti}_2(\text{N}(\text{Ph}_2\text{PS})_2)_2(\mu\text{-S})_2\text{Cl}][\text{Ti}_2\text{Cl}_9]$ (right).

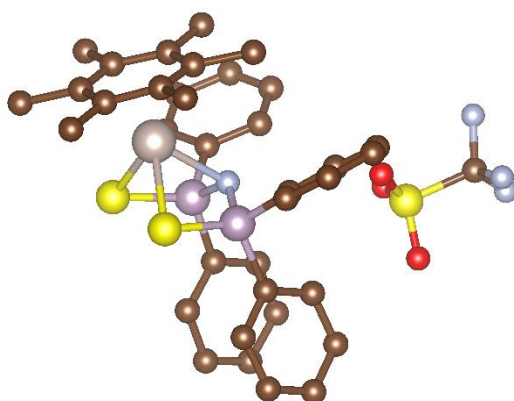


Figure 2.45: Molecular structure of $[\text{Ru}(\text{N}(\text{Ph}_2\text{PS})_2)(\text{C}_6(\text{Me})_6)]$, (built in VESTA).

For the trivalent cations of yttrium, the lanthanides lanthanum, cerium and ytterbium and the actinides uranium and plutonium, two types of complexes are known with the structures $[M(N(Ph_2PS)_2)_3]$ (where $M = Y^{3+}, La^{3+}, Ce^{3+}, U^{3+}$ and Pu^{3+})^{229–231} and $[M(N(Ph_2PS)_2)Cp_2]$ (where $M = Y^{3+}, Ce^{3+}$ and Yb^{3+})^{232–234} as given in Figures 2.46. All these compounds were prepared under inert conditions using $[M(N(SiMe_3)_2)_3]$ and $[MCp_3]$ as starting reagents respectively. In all these cases, except for the ruthenium complex, complexes showed flat S–P–N–P–S structures indicating very good charge dispersion about this group. This is in fact contrary to the isoelectronic carbenes discussed prior in Section 2.6.2, where puckering in the structures is typical, however no discussion of the relation between puckering and charge distribution was noted in literature. It should also be noted that the N–M bond lengths for these complexes were as given in Table 2.2.

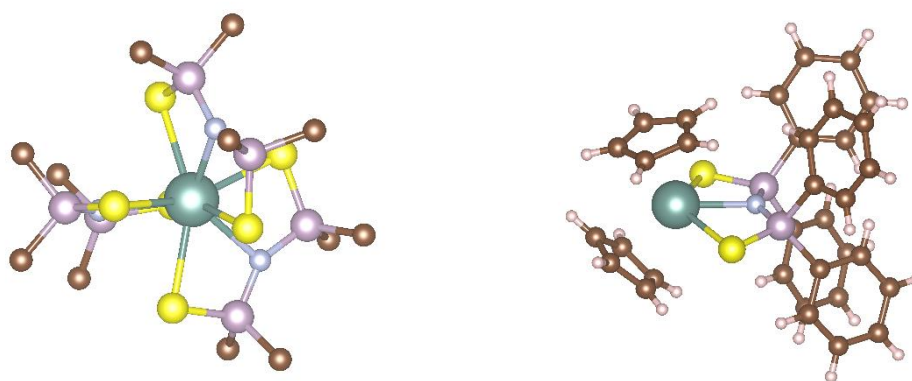


Figure 2.46: Molecular structures of $[M(N(Ph_2PS)_2)_3]$ (left) and $[M(N(Ph_2PS)_2)Cp_2]$ (right) typical for the metals described in text.

Table 2.2: Bond lengths of N–M bonds given in literature.

Compound	N–M bond length
$[Ti(N(Ph_2PS)_2)(HN(Ph_2PS)_2)Cl_2][Ti_2Cl_9]$	2.066 Å
$[Ti_2(N(Ph_2PS)_2)_2-\mu-S_2,Cl][Ti_2Cl_9]$	2.103 Å
$[Ru(N(Ph_2PS)_2)(C_6(Me)_6)]$	2.282 Å
$[M(N(Ph_2PS)_2)_3]$	2.560–2.652 Å
$[M(N(Ph_2PS)_2)Cp_2]$	2.374–2.567 Å

2.7.3. Compounds with the structure X(R₂PY)₂, where X = HN, Y = O, and their complexes

Similar to the compounds of the HN(R₂PS)₂ ligand and its derivatives a number of HN(R₂PO)₂ have been synthesised and structurally characterised. In these cases only two structural analogues were characterised, namely the ligands HN(*i*Pr₂PO)₂ and HN((C₆F₅)₂PO)₂.^{220,235} As with some of the HN(R₂PS)₂ analogues both were prepared under inert conditions using R₂PBr and HN(SiMe₃)₂.^{220,235} The tautomeric compound [N⁺(Ph₂PO⁻)(Ph₂POH)] was synthesised by Fluck and Goldmann in 1963, but only structurally characterised by Nöth in 1982, as having the structure given in Figure 2.47.^{37,236} The synthetic route was not typical to those described previously for the HN(R₂PS)₂ and HN(R₂PO)₂ analogues but was undertaken through the reaction given in Scheme 2.9, which was undergone under inert conditions due to the reactivity of the starting reagents.

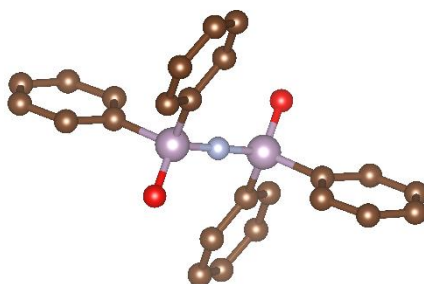
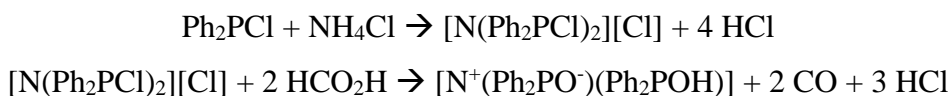


Figure 2.47: Molecular diagram of tautomer structure for HN(Ph₂PO)₂ published by Nöth in 1982.²³⁶



Scheme 2.9: Synthesis of [N⁺(Ph₂PO⁻)(Ph₂POH)]

Complexes of HN(*i*Pr₂PO)₂, HN((C₆F₅)₂PO)₂ and [N⁺(Ph₂PO⁻)(Ph₂POH)] with transition metals have been studied extensively and all these complexes, to the author's knowledge, show chelation through the oxygen atoms.²²⁵ It is interesting to note that the compound [N⁺(Ph₂PO⁻)(Ph₂POH)] forms, on deprotonation and complexation, the [N(Ph₂PO)₂]⁻ chelate. A N–M bond has not been published in current literature for these compounds.²²⁵ The complexes of interest in the current study are the complexes of these three ligands with lanthanides.

For the ligand species $\text{HN}((\text{C}_6\text{F}_5)_2\text{PO})_2$ and $[\text{N}^+(\text{Ph}_2\text{PO}^-)(\text{Ph}_2\text{POH})]$ complexes with the basic formula of $[\text{Ln}(\text{N}(\text{R}_2\text{PO})_2)_3]$ (where Ln = La, Ce, Pr, Nd, Sm, Eu, Gd, Tb, Dy or Er) have been synthesised and characterised in published literature.^{32,235,237–245} Unlike the lanthanide $[\text{Ln}(\text{N}(\text{Ph}_2\text{PS})_2)_3]$ complexes, in the cases for the $[\text{Ln}(\text{N}(\text{R}_2\text{PO})_2)_3]$ analogues no N–M bonds have been published in literature. All these have been noted as having both octahedral and trigonal prismatic geometry as given in Figure 2.48 for $[\text{Tb}(\text{N}(\text{Ph}_2\text{PO})_2)_3] \cdot 0.75\text{H}_2\text{O}$, in which both coordination geometries were noted.²⁴⁰ In all cases two main preparation procedures were undertaken in numerous solvents through either the complexation of the lanthanide(III) salts, typically chlorides, with $\text{K}[\text{N}(\text{R}_2\text{PO})_2]$,^{32,235,238,240,246} which was undertaken under typical laboratory conditions or the reaction of the neutral ligand with $[\text{Ln}(\text{NSiMe}_3)_2]$, which was undertaken under inert conditions.²⁴¹

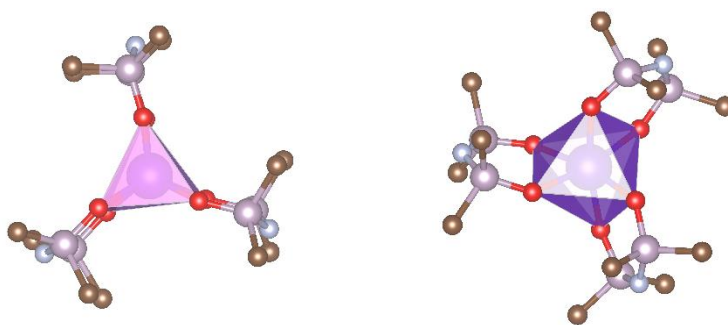


Figure 2.48: Trigonal prismatic (left) and Octahedral $[\text{Tb}(\text{N}(\text{Ph}_2\text{PO})_2)_3] \cdot 0.75\text{H}_2\text{O}$.

For the ligands $\text{HN}((\text{C}_6\text{F}_5)_2\text{PO})_2$ and $[\text{N}^+(\text{Ph}_2\text{PO}^-)(\text{Ph}_2\text{POH})]$, the inclusion of a monodentate secondary ligand to the complexes $[\text{Ln}(\text{N}(\text{R}_2\text{PO})_2)_3]$ to give complexes of the formula $[\text{Ln}(\text{N}(\text{R}_2\text{PO})_2)_3\text{L}]$ have been noted in literature with L = MeCN, MeCO₂Et, THF, Me₂SO, Me₂CO and H₂O for R = Ph and L = MeOH for R = *i*Pr,^{200,235,239,241,242,245} with no overarching coordination geometry common for these species. Many of the $[\text{Ln}(\text{N}(\text{Ph}_2\text{PO})_2)_3]$ complexes were also noted as solvates of MeCN, H₂O, THF, CHCl₃ and hexane.^{32,235,238–245} The presence of both aqua complexes and hydrates indicated that the complexes thus formed were stable to some degree on exposure to moisture.

For the ligand $[\text{N}((i\text{Pr})_2\text{PO})_2]^-$ only cerium(IV) complexes have been characterised by XRD methods to give molecular structures. The cerium(III) $[\text{Ce}(\text{N}(i\text{Pr}_2\text{PO})_2)_3]$ has not been structurally characterised although the cerium(IV) complexes $[\text{Ce}(\text{N}(i\text{Pr}_2\text{PO})_2)_3\text{Cl}]$ and $[\text{Ce}(\text{N}(i\text{Pr}_2\text{PO})_2)_3(\text{OI}(\text{Ph})(\text{Cl}))]$ with the same

formula and structure of $[\text{Ln}(\text{N}(\text{R}_2\text{PO})_2)_3\text{L}]$ have been published.^{200,247} The cerium clusters $[\text{Ce}(\text{N}(\text{iPr}_2\text{PO})_2)_2(\text{O}_2)]_2$ and $[\text{Ce}(\text{N}(\text{iPr}_2\text{PO})_2)_2\text{Cl}]_2[\mu\text{-N}(\text{iPr}_2\text{PO})_2](\mu\text{-O})$ were also published.^{200,247} Finally, two complexes of structure $[\text{Ce}(\text{N}(\text{iPr}_2\text{PO})_2)_2(\text{L})_2]$ namely, $[\text{Ce}(\text{N}(\text{iPr}_2\text{PO})_2)_2(\text{NO}_3)_2]$ and $[\text{Ce}(\text{N}(\text{iPr}_2\text{PO})_2)_2(\text{MoO}_3\text{Cp})_2]$ have also been published.²⁴⁸ These indicated that using a less bulky R group than phenyl and an early lanthanide cation, which typically have greater coordination numbers could form complexes with secondary ligands of interest which can replace at least one of the chelates. This could increase the chemistry of such complexes, which is of general interest.

In all cases little puckering of the O–P–N–P–O structures on coordination was noted in the structures published in literature, regardless of the structure of the complex. However, it was noted that the structures for the coordinated S–P–N–P–S moieties were more planar, possibly indicating a higher degree of charge distribution than the coordinated O–P–N–P–O moieties. This preference for planar S–P–N–P–S moieties as compared to the O–P–N–P–O moieties could be the reason for the formation of N–M bonding in the former but not the latter. The reason for this could be the preference of the ylide form $\text{P}^+\text{-S}^-$ for P=S bonds as compared to the $\text{P}^+\text{-O}^-$ form for the P=O bond,^{99,249} which could cause better charge distribution in the latter.

2.8. Stabilisation of compounds by co-crystallisation

Co-crystals are typically defined as crystalline materials which contain two or more molecular components in definite stoichiometric amounts, bound together by intermolecular interactions within a singular crystal lattice.^{250,251} It is commonly accepted that co-crystals have physical and chemical properties that are different from those of the solids of the individual components.²⁵² This is indeed the most important difference between co-crystals and the solid state forms of the individual components that has pushed co-crystals into the forefront of crystal engineering.

Although in most studies the components of the co-crystals are molecular and neutral in nature, co-crystals are also known for charged components such as organic salts and charged metallic complexes.²⁵³ Numerous metallic complex – organic compound co-crystals have been published, using a wide range of metallic complexes ranging from organometallic compounds to ionic complexes such as lanthanide nitrate hydrates.^{254–256} Although ionic species are considered to be able to form co-crystals, neutral acidic and

basic co-formers, which are very common, must not react with each other to form ionic species, namely the conjugate base or acid.^{257,258} The most well described intermolecular bond used in co-crystallisation is the hydrogen bond, although other types of bonding such as ionic, π to π interactions and hydrophobic interactions are well known.²⁵⁰

In many cases the properties that have been discussed in the study of co-crystals are physical properties, such as solubility.^{259,260} A second characteristic which is somewhat less discussed is the stability of these co-crystals as compared to the original compounds. Research into the difference in stability was mainly concentrated on APIs, wherein the presence of co-formers in the crystalline form diminishes the possibility and rate of formation of other crystalline forms, especially hydrates.²⁶¹

Less work has been published on the chemical stabilisation of compounds using co-crystallisation but examples from such works are provided hereunder. The earliest discussion on stabilisation of compounds through co-crystallisation was published in 1931 by Fischer and Taurinsch, when the field of co-crystallisation was not established.²⁶² The authors dealt with a number of acyl and thionyl halides and a number of inorganic sulphur and phosphorus halides which were crystallised in stoichiometric amounts with numerous (phenylazo)phenyl derivatives. These gave crystals in which the halides did not react with atmospheric moisture to release the respective hydrogen halides.²⁶² The cause of this stability is not well known and is not expanded upon in the study. Simple molecules that are known to be unstable in both the solid state and in solution to varying degrees are the 1,1,4,4-tetrahalobutatrienes. Although 1,1,4,4-tetrafluorobutatriene is the least stable of the series, in the solid state it was nonetheless elucidated in single crystals.²⁶³ This however was not the case for the more stable 1,1,4,4-tetrabromobutatriene, although still sensitive to decomposition, which could only be obtained in a crystalline and stable form in co-crystals with phenazine.²⁶⁴ This is therefore an example of the use of co-crystallisation in the stabilisation of highly reactive compounds in the attempt to produce crystals which were suitable for SXRD.

An area of study that is of interest in the field of chemical stability of compounds in crystalline form is the co-crystallisation of energetic materials in an attempt to control the sensitivity of these materials to reaction.²⁶⁵ Crystallographic studies have shown that in many cases thermal and chemical stability is mainly influenced by increasing the density of the crystal.^{266,267} This may be due in part to a correlation between density and a greater intermolecular bonding which increases the lattice energy and therefore thermal stability.²⁶⁸

In this regard a number of studies have been undertaken that address the co-crystallisation of 2,4,6-trinitrotoluene (TNT) with a number of co-formers. In these studies this highly energetic and reactive compound was stabilised for purposes of storage by co-crystallisation. In the first study of the kind TNT was co-crystallised, mainly in a 1:1 molar ratio, with a number of highly aromatic compounds. The intermolecular bonding was found to be donor-acceptor π - π bonding which through the formation of stacked crystal structures increased the density of the co-crystals as compared to that of crystalline TNT.²⁶⁹

Isoniazid, as shown in Figure 2.49, is known to be stable at room conditions but decomposes on storage when mixed with a number of other APIs with which it is commonly prescribed.²⁷⁰ As may be expected decomposition of this compound occurs mainly due to the reaction of the hydrazine group, resulting in the formation of numerous degradation products.²⁷¹ Co-crystallisation of isoniazid with cinnamic, succinic, glutaric, adipic, pimelic, sebacic and suberic acids yielded a number of co-crystals which were stable in storage conditions.^{272,273} However with the co-formers malonic and benzoic acid it yielded co-crystals which decomposed on storage.²⁷³

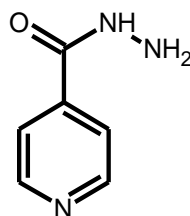


Figure 2.49: Structure of Isoniazid

In all cases the acid co-formers bonded to the pyridine electron donating nitrogen, while numerous different synthons were noted for the hydrazine moiety. A clear relationship between the synthons formed in each co-crystal and the stability or lack thereof was not concluded, as apart from the carboxylic to pyridine synthon co-crystals containing malonic and benzoic acid did not have other similar synthons. Meanwhile the stable co-crystals showed a wide variety of synthons, many being different between one co-crystal and the next.^{272,273}

3. EXPERIMENTAL

3.1. Instrumentation and software used for product characterisation

A number of instruments were used to analyse the resultant products obtained from the reactions performed during this study.

Infra-red Spectra were obtained by a Shimadzu IRAffinity-1 FTIR spectrophotometer, with a detection range of 4000–400 cm^{-1} . Solid samples were prepared using the pellet method by FT-IR grade ($\geq 99\%$) KBr (Sigma Aldrich), which was heated to dryness overnight before and after use and stored in a vacuum desiccator at room temperature before use, to ensure that no changes occur in the solid state of the sample due to heat transfer from the KBr to the sample. This was the main sample preparation technique for the products to be analysed by IR spectroscopy used during this study, since the focus was on products in the solid state. Other sample preparation methods used are described where applicable.

UV-visible light spectroscopy was undergone using a Jasco V-650 Spectrophotometer. Liquid samples were prepared by dissolving an amount of solid in the relevant solvent and the sample transferred to a quartz cuvette. All solvents used were dried as described in Section 3.2.3. Raman spectroscopy was undergone using a LabRAM HR evolution spectrometer. Samples were analysed sealed in glass capillaries. IR spectra, UV spectra and Raman spectra were plotted and analysed using Spectragryph - optical spectroscopy software.²⁷⁴

^1H and ^{31}P NMR spectroscopy was undertaken using a Bruker Biospin GmbH Ascend NMR spectrometer with a probe having a set frequency of 500.13 MHz for ^1H NMR and a set frequency of 202.457 MHz for ^{31}P . ^1H NMR samples were prepared by dissolving 1-5 mg of the solid to be tested in 0.8 ml of deuterated solvent in which the solid is soluble. Tetramethylsilane (TMS) was used as an internal standard for ^1H NMR spectroscopy. ^{31}P NMR samples were prepared by dissolving 10-20 mg of the solid to be tested in 0.4 ml of the deuterated solvent in which the solid was soluble. 0.1%(w/v) $\text{H}_3\text{PO}_{4(\text{aq})}$ solution was prepared and used as an external standard for ^{31}P NMR spectrometry. The deuterated solvent used for the sample was also used to lock the frequency. All data was collected at a temperature of 298 K, unless otherwise stated. ^1H and ^{31}P NMR spectra were plotted and analysed using TopSpin 3.5pl6 and MNova 14.1.0.

Gas chromatography mass spectroscopy (GC-MS) data was collected using Thermo DSQ II GC/MS spectrometer. Samples were prepared by dissolving 5-10 mg of the solid to be tested in 0.75-0.8 ml of chloroform. As with the NMR spectra the gas chromatographs and mass spectra obtained were plotted and analysed using MNova 14.1.0.

Detailed photographs of crystals, crystalline powders and amorphous solids were obtained using a Leica Z16 APO microscope and a QICAM Fast 1394 camera along with the software Q-Capture Pro 7. All hot stage techniques were undergone using the same microscope and camera and the hot stage apparatus THMS600 controlled and used via the Linksys32 software.

SXRD data was collected using a STOE STADIVARI diffractometer for both Cu- $K_{\alpha 1}$ or Mo- $K_{\alpha 1}$ radiation and the BM01 beamline at the European Synchrotron Radiation Facility (ESRF) using 0.6407 Å radiation. Powder data was also collected using the BM01 beamline at the ESRF using 0.6407 Å radiation and a STOE Stadi MP- and P-powder diffractometer as well as STOE STADI P Essentials powder diffractometer for both Cu- $K_{\alpha 1}$ or Mo- $K_{\alpha 1}$ radiation.

3.2. Schlenk line techniques

Throughout this study reactions had to be undergone in a moisture free and inert atmosphere. Therefore, standard Schlenk line techniques were used as detailed out in Appendix 1.

3.2.1. Argon Purification

The most critical aspect was to ensure dry and inert conditions. The biggest challenge encountered was due to the fact that commercially available argon is typically not of high enough purity for research purposes. Therefore, a number of purification columns were prepared or purchased to remove reactive agents, mainly moisture and oxygen. The preparation of the purification columns used in this study is detailed out in Appendix 1 and is based on the preparations which enjoy widespread use in the field of air and moisture sensitive chemistry.²⁷⁵

3.2.2. General conditions and procedures

All reactions performed during this study were undergone under an argon atmosphere. Any variations will be detailed out in the specific procedures. All glassware used was heated overnight at 150 °C and flame dried under vacuum for 5 minutes to obtain dry glass conditions. Glassware was purged for 5 minutes under vacuum and 2 minutes under argon three times over, to ensure an argon atmosphere. All solvents and solid reagents used in reactions were stored under argon. Solvents were stored in Schlenk tubes under argon over a desiccant. Most solids obtained commercially were stored under argon in screw cap bottles. The argon atmosphere was maintained by resupplying the bottles with argon, whereby argon was allowed to flow over the solid in the open bottles covered by the screw cap. After this procedure, these were further stored in vacuum desiccators over activated coloured silica beads. Solid products prepared throughout the study were mainly stored in sealed ampoules or in small Schlenk tubes the latter being inspected and purged with argon regularly. All wet chemistry was undertaken using well established procedures. Weighing was undertaken using a simple benchtop mass balance using a special set up. All of these techniques are described in detail in Appendix 1. In all cases the purchased reagents were used as purchased without further purification unless specified. Reagents which were synthesised previously in the current study are identified in the Experimental section and characterisation is given in the Results and Discussion section.

3.2.3. Drying of solvents

All solvents used in the current study had to be dried and purified from impurities before use. The main drying procedure for solvents was the distillation of the solvent over a desiccant. The set up used in the current study and the specific techniques used for each solvent are given in detail in Appendix 2. Solvents which were used as purchased or dried using other techniques are noted as such while solvents dried using the techniques given in Appendix 2 are noted as dry.

3.3. Reaction procedures

3.3.1. Synthesis of Lanthanide carbene complexes

3.3.1.1. Ligand synthesis

Since the phosphorane ligands used in this study were not commercially available these had to be synthesised by following the procedures described in literature. On a number of occasions deviations from the published procedures were made, mainly due to the unavailability of equipment and a lack of details given in the published procedures.

3.3.1.1.1. Synthesis of $K[HC(Ph_2PNiPr)_2]$ through the Kirsanov method

The synthesis of the potassium salt of bis(diphenyl-*N*-*iso*-propyl phosphorano)methane, $K[HC(Ph_2PNiPr)_2]$, was undertaken several times during this study, with the aim of obtaining the required product and yield. In each case the Kirsanov method as employed by Demange and co-workers and Klemp, *et al.* was used.^{36,121} The synthesis of the salt was undergone in two steps. The first step was the synthesis of the aminophosphonium derivative ($[H_2C(Ph_2PNH(iPr))_2]Br_2$) using the procedure described by Demange *et al.*, which is a modification of the previously published Kirsanov method.^{119,120} The molecular diagram of the expected product $[H_2C(Ph_2PNH(iPr))_2]Br_2$ is given in Figure 3.1.

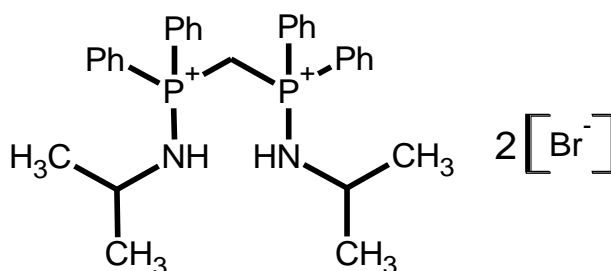


Figure 3.1: Molecular diagram of $[H_2C(Ph_2PNH(iPr))_2]Br_2$.

The second step involved the preparation of the actual salt $\text{K}[\text{HC}(\text{Ph}_2\text{PN}i\text{Pr})_2]$ through the simple deprotonation of the aminophosphonium salt $[\text{H}_2\text{C}(\text{Ph}_2\text{PNH}(i\text{Pr}))_2]\text{Br}_2$ with potassium bis(trimethylsilyl)amide (KHMDS) as described by Klemps and co-workers.¹²¹ The molecular diagram of the expected product $\text{K}[\text{HC}(\text{Ph}_2\text{PN}i\text{Pr})_2]$ is given in Figure 3.2.

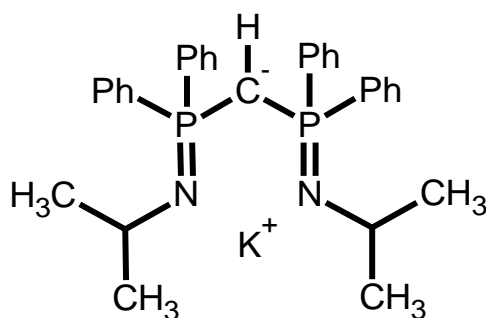


Figure 3.2: Molecular diagram of $\text{K}[\text{HC}(\text{Ph}_2\text{PN}i\text{Pr})_2]$.

3.3.1.1.1.1 Synthesis of $[\text{H}_2\text{C}(\text{Ph}_2\text{PNH}(i\text{Pr}))_2]\text{Br}_2$

3.3.1.1.1.1.1 Reagents used

The chemicals used in the procedures described in this section were 1,1-bis(diphenylphosphino)methane (dppm) (99%), *iso*-Propyl amine (99%), tributylamine (98%), bromine (>99%), dichloromethane (dry) and THF (dry).

3.3.1.1.1.1.2 $[\text{H}_2\text{C}(\text{Ph}_2\text{PNH}(i\text{Pr}))_2]\text{Br}_2_1$

A 100 ml Schlenk flask was charged with 30 ml of dry CH_2Cl_2 via cannula, after which 1.001g (2.6 mmol) of Bis(diphenylphosphino)methane (dppm) were added. Full dissolution occurred, yielding a clear solution. This was cooled to $-78\text{ }^\circ\text{C}$ in a dry ice-acetone bath under constant stirring. A 100 μl syringe was used to transfer 267 μl (5.18 mmol) bromine liquid to the reaction solution at $-78\text{ }^\circ\text{C}$. Transfer of bromine was undergone in a dropwise manner during which a bright orange suspension was formed. After all the bromine was added the bath was removed and the mixture allowed to reach room temperature, yielding a white precipitate along with a yellow suspension. The reaction mixture was allowed to stir for 1 hour at room temperature.

Afterwards the reaction flask was again cooled down to $-78\text{ }^{\circ}\text{C}$ and $\sim 1.3\text{ ml}$ (5.5 mmol) of tributylamine and $\sim 0.5\text{ ml}$ (5.8 mmol) of *iso*-propyl amine were added to the reaction mixture via glass syringes. These were both added in slight excess of the amounts required. After this addition the reaction mixture was left stirring until it reached room temperature, whereupon it was left stirring for a further 2 hours. Immediately on the addition of the reagents, the suspension started to clear until on reaching room temperature a yellow solution was formed. The solvent was removed under vacuum to give a foamy white residue. Dry THF (20 ml) was then added to dissolve the majority of the residue. This was allowed to stir at room temperature for 5 hours. The mixture was filtered through a filtration tube set up and the solid washed with another 20 ml of THF. The solid was dried under vacuum and afterwards further dried under argon flow. The solid was collected as the final product in an ampoule under argon. Yield: 0.905 g, 52.7 %.

3.3.1.1.1.3 Characterisation data

$[\text{H}_2\text{C}(\text{Ph}_2\text{PNH}(i\text{Pr}))_2]\text{Br}_2\text{-1}$ FT-IR (KBr, cm^{-1}): 3494 (m), 3423 (m), 3054 (m), 2967 (w), 2826 (w), 2761 (wb), 1587 (w), 1439 (s), 1371 (w), 1320 (w), 1222 (w), 1190 (w), 1166 (w), 1114 (s), 1075 (w), 1042 (m), 994 (w), 909 (w), 822 (m), 802 (m), 784 (m), 750 (s), 717 (w), 690 (s), 490 (s). ^1H NMR (CDCl_3): 8.00 ppm (dd, $^3J_{\text{HP}} = 13.38\text{ Hz}$, $^3J_{\text{HH}} = 7.33\text{ Hz}$, 8.34H, o-H), 7.40 ppm (t, $^3J_{\text{HH}} = 7.30\text{ Hz}$, 4.34H, p-H), 7.61 ppm (dt, $J_1 = 7.88\text{ Hz}$, $J_2 = 3.30\text{ Hz}$, 8.34, m-H), 6.96 ppm (t, $^2J_{\text{HP}} = 10.45\text{ Hz}$, $^3J_{\text{HH}} = 5.60\text{ Hz}$, 2.34H, NH), 6.56 ppm (t, $^3J_{\text{HH}} = 16.03\text{ Hz}$, 4.34H, PCH₂P), 3.06 ppm (bm, 2.34H, NCH(*i*Pr)), 0.95 ppm (d, $^3J_{\text{HH}} = 6.40\text{ Hz}$, 14H, CH₃(*i*Pr)).

3.3.1.1.1.2 Synthesis of $\text{K}[\text{HC}(\text{Ph}_2\text{PNiPr})_2]$

3.3.1.1.1.2.1 Reagents used

The chemicals used in the procedures described in this section were $[\text{H}_2\text{C}(\text{Ph}_2\text{PNH}(i\text{Pr}))_2][\text{Br}]_2\text{-1}$ (synthesised in current study), KHMDS (94-106%) and THF (dry).

3.3.1.1.2.2 General procedure for $\text{K}[\text{HC}(\text{Ph}_2\text{PNiPr})_2]$

A 100 ml Schlenk flask was charged with 25 ml of THF and stirring was commenced. Subsequently 0.2g (0.302 mmol) of $[\text{H}_2\text{C}(\text{Ph}_2\text{PNH}(i\text{Pr}))_2]\text{Br}_2\text{-1}$ were dissolved in the THF and afterwards 0.184g (0.922 mmol) of KHMDS were added in portions to the solution, at room temperature. The solution turned into a very pale yellow colour and remained slightly murky. This solution was allowed to stir at room temperature for 2 hours. During these 2 hours an off-white to pale yellow suspension started to form. The suspension was allowed to stand for 4 days, after which it was filtered through cannula filtration to yield a slightly murky pale yellow suspension. The solid left behind was washed with THF and the washing was added to the filtrate, which was left to stand overnight. A second cannula filtration was undergone to yield a pale yellow solution which was dried under vacuum to yield a sticky off-white precipitate. This precipitate was collected as the final product in an ampoule under argon.

3.3.1.1.2.3 $\text{K}[\text{HC}(\text{Ph}_2\text{PNiPr})_2]\text{-1}$

In this attempt 10 ml of dry THF, 0.121g (0.183 mmol) of $[\text{H}_2\text{C}(\text{Ph}_2\text{PNH}(i\text{Pr}))_2]\text{Br}_2\text{-1}$ and 0.110g (0.551 mmol) of KHMDS were used. Precipitation was allowed for 3 days rather than 4 days while washing with THF and the second cannula filtration were not undertaken. The final product was labelled as $\text{K}[\text{HC}(\text{Ph}_2\text{PNiPr})_2]\text{-1}$. Yield: Negligible.

3.3.1.1.2.4 $\text{K}[\text{HC}(\text{Ph}_2\text{PNiPr})_2]\text{-2}$

The solid $\text{K}[\text{HC}(\text{Ph}_2\text{PNiPr})_2]\text{-2}$ was collected as a final product through the general procedure described prior with no modifications. Yield: 0.102 g, 62 %.

3.3.1.1.2.5 Characterisation data

$\text{K}[\text{HC}(\text{Ph}_2\text{PNiPr})_2]\text{-1}$ FT-IR (KBr, cm^{-1}): 3370 (bw), 3176 (bw), 3055 (w), 2964 (m), 2925 (m), 2855 (w), 1653 (w), 1437 (s), 1365 (w), 1260 (m), 1183 (s), 1109 (s), 1026 (s), 978 (sh), 886 (m), 802 (s), 743 (s), 718 (m), 695 (s), 503 (m). ^1H NMR (CDCl_3): 8.00-

7.40 ppm (phenyl) 3.37 ppm (m, $^3J_{\text{HH}} = 6.29$ Hz, $^3J_{\text{HP}} = 19.2$ Hz, 2.0H, NCH(*i*Pr)), 1.24 ppm (d, $^3J_{\text{HH}} = 6.5$ Hz, 29.32H, CH₃(*i*Pr)), 0.88 ppm (t, $^2J_{\text{HP}} = 6.9$ Hz, 18.64H, PCHP).

K[HC(Ph₂PNiPr)₂]₂ FT-IR (KBr, cm⁻¹): 3419 (bw), 3122 (m), 3059 (w), 2963 (m), 2927 (w), 2856 (w), 1655 (bw), 1470 (w), 1438 (s), 1261 (s), 1203 (s), 1185 (s), 1173 (m), 1107 (s), 1071 (w), 1016 (s), 890 (m), 801 (s), 754 (m), 747 (m), 742 (m), 723 (m), 715 (w), 699 (s), 692 (s), 563 (s), 523 (m). ¹H NMR (CDCl₃): 8.00-7.40 ppm (phenyl) 3.37 ppm (m, $^3J_{\text{HH}} = 6.29$ Hz, $^3J_{\text{HP}} = 19.2$ Hz, 2.0H, NCH(*i*Pr)), 1.24 ppm (d, $^3J_{\text{HH}} = 6.5$ Hz, 13.14H, CH₃(*i*Pr)), 0.88 ppm (t, $^2J_{\text{HP}} = 6.9$ Hz, 1.40H, PCHP).

3.3.1.1.2. Synthesis of H₂C(Ph₂PNSiMe₃)₂

The synthesis of the compound, H₂C(Ph₂PNSiMe₃)₂, was published by Appel and Rupert in 1974.³⁴ The authors used the Phospho-Staudinger method wherein λ³σ³-phosphanes were reacted with azides to produce iminophosphoranes and nitrogen gas as a side product, as described in Section 2.4.3.1.1.¹¹⁷ During the current study, the synthesis of the H₂C(Ph₂PNSiMe₃)₂ through this method was undergone by reacting dppm with trimethylsilyl azide. The reaction was attempted several times and a number of batches were prepared. The molecular diagram of the expected product, H₂C(Ph₂PNSiMe₃)₂, is given in Figure 3.3.

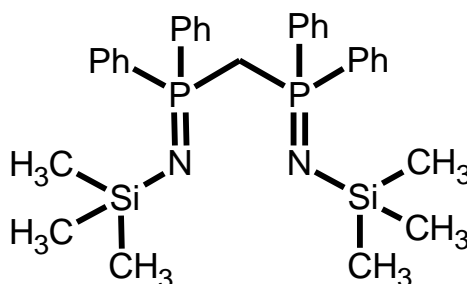


Figure 3.3: Molecular diagram of the ligand H₂C(Ph₂PNSiMe₃)₂.

3.3.1.1.2.1 Reagents used

The chemicals used in the procedures described in this section were dppm (99%), trimethylsilyl azide (94%) and acetonitrile (dry).

3.3.1.1.2.2 General procedure

In this reaction 2 ml (15 mmol) of trimethylsilyl azide were transferred by syringe to a 50 ml Schlenk flask, followed by 2.330g (5.99 mmol) of dppm, to give a thick white suspension. The mixture was stirred at 80 rpm. On heating to 90-100 °C full dissolution was obtained along with heavy effervescence. The temperature was then increased to 140 °C over a period of approximately 10 hours at a rate of 4 °C/hour. Full dissolution of the solid occurred at ~87 °C. The solution was kept at 140 °C until no more effervescence was observed. This mixture was allowed to cool to 100 °C and vacuum applied for 6 hours to remove volatile reagents and by-products. The mixture was cooled to room temperature yielding an off-white crystalline mass as expected. The mass was broken into smaller pieces and an off-white powder obtained. The solid proved to be crystalline on inspection under polarised light. The solid was collected in an ampoule under argon as the final product.

3.3.1.1.2.3 H₂C(Ph₂PNSiMe₃)₂_1

In this attempt the final product was recrystallised from acetonitrile as described by Müller and co-workers in 1999.²⁷⁶ Dry acetonitrile was heated to reflux in a temperature range of 75-81°C and 5 ml was transferred by cannula onto the solid product. The mixture was heated to 81 °C giving two liquid phases which were miscible, forming a clear liquid. This was cooled to -10 °C in a salt-ice bath to yield a white precipitate containing a small amount of dark grey solid mixed with the white solid. The mixture was filtered by cannula filtration and the solid dried under vacuum for several hours. The solid was collected as H₂C(Ph₂PNSiMe₃)₂_1 in an ampoule under argon. Yield: 1.195 g, 35 %.

3.3.1.1.2.4 H₂C(Ph₂PNSiMe₃)₂_2

In this attempt the solution was heated directly to 140 °C and left at this temperature for 10 hours, after which no more effervescence was observed. The mixture was allowed to cool to room temperature overnight after which the solid was heated under vacuum at 100 °C to remove volatiles, yielding the final product H₂C(Ph₂PNSiMe₃)₂_2. Yield: 3.268 g, 96.7 %.

3.3.1.1.2.5 H₂C(Ph₂PNSiMe₃)₂_3

A solid H₂C(Ph₂PNSiMe₃)₂_3 was collected as a final product through the general procedure described prior with no modifications. Yield: 2.4895 g, 74.4 %.

3.3.1.1.2.6 Characterisation data

H₂C(Ph₂PNSiMe₃)₂_1, _2, _3 FT-IR (KBr, cm⁻¹): 3049 (m), 2948 (m), 2891 (w), 1961 (w), 1914 (w), 1829 (w), 1481 (w), 1435 (s) 1273 (bs), 1238 (s), 1184 (w), 1175 (w), 1157 (w), 1127 (m), 1114 (m), 1103 (m), 1027 (m), 998 (w), 864 (w), 851 (s), 831 (s), 802 (s) 776 (m), 751 (m), 741 (s), 730 (m), 710 (w), 696 (s), 633 (s), 573 (m), 532 (s), 510 (s), 500 (s), 460 (m). ¹H NMR (C₆D₆): 7.93 ppm (m, 2.97H, o-H), 7.65 ppm (m, 9.43H, m-H), 7.41 ppm (td, J₁ = 1.65 Hz, J₂ = 7.68 Hz, 1.81H, p-H) 3.29 ppm (t, ²J_{HP} = 13.87 Hz, 1H, PCH₂P), 0.26 ppm (s, 18.18H, SiMe₃).

3.3.1.1.3. Synthesis of H₂C(Ph₂PS)₂

The synthesis and SXRD characterisation of bis(diphenylthiophosphinoyl)methane, H₂C(Ph₂PS)₂, was published by Carmalt and co-workers in 1996.³⁵ The reaction undergone was the oxidation of the phosphorus(III) dppm to the phosphorus(V) H₂C(Ph₂PS)₂ by the reduction of elemental sulphur, as described in Section 2.4.3.2. This has remained the main method for the preparation of this ligand and is described in various publications wherein this ligand is used to complex with lanthanide metal centres.^{8,123,124} In this study this procedure was used to prepare multiple batches of H₂C(Ph₂PS)₂. The molecular diagram of the expected product, H₂C(Ph₂PS)₂, is given in Figure 3.4.

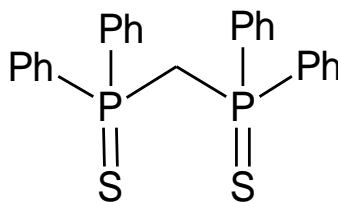


Figure 3.4: Molecular diagram of H₂C(Ph₂PS)₂.

3.3.1.1.3.1 Reagents used

The chemicals used in the procedures described in this section were dppm (99%), sulphur (94%) and toluene (dry).

3.3.1.1.3.2 General procedure

A 200 ml Schlenk flask was charged with 25 ml of dry toluene and 2.143g (5.6 mmol) of dppm. The mixture was stirred at room temperature and a colourless solution was formed. Subsequently 0.358g (11.1 mmol) of sulphur was added to this solution to obtain a 1:2 molar ratio of dppm to sulphur. The added sulphur dissolved after 10 minutes of stirring at room temperature, to yield a very pale yellow solution. The solution was heated in an oil bath at 111 °C for 30 minutes, to induce reflux within the flask. The solution was placed in a liquid nitrogen-chloroform bath at -60 °C and allowed to stand at this temperature for 2 days, with the bath being replenished each day. This yielded a highly crystalline solid composed of colourless crystals clearly visible to the naked eye. The solvent was removed by cannula filtration at a temperature of -60 °C. The solid was dried under vacuum and collected as the final product in a dry ampoule under argon.

3.3.1.1.3.3 H₂C(Ph₂PS)_{2_1}

A solid labelled H₂C(Ph₂PS)_{2_1} was collected as a final product through the general procedure described prior with no modifications. Yield: 2.183 g, 87 %.

3.3.1.1.3.4 H₂C(Ph₂PS)_{2_2}

In this reaction two solids were obtained, namely the final product as described in the general procedure, H₂C(Ph₂PS)_{2_2a}, and a secondary solid also collected under argon and labelled as H₂C(Ph₂PS)_{2_2b}. The second solid was collected on removal of volatiles under vacuum from the final cannula filtration filtrate. Yield H₂C(Ph₂PS)_{2_2a}: 2.156 g, 85.8 %. Yield H₂C(Ph₂PS)_{2_2b}: 0.211 g, 8.40 %.

3.3.1.1.3.5 H₂C(Ph₂PS)_{2_3}

In this attempt the reaction was undergone at 116 °C rather than 111 °C. Two solids were obtained namely the final product as described in the general procedure, H₂C(Ph₂PS)_{2_3a}, and a secondary solid also collected under argon and labelled as H₂C(Ph₂PS)_{2_3b}. The second solid was collected on removal of volatiles under vacuum from the final cannula filtration filtrate. Yield H₂C(Ph₂PS)_{2_3a}: 1.999 g, 79.58 %. Yield H₂C(Ph₂PS)_{2_3b}: 0.275 g, 10.95 %.

3.3.1.1.3.6 Characterisation data

H₂C(Ph₂PS)_{2_1, _2a, _3a} FT-IR (KBr, cm⁻¹): 3053 (w), 2937 (w), 2888 (w), 1966 (w), 1895 (w), 1821 (w), 1490 (m), 1435 (s), 1356 (m), 1309 (m), 1181 (w), 1155 (s), 1103 (s), 1066 (w), 1026 (w), 999 (w), 926 (w), 850 (m), 783 (s), 771 (s), 763 (w), 752 (s), 746 (s), 735 (s), 708 (s), 690 (s), 625 (s), 613 (s), 594 (s), 522 (m), 497 (s), 477 (s). ¹H NMR (C₆D₆): 7.89 ppm (m, 3.79H, o-H), 6.92 ppm (m, 5.91, m/p-H), 3.84 ppm (t, ²J_{HP} = 13.5 Hz, 1H, PCH₂P). ¹H NMR (CDCl₃): 7.82 ppm (dd, J₁ = 7.62 Hz, J₂ = 13.13 Hz, 2H, o-H), 7.42 ppm (t, 1H, p-H), 7.33 ppm (t, 2H, m-H), 3.98 ppm (t, ²J_{HP} = 13.43 Hz, 0.5H, PCH₂P). MP: 186–192 °C.

H₂C(Ph₂PS)_{2_2b, _3b} FT-IR (KBr, cm⁻¹): 3053 (w), 2937 (w), 2888 (w), 1966 (w), 1895 (w), 1821 (w), 1490 (m), 1435 (s), 1356 (w), 1307 (m), 1165 (s), 1155 (m), 1102 (s), 1066 (w), 1026 (w), 999 (w), 926 (w), 848 (m), 803 (s), 771 (s), 747 (s), 737 (s), 708 (w), 690 (s), 619 (m), 603 (s), 522 (m), 497 (s), 477 (s). ¹H NMR (CDCl₃): 7.82 ppm (dd, J₁ = 7.62 Hz, J₂ = 13.13 Hz, 2H, o-H), 7.42 ppm (t, 1H, p-H), 7.33 ppm (t, 2H, m-H), 3.98 ppm (t, ²J_{HP} = 13.43 Hz, 0.5H, PCH₂P).

3.3.1.2. Lanthanide starting reagents

Although as described in Section 2.5. numerous lanthanide starting reagents have been used in similar studies focusing on the synthesis of lanthanide carbenes, the lanthanide iodides remain the most widely used. Lanthanide iodide starting reagents were also used in the current study and therefore the preparation of relevant starting reagents formed an important part of this research.

3.3.1.2.1. Synthesis of $\text{LnI}_3(\text{THF})_{3.5}$ complexes

Attempts at synthesising anhydrous lanthanide iodides were undertaken for neodymium and samarium. In both cases the respective $\text{LnI}_3(\text{THF})_{3.5}$ ($\text{Ln} = \text{Nd}$ and Sm) was the desired product. These complexes are known to form as salt structures of the type $[\text{LnI}_2(\text{THF})_5][\text{LnI}_4(\text{THF})_2]$, given in Figure 3.5 for the Nd^{3+} analogue. These compounds were required as starting reagents in the attempts to synthesise complexes of the respective metals. The synthesis of these iodides was undergone as described by Izod and co-workers in 2004 and as detailed out hereunder.¹³⁷ In the current study numerous attempts, using variants to this methodology, were made to prepare these compounds. In the case of the neodymium iodides Soxhlet extraction as described in literature could not be undergone and therefore the procedure was also modified to employ a number of other methods for the removal of iodine and further purification.¹³⁷ In the case of the samarium iodide Soxhlet extraction as described in literature was undertaken both for the removal of iodine and for the recrystallisation of the crude product into a clear crystalline solid.¹³⁷ The synthesis attempts that gave the best yields and the best characterisation data are described hereunder.

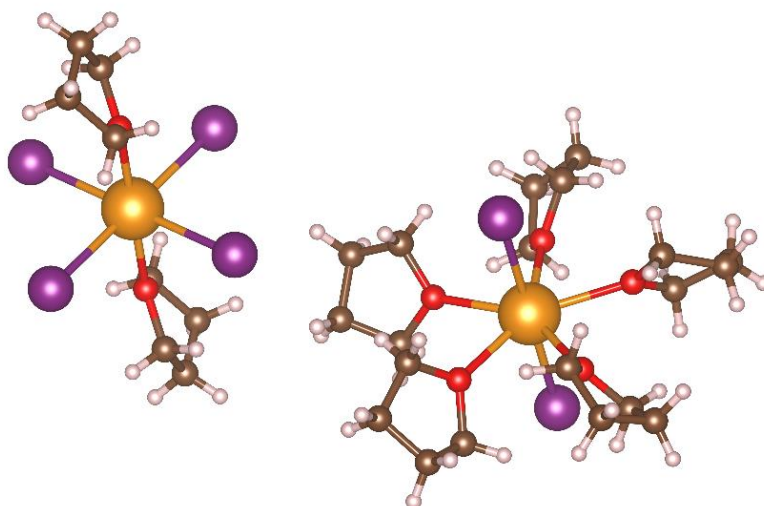


Figure 3.5: Structure of $[\text{NdI}_2(\text{THF})_5][\text{NdI}_4(\text{THF})_2]$ (built in VESTA from cif data obtained from CSD).

3.3.1.2.1.1 Reagents used

The chemicals used in the procedures described in this section were Neodymium metal (99.9%), Samarium metal (99.9%), iodine (99%), THF (dry), 40-60 °C petroleum ether (dry) and n-hexane (dry).

3.3.1.2.1.2 NdI₃(THF)_{3.5_1}

In this reaction a 100 ml Schlenk tube was charged with 15 ml dry THF. Afterwards 0.996g (6.91 mmol) of neodymium metal were weighed and added to the THF, yielding a black suspension on stirring. The flask was placed in a salt-ice bath at a temperature of -10 °C and allowed to equilibrate with the bath. When the mixture reached a temperature of 0 °C 2.629g (10.36 mmol) of iodine were added to the reaction mixture. Immediately on addition of iodine a dark brown suspension was formed along with some effervescence. On reaching room temperature the precipitate in suspension was observed to be yellow in colour. Dry 40-60 °C petroleum ether (40 ml) was then added to the reaction mixture yielding a yellow-green solid, in addition to the solid already present, and a light yellow filtrate.

The mixture was filtered through a filtration tube set up leaving a pale yellow filtrate along with a green-yellow solid. The solid was then dried under vacuum and collected. The solid was allowed to stand under vacuum in a 140 °C oil bath for 9 hours, giving a light grey solid. The flask was attached to the Schenk line through dry ice-acetone traps to minimise the burden on the main Schlenk line liquid nitrogen trap. Afterwards the solid was transferred to another filtration tube and was washed 5 times with 10 ml portions of 40-60 °C petroleum ether followed by 5 times with 20 ml portions of dry THF, after which the solid was recollected. Yield: 1.199 g, 21.5 %.

3.3.1.2.1.3 SmI₃(THF)_{3.5_1} and SmI₃(THF)_{3.5_2}

For this reaction 2.002 g (13.3 mmol) of samarium metal were weighed under argon flow and transferred into a 200 ml Schlenk tube. Subsequently 20 ml of dry THF were added via cannula and the solid was suspended by stirring the mixture using a magnetic stirrer. This mixture was cooled to 0 °C using an ice bath. On cooling 5.069 g

(20 mmol) of solid iodine were added to the stirred mixture to yield a dark brown suspension. This was allowed to equilibrate to room temperature overnight with constant stirring.

After the reaction was stopped, 50 ml of dry n-hexane were added via cannula to the mixture to yield a yellow precipitation. The resultant mixture was filtered using a 24/29 filtration tube to collect the yellow precipitate and a clear dark brown filtrate. The solid obtained was washed with 10 ml dry THF. The flask containing the filtrate was replaced with another flask containing dry THF to prepare a set up as described in Figure 3.6. The THF was heated to reflux until the solvent front reached above the level of the solid in the filtration tube. On suspension of the solid in THF heating was stopped and the THF was filtered automatically back to the Schlenk flask thus washing the solid. This was repeated for 10 runs to yield a dark brown THF solution, whilst at the same time the solid colouration did not change. The solid was then transferred to a Schlenk tube attached to the Schlenk line through a dry ice-acetone trap. The solid was set under vacuum and heated to 150 °C for 4 hours with constant stirring. The resultant product was weighed to give a mass of 5.444 g and was labelled as $\text{SmI}_3(\text{THF})_{3.5_1}$.

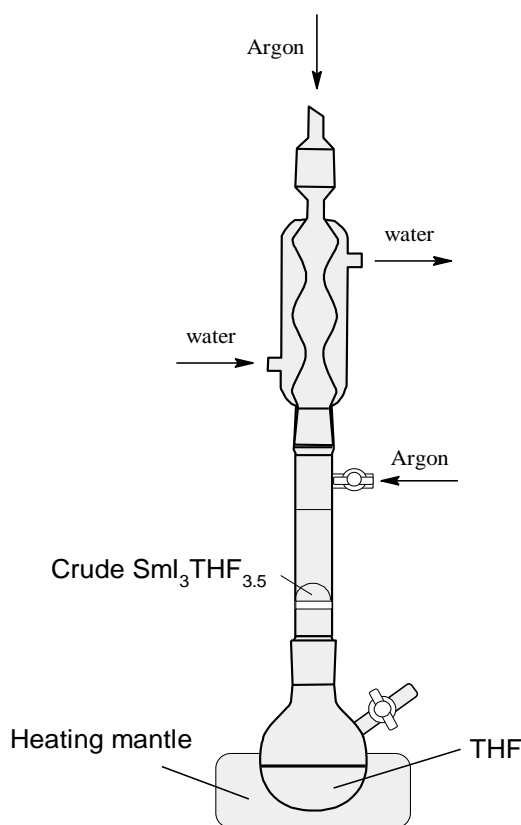


Figure 3.6: Second set up used to remove iodine from crude $\text{SmI}_3 \cdot \text{THF}_{3.5}$.

A Soxhlet extraction set up was prepared using a 250 mm Allihn condenser, a 100 ml Soxhlet extractor with a glass thimble and a 250 ml round bottom flask to act as a THF reservoir with a side arm attached to the Schlenk line. The glass thimble was charged with 1.070 g of the crude solid $\text{SmI}_3(\text{THF})_{3.5_1}$, while the reservoir flask was filled with 150 ml of dry THF. Soxhlet extraction was undertaken overnight. Most of the solid in the glass thimble was transferred to the reservoir flask. This solution was left at room temperature for 2 days, and an orange crystalline solid was formed in the THF reservoir. This solid was collected and labelled as $\text{SmI}_3(\text{THF})_{3.5_2}$ and its mass recorded to be 0.669 g. This procedure was repeated using the same amount of dry THF and 2.008 g of $\text{SmI}_3(\text{THF})_{3.5_1}$ to yield another orange crystalline solid with a mass of 1.906 g. The IR spectra of the two solids indicated that both solids had the same composition and therefore they were collected in an ampoule as a single solid and labelled as $\text{SmI}_3(\text{THF})_{3.5_2}$. Yield $\text{SmI}_3(\text{THF})_{3.5_1}$: 5.444 g, 52.24 %. Yield $\text{SmI}_3(\text{THF})_{3.5_2}$: 2.574 g, 24.7 %.

3.3.1.2.1.4 Characterisation data

$\text{NdI}_3(\text{THF})_{3.5_1}$ FT-IR (Nujol, cm^{-1}): 3330 (bs), 1300 (m), 1233 (sh), 1172 (w), 1154 (w), 1076 (w), 1034 (w), 1005 (s), 849 (m), 832 (w), 665 (w).

$\text{SmI}_3(\text{THF})_{3.5_1}$ FT-IR (Nujol, cm^{-1}): 3380 (bs), 1606 (bm), 1168 (m), 1154 (m), 1074 (m), 1005 (w), 965 (m), 934 (w), 917 (w), 890 (m), 846 (m).

$\text{SmI}_3(\text{THF})_{3.5_2}$ FT-IR (Nujol, cm^{-1}): 3380 (bw), 1606 (bw), 1170 (m), 1074 (m), 1036 (m), 1005 (w), 953 (w), 917 (m), 846 (w).

3.3.1.2.2. Synthesis of $[\text{Sm}(\text{NCy}_2)_3\text{THF}] \cdot \text{C}_6\text{H}_5\text{CH}_3$

In the current study the compound $[\text{Sm}(\text{NCy}_2)_3\text{THF}] \cdot \text{C}_6\text{H}_5\text{CH}_3$ was required as a starting reagent in the attempted synthesis of the carbene $[\text{Sm}(\text{C}(\text{Ph}_2\text{PNSiMe}_3)_2)(\text{NCy}_2)(\text{THF})]$, as discussed in Section 2.5.3 of the Literature Review.⁷ This compound is used as a starting reagent since it acts as a strong base where the amide ligand should be a strong enough base to deprotonate the di- $\lambda^5\sigma^4$ -phosphorane carbene precursor.⁷ The synthesis and structural characterisation of this compound were published by Minhas, R.K. and co-workers in 1996.¹⁶² The published molecular structure of this compound is given in Figure 3.7.

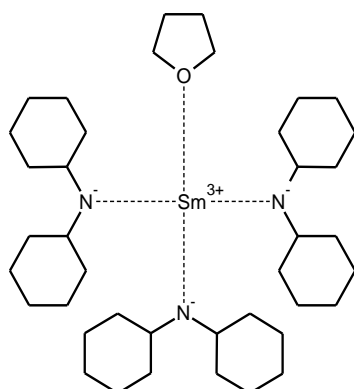


Figure 3.7: Molecular diagram of [Sm(NCy₂)₃THF]·C₆H₅CH₃.

In literature the synthesis of this compound was undertaken through a simple salt metathesis reaction as given in Scheme 3.1. The reaction was undertaken in THF and the product was separated from the LiCl by-product by recrystallisation from toluene.



Scheme 3.1: Synthesis of [Sm(NCy₂)₃THF].

The reaction undertaken in the current study was based on the published synthesis, with minor modifications. Multiple synthesis attempts were made with the one that gave the best product being described hereunder.

3.3.1.2.2.1 Reagents used

The chemicals used in the procedure described in this section were SmCl₃ (99.9%), LiNCy_{2_1} (synthesised in current study as detailed in Appendix 3), THF (dry) and toluene (dry).

3.3.1.2.2.2 [Sm(NCy₂)₃THF]·C₆H₅CH_{3_1}

A 100 ml Schlenk flask was purged under argon and charged with 0.992 g (3.86 mmol) of SmCl₃ and 10 ml dry THF. The mixture was stirred and heated to reflux overnight. This mixture was then cooled to room temperature with constant stirring and

2.166 g (11.6 mmol) of LiNCy₂_1 were added to it. This addition changed the colour of the mixture immediately to an orange colour. The resultant mixture was allowed to stir for 30 minutes. The volatiles of this reaction mixture were removed under vacuum and subsequently 50 ml dry toluene were added to the remaining solid via cannula. The orange mixture obtained in this reaction was filtered using a filtration tube set up to yield an orange filtrate and a white solid. This white solid proved to be the LiCl salt. The filtrate was then allowed to stand at -41 °C overnight yielding the precipitation of a light orange solid as the final product which was collected in an ampoule under argon and labelled [Sm(NCy₂)₃THF]·C₆H₅CH₃_1. Yield: 0.103 g, 9.17 %.

3.3.1.2.2.3 Characterisation data

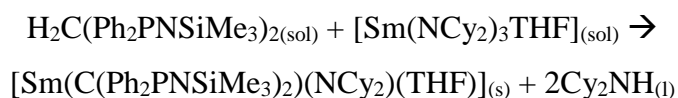
[Sm(NCy₂)₃THF]·C₆H₅CH₃_1 FT-IR (Nujol, cm⁻¹): 3564 (bs), 1458 (s), 1375 (s), 1344 (w), 1259 (m), 1144 (m), 1123 (m), 1079 (w), 1047 (w), 1027 (w), 958 (w), 889 (m), 847 (w), 800 (w), 728 (s), 694 (m).

3.3.1.3. Complexation

Lanthanide carbene complexes were prepared in the current study using the ligand, ligand precursors and lanthanide starting reagents prepared as described in Sections 3.3.1.1 and 3.3.1.2. The attempts at synthesising these lanthanide carbenes were undertaken following the procedures described in literature. On many occasions deviations from the published procedures were made.

3.3.1.3.1. Synthesis of [Sm(C(Ph₂PNSiMe₃)₂)(NCy₂)(THF)]·0.5(C₆H₅CH₃)

The synthesis of this lanthanide carbene complex was previously published by Aparna, K. and co-workers in 2000 and was one of the earliest phosphorus(V) stabilised lanthanide carbenes described in literature.⁷ This compound was synthesised in literature through the acid-base reaction of the carbene precursor H₂C(Ph₂PNSiMe₃)₂, which was used as a diprotic acid, with two of the amide ligands of the [Sm(NCy₂)₃THF]·C₆H₅CH₃ starting reagent acting as mono basic bases, as given in Scheme 3.2. The structure of this compound is given in Figure 2.22 (left). It should be noted that this compound was stable under an inert atmosphere, however it was not thermally stable.



Scheme 3.2: Synthesis of [Sm(C(Ph₂PNSiMe₃)₂)(NCy₂)(THF)].

3.3.1.3.1.1 Reagents used

The chemicals used in the procedures described in this section were SmCl₃ (99.9%), LiNCy₂_2 (synthesised in current study as detailed in Appendix 3), [Sm(NCy₂)₃THF]·C₆H₅CH₃_1 (synthesised in current study), H₂C(Ph₂PNSiMe₃)₂_2 and_3 (synthesised in current study), THF (dry) and toluene (dry).

3.3.1.3.1.2 General procedure

A 100 ml Schlenk flask was charged with 0.103 g (0.135 mmol) of [Sm(NCy₂)₃THF]·C₆H₅CH₃_1, which was suspended in 5 ml of dry toluene to give an orange-yellow suspension. Approximately 0.080 g (0.148 mmol) of H₂C(Ph₂PNSiMe₃)₂ were weighed and transferred to the orange-yellow suspension at room temperature with constant stirring. The ligand was dissolved but no further changes were observed. This reaction was left for 24 hours at room temperature. The stirred mixture was then heated in the range of 80 °C for 20 minutes. Stirring was stopped and the mixture cooled to room temperature. This was left over 2 days to form a pale yellow precipitation. This mixture was filtered using cannula filtration to yield a pale yellow filtrate and pale yellow solid as the initial products.

3.3.1.3.1.3 [Sm(C(Ph₂PNSiMe₃)₂)(NCy₂)(THF)]_1

This reaction was undergone as described prior with the following modifications. Immediately on cooling to room temperature a pale yellow suspension was formed. This was filtered using cannula filtration. The filtrate was collected, concentrated to 2 ml and allowed to stand at room temperature over 2 days. The first precipitate was analysed with IR spectroscopy and it proved to be an intractable water containing solid. Standing at room temperature over 2 days did not yield the desired crystallisation and therefore the

filtrate was cooled to -78 °C. This yielded the precipitation of a yellow solid. This solid was collected by filtration, ampouled and labelled [Sm(C(Ph₂PNSiMe₃)₂)(NCy₂)(THF)]₁. Yield: 0.034 g, 25 %.

3.3.1.3.1.4 [Sm(C(Ph₂PNSiMe₃)₂)(NCy₂)(THF)]₂

A total of 0.057 g (0.068 mmol) of [Sm(NCy₂)₃THF]·C₆H₅CH₃₁ and 0.042 g (0.075 mmol) of H₂C(Ph₂PNSiMe₃)₂₂ were used in 4 ml of dry toluene. Reaction at 80 °C was allowed for 30 minutes. Standing at room temperature over 2 days did not yield the desired crystallisation and therefore the filtrate was cooled to -78 °C. Subsequently a small crop of clear pale yellow crystals was formed. This solid was collected by removal of the majority of the solution by cannula and the small crop of crystals was transferred to an NMR tube. This was labelled as [Sm(C(Ph₂PNSiMe₃)₂)(NCy₂)(THF)]₂. Some of the mother liquor was added to the NMR tube and this was sealed under vacuum by freezing the mother liquor in liquid nitrogen. Yield: negligible.

3.3.1.3.1.5 [Sm(C(Ph₂PNSiMe₃)₂)(NCy₂)(THF)]₃

In this reaction the required [Sm(NCy₂)₃THF]·C₆H₅CH₃ starting reagent was prepared *in situ*. A 100 ml Schlenk tube was purged under inert argon and dried. This was charged with 11 ml dry THF, followed by 0.2295 g (0.894 mmol) of SmCl₃ giving a white suspension. The mixture was refluxed in the flask for 2.5 hours. To the stirred suspension at room temperature 0.5015 g (2.678 mmol) of LiNCy₂₂ were added. During addition an intense orange colour was obtained in the suspension, which turned into a yellow solution immediately after the full addition of LiNCy₂₂. This was left stirring at room temperature for 1 hour after which the THF was removed under vacuum and 13 ml dry toluene were added. After 1 hour full precipitation of the suspended LiCl_(s) by-product was obtained. The mixture obtained was filtered to a second 100 ml Schlenk flask using cannula filtration whereby a clear yellow filtrate was collected.

To this filtrate, 0.498 g (0.891 mmol) of H₂C(Ph₂PNSiMe₃)₂₃ were added and the general procedure described prior was followed. On cooling to room temperature an increase in precipitation was observed and this solution was left at 0 °C over 2 days. The

mixture obtained was filtered using a cannula filtration set up. The pale yellow precipitate was collected as the 1st precipitate of $[\text{Sm}(\text{C}(\text{Ph}_2\text{PNSiMe}_3)_2)(\text{NCy}_2)(\text{THF})]_3$. The filtrate later yielded a second precipitate. The solvent was removed by filtration and the remaining volatiles were removed by allowing the solid to dry under argon over time. A pale yellow powder was obtained as the 2nd precipitate of $[\text{Sm}(\text{C}(\text{Ph}_2\text{PNSiMe}_3)_2)(\text{NCy}_2)(\text{THF})]_3$. Yield: 0.1302 g, 14.5 %.

3.3.1.3.1.6 $[\text{Sm}(\text{C}(\text{Ph}_2\text{PNSiMe}_3)_2)(\text{NCy}_2)(\text{THF})]_4$

This attempt at preparing $[\text{Sm}(\text{C}(\text{Ph}_2\text{PNSiMe}_3)_2)(\text{NCy}_2)(\text{THF})]$ was undertaken using the moisture and oxygen scavenging set up given in Section A-1.1.3. of Appendix 1. In this reaction the required $[\text{Sm}(\text{NCy}_2)_3\text{THF}] \cdot \text{C}_6\text{H}_5\text{CH}_3$ starting reagent was prepared *in situ* as described in Section 3.3.1.3.1.5. using the same reagents: 0.2303 g (0.897 mmol) of SmCl_3 and 0.5035 g (2.689 mmol) of LiNCy_2_2 . The mixture obtained was filtered to a second 100 ml Schlenk flask using cannula filtration, whereby a clear bright yellow filtrate was collected. To this filtrate 0.4980 g (0.891 mmol) of $\text{H}_2\text{C}(\text{Ph}_2\text{PNSiMe}_3)_2_3$ were added with constant stirring. The general procedure described prior was followed. The heating at 80 °C for 20 minutes yielded a light yellow solution with a noticeable increase in turbidity. The reaction mixture was cooled to room temperature and allowed to stand for 2 days. An increase in precipitation was observed and therefore the mixture was filtered using cannula filtration to yield a colourless solution and a mixture of light yellow and off-white solids, which could not be separated. The light yellow solid mixture was collected as $[\text{Sm}(\text{C}(\text{Ph}_2\text{PNSiMe}_3)_2)(\text{NCy}_2)(\text{THF})]_4$. Yield: 0.2340 g, 26.1 %.

3.3.1.3.1.7 Characterisation data

$[\text{Sm}(\text{C}(\text{Ph}_2\text{PNSiMe}_3)_2)(\text{NCy}_2)(\text{THF})]_1$ FT-IR (KBr, cm^{-1}): 3174 (w), 1435 (m), 1258 (m), 1241 (m), 1145 (s), 1116 (s), 1085 (w), 1070 (w), 1028 (w), 889 (s), 847 (s), 828 (m), 800 (w), 772 (w), 747 cm^{-1} (w), 737 (s), 721 (s), 693 (m).

$[\text{Sm}(\text{C}(\text{Ph}_2\text{PNSiMe}_3)_2)(\text{NCy}_2)(\text{THF})]_2$ FT-IR (KBr, cm^{-1}): 3450 (bs), 1635 (bm), 1437 (s), 1175 (s), 1125 (s), 1109 (s), 1071 (w), 1026 (w), 911 (m), 756 (m), 745 (m), 722 (m), 698 (m), 692 (m).

[Sm(C(Ph₂PNSiMe₃)₂(NCy₂)(THF)]₃ FT-IR (KBr, cm⁻¹): 3353 (bs), 3086 (w), 3059 (w), 1650 (bm), 1435 (s), 1313 (s), 1260 (s), 1238 (w), 1176 (s), 1126 (s), 1109 (s), 1082 (w), 1070 (w), 1028 (m), 916 (w), 890 (w), 846 (m), 863 (m), 827 (s), 743 (m), 692 (m), 718 (m), 728 (m), 692 (s).

[Sm(C(Ph₂PNSiMe₃)₂(NCy₂)(THF)]₄ FT-IR (KBr, cm⁻¹): 3400 (bs), 3055 (w), 2929 (s), 2853 (s), 1645 (bw), 1437 (s), 1310 (w), 1253 (s), 1180 (s), 1127 (s), 1115 (s), 1070 (w), 1028 (w), 998 (s), 918 (m), 890 (m), 847 (m), 828 (w), 787 (m), 747 (s), 722 (m), 695 (s).

3.3.1.3.2. Synthesis of [Nd(C(Ph₂PNiPr)₂)(HC(Ph₂PNiPr)₂)]·2THF

The lanthanide carbene complex [Nd(C(Ph₂PNiPr)₂)(HC(Ph₂PNiPr)₂)]·2THF was of interest in the current study since it has been shown to initiate lactide polymerisation as discussed in Section 2.6.2.2.2 in the literature review. This introduces the possibility of using these lanthanide carbenes in polymerisation and catalysis. The synthesis and structural characterisation of this lanthanide carbene was first published by Buchard, A. and co-workers in 2009.⁴⁰ The structure of this complex is given in Figure 3.8.

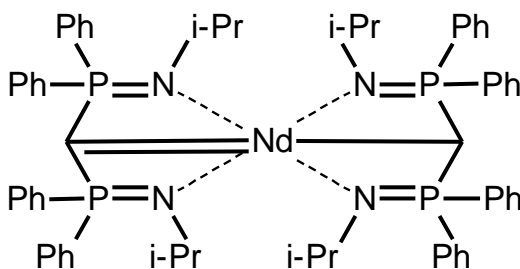
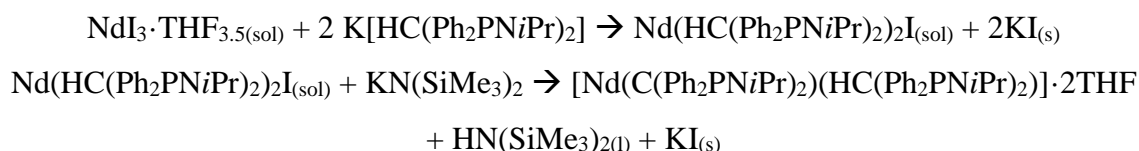


Figure 3.8: Molecular diagram of [Nd(C(Ph₂PNiPr)₂)(HC(Ph₂PNiPr)₂)]·2THF.

This synthesis was undertaken in a stepwise reaction as given in Scheme 3.3. In the first step Nd(HC(Ph₂PNiPr)₂)₂I was prepared through salt metathesis while in the second step the final complex [Nd(C(Ph₂PNiPr)₂)(HC(Ph₂PNiPr)₂)]·2THF was prepared through an acid-base reaction. In the current study the synthesis of this complex was attempted using two different modifications of the methods published by Buchard, A. and co-workers and Klemp C. and co-workers.^{40,121}



Scheme 3.3: Synthesis of [Nd(C(Ph₂PNiPr)₂)(HC(Ph₂PNiPr)₂)]·2THF.

3.3.1.3.2.1 Reagents used

The chemicals used in the procedures described in this section were NdI₃THF_{3.5_1} (synthesised in current study), [H₂C(Ph₂PNH(*i*Pr))₂]Br_{2_1} (synthesised in current study), K(HC(Ph₂PNiPr)₂)₂ (synthesised in current study), KHMDS (94-106%), THF (dry) and 40-60 °C petroleum ether (dry).

3.3.1.3.2.2 [Nd(C(Ph₂PNiPr)₂)(HC(Ph₂PNiPr)₂)]·2THF_1

The initial step of the reaction involved the preparation of K[HC(Ph₂PNiPr)₂] *in situ*. A 50 ml Schlenk tube was purged under argon, dried under vacuum and charged with 0.111 g (0.168 mmol) of [H₂C(Ph₂PNH(*i*Pr))₂]Br_{2_1}, which had been weighed under argon. To this solid 10 ml dry THF were added to yield a pale yellow solution. Subsequently, 0.101 g (0.506 mmol) of KHMDS were weighed under argon and added at room temperature to the mixture in the Schlenk tube, with constant stirring. On reaction a light yellow suspension was produced. This reaction mixture was allowed to stir for 2 hours at room temperature, after which 64 mg (0.082 mmol) of NdI₃THF_{3.5_1} were added to yield a yellow suspension. The mixture obtained was filtered using a 19/26 filtration tube set up to yield a white solid and a yellow filtrate. On analysis by IR spectroscopy it was determined that the solid was most likely the KI salt.

An amount of 0.016 g (0.080 mmol) of KHMDS were then added to the filtrate at room temperature with constant stirring and this yielded a light yellow suspension. Stirring was continued for 1 hour after which it was stopped and the mixture was filtered using a 19/26 filtration tube. This was followed by cannula filtration. These filtrations yielded an off-white solid. On analysis by IR spectroscopy it was determined that the solid was most likely the KI salt. Approximately 5 ml of dry 40-60 °C petroleum ether were then added via cannula to the filtrate and the resultant solution was cooled to -78 °C

and maintained at this temperature overnight. This yielded a grey precipitate which was collected in an ampoule and labelled as $[\text{Nd}(\text{C}(\text{Ph}_2\text{PNiPr})_2)(\text{HC}(\text{Ph}_2\text{PNiPr})_2)] \cdot 2\text{THF}_1$. Yield: Negligible.

3.3.1.3.2.3 $[\text{Nd}(\text{C}(\text{Ph}_2\text{PNiPr})_2)(\text{HC}(\text{Ph}_2\text{PNiPr})_2)] \cdot 2\text{THF}_2$

In this reaction a 100 ml Schlenk tube was charged with 0.102 g (0.189 mmol) of $\text{K}(\text{HC}(\text{Ph}_2\text{PNiPr})_2)_2$, which had been weighed under argon. This solid was dissolved in 15 ml dry THF with constant stirring to yield a slight yellow solution. Subsequently, 0.078 g (0.100 mmol) of $\text{NdI}_3\text{THF}_{3.5}_1$, which was also weighed under argon, were added at room temperature to this solution. This addition did not yield a significant change, except for the formation of a slight suspension. After 1 hour, 20 mg (0.100 mmol) of KHMDS were added to this mixture and it was allowed to stir at room temperature for 2 hours. This led to the formation of a green-brown suspension. The mixture was then filtered through a cannula filtration set up to yield an off-white solid and a yellow filtrate. On analysis by IR spectroscopy it was determined that the solid was most likely the KI salt. The volatiles in the filtrate were removed under vacuum to yield a sticky brown residue. This residue was dissolved in 5 ml 40-60 °C petroleum ether and the resultant solution cooled to -78 °C, whereby a brown suspension was obtained. On cannula filtration the solid remained a sticky brown residue. This was collected and labelled as $[\text{Nd}(\text{C}(\text{Ph}_2\text{PNiPr})_2)(\text{HC}(\text{Ph}_2\text{PNiPr})_2)] \cdot 2\text{THF}_2$. Yield: Negligible.

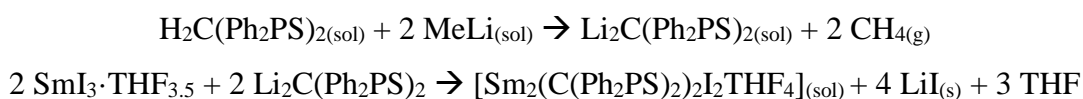
3.3.1.3.2.4 Characterisation data

$[\text{Nd}(\text{C}(\text{Ph}_2\text{PNiPr})_2)(\text{HC}(\text{Ph}_2\text{PNiPr})_2)] \cdot 2\text{THF}_1$ FT-IR (KBr, cm^{-1}): 3564 (bs), 3056 (w), 2959 (s), 2859 (s), 1620 (w), 1590 (w), 1438 (w), 1314 (w), 1297 (w), 1260 (s), 1203 (m), 1110 (m), 1076 (s), 1015 (m), 910 (s), 806 (s), 747 (m), 728 (m), 693 (m).

$[\text{Nd}(\text{C}(\text{Ph}_2\text{PNiPr})_2)(\text{HC}(\text{Ph}_2\text{PNiPr})_2)] \cdot 2\text{THF}_2$ FT-IR (KBr, cm^{-1}): 3188 (w), 3056 (w), 2962 (s), 2925 (s), 2855 (m), 1620 (w), 1590 (w), 1438 (m), 1314 (w), 1297 (w), 1261 (s), 1145 (s), 1123 (s), 1096 (s), 1021 (s), 997 (m), 888 (s), 802 (s), 747 (s), 728 (m), 692 (s).

3.3.1.3.3. Synthesis of $[\text{Sm}_2(\text{C}(\text{Ph}_2\text{PS})_2)_2\text{I}_2\text{THF}_4] \cdot 4(\text{C}_6\text{H}_5\text{CH}_3)$

The compound $[\text{Sm}_2(\text{C}(\text{Ph}_2\text{PS})_2)_2\text{I}_2\text{THF}_4]$ was first synthesised and characterised by Cantat, T. and co-workers in 2005.⁸ In the published literature the complex was prepared through a salt metathesis reaction of the lithium salt of $\text{H}_2\text{C}(\text{Ph}_2\text{PS})_2$, $\text{Li}_2\text{C}(\text{Ph}_2\text{PS})_2$, prepared *in situ* with the samarium iodide salt $\text{SmI}_3 \cdot \text{THF}_{3.5}$ in toluene and crystallised by layering the solution with diethyl ether. The complete reaction is given in Scheme 3.4.



Scheme 3.4: Synthesis of $[\text{Sm}_2(\text{C}(\text{Ph}_2\text{PS})_2)_2\text{I}_2\text{THF}_4]$.

In the current study multiple attempts were made in preparing this compound, using the procedure published by Cantat, T. and co-workers in 2005,⁸ with minor modifications. The attempts with the best yield and most interesting results are described hereunder. The structure of the expected complex is given in Figure 3.9. In the publication the compound was obtained as a solvate of toluene, with the structure $[\text{Sm}_2(\text{C}(\text{Ph}_2\text{PS})_2)_2\text{I}_2\text{THF}_4] \cdot 4(\text{C}_6\text{H}_5\text{CH}_3)$.

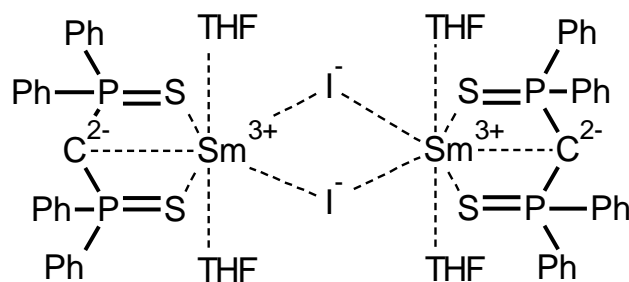


Figure 3.9: Molecular diagram of $[\text{Sm}_2(\text{C}(\text{Ph}_2\text{PS})_2)_2\text{I}_2\text{THF}_4] \cdot 4(\text{C}_6\text{H}_5\text{CH}_3)$.

3.3.1.3.3.1 Reagents used

The chemicals used in the procedures described in this section were $\text{H}_2\text{C}(\text{Ph}_2\text{PS})_{2_1}$ and $_3\text{a}$ (synthesised in current study), $\text{SmI}_3\text{THF}_{3.5_2}$ (synthesised in current study), MeLi (1.6 mol dm⁻³ in diethyl ether), toluene (dry), THF (dry), diethyl ether (dry) and n-hexane (dry).

3.3.1.3.3.2 General procedure

In this reaction a 25 ml Schlenk tube was purged and dried before being charged with 0.359 g (0.8 mmol) of $\text{H}_2\text{C}(\text{Ph}_2\text{PS})_2$ and 6 ml of dry toluene, yielding a white suspension. The mixture was cooled to $-78\text{ }^\circ\text{C}$, with constant stirring. When the mixture reached this temperature 1 ml (1.6 mmol) of 1.6 mol dm^{-1} MeLi in diethyl ether was added via a 5 ml glass syringe. The resultant mixture was then left to equilibrate to room temperature to yield a yellow solution with a slight turbidity. Subsequently 0.628 g (0.802 mmol) of $\text{SmI}_3\text{THF}_{3.5_2}$ were added to the solution to yield a bright yellow suspension. This was left stirring at room temperature overnight and afterwards filtered using a 19/26 filtration tube set up, to yield a light yellow solid and a yellow filtrate. This solid, expected to be LiI, was labelled as $[\text{Sm}_2(\text{C}(\text{Ph}_2\text{PS})_2)_2\text{I}_2\text{THF}_4]\cdot 4(\text{C}_6\text{H}_5\text{CH}_3)$ _1a, _2a, _3a and _4a for respective reactions. The yield of each of these four solids was calculated assuming that the solid was anhydrous LiI, giving values $> 100\%$. This indicated the presence of hydrates of LiI and/or mixtures of various products and side products of the reaction. Both these possibilities were confirmed by IR spectroscopy. Different work up procedures of the yellow filtrate were undergone for each reaction described and therefore these are given in the relevant sections hereunder. Further reactions and work up were also undertaken using $[\text{Sm}_2(\text{C}(\text{Ph}_2\text{PS})_2)_2\text{I}_2\text{THF}_4]\cdot 4(\text{C}_6\text{H}_5\text{CH}_3)$ _2a and _4a, as described hereunder, in attempts to collect samarium complexes of $\text{H}_2\text{C}(\text{Ph}_2\text{PS})_2$ derivatives from the mixture of compounds obtained.

3.3.1.3.3.3 $[\text{Sm}_2(\text{C}(\text{Ph}_2\text{PS})_2)_2\text{I}_2\text{THF}_4]\cdot 4(\text{C}_6\text{H}_5\text{CH}_3)$ _1

The filtrate was layered using 10 ml of dry THF and left overnight at room temperature to yield a yellow paste. A cannula filtration setup was used to collect this residue. The solid was labelled as $[\text{Sm}_2(\text{C}(\text{Ph}_2\text{PS})_2)_2\text{I}_2\text{THF}_4]\cdot 4(\text{C}_6\text{H}_5\text{CH}_3)$ _1b. Analysis by plane polarised light microscopy indicated that the solid was an amorphous paste. $[\text{Sm}_2(\text{C}(\text{Ph}_2\text{PS})_2)_2\text{I}_2\text{THF}_4]\cdot 4(\text{C}_6\text{H}_5\text{CH}_3)$ _1b was afterwards dissolved in 2 ml of dry toluene and 10 ml dry n-hexane to yield a white powder which was collected by filtration. This third solid was labelled as $[\text{Sm}_2(\text{C}(\text{Ph}_2\text{PS})_2)_2\text{I}_2\text{THF}_4]\cdot 4(\text{C}_6\text{H}_5\text{CH}_3)$ _1c. Yield $[\text{Sm}_2(\text{C}(\text{Ph}_2\text{PS})_2)_2\text{I}_2\text{THF}_4]\cdot 4(\text{C}_6\text{H}_5\text{CH}_3)$ _1a: 0.785 g, 366 %. Yield $[\text{Sm}_2(\text{C}(\text{Ph}_2\text{PS})_2)_2\text{I}_2\text{THF}_4]\cdot 4(\text{C}_6\text{H}_5\text{CH}_3)$ _1b: Negligible. Yield $[\text{Sm}_2(\text{C}(\text{Ph}_2\text{PS})_2)_2\text{I}_2\text{THF}_4]\cdot 4(\text{C}_6\text{H}_5\text{CH}_3)$ _1c: 0.185 g, 21.9 %.

3.3.1.3.3.4 [Sm₂(C(Ph₂PS)₂)₂I₂THF₄].4(C₆H₅CH₃)₂

On addition of SmI₃THF_{3.5}₂ the reaction was left stirring for 3 hours instead of overnight. The first solid [Sm₂(C(Ph₂PS)₂)₂I₂THF₄].4(C₆H₅CH₃)₂a was a pale yellow waxy solid rather than a light yellow solid. The filtrate was concentrated under vacuum to approximately half its volume and 12 ml of dry diethyl ether were then added to it, to yield a white precipitate, which was collected and labelled as [Sm₂(C(Ph₂PS)₂)₂I₂THF₄].4(C₆H₅CH₃)₂b.

In a different set-up, 0.308 g of the product [Sm₂(C(Ph₂PS)₂)₂I₂THF₄].4(C₆H₅CH₃)₂a were suspended in toluene to yield a yellow suspension which was filtered. The solid obtained was a bright yellow solid and it was collected and labelled as [Sm₂(C(Ph₂PS)₂)₂I₂THF₄].4(C₆H₅CH₃)₂a₁, while the filtrate remained a clear, colourless filtrate. This solid was ampouled under argon and the colour was observed to change from a bright yellow to orange. All the volatiles from the filtrate were removed under vacuum to yield a gelatinous solid in which crystallites were observed when the product, labelled as [Sm₂(C(Ph₂PS)₂)₂I₂THF₄].4(C₆H₅CH₃)₂a₂, was inspected under a microscope. Yield [Sm₂(C(Ph₂PS)₂)₂I₂THF₄].4(C₆H₅CH₃)₂a: 0.665 g, 309 %. Yield [Sm₂(C(Ph₂PS)₂)₂I₂THF₄].4(C₆H₅CH₃)₂b: 0.276 g, 32.7 %. Yield [Sm₂(C(Ph₂PS)₂)₂I₂THF₄].4(C₆H₅CH₃)₂a₁: 0.221 g, 26.1 %. Yield [Sm₂(C(Ph₂PS)₂)₂I₂THF₄].4(C₆H₅CH₃)₂a₂: 0.154 g, 18.2 %.

3.3.1.3.3.5 [Sm₂(C(Ph₂PS)₂)₂I₂THF₄].4(C₆H₅CH₃)₃

The yellow filtrate was left to stand overnight and precipitation was observed. Filtration yielded a white solid and a clear colourless filtrate. The latter filtrate was left to stand for a week at room temperature, after which a small crop of crystals was produced. The white solid was collected and labelled as [Sm₂(C(Ph₂PS)₂)₂I₂THF₄].4(C₆H₅CH₃)₃b₁, while the small crop of crystals was collected and labelled as [Sm₂(C(Ph₂PS)₂)₂I₂THF₄].4(C₆H₅CH₃)₃b₂. Yield [Sm₂(C(Ph₂PS)₂)₂I₂THF₄].4(C₆H₅CH₃)₃a: 0.298 g, 139 %. Yield [Sm₂(C(Ph₂PS)₂)₂I₂THF₄].4(C₆H₅CH₃)₃b₁: 0.254 g, 30.1 %. Yield [Sm₂(C(Ph₂PS)₂)₂I₂THF₄].4(C₆H₅CH₃)₃b₂: Negligible.

3.3.1.3.3.6 [Sm₂(C(Ph₂PS)₂)₂I₂THF₄].4(C₆H₅CH₃)₄

In this attempt 0.126 g (0.281 mmol) of H₂C(Ph₂PS)₂_3a, 2 ml of dry toluene and 0.4 ml (0.64 mmol) of 1.6 moldm⁻¹ MeLi in diethyl ether were used in the deprotonation reaction of H₂C(Ph₂PS)₂. A second 25 ml Schlenk tube was charged with 0.220 g (0.281 mmol) of SmI₃THF_{3.5}_2 and the solution prepared prior was added via cannula to the stirred solid. This yielded a pale yellow suspension. This was left stirring at room temperature for 1.5 hours and afterwards filtered using a 19/26 filtration tube set up, to yield a very pale yellow residue, expected to be LiI, which was collected and labelled as [Sm₂(C(Ph₂PS)₂)₂I₂THF₄].4(C₆H₅CH₃)₄a, along with a yellow filtrate. The filtrate was allowed to stand over a week, after which a small crop of very pale yellow crystals was produced. These were collected and labelled as [Sm₂(C(Ph₂PS)₂)₂I₂THF₄].4(C₆H₅CH₃)₄b.

The solid [Sm₂(C(Ph₂PS)₂)₂I₂THF₄].4(C₆H₅CH₃)₄a was dissolved in 2 ml of dry toluene and the mixture was cooled to -78 °C. Afterwards 0.6 ml (0.96 mmol) of 1.6 moldm⁻¹ of MeLi in diethyl ether were added to this mixture to yield a yellow suspension. This suspension was left to equilibrate to room temperature and then left stirring overnight. This mixture was filtered via cannula to yield a white powder and a golden yellow filtrate. The solid was collected and labelled as [Sm₂(C(Ph₂PS)₂)₂I₂THF₄].4(C₆H₅CH₃)₄a_1. The resultant filtrate was layered with 10 ml of dry diethyl ether to yield a yellow suspension which on filtration gave a pale yellow gelatinous solid, which was collected and labelled as [Sm₂(C(Ph₂PS)₂)₂I₂THF₄].4(C₆H₅CH₃)₄a_2.

Yield [Sm₂(C(Ph₂PS)₂)₂I₂THF₄].4(C₆H₅CH₃)₄a: 0.099 g, 132 %. Yield [Sm₂(C(Ph₂PS)₂)₂I₂THF₄].4(C₆H₅CH₃)₄b: Negligible. Yield [Sm₂(C(Ph₂PS)₂)₂I₂THF₄].4(C₆H₅CH₃)₄a_1: 0.067 g, 22.61 %. Yield [Sm₂(C(Ph₂PS)₂)₂I₂THF₄].4(C₆H₅CH₃)₄a_2: Negligible.

3.3.1.3.3.7 Characterisation data

[Sm₂(C(Ph₂PS)₂)₂I₂THF₄].4(C₆H₅CH₃)₄_1a, _1c, _2a_2, _3a, _3a_1, _3b_1 FT-IR (KBr, cm⁻¹): 3455 (bs), 1606 (bs), 1435 (s), 1308 (w), 1261 (w), 1153 (w), 1126 (w), 1103 (s), 1064 (w), 1040 (w), 1028 (w), 997 (w), 782 (s), 772 (s), 752 (m), 732 (s), 707 (w), 689 (s), 623 (s), 613 (m), 594 (w).

[Sm₂(C(Ph₂PS)₂)₂I₂THF₄]·4(C₆H₅CH₃)_1c, _2a, _4a, _4a_1 FT-IR (KBr, cm⁻¹): 1734 (w), 1431 (s), 1371 (s), 1165 (w), 1153 (w), 1114 (w), 1101 (s), 1070 (w), 1025 (w), 997 (w), 801 (s), 770 (s), 744 (sh), 736 (s), 721 (sh), 708 (m), 688 (m), 619 (m), 602 (s). ¹H NMR (CDCl₃): 7.82 ppm (m, 2H, o-H), 7.42 ppm (m, 1H, p-H), 7.34 ppm (m, 2H, m-H), 3.98 ppm (t, J = 13.45 Hz, 0.5H, PCH₂P), 3.48 ppm (q, 1H, CH₂(DEE)) 1.21 ppm (t, 2H, CH₃(DEE))

[Sm₂(C(Ph₂PS)₂)₂I₂THF₄]·4(C₆H₅CH₃)_1b FT-IR (KBr, cm⁻¹): 3416 (bs), 3051 (w), 2962 (s), 2878 (s), 2692 (w), 1619 (bw), 1458 (s), 1377 (s), 1292 (w), 1236 (w), 1186 (m), 1102 (s), 1042 (s), 914 (s), 890 (s), 784 (m), 731 (s), 692 (m), 645 (m) 629 (m), 614 (m), 597 (sh), 585 (w).

[Sm₂(C(Ph₂PS)₂)₂I₂THF₄]·4(C₆H₅CH₃)_2a_1 FT-IR (KBr, cm⁻¹): 3420 (bs), 1615 (bm), 1520 (s), 1402 (s), 1140 (w), 1102 (w), 1022 (w), 916 (w), 889 (w).

[Sm₂(C(Ph₂PS)₂)₂I₂THF₄]·4(C₆H₅CH₃)_2b FT-IR (KBr, cm⁻¹): 3433 (bs), 1616 (bs), 1435 (s), 1261 (s), 1154 (w), 1101 (s), 1062 (w), 1025 (m), 817 (sh), 799 (s), 785 (s), 771 (m), 746 (w), 737 (s), 687 (s), 585 (w). ¹H NMR (CDCl₃): 7.82 ppm (m, 2H, o-H), 7.42 ppm (m, 1H, p-H), 7.34 ppm (m, 2H, m-H), 3.98 ppm (t, J = 13.45 Hz, 0.5H, PCH₂P), 3.48 ppm (q, 1H, CH₂(DEE)) 1.21 ppm (t, 2H, CH₃(DEE))

[Sm₂(C(Ph₂PS)₂)₂I₂THF₄]·4(C₆H₅CH₃)_3b_2 FT-IR (KBr, cm⁻¹): 1170 (w), 1152 (w), 1084 (w), 1017 (w), 935 (w), 917 (w), 890 (w), 845 (w), 799 (w), 770 (w). ¹H NMR (C₆D₆): 7.89 ppm (m, 4H, o-H), 6.92 ppm (m, 6H, m/p-H and the triplet at 3.84 ppm (t, J = 13.55 Hz, 1H, PCH₂P)

[Sm₂(C(Ph₂PS)₂)₂I₂THF₄]·4(C₆H₅CH₃)_4a_2 FT-IR (KBr, cm⁻¹): 3029 (w), 2962 (s), 2905 (m), 2862 (m), 1260 (s), 1101 (s), 1026 (s), 864 (m), 728 (m), 705 (sh) 695 (s), 605 (w), 542 (w).

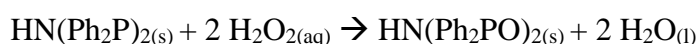
3.3.2. Synthesis of Lanthanide non-carbene di-λ⁵σ⁴-phosphorane complexes

3.3.2.1. Ligand synthesis

As with the ligands and ligand precursors prepared for the preparation of lanthanide carbenes the ligand and ligand precursors prepared for these non-carbene lanthanide complexes were prepared using previously published methods. In many cases the methods published were modified to obtain better results.

3.3.2.1.1. Synthesis of HN(Ph₂PO)₂

The synthesis of HN(Ph₂PO)₂ and various other HN(R₂PO)₂ analogues are attested in literature.^{38,238,277} These are typically published in studies dealing with the complexation of these HN(R₂PO)₂ analogues. The basic synthesis used in many of these publications is the oxidation of N,N-bis(diphenylphosphino)amine (HN(Ph₂P)₂), as given in the Scheme 3.5.



Scheme 3.5: Synthesis of HN(Ph₂PO)₂.

The HN(Ph₂PO)₂ ligand itself is not moisture or oxygen sensitive and therefore could be handled using aqueous solutions in normal laboratory conditions. However, synthesis was still undergone under an inert atmosphere due to the moisture sensitivity of the starting reagent, HN(Ph₂P)₂. The molecular diagram of the expected product HN(Ph₂PO)₂ is given in Figure 3.10.

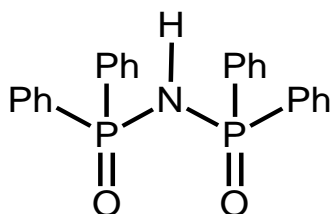


Figure 3.10: Molecular diagram of the ligand HN(Ph₂PO)₂.

3.3.2.1.1.1 Reagents used

The chemicals used in the procedure described in this section were HN(Ph₂P)₂ (98%), H₂O_{2(aq)} (30% w/w), THF (dry), chloroform (GPR, used as purchased) and methanol (GPR, used as purchased).

3.3.2.1.1.2 HN(Ph₂PO)₂_1

A 25 ml Schlenk flask was set up with a magnetic stirring bar and charged with 1 g (2.6 mmol) of HN(Ph₂P)₂. Via cannula, 5 ml dry THF were added and the solid reagent dissolved to yield a clear colourless solution. This solution was cooled down to 0 °C via an ice bath. Using a glass pipette, 0.6 ml (5.7 mmol) of 30% w/w aqueous hydrogen peroxide were added dropwise to the solution. This immediately gave a white precipitate. The mixture was left to stir for 1 hour at room temperature. The reaction solution was filtered using a filtration tube and the white solid that was collected was washed with 20 ml water. The solid was recrystallised in a mixture of 20 ml CHCl₃ and 5 ml methanol and left in a refrigerator at 8 °C for 16 hours. This procedure yielded a white crystalline mass as a product, labelled HN(Ph₂PO)₂_1. Yield: 0.897 g, 82 %.

3.3.2.1.1.3 Characterisation data

HN(Ph₂PO)₂_1 FT-IR (KBr, cm⁻¹): 3104 (bs), 1645 (s), 1437 (s), 1325 (m), 1309 (w), 1227 (w), 1180 (w), 1148 (s), 1110 (s), 1089 (s), 939 (m), 928 (s), 923 (s), 784 (m), 754 (m), 742 (m), 740 (m), 689 (s), 649 (m), 638 (m), 625 (s) 575 (w). ¹H NMR (CDCl₃): 7.83 ppm (dd, J₁ = 7.75 Hz and ³J_{HP} = 12.67 Hz, 8H, o-H), 7.41 ppm (t, J₁ = 7.75 Hz, 4H, p-H) and 7.32 ppm (m, 8H, m-H). MP: 274.1–276.1 °C.

3.3.2.1.2. Synthesis of HN(Ph₂PS)₂

In the investigation of the complexation of di-λ⁵σ⁴-phosphorane compounds which are more stable than the respective carbenes, it was of interest to study the complexation of the compound HN(Ph₂PS)₂, having the structure given in Figure 3.11. This compound is the thio analogue of HN(Ph₂PO)₂. The synthesis of HN(Ph₂PS)₂ was first published by Wang and co-workers, in 1978.²⁷⁸ In the published reaction bis(diphenylphosphino)imine (HN(Ph₂P)₂) was reacted with elemental Sulphur in toluene and the crude product was washed with toluene, petroleum ether and carbon disulfide and then recrystallised from iso-propanol. The reaction was a simple oxidation of the phosphorus centers in HN(Ph₂P)₂ with Sulphur, as given in Scheme 3.6. The reaction described hereunder is a modification of the reaction published previously.

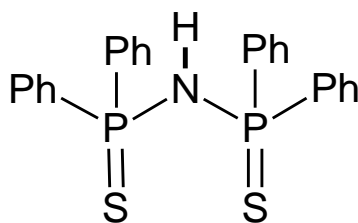


Figure 3.11: Molecular diagram of HN(Ph₂PS)₂.



Scheme 3.6: Synthesis of HN(Ph₂PS)₂.

3.3.2.1.2.1 Reagents used

The chemicals used in the procedure described in this section were HN(Ph₂P)₂ (98%), sulphur (GPR), toluene (dry), diethyl ether (dry), *iso*-propanol (GPR, used as purchased) and chloroform (GPR, used as purchased).

3.3.2.1.2.2 HN(Ph₂PS)_{2_1}

A 25 ml Schlenk flask, equipped with a Liebig condenser, was charged with 1g (2.6 mmol) of HN(Ph₂P)₂ and 0.183 g (5.7 mmol) of Sulphur. The reagents were dissolved by adding 5 ml of the dried toluene to the solid mixture, via cannula. The solution was stirred for 15 minutes at room temperature, after which it was refluxed for 4 hours at 100 °C. Subsequently, the solution was cooled down to 0 °C, yielding a white precipitate. The mixture was filtered using a filtration tube and the precipitate was washed with 10 ml of toluene and 10 ml diethyl ether. The crude solid was recrystallised in a mixture of 10 ml *iso*-propanol and 5 ml chloroform, yielding a colourless crystalline solid. Yield: 0.783 g, 69 %.

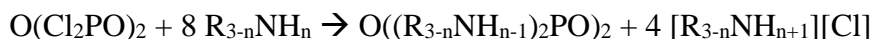
3.3.2.1.2.3 Characterisation data

HN(Ph₂PS)_{2_1} FT-IR (KBr, cm⁻¹): 3030 (bs), 2631 (m), 1972 (w), 1910 (w), 1829 (w), 1585 (m), 1478 (m), 1438 (s), 1325 (s), 1309 (m), 1180 (m) 1162 (w), 1106 (s) 1074 (w), 1023 (w), 996 (m), 937 (w), 924 (s), 785 (s), 742 (s), 717 (s), 687 (s), 648 (s), 613 (s),

569 (m), 532 (s), 499 (s), 491 (m), 477 (m), 462 (m), 408 (m). ^1H NMR (CDCl_3): 7.89 ppm (ddt, $J_1 = 6.94$ Hz and $^3J_{\text{HP}} = 12.59$ Hz, 1.95H, o-H), 7.43 ppm (m, 1H, p-H), 7.34 ppm (m, $J_1 = 3.43$ Hz and $J_2 = 7.59$ Hz, 2.02H, m-H). MP: 212–213 °C.

3.3.2.1.3. Synthesis of $\text{O}((\text{Et}_2\text{N})_2\text{PO})_2$

In this study the preparation of $\text{O}((\text{Et}_2\text{N})_2\text{PO})_2$ was undergone using a modification on the synthesis of the analogous pesticide Schradan, $\text{O}((\text{Me}_2\text{N})_2\text{PO})_2$; the synthesis of which was described by Goehring and Niedenzu in 1956.^{199,211} The general reaction for the formation of the analogous compounds having a structure of $\text{O}((\text{R}_{3-n}\text{NH}_{n-1})_2\text{PO})_2$, which include the published Schradan and its analogues, is given in Scheme 3.7. This reaction could be undertaken using primary and secondary amines, where $n = 1$ or 2 .



Scheme 3.7: General synthesis reaction for the preparation of $\text{O}((\text{R}_{3-n}\text{NH}_{n-1})_2\text{PO})_2$ compounds.

In the case of Schradan, literature describes that this compound was prepared by reacting the two reagents at decreased temperatures, without the use of a solvent. The desired product was then extracted using ether and afterwards vacuum distillation.¹⁹⁹ In the preparations undertaken in this study and recorded below, the reaction was undergone in an argon atmosphere due to the moisture sensitivity of the starting reagent pyrophosphoryl tetrachloride (PPTC). The molecular diagram of the expected product $\text{O}((\text{Et}_2\text{N})_2\text{PO})_2$ is given in Figure 3.12.

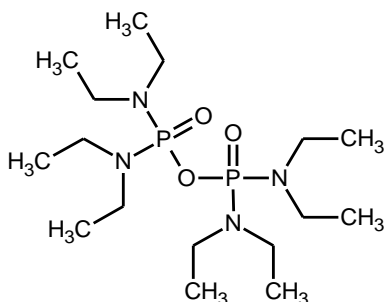


Figure 3.12: Molecular diagram of $\text{O}((\text{Et}_2\text{N})_2\text{PO})_2$.

3.3.2.1.3.1 Reagents used

The chemicals used in the procedure described in this section were PPTC (purified and stored as described in Appendix 4), diethylamine (GPR), methanol (HPLC, dried over 3 Å molecular sieves), chloroform (GPR, dried over 4 Å molecular sieves), n-pentane (GPR, dried over 4 Å molecular sieves), dichloromethane (GPR, used as purchased), diethyl ether (GPR, used as purchased), acetonitrile (GPR, used as purchased) and dimethylformamide (GPR, used as purchased).

3.3.2.1.3.2 (O((Et₂N)₂PO)₂_1

For this attempt a 100 ml Schlenk tube was charged with 7.6 ml (0.073 mol) diethyl amine dissolved in 10 ml of chloroform as a solvent. The amount of amine used was in excess of that required. This mixture was cooled to -78 °C using a dry ice-acetone bath and stirred using a magnetic stirrer. When the required temperature was reached, 1 ml (0.007 mol) PPTC was added dropwise to the reaction solution using a glass syringe. After addition of the PPTC the cooling bath was removed and the reaction mixture was allowed to react at room temperature overnight, with continuous stirring. This yielded a thick wine coloured suspension. Approximately 15 ml of n-pentane were added to this mixture via a glass syringe to yield a wine coloured suspension and this was left overnight to allow precipitation. The suspension was filtered via a series of cannula filtrations to remove the colourless precipitates that formed after each filtration. Finally, after a filtration from which very little precipitation occurred, the volatile solvents (chloroform and n-pentane) were removed under vacuum at 50 °C. This yielded a viscous wine liquid, labelled as (O((Et₂N)₂PO)₂_1.

The product (O((Et₂N)₂PO)₂_1 was analysed by ³¹P-NMR spectroscopy and it was revealed to contain numerous phosphorus species. Therefore, it was decided that column chromatography would be the best method to separate these species. Column chromatography of a sample of O((Et₂N)₂PO)₂_1 in dichloromethane was undertaken using a column of 6 g activated Keisegel 60, and using diethyl ether as the eluent. This was undertaken under normal atmosphere. Given the volume of the column, fractions were collected each having a volume of 12 ml, unless otherwise specified. Details of the chromatography are given in Table 3.1.

Table 3.1: Details of the column chromatography fractions of O((Et₂N)₂PO)₂_1.

Fraction	Notes
1	Clear fraction, little movement of the coloured band
2	
3	
4	
5	
6	
7	
8	
9	
10	After collection eluent changed to acetonitrile
11	Clear fraction, movement of a pink band
12	
13	Pink fraction collected, with a total volume of 60 ml
14	Clear fraction, movement of a second pink band
15	After collection eluent changed to DMF
16	Pink fraction collected, with a total volume of 20 ml

In each case the volatiles were removed by evaporation at room temperature and pressure for two days. Fraction 13 yielded a dark pink viscous liquid. A small number of colourless single crystals were obtained from the pink viscous liquid O((Et₂N)₂PO)₂_1_f13 (fraction 13). Yield O((Et₂N)₂PO)₂_1: 2.130 g (1.8 ml), 75 %.

3.3.2.1.3.3 Characterisation data

O((Et₂N)₂PO)₂_1 FT-IR (NaCl, cm⁻¹): 3425 (bm), 2972 (s), 2931 (s), 2873 (s) 2722 (bw), 2481 (bm), 2404 (w), 1632 (bw), 1466 (s), 1381 (s), 1350 (sh), 1294 (m), 1240 (s), 1211 (s), 1194 (w), 1175 (s), 1102 (s), 1064 (m), 1027 (s), 957 (s), 930 (s), 902 (s), 790 (s), 751 (s), 716 (s), 662 (s). ¹H NMR (CDCl₃): 9.90 ppm (bs, 0.12H), 3.16 ppm (bs, 4.39H), 3.07 ppm (bs, 4.52H), 3.11 ppm (bd, J = 43.11 Hz, 8.90H), 2.95 ppm (t, J = 7.25 Hz, 0.68H), 1.39 ppm (t, J = 7.38 Hz, 1.00H), 1.13 ppm (t, J = 7.15 Hz, 13.8H). ³¹P{¹H} NMR (CDCl₃): 8.45 ppm (s). GC-MS (EI; 70 eV) m/z: 71.99 m/z, 72.14 m/z, 191.09 m/z, 209.15 m/z, 280.23 m/z, 326.18 m/z, 398.30 m/z [M⁺].

O((Et₂N)₂PO)₂_1_f13 FT-IR (NaCl, cm⁻¹): 2971 (m), 2929 (m), 2874 (w), 2722 (bw), 1432 (s), 1381 (s), 1360 (sh), 1315 (w), 1240 (s), 1211 (s), 1194 (w), 1170 (s), 1102 (w), 1064 (w), 1027 (s), 958 (m), 930 (m), 902 (s), 790 (s), 751 (s), 716 (s), 662 (s). ¹H NMR (CDCl₃): 3.10 ppm (bd, J = 40.11 Hz, 1H, CH₂), 1.12 ppm (t, J = 7.15 Hz, 1.37H, CH₃) ³¹P{¹H} NMR (CDCl₃): 9.38 ppm (s). GC-MS (EI; 70 eV) m/z: 71.99, 72.14, 191.09, 209.15, 280.23, 326.18, 398.30 [M⁺].

3.3.2.1.4. Synthesis of O((iPrNH)₂PO)₂

As in the case of the preparation of O((Et₂N)₂PO)₂, described in Section 3.3.2.1.3, the synthesis of O((iPrNH)₂PO)₂ in this study was undergone using a modification on the synthesis of the analogous pesticide Schradan, O((Me₂N)₂PO)₂; the synthesis of which was described by Goehring and Niedenzu in 1956.^{199,211} The general reaction for the formation of the analogous compounds having a structure of O((R_{3-n}NH_{n-1})₂PO)₂, which include the published Schradan and its analogues, is given in Scheme 3.7. In the preparations undertaken in this study and recorded below, the reaction was undergone in an argon atmosphere due to the moisture sensitivity of the starting reagent pyrophosphoryl tetrachloride (PPTC). The molecular diagram of the expected product O((iPrNH)₂PO)₂ is given in Figure 3.13. The reaction was attempted several times using slight variations in the methodology and different product batches were prepared. The reaction that gave the most noteworthy products is described hereunder.

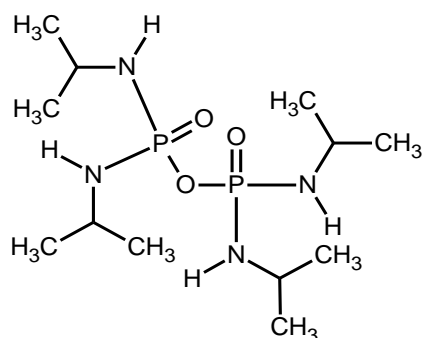


Figure 3.13: Molecular diagram of $O((iPrNH)_2PO)_2$.

3.3.2.1.4.1 Reagents used

The chemicals used in the procedure described in this section were PPTC (purified and stored as described in Appendix 4), *iso*-propylamine (99%), chloroform (GPR, dried over 4 Å molecular sieves), 30-40 °C petroleum ether (GPR, used as purchased), dichloromethane (GPR, used as purchased), diethyl ether (GPR, used as purchased), THF (GPR, used as purchased) and acetonitrile (GPR, used as purchased).

3.3.2.1.4.2 $O((iPrNH)_2PO)_2$ _1

For this reaction a 100 ml Schlenk tube was charged with 5 ml (0.058 mol) *iso*-propyl amine dissolved in 10 ml of chloroform as a solvent. The amount of amine used was in excess of that required. This mixture was cooled to -78 °C using a dry ice-acetone bath and stirred at 200 rpm using a magnetic stirrer. When the required temperature was reached, 1 ml (0.007 mol) PPTC was added dropwise to the reaction solution using a glass syringe. The formation of white fumes was observed during the addition of the PPTC, along with the formation of a solid crystalline mass. The stirred reaction mixture was allowed to react at room temperature overnight. On reaching room temperature the solid melted to give a thick white suspension and this was subsequently heated to 60 °C for 3 hours to complete the reaction. This reaction yielded a pale yellow solution. After leaving this solution overnight, the formation of clear colourless single crystals was observed.

The mixture was filtered via cannula filtration. The crystals were collected and labelled as $O((iPrNH)_2PO)_2$ _1_a. On characterisation by IR and 1H NMR spectroscopy this solid proved to be the expected salt by-product *iPrNH*₃Cl. The filtrate was

concentrated and layered with diethyl ether. This yielded crystallisation overnight. The crystals were collected by cannula filtration and labelled $O((iPrNH)_2PO)_2_1_b$ and the filtrate was again layered using 30-40 petroleum ether. This yielded another residue, labelled as $O((iPrNH)_2PO)_2_1_c1$. The filtrate showed further crystallisation after it was left standing at room temperature for a number of weeks. This product was labelled $O((iPrNH)_2PO)_2_1_c2$. A sample of $O((iPrNH)_2PO)_2_1_b$ was recrystallized by dissolving in $CHCl_3$ and layering with petroleum ether to yield crystalline $O((iPrNH)_2PO)_2_1_b1$.

The product $O((iPrNH)_2PO)_2_1_c1$ was analysed by ^{31}P NMR spectroscopy and it was revealed to contain numerous phosphorus species. Therefore, it was decided that column chromatography would be the best method to separate these species. Column chromatography was undergone on a sample of the amorphous solid, $O((iPrNH)_2PO)_2_1_c1$. A sample of the solid was dissolved in dichloromethane and passed through a column of 6 g activated Keiselgel 60 as the stationary phase. Diethyl ether was used as the eluent. This technique was undertaken under normal atmospheric conditions. Given the volume of the column, fractions were collected each having a volume of 12 ml, unless otherwise specified. Details of the chromatography are given in Table 3.2.

Table 3.2: Details of the column chromatography fractions of $O((iPrNH)_2PO)_2_1_c1$

Fraction	Notes
1	Contains 1 st band visible in the column, no UV luminescence noted
2	After collection eluent changed to a 1:3 by volume THF/diethyl ether mixture
3	During collection a number of new bands became visibly separated
4	Contains 2 nd band obtained
5	
6	
7	After collection eluent changed to a 1:1 by volume THF/acetonitrile mixture
8	

9	No movement of final band obtained
10	
11	
12	
13	
14	
15	
16	3 rd band was collected by flushing column with 50 ml of the current eluent

In each case the volatiles were removed by evaporation at room temperature and pressure for a number of days. The fractions 5, 7, 9, 10, and 15 proved interesting, yielding solid products, both amorphous and crystalline. Given the small amount of products $O((iPrNH)_2PO)_2_1_b1$, $O((iPrNH)_2PO)_2_1_c1$ and $O((iPrNH)_2PO)_2_1_c2$ obtained the yield for these could not be calculated. Yield $O((iPrNH)_2PO)_2_1_b$: 0.975 g, 40.6 %.

3.3.2.1.4.3 Characterisation data

$O((iPrNH)_2PO)_2_1_b, _1_b1$ FT-IR (KBr, cm^{-1}): 3400 (w), 3252 (sb), 2965 (s), 2870 (m), 1637 (m), 1527 (m), 1466 (m), 1432 (m), 1396 (m), 1367 (m), 1257 (s), 1229 (s), 1167 (m), 1137 (w), 1055 (s), 1026 (s), 945 (m), 914 (m), 886 (s), 804 (m), 750 (m). 1H NMR ($CDCl_3$): 8.31 ppm (s, 1H, NH_3), 3.64 ppm (td, 1.17H, CH), 3.40 ppm (m, 1H, CH), 2.26 ppm (s, 1.17H, NH), 1.39 ppm (d, 2.39H, CH_3) and at 1.14 ppm (t, 6.15H, CH_3). $^{31}P\{^1H\}$ NMR ($CDCl_3$): 14.33 ppm (s). GC-MS (EI; 70 eV) m/z: 44.12, 58.08, 79.01, 93.97, 137.07, 179.10 [$(iPrNH)_2PO_2$]⁺, 195.16.

$O((iPrNH)_2PO)_2_1_c1_{f10}$ FT-IR (KBr, cm^{-1}): 3414 (w), 3255 (bm), 2965 (s), 2870 (m), 1465 (m), 1428 (m), 1367 (m), 1257 (s), 1205 (s), 1167 (m), 1137 (m), 1051 (s), 1021 (s), 916 (m), 886 (m), 833 (sh), 800 (vw), 771 (m). 1H NMR ($CDCl_3$): 3.37 (m, 1H, CH), 2.29 (bt, 0.96H, NH), 1.16 (t, 6.28H, CH_3). $^{31}P\{^1H\}$ NMR ($CDCl_3$): 14.33 ppm (s). GC-MS (EI; 70 eV) m/z: 44.12, 58.11, 79.01, 93.93, 137.09, 179.10 [$(iPrNH)_2PO_2$]⁺, 195.16.

3.3.2.2. Complexation

Complexation of $[\text{N}(\text{Ph}_2\text{PO})_2]^-$, $[\text{N}(\text{Ph}_2\text{PS})_2]^-$ and $\text{O}((\text{Et}_2\text{N})_2\text{PO})_2$ were all attempted in the current study using preparations modified from procedures published in literature.

3.3.2.2.1. Synthesis of $[\text{Eu}(\text{N}(\text{Ph}_2\text{PO})_2)_3]$

The complex $[\text{Eu}(\text{N}(\text{Ph}_2\text{PO})_2)_3]$ has been studied by various groups, both in structural studies and in luminescence studies.^{32,240,244} Two main crystal structures have been published for this compound, namely $[\text{Eu}(\text{N}(\text{Ph}_2\text{PO})_2)_3]$ and $[\text{Eu}(\text{N}(\text{Ph}_2\text{PO})_2)_3] \cdot 0.67(\text{H}_2\text{O})$. The first structure was published by Pietraszkiewicz and co-workers in 2012, whilst the second structure was published by Magennis and co-workers in 1999.^{240,244} In each case the potassium salt $[\text{K}][\text{N}(\text{Ph}_2\text{PO})_2]$ was reacted with $\text{EuCl}_3 \cdot 6(\text{H}_2\text{O})$ in an aqueous solution, in a molar ratio of 3:1 yielding a crystalline white precipitate. The molecular structure of the complex present in each case was as given in Figure 3.14, with the structure published by Magennis and co-workers being a hydrate of the polymorph, $[\text{Eu}(\text{N}(\text{Ph}_2\text{PO})_2)_3]$. In the current study the synthesis of this compound using the hydrated europium chloride was found to be problematic and therefore the more soluble and less coordinating nitrate counter ion was used instead of the chloride, as shown in Scheme 3.8.

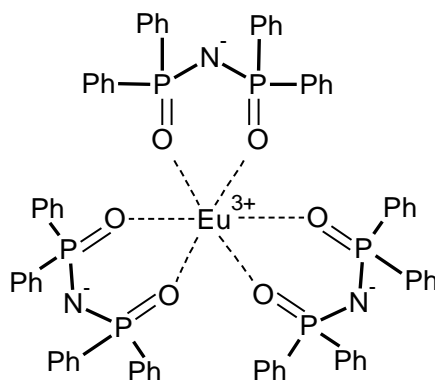
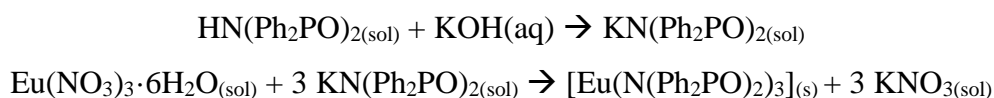


Figure 3.14: Molecular diagram $[\text{Eu}(\text{N}(\text{Ph}_2\text{PO})_2)_3]$.



Scheme 3.8: Synthesis of $[\text{Eu}(\text{N}(\text{Ph}_2\text{PO})_2)_3]$.

3.3.2.2.1.1 Reagents used

The chemicals used in the procedures described in this section were HN(Ph₂PO)₂_1 (synthesised in current study), KOH_(aq) (2 w/w %), Eu(NO₃)₃ (prepared by dissolution of Eu₂O₃ in conc. HNO₃ followed by crystallisation, after which solid was dried under active vacuum) and methanol (HPLC, dried over 3 Å molecular sieves).

3.3.2.2.1.2 General procedure

A reflux set up was prepared using a 50 ml flask. The flask was charged with 0.867 g (2.1 mmol) HN(Ph₂PO)₂_1. Approximately 6 ml of a 2 w/w % KOH_(aq) solution was mixed with 30 ml methanol. When a singular phase was obtained, this mixture was added to the reflux set up. The resultant mixture was stirred at room temperature for 1 hour to obtain full dissolution. Subsequently 0.229 g (0.68 mmol) dehydrated Eu(NO₃)₃ were added to this solution and this mixture was refluxed for 1 hour. The resultant mixture was filtered under vacuum and the filtrate was allowed to stand at 6-8 °C for 72 hours yielding colourless crystals, which were collected as the final product.

3.3.2.2.1.3 [Eu(N(Ph₂PO)₂)₃]₁

In this reaction attempt the main reflux was undergone for 30 minutes and no precipitation or crystallization occurred after standing at 6-8 °C for 72 hours. Removal of the volatiles from this filtrate did not yield any solid. The precipitate obtained from the first filtration was collected and labelled as [Eu(N(Ph₂PO)₂)₃]₁. Yield: 0.420 g, 39 %.

3.3.2.2.1.4 [Eu(N(Ph₂PO)₂)₃]₂

A solid labelled [Eu(N(Ph₂PO)₂)₃]₂ was collected as a final product through the general procedure described prior with no modifications. Yield: 0.185 g, 17 %.

3.3.2.2.1.5 Characterisation data

[Eu(N(Ph₂PO)₂)₃]₁ FT-IR (KBr, cm⁻¹): 3069 (m), 3007 (w), 1965 (w), 1895 (w), 1577 (s), 1467 (bs) 1336 (m), 1309 (s), 1184 (s), 1124 (s), 1028 (s), 787 (bs), 690 (bs), 522 (s).

¹H NMR (CDCl₃): 7.90 ppm (m, 2H, o-H), 7.43 ppm (t, 1H, p-H) 7.34 ppm (t, 2H, m-H).

[Eu(N(Ph₂PO)₂)₃]₂ FT-IR (KBr, cm⁻¹): 3389 (bs), 1650 (s), 1515 (s), 1384 (s), 1110 (m), 1090 (m), 849 (m), 826 (m), 784 (w), 752 (w), 725 (w), 697 (m). ¹H NMR (CDCl₃): 7.55 ppm (bd, 2H), 7.24 ppm (bs, 1H), 7.01 ppm (bd, 2H).

3.3.2.2.2. Synthesis of HN(Ph₂PS)₂+Eu(ClO₄)₃·n(H₂O)

To the author's knowledge the sulphide analogue of the Eu(N(Ph₂PO)₂)₃ complex has not been described in published literature. This is in contrast with Eu(N(Ph₂PO)₂)₃ as crystal structures for this complex have been published by various groups.^{240,244} It was therefore of interest to see if this analogous compound could be prepared from HN(Ph₂PS)₂. Analogous structures were published in the form of Ln(N(Ph₂PS)₂)₃·C₆H₅CH₃ and Ln(N(*i*Pr₂PS)₂)₃ (where Ln = La³⁺ and Ce³⁺).²⁷⁹ In all published cases these complexes were prepared on reaction of HN(Ph₂PS)₂ with Ln(N(SiMe₃)₂)₃.²⁷⁹ However in this study a method which did not require stringent conditions was desired. In the current research a series of reactions were undergone in an attempt to produce the expected product, using the conditions given in Table 3.3. Several europium salts were used namely the nitrate, acetate and perchlorate, on the basis of their enhanced solubility and the anions' decreased coordination ability. The ligand salts were prepared before each reaction by reacting the ligand, HN(Ph₂PS)₂, with KOH and *n*-BuLi to yield KN(PSPPh₂)₃ and LiN(PSPPh₂)₃ respectively.

Unfortunately, characterisation by IR spectroscopy concluded that in each case no coordination products were obtained, with the major product always being the starting ligand. Therefore, in a final attempt, the reaction of the free ligand with Eu(ClO₄)₃·6H₂O was undertaken in non-inert conditions in an effort to induce coordination of the ligand, even protonated, with the Eu³⁺ metal center. Perchlorate was used as a counter ion since this has a very low coordination ability.

Table 3.3: Synthesis attempts for $\text{Eu}(\text{N}(\text{Ph}_2\text{PS})_2)_3$ through wet chemical methods.

Reagents	Solvent	Temp., °C	Reaction duration, hours
$\text{KN}(\text{PSPH}_2)_3 + \text{Eu}(\text{NO}_3)_3$	methanol	room temperature	16
$\text{KN}(\text{PSPH}_2)_3 + \text{Eu}(\text{NO}_3)_3$	methanol	reflux	16
$\text{KN}(\text{PSPH}_2)_3 + \text{Eu}(\text{NO}_3)_3$	THF	reflux	1
$\text{LiN}(\text{PSPH}_2)_3 + \text{Eu}(\text{NO}_3)_3$	THF	reflux	16
$\text{LiN}(\text{PSPH}_2)_3 + \text{Eu}(\text{NO}_3)_3$	toluene	room temperature	16
$\text{LiN}(\text{PSPH}_2)_3 + \text{Eu}(\text{OAc})_3$	acetone	room temperature	16
$\text{LiN}(\text{PSPH}_2)_3 + \text{Eu}(\text{ClO}_4)_3$	toluene	room temperature	72

3.3.2.2.2.1 Reagents used

The chemicals used in the procedure described in this section were $\text{HN}(\text{Ph}_2\text{PS})_2$ _1 (synthesised in current study) and $\text{Eu}(\text{ClO}_4)_3 \cdot 6\text{H}_2\text{O}$ (prepared by dissolution of Eu_2O_3 in Grade A $\text{HClO}_{4(\text{aq})}$ and crystallisation; after which solid was dried under active vacuum).

3.3.2.2.2.2 $\text{HN}(\text{Ph}_2\text{PS})_2 + \text{Eu}(\text{ClO}_4)_3 \cdot n(\text{H}_2\text{O})$ _1

Exactly 30 mg (0.07 mmol) of $\text{HN}(\text{Ph}_2\text{PS})_2$ and 13 mg (0.02 mmol) of $\text{Eu}(\text{ClO}_4)_3 \cdot 6\text{H}_2\text{O}$ were ground together using a pestle and mortar, to yield a fine white powder. The mixture was then heated on the hot stage set up using the heating profile given in Table 3.4.

Table 3.4: Hot Stage microscopy temperature profile used in the synthesis of $\text{HN}(\text{Ph}_2\text{PS})_2+\text{Eu}(\text{ClO}_4)_3\cdot n(\text{H}_2\text{O})_1$.

Step	Rate, °Cmin ⁻¹	Holding temperature, °C	Holding time, minutes
1	50	200	10
2	10	230	30

Maintaining the temperature at 200 °C for 10 minutes was intended to determine if any reaction occurred between the two solid reagents prior to the temperature being raised to the melting point of the ligand. Since no visible reaction occurred at 200 °C heating was undertaken at a slower rate to establish if any change was affected during the melting of the ligand at 212–213 °C. Finally, the temperature was maintained at 230 °C, since at this temperature the ligand was fully melted and the Europium salt was fully dissolved in the melt. After holding the mixture at this temperature for 30 minutes the melt was allowed to cool to room temperature to yield a crystalline solid. This solid started to form as soon as the mixture started to cool. The crystalline solid was ground into a brownish white powder. The product obtained was collected and labelled as $\text{HN}(\text{Ph}_2\text{PS})_2+\text{Eu}(\text{ClO}_4)_3\cdot n(\text{H}_2\text{O})_1$. Given the nature of the reaction technique and that no further work up was undergone, the yield of the product could not be calculated as the solid mixture had the same mass as the starting reagents.

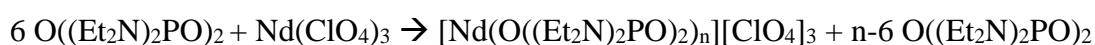
3.3.2.2.2.3 Characterisation data

$\text{HN}(\text{Ph}_2\text{PS})_2+\text{Eu}(\text{ClO}_4)_3\cdot n(\text{H}_2\text{O})_1$ FT-IR (KBr, cm⁻¹): 3021 (bs), 2631 (s), 1972 (w), 1910 (w), 1829 (w), 1585 (m), 1475 (m), 1438 (s), 1325 (s), 1145 (m), 1129 (m), 1102 (s), 921 (s), 1051 (m), 784 (s), 742 (s), 717 (s), 687 (s), 648 (s), 613 (s), 569 (m), 532 (s), 499 (s), 491 (m), 477 (m), 462 (m), 408 (m). ¹H NMR (CDCl₃): 7.90 ppm (bs, 2H), 7.38 ppm (bd, 1H), 7.14 ppm (bd, 2H).

3.3.2.2.3. Synthesis of $\text{O}((\text{Et}_2\text{N})_2\text{PO})_2+\text{Nd}(\text{ClO}_4)_3$ complex

In this study the complexation of $\text{O}((\text{Et}_2\text{N})_2\text{PO})_2$ with lanthanide metal centres was desired and therefore an attempt was made to produce a complex of this ligand with neodymium perchlorate, $\text{Nd}(\text{ClO}_4)_3$. Since such complexes are not known in published

literature the procedure undertaken in this research was established by implementing modifications to numerous reactions used to produce complexes of the analogous Schradan ($\text{O}((\text{Me}_2\text{N})_2\text{PO})_2$) ligand with both transition, alkali earth and actinide metals.^{207–209} Given that lanthanides typically have chemistry more similar to the alkali earth metals than the transition metals, a method similar to the preparation of alkali earth metal complexes for Schradan was employed in this study.^{208,209} During the preparation more ligand was used and the reaction was undertaken in the presence of 2,2-DMP to reduce the possibility of complexation of water and other unwanted small molecules. The general reaction for the attempted reaction, is given in Scheme 3.9.



Scheme 3.9: Reaction expected in the current study to form a $\text{O}((\text{Et}_2\text{N})_2\text{PO})_2+\text{Nd}(\text{ClO}_4)_3$ complex.

3.3.2.2.3.1 Reagents used

The chemicals used in the procedures described in this section were $\text{O}((\text{Et}_2\text{N})_2\text{PO})_2$ _1 (synthesised in current study), Nd_2O_3 (99.9%), $\text{HClO}_{4(\text{aq})}$ (A Grade), Acetone (GPR, used as purchased), 2,2-dimethoxypropane (2,2-DMP) (GPR), 30-40 °C petroleum ether (GPR, used as purchased) and diethyl ether (dry).

3.3.2.2.3.2 $\text{O}((\text{Et}_2\text{N})_2\text{PO})_2+\text{Nd}(\text{ClO}_4)_3$ _1

$\text{Nd}(\text{ClO}_4)_3 \cdot 6(\text{H}_2\text{O})$ was prepared by suspending 1.082 g (3.22 mmol) of Nd_2O_3 in 20 ml distilled water and 2 ml (excess) of A Grade $\text{HClO}_{4(\text{aq})}$. The mixture was heated and stirred to yield a pale purple solution. This was concentrated by evaporation to produce a purple viscous liquid, which was allowed to cool to yield a bed of purple crystalline solid. The solid was washed with 30-40 °C petroleum ether to yield a deliquescent crystalline mass.

A 100 ml Schlenk tube was charged with 0.158 g (0.470 mmol) of $\text{Nd}(\text{ClO}_4)_3 \cdot 6(\text{H}_2\text{O})$ dissolved in 1 ml of acetone. Afterwards an extra 5 ml of acetone were added to this mixture along with 6 ml (48.97 mmol) of 2,2-DMP, to yield a very pale purple solution. The solution was stirred at room temperature for 1.5 hours. After

approximately 30 minutes the solution changed colour to a distinctly dark brown colour. Using a 10 ml glass syringe, 0.4 ml (2.96 mmol) of $O((Et_2N)_2PO)_2_1$ were added to the reaction mixture at room temperature, while the mixture was continuously stirred. Problems were noted during the transfer of the $O((Et_2N)_2PO)_2_1$, due to the viscosity of the liquid and the dark colour made it very difficult to read the meniscus. No immediate changes were noted and stirring was stopped after 1 hr. There seemed to be a slight darkening of the colour, although no precipitation was observed.

An equivolume amount of diethyl ether was subsequently added to the reaction mixture to yield a wine red solution. A dark wine coloured viscous liquid phase formed after the mixture was allowed to settle. Cooling the mixture to $-78\text{ }^\circ\text{C}$ did not yield significant solidification, but increased the viscosity of the liquid. This liquid was filtered using a filtration tube set up. This yielded a dark brown viscous liquid as a residue, and a pale wine red coloured filtrate. The viscous liquid was washed with diethyl ether to remove impurities. About 5 ml of diethyl ether were then added to the dark brown viscous liquid and the resultant mixture was refluxed for 2 hours. No changes were observed and on filtration the same residue was obtained. This product was labelled $O((Et_2N)_2PO)_2+Nd(ClO_4)_3_1$. Yield $O((Et_2N)_2PO)_2+Nd(ClO_4)_3_1$: 0.261 g, 33.94 % (The yield assumes the lack of impurities and a 3:1 stoichiometric ratio for the ligand and the Nd^{3+} centre ($M = 1636.41\text{ gmol}^{-1}$), as was typical for similar Schradan complexes described earlier)

3.3.2.2.3.3 Characterisation data

$O((Et_2N)_2PO)_2+Nd(ClO_4)_3_1$ FT-IR (KBr, cm^{-1}): 2974 (s), 2937 (s), 2876 (w), 1732 (m), 1460 (m), 1385 (m), 1360 (m), 1292 (w), 1260 (w), 1217 (s), 1177 (s), 1101 (s), 1072 (w), 1032 (s), 972 (w), 958 (w), 930 (m), 907 (s), 796 (s), 723 (m), 624 (m), 527 (m). 1H NMR ($CDCl_3$): 1.14 ppm (bs, OH(MeOH)), 1.22 ppm (t, $J = 7.04\text{ Hz}$, 1.72H, CH_3 (product)), 1.38 ppm (t, 1.45H, CH_3 (product)), 1.86 ppm (s, 0.35H, NH(product)), 2.17 ppm (s, CH_3 (Acetone)), 3.11 ppm (bs, 1H, CH_2 (product)), 3.39 ppm (s, CH_3 (MeOH)), 5.72 ppm (bs, 0.47H), 6.61 ppm (bs, 0.45H). ^{31}P $\{^1H\}$ NMR ($CDCl_3$): 86.34 ppm (s). GC-MS (EI; 70 eV) m/z: 43.11, 57.10, 71.12, 83.12, 279.21, 149.01.

3.3.3. Co-Crystallisation

Co-crystallisation has been shown in literature to produce solids which were more stable to decomposition than the solids of individual co-formers.^{252,265,268} In this study co-crystallisation was only undertaken for the complex $[\text{Sm}(\text{C}(\text{Ph}_2\text{PNSiMe}_3)_2)(\text{NCy}_2)(\text{THF})]$.

This technique was considered advantageous over other possible stabilisation techniques for numerous reasons. In general this technique could be undertaken using no or little solvent making it a green chemical method, it is a simple technique which is easy to implement, both in the current study and in the industrial sphere and the easiest technique to expand upon making it more versatile than the remaining techniques.

3.3.3.1. Co-crystallisation attempts of $[\text{Sm}(\text{C}(\text{Ph}_2\text{PNSiMe}_3)_2)(\text{NCy}_2)(\text{THF})] \cdot 0.5(\text{C}_6\text{H}_5\text{CH}_3)$

The main attempts were undertaken using the previously synthesised $[\text{Sm}(\text{C}(\text{Ph}_2\text{PNSiMe}_3)_2)(\text{NCy}_2)(\text{THF})]_3$ and $[\text{Sm}(\text{C}(\text{Ph}_2\text{PNSiMe}_3)_2)(\text{NCy}_2)(\text{THF})]_4$ which were produced as described in Section 3.3.1.3.1.5 and 3.3.1.3.1.6 respectively. $[\text{Sm}(\text{C}(\text{Ph}_2\text{PNSiMe}_3)_2)(\text{NCy}_2)(\text{THF})]_3$ was used as opposed to the other products described in the same section due to its higher yield, which was enough to undertake a number of co-crystallisation procedures. $[\text{Sm}(\text{C}(\text{Ph}_2\text{PNSiMe}_3)_2)(\text{NCy}_2)(\text{THF})]_4$ was used given the better yield and quality of IR data which indicated the formation of a $[\text{HC}(\text{Ph}_2\text{PNSiMe}_3)_2]^-$ samarium derivative. Di- $\lambda^5\sigma^4$ -phosphorane lanthanide carbene and methanide complexes of $\text{H}_2\text{C}(\text{Ph}_2\text{PNSiMe}_3)_2$ have two main groups of interest in relation to co-crystallisation and intermolecular interactions. The first group consists of the P-Ph moieties of the ligand. The second group consists of the central negative hyperconjugation stabilised moiety composed of the $\text{N}^--\text{P}^+-\text{C}^{2-}-\text{P}^+-\text{N}^-$ and $\text{Ln}=\text{C}$ groups and the $\text{N}^--\text{P}^+-\text{CH}^--\text{P}^+-\text{N}^-$ and $\text{Ln}-\text{C}$ groups for the carbene and methanide respectively. Therefore, co-formers which could interact strongly with these two groups were required. The three co-formers used were biphenyl, 4,4'-bipyridine and 4,4'-oxydianiline, the structures of which are given in Figure 3.15.

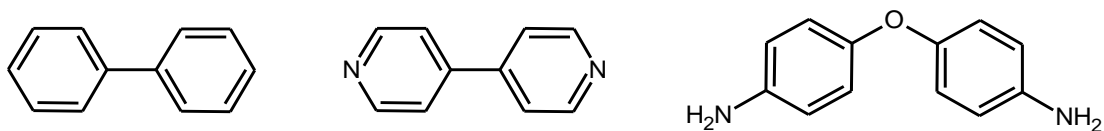


Figure 3.15: Molecular diagrams of co-formers, biphenyl (left), 4,4'-bipyridine (centre) and 4,4'-oxydianiline (right).

The reason for the choice of these co-formers was the various intermolecular bonding modes available to these compounds. Three main intermolecular interactions were available for these co-formers namely, alkyl hydrogen to aromatic ring interactions (C–H \cdots π), lateral pi to pi orbital interactions ($\pi \cdots \pi$), and classical hydrogen bonding with the co-formers acting as either a base or an acid (B \cdots H–A). The degree of availability of these interactions varied from one co-former to the other. The viable interactions between the various co-formers and the possible moieties within the expected carbene and methanide complexes are given in Table 3.5, divided in columns according to the carbene and methanide moieties which could be involved in such interactions.

Table 3.5: Intermolecular interactions believed to be available for co-formers used in this study.

	P–Ph	P–Ph, P=N, C=Sm, C–Sm	P–Ph, –SiMe₃	P⁺–C²⁻–P⁺, P⁺–CH⁻–P⁺, P⁺–N⁻
Biphenyl	C–H \cdots π	$\pi \cdots \pi$		
4,4'-bipyridine	C–H \cdots π	$\pi \cdots \pi$	N \cdots H–A	
4,4'-oxydianiline	C–H \cdots π	$\pi \cdots \pi$	O \cdots H–A	N–H \cdots B

3.3.3.1.1. Reagents used

The chemicals used in the procedures described in this section were [Sm(C(Ph₂PNSiMe₃)₂)(NCy₂)(THF)]₃ (synthesised in current study), [Sm(C(Ph₂PNSiMe₃)₂)(NCy₂)(THF)]₄ (synthesised in current study), 4,4'-bipyridine (99%, dried by melting and heating at 120 °C under vacuum with constant stirring for 4 hours), biphenyl (Analytical), 4,4'-oxydianiline (98%) and toluene (dry).

3.3.3.1.2. General considerations

All samples were weighed and prepared under an inert oxygen and moisture free nitrogen atmosphere, in a glovebox. Given the possibility of solvate toluene loss, the masses of $[\text{Sm}(\text{C}(\text{Ph}_2\text{PNSiMe}_3)_2(\text{NCy}_2)(\text{THF})]_{\text{3}}$ and $[\text{Sm}(\text{C}(\text{Ph}_2\text{PNSiMe}_3)_2(\text{NCy}_2)(\text{THF})]_{\text{4}}$ used were calculated using a $M = 959.56 \text{ g mol}^{-1}$, that is the molar mass of the carbene complex expected without the mass of the $0.5(\text{C}_6\text{H}_5\text{CH}_3)$ solvate.

3.3.3.1.3. Co-crystallisation procedures

Equimolar amounts of the inorganic co-formers $[\text{Sm}(\text{C}(\text{Ph}_2\text{PNSiMe}_3)_2(\text{NCy}_2)(\text{THF})]_{\text{3}}$ and $_{\text{4}}$ and the respective organic co-former were weighed and transferred into a clean agate mortar and ground for 3 minutes. The grinding procedure for the mixture was undertaken twice more for a total of three times. After grinding the solid was collected for analysis. The masses and amounts used for the various procedures are given in Table 3.6.

Table 3.6: Details of co-crystallisation procedures undertaken.

Inorganic Co-former			Organic co-former		
Name	Mass (g)	Amount (mmol)	Name	Mass (g)	Amount (mmol)
_3	0.0410	0.0427	Biphenyl	0.0069	0.0447
	0.0407	0.0421	4,4'-bipyridine	0.0068	0.0435
	0.0299	0.0312	4,4'-oxydianiline	0.0068	0.0395
_4	0.0509	0.0531	Biphenyl	0.0086	0.0558
	0.0505	0.0526	4,4'-bipyridine	0.0085	0.0544
	0.0502	0.0523	4,4'-oxydianiline	0.0115	0.0574

In all cases, except for the two biphenyl co-crystallisation attempts, very pale yellow powders were obtained. During the $[\text{Sm}(\text{C}(\text{Ph}_2\text{PNSiMe}_3)_2)(\text{NCy}_2)(\text{THF})]_3$:biphenyl preparation, on each grinding procedure a yellow paste was formed which on collection by spatula yielded a waxy solid with a deeper yellow colour than the yellow colouration of $[\text{Sm}(\text{C}(\text{Ph}_2\text{PNSiMe}_3)_2)(\text{NCy}_2)(\text{THF})]_3$. This was also the case during the preparation of $[\text{Sm}(\text{C}(\text{Ph}_2\text{PNSiMe}_3)_2)(\text{NCy}_2)(\text{THF})]_4$:biphenyl. This solid was placed under vacuum for 1 hour to yield a dry pale yellow solid which on grinding did not yield the same paste.

3.3.3.1.4. Single crystal preparation and collection

For the co-crystallisation products of $[\text{Sm}(\text{C}(\text{Ph}_2\text{PNSiMe}_3)_2)(\text{NCy}_2)(\text{THF})]_4$ single crystals were prepared by transferring between 0.01 g and 0.03 g of the product to a 10 ml Schlenk tube which was transferred to the Schlenk line. Dry toluene was added in 1 ml aliquots via cannula and the mixture was heated to 65 °C for 30 minutes with constant stirring. This was repeated until a solution was obtained. The solutions were allowed to stand for 1 week in a refrigerator. Details of these crystallisations are given in Table 3.7.

Table 3.7: Details of crystallisation from toluene of $[\text{Sm}(\text{C}(\text{Ph}_2\text{PNSiMe}_3)_2)(\text{NCy}_2)(\text{THF})]_4$ co-crystallisation products.

Co-former	Mass (g)	Toluene Vol. (ml)	Observations
Biphenyl	0.0262	1	Clear solution Amorphous precipitate collected
4,4'-bipyridine	0.0246	1	Slightly turbid solution Small needle-like crystals collected
4,4'-oxydianiline	0.0105	2	Turbid solution Crystal microbundles collected

3.3.3.1.5. Characterisation techniques used for co-crystal samples

In all cases the samples obtained were stored under dry nitrogen in a glovebox and characterised by IR spectroscopy. PXRD, SXRD and Raman spectroscopy was undertaken for samples of the co-crystallisation products of $[\text{Sm}(\text{C}(\text{Ph}_2\text{PNSiMe}_3)_2)(\text{NCy}_2)(\text{THF})]_4$. Given the small amounts of products available and the fact that no reaction was expected, yields were not calculated.

$[\text{Sm}(\text{C}(\text{Ph}_2\text{PNSiMe}_3)_2)(\text{NCy}_2)(\text{THF})]_3$:biphenyl FT-IR (KBr, cm^{-1}): 2963 (w), 2924 (w), 2852 (w), 1260 (s), 1189 (m), 1180 (w), 1169 (w), 1160 (m), 1155 (w), 1103 (s), 1070 (w), 1018 (s), 925 (w), 876 (w), 845 (w), 825 (w), 800 (s), 738 (m), 719 (m).

$[\text{Sm}(\text{C}(\text{Ph}_2\text{PNSiMe}_3)_2)(\text{NCy}_2)(\text{THF})]_3$:4,4'-bipyridine FT-IR (Nujol, cm^{-1}): 1260 (s), 1168 (w), 1159 (w), 1123 (wsh), 1097 (s), 1067 (w), 1020 (s), 962 (w), 890 (w), 876 (w), 864 (w), 845 (w), 820 (w), 800 (s), 738 (w), 722 (m).

$[\text{Sm}(\text{C}(\text{Ph}_2\text{PNSiMe}_3)_2)(\text{NCy}_2)(\text{THF})]_3$:4,4'-oxydianiline FT-IR (KBr, cm^{-1}): 2963 (w), 2924 (w), 2852 (w), 1260 (s), 1225 (w), 1157 (w), 1091 (s), 1019 (s), 869 (w), 862 (w), 820 (w), 800 (s), 738 (w), 719 (w).

$[\text{Sm}(\text{C}(\text{Ph}_2\text{PNSiMe}_3)_2)(\text{NCy}_2)(\text{THF})]_4$:biphenyl FT-IR (KBr, cm^{-1}): 3400 (bs), 3055 (w), 2929 (s), 2853 (s), 1645 (bw), 1437 (s), 1310 (w), 1253 (s), 1240 (s), 1180 (s), 1127 (s), 1115 (s), 1070 (w), 1028 (w), 890 (m), 747 (s), 722 (s), 695 (s). Raman (cm^{-1}): 1598 (bw), 1318 (bw), 1171 (bw).

$[\text{Sm}(\text{C}(\text{Ph}_2\text{PNSiMe}_3)_2)(\text{NCy}_2)(\text{THF})]_4$:4,4'-bipyridine FT-IR (KBr, cm^{-1}): 3400 (bs), 3055 (w), 2929 (s), 2853 (s), 1645 (bw), 1592 (s), 1532 (m), 1486 (m), 1437 (s), 1406 (m), 1310 (w), 1256 (w), 1238 (w), 1217 (w), 1180 (s), 1127 (s), 1115 (s), 1069 (w), 998 (s), 994 (w), 918 (w), 890 (m), 847 (m), 828 (w), 806 (s), 787 (m), 747 (s), 722 (m), 695 (s), 610 (m). Raman (cm^{-1}): 1868 (bs), 1000 (w)

$[\text{Sm}(\text{C}(\text{Ph}_2\text{PNSiMe}_3)_2)(\text{NCy}_2)(\text{THF})]_4$:4,4'-oxydianiline FT-IR (KBr, cm^{-1}): 3444 (w), 3386 (w), 3400 (bs), 3055 (w), 2929 (s), 2853 (s), 1630 (bw), 1499 (s), 1437 (s), 1310 (w), 1255 (w), 1222 (s), 1180 (s), 1127 (s), 1115 (s), 1070 (w), 1028 (w), 998 (m), 890 (m), 873 (w), 828 (w), 826 (s), 787 (w), 747 (s), 722 (m), 695 (s). Raman (cm^{-1}): 3100 (bs).

4. RESULTS AND DISCUSSION

4.1. Lanthanide carbene complexes

4.1.1. Ligands and ligand precursors

4.1.1.1. Characterisation of $[\text{H}_2\text{C}(\text{Ph}_2\text{PNH}(i\text{Pr}))_2]\text{Br}_2$ and $\text{K}[\text{HC}(\text{Ph}_2\text{PN}i\text{Pr})_2]$.

As described in Section 2.4.3.1.2. bis(diphenyliminophosphorano)methane analogues can be synthesised through the Kirsanov route.³⁶ In the current study this method was used in the preparation of the ligand salt potassium bis(diphenyl-N-*iso*-propyl-iminophosphorano)methanide, $\text{K}[\text{HC}(\text{Ph}_2\text{PN}i\text{Pr})_2]$, as described in Section 3.3.1.1.1. The synthesis of this methanide required the preparation of the cationic phosphonium bis(diphenyl-N-*iso*-propyl-aminophosphonium)methane di-bromide, $[\text{H}_2\text{C}(\text{Ph}_2\text{PNH}(i\text{Pr}))_2]\text{Br}_2$, as a product of the initial step of the Kirsanov reaction.^{36,99,117,119,120}

4.1.1.1.1. Characterisation of $[\text{H}_2\text{C}(\text{Ph}_2\text{PNH}(i\text{Pr}))_2]\text{Br}_2$.

The reaction to prepare $[\text{H}_2\text{C}(\text{Ph}_2\text{PNH}(i\text{Pr}))_2]\text{Br}_2$ was undergone as described in Section 3.3.1.1.1. through a modification of the Kirsanov route. The product obtained in this reaction, at a yield of 52.7%, was labelled as $[\text{H}_2\text{C}(\text{Ph}_2\text{PNH}(i\text{Pr}))_2]\text{Br}_2_1$. This product was used in order to prepare the potassium salt ligand $\text{K}[\text{HC}(\text{Ph}_2\text{PN}i\text{Pr})_2]$.

4.1.1.1.1.1 Analysis by Infra-red spectroscopy

The IR spectrum of $[\text{H}_2\text{C}(\text{Ph}_2\text{PNH}(i\text{Pr}))_2]\text{Br}_2_1$, collected in KBr, is given in Figure 4.1. The solid was evidently a dppm derivative, with many of the expected P–Ph bands visible. Given the lack of band assignments for this product in literature tentative assignments are also given in Figure 4.1. These assignments were used for comparative purposes for derivatives of this compound produced in this study.

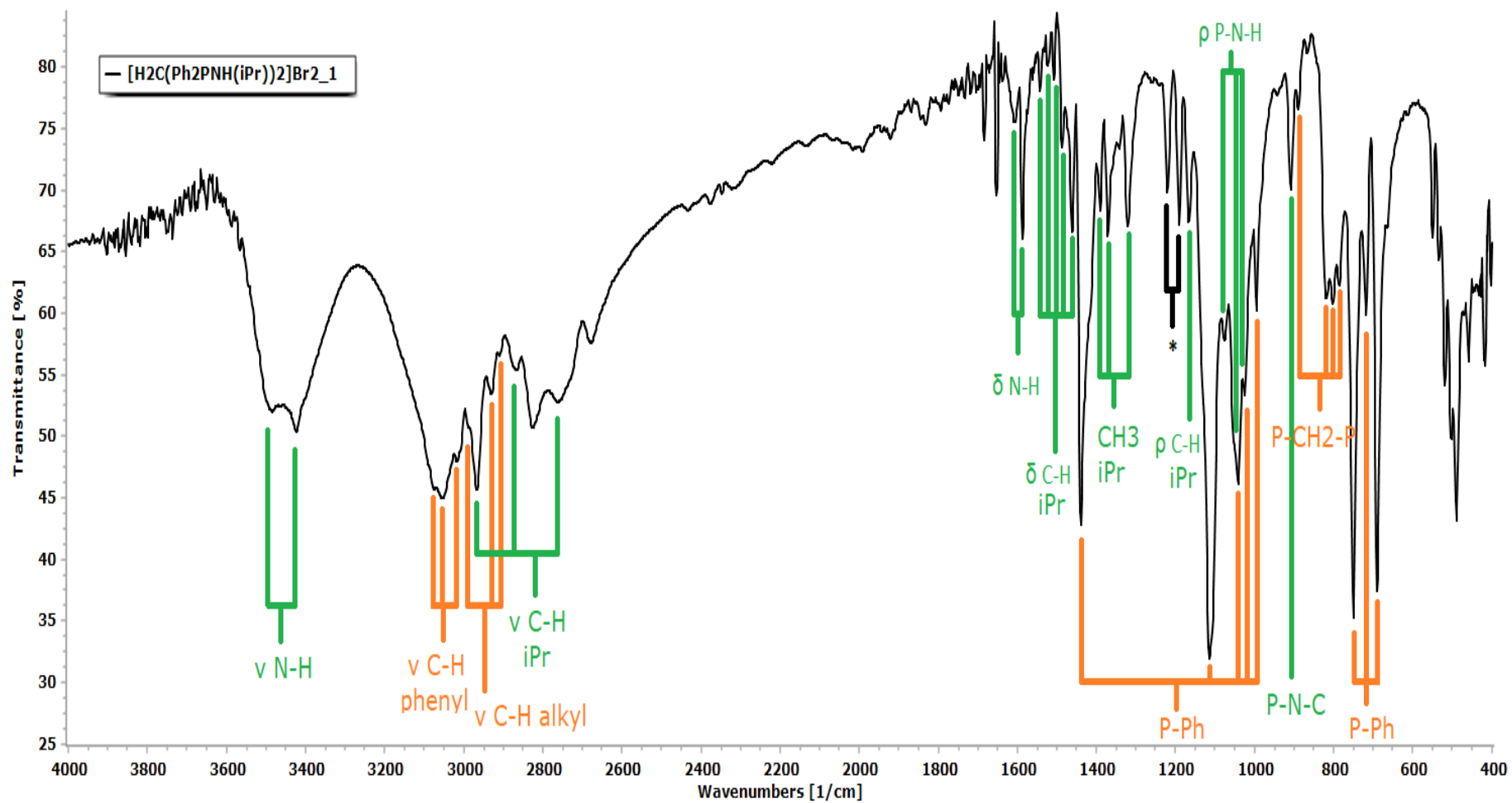


Figure 4.1: Tentative band assignment for IR spectrum for product $[H_2C(Ph_2PNH(iPr))_2]Br_2_1$.

In this figure the bands attributed to vibrations from the original dppm molecular structure (IR data for the dppm used in this study is given in Appendix 5) are given in orange and labelled according to the moiety most likely leading to the vibration. Bands labelled in green are believed to be due to the presence of the *iso*-propyl amine moiety – NH(*i*Pr) including bands believed to be due to the bonds formed between the –NH(*i*Pr) moiety and the dppm molecular structure, mainly the P–N–H and P–N–C vibrations.⁹⁹ The importance of the bands assigned to P–N–H, in the range of 1075-1024 cm⁻¹, and P–N–C, at 909 cm⁻¹, is that they affirm the bonding of the amine *iso*-propyl moiety to the dppm molecular structure as expected in the product. The P–N–C bands may also occur in the range for P–N–H vibrations. The P–N–H vibration indicated that this moiety was still an amine, as expected. The region in 1075-1024 cm⁻¹, in [H₂C(Ph₂PNH(*i*Pr))₂Br₂]₁, may also contain the band due to the ν C–N vibration but this could not be specifically identified. The two bands labelled in black by an asterisk could not be assigned with any reasonable certainty, although they do lie in the regions typical for the ν P=C vibration. This may result from some form of hyperconjugation between the methane carbon and the phosphonium center. The bands labelled in black may also be due to the presence of ν C–N.

The assignment of C–H bands of the *i*Pr group was undergone by comparison to spectra of the *iso*-propyl amine, *iso*-propyl amine HCl salt and other aliphatic amines, both primary and secondary.^{280,281} The ν N–H and δ N–H bands were still indicative of primary amines with two bands present for the former and a single band present for the latter. However this is not what was expected for amine moieties in the product which should have contained a single hydrogen on the amine nitrogen.²⁸¹ This may indicate the presence of unreacted *iso*-propyl amine or a lack of reaction in contrast to the reaction attested by the presence of the P–N–H and P–N–C vibrations. There is no literature data to attest whether the phosphonium centre has an influence on the N–H vibrations which could explain the discrepancy and therefore any difference in the two bands due to this is unknown.

The bands attributed to P–CH₂–P vibrations were assigned as such, because for phosphorus containing compounds they are the only vibrations normally occurring in this region.⁹⁹ However, only two bands should be caused by the P–CH₂–P group, namely from the symmetric and asymmetric stretching vibrations. Fingerprint bands for the *iso*-propyl moiety cannot be disregarded in this region. P–CH₂–P vibrations can also include bands up to the band at 995 cm⁻¹, which could also be due to the presence of the *iso*-propyl

moiety.⁹⁹ The band at 908 cm⁻¹ ascribed to P–CH₂–P vibrations could also be tentatively ascribed to the P–N–C vibrations but was considered a possible shift of the 918 cm⁻¹ band attributed to ν_{as} P–CH₂–P in dppm.

Some bands were also assigned twice, for two different vibrations, as both are possible assignments with no particular reason to discriminate in favour of one assignment. Unassigned bands could not be ascribed to specific bond vibrations with any level of accuracy. The effect of the phosphonium centres has not been well studied and most IR studies of phosphorus centred compounds relate to neutral compounds.⁹⁹

4.1.1.1.1.2 Analysis by ¹H NMR spectroscopy

¹H NMR spectroscopy was used to further characterise the product [H₂C(Ph₂PNH(*i*Pr))₂]Br₂. ¹H NMR spectroscopy data on the characterisation of the [H₂C(Ph₂PNH(*i*Pr))₂]Br₂ product was published in literature.³⁶ This data is reproduced in Table 4.1.³⁶

Table 4.1: ¹H NMR spectroscopy data for [H₂C(Ph₂PNH(*i*Pr))₂]Br₂ in CDCl₃ as given in literature.³⁶

¹H NMR spectroscopy data for [H₂C(Ph₂PNH(<i>i</i>Pr))₂]Br₂ in CDCl₃, as given in literature				
ppm	Assignment	Multiplicity	Number of ¹H	Coupling
7.96	m-H	doublet of doublets	8	⁴ J _{HP} = 13.5 Hz ³ J _{HH} = 7.0 Hz
7.70	p-H	triplet	4	³ J _{HH} = 7.0 Hz
7.57	o-H	doublet of doublets	8	³ J _{HP} = 13.5 Hz ³ J _{HH} = 7.0 Hz
6.86	NH	doublet of doublets	2	² J _{HP} = 10.0 Hz ³ J _{HH} = 6.4 Hz
6.41	PCH ₂ P	triplet	2	² J _{HP} = 16.0 Hz
3.01	NCH(<i>i</i> Pr)	singlet broad	2	N/A
0.94	CH ₃ (<i>i</i> Pr)	doublet	12	³ J _{HH} = 6.5 Hz

The spectrum of the product $[\text{H}_2\text{C}(\text{Ph}_2\text{PNH}(i\text{Pr}))_2]\text{Br}_2\text{-1}$ in CDCl_3 was found to be in close agreement with the data given in literature, although all the peaks were found to be slightly downfield to those presented in literature. The spectrum of $[\text{H}_2\text{C}(\text{Ph}_2\text{PNH}(i\text{Pr}))_2]\text{Br}_2\text{-1}$ is given in Figure 4.2, while important data is summarised in Table 4.2. The experimental data was in agreement with both chemical shifts and multiplicity values given in literature. Impurity peaks were noted at 1.59 ppm (water), at 1.26 ppm and 0.86 ppm likely due to grease and at 0.07 ppm due to silicone grease.

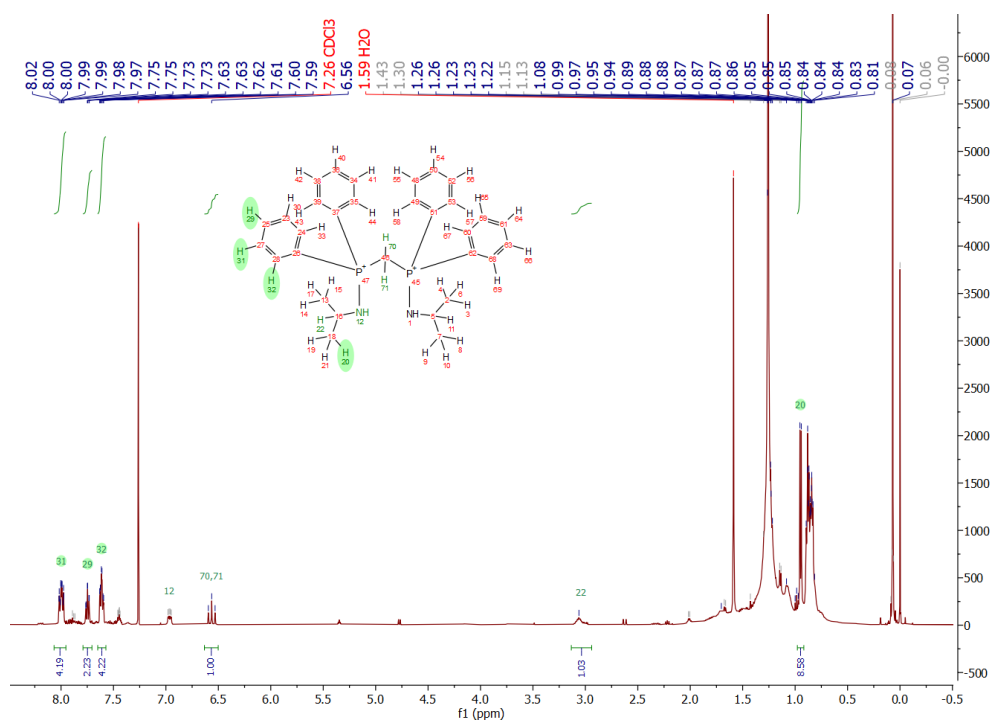


Figure 4.2: Full ^1H NMR spectrum of $[\text{H}_2\text{C}(\text{Ph}_2\text{PNH}(i\text{Pr}))_2]\text{Br}_2\text{-1}$ in CDCl_3 .

Table 4.2: ^1H NMR experimental data for $[\text{H}_2\text{C}(\text{Ph}_2\text{PNH}(i\text{Pr}))_2]\text{Br}_2\text{-1}$ in CDCl_3

^1H NMR experimental data for $[\text{H}_2\text{C}(\text{Ph}_2\text{PNH}(i\text{Pr}))_2]\text{Br}_2\text{-1}$ in CDCl_3				
Ppm	Assignment	Multiplicity	Calc. no. of ^1H	Coupling
8.00	o-H	doublet of doublets	8.34	$^3J_{\text{HP}} = 13.38 \text{ Hz}$ $^3J_{\text{HH}} = 7.33 \text{ Hz}$
7.4	p-H	triplets	4.34	$^3J_{\text{HH}} = 7.30 \text{ Hz}$
7.61	m-H	doublet of triplets	8.34	7.88 Hz 3.30 Hz

6.96	NH	doublet of doublets	2.34	${}^2J_{\text{HP}} = 10.45 \text{ Hz}$ ${}^3J_{\text{HH}} = 5.60 \text{ Hz}$
6.56	PCH ₂ P	triplet	2	${}^2J_{\text{HP}} = 16.03 \text{ Hz}$
3.06	NCH(<i>i</i> Pr)	broad multiplet	2.34	N/A
0.95	CH ₃ (<i>i</i> Pr)	doublet	14	${}^3J_{\text{HH}} = 6.40 \text{ Hz}$

As expected the triplet due to the PCH₂P protons, shown in detail in Figure 4.3, was found at 6.56 ppm. This was significantly downfield to the 2.80 ppm triplet found in the spectrum of dppm (¹H NMR data for the dppm used in this study is given in Appendix 5). This shift may be due to the increased electronegativity of the phosphorus centres due to their bonding with the nitrogen and the presence of a phosphonium centre. Another issue known to cause a similar effect is the increase in valency in metal centres, in which the ¹H NMR peaks of protons bound to ligands are found downfield from their position in the spectrum of the un-coordinated ligands.²⁸²

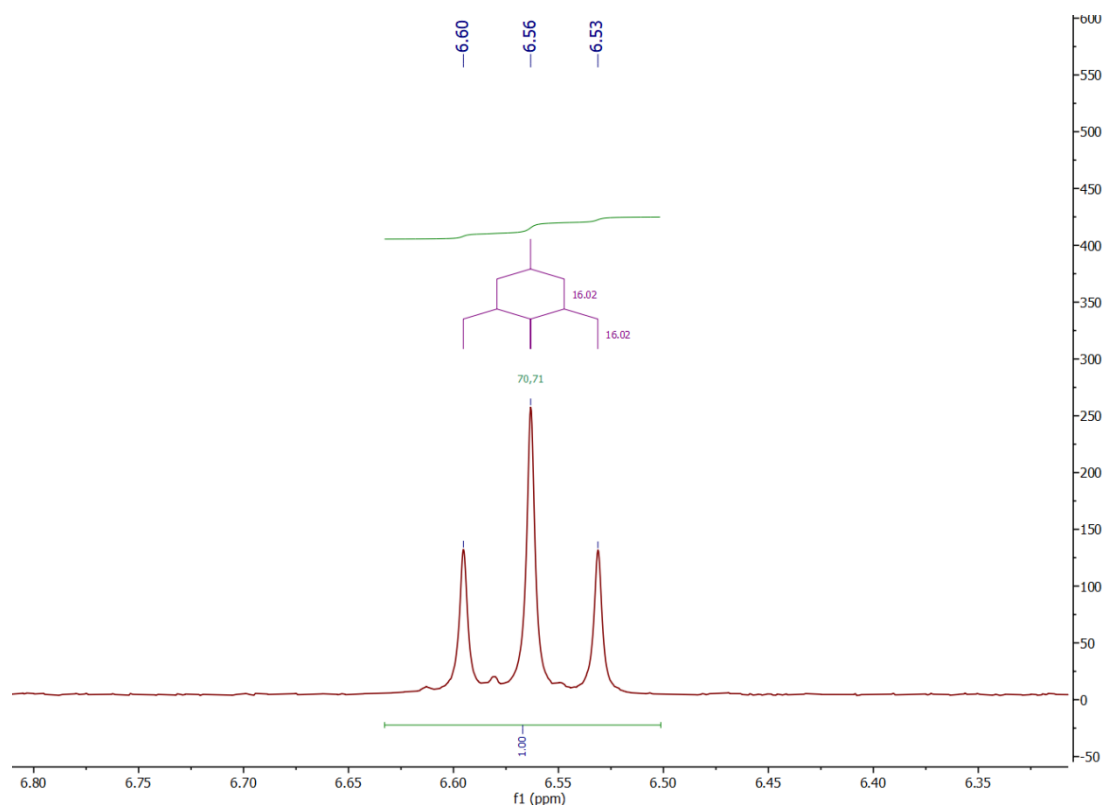


Figure 4.3: Detail of the spectrum for [H₂C(Ph₂PNH(*i*Pr))₂]Br₂_1 showing triplet at 6.56 ppm.

The increase in ${}^2J_{\text{HP}}$ from 1.5 Hz in the triplet in dppm to 16.03 Hz in the triplet in the spectrum of the product was also indicative of the increased electronegativity of the phosphorus through the bonding of an electronegative substituent (nitrogen in this case) to the NMR active phosphorus centres.²⁸² The presence of such an electronegative substituent on one of the active nuclei causes an increase in the reduced coupling constant, 2K , which is in turn proportional to the value of 2J , causing this to increase under the same circumstances.²⁸² The close agreement of this ${}^2J_{\text{HP}}$ coupling constant to literature data was strongly indicative of the formation of the desired phosphorus species as these coupling constants vary widely for derivatives of dppm according to the nature of the phosphorus centres and the charge on the central carbon.

Three multiplets were found in the spectrum of $[\text{H}_2\text{C}(\text{Ph}_2\text{PNH}(i\text{Pr}))_2]\text{Br}_2\text{-1}$ in the region typical for phenyl protons, as shown in Figure 4.4. The chemical shifts of these peaks, as with all peaks, were found to be slightly downfield to the values found in literature data for the ligand but were still in good agreement with the literature data. The assignment of the phenyl peaks was undergone through comparison with the assignment given by Demange *et al.*³⁶ The assignment of the p-H protons to the triplet at 7.40 ppm was confirmed by the integration ratio of 2:1:2 with both remaining peaks in the aromatic region. This indicated the presence of a mesomeric electron donor or acceptor at the aminophosphonium centre.

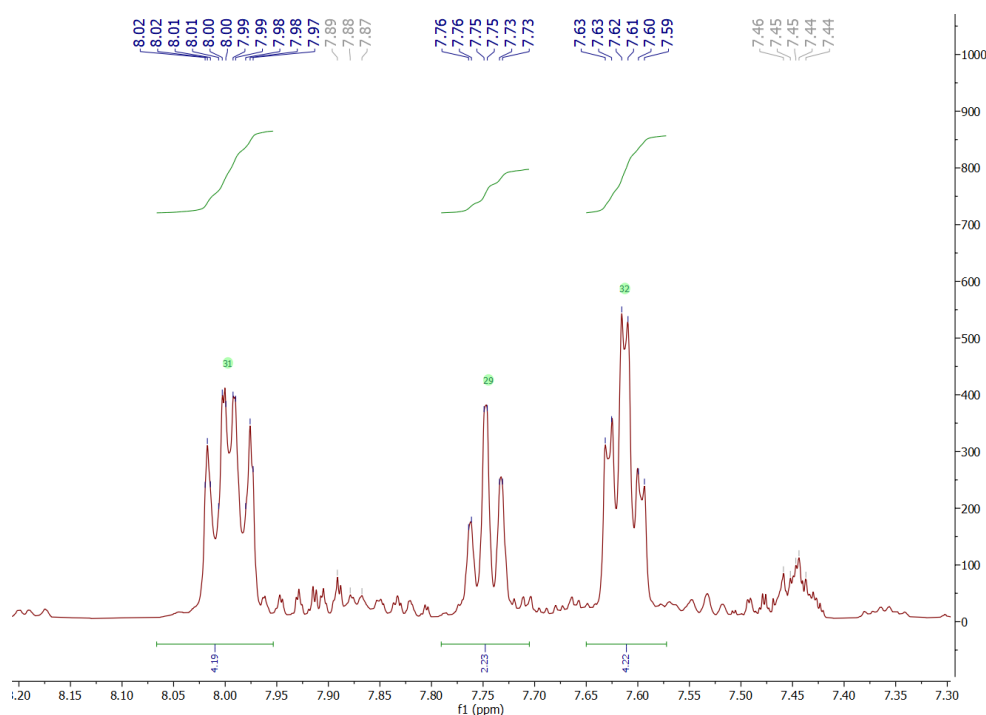


Figure 4.4: ${}^1\text{H}$ NMR peaks for $[\text{H}_2\text{C}(\text{Ph}_2\text{PNH}(i\text{Pr}))_2]\text{Br}_2\text{-1}$ believed to be due to phenyl protons.

The assignment of the o-H and m-H protons proved more difficult. The main difference between the literature and the experimental data was in the phenyl proton peak at 7.61 ppm. Literature data describes the analogous peak (7.57 ppm), assigned to the o-H protons, as being a doublet of doublets with coupling constants $^3J_{HP} = 13.5$ Hz and $^3J_{HH} = 7.0$ Hz. These details were identical to the literature peak at 7.96 ppm assigned to the m-H protons and therefore these peaks could not be distinguished by the coupling observed, as shown in Table 4.1. The results of the current study however gave what could best be described as a doublet of triplets at 7.61 ppm with coupling constants of 7.88 Hz and 3.30 Hz, as shown in Figure 4.5. The two coupling constants were similar to aromatic $^3J_{HH}$ and $^4J_{HH}$ coupling constant respectively. A coupling constant of >10 Hz, typical of $^3J_{HP}$, could not be described for the peak at 7.61 ppm. This $^3J_{HP}$ would be expected for the o-H protons.

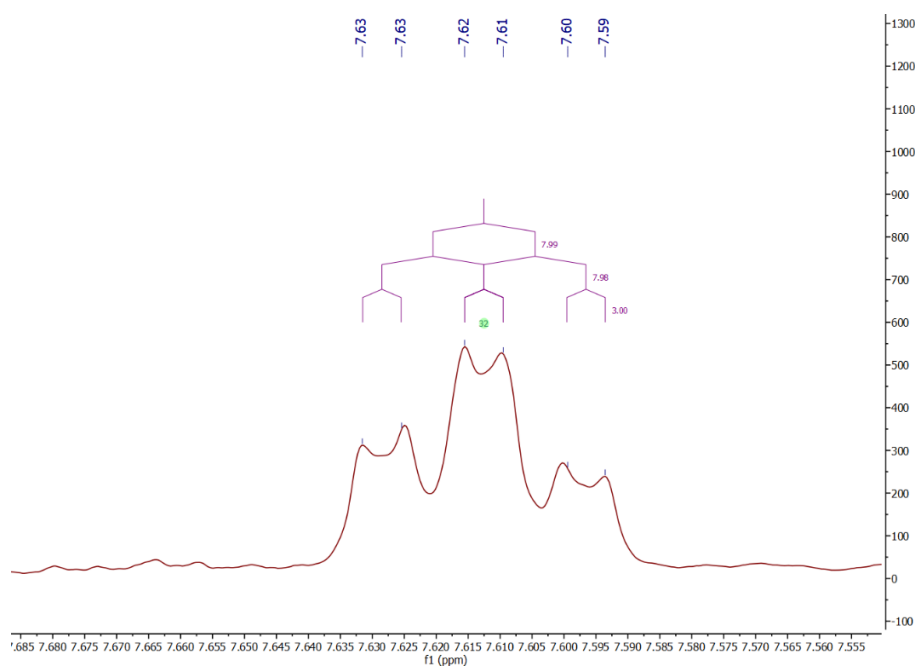


Figure 4.5: Doublet of triplets structure fit for the peaks around 7.61 ppm.

In the current study the more deshielded protons at 8.00 ppm were the only protons with coupling constants indicative of $^3J_{HP}$ coupling ($^3J_{HP} = 13.38$ Hz) and therefore were more likely due to o-H protons, while the peak at 7.61 ppm was considered more likely due to the m-H protons. This would indicate that the aminophosphonium centre acts as a mesomeric electron withdrawing group rather than a mesomeric electron donating group as described in literature. These observations, along with the overall

downfield shift from the dppm values for o-H and m/p-H, were in line with the expected change in electronegativity of the phosphorus centre in the aminophosphonium product. The cause for the formation of a doublet of triplets at 7.61 ppm is unknown, although other analogous compounds show this type of splitting for m-H.³⁶

For all other peaks present in the spectrum the coupling is in agreement with the literature data, although the 5.60 Hz constant for the NH peaks is smaller than the expected value of 6.4 Hz. Another major difference was the number of calculated protons for the peaks assigned to the CH₃(*i*Pr) protons; this being 14 as opposed to the expected value of 12. This may be due to an amount of strong peaks present on either side of this doublet, possibly due to grease contamination of the deuterated solvent used as described previously.

4.1.1.1.3 Conclusion

The similarities observed between the ¹H NMR experimental data for [H₂C(Ph₂PNH(*i*Pr))₂]Br_{2_1} and the data produced in literature, along with the data obtained from the IR spectra, led to the conclusion that [H₂C(Ph₂PNH(*i*Pr))₂]Br_{2_1} was most likely the required product.

4.1.1.1.2. Characterisation of K[HC(Ph₂PN*i*Pr)₂]

Two batches of the methanide, K[HC(Ph₂PN*i*Pr)₂], which will be discussed hereunder, were prepared from [H₂C(Ph₂PNH(*i*Pr))₂]Br_{2_1}, with the reagent ratio and yield for each batch given in Table 4.3. In each case the product was reacted with KHMDS following the procedure described in Section 3.3.1.1.1 and published by Klemps and co-workers in 2009 and similar to the synthesis of the analogous lithium salt as described by Demange and collaborators in 2006.^{36,121}

Table 4.3: Reaction data for the synthesis of K[HC(Ph₂PN(*i*Pr))₂] from [H₂C(Ph₂PNH(*i*Pr))₂]Br_{2_1}.

Code	KHMDS:[H ₂ C(Ph ₂ PNH(<i>i</i> Pr)) ₂]Br _{2_1}	Yield
K[HC(Ph ₂ PN <i>i</i> Pr) ₂] ₁	3.01:1	Negligible
K[HC(Ph ₂ PN <i>i</i> Pr) ₂] ₂	3.04:1	62%

In each case a dry solid could not be collected and the product obtained was in the form of a white sticky powder.

4.1.1.1.2.1 Analysis by Infra-red spectroscopy

IR spectroscopy was used to characterise the two products. The IR spectra of $\text{K}[\text{HC}(\text{Ph}_2\text{PNiPr})_2]_1$ and $\text{K}[\text{HC}(\text{Ph}_2\text{PNiPr})_2]_2$ were found to be similar to each other and are presented in Figure 4.6.

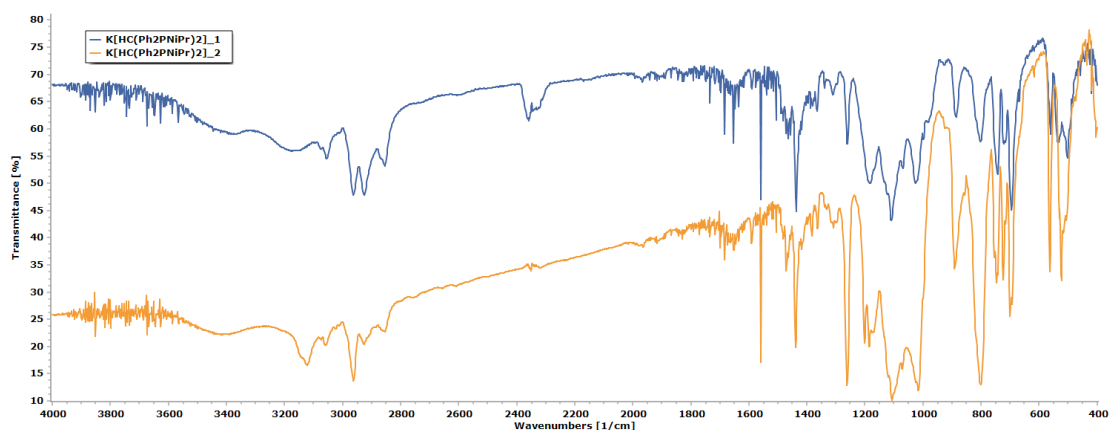


Figure 4.6: IR spectra of $\text{K}[\text{HC}(\text{Ph}_2\text{PN}(\text{iPr}))_2]_1$ (blue) and $\text{K}[\text{HC}(\text{Ph}_2\text{PN}(\text{iPr}))_2]_2$ (orange).

The main differences between the two spectra arise in three regions. The typical aromatic ν C–H band was well presented in the spectrum of $\text{K}[\text{HC}(\text{Ph}_2\text{PNiPr})_2]_2$ (at 3122 cm^{-1}) but not in the spectrum of $\text{K}[\text{HC}(\text{Ph}_2\text{PNiPr})_2]_1$, wherein this band seems to be replaced with a rather broad band centered around 3176 cm^{-1} . Nonetheless the numerous skeletal P–Ph bands in the fingerprint region, as presented in Figure 4.6, were present in the spectrum for $\text{K}[\text{HC}(\text{Ph}_2\text{PNiPr})_2]_1$, thus indicating the presence of the aromatic rings in this product.

The second major difference occurred with regards to the single strong and broad band at 1183 cm^{-1} in the spectrum of $\text{K}[\text{HC}(\text{Ph}_2\text{PNiPr})_2]_1$, which was replaced by a similar band at 1171 cm^{-1} and two sharp bands at 1202 cm^{-1} and 1185 cm^{-1} in the spectrum of $\text{K}[\text{HC}(\text{Ph}_2\text{PNiPr})_2]_2$.⁹⁹ The sharp nature of the latter two bands indicated that they represent some moieties that do not occur in $\text{K}[\text{HC}(\text{Ph}_2\text{PNiPr})_2]_1$. This region usually has bands attributable to P=N and P=C vibrations, which would indicate the formation of the expected product. The P=N moiety is expected for the molecule, while the P=C

vibration may be due to some type of delocalisation between the methanide carbon and the phosphorus centres. However the impact of the P=C bond may not be significant since similar bands are given in the neutral $\text{H}_2\text{C}(\text{Ph}_2\text{PNSiMe}_3)_2$ products discussed in Section 4.1.1.2. The final difference lies in the range below 600 cm^{-1} where bands are typically assigned to P–Ph vibrations and to which no reasonable explanation can be given in this study.⁹⁹

The tentative assignment of the bands in the IR spectrum of $\text{K}[\text{HC}(\text{Ph}_2\text{PN}i\text{Pr})_2]_2$ was undergone in more detail and special attention was given to the assignment of the bands similar to those for the starting reagent $[\text{H}_2\text{C}(\text{Ph}_2\text{PNH}(i\text{Pr}))_2]\text{Br}_2_1$. This tentative assignment is given in Figure 4.7.

Firstly the amine bands assigned to $\nu\text{ N-H}$ and $\delta\text{ N-H}$ were retained, although at significantly reduced intensities. This was expected since the P–N bonds are replaced by P=N in the reaction.¹²¹ The skeletal vibrations, mainly the dppm skeletal phenyl and alkyl $\nu\text{ C-H}$ and the P–Ph vibrations, along with the vibrations of the *iso*-propyl moiety given in green in Figure 4.7,⁹⁹ remained mainly unchanged from the spectrum of $[\text{H}_2\text{C}(\text{Ph}_2\text{PNH}(i\text{Pr}))_2]\text{Br}_2_1$.

The most important bands in the spectrum of $\text{K}[\text{HC}(\text{Ph}_2\text{PN}i\text{Pr})_2]_2$ are presented in black in Figure 4.7. The first group contains the strong and sharp bands at 1261 cm^{-1} , 1202 cm^{-1} and 1185 cm^{-1} , the latter two already described prior. All three bands fell in the range normally containing bands due to the $\nu\text{ P=N}$ and $\nu\text{ P=C}$ bonds vibrations, as described Figure 4.6.⁹⁹ The bands 1202 cm^{-1} and 1185 cm^{-1} may be due to both these moieties and their presence indicate electron delocalisation over the methanide carbon, phosphorus and nitrogen centres. The band at 1261 cm^{-1} was also possibly due to the $\nu\text{ P=N}$ vibration, although at this higher wavenumber this is more typical of the neutral precursors.⁹⁹ This band also falls in a region typical for $\nu\text{ C-N}$ vibrations and could be indicative of the *iso*-propyl amine moiety, although an analogous band in the IR spectra of $[\text{H}_2\text{C}(\text{Ph}_2\text{PNH}(i\text{Pr}))_2]\text{Br}_2_1$ could not be definitively assigned. Unfortunately the band attributed to the vibration of the $\nu\text{ P-C}$ lies in a range which makes it non-diagnostic and therefore the effect of delocalisation on this bond cannot be directly observed in IR spectra.⁹⁹

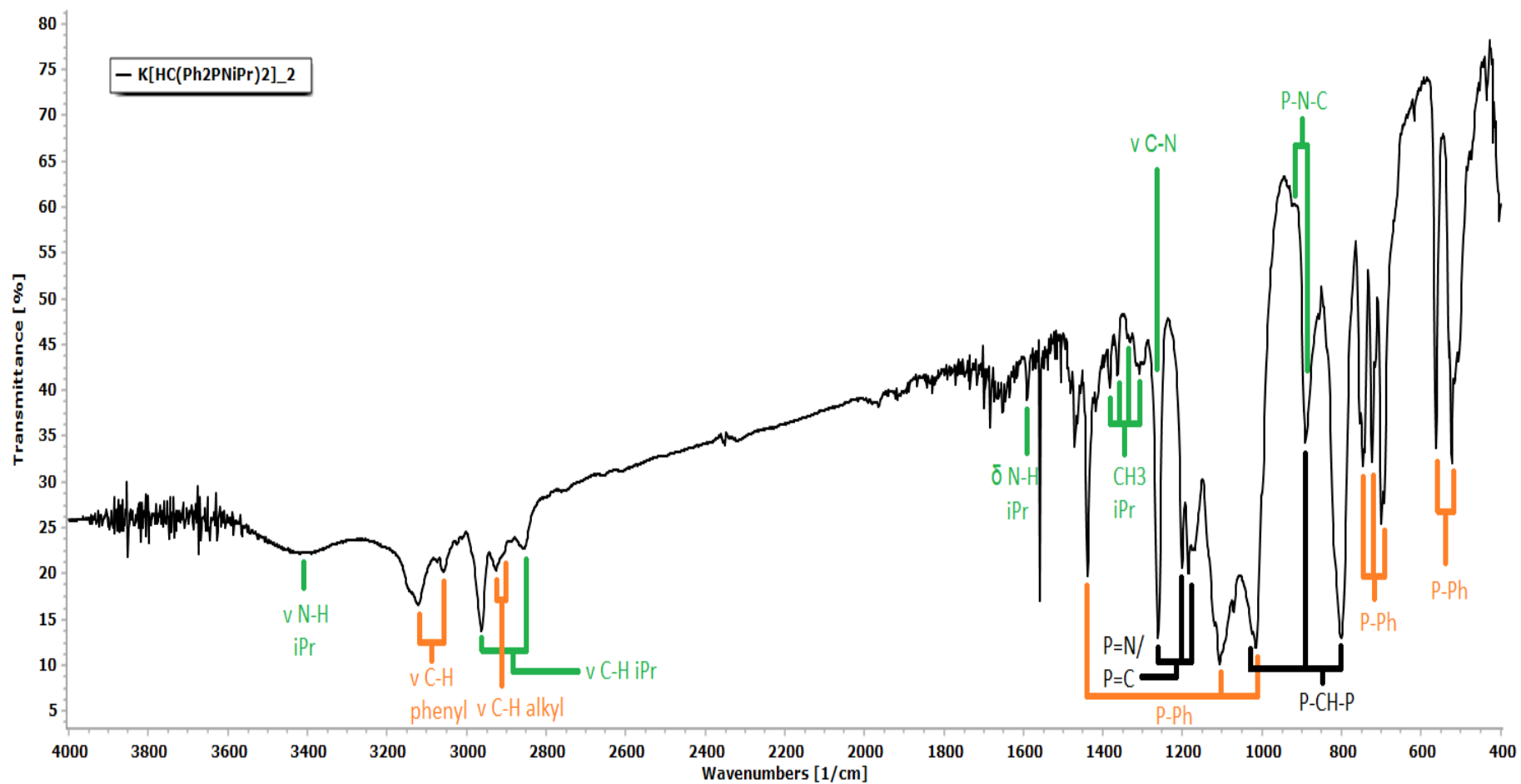


Figure 4.7: Tentative band assignment for IR spectrum of product $K[HC(Ph_2PNiPr)_2]_2$.

The bands at 1016 cm⁻¹, 890 cm⁻¹ and 801 cm⁻¹ comprise the other group of bands that may be diagnostic to the formation of the methanide salt. The latter falls in the range known for the stretching vibrations of the P–CH₂–P moiety. The expected bonding present in the product is P–CH–P but no IR studies are known dedicated specifically for this moiety and therefore no direct comparisons could be made. Given the expected change in symmetry of the moiety a shift was expected but since no data is known from literature only a very tentative discussion could be posited. The bands at 1016 cm⁻¹ and 890 cm⁻¹ are commonly in a higher range than expected for P–CH₂–P.⁹⁹ An increase in the bond order of the P–C(methanide), due to increased electron delocalisation from the anionic methanide to the higher energy orbitals of the phosphorus, could cause such a shift.^{99,281} The two bands at 1016 cm⁻¹ and 890 cm⁻¹ can therefore be attributed to ν_{as} P⁺–CH⁻–P⁺ vibrations while the band at 801 cm⁻¹ can be attributed to the ν_s P⁺–CH⁻–P⁺ vibration, if such a shift were to occur. It should be noted that the strong band at 1016 cm⁻¹ can also be due to P–Ph vibrations and therefore the assignment is not definitive. Finally the shoulder at 926 cm⁻¹ and the band at 890 cm⁻¹ can also be attributed to the P–N–C bending vibration. The shoulder could be due to minute amounts of unreacted reagent and it might be shifted from the 908 cm⁻¹ band observed in the [H₂C(Ph₂PNH(*i*Pr))₂]Br₂_1 spectrum. The band at 890 cm⁻¹ can be due to the formation of the P=N–C moiety and its related bending vibration.⁹⁹

4.1.1.1.2.2 Analysis by ¹H NMR spectroscopy

Similarly to the IR spectra, the products K[HC(Ph₂PN*i*Pr)₂]₁ and K[HC(Ph₂PN*i*Pr)₂]₂ gave similar ¹H NMR spectra, with the respective spectra being shown in Figure 4.8 and Figure 4.9. Both spectra were obtained in CDCl₃ as solvent. Literature data for the ¹H NMR of this compound has not been published, although Demange and co-workers published the ¹H NMR data of the lithium salt of bis(diphenyl-*N-iso*-propyl-iminophosphorano)methanide in THF-*d*₈. This literature data has been reproduced in Table 4.4.

Table 4.4: ^1H NMR literature data published for $\text{Li}[\text{HC}(\text{Ph}_2\text{PNiPr})_2]$ in THF-d_8 .³⁶

^1H NMR Literature Data published for $\text{Li}[\text{HC}(\text{Ph}_2\text{PNiPr})_2]$ in THF-d_8				
ppm	Assignment	Multiplicity	Calc. no. ^1H	Coupling
7.59	m-H	triplet	8	N/A
7.34	p-H	triplet	4	$^3J_{\text{HH}} = 7.5 \text{ Hz}$
7.26	o-H	triplet	8	$^3J_{\text{HH}} = 7.5 \text{ Hz}$ $^3J_{\text{HH}} = 7.0 \text{ Hz}$
3.18	$\text{NCH}(i\text{Pr})$	septet of doublets	2	$^3J_{\text{HH}} = 6.0 \text{ Hz}$ $^3J_{\text{HP}} = 19.5 \text{ Hz}$
1.05	$\text{CH}_3(i\text{Pr})$	doublet	12	$^3J_{\text{HH}} = 6.0 \text{ Hz}$
0.86	PCHP	triplet	1	$^2J_{\text{HP}} = 3.0 \text{ Hz}$

The two spectra of the products were very similar and there was also a correlation in specific data details. This similarity indicated that the two products obtained were the same or very similar. In both cases the last three peaks listed in the literature data were found to be present in the experimental data. Figures 4.10 and 4.11 show details from the full spectra of the products, highlighting the three peaks found in the range 4 ppm to 0 ppm.

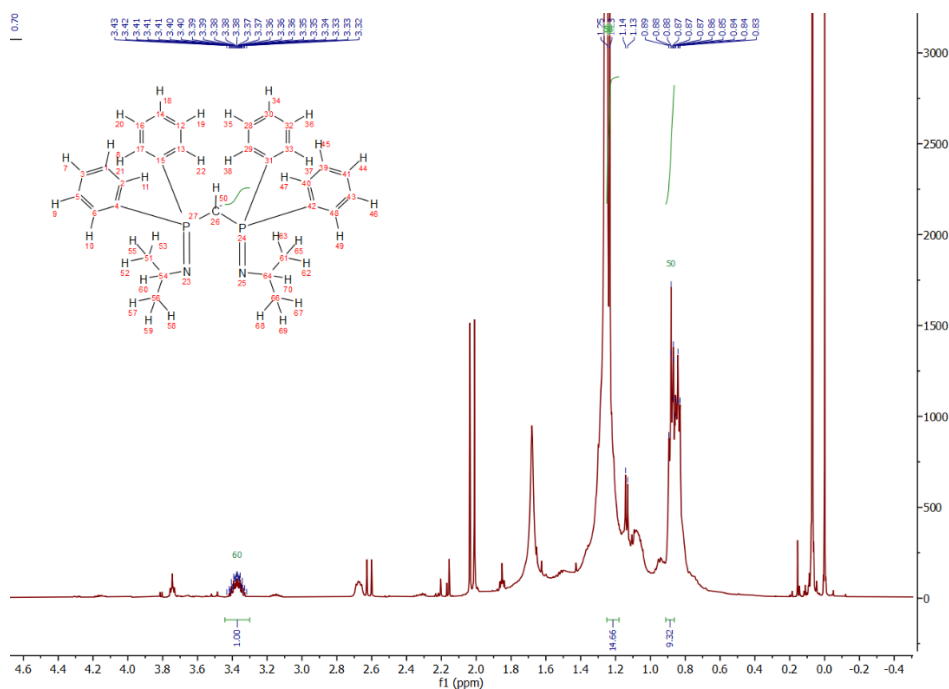


Figure 4.10: ^1H NMR spectrum in the range of 4-0 ppm for $\text{K}[\text{HC}(\text{Ph}_2\text{PNiPr})_2]_1$ in CDCl_3 .

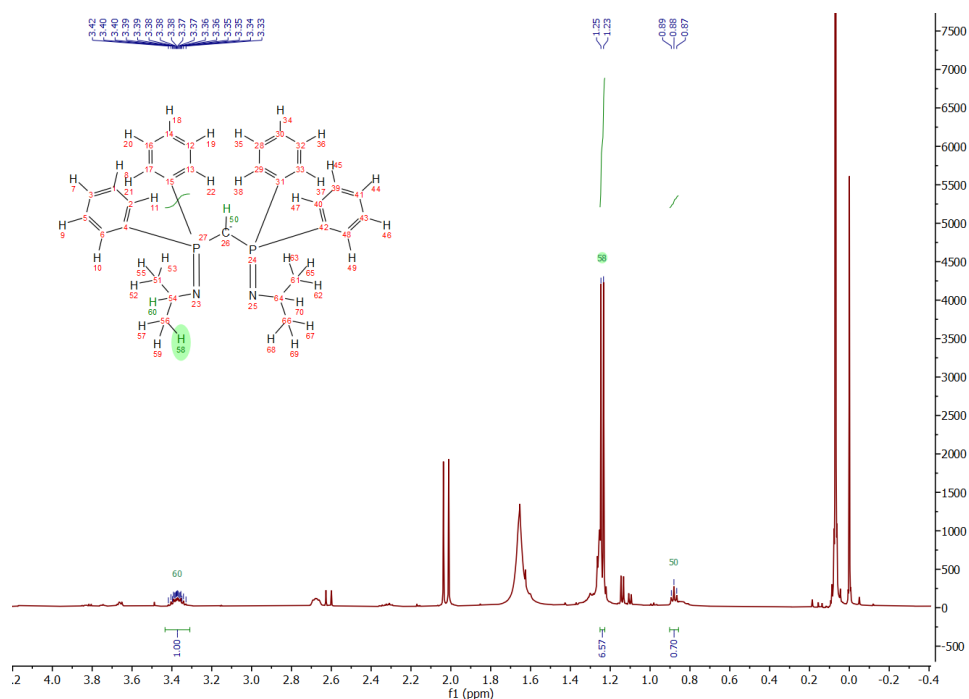


Figure 4.11: ^1H NMR spectrum in the range of 4-0 ppm for $\text{K}[\text{HC}(\text{Ph}_2\text{PNiPr})_2]_2$ in CDCl_3 .

In both figures the peaks of interest are labelled. In both spectra other peaks were present and it is believed that these were due to impurities such as water (1.65 ppm) and grease (1.26 ppm and 0.85 ppm) or by-products (2.02 ppm). The assignment, chemical shifts and peak integration values from the experimental data are listed and compared to the literature data in Table 4.5.

Table 4.5: Comparison of data for the literature Li salt (in THF-d_8) and the two products $\text{K}[\text{HC}(\text{Ph}_2\text{PNiPr})_2]_1$ (1) and $\text{K}[\text{HC}(\text{Ph}_2\text{PNiPr})_2]_2$ (2) (both in CDCl_3).

Comparison of Experimental Data for Products $\text{K}[\text{HC}(\text{Ph}_2\text{PNiPr})_2]_1$ (<u>1</u>) and $\text{K}[\text{HC}(\text{Ph}_2\text{PNiPr})_2]_2$ (<u>2</u>) to Literature Data						
Assignment	ppm			Calc. No. of ^1H		
	Literature	Experimental		Literature	Experimental	
		<u>1</u>	<u>2</u>		<u>1</u>	<u>2</u>
NCH(<i>i</i> Pr)	3.18	3.37	3.37	2	2.0	2.0
CH ₃ (<i>i</i> Pr)	1.05	1.24	1.24	12	29.32	13.14
PCHP	0.86	0.88	0.88	1	18.64	1.40

The chemical shifts of the two products were in agreement with each other and the triplet at 0.88 ppm for both products was also in close agreement with the literature value of 0.86 ppm. These triplets showed an upfield shift from the analogous triplet found in the spectrum of dppm at 2.80 ppm and that found in the spectrum of $[\text{H}_2\text{C}(\text{Ph}_2\text{PNH}(i\text{Pr}))_2]\text{Br}_2\text{-1}$ at 6.56 ppm. This was attributed in literature to the concentration of the anionic lone pair on a sp^3 hybridised methanide centre.³⁶ However the peaks in the spectra of the products assigned to $\text{CH}_3(i\text{Pr})$ and $\text{NCH}(i\text{Pr})$ were distinctly downfield by a value of 0.19 ppm as compared to the values given in literature. Whether this shift was due to structural differences, the presence of impurities or the differences in solvent is unknown, although the latter is unlikely given that the *iso*-propyl hydrogens are believed to be non H-bonding.

In both samples integration was undergone with the multiplet assigned to $\text{NCH}(i\text{Pr})$ set as the reference 1.00. The experimental integration data for the product $\text{K}[\text{HC}(\text{Ph}_2\text{PN}i\text{Pr})_2]\text{-2}$ was found to be more in agreement with the literature integration data as compared to that of $\text{K}[\text{HC}(\text{Ph}_2\text{PN}i\text{Pr})_2]\text{-1}$. The calculated number of protons for the PCHP, $\text{CH}_3(i\text{Pr})$ and $\text{NCH}(i\text{Pr})$ multiplets in $\text{K}[\text{HC}(\text{Ph}_2\text{PN}i\text{Pr})_2]\text{-2}$ were found to be 1.4, 13.14 and 2 respectively, with the former two being slightly larger than the values expected. The increased value for the doublet assigned to $\text{CH}_3(i\text{Pr})$ could have resulted from the overlap of the doublet with a small broad peak downfield of it, thus altering the calculated value of the integration. The same can be said for the triplet at 0.88 ppm wherein the increase in the integration value is due to the triplet overlapping with the multiplet upfield to it. The integration data for the product $\text{K}[\text{HC}(\text{Ph}_2\text{PN}i\text{Pr})_2]\text{-1}$ was found to be uncharacteristic of the expected composition, with little information being attainable from the results. This could be due to a number of peaks resulting from the presence of impurities which overlap with the peaks of the product and therefore make the calculation of the peak integration unreliable. These impurity peaks were visible as a singlet downfield of the doublet at 1.24 ppm and a multiplet upfield of the triplet at 0.88 ppm both previously attributed to grease contamination.

The coupling constants of the experimental peaks in the spectra of both products were found to be identical and therefore the following discussion will focus on the data for the product $\text{K}[\text{HC}(\text{Ph}_2\text{PN}i\text{Pr})_2]\text{-2}$ only. The coupling constants described in literature and those obtained in the experimental spectrum of $\text{K}[\text{HC}(\text{Ph}_2\text{PN}i\text{Pr})_2]\text{-2}$ are given in Table 4.6. The coupling constants in the spectrum of the product are presented for each multiplet in Figures 4.12, 4.13 and 4.14.

Table 4.6: Comparison of coupling constants for literature data and experimental data for $K[HC(Ph_2PNiPr)_2]_2$.

Coupling Constants for Literature Data and Experimental Data for $K[HC(Ph_2PNiPr)_2]_2$				
Ppm	Assignment	Multiplet	Literature	$K[HC(Ph_2PNiPr)_2]_2$
3.37	NCH(<i>i</i> Pr)	Multiplet/Septet of doublets	$^3J_{HH} = 6.0$ Hz $^3J_{HP} = 19.5$ Hz	$^3J_{HH} = 6.29$ Hz $^3J_{HP} = 19.2$ Hz
1.24	CH ₃ (<i>i</i> Pr)	Doublet	$^3J_{HH} = 6.0$ Hz	$^3J_{HH} = 6.5$ Hz
0.88	PCHP	Triplet	$^2J_{HP} = 3.0$ Hz	$^2J_{HP} = 6.9$ Hz

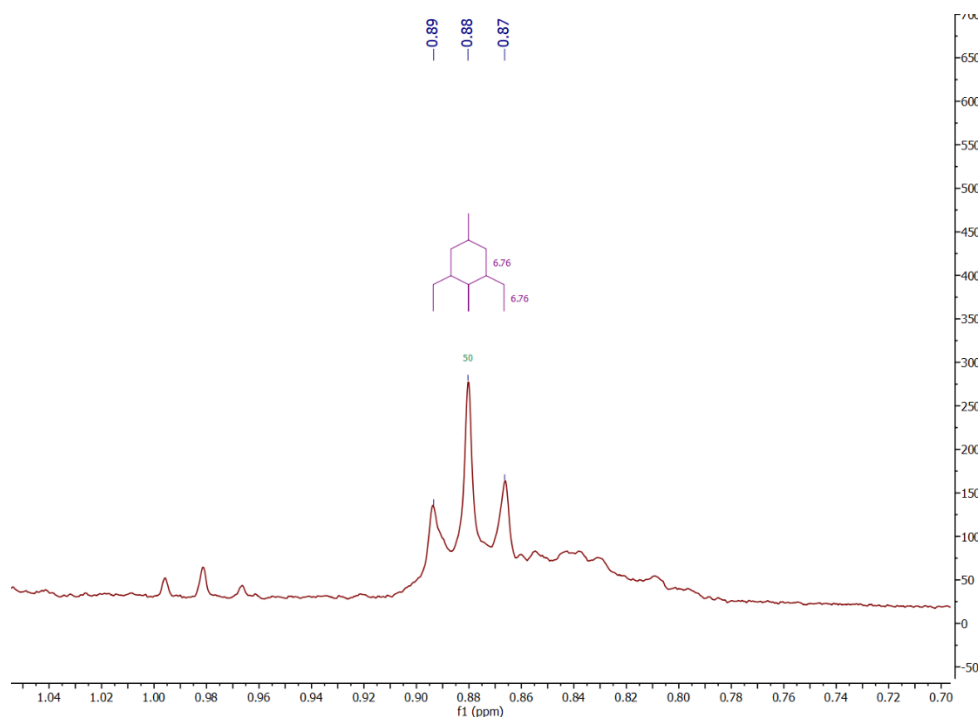


Figure 4.12: Triplet attributed to the PCHP protons in the 1H NMR spectrum of $K[HC(Ph_2PNiPr)_2]_2$.

Although the chemical shift of the triplet attributed to PCHP in $K[HC(Ph_2PNiPr)_2]_2$ was in good agreement with the literature data for the lithium analogue, the coupling constant was distinctly larger at 6.9 Hz against the expected 3.0 Hz. In both literature and experimental data the coupling constant was markedly decreased from the value of the PCH₂P triplet in $[H_2C(Ph_2PNH(*i*Pr))_2]Br_2$, which was of

16.0 Hz. The methanide anion may be electropositive enough to effect this marked decrease in the ${}^2J_{\text{HP}}$ given that both NMR active atoms are bound directly to it. Such a relationship between the decreased electronegativity of an atom bound to an NMR active atom is known through the relationship of the electronegativity with the reduced coupling constant, 2K .²⁸² This does not explain the marked difference between the experimental and literature values, although it gives an indication as to the formation of the anionic methanide from the aminophosphonium derivative.

The doublet attributed to the $\text{CH}_3(i\text{Pr})$ protons shown in Figure 4.13 gave a ${}^3J_{\text{HH}} = 6.5$ Hz which was similar to the expected value of 6.0 Hz. This clearly indicated the presence of the iso-propyl group.

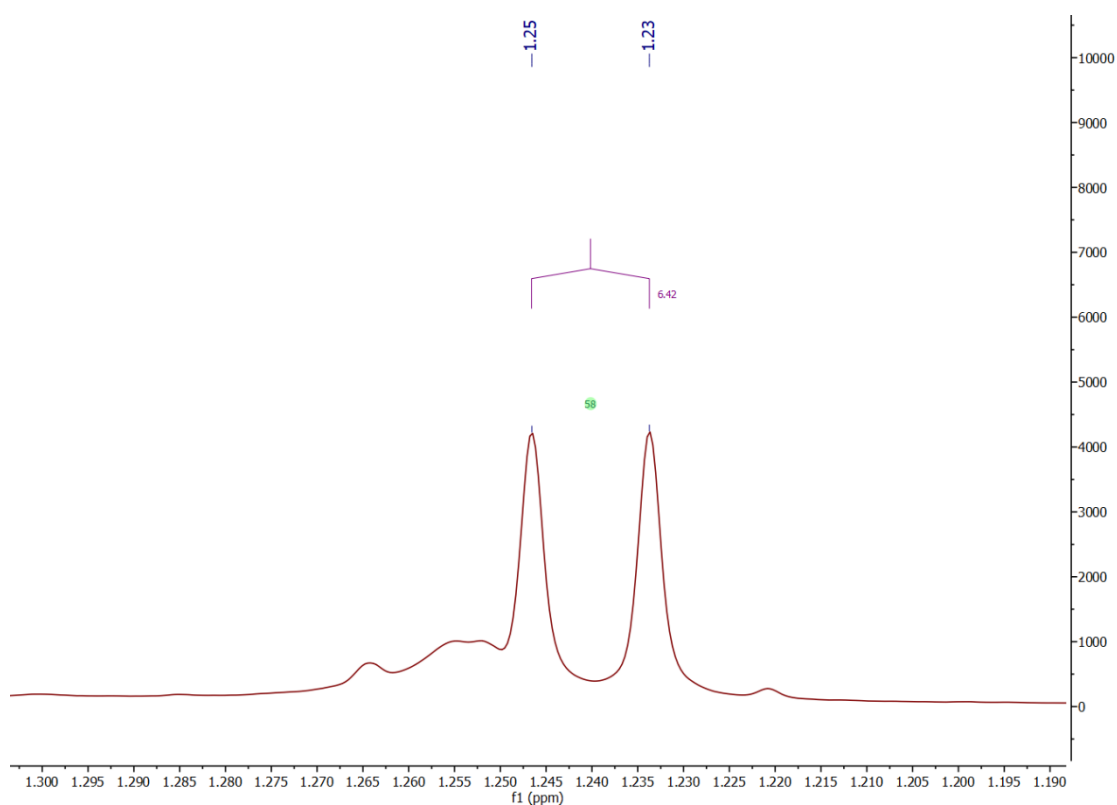


Figure 4.13: Doublet associated with the $\text{CH}_3(i\text{Pr})$ protons in the ${}^1\text{H}$ NMR spectrum of $\text{K}[\text{HC}(\text{Ph}_2\text{PNiPr})_2]_2$.

Figure 4.14 shows in detail the multiplet assigned to the $\text{NCH}(i\text{Pr})$ protons in the spectrum of the product. The chemical shift and the integration of this multiplet gave expected values, however the multiplicity proved complex. Despite the complex nature of the multiplet, coupling similar to that observed in literature for the analogous lithium salt was apparent. A doublet of septets superstructure was visible, with coupling constants $J_1 = 19.2$ Hz (d) and $J_2 = 6.29$ Hz (sept), as given in Figure 4.15. These coupling constants

were in agreement with the two literature values of ${}^3J_{\text{HP}} = 19.5 \text{ Hz}$ and ${}^3J_{\text{HH}} = 6.0 \text{ Hz}$. For the expected structure the doublet of septets obtained in the current study was more in line with expected observations than a septet of doublets as described in literature. This indicated that the proton in question was likely the $\text{NCH}(i\text{Pr})$ proton, coupled with both the $\text{CH}_3(i\text{Pr})$ protons (${}^3J_{\text{HH}} = 6.29 \text{ Hz}$) and the phosphorus (V) centres to yield ${}^3J_{\text{HP}} = 19.2 \text{ Hz}$. The latter coupling may also support the formation of the desired compound given that J_{HP} coupling constants are sensitive to the oxidation state and chemical environment on the phosphorus centres.²⁸²

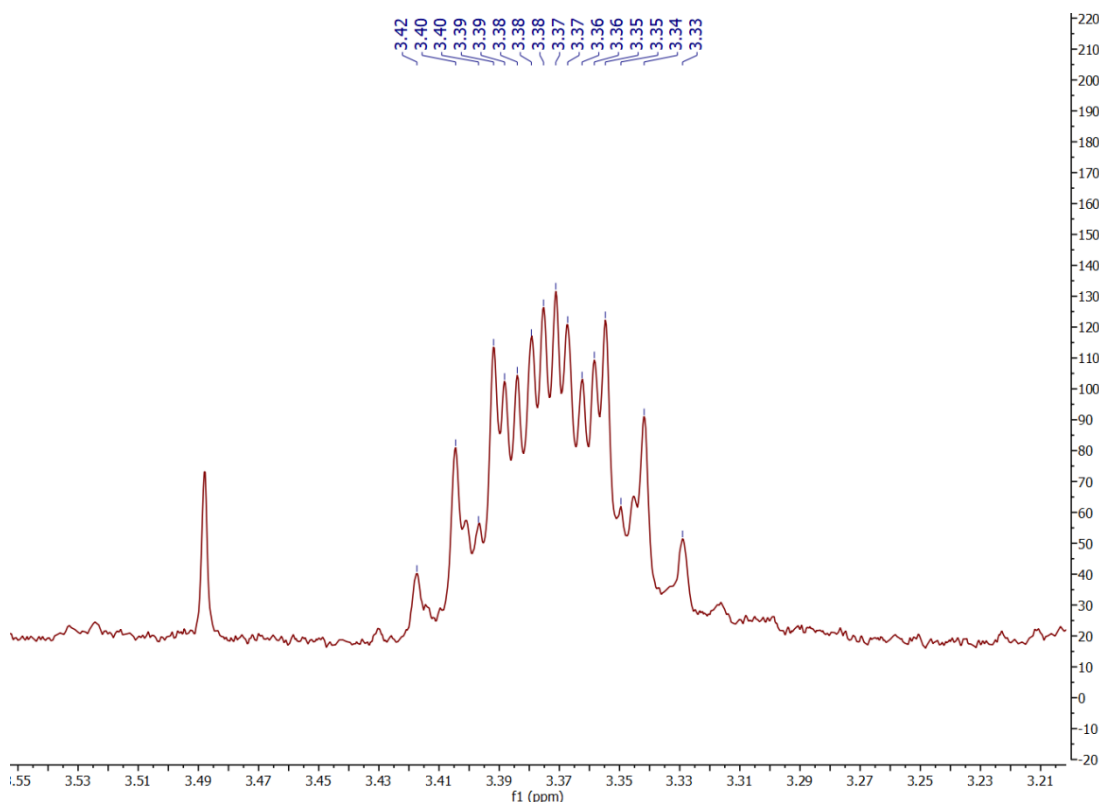


Figure 4.14: Multiplet associated with the $\text{NCH}(i\text{Pr})$ protons in the ${}^1\text{H}$ NMR spectrum of $\text{K}[\text{HC}(\text{Ph}_2\text{PN}i\text{Pr})_2]_2$.

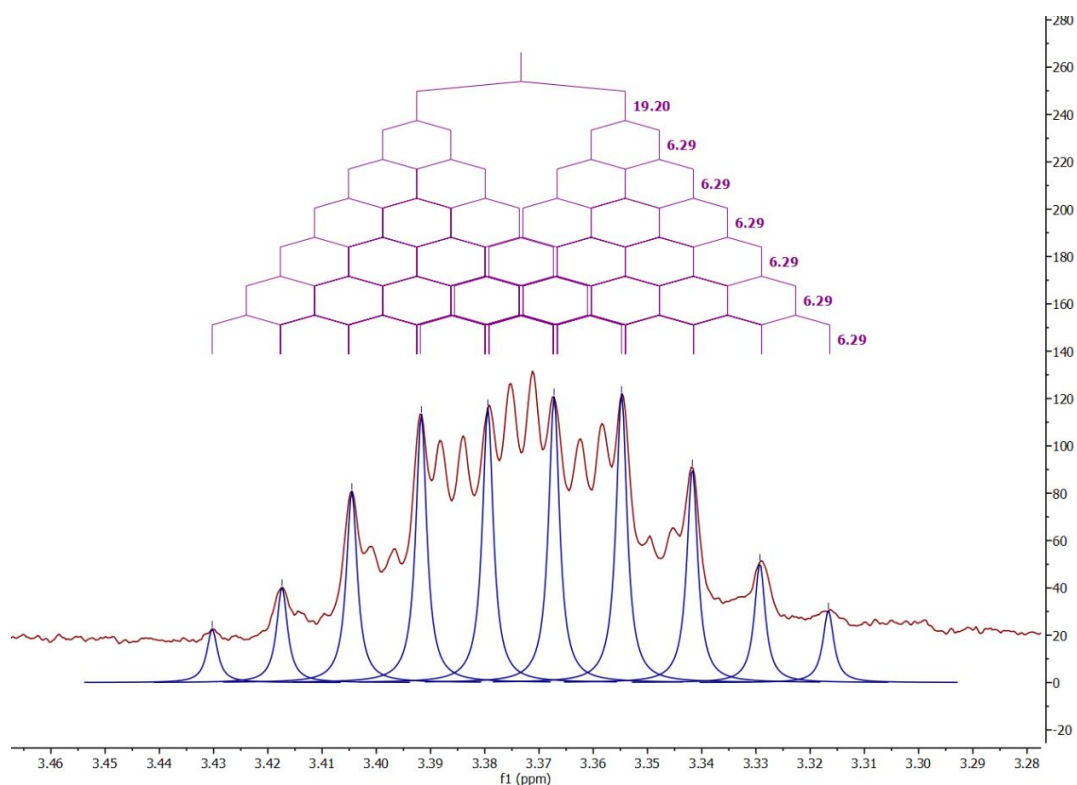


Figure 4.15: Basic coupling observable for the multiplet associated with the NCH(*i*Pr) protons in the ^1H NMR spectrum of $\text{K}[\text{HC}(\text{Ph}_2\text{PNiPr})_2]_2$.

The remaining peaks were more difficult to describe and therefore little characterisation data could be collected. The symmetric nature of the peaks suggests that the multiplet was due to chemically equivalent protons as would be expected for the two NCH(*i*Pr) protons in the expected symmetric molecule and that this multiplet formation was possibly due to further coupling. The further coupling could be due to numerous effects. Coupling with nitrogen is a possibility though this is rarely observed and described. The nucleus of the major isotope of nitrogen (^{14}N) is quadrupolar with a quantum spin number of 1 ($I=1$) and a strong quadrupolar moment.²⁸³ The quantum spin number of 1 leads to a basic theoretical J_{HN} coupling which should be a triplet of equally intense peaks, although various factors can cause a change in relative intensity of the triplet peaks.^{284–286} The strong quadrupole moment also leads to rapid quadrupole relaxation, causing peak broadening which makes description of such multiplets more difficult.²⁸⁶ It is also known that such J_{HN} coupling can be negative, further complicating description.²⁸⁷ Therefore this complex coupling could be related to this type of coupling, further to the doublet of septets described prior. Such complex coupling however is not typically described for other species containing the P=N–C–H moiety, although in some cases multiplets are described wherein no further detail is given.^{288–292}

Coordination with the K^+ cation in solution may be another possibility for the complex nature of the multiplet. Alkali metal complexes of various bis(iminophosphorane)methanides do not form planar species about the cation to methanide carbon axis but rather partially puckered rings, the stability of which can be influenced by numerous factors.^{191,192} This is true for $Li[HC(Ph_2PN*i*Pr)_2] \cdot THF$, the closest analogue to $K[HC(Ph_2PN*i*Pr)_2]$. Coordination in $K[HC(Ph_2PN*i*Pr)_2]$ is expected to be similar to that of such analogues. The $NCH(*i*Pr)$ protons can interact with the K^+ cation through electrostatic $K \cdots H$ interactions in different conformations should these prove beneficial to the stability of the complex.²⁹³ Such interactions are not known for the $Li[HC(Ph_2PN*i*Pr)_2] \cdot THF$ species,²⁹⁴ however similar interactions have been described for K^+ salts of other bis(iminophosphorane)methanides.^{191,192} These interactions could constrain one or both of the two $NCH(*i*Pr)$ protons to different chemical or magnetic environments leading to the observation of a complex multiplet. Such complex multiplets could occur due to the overlapping unique peaks obtained for the newly non-equivalent $NCH(*i*Pr)$ protons although asymmetric multiplets would be more likely in such a case. These interactions are also more likely preserved in the nonpolar $CDCl_3$ used in the current study than the coordinating $THF-d_8$ used in literature.

Peaks attributable to the phenyl protons, which are usually found in the region of 8.00 to 7.00 ppm, were clearly visible in the spectra of the two products and closer inspection revealed near identical spectra in this region. This corroborated the evidence that the two products were identical in composition. The peaks found in this region of the 1H NMR spectrum of $K[HC(Ph_2PN*i*Pr)_2]_2$ are given in Figure 4.16. These peaks had limited similarity to those reported in literature data, with no obvious identifiable triplets. Furthermore they were all shifted downfield to a range between 8.00-7.40 ppm, as compared to the literature range of 7.59-7.26 ppm (in $THF-d_8$). Information from the integration of the peaks in this range did not yield results which could corroborate the molecular structure expected, as the values obtained indicated a species containing approximately 35 aromatic protons (per 1 NCH proton), which is greater than the expected 20 protons. This difference in integration values indicated that other aromatic species may have been present in the sample, accounting for the excess proton integration values.

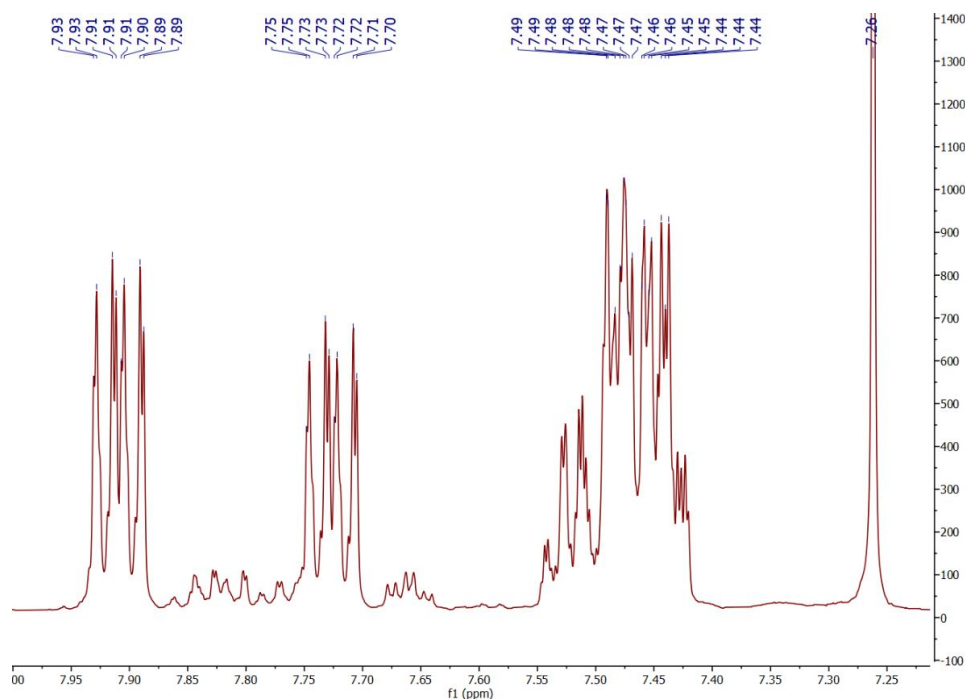


Figure 4.16: Peaks in the ^1H NMR spectrum of $\text{K}[\text{HC}(\text{Ph}_2\text{PNiPr})_2]_2$ in CDCl_3 found in the range typical of phenyl protons.

In both spectra numerous peaks, shown in Figures 4.10 and 4.11, were attributed to other impurities. The doublet at 2.02 ppm, with $J = 13.3$ Hz, is of interest in the discussion of the aromatic peaks. This peak was likely due to the methyl protons of methyldiphenylphosphine oxide, $\text{Ph}_2\text{P}(\text{O})\text{Me}$, a known moisture induced decomposition product for bis(diphenyliminophosphorane)methylene derivatives, such as the expected product and the main starting reagent.^{295,296} Therefore the respective peaks in the aromatic region for this decomposition product were also expected. This can help explain the difference in integration values for the experimental aromatic peaks, due to overlap of the aromatic peaks expected for the product and decomposition product.

The integration ratio of the peaks attributed to the combined aromatic protons, the product NCH protons and the $\text{Ph}_2\text{P}(\text{O})\text{Me}$ methyl protons was of 17.8:1:2.55. It was clear that the integration of the aromatic peaks is a summation of integration values of the aromatic protons for both species as per their relative concentrations in the sample. The presence of $\text{Ph}_2\text{P}(\text{O})\text{Me}$ could indicate some level of decomposition on reaction, storage or sample preparation. The presence of $\text{Ph}_2\text{P}(\text{O})\text{Me}$ could not be determined through the IR data presented in Section 4.1.1.1.2.1. as only the band at 1170 cm^{-1} could be related to literature IR data and the diagnostic peak at 1304 cm^{-1} related to $\nu\text{ P-CH}_3$ vibration was not obtained in the experimental spectrum.²⁹⁶ This supports the possibility of decomposition on sample preparation.

Two multiplets at 7.90 ppm and 7.70 ppm ($J_1 = 1.48$ Hz, $J_2 = 8.07$ Hz, $J_3 = 11.9$ Hz), as shown in Figure 4.17, were of interest. The coupling constant of 11.9 Hz could be due to $^3J_{\text{HP}}$ coupling, indicating that both these peaks are due to o-H protons. These two peaks could be due to two distinct o-H multiplets for the expected product and $\text{Ph}_2\text{P}(\text{O})\text{Me}$, although further assignment was not possible. However the similarity in structure and the presence of the same coupling constants in both peaks indicated that the respective protons were present in the same species. Therefore, for both the expected product and the decomposition product a strict assignment of the various aromatic protons, typically in terms of ortho, meta and para protons, could not be made, as was the case for the starting reagent $[\text{H}_2\text{C}(\text{Ph}_2\text{PNH}(i\text{Pr}))_2]\text{Br}_2_1$. Further characterisation information from the multiplet at 7.45 ppm was not possible, as this was clearly composed of overlapping aromatic proton peaks. Integration values for all three peaks at 7.90 ppm, 7.70 ppm and 7.45 ppm could not help in assignment of the specific aromatic protons.

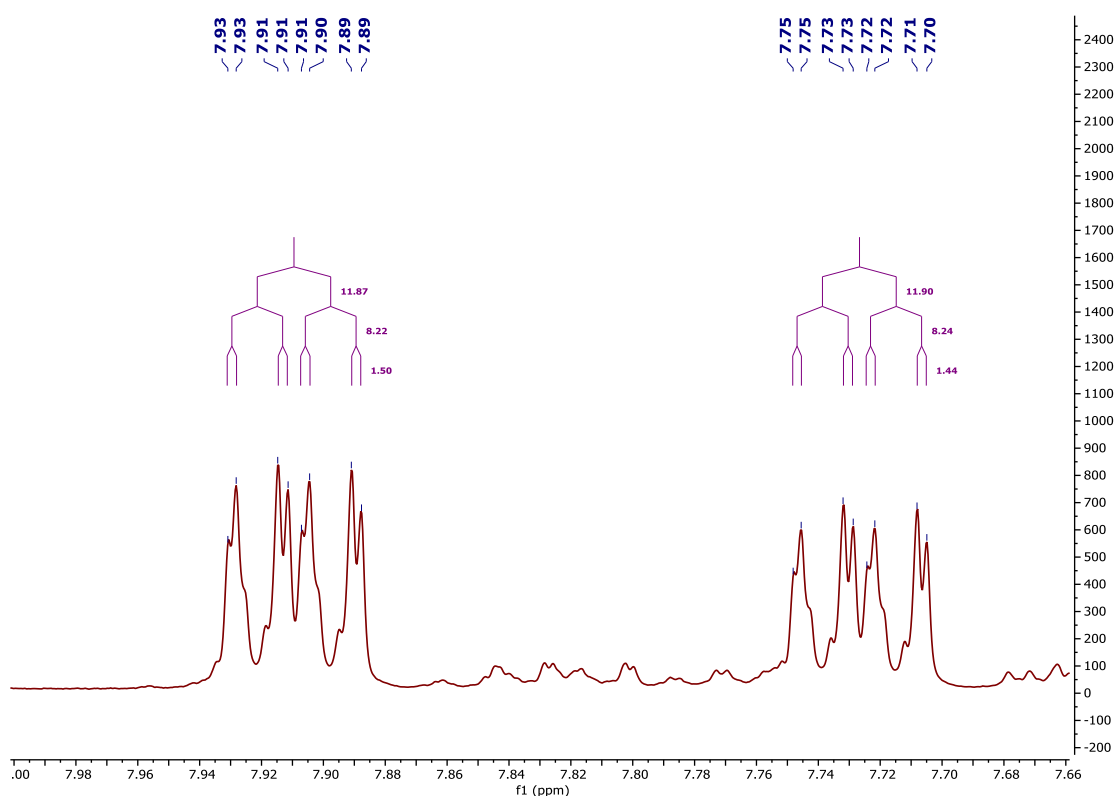


Figure 4.17: Structure of coupling for peaks around 7.90 ppm and 7.70 ppm for the ^1H NMR spectrum of $\text{K}[\text{HC}(\text{Ph}_2\text{PNiPr})_2]_2$ in CDCl_3 .

4.1.1.1.2.3 Analysis by Powder X-ray diffraction

Powder X-ray diffraction data for $\text{K}[\text{HC}(\text{Ph}_2\text{PNiPr})_2]_2$ was collected from powder packed in a 0.5 mm capillary which was sealed under dry nitrogen. The data was collected using $\text{Mo-K}\alpha_1$ radiation. The sample data was compared to the calculated powder pattern for the starting reagent $[\text{H}_2\text{C}(\text{Ph}_2\text{PNH}(i\text{Pr}))_2]\text{Br}_2$ (CCDC Refcode: WERRUH), as given in Figure 4.18. The data for the reagent was obtained from literature data and calculated using Mercury.^{36,297} Although the two patterns showed superficial similarities a closer examination revealed that there were no analogous peaks. Therefore, the product $\text{K}[\text{HC}(\text{Ph}_2\text{PNiPr})_2]_2$ was not the starting reagent $[\text{H}_2\text{C}(\text{Ph}_2\text{PNH}(i\text{Pr}))_2]\text{Br}_2$ and this reagent was unlikely to have remained in the solid product. This supported the IR and ^1H NMR data for $\text{K}[\text{HC}(\text{Ph}_2\text{PNiPr})_2]_2$. Detailed analysis and structure solution of this novel PXRD pattern is currently being undertaken in order to describe the structure of $\text{K}[\text{HC}(\text{Ph}_2\text{PNiPr})_2]_2$. Although some deviation was observed in the ^1H NMR data for $\text{K}[\text{HC}(\text{Ph}_2\text{PNiPr})_2]_2$, on comparison with literature data for the lithium analogue, the solid was believed to be $\text{K}[\text{HC}(\text{Ph}_2\text{PNiPr})_2]$ and the powder pattern obtained was novel and therefore the structure in question is believed to be previously unreported.

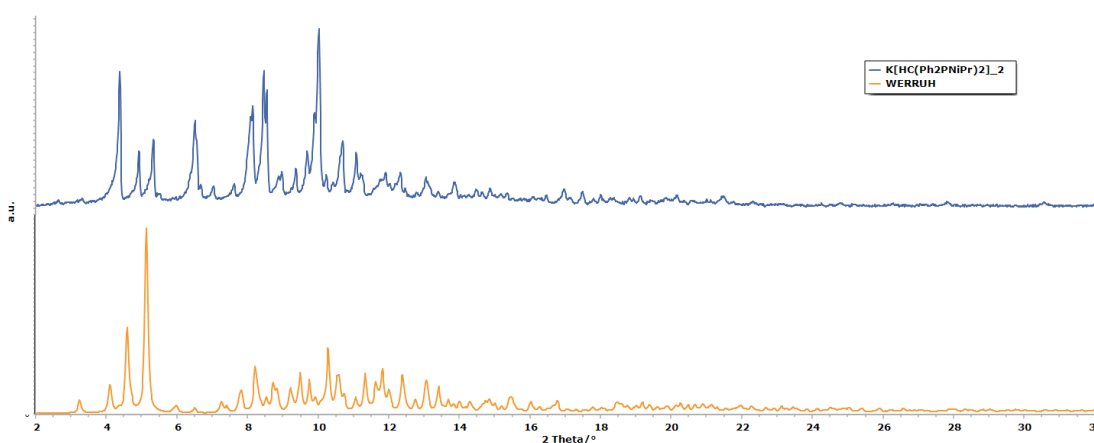


Figure 4.18: PXRD patterns of $\text{K}[\text{HC}(\text{Ph}_2\text{PNiPr})_2]_2$ (blue) and $[\text{H}_2\text{C}(\text{Ph}_2\text{PNH}(i\text{Pr}))_2]\text{Br}_2$ REFCODE: WERRUH (orange).

4.1.1.1.2.4 Conclusion

Although the IR spectroscopy data for both $\text{K}[\text{HC}(\text{Ph}_2\text{PNiPr})_2]_1$ and $\text{K}[\text{HC}(\text{Ph}_2\text{PNiPr})_2]_2$ were promising and indicated that many of the expected moiety changes from the $[\text{H}_2\text{C}(\text{Ph}_2\text{PNH}(i\text{Pr}))_2]\text{Br}_2$ reagent occurred, these could not definitely

characterise the composition of the product. ^1H NMR data was in line with the expected data in relation to the anionic methanide and the $\text{P}=\text{N}-i\text{Pr}$ group, which corroborated the formation of the desired salt. The main differences between the experimental and literature ^1H NMR spectroscopy data for the lithium analogue occurred in the region typically containing phenyl proton peaks. These differences along with the presence of a doublet at 2.02 ppm indicated that the product obtained partially decomposed some time during ^1H NMR sample preparation. PXRD data indicated the formation of a crystalline solid which was not composed of the XRD characterised $[\text{H}_2\text{C}(\text{Ph}_2\text{PNH}(i\text{Pr}))_2]\text{Br}_2$ or other structurally characterised co-products. Therefore the solid obtained for $\text{K}[\text{HC}(\text{Ph}_2\text{PN}i\text{Pr})_2]_2$ could be $\text{K}[\text{HC}(\text{Ph}_2\text{PN}i\text{Pr})_2]$ and the PXRD pattern obtained indicated a novel structure which should be the first described for this compound.

4.1.1.2. Characterisation of $\text{H}_2\text{C}(\text{Ph}_2\text{PNSiMe}_3)_2$.

Three batches of $\text{H}_2\text{C}(\text{Ph}_2\text{PNSiMe}_3)_2$ were initially prepared by following the Phospha-Staudinger method as described in Section 2.4.3.1.1. All three products yielded white or off-white solids with yields of 96.7% and 74.4% for crystalline solids obtained directly from reaction and 35% for $\text{H}_2\text{C}(\text{Ph}_2\text{PNSiMe}_3)_2_1$ which was recrystallized from acetonitrile. The products were analysed by IR and ^1H NMR spectroscopy. Literature data for both these techniques is available and therefore the characterisation of the products obtained was mainly undergone by comparison to the literature data.^{34,276}

4.1.1.2.1. Analysis by Infra-red spectroscopy

IR spectra of $\text{H}_2\text{C}(\text{Ph}_2\text{PNSiMe}_3)_2_1$, $\text{H}_2\text{C}(\text{Ph}_2\text{PNSiMe}_3)_2_2$ and $\text{H}_2\text{C}(\text{Ph}_2\text{PNSiMe}_3)_2_3$ were compared to IR spectra of the two main reagents dppm and trimethylsilyl azide.²⁹⁸ The loss of the diagnostic $\nu_{\text{as}} \text{N}=\text{N}=\text{N}$ azide band at 2140 cm^{-1} for trimethylsilyl azide indicated that a reaction occurred. The presence of bands at 1273 cm^{-1} and 851 cm^{-1} for the products indicated the formation of a $\text{P}=\text{N}$ bond and a trimethylsilyl group containing compound similar to what was expected. Comparison of this experimental data with literature data confirmed the formation of the desired ligand in all three cases. Tentative assignments of the most characteristic bands are given in Table 4.7.

Table 4.7: Tentative assignment of characteristic IR bands of $\text{H}_2\text{C}(\text{Ph}_2\text{PNSiMe}_3)_2$ prepared in this study.

Wavenumber, cm^{-1}	Description	Assignment
2948	m	ν C–H (alkyl, SiMe_3)
1435	s	P–Ph
1273	s,b	ν P=N
1238	s	δ C–H (SiMe_3)
1184–998	variable	Fingerprint region peaks
864	w	ν_{as} P–CH ₂ –P or other P–CH ₂ –P vibration
851	s	ρ CH ₃ + ν Si–C or ν P–CH ₂ –P
831	s	ν_{as} P–CH ₂ –P or other P–CH ₂ –P vibration
802	s	ν_{as} P–CH ₂ –P or other P–CH ₂ –P vibration
776	m	ν_{as} P–CH ₂ –P or other P–CH ₂ –P vibration
751–680	variable	P–Ph and ν_{s} P–CH ₂ –P
460	m	Si–N

Where, w = weak, b = broad, m = medium, s = strong, sh = sharp, N/A = non-assigned.

4.1.1.2.2. Analysis by ^1H NMR spectroscopy

Characterisation using this technique was mainly undergone for $\text{H}_2\text{C}(\text{Ph}_2\text{PNSiMe}_3)_2_1$ in benzene- d_6 given the confirmation of the same product being present in all three cases by IR spectroscopy. The most important feature that was observed was the presence of a triplet at 3.29 ppm attributed to the PCH₂P group with a $^2J_{\text{HP}}$ of 13.87 Hz. The chemical shift was slightly upfield to the recorded literature value of 3.42 ppm,³⁴ but still lying in the typical range for such dppm analogues. The coupling constant showed a marked and expected change from the 1.5 Hz observed for the analogous group in dppm. This also agreed with literature data for the compound where the coupling constant was reported as 14 Hz.³⁴ A singlet at 0.26 ppm also corroborated the presence of the trimethylsilyl groups in the amounts expected. Other peaks in the region 0.40 to 0.00 ppm indicated the presence of silicone grease and other simple trimethylsilyl species as significant impurities.

Data regarding the phenyl group protons of the compound $\text{H}_2\text{C}(\text{Ph}_2\text{PNSiMe}_3)_2$ is much less present in the literature. However, the peaks observed for these protons in the spectrum of $\text{H}_2\text{C}(\text{Ph}_2\text{PNSiMe}_3)_{2_1}$ were in the region described in literature and showed definition of the o-H, m-H and p-H protons although only the latter group could be tentatively assigned to the peak at 7.41 ppm. The o-H and m-H protons could be related to the multiplets at 7.93 ppm and 7.65 ppm respectively. This assignment is not strict as the peak at 7.65 ppm had integration values greater than expected, indicating that it was composed of two superimposed peaks. The presence of a large peak at 7.03 ppm also indicated the presence of a secondary phenyl species containing an electron donating group, most likely a silane, but no further details could be given.

4.1.1.2.3. Conclusion

In conclusion the IR spectroscopic data for the products $\text{H}_2\text{C}(\text{Ph}_2\text{PNSiMe}_3)_{2_1}$, $\text{H}_2\text{C}(\text{Ph}_2\text{PNSiMe}_3)_{2_2}$ and $\text{H}_2\text{C}(\text{Ph}_2\text{PNSiMe}_3)_{2_3}$ was in accordance with the literature data and with the expected changes from dppm on reaction. In the former case the recrystallisation from acetonitrile did not affect the composition of the solid. ^1H NMR spectroscopy of the product $\text{H}_2\text{C}(\text{Ph}_2\text{PNSiMe}_3)_{2_1}$ was in agreement with the literature data. A multiplet was tentatively assigned to the p-H protons whilst a singlet was tentatively assigned to the trimethylsilylamine protons further corroborating the formation of the desired ligand. No novel or noteworthy features were observed in the spectra of these products. The relevant spectra and data used for the above discussion are given in Appendix 6.

4.1.1.3. Characterisation of $\text{H}_2\text{C}(\text{Ph}_2\text{PS})_2$.

Bis(diphenylthiophosphinoyl)methane, $\text{H}_2\text{C}(\text{Ph}_2\text{PS})_2$, was prepared multiple times as described in Section 3.3.1.1.3. using the procedure published by Carmalt *et al.* in 1996.³⁵ The singular product obtained in the first attempt and labelled as $\text{H}_2\text{C}(\text{Ph}_2\text{PS})_{2_1}$, was a colourless crystalline solid with a yield of 87%. Subsequent reactions, $\text{H}_2\text{C}(\text{Ph}_2\text{PS})_{2_2}$ and $\text{H}_2\text{C}(\text{Ph}_2\text{PS})_{2_3}$, yielded two distinct products each. The first solids deposited were labelled $\text{H}_2\text{C}(\text{Ph}_2\text{PS})_{2_2\text{a}}$ and $\text{H}_2\text{C}(\text{Ph}_2\text{PS})_{2_3\text{a}}$ and these were obtained as colourless rhombic crystals on cooling the solutions to $-60\text{ }^\circ\text{C}$. The respective

yield of these solids was of 85.8 % and 79.58 %. Products labelled as $\text{H}_2\text{C}(\text{Ph}_2\text{PS})_2_2\text{b}$ and $\text{H}_2\text{C}(\text{Ph}_2\text{PS})_2_3\text{b}$ were obtained as white crystalline powders on the removal of volatiles from the initial filtrates. The respective yield of these solids was of 8.40 % and 10.95 %.

4.1.1.3.1. Analysis by Infra-red spectroscopy

The IR spectrum of the product $\text{H}_2\text{C}(\text{Ph}_2\text{PS})_2_1$ was initially compared to the spectrum of dppm. As expected both spectra were very similar.³⁵ The only new bond expected was the P=S and therefore it is new bands assigned to the vibrations of this bond that were of interest. It is known that the wavenumber range for the diagnostic ν P=S vibration of P=S bonds is $800\text{--}500\text{ cm}^{-1}$.⁹⁹ Therefore a number of bands in this region were assigned to this vibrational mode. Of the bands within this region the three bands at 625 cm^{-1} , 613 cm^{-1} and 594 cm^{-1} were the most likely due to the P=S vibrations, as no other moieties in the expected products or reagents give bands in this region. This was corroborated by literature data.^{299,300}

The IR spectra of $\text{H}_2\text{C}(\text{Ph}_2\text{PS})_2_2\text{a}$ and $\text{H}_2\text{C}(\text{Ph}_2\text{PS})_2_3\text{a}$ were similar to the IR spectrum of $\text{H}_2\text{C}(\text{Ph}_2\text{PS})_2_1$. However, IR data for the products $\text{H}_2\text{C}(\text{Ph}_2\text{PS})_2_2\text{b}$ and $\text{H}_2\text{C}(\text{Ph}_2\text{PS})_2_3\text{b}$ indicated structural differences from the three previously mentioned products. In the range $805\text{--}590\text{ cm}^{-1}$ two distinct sets of bands were noted for different products as shown in Table 4.8. The bands at 803 cm^{-1} and 783 cm^{-1} were assigned to the ν P-CH₂-P vibration while the remaining bands were most likely due to the ν P=S vibrations. The assignment of the band at 752 cm^{-1} was difficult since it appeared in all spectra. The remaining bands in this region that were not discussed were considered as being due to P-Ph vibrations. It was therefore concluded that the two sets of IR spectra were indicative of two different solid state species of the same chemical compound, most easily identified by the unique bands at 803 cm^{-1} and 783 cm^{-1} respectively. $\text{H}_2\text{C}(\text{Ph}_2\text{PS})_2_3\text{a}$ proved to be a mixture of both species. This difference is further highlighted in Figure 4.19 where the IR spectra of $\text{H}_2\text{C}(\text{Ph}_2\text{PS})_2_2\text{a}$, $\text{H}_2\text{C}(\text{Ph}_2\text{PS})_2_2\text{b}$ and dppm are compared. The figure clearly shows the differences in bands assigned to ν P-CH₂-P and ν P=S vibrations for $\text{H}_2\text{C}(\text{Ph}_2\text{PS})_2_2\text{a}$, $\text{H}_2\text{C}(\text{Ph}_2\text{PS})_2_2\text{b}$ and dppm.

Table 4.8: Bands of interest in the IR spectra of all products of $\text{H}_2\text{C}(\text{Ph}_2\text{PS})_2$ in the range 805 to 590 cm^{-1} .

Solids	Bands (cm^{-1})								
$\text{H}_2\text{C}(\text{Ph}_2\text{PS})_2_1$		783	771	752	625		613		594
$\text{H}_2\text{C}(\text{Ph}_2\text{PS})_2_2\text{a}$		783	771	752	625		613		594
$\text{H}_2\text{C}(\text{Ph}_2\text{PS})_2_2\text{b}$	803		771				619		605
$\text{H}_2\text{C}(\text{Ph}_2\text{PS})_2_3\text{a}$	802	783	771	755	626	620	619	605	593
$\text{H}_2\text{C}(\text{Ph}_2\text{PS})_2_3\text{b}$	802		771				619		605

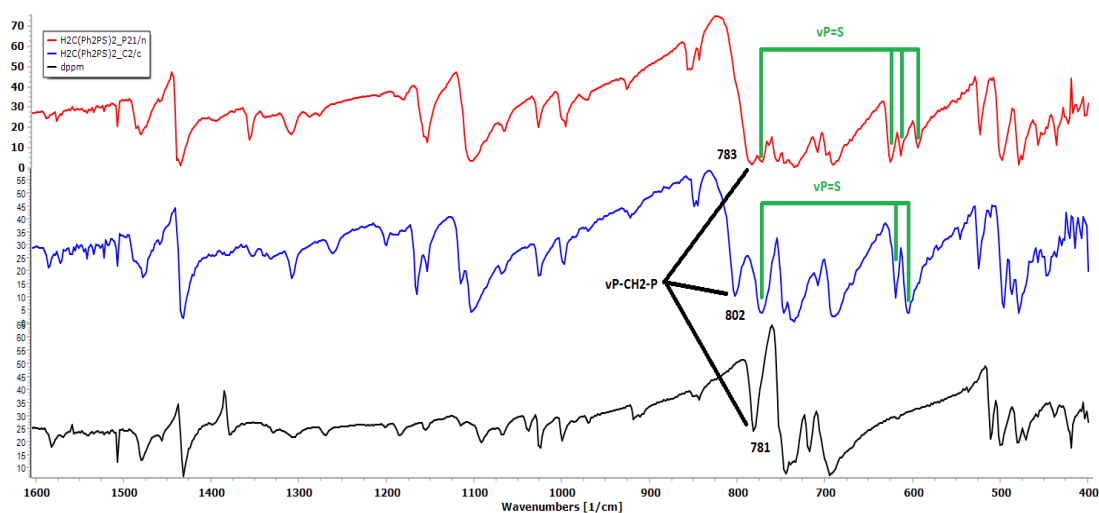


Figure 4.19: IR spectra of dppm (black), $\text{H}_2\text{C}(\text{Ph}_2\text{PS})_2_2\text{a}$ (red) and $\text{H}_2\text{C}(\text{Ph}_2\text{PS})_2_2\text{b}$ (blue).

4.1.1.3.2. Analysis by ^1H NMR spectroscopy

The ligand $\text{H}_2\text{C}(\text{Ph}_2\text{PS})_2_1$ was also analysed by ^1H NMR spectroscopy. Samples were prepared in benzene- d_6 as was described in literature. The most important observation was that of a triplet at around 3.84 ppm. This was attributed to the methylene protons (PCH₂P) in $\text{H}_2\text{C}(\text{Ph}_2\text{PS})_2_1$, forming from a downfield shift of the analogous triplet found at 2.80 ppm in the spectrum of dppm. A change in the coupling constant $^2J_{\text{HP}}$ was also observed from 1.5 Hz in dppm to 13.5 Hz in $\text{H}_2\text{C}(\text{Ph}_2\text{PS})_2_1$. These experimental values were in good agreement with the literature data available, where $\delta = 3.9$ ppm and $^2J_{\text{HP}} = 13.4$ Hz for the methylene protons of $\text{H}_2\text{C}(\text{Ph}_2\text{PS})_2$.^{301,302} Two

multiplets at 6.92 and 7.89 ppm were observed in the spectrum of $\text{H}_2\text{C}(\text{Ph}_2\text{PS})_2_1$. These were easily assigned to the m/p-H and o-H protons on comparison of literature data with the experimental integration data.³⁰¹ The o-H peaks proved to be shifted downfield to those of dppm while the m/p-H peaks proved to be shifted upfield. This trend was observed in literature but to a lesser degree showing that the P=S may exhibit multiple electronic effects on the phenyl protons.

All the products of reactions $\text{H}_2\text{C}(\text{Ph}_2\text{PS})_2_2$ and $\text{H}_2\text{C}(\text{Ph}_2\text{PS})_2_3$ proved to be the same compound as $\text{H}_2\text{C}(\text{Ph}_2\text{PS})_2_1$ on characterisation by ^1H NMR spectroscopy. The ^1H NMR spectra of products of reactions $\text{H}_2\text{C}(\text{Ph}_2\text{PS})_2_2$ and $\text{H}_2\text{C}(\text{Ph}_2\text{PS})_2_3$ were collected in CDCl_3 . The P-CH₂-P methylene triplet was visible in all these spectra at 3.98 ppm with a $^2J_{\text{HP}}$ in the region 13.43–13.35 Hz. This was in close agreement with the analogous peak at 3.84 ppm for the spectrum of $\text{H}_2\text{C}(\text{Ph}_2\text{PS})_2_1$ in benzene-d₆. In these CDCl_3 samples the phenyl protons were fully resolved with peaks at 7.82, 7.42 and 7.33 ppm in a 2:1:2 integration ratio. The triplet at 7.42 ppm was assigned to the p-H protons while the doublet of doublets at 7.82 ppm was assigned to the o-H since it was the only aromatic peak with a coupling constant indicative of the expected $^3J_{\text{HP}}$ (13.13 Hz). The remaining peak was assigned to the m-H. These assignments indicated that the phosphorus centre acts as a mesomeric electron withdrawing group.

4.1.1.3.3. Analysis by Microscopy

The solid $\text{H}_2\text{C}(\text{Ph}_2\text{PS})_2_1$ was checked under the microscope given that relatively large brick like crystals precipitated during work up of the reaction mixture. The blocks were found to be single crystals as they extinguished plane polarised light completely on rotation.

4.1.1.3.4. Analysis by Powder X-ray diffraction

PXRD data was obtained for the crystalline powder $\text{H}_2\text{C}(\text{Ph}_2\text{PS})_2_2\text{b}$. This data was collected at the European Synchrotron Radiation Facility (ESRF), with sample preparation undertaken under an inert atmosphere to ensure minimal exposure to moisture which may change the crystal structure. The data obtained was compared to calculated PXRD patterns of the two $C2/c$ and $P2_1/n$ polymorphs of $\text{H}_2\text{C}(\text{Ph}_2\text{PS})_2$, obtained in

literature, calculated in Mercury.^{35,297,303} This showed that the product H₂C(Ph₂PS)_{2_2b} was mainly composed of the *C2/c* polymorph of H₂C(Ph₂PS)₂, which was first published by Thirumoorthi and co-workers.³⁹ Quantitative Rietveld refinement of the experimental PXRD data for H₂C(Ph₂PS)_{2_2b} indicated the presence of both polymorphs. The major polymorph was confirmed as *C2/c* and it was found to be at a percentage of 80.62 % while the *P2₁/n* polymorph was found to be present at a percentage of 19.38 %.

4.1.1.3.5. H₂C(Ph₂PS)₂ polymorphism

¹H NMR data indicated that all products discussed in Section 4.1.1.3. were the same chemical compound. IR data indicated the possible formation of two distinct solid state species for this compound. The spectra for H₂C(Ph₂PS)_{2_1} and H₂C(Ph₂PS)_{2_2a} showed the formation of one species, whilst the spectra of H₂C(Ph₂PS)_{2_2b} and H₂C(Ph₂PS)_{2_3b} indicated the presence of the second species. The spectrum of H₂C(Ph₂PS)_{2_3a} showed a mixture of both. PXRD data indicated that H₂C(Ph₂PS)_{2_2b} was composed mainly of the *C2/c* polymorph of H₂C(Ph₂PS)₂ with the *P2₁/n* polymorph being a minor component. This indicated that H₂C(Ph₂PS)_{2_2b} and H₂C(Ph₂PS)_{2_3b} crystallised mainly in the *C2/c* polymorph, while H₂C(Ph₂PS)_{2_1} and H₂C(Ph₂PS)_{2_2a} likely crystallised in the *P2₁/n* polymorph.

Investigation of the published crystal structures of these polymorphs also showed the interactions which may have caused the distinct differences between the IR spectra of the two polymorphs. The intermolecular bonding about the P=S moiety for the *P2₁/n* and *C2/c* polymorphs are given in Figures 4.20 and 4.21 respectively. In both cases the intermolecular bonding is P=S---H-C in nature. However, in the case of the former polymorph the H-C occurs as a meta proton on the aromatic ring while for the latter polymorph the H-C group refers to the central methylene moiety.

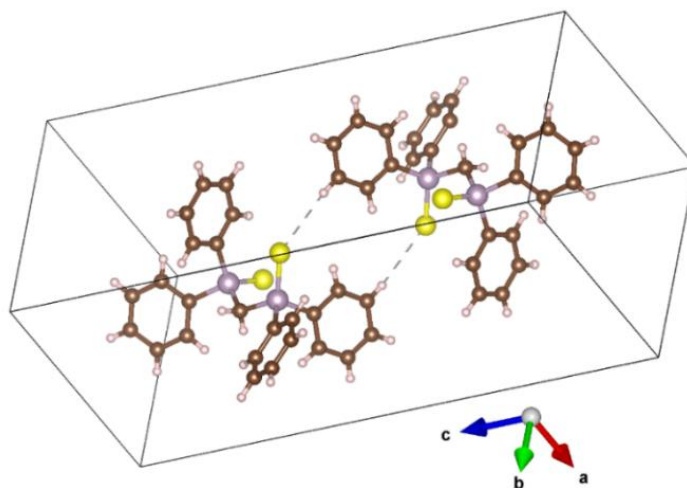


Figure 4.20: Unit cell of $P2_1/n$ polymorph of $H_2C(Ph_2PS)_2$ showing the $P=S\cdots H-C(\text{phenyl})$ interactions.

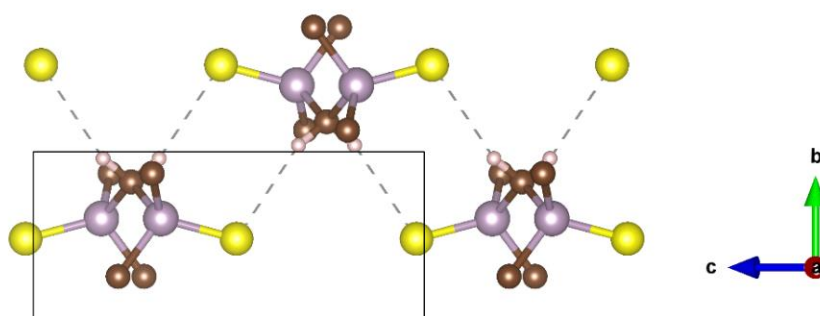


Figure 4.21: Unit cell of $C2/c$ polymorph of $H_2C(Ph_2PS)_2$ showing the $P=S\cdots H-C(\text{methylene})$ interactions.

It is therefore believed that the initial changes in the IR spectra observed for the two groups as classified above was due to some increased restriction on the ν P-CH₂-P vibration in the $C2/c$ polymorph, as compared to the $P2_1/n$ polymorph. It seems that in the $C2/c$ polymorph the $P=S\cdots H-C(\text{methylene})$ interaction causes an increase in stiffness of the P-CH₂-P bonds and therefore a slight increase in wavenumber from 783 cm⁻¹ to 802 cm⁻¹. The exact reason for the impact of the $P=S\cdots H-C(\text{methylene})$ intermolecular bonding on the intramolecular bonding C-P in the P-CH₂-P group does not seem to be straightforward. However, it seems that this interaction is what effects the wavenumber shift since the published structures offer no other explanations.

It was observed that the IR bands in the regions typical of ν P=S changed dramatically between the two polymorphs, indicating that the P=S bond is central to and effected by the polymorphism. The problem is that there are multiple bands that can be attributed to this vibration and the changes do not give any information because the multiple bands remain in the same region.

4.1.1.3.6. Conclusion

The synthesis of this ligand was confirmed for all the products formed by ^1H NMR spectroscopy, as these spectra were in agreement with literature values for the PCH_2P group protons and showed evidence of the effect of the $\text{P}=\text{S}$ bond on the entire ^1H NMR spectrum in all cases. The IR spectra of all the $\text{H}_2\text{C}(\text{Ph}_2\text{PS})_2$ products indicated the formation of two solid state species in different precipitation conditions. PXRD data confirmed that both the $C2/c$ and $P2_1/n$ polymorphs were formed in $\text{H}_2\text{C}(\text{Ph}_2\text{PS})_2$ _2b, with the former being the major component. This data along with the IR data for each solid obtained indicated that the $P2_1/n$ polymorph was the major form collected for $\text{H}_2\text{C}(\text{Ph}_2\text{PS})_2$ _1 and $\text{H}_2\text{C}(\text{Ph}_2\text{PS})_2$ _2a while the $C2/c$ polymorph was the major form collected for $\text{H}_2\text{C}(\text{Ph}_2\text{PS})_2$ _2b and $\text{H}_2\text{C}(\text{Ph}_2\text{PS})_2$ _3b. $\text{H}_2\text{C}(\text{Ph}_2\text{PS})_2$ _3a was likely a mixture of both. The spectra and diffraction patterns that support these conclusions are given in Appendix 7.

4.1.1.4. Summary

This section addressed the characterisation of the ligands and ligand precursors which were synthesised as described in Section 3.3.1.1, to be used in the synthesis of the lanthanide carbene complexes. For most ligands various attempts were undertaken either because the first product did not show the expected characteristics or to increase yield. The ligand precursors $\text{H}_2\text{C}(\text{Ph}_2\text{PNSiMe}_3)_2$ and $\text{H}_2\text{C}(\text{Ph}_2\text{PS})_2$ were synthesised and characterised using mainly IR and ^1H NMR spectroscopy. The desired compounds were clearly confirmed by these analytical techniques. IR and PXRD data indicated that both the $P2_1/n$ and the $C2/c$ polymorphs of $\text{H}_2\text{C}(\text{Ph}_2\text{PS})_2$, previously recorded in literature, were formed through the same reaction. Previously these two polymorphs were obtained from different reaction procedures. The product $[\text{H}_2\text{C}(\text{Ph}_2\text{PNH}(i\text{Pr}))_2]\text{Br}_2$ _1 was believed to be the desired compound as inferred from the ^1H NMR data and therefore was used in the synthesis of $\text{K}[\text{HC}(\text{Ph}_2\text{PN}i\text{Pr})_2]$ and $[\text{Nd}(\text{C}(\text{Ph}_2\text{PN}i\text{Pr})_2)(\text{HC}(\text{Ph}_2\text{PN}i\text{Pr})_2)] \cdot 2\text{THF}$. The characterisation of $\text{K}[\text{HC}(\text{Ph}_2\text{PN}i\text{Pr})_2]$ was found to be difficult. IR spectroscopy was promising but could not definitively conclude the formation of the desired compound as was the case for $\text{H}_2\text{C}(\text{Ph}_2\text{PNSiMe}_3)_2$. ^1H NMR data was in good agreement for all protons expected in the spectrum of $\text{K}[\text{HC}(\text{Ph}_2\text{PN}i\text{Pr})_2]$, barring the phenyl protons due to

impurities, which was promising. However the J_{HP} for the PCHP proton diverged significantly, the reason for which could not be confirmed. PXRD data for $K[HC(Ph_2PNiPr)_2]_2$ indicated the formation of a novel crystalline solid.

4.1.2. Lanthanide starting reagents

4.1.2.1. Characterisation of $LnI_3(THF)_{3.5}$ complexes

In the current study the synthesis of $NdI_3(THF)_{3.5}$ and $SmI_3(THF)_{3.5}$ both having the structure $LnI_3(THF)_{3.5}$, were attempted using the procedure published by Izod and co-workers, with various modifications,¹³⁷ as described in Section 3.3.1.2.1. The respective yields and other details are given in Table 4.9.

Table 4.9: Yields of $LnI_3(THF)_{3.5}$ products.

Compound label	Yield	Notes
$NdI_3(THF)_{3.5_1}$	21.5%	N/A
$SmI_3(THF)_{3.5_1}$	52.24 %	Used to prepare $SmI_3(THF)_{3.5_2}$
$SmI_3(THF)_{3.5_2}$	24.7 %	Recrystallised

4.1.2.1.1. Analysis by Infra-red spectroscopy

All solids obtained were initially analysed using IR spectroscopy. All solid samples were prepared in nujol as this proved to yield better spectra for these compounds as compared to KBr. Moisture intrusion was observed in all samples to varying degrees. During the research IR spectra of the solids were obtained both before and after iodine removal under vacuum and by washing. No significant differences were observed between the wavenumber of bands present in the two spectra for each respective product, although iodine contaminated samples were found to have very intensity reduced bands. Therefore, unless otherwise stated, all spectra discussed below are for the final product.

4.1.2.1.1.1 NdI₃(THF)_{3.5_1}

The IR spectrum of NdI₃(THF)_{3.5_1} was collected. A broad band in the range of 3420-3330 cm⁻¹ and a band at about 1602 cm⁻¹ were observed. These were undoubtedly due to the presence of water. It is reasonable to assume that moisture was present in the sample. In fact during the course of sample preparation it was observed that although the process was undergone under argon flow, the samples tended to darken in colour and become stickier during their transfer from the Schlenk flask to the sample cell.

The spectrum of NdI₃(THF)_{3.5_1} in Nujol mull was compared with the literature data for NdI₃(THF)_{3.5} (in Nujol Mull),¹³⁷ NdI₃(THF)₄ (in KBr) and THF (liquid film).^{151,298} The most significant bands that occurred in the product spectrum were the bands at 1005 cm⁻¹ and 849 cm⁻¹. Although these bands were weak they were in agreement with the strong bands at 1004 cm⁻¹ and 851 cm⁻¹ presented in literature for NdI₃(THF)_{3.5}.¹³⁷ These bands are believed to be due to the ν_{as} C–O–C and the ν_s C–O–C or ring relaxation vibrations in THF coordinated to the neodymium (III) centres, respectively. The analogous bands in uncoordinated THF are found either at 1184 cm⁻¹ or 1070 cm⁻¹ for ν_{as} C–O–C and at 912 cm⁻¹ for the ν_s C–O–C or ring relaxation vibrations.^{304–309}

A number of unexpected bands were observed in the spectrum for NdI₃(THF)_{3.5_1}, namely the shoulder at 1233 cm⁻¹, the weak band at 1154 cm⁻¹, the strong band at 1034 cm⁻¹ and the weak bands at 832 cm⁻¹ and 665 cm⁻¹. All of these bands were found to be similar to the bands expected for the IR spectrum of NdI₃(THF)₄ in KBr, as described by Balashova and co-workers in 2006.¹⁵¹ Therefore NdI₃(THF)₄ was possibly present as a secondary component in the solid although it was considered unlikely to form in the conditions used in the current study. It should however be noted that the most prominent of the unexpected bands was the one at 1034 cm⁻¹, which could indicate the presence of free THF.

4.1.2.1.1.2 SmI₃(THF)_{3.5_1} and SmI₃(THF)_{3.5_2}

The solid SmI₃(THF)_{3.5_1} was obtained after iodine removal under vacuum at 140 °C, while SmI₃(THF)_{3.5_2} was collected as the product of Soxhlet extraction recrystallisation. In both cases bands indicative of water were visible at around

3380 cm^{-1} and 1606 cm^{-1} , due to the ν O–H and the δ O–H vibrations respectively. This was most likely due to the absorption of atmospheric moisture during the preparation of the samples for the IR studies. The smaller bands at 3380 cm^{-1} and 1606 cm^{-1} in the spectrum of the product $\text{SmI}_3(\text{THF})_{3.5_2}$ as compared to those in the spectrum of the product $\text{SmI}_3(\text{THF})_{3.5_1}$ may be due to the increased kinetic stability of the crystalline $\text{SmI}_3(\text{THF})_{3.5_2}$.

The spectra of the products obtained during synthesis were similar, with many of the bands present at the same wavenumber and having the same relative intensity in both spectra. The main difference between the experimental spectra was in the intensities of three bands located at 965 cm^{-1} , 917 cm^{-1} and 890 cm^{-1} . The first and third bands were found to be more intense in the product $\text{SmI}_3(\text{THF})_{3.5_1}$, while the second band was found to be more intense in the product $\text{SmI}_3(\text{THF})_{3.5_2}$. The IR bands in the experimental spectra which were assigned to the samarium salt (excluding nujol and moisture bands) were similar to those bands published in literature by Izod and co-workers for this samarium compound.¹³⁷ The literature bands were found to be in very good correlation with the experimental data in the range of 1200–800 cm^{-1} , with the greatest agreement being with the spectrum of the product $\text{SmI}_3(\text{THF})_{3.5_2}$.

The two main bands which were indicative of the formation of the THF coordinated samarium iodide were visible in both the spectra of $\text{SmI}_3(\text{THF})_{3.5_1}$ and $\text{SmI}_3(\text{THF})_{3.5_2}$, as the shoulder at 1005 cm^{-1} and the band at ~ 846 cm^{-1} for the former product and the shoulders at 1005 cm^{-1} and ~ 846 cm^{-1} for the latter.

4.1.2.1.2. Analysis by UV-visible light spectroscopy

UV-visible light spectroscopy for $\text{NdI}_3(\text{THF})_{3.5_1}$ in THF was undertaken. The solution was prepared by heating and stirring a small suspension of the solid in THF. During this analysis $\text{NdCl}_3 \cdot n\text{H}_2\text{O}$ was used as a reference to indicate the presence of the Nd^{3+} in a THF solution, since the absorption peaks of lanthanides are typically unaffected by ligands present and therefore unlikely to shift drastically between the iodides and the chloride.²³ The first spectrum was collected using a sample of $\text{NdI}_3(\text{THF})_{3.5_1}$ which had been left under vacuum at 140 °C but was not washed to remove excess iodine. The presence of Nd^{3+} in the THF solution of the product was confirmed by the comparison of the resultant spectrum with that of $\text{NdCl}_3 \cdot n\text{H}_2\text{O}$. All peaks obtained for the $\text{NdCl}_3 \cdot n\text{H}_2\text{O}$

reference were visible in the spectrum of $\text{NdI}_3(\text{THF})_{3.5_1}$, although the intensity of the peaks was very diminished. This was due to the partial solubility of the product in THF.

Another UV-visible spectrum was obtained after the final washing of the solid. The two spectra obtained were compared with each other. The main difference between the two spectra was that the peak at 233 nm, attributed to I^- in equilibrium with I_2 and I_3^- ,^{310,311} was lost after the washing procedure and at the same time giving rise to the peaks at 213 nm and 254 nm. However, these new peaks remained less intense than the peaks at 294 nm and 367 nm. The peaks at 294 nm and 367 nm are believed to be due to the presence of the tri-iodide anion, I_3^- ,^{310,311} indicating that elemental iodine was still present. This in turn indicated that there may be dissociation of I^- ligands from the $\text{NdI}_3(\text{THF})_{3.5}$ in solution.

The peaks at 213 nm and 254 nm are commonly attributed to free I^- anion which indicated that after the washing procedure free I^- anion was found in solution along with I_3^- .^{310,311} The presence of both peaks may indicate that although elemental iodine was still present the amount had decreased significantly. This decrease therefore indicated that the washing procedure did reduce the amount of iodine enough to allow free I^- in the presence of iodine in solution.³¹¹

4.1.2.1.3. Analysis by Powder X-ray Diffraction

In the current study only the solid $\text{SmI}_3(\text{THF})_{3.5_2}$ could be characterised using PXRD. The solid was prepared in a 0.3 mm capillary, sealed under dry nitrogen, and data was collected using synchrotron radiation. It was clear from the comparison of the experimental powder pattern and the calculated powder pattern of $\text{SmI}_3(\text{THF})_{3.5}$ obtained from literature,^{137,297} that $\text{SmI}_3(\text{THF})_{3.5_2}$ was the desired complex. Very minor peaks in the powder pattern could also indicate the presence of a very minor crystalline phase, possibly iodine.

4.1.2.1.4. Conclusion

In all cases the IR data indicated that complexes containing coordinated THF were obtained. The differences in the IR spectra of the various products and the literature data indicated that all contained some impurity and that the most congruent products were $\text{NdI}_3(\text{THF})_{3.5_1}$ and $\text{SmI}_3(\text{THF})_{3.5_2}$. UV data indicated that some I_2 remained in the Nd^{3+}

product. The PXRD analysis of $\text{SmI}_3(\text{THF})_{3.5_2}$ indicated that although the reactions used for both lanthanides produced iodides the recrystallisation by Soxhlet extraction is necessary to obtain the desired crystallographic product with the required THF stoichiometry. The relevant spectra, powder patterns and data used for the above discussion are given in Appendix 8.

4.1.2.2. Characterisation of $[\text{Sm}(\text{NCy}_2)_3\text{THF}] \cdot \text{C}_6\text{H}_5\text{CH}_3$

During the attempts undertaken to synthesise this starting reagent a single product of $[\text{Sm}(\text{NCy}_2)_3\text{THF}] \cdot \text{C}_6\text{H}_5\text{CH}_3$ was prepared as described in Section 3.3.1.2.2. The synthesis procedure was based on the method published by Minhas, R.K. and co-workers in 1996, with minor modifications.¹⁶² This reaction yielded a single light orange coloured solid labelled as $[\text{Sm}(\text{NCy}_2)_3\text{THF}] \cdot \text{C}_6\text{H}_5\text{CH}_3_1$. The yield of the product was 9.17 %.

4.1.2.2.1. Analysis by Infra-red spectroscopy

IR spectroscopic data for $[\text{Sm}(\text{NCy}_2)_3\text{THF}] \cdot \text{C}_6\text{H}_5\text{CH}_3_1$ was collected using nujol mull and the spectrum is given in Figure 4.22. IR data, in nujol, for this compound was published by Minhas and co-workers but detailed discussion of this data was not undertaken.¹⁶² Therefore the IR data collected in the current study was also compared to the data provided in literature, as shown in Figure 4.23.

In the desired compound there are three components of interest, namely the amide ligand NCy_2^- , THF and the toluene as solvate. Unfortunately, the spectrum for $[\text{Sm}(\text{NCy}_2)_3\text{THF}] \cdot \text{C}_6\text{H}_5\text{CH}_3_1$ prepared in the current study showed some water intrusion with a broad band covering the 3680-3200 cm^{-1} region centred around 3564 cm^{-1} of the spectrum. This region typically contains bands of the ν O-H vibration. The complementary band at about 1620 cm^{-1} , typically assigned to δ O-H vibrations, was also visible as a relatively weak band.

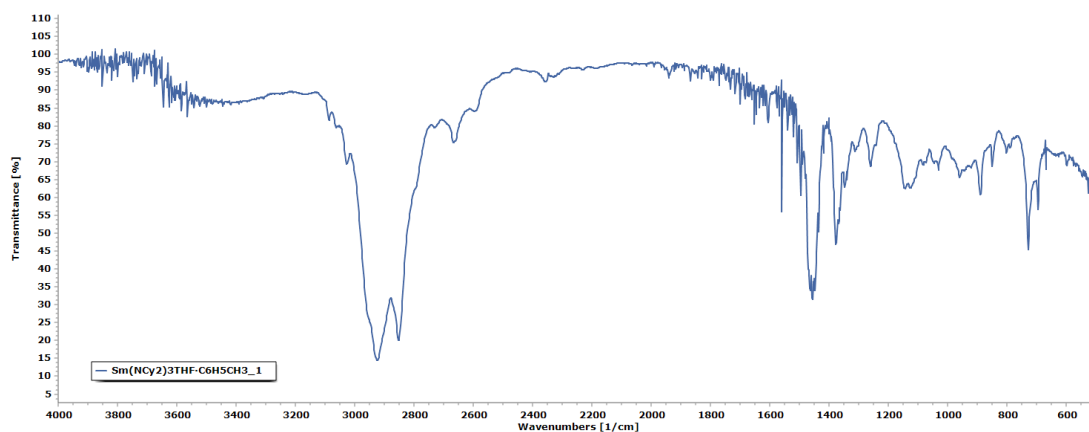


Figure 4.22: IR spectrum of $[\text{Sm}(\text{NCy}_2)_3\text{THF}] \cdot \text{C}_6\text{H}_5\text{CH}_3_1$ in nujol.

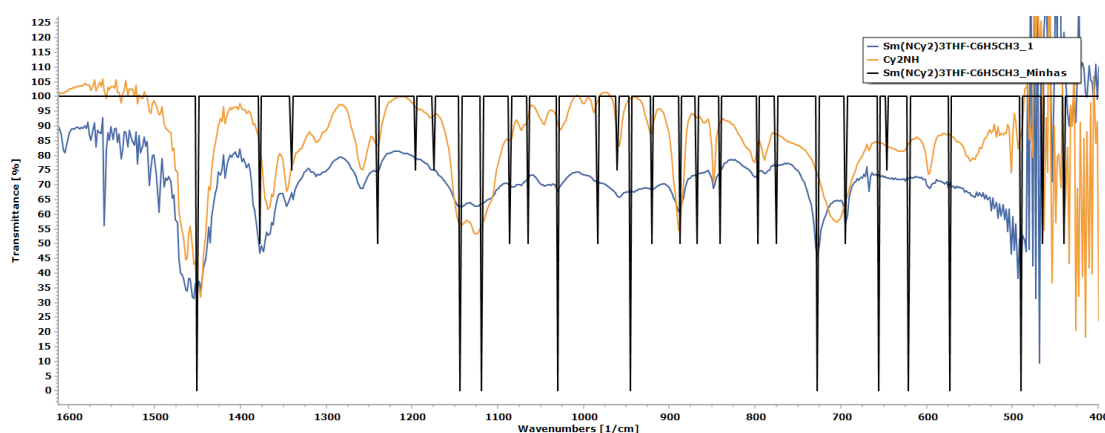


Figure 4.23: Details of the IR spectra of $[\text{Sm}(\text{NCy}_2)_3\text{THF}] \cdot \text{C}_6\text{H}_5\text{CH}_3_1$ (blue), Cy_2NH (orange) and the data provided in literature for $[\text{Sm}(\text{NCy}_2)_3\text{THF}] \cdot \text{C}_6\text{H}_5\text{CH}_3$ (black).

The bands at 1458 cm^{-1} , 1375 cm^{-1} and 1344 cm^{-1} in the experimental spectrum were believed to be analogous to the bands at 1450 cm^{-1} , 1376 cm^{-1} and 1340 cm^{-1} recorded in literature. In all cases these bands were assigned to the δ C–H vibrations which are common to all the organic groups, that is NCy_2^- , THF, toluene and nujol which was used in sample preparation. The strong band at 721 cm^{-1} could be analogous to the literature band at 727 cm^{-1} , both of which could be assigned to the ω C–H vibrations. Given that these vibrations are common to so many groups that could be present in the product they could not be used for characterisation purposes.

The two sharp bands which were described in literature at 1143 cm^{-1} and 1118 cm^{-1} were found to have strong yet slightly broad analogue bands in the spectrum of the $[\text{Sm}(\text{NCy}_2)_3\text{THF}] \cdot \text{C}_6\text{H}_5\text{CH}_3$ sample prepared in the current study. These bands could also be analogous to the two bands at 1144 cm^{-1} and 1125 cm^{-1} for the Cy_2NH , as shown in Figure 4.23. In this reagent these bands were assigned to the ν C–N vibrations.

However an increase in wavenumber was expected for these bands on deprotonation, due to back donation of the lone pair electron density to the C–N bonds.³¹² This shift was not observed in the experimental data of the current study or the literature data and the reason for this is not known.

The shoulder at 1240 cm⁻¹ could be due to this expected shift. This band could also be analogous to multiple different bands observed. The first such band was the band at 1240 cm⁻¹ observed in the literature data for the desired compound while the second possible band was the band at the same wavenumber for the spectrum of Cy₂NH. The latter assignment is supported by the presence of the band at 1259 cm⁻¹ found in the experimental spectrum. This band could be analogous to a band at 1259 cm⁻¹ for the Cy₂NH. When comparing the data from the product with the spectrum of Cy₂NH, the loss of the Cy₂NH spectrum band at 705 cm⁻¹ indicated that the compound obtained should not contain the N–H moiety, since this band may be confidently assigned to the ω N–H vibration which should be lost on deprotonation. The loss of this band therefore indicated that even if not coordinated with the Sm³⁺ cation the deprotonated amide may be present. However, given that the spectrum still contained bands which were very similar to those of the amine, definite conclusions on the structure of [Sm(NCy₂)₃THF]·C₆H₅CH₃_1 were difficult.

The bands at 1027 cm⁻¹, 958 cm⁻¹, 889 cm⁻¹ and 847 cm⁻¹, were visible in the spectrum of [Sm(NCy₂)₃THF]·C₆H₅CH₃_1 although the broad nature of the band at 958 cm⁻¹ severely diminished the visibility of the remaining bands. These bands could be analogous to the bands at 1030 cm⁻¹, 944 cm⁻¹, 887 cm⁻¹ and 840 cm⁻¹ given in literature. Comparison of the strength of the experimental bands of [Sm(NCy₂)₃THF]·C₆H₅CH₃_1 with that in the published data showed an overall similarity except for the experimental band at 1027 cm⁻¹ which remained a shoulder like band unlike what was described in literature for the 1030 cm⁻¹ band. On comparison the latter two bands (at 889 cm⁻¹ and 847 cm⁻¹) seem to be also common for the spectra of NCy₂⁻, toluene and nujol. Therefore, the latter two bands could not be assigned properly and did not yield significant structural data.

The assignment of these bands was made more difficult by the fact that a number of them fell in the fingerprint region. The band at 1027 cm⁻¹ may however be assigned to the THF vibration of ν_{as} C–O–C for coordinated THF. This band would be analogous to the THF bands at 1184 cm⁻¹ and 1070 cm⁻¹, both of which have been assigned to the ν_{as} C–O–C vibration in numerous publications.^{304–307} The shift of these bands to lower

wavenumbers is well attested on coordination of the THF to metal centres.^{308,309} Therefore, the band at 1027 cm^{-1} could be analogous to either the band at 1184 cm^{-1} or 1070 cm^{-1} for free THF, which would indicate clear coordination of the THF. The similar shifts expected for the free THF ν_s C–O–C and ring relaxation bands assigned to the bands at 1070 cm^{-1} and 912 cm^{-1} were not observed in the spectrum of the product obtained.^{306,307}

Bands at 800 cm^{-1} and 789 cm^{-1} were observed in this experimental spectrum of $[\text{Sm}(\text{NCy}_2)_3\text{THF}] \cdot \text{C}_6\text{H}_5\text{CH}_3_1$. These were in agreement with the data for the Cy_2NH spectrum, however they could also be analogous with the literature data bands at 796 cm^{-1} and 775 cm^{-1} respectively. Although these bands are in agreement with literature data, no assignment was possible due to the numerous amount of possible vibrations typical for this region. The medium strength band at 693 cm^{-1} could be analogous to the literature band at 694 cm^{-1} . This band could not be assigned to any particular vibration, although the presence of this band was indicative of the preparation of the desired product since it was in agreement with literature.

It is important to note that the colour of the product $[\text{Sm}(\text{NCy}_2)_3\text{THF}] \cdot \text{C}_6\text{H}_5\text{CH}_3$ given in literature was a pale yellow. This was in disagreement with the colour observed in $[\text{Sm}(\text{NCy}_2)_3\text{THF}] \cdot \text{C}_6\text{H}_5\text{CH}_3_1$ which was a light orange. Minhas and co-workers also published the preparation of a second compound, $[(\text{Cy}_2\text{N})_2\text{Sm}(\mu\text{-Cl})(\text{THF})]_2$,¹⁶² using the same reaction method but with an alternative stoichiometry. This product was obtained as an orange crystalline solid. The spectral data of both products published in this publication is given in Figure 4.24, showing the clear similarities in the IR spectra of the two compounds. These similarities were expected since most of the same vibrations are present in both compounds and the differences are due to symmetry differences.

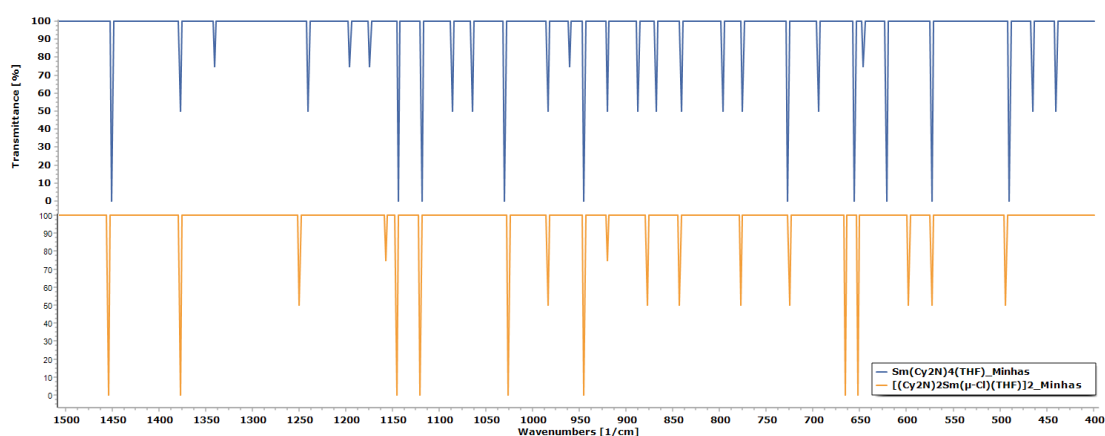


Figure 4.24: IR spectra of $[\text{Sm}(\text{NCy}_2)_3\text{THF}] \cdot \text{C}_6\text{H}_5\text{CH}_3$ (blue) and $[(\text{Cy}_2\text{N})_2\text{Sm}(\mu\text{-Cl})(\text{THF})]_2$ (orange).

These similarities indicated that the product obtained in the current study could also be this compound or a mixture of both published compounds. However this cannot be determined by this IR data. With regards to the bands discussed prior all these bands have clear analogues for both published products.

4.1.2.2.2. Analysis by Microscopy

The product $[\text{Sm}(\text{NCy}_2)_3\text{THF}] \cdot \text{C}_6\text{H}_5\text{CH}_3_1$ obtained from the reaction undergone to produce $[\text{Sm}(\text{NCy}_2)_3\text{THF}] \cdot \text{C}_6\text{H}_5\text{CH}_3$ was observed under polarised light using a microscopy to determine whether the product was crystalline. A micrograph of the product $[\text{Sm}(\text{NCy}_2)_3\text{THF}] \cdot \text{C}_6\text{H}_5\text{CH}_3_1$ is given in Figure 4.25.



Figure 4.25: Micrograph of $[\text{Sm}(\text{NCy}_2)_3\text{THF}] \cdot \text{C}_6\text{H}_5\text{CH}_3_1$.

The crystallinity of the sample could not be concluded definitively as no clear extinction of polarised light was observed on the shifting of the sample. This lack of polarised light extinction would indicate that the product was amorphous in nature.

4.1.2.2.3. Conclusion

The IR spectrum of the product $[\text{Sm}(\text{NCy}_2)_3\text{THF}] \cdot \text{C}_6\text{H}_5\text{CH}_3_1$ in nujol yielded weak bands which could not be thoroughly assigned. However similarities with the data provided in literature were observed. These similarities indicated that the product obtained most likely contained coordinated THF. However, coordination with the amide ligands could not be described by IR bands' assignments. Bands nearly identical to the

bands assigned to the ν C–N vibration in the IR spectrum of CyN₂H were observed in the experimental data and the literature data, which was unexpected. A lack of crystallinity was noticeable for [Sm(NCy₂)₃THF]·C₆H₅CH₃_1, which was problematic given that the expected compound was crystalline. The light orange colouration of the product could indicate that the desired compound, which was reported to be yellow in literature, was either not obtained or that it was mixed with other Sm³⁺ derivatives of the lithium amide used, which were reported to be orange in colour.¹⁶² The presence of either compound could not be defined through IR. Numerous bands in the IR spectrum of the product indicated that the desired product was obtained, however differences from IR data and physical properties reported in literature cast certain doubts on the composition of [Sm(NCy₂)₃THF]·C₆H₅CH₃_1.

4.1.2.3. Summary

This section addressed the characterisation of the lanthanide containing starting reagents which were synthesised as described in Section 3.3.1.2., to be used in the synthesis of the lanthanide carbene complexes. Both crude and re-crystallised lanthanide iodide THF solvate salts were used in the synthesis attempts for lanthanide carbenes. Re-crystallisation through Soxhlet extraction yielded the desired crystalline phase and it is believed that the specific stoichiometry of the LnI₃THF_{3.5} salt may only be achieved through Soxhlet extraction re-crystallisation. It was observed that the removal of iodine was the major problem in purification and could have effected their use in lanthanide carbene synthesis. The synthesis of the non-iodide starting reagent [Sm(NCy₂)₃THF]·C₆H₅CH₃ was found to be more problematic with characterisation undertaken mainly by IR spectroscopy. In the product [Sm(NCy₂)₃THF]·C₆H₅CH₃_1 the IR spectrum indicated the presence of a [NCy₂]⁻ derivative which could have been due to the presence of the expected compound or a similar species. [Sm(NCy₂)₃THF]·C₆H₅CH₃_1 was also likely to be amorphous from the analysis undertaken using plane polarised light microscopy.

4.1.3. Complexation products

4.1.3.1. Characterisation of $[\text{Sm}(\text{C}(\text{Ph}_2\text{PNSiMe}_3)_2)(\text{NCy}_2)(\text{THF})] \cdot 0.5(\text{C}_6\text{H}_5\text{CH}_3)$

In the attempts undertaken in this study to synthesise this lanthanide carbene complex, as described in Section 3.3.1.3.1, four products were obtained namely, $[\text{Sm}(\text{C}(\text{Ph}_2\text{PNSiMe}_3)_2)(\text{NCy}_2)(\text{THF})]_1$, $[\text{Sm}(\text{C}(\text{Ph}_2\text{PNSiMe}_3)_2)(\text{NCy}_2)(\text{THF})]_2$, $[\text{Sm}(\text{C}(\text{Ph}_2\text{PNSiMe}_3)_2)(\text{NCy}_2)(\text{THF})]_3$ and $[\text{Sm}(\text{C}(\text{Ph}_2\text{PNSiMe}_3)_2)(\text{NCy}_2)(\text{THF})]_4$. The syntheses undergone were modifications of the method published by Aparna and co-workers in 2000.⁷ The products obtained were all a light yellow powder or crystalline solid. These compounds were obtained in yields of 25 %, 14.5 % and 26.1% for $[\text{Sm}(\text{C}(\text{Ph}_2\text{PNSiMe}_3)_2)(\text{NCy}_2)(\text{THF})]_1$, $[\text{Sm}(\text{C}(\text{Ph}_2\text{PNSiMe}_3)_2)(\text{NCy}_2)(\text{THF})]_3$ and $[\text{Sm}(\text{C}(\text{Ph}_2\text{PNSiMe}_3)_2)(\text{NCy}_2)(\text{THF})]_4$ respectively while only a small crop of crystals was obtained for the product $[\text{Sm}(\text{C}(\text{Ph}_2\text{PNSiMe}_3)_2)(\text{NCy}_2)(\text{THF})]_2$, and this was collected for SXR D analysis before the yield could be calculated. The reason for the poor yields obtained when compared to the literature yield of 54.4 % is unknown, although the presence of moisture or oxygen could have decomposed the starting reagents thus reducing their availability for the reaction. These products are discussed since they were obtained using different modified procedures and had different characterisation results.

4.1.3.1.1. Analysis by Infra-red spectroscopy

Comparison of the IR spectra of the four products obtained in these reactions showed that there were substantial differences between them. Therefore, these spectra will be discussed separately. In the publication by Aparna and co-workers the IR data was published, however no assignment or interpretation of this data was given.⁷

In the reactions undertaken as described in Section 3.3.1.3.1, the main structural transformations which should be visible in the IR spectra are the changes in the bond order of the ligand P=N and P–C bonds of the central group. In this reaction the ligand becomes deprotonated stepwise from $[\text{H}_2\text{L}^{\text{TMS}}]$ to $[\text{HL}^{\text{TMS}}]^-$ to $[\text{L}^{\text{TMS}}]^{2-}$. In this stepwise deprotonation it is known through published SXR D and PXR D data that the P=N and P–C bonds undergo an increase and decrease in bond length respectively.^{7,9,36,41,42,118,122,178,188,191,313–321} This change is effected by the strength and

nature of coordination, however the general trend is always true.^{7,9,36,41,42,118,122,178,188,191,313–321} It is believed that these changes are a result of the decrease in bond order on the P=N bond and the respective increase in bond order on the P–C bond during the structural change depicted in Figure 4.26. The P⁺–C²⁻ bond is stabilised by negative hyperconjugation and electron charge distribution about the entire charged system in the di-anion shown in Figure 4.26. The negative hyperconjugation increases the P–C bond order.

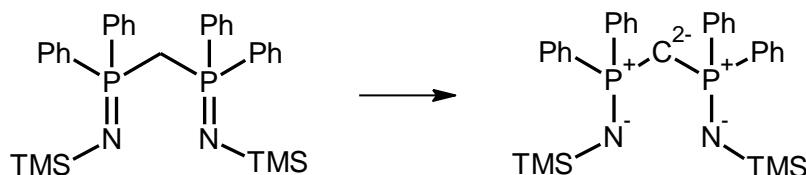


Figure 4.26: Change in structure on deprotonation of $\text{H}_2\text{C}(\text{Ph}_2\text{PNSiMe}_3)_2$.

These changes in bond order are expected to be present in the IR spectra as shifts to lower wavenumbers of the ν P=N vibration band and an increase in wavenumber for the ν_{as} P–C–P vibration on deprotonation. In the IR spectrum of the ligand, $\text{H}_2\text{C}(\text{Ph}_2\text{PNSiMe}_3)_2$, the bands at 864 cm^{-1} , 851 cm^{-1} , 802 cm^{-1} and 776 cm^{-1} could all be due to the ν_{as} P–CH₂–P vibrations, with the bands at 864 cm^{-1} and 802 cm^{-1} best assigned to this vibration as discussed in Section 4.1.1.2.1. No literature data is given to assign bands in published IR spectra of the $(\text{C}(\text{Ph}_2\text{PNSiMe}_3)_2)^{2-}$ salts and carbenes to the ν_{as} P–C–P vibration.^{7,9,41,42,122,188,316,317} Therefore the use of this vibration in the characterisation of these compounds was problematic. It was however noted that in the IR data for numerous $(\text{C}(\text{Ph}_2\text{PNSiMe}_3)_2)^{2-}$ complexes published in literature the number of bands in this region diminished on deprotonation from $[\text{H}_2\text{L}^{\text{TMS}}]$ to $[\text{HL}^{\text{TMS}}]^-$ to $[\text{L}^{\text{TMS}}]^{2-}$, with the final species having only one to two bands, typically in the region of $860\text{--}820\text{ cm}^{-1}$. The band which is always observed is believed to be due to the ρ CH₃ + ν Si–C vibration, previously assigned to the ligand band at 851 cm^{-1} ,³²² rather than the ν_{as} P–C–P vibration. In the light of the IR data available for numerous $(\text{C}(\text{Ph}_2\text{PNSiMe}_3)_2)^{2-}$ salts and lanthanide carbenes, four general groups of bands are expected in the IR spectra of products containing this di-anion. These groups fall in the following ranges:

- $1265\text{--}1240\text{ cm}^{-1}$
- $1110\text{--}1025\text{ cm}^{-1}$
- $860\text{--}820\text{ cm}^{-1}$
- $775\text{--}680\text{ cm}^{-1}$

The bands observed in the regions 1265–1240 cm⁻¹ and 860–820 cm⁻¹ are believed to be due to the trimethylsilyl group δ C–H and ρ CH₃ + ν Si–C vibrations respectively. These would be analogous to the bands at 1238 cm⁻¹ and 851 cm⁻¹ for the IR spectrum of H₂C(Ph₂PNSiMe₃)₂, as described in Section 4.1.1.2.1. If this assignment is correct these bands offer no structural information regarding protonation and coordination of the ligand, as the trimethylsilyl group is unaffected by these changes. In the region 775–680 cm⁻¹ bands for the P–Ph and ν_s P–C–P vibrations are typically expected. This region contains numerous bands for the P–Ph vibrations and bands for ν_{as} P–C–P vibrations which is used for many of the samples discussed. Therefore, the use of shifts in this region is unsuitable for structural determination. As detailed above, deprotonation of the P–CH₂–P group should give an increase in the wavenumber of the ν_s P–C–P bands. However, the region at higher wavenumbers where such a band or bands is/are expected is unknown, thus these are discussed together with the ν_{as} P–C–P bands.

For all published IR data at least two or more bands are always present in the 1110–1025 cm⁻¹ region. At least some of these bands can be tentatively assigned to the ν P=N vibrations at a lower wavenumber when compared to the ligand band at 1273 cm⁻¹, which is assigned to the same vibrations. This significant shift is backed by the typical change in the P⁺–N⁻ bond length from 1.534–1.574 Å for H₂C(Ph₂PNR)₂ to the range 1.609–1.630 Å for [C(Ph₂PNR)₂]²⁻ complexes.^{323–331} The P⁺–N⁻ bond lengths in these complexes are shorter than those typical for P(V)–N and P(III)–N, which are in the ranges of 1.676–1.754 Å and 1.646–1.704 Å respectively. This indicates a higher bond order for the carbene P⁺–N⁻ bond when compared to typical P(V)–N and P(III)–N bonds.^{332–347} Given this information the bands for the ν P⁺–N⁻ vibration are expected to lie in the 1110–1025 cm⁻¹ region, which lies between the regions typically containing ν P=N and ν P–N vibrations. In contrast the ν P⁺–N⁻ vibration bands of the analogous mono-anion [HC(Ph₂PNSiMe₃)₂]⁻ fall in the intermediate range of 1220–1100 cm⁻¹, as supported mainly through IR data for alkali metal salts.³¹⁸ However, overlap with the di-anionic ν P⁺–N⁻ vibrational modes cannot be completely discarded, as previously published IR data does not give sufficient discrimination between the two.

It should also be noted that other vibrations for organic phosphorus (V) compounds are known in the 1220–1100 cm⁻¹ and 1110–1025 cm⁻¹ regions. Low bond order P=O/P⁺–O⁻ stretching vibrations, including phosphate bands, are known to fall in these ranges. High bond order ν P–NH–P stretching vibrations can also fall in these

ranges but not the typical ν P–N vibrations. In the case of the formation of other derivatives of $\text{H}_2\text{C}(\text{Ph}_2\text{PNSiMe}_3)_2$, other than these anionic species, only ν P=O vibrations would be expected in this region.

On transition from $\text{H}_2\text{C}(\text{Ph}_2\text{PNR})_2$ to $[\text{C}(\text{Ph}_2\text{PNR})_2]^{2-}$ complexes, the P–C bond length shifts from the range of 1.810–1.860 Å to the range of 1.637–1.700 Å.^{7,9,36,41,42,118,122,178,188,191,313–321} The P=C bonds in simple, symmetric and un-coordinated compounds have a very broad range of bond lengths from 1.669 Å to 1.757 Å, which overlaps significantly with the range for the $[\text{C}(\text{Ph}_2\text{PNR})_2]^{2-}$ complexes.^{323–331} This similarity in bond lengths would indicate that the IR bands for these complexes should lie in the region typical for P=C bands; that is in the region 1220–1150 cm^{-1} . These bands fall between the above mentioned regions at 1265–1240 cm^{-1} and 1110–1025 cm^{-1} . It should be noted that bands in this region for complexes were not typically found in published data and therefore the $\nu_{\text{as/s}} \text{P}^+-\text{C}^{2-}-\text{P}^+$ vibrations cannot be used for structural determination. Another issue for the use of this moiety in structure determination is the overlap of the range in which $\nu_{\text{as/s}} \text{P}^+-\text{C}^{2-}-\text{P}^+$ vibrations are expected with the ranges typical for ν P=O and ν P=N vibrations. Overlap is also possible with the mono-anionic $\nu \text{P}^+-\text{N}^-$ modes discussed earlier if both anions are present, as these vibrations fall in similar regions.

In comparison the expected wavenumber range for the bands of the analogous mono-anionic $[\text{HC}(\text{Ph}_2\text{PNSiMe}_3)_2]^- \nu_{\text{as/s}} \text{P}^+-\text{CH}^--\text{P}^+$ stretching vibrations lies in between the ranges in which the $\nu_{\text{as/s}} \text{P}-\text{CH}_2-\text{P}$ and $\nu_{\text{as/s}} \text{P}^+-\text{C}^{2-}-\text{P}^+$ bands fall, as the P–C bond lengths of the mono-anions are given in literature in the range of 1.724–1.747 Å. This range is difficult to describe, however literature IR data for lanthanide complexes of $[\text{HC}(\text{Ph}_2\text{PNSiMe}_3)_2]^-$ indicates a range of 1050–850 cm^{-1} .^{9,191,192} In relation to the mono-anion numerous organic phosphorus (V) compound moieties are known to show bands in the same region in which the $\nu_{\text{as/s}} \text{P}^+-\text{CH}^--\text{P}^+$ stretching vibrations are expected. This region typically shows bands for the ν P=O, ν P–N, ν P–O, ν P–F and ν P–H, along with bending vibrations such as δ P–H, of which only the former three are of interest in the current study.^{99,348}

From this discussion it can be concluded that the most diagnostic feature for the di-anion in the spectra of the complexes obtained would be the assignment of the $\nu \text{P}^+-\text{N}^-$ vibration band in the region of 1110–1025 cm^{-1} . This is the best feature due to its presence in all literature IR data, strong intensity, clear theoretical connection to the band recorded for the neutral precursors and a minimum number of other phosphorus

moieties that show bands in this region. The discussion of the IR spectra of the products obtained in this study will be undertaken with this theoretical framework regarding the mono and di-anionic species in mind.

The first noticeable difference between the literature and experimental data for the product $[\text{Sm}(\text{C}(\text{Ph}_2\text{PNSiMe}_3)_2)(\text{NCy}_2)(\text{THF})]_1$ in nujol was that the literature band at 1435 cm^{-1} was not clearly visible in the spectrum of the product, as given in Figure 4.27. This band could be assigned to P–Ph vibrations analogous to the band at the same wavenumber in the IR spectrum of $\text{H}_2\text{C}(\text{Ph}_2\text{PNSiMe}_3)_2$. Alternatively it could be analogous to the band at 1450 cm^{-1} in the starting reagent $[\text{Sm}(\text{NCy}_2)_3\text{THF}] \cdot (\text{C}_6\text{H}_5\text{CH}_3)$ as shown in Figure 4.28. This was assigned in Section 4.1.2.2.1. to δ C–H vibrations for either the NCy_2^- or THF, given that both these ligands were expected in the product. This band was not visible in the spectrum of the product because it was obscured by the band for the nujol, which is found in this same region. A strong band at 1258 cm^{-1} and a shoulder at 1241 cm^{-1} were observed in the experimental spectrum of $[\text{Sm}(\text{C}(\text{Ph}_2\text{PNSiMe}_3)_2)(\text{NCy}_2)(\text{THF})]_1$, as given in Figure 4.27. These could both be analogous to the literature band at 1244 cm^{-1} , which is in line with the previous discussion and could tentatively be assigned to the δ C–H vibrations of the trimethylsilyl group. Although this was expected, the presence of two bands in this region could indicate that some fully protonated ligand was still present in the product mixture. This would not be the case if the band at 1258 cm^{-1} was analogous to the literature band.

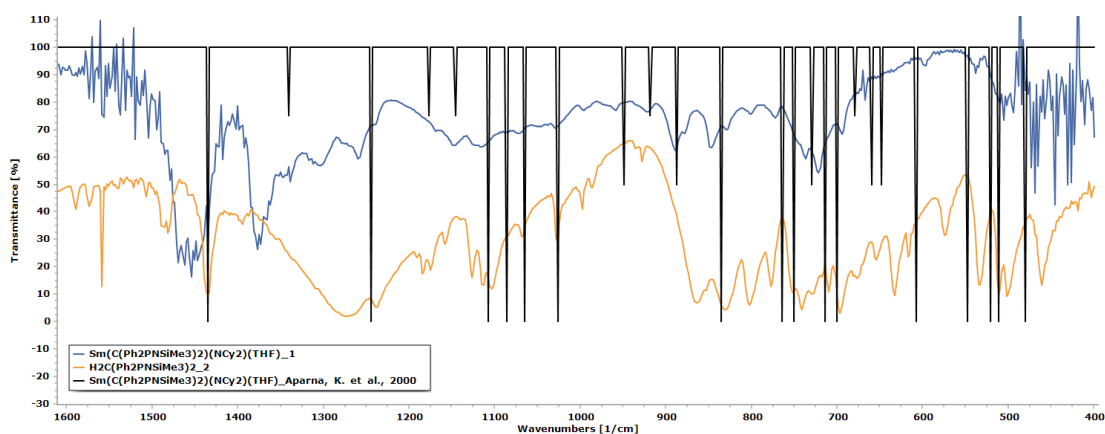


Figure 4.27: IR spectra of $[\text{Sm}(\text{C}(\text{Ph}_2\text{PNSiMe}_3)_2)(\text{NCy}_2)(\text{THF})]_1$ in nujol (blue), $\text{H}_2\text{C}(\text{Ph}_2\text{PNSiMe}_3)_2$ (orange) and $[\text{Sm}(\text{C}(\text{Ph}_2\text{PNSiMe}_3)_2)(\text{NCy}_2)(\text{THF})]$ literature data (black).

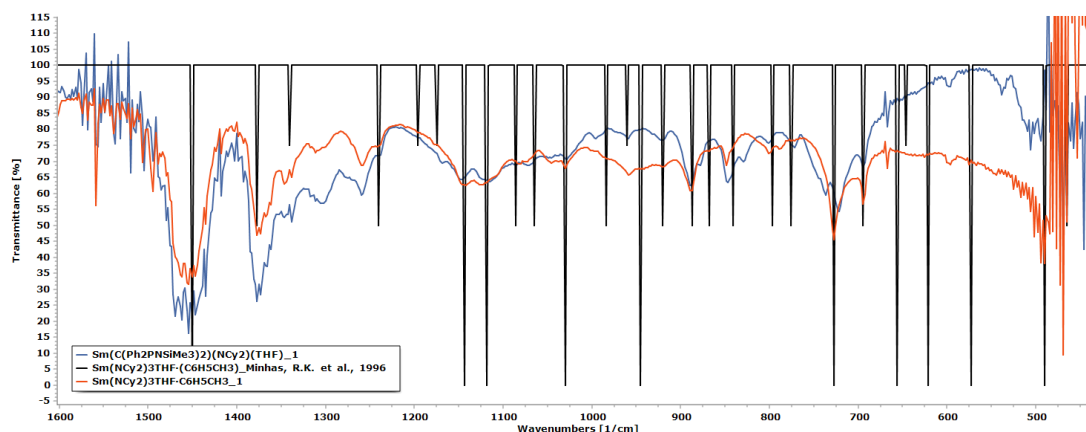


Figure 4.28: IR spectra of $[\text{Sm}(\text{C}(\text{Ph}_2\text{PNSiMe}_3)_2)(\text{NCy}_2)(\text{THF})]_1$ in *nujol* (blue), $[\text{Sm}(\text{NCy}_2)_3\text{THF}] \cdot \text{C}_6\text{H}_5\text{CH}_3_1$ (orange) and $[\text{Sm}(\text{NCy}_2)_3\text{THF}] \cdot \text{C}_6\text{H}_5\text{CH}_3$ literature data (black).

In the region $775\text{--}680\text{ cm}^{-1}$ five bands were observed at 772 cm^{-1} (weak), 747 cm^{-1} (shoulder), 737 cm^{-1} (strong), 721 cm^{-1} (strong) and 693 cm^{-1} (medium) in the spectrum of the product. These could be analogous to the literature bands observed in this region for this complex and which are given at 763 cm^{-1} (strong), 749 cm^{-1} (strong), 729 cm^{-1} (medium), 713 cm^{-1} (strong), and 699 cm^{-1} (strong) respectively. Although not an exact match, these bands would indicate the presence of the ligand P–Ph vibrations in the product, as these are typically present in this region. The bands at 772 cm^{-1} , 721 cm^{-1} and 693 cm^{-1} , along with a weak band at 800 cm^{-1} , could also be analogous to the $[\text{Sm}(\text{NCy}_2)_3\text{THF}] \cdot \text{C}_6\text{H}_5\text{CH}_3$ bands given in literature at 775 cm^{-1} , 727 cm^{-1} , 694 cm^{-1} and 769 cm^{-1} respectively. This could indicate the presence of the NCy_2^- ligand, although proper assignment of these bands was not definitive, as described in Section 4.1.2.2.1. It should be noted that the band at 693 cm^{-1} was also observed for the starting reagent used in this synthesis, namely $[\text{Sm}(\text{NCy}_2)_3\text{THF}] \cdot \text{C}_6\text{H}_5\text{CH}_3_1$. The bands at 800 cm^{-1} and 772 cm^{-1} also lie in the same region as the $\text{H}_2\text{C}(\text{Ph}_2\text{PNSiMe}_3)_2$ bands at 802 cm^{-1} and 776 cm^{-1} , which could be assigned to the $\nu_{\text{as}}\text{ P-CH}_2\text{-P}$ and $\nu_{\text{s}}\text{ P-CH}_2\text{-P}$ vibrations. This indicated the presence of this ligand, however the loss of the ligand band at 864 cm^{-1} in the spectrum of the product and the clear decrease in intensity for the bands at 800 cm^{-1} and 772 cm^{-1} would indicate that if the protonated ligand was present it was most likely an impurity rather than the major component.

Two bands, a strong band at 847 cm^{-1} and a weak band at 828 cm^{-1} were observed in the spectrum of $[\text{Sm}(\text{C}(\text{Ph}_2\text{PNSiMe}_3)_2)(\text{NCy}_2)(\text{THF})]_1$. Both these bands fell in the $860\text{--}820\text{ cm}^{-1}$ region and therefore they could be tentatively assigned to the expected $\rho\text{ CH}_3 + \nu\text{ Si-C}$ vibrations. Notwithstanding its intensity the strong band at 889 cm^{-1} could

not be assigned to any particular vibration or to any analogue in the spectra of the reagents used or the expected product. The loss of most of the major bands in the region 870–750 cm^{-1} , apart from the bands at 847 cm^{-1} and 889 cm^{-1} , was in line with the expected decrease in the number of bands in this region which is typically observed on deprotonation of the ligand and thus indicating deprotonation and coordination. However the band at 889 cm^{-1} could be indicative of a ν_{as} P–C–P or ν_{s} P–C–P vibration which in this region could indicate the presence of the $[\text{HC}(\text{Ph}_2\text{PNSiMe}_3)_2]^-$ anion, since for the di-anion species bands are not typically found in this range.

Discussion on the bands observed in the IR spectrum of $[\text{Sm}(\text{C}(\text{Ph}_2\text{PNSiMe}_3)_2)(\text{NCy}_2)(\text{THF})]_1$ in the region of 1110–1025 cm^{-1} was difficult, given that although the bands were strong, numerous bands were present and all appeared to be very broad and overlapping. The literature data described four strong bands in this region, at 1107 cm^{-1} , 1086 cm^{-1} , 1065 cm^{-1} and 1026 cm^{-1} . The experimental data yielded broad bands of varying intensity at 1116 cm^{-1} (strong), 1085 cm^{-1} (very weak), 1070 cm^{-1} (shoulder) and 1028 cm^{-1} (shoulder). In each case the intensities of these bands were hard to describe given the overlaps. All four bands were in agreement with the literature data although the intensity was less than expected. All the bands in this range could be assigned to the new $\nu \text{P}^+-\text{N}^-$ vibrations, as described earlier. It should however be noted that all these bands observed in both the data of $[\text{Sm}(\text{C}(\text{Ph}_2\text{PNSiMe}_3)_2)(\text{NCy}_2)(\text{THF})]_1$ and the literature data could be analogous to bands in this region which were observed in the $[\text{Sm}(\text{NCy}_2)_3\text{THF}] \cdot \text{C}_6\text{H}_5\text{CH}_3_1$ IR spectrum, indicating that the bands could be due to vibrations in the $\text{Sm}(\text{NCy}_2)(\text{THF})$ fragment. In this study the band at 1028 cm^{-1} was thus tentatively assigned to the ν_{as} C–O–C vibration for coordinated THF typical in the region.^{305,307–309,349} Another similar observation was the band at 1145 cm^{-1} which was present in the spectrum of $[\text{Sm}(\text{C}(\text{Ph}_2\text{PNSiMe}_3)_2)(\text{NCy}_2)(\text{THF})]_1$ but not described in the literature data. This was however observed in the spectrum of the $[\text{Sm}(\text{NCy}_2)_3\text{THF}] \cdot \text{C}_6\text{H}_5\text{CH}_3_1$ and on comparison of the spectra of the product and the starting reagent, as given in Figure 4.28, the similarities indicated that the product could contain this starting reagent as a major component.

It should be noted that the bands at higher wavenumbers than those described in literature may not only have been due to this unreacted $[\text{Sm}(\text{NCy}_2)_3\text{THF}] \cdot \text{C}_6\text{H}_5\text{CH}_3_1$ starting reagent but also to the presence of $\nu \text{P}=\text{C}$ vibrations expected in this region. This assumption was based on the bond length values published for these lanthanide carbene

complexes. The issue remained that such bands have not been reported in literature as can be seen in Figure 4.28. It is also possible that these bands indicate the formation of $[\text{HC}(\text{Ph}_2\text{PNSiMe}_3)_2]^-$ containing complexes, wherein bands in the region of $1220\text{--}1100\text{ cm}^{-1}$ are expected. These bands would be due to the presence of $\nu\text{ P}^+\text{--N}^-$ vibrations for the mono-anions.

In the case of the small crop of crystals labelled as product $[\text{Sm}(\text{C}(\text{Ph}_2\text{PNSiMe}_3)_2)(\text{NCy}_2)(\text{THF})]_2$, a very different IR spectrum was obtained when compared to that of the product $[\text{Sm}(\text{C}(\text{Ph}_2\text{PNSiMe}_3)_2)(\text{NCy}_2)(\text{THF})]_1$. Therefore an attempt was made to obtain a better spectrum using KBr disk method, as given in Figure 4.29. The IR spectrum obtained showed two strong broad bands at 3450 cm^{-1} and 1635 cm^{-1} , which are typically assigned to water $\nu\text{ O--H}$ and $\delta\text{ O--H}$ vibrations respectively. This could be due to moisture absorption during the preparation of the KBr disk, although the large intensities could also indicate the presence of moisture in the product. This would indicate that the desired product was not obtained, because of this compound's instability in non-dry conditions. The decreased amount of bands in the regions of $1265\text{--}1240\text{ cm}^{-1}$ and $860\text{--}820\text{ cm}^{-1}$, indicative of the loss of the trimethylsilyl group, and the significant water intrusion, indicated the potential presence of a decomposition product. As described in Section 4.1.3.1.3., SXRD studies indicated that diphenylphosphinamide, $\text{Ph}_2\text{P}(\text{O})\text{NH}_2$, was a component of this solid. This is a moisture induced decomposition product of $\text{H}_2\text{C}(\text{Ph}_2\text{PNSiMe}_3)_2$.^{295,350} Comparison of the IR data of the product $[\text{Sm}(\text{C}(\text{Ph}_2\text{PNSiMe}_3)_2)(\text{NCy}_2)(\text{THF})]_2$ with the IR data of $\text{Ph}_2\text{P}(\text{O})\text{NH}_2$, as given in Figure 4.29, indicated that the bulk of the solid was mainly $\text{Ph}_2\text{P}(\text{O})\text{NH}_2$.

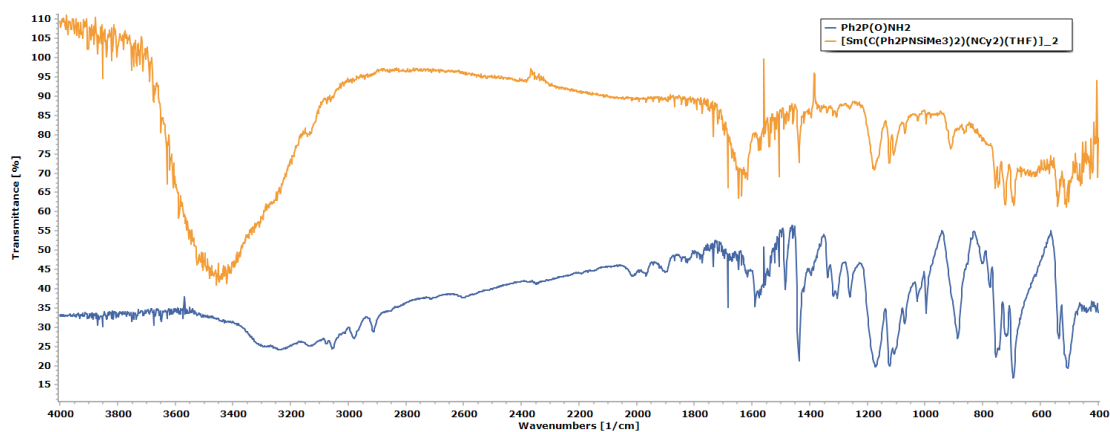


Figure 4.29: IR spectra of $[\text{Sm}(\text{C}(\text{Ph}_2\text{PNSiMe}_3)_2)(\text{NCy}_2)(\text{THF})]_2$ (orange) and $\text{Ph}_2\text{P}(\text{O})\text{NH}_2$ (blue).

The product $[\text{Sm}(\text{C}(\text{Ph}_2\text{PNSiMe}_3)_2)(\text{NCy}_2)(\text{THF})]_3$ was collected as described in Section 3.3.1.3.1.5 in two solid products. The IR spectra were significantly similar, as shown in Figure 4.30. It should be noted that the IR spectra obtained for these products were not of very good quality and therefore only a conservative discussion is given hereunder. In the IR spectrum of the second precipitate bands indicative of moisture intrusion were present. The spectra for these two products are shown in Figure 4.31, together with the spectra of the starting reagents $\text{H}_2\text{C}(\text{Ph}_2\text{PNSiMe}_3)_2$ and $[\text{Sm}(\text{NCy}_2)_3\text{THF}] \cdot \text{C}_6\text{H}_5\text{CH}_3_1$ and the spectrum presented in literature for the expected product. Given the similarities highlighted above, in this discussion similar bands in the two spectra of the two products are discussed as being bands for the spectrum of the product $[\text{Sm}(\text{C}(\text{Ph}_2\text{PNSiMe}_3)_2)(\text{NCy}_2)(\text{THF})]_3$.

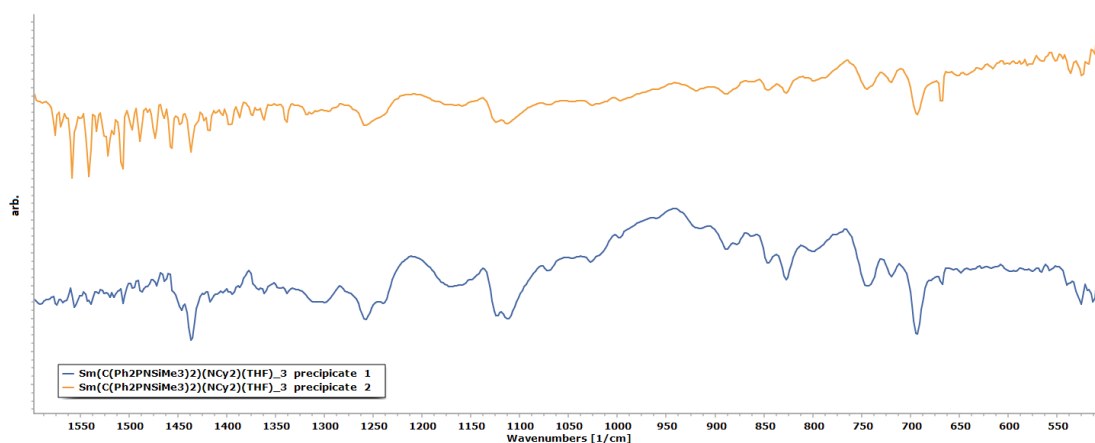


Figure 4.30: IR spectra of the two precipitates constituting $[\text{Sm}(\text{C}(\text{Ph}_2\text{PNSiMe}_3)_2)(\text{NCy}_2)(\text{THF})]_3$ (1st precipitate in blue and 2nd in orange).

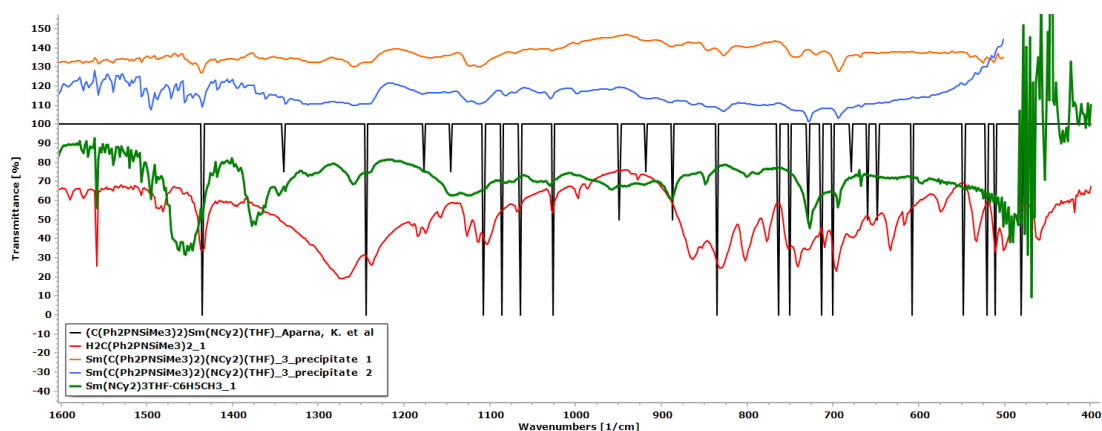


Figure 4.31: IR spectra of $[\text{Sm}(\text{C}(\text{Ph}_2\text{PNSiMe}_3)_2)(\text{NCy}_2)(\text{THF})]_3$ (1st precipitate in blue and 2nd in orange), $[\text{Sm}(\text{C}(\text{Ph}_2\text{PNSiMe}_3)_2)(\text{NCy}_2)(\text{THF})]$ literature data (black), $\text{H}_2\text{C}(\text{Ph}_2\text{PNSiMe}_3)_2$ (red) and $[\text{Sm}(\text{NCy}_2)_3\text{THF}] \cdot \text{C}_6\text{H}_5\text{CH}_3_1$ (green).

For the product $[\text{Sm}(\text{C}(\text{Ph}_2\text{PNSiMe}_3)_2)(\text{NCy}_2)(\text{THF})]_3$ a weak band at 1435 cm^{-1} was observed which could be analogous to the P–Ph band noted at the same wavenumber in the literature data for the expected product. Another two bands, namely a strong band at 1260 cm^{-1} and a shoulder at 1238 cm^{-1} were also observed in the spectrum of the product. Both these bands fell in the $1265\text{--}1240\text{ cm}^{-1}$ region which is associated with the δ C–H vibration of the trimethylsilyl group and these could be analogous to the literature band at 1243 cm^{-1} . This was in agreement with the band at 827 cm^{-1} observed for this product, which fell in the expected range of $860\text{--}820\text{ cm}^{-1}$ associated with the ρ $\text{CH}_3 + \nu$ Si–C vibrations. These bands indicated the presence of the trimethylsilyl moiety in the product obtained. The lack of further bands in the region $900\text{--}765\text{ cm}^{-1}$ was indicative of deprotonation, indicating the possible formation of the desired product. Weak bands at 916 cm^{-1} , 890 cm^{-1} and 846 cm^{-1} , and the band at 863 cm^{-1} observed only for the second precipitate, could not be related to any reagent IR bands and only the bands at 916 cm^{-1} and 890 cm^{-1} could be associated with bands described in literature data for the desired compound, with the latter most likely due to vibrations of the NCy_2^- ligand.

In the region $775\text{--}680\text{ cm}^{-1}$ there were some differences between the spectra of the two precipitates. In each case strong bands at 743 cm^{-1} and 692 cm^{-1} were observed, while for the first precipitate a medium intensity band was observed at 718 cm^{-1} and for the second precipitate a band at 728 cm^{-1} was observed. Typically, more bands are observed in this region normally assigned to P–Ph vibrations. The two bands present in both precipitates could be analogous to the literature bands at 749 cm^{-1} and 699 cm^{-1} , while the two bands at 718 cm^{-1} and 728 cm^{-1} could be analogous to the band at 729 cm^{-1} given their medium intensity as compared to that of the other two bands. The lack of bands analogous to the remaining two bands from literature could be due to overlap and the quality of the experimental spectra. In the second precipitate the bands at 728 cm^{-1} and 692 cm^{-1} showed similarity to bands present in the spectrum of $[\text{Sm}(\text{NCy}_2)_3\text{THF}] \cdot \text{C}_6\text{H}_5\text{CH}_3_1$, indicating that this solid still contained some of this reagent after reaction.

As detailed above numerous bands are expected in the region of $1110\text{--}1025\text{ cm}^{-1}$, especially due to the expected ν $\text{P}^+\text{--N}^-$, ν_{as} C–O–C for coordinated THF and skeletal NCy_2^- ligand vibrations. In this region three common bands were observed for both precipitates, at 1109 cm^{-1} (strong), 1070 cm^{-1} (shoulder) and 1028 cm^{-1} (medium), while for the second precipitate a fourth band was observed at 1082 cm^{-1} (strong). The three bands found in common for both spectra could be analogous to the strong literature bands

at 1107 cm^{-1} , 1065 cm^{-1} and 1026 cm^{-1} , while the experimental band at 1082 cm^{-1} could be analogous to the literature band at 1086 cm^{-1} . Therefore, these bands seemed to be in agreement with literature data, although the intensity of the bands differed from that reported in literature. As described prior the band at 1028 cm^{-1} was associated with the ν_{as} C–O–C vibrations for coordinated THF, while the band at 1109 cm^{-1} was tentatively assigned to the ν P^+-N^- vibration for the di-anion $[\text{C}(\text{Ph}_2\text{PNSiMe}_3)_2]^{2-}$ species. At a higher wavenumber than this range two bands were observed, namely the weak broad band at 1176 cm^{-1} and the strong band at 1126 cm^{-1} . The former band could be analogous to the band at 1177 cm^{-1} described in literature, however no analogous band was known for the latter band. The presence of the band at 1176 cm^{-1} could support the formation of the desired product since this band was described in literature and is unique to this complex as compared to the IR data of other lanthanide carbene complexes. It should be noted that the two bands at 1176 cm^{-1} and 1126 cm^{-1} also fell in the range 1220–1100 cm^{-1} wherein ν P^+-N^- vibrational bands for $[\text{HC}(\text{Ph}_2\text{PNSiMe}_3)_2]^-$ are expected. This could indicate that a $[\text{HC}(\text{Ph}_2\text{PNSiMe}_3)_2]^-$ species is a minor component of this product.

Given the similarities in both IR spectra of the two precipitates these were considered to be the same product and therefore collected together as product $[\text{Sm}(\text{C}(\text{Ph}_2\text{PNSiMe}_3)_2)(\text{NCy}_2)(\text{THF})]_3$.

The product $[\text{Sm}(\text{C}(\text{Ph}_2\text{PNSiMe}_3)_2)(\text{NCy}_2)(\text{THF})]_4$ was analysed using IR spectroscopy with the IR spectrum of the solid in KBr given in Figure 4.32.

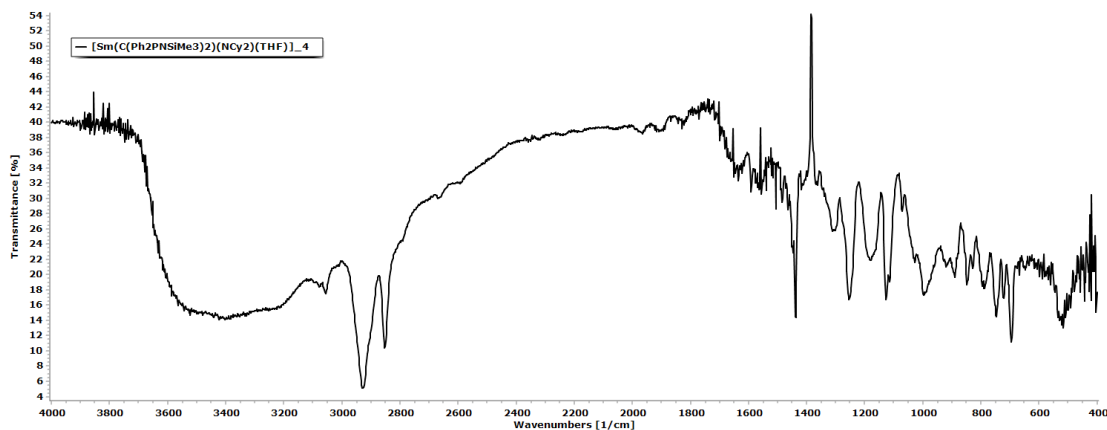


Figure 4.32: IR spectrum of $[\text{Sm}(\text{C}(\text{Ph}_2\text{PNSiMe}_3)_2)(\text{NCy}_2)(\text{THF})]_4$ in KBr .

The first noticeable feature of the spectrum was the presence of the two bands at 3400 cm^{-1} and 1645 cm^{-1} . These bands were assigned to the ν O–H and δ O–H vibrations respectively and are typical of water trapped in the solid. This water may be present in

the form of moisture intrusion or water of crystallisation. The presence of these two bands indicated that any compounds obtained were unlikely to be the desired carbene given the sensitivity of this compound to moisture.

The presence of an organic compound was attested through the presence of a number of bands. The band at 3055 cm^{-1} , bands in the region of 2000 to 1800 cm^{-1} and bands at 1437 cm^{-1} , 787 cm^{-1} , 747 cm^{-1} , 722 cm^{-1} and 695 cm^{-1} were all indicative of the presence of phenyl groups. The band at 3055 cm^{-1} was due to the $\nu\text{ C-H}$ vibration while the weak bands in the range 2000 to 1800 cm^{-1} could be attributed to phenyl ring overtone bands, both groups being typical of all phenyl groups which could be due to any $\text{H}_2\text{C}(\text{Ph}_2\text{PNSiMe}_3)_2$ derivatives or toluene. The bands at 1437 cm^{-1} , 787 cm^{-1} , 747 cm^{-1} , 722 cm^{-1} and 695 cm^{-1} could all be assigned to P-Ph vibrations expected for the ligand $\text{H}_2\text{C}(\text{Ph}_2\text{PNSiMe}_3)_2$ and any anionic and other derivatives. The two strong bands at 2929 cm^{-1} and 2853 cm^{-1} were also assigned to the $\nu\text{ C-H}$ vibrations for aliphatic groups which could be tentatively attributed to toluene, the methylene group of the neutral $\text{H}_2\text{C}(\text{Ph}_2\text{PNSiMe}_3)_2$, and the organic moieties in the $\text{Sm}(\text{NCy}_2)(\text{THF})$ fragment. In general, these bands do not give much information on the chemical structure of the solid except for the indication of the presence of P-Ph containing $\text{H}_2\text{C}(\text{Ph}_2\text{PNSiMe}_3)_2$ derivatives.

The remaining bands could provide more detailed structural information. These bands could be initially discussed in the light of the expected theoretical changes that occur on the deprotonation of $\text{H}_2\text{C}(\text{Ph}_2\text{PNSiMe}_3)_2$, as discussed prior in this section. The strong bands at 1253 cm^{-1} , 1240 cm^{-1} , 847 cm^{-1} and 828 cm^{-1} could be tentatively assigned to the $\delta\text{ C-H}$ and $\rho\text{ CH}_3 + \nu\text{ Si-C}$ vibrations typical of the trimethylsilyl moiety. These fall in the ranges described for the various di-anionic species published in literature and described prior, namely $1265\text{--}1240\text{ cm}^{-1}$ and $860\text{--}820\text{ cm}^{-1}$. These bands are indicative of the presence of trimethylsilyl containing $\text{H}_2\text{C}(\text{Ph}_2\text{PNSiMe}_3)_2$ derivatives. Given that both aliphatic $\nu\text{ C-H}$ and these trimethylsilyl vibrations were visible in the spectrum, the presence of $\text{H}_2\text{C}(\text{Ph}_2\text{PNSiMe}_3)_2$ was possible. However, the lack of a strong band at 1273 cm^{-1} , due to the P=N bond, indicated that this compound was unlikely to be present in the solid. Therefore, it was likely that either the mono-anionic or di-anionic derivative of this compound was present. Detailed discussion was more viable using more diagnostic features of the IR spectrum in the fingerprint region, specifically in the range of $1180\text{--}787\text{ cm}^{-1}$.

As was described prior the main diagnostic feature of the IR spectrum of the di-anion $[\text{C}(\text{Ph}_2\text{PNSiMe}_3)_2]^{2-}$ should be the expected strong $\nu \text{P}^+-\text{N}^-$ vibration bands in the region $1110\text{--}1025 \text{ cm}^{-1}$. The bands at 1115 cm^{-1} , 1070 cm^{-1} and 1028 cm^{-1} could all be tentatively assigned to this vibrational mode. However, the former band seemed to be paired with the band at 1127 cm^{-1} , typical of the NCy_2^- ligand, and the latter band could also be assigned to the $\nu_{\text{as}} \text{C-O-C}$ for coordinated THF. The band at 1070 cm^{-1} was observed to be very weak, which contrasts with the strong bands at 1086 cm^{-1} and 1065 cm^{-1} given in literature for $[\text{Sm}(\text{C}(\text{Ph}_2\text{PNSiMe}_3)_2)(\text{NCy}_2)(\text{THF})]$. The bands at 1180 cm^{-1} and 1127 cm^{-1} could fall in the range in which the $\nu \text{P}^+-\text{C}^{2-}-\text{P}^+$ vibrations are expected, although no bands in this region are typically given in data for published carbene structures. Stronger bands were observed in the region $1220\text{--}1100 \text{ cm}^{-1}$ wherein $\nu \text{P}^+-\text{N}^-$ vibrational bands for $[\text{HC}(\text{Ph}_2\text{PNSiMe}_3)_2]^-$ are expected. The main bands that fell in this range were the broad band at 1180 cm^{-1} and the paired strong bands at 1127 cm^{-1} and 1115 cm^{-1} . All of these could be tentatively assigned to the $\nu \text{P}^+-\text{N}^-$ vibrational bands of the mono-anion. As described prior the latter two bands could also be due to the $\nu \text{C-N}$ vibration of the NCy_2^- ligand and therefore only the band at 1180 cm^{-1} was diagnostic of the mono-anion. The bands at 1127 cm^{-1} and 1115 cm^{-1} could be analogous to the literature band of $[\text{Sm}(\text{C}(\text{Ph}_2\text{PNSiMe}_3)_2)(\text{NCy}_2)(\text{THF})]$ at 1107 cm^{-1} and the $[\text{Sm}(\text{NCy}_2)_3\text{THF}] \cdot \text{C}_6\text{H}_5\text{CH}_3$ literature bands at 1143 cm^{-1} and 1118 cm^{-1} . The similarity and profile of the two bands further support this assignment.

The bands in the range $998\text{--}828 \text{ cm}^{-1}$ were the most diagnostic in determining the main $\text{H}_2\text{C}(\text{Ph}_2\text{PNSiMe}_3)_2$ derivative present in the solid. In this range only trimethylsilyl bands are expected for the $[\text{C}(\text{Ph}_2\text{PNSiMe}_3)_2]^{2-}$ di-anion. Therefore, strong or noticeable bands in this region, especially at higher wavenumbers, indicated the possible lack of the $[\text{C}(\text{Ph}_2\text{PNSiMe}_3)_2]^{2-}$ di-anion species. Fingerprint region bands for THF, toluene and NCy_2^- are known, however these are rarely of the intensity observed in this spectrum. The bands at 998 cm^{-1} , 890 cm^{-1} , 847 cm^{-1} and 828 cm^{-1} could all be assigned or related to the $\nu \text{P}^+-\text{CH}^--\text{P}^+$ vibration typical of the mono-anion $[\text{HC}(\text{Ph}_2\text{PNSiMe}_3)_2]^-$, as theoretically described in this section. The latter two could be assigned to the trimethylsilyl group $\rho \text{CH}_3 + \nu \text{Si-C}$ vibrations and therefore the assignment would indicate either overlap or a region containing both band types wherein further distinction is not possible. The former two bands are on the other hand unlikely to be assigned to other possible vibrational modes. This assignment was further supported by the high intensity of the band at 998 cm^{-1} . The band at 1028 cm^{-1} could also be assigned to this

vibrational mode but was more likely due to the expected $\nu_{\text{as}} \text{C-O-C}$ for coordinated THF vibrations, indicating the possible presence of the $\text{Sm}(\text{NCy}_2)(\text{THF})$ fragment and specifically the Sm-THF moiety. The presence of these bands, along with the loss of the $\nu \text{P=N}$ band of $\text{H}_2\text{C}(\text{Ph}_2\text{PNSiMe}_3)_2$ and the lack of strong bands in the region of $1110\text{--}1025 \text{ cm}^{-1}$ indicating the presence of the di-anion derivative, indicated that the main product of the solid $[\text{Sm}(\text{C}(\text{Ph}_2\text{PNSiMe}_3)_2)(\text{NCy}_2)(\text{THF})]_4$ was a salt or complex of the mono-anion $[\text{HC}(\text{Ph}_2\text{PNSiMe}_3)_2]^-$.

Further to this discussion it is also observed that some bands in the IR spectrum of $[\text{Sm}(\text{C}(\text{Ph}_2\text{PNSiMe}_3)_2)(\text{NCy}_2)(\text{THF})]_4$ could indicate the presence of the decomposition product $\text{Ph}_2\text{P}(\text{O})\text{NH}_2$. The bands at 1180 cm^{-1} and 1127 cm^{-1} , previously assigned to the mono-anionic $\nu \text{P}^+-\text{N}^-$ and the NCy_2^- group, could also be assigned to $\nu \text{P=O}$ vibrations observed for $\text{Ph}_2\text{P}(\text{O})\text{NH}_2$. The unassigned weak bands at 1564 cm^{-1} and 920 cm^{-1} further indicated the presence of $\text{Ph}_2\text{P}(\text{O})\text{NH}_2$. However, the decreased intensity of the band at 1180 cm^{-1} compared to the intensity of the bands at 1127 cm^{-1} and 1115 cm^{-1} , the weakness of the bands at 1564 cm^{-1} and 920 cm^{-1} and the presence of other strong bands in the region of $998\text{--}828 \text{ cm}^{-1}$ clearly indicated that $\text{Ph}_2\text{P}(\text{O})\text{NH}_2$ was most likely a secondary component.

Therefore it may be tentatively concluded that the solid obtained was most likely a hydrated form of a $[\text{HC}(\text{Ph}_2\text{PNSiMe}_3)_2]^-$ complex, with the possible presence of a $\text{Sm}(\text{NCy}_2)(\text{THF})$ fragment or some such derivative. This could indicate the presence of a samarium complex of $[\text{HC}(\text{Ph}_2\text{PNSiMe}_3)_2]^-$. It could also be concluded that $\text{Ph}_2\text{P}(\text{O})\text{NH}_2$ was likely a minor component of the solid.

4.1.3.1.2. Analysis by Microscopy

Samples obtained during the first three synthesis reactions undertaken to produce $[\text{Sm}(\text{C}(\text{Ph}_2\text{PNSiMe}_3)_2)(\text{NCy}_2)(\text{THF})]$, were observed under the microscope using plane polarised light. Micrographs of the solids obtained are given in Figures 4.33, 4.34 and 4.35 for $[\text{Sm}(\text{C}(\text{Ph}_2\text{PNSiMe}_3)_2)(\text{NCy}_2)(\text{THF})]_1$, $[\text{Sm}(\text{C}(\text{Ph}_2\text{PNSiMe}_3)_2)(\text{NCy}_2)(\text{THF})]_2$ and $[\text{Sm}(\text{C}(\text{Ph}_2\text{PNSiMe}_3)_2)(\text{NCy}_2)(\text{THF})]_3$ respectively.

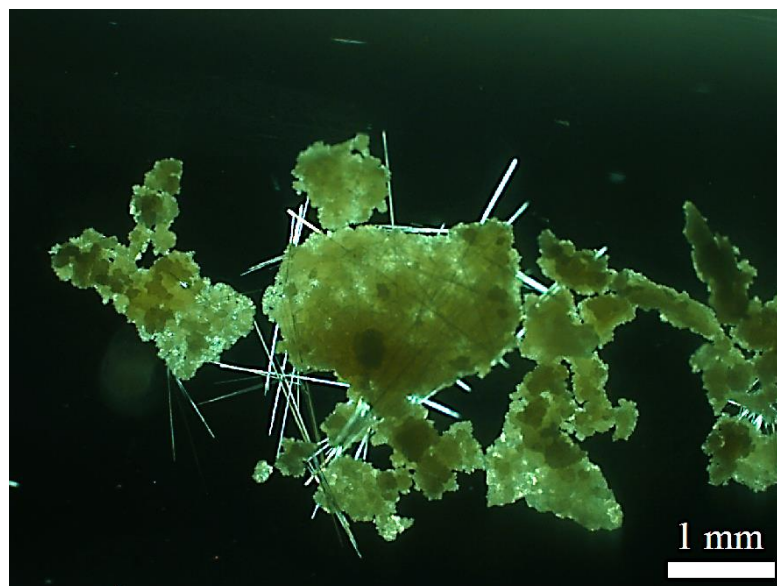


Figure 4.33: Micrograph of $[\text{Sm}(\text{C}(\text{Ph}_2\text{PNSiMe}_3)_2)(\text{NCy}_2)(\text{THF})]_1$.

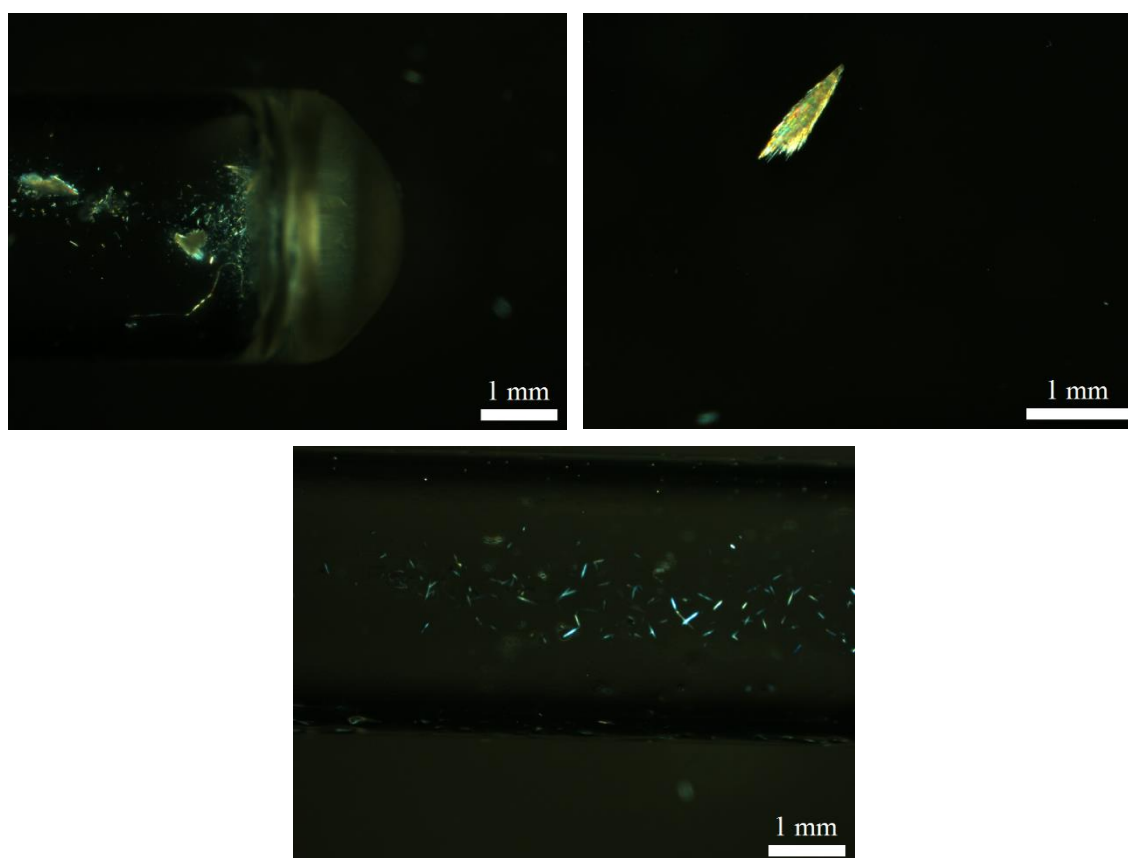


Figure 4.34: Micrographs of $[\text{Sm}(\text{C}(\text{Ph}_2\text{PNSiMe}_3)_2)(\text{NCy}_2)(\text{THF})]_2$, top left shows the crystalline bed stored under mother liquor, while the ones on the top right and bottom show a crop of crystals and single crystals stored in the NMR tube above the mother liquor.

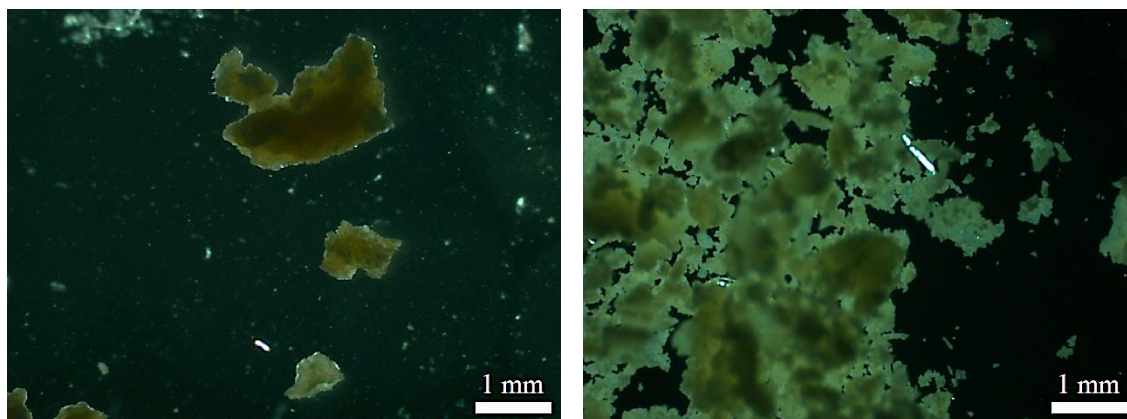


Figure 4.35: Two micrographs of the product $[\text{Sm}(\text{C}(\text{Ph}_2\text{PNSiMe}_3)_2)(\text{NCy}_2)(\text{THF})]_3$.

In the case of both $[\text{Sm}(\text{C}(\text{Ph}_2\text{PNSiMe}_3)_2)(\text{NCy}_2)(\text{THF})]_1$ and $[\text{Sm}(\text{C}(\text{Ph}_2\text{PNSiMe}_3)_2)(\text{NCy}_2)(\text{THF})]_2$ the products obtained were clearly crystalline. The product $[\text{Sm}(\text{C}(\text{Ph}_2\text{PNSiMe}_3)_2)(\text{NCy}_2)(\text{THF})]_2$ was obtained as a bed of single crystals which were stored under the toluene based mother liquor in an sealed NMR tube. Crystals which were viable for SXRD studies were observed on the walls of the sealed NMR tube, as shown in the bottom micrograph in Figure 4.34. The solid $[\text{Sm}(\text{C}(\text{Ph}_2\text{PNSiMe}_3)_2)(\text{NCy}_2)(\text{THF})]_1$ was initially collected as a somewhat sticky pale yellow powder, similar to the clumps observed in Figure 4.33. This was collected under dry argon in a sealed ampoule and stored for over a year, since the small yield was insufficient for further work. On examining this solid, during the preparation of PXRD capillary samples, it was observed that the clear single crystals shown in Figure 4.33 had formed. This spontaneous crystallisation was of great interest although the reason for its occurrence was unknown. The solid obtained for $[\text{Sm}(\text{C}(\text{Ph}_2\text{PNSiMe}_3)_2)(\text{NCy}_2)(\text{THF})]_3$ proved to be similar in texture to $[\text{Sm}(\text{C}(\text{Ph}_2\text{PNSiMe}_3)_2)(\text{NCy}_2)(\text{THF})]_1$, however the crystallinity was more difficult to describe under plane polarised light as given in Figure 4.35. No further information could be obtained from this physical data.

4.1.3.1.3. Analysis by Single crystal X-ray diffraction

In the case of $[\text{Sm}(\text{C}(\text{Ph}_2\text{PNSiMe}_3)_2)(\text{NCy}_2)(\text{THF})]_2$ the opening of the sealed tube and the removal of the mother liquor forced the loss of many of the crystals on the walls but the bed and cluster shown in the top left and right photographs in Figure 4.34 were collected. Single crystal samples of $[\text{Sm}(\text{C}(\text{Ph}_2\text{PNSiMe}_3)_2)(\text{NCy}_2)(\text{THF})]_2$ were

collected in dry nitrogen conditions in a glove box and sealed in 0.5 mm capillaries under the same conditions. Crystals were not collected for $[\text{Sm}(\text{C}(\text{Ph}_2\text{PNSiMe}_3)_2)(\text{NCy}_2)(\text{THF})]_1$ as these proved too fragile.

Data was collected for a $[\text{Sm}(\text{C}(\text{Ph}_2\text{PNSiMe}_3)_2)(\text{NCy}_2)(\text{THF})]_2$ single crystal using a STOE Stadivari diffractometer with a microfocus $\text{Cu-K}\alpha_1$ source. Unit cell and space group determination was undertaken using X-Area and structure solution was undergone using Olex2.^{351,352} This structure solution showed that the crystal collected from the compound $[\text{Sm}(\text{C}(\text{Ph}_2\text{PNSiMe}_3)_2)(\text{NCy}_2)(\text{THF})]_2$ was in fact diphenylphosphinamide, $\text{Ph}_2\text{P}(\text{O})\text{NH}_2$. The structure obtained had an orthorhombic unit cell with cell parameters $a = 5.58(3) \text{ \AA}$, $b = 11.85(8) \text{ \AA}$, $c = 16.13(11) \text{ \AA}$ and $\alpha = \beta = \gamma = 90^\circ$ and a spacegroup of $P2_12_12_1$, as shown in Figure 4.36. This is in good general agreement with the structure of a known polymorph of $\text{Ph}_2\text{P}(\text{O})\text{NH}_2$ which was published by Oliva, G. and Castellano, E.E. in 1981.³⁵³ Comparison of the IR data described in Section 4.1.3.1.1. with IR data of pure $\text{Ph}_2\text{P}(\text{O})\text{NH}_2$ indicated that this was the major component of the solid $[\text{Sm}(\text{C}(\text{Ph}_2\text{PNSiMe}_3)_2)(\text{NCy}_2)(\text{THF})]_2$. Literature data indicated that $\text{Ph}_2\text{P}(\text{O})\text{NH}_2$ was a common moisture induced decomposition product of $\text{H}_2\text{C}(\text{Ph}_2\text{PNSiMe}_3)_2$.^{295,350} Therefore in the case of $[\text{Sm}(\text{C}(\text{Ph}_2\text{PNSiMe}_3)_2)(\text{NCy}_2)(\text{THF})]_2$ it appeared that the major mode of reaction was the moisture induced decomposition of the $\text{H}_2\text{C}(\text{Ph}_2\text{PNSiMe}_3)_2$ ligand precursor. A discussion of the decomposition mechanism which was likely to have occurred is given in Section 4.1.3.1.4.

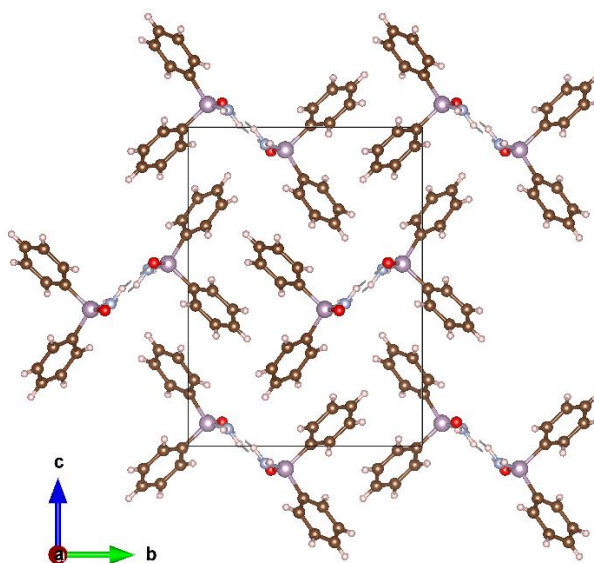
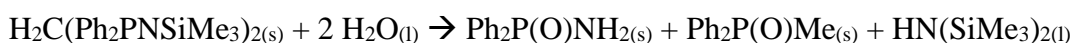


Figure 4.36: Crystal structure obtained from $[\text{Sm}(\text{C}(\text{Ph}_2\text{PNSiMe}_3)_2)(\text{NCy}_2)(\text{THF})]_2$ showing clearly that the compound obtained was diphenylphosphinamide.

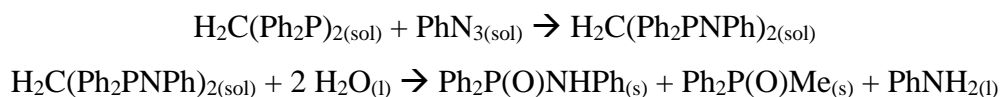
4.1.3.1.4. Decomposition of $\text{H}_2\text{C}(\text{Ph}_2\text{PNSiMe}_3)_2$

Single crystal X-ray diffraction of a single crystal from the solid $[\text{Sm}(\text{C}(\text{Ph}_2\text{PNSiMe}_3)_2)(\text{NCy}_2)(\text{THF})]_2$ showed that the single crystal analysed was $\text{Ph}_2\text{P}(\text{O})\text{NH}_2$. This was confirmed for the bulk of $[\text{Sm}(\text{C}(\text{Ph}_2\text{PNSiMe}_3)_2)(\text{NCy}_2)(\text{THF})]_2$ through IR spectroscopy. An account of the decomposition of the di- $\lambda^5\sigma^4$ -iminophosphorane $\text{H}_2\text{C}(\text{Ph}_2\text{PNSiMe}_3)_2$ was published by Schlecht and co-workers in 1998.³⁵⁰ A decomposition reaction, as provided in Scheme 4.1, was proposed in the publication.³⁵⁰



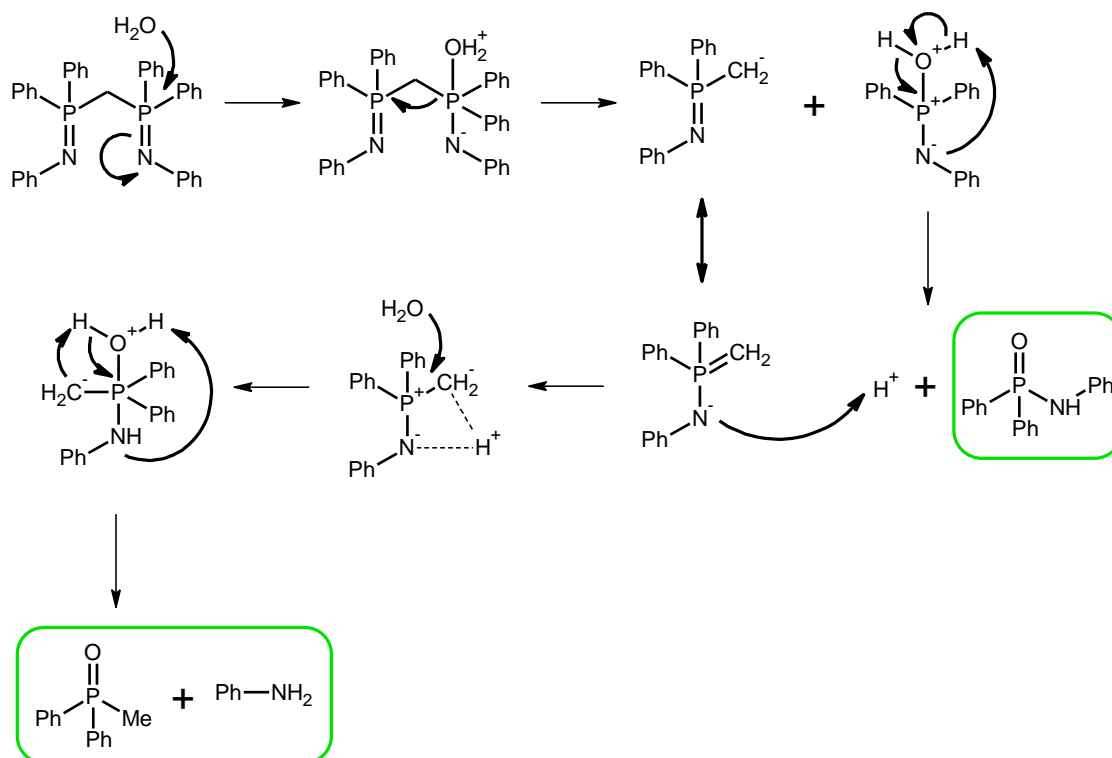
Scheme 4.1: General moisture induced decomposition reaction of $\text{H}_2\text{C}(\text{Ph}_2\text{PNSiMe}_3)_2$.

Support for this reaction was given in reference to an older publication by Aguiar and Biesler, published in 1964.²⁹⁵ This publication discussed the hydrolysis decomposition of other di- $\lambda^5\sigma^4$ -iminophosphorane compounds, namely $(\text{H}_2\text{CPh}_2\text{PNPh})_2$ and $\text{H}_2\text{C}(\text{Ph}_2\text{PNPh})_2$. In an effort to synthesis $\text{H}_2\text{C}(\text{Ph}_2\text{PNPh})_2$ through the phosphor-Staudinger method the mono-N-substituted phosphinamide N-phenyl(diphenyl)phosphinamide, $\text{Ph}_2\text{P}(\text{O})\text{NHPh}$, and methyldiphenylphosphine oxide, $\text{Ph}_2\text{P}(\text{O})\text{Me}$, were obtained, indicating that dppm was cleaved on reaction with PhN_3 in the presence of an oxygen containing reagent. Aguiar and Beisler reported that they could not collect the desired iminophosphorane, $\text{H}_2\text{C}(\text{Ph}_2\text{PNPh})_2$, but as stated above collected $\text{Ph}_2\text{P}(\text{O})\text{NHPh}$ and $\text{Ph}_2\text{P}(\text{O})\text{Me}$, which they described as forming through the reactions given in Scheme 4.2.²⁹⁵



Scheme 4.2: Hydrolysis reaction for $\text{H}_2\text{C}(\text{Ph}_2\text{PNPh})_2$ proposed by Aguiar and Beisler.²⁹⁵

This was explained by Aguiar and Beisler, through a nucleophilic substitution reaction of water on the phosphorus centres, followed by numerous rearrangements and a secondary nucleophilic substitution and elimination.²⁹⁵ An overview of this nucleophilic substitution and rearrangement mechanism is given in Scheme 4.3.

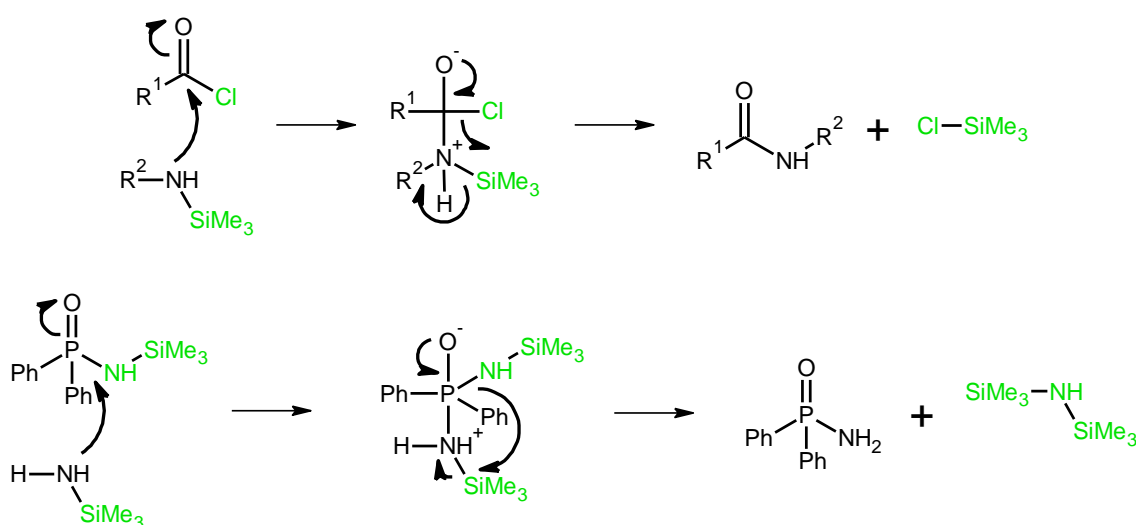


Scheme 4.3: Overview of the hydrolysis decomposition mechanism of $\text{H}_2\text{C}(\text{Ph}_2\text{PNPh})_2$; products obtained highlighted in green.

This decomposition mechanism was likely analogous to that which occurred to some degree for $\text{K}[\text{HC}(\text{Ph}_2\text{PNiPr})_2]_2$, where $\text{Ph}_2\text{P}(\text{O})\text{Me}$ was collected as an impurity in the ^1H NMR sample of the product, as described in Section 4.1.1.1.2.2. This mechanism described by Aguiar and Beisler may be considered the basis for the decomposition reaction published by Schlecht and co-workers. If this same mechanism was followed during the decomposition of $\text{H}_2\text{C}(\text{Ph}_2\text{PNSiMe}_3)_2$ one would expect the formation of $\text{Ph}_2\text{P}(\text{O})\text{NHSiMe}_3$, $\text{Ph}_2\text{P}(\text{O})\text{Me}$ and H_2NSiMe_3 . However as per Scheme 4.1 this was not the case and no further discussion was given in literature regarding this important difference. Thus a tentative mechanism which reconciles these differences is proposed hereunder.

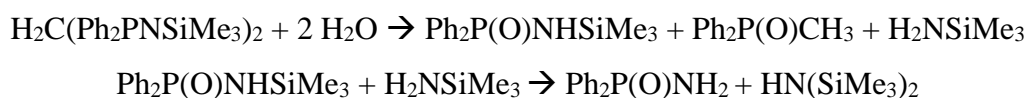
The synthesis of trimethylsilylamine, H_2NSiMe_3 , is very rarely attested in literature and publications mentioning this compound indicate that it has a short lifetime with decomposition at room temperature.^{354,355} It is clearly attested from experimental data that all mono-N-substituted silyl amines tend to decompose through condensation of ammonia to form di-N-substituted silyl amines.³⁵⁶ This trend indicates that the formation of $\text{HN}(\text{SiMe}_3)_2$ would be preferential to the formation of H_2NSiMe_3 , supporting the reaction proposed by Schlecht and co-workers.

It should be noted that the cleavage of the Si–N bond is also known in reactions with organic acid chlorides through nucleophilic substitution wherein amides are produced, leaving the silyl chlorides as the main side products.³⁵⁷ Such nucleophilic reactions are also known for phosphorus (V) compounds as described prior.⁹⁹ The nucleophilic substitution of acid chlorides by silyl amines, as described in literature, and the analogous mechanism for the reaction of $\text{Ph}_2\text{P}(\text{O})\text{NHSiMe}_3$ with H_2NSiMe_3 , being proposed in this study, are given in Scheme 4.4. The moieties represented in black in the reagents are the ones that produce the organic or phosphorus centred compound, while the green moieties in the reagents are the ones that form the respective silyl by-product.



Scheme 4.4: Nucleophilic substitution by silyl amine with organic acid chloride (top) and the nucleophilic substitution of $\text{Ph}_2\text{P}(\text{O})\text{NHSiMe}_3$ with H_2NSiMe_3 in an analogous mechanism (bottom).

Therefore, the decomposition of $\text{H}_2\text{C}(\text{Ph}_2\text{PNSiMe}_3)_2$ as described in literature can be described through the analogous stepwise mechanisms for this ligand as given in Schemes 4.3 and 4.4. The full proposed reaction for the decomposition of $\text{H}_2\text{C}(\text{Ph}_2\text{PNSiMe}_3)_2$ is summarised in Scheme 4.5. The two main driving forces are most likely thermodynamic. These are the formation of the very strong and stable P=O bonds and the formation of the silazane instead of the less stable mono-N-substituted silyl amine.



Scheme 4.5: Full multi-step moisture induced decomposition reaction of $\text{H}_2\text{C}(\text{Ph}_2\text{PNSiMe}_3)_2$.

4.1.3.1.5. Analysis by Powder X-ray diffraction

PXRD analysis of $[\text{Sm}(\text{C}(\text{Ph}_2\text{PNSiMe}_3)_2)(\text{NCy}_2)(\text{THF})]_4$ was undertaken using samples of the solid prepared and sealed in a 0.5 mm capillary under nitrogen in a glove box. The data was collected using $\text{Mo-K}\alpha_1$ radiation to eliminate expected absorption issues due to the presence of Sm^{3+} . The PXRD pattern of the solid $[\text{Sm}(\text{C}(\text{Ph}_2\text{PNSiMe}_3)_2)(\text{NCy}_2)(\text{THF})]_4$ is given in Figure 4.37. On initial inspection of the PXRD pattern it was clear that the major phase of the solid was amorphous. A minor crystalline phase was observed with peaks in the region of 4° to 11° . Given that the major phase was amorphous no structure solution of the main chemical components could be undertaken. The nature of the minor crystalline phase would be best described by comparison of the pattern with calculated powder patterns of the reagents used, products expected and other possible solid by-products. Comparison of the experimental pattern with the calculated powder pattern of the desired product $[\text{Sm}(\text{C}(\text{Ph}_2\text{PNSiMe}_3)_2)(\text{NCy}_2)(\text{THF})]$, as given in Figure 4.38,⁷ indicated that this was not present in the solid in any significant amount. This was in agreement with the IR data discussed previously.

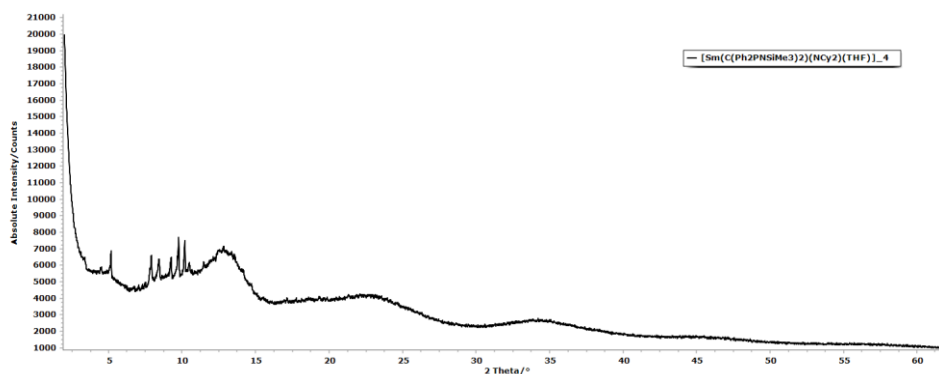


Figure 4.37: PXRD pattern of $[\text{Sm}(\text{C}(\text{Ph}_2\text{PNSiMe}_3)_2)(\text{NCy}_2)(\text{THF})]_4$.

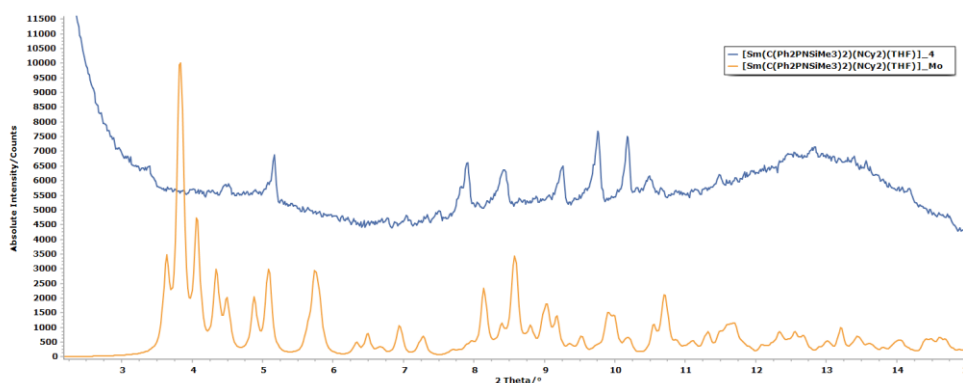


Figure 4.38: PXRD patterns of $[\text{Sm}(\text{C}(\text{Ph}_2\text{PNSiMe}_3)_2)(\text{NCy}_2)(\text{THF})]_4$ (blue) and literature $[\text{Sm}(\text{C}(\text{Ph}_2\text{PNSiMe}_3)_2)(\text{NCy}_2)(\text{THF})]$ (orange).

The powder pattern of $[\text{Sm}(\text{C}(\text{Ph}_2\text{PNSiMe}_3)_2)(\text{NCy}_2)(\text{THF})]_4$ was also compared with the calculated powder patterns of the reagents used, namely $\text{H}_2\text{C}(\text{Ph}_2\text{PNSiMe}_3)_2$, $[\text{Sm}(\text{NCy}_2)_3\text{THF}] \cdot \text{C}_6\text{H}_5\text{CH}_3$ and LiNCy_2 ,^{34,162,358} as given in Figure 4.39. None of these reagents were present in the solid, as no analogous peaks for the reagents' patterns were observed in the experimental powder pattern. Given that the $[\text{Sm}(\text{NCy}_2)_3\text{THF}] \cdot \text{C}_6\text{H}_5\text{CH}_3$ was prepared in-situ comparison with other products of the reaction of SmCl_3 with LiNCy_2 at different stoichiometry was undergone. This again yielded no analogous peaks between the calculated PXRD patterns and the experimental powder pattern.

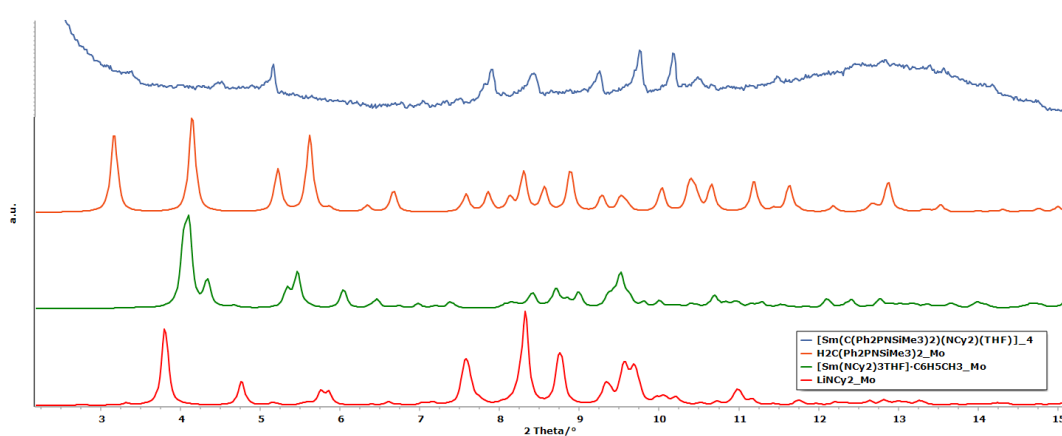


Figure 4.39: Experimental PXRD pattern of $[\text{Sm}(\text{C}(\text{Ph}_2\text{PNSiMe}_3)_2)(\text{NCy}_2)(\text{THF})]_4$ (blue) and the calculated PXRD patterns of $\text{H}_2\text{C}(\text{Ph}_2\text{PNSiMe}_3)_2$ (orange), $[\text{Sm}(\text{NCy}_2)_3\text{THF}] \cdot \text{C}_6\text{H}_5\text{CH}_3$ (green) and LiNCy_2 (red).

Since it was clear that the crystalline phase present in $[\text{Sm}(\text{C}(\text{Ph}_2\text{PNSiMe}_3)_2)(\text{NCy}_2)(\text{THF})]_4$ was not due to the expected products and the reagents used it was determined that this significant minor phase was likely due to some decomposition or side reaction product. Comparison with the two known polymorphs of the decomposition product $\text{Ph}_2\text{P}(\text{O})\text{NH}_2$,^{350,353} as given in Figure 4.40, indicated that the $P2_12_12_1$ polymorph was a possible minor component of the solid.³⁵³ The two highest intensity peaks of this $\text{Ph}_2\text{P}(\text{O})\text{NH}_2$ polymorph at 8.50° and 10.13° were analogous to the peaks at 8.42° and 10.18° in the experimental pattern. The presence of the strong experimental peak at 5.16° could indicate the presence of the $P2_1/c$ polymorph of $\text{Ph}_2\text{P}(\text{O})\text{NH}_2$, although this peak could be due to some other solid given that the analogous calculated peak was not strong and that no other stronger peaks were observed in the experimental pattern.³⁵⁰ The presence of this compound as a minor component could be supported by the presence of a number of bands in the IR spectrum of the product.

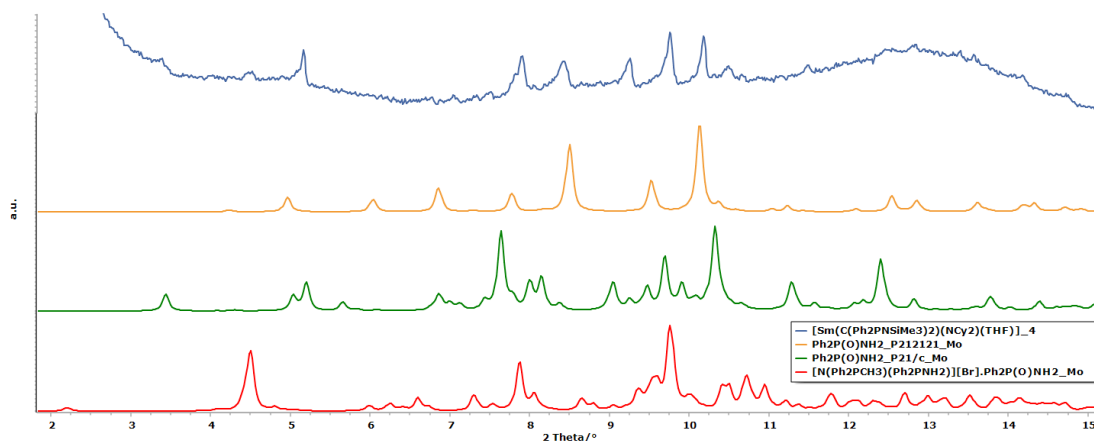


Figure 4.40: Experimental PXRD pattern of $[\text{Sm}(\text{C}(\text{Ph}_2\text{PNSiMe}_3)_2)(\text{NCy}_2)(\text{THF})]_4$ (blue) and the calculated PXRD patterns of $\text{Ph}_2\text{P}(\text{O})\text{NH}_2_{\text{P}212121}$ (orange), $\text{Ph}_2\text{P}(\text{O})\text{NH}_2_{\text{P}21/c}$ (green) and $[\text{N}(\text{Ph}_2\text{PCH}_3)(\text{Ph}_2\text{PNH}_2)][\text{Br}] \cdot \text{Ph}_2\text{P}(\text{O})\text{NH}_2$ (red).

The presence of the three strong peaks at 4.50° , 7.90° and 9.76° was found to indicate the possible presence of $[\text{N}(\text{Ph}_2\text{PCH}_3)(\text{Ph}_2\text{PNH}_2)][\text{Br}] \cdot \text{Ph}_2\text{P}(\text{O})\text{NH}_2$, as shown in Figure 4.40.³⁵⁹ This is another moisture induced decomposition product for the ligand used, the formation of which was published by Hagenbach, A. and co-workers in 2004.³⁵⁹ This is a decomposition product obtained from acidic or moisture containing conditions through a different route from that described in section 4.1.3.1.4. This product can also produce $\text{Ph}_2\text{P}(\text{O})\text{NH}_2$ if exposed to further moisture. There are two main issues with the possible presence of this compound. The first issue is that the presence of the $[\text{N}(\text{Ph}_2\text{PCH}_3)(\text{Ph}_2\text{PNH}_2)]^+$ cation could not be described in the IR spectrum of the product. The second issue is the presence of the bromide anion which was not present in the reaction. Therefore, this could indicate the presence of a similar decomposition product not containing bromide.

The presence of the strong peaks at 5.16° , 7.82° , 9.25° and 10.50° and the minor peaks at 6.77° , 7.05° , 7.33° and 7.50° indicated the presence of a minor undescribed crystalline solid, as these peaks could not be assigned to any of the compounds discussed prior.

4.1.3.1.6. Conclusion

With regards to the IR spectrum of $[\text{Sm}(\text{C}(\text{Ph}_2\text{PNSiMe}_3)_2)(\text{NCy}_2)(\text{THF})]_1$ some deprotonation was believed to have occurred given that bands which could support the presence of either anionic species of $\text{H}_2\text{C}(\text{Ph}_2\text{PNSiMe}_3)_2$ were observed, as discussed

prior. No water intrusion was observed indicating that any differences from the expected spectra were not due to moisture inclusion. The presence of the two secondary ligands was also indicated, although the bands in the two ranges of 1220–1100 cm^{-1} and 1110–1025 cm^{-1} indicated the possibility that the starting reagent $[\text{Sm}(\text{NCy}_2)_3\text{THF}]\cdot\text{C}_6\text{H}_5\text{CH}_3_1$ was a significant component of this product.

The product $[\text{Sm}(\text{C}(\text{Ph}_2\text{PNSiMe}_3)_2)(\text{NCy}_2)(\text{THF})]_2$ showed moisture contamination in the IR spectrum. The structure solution from the SXRD data for the crystal collected from the product $[\text{Sm}(\text{C}(\text{Ph}_2\text{PNSiMe}_3)_2)(\text{NCy}_2)(\text{THF})]_2$, concluded that the crystal analysed was composed of a $\text{Ph}_2\text{P}(\text{O})\text{NH}_2$ polymorph, a known moisture induced decomposition product of $\text{H}_2\text{C}(\text{Ph}_2\text{PNSiMe}_3)_2$. Comparison of the IR data of the product with that of pure $\text{Ph}_2\text{P}(\text{O})\text{NH}_2$ indicated that this was the major product in the solid and therefore the major mode of reaction in this case was in fact decomposition.

With regards to the product $[\text{Sm}(\text{C}(\text{Ph}_2\text{PNSiMe}_3)_2)(\text{NCy}_2)(\text{THF})]_3$ although the bands in the regions $< 900 \text{ cm}^{-1}$ indicated the possible presence of free $[\text{Sm}(\text{NCy}_2)_3\text{THF}]\cdot\text{C}_6\text{H}_5\text{CH}_3_1$ reagent, similarities at higher wavenumbers showed less agreement with this conclusion than was noted for the spectrum of $[\text{Sm}(\text{C}(\text{Ph}_2\text{PNSiMe}_3)_2)(\text{NCy}_2)(\text{THF})]_1$, indicating a purer product. The bands in the region of 1110–1025 cm^{-1} , along with the band at 1176 cm^{-1} , could be indicative of the formation of a $[\text{C}(\text{Ph}_2\text{PNSiMe}_3)_2]^{2-}$ species. The lack of unexpected strong bands in the region of 900–765 cm^{-1} could also support the presence of this species and diminish the possibility of the presence of the $[\text{HC}(\text{Ph}_2\text{PNSiMe}_3)_2]^-$ species. The presence of the weak band at 1176 cm^{-1} could also indicate the presence of an amount of $\text{Ph}_2\text{P}(\text{O})\text{NH}_2$ in the solid.

IR data for the product $[\text{Sm}(\text{C}(\text{Ph}_2\text{PNSiMe}_3)_2)(\text{NCy}_2)(\text{THF})]_4$ was also collected and on initial analysis indicated that the major component was most likely a $[\text{HC}(\text{Ph}_2\text{PNSiMe}_3)_2]^-$ containing species. The possible presence of THF and NCy_2^- bands indicated that this could be a samarium complex of $[\text{HC}(\text{Ph}_2\text{PNSiMe}_3)_2]^-$. A number of bands also indicated the possible presence of the decomposition product $\text{Ph}_2\text{P}(\text{O})\text{NH}_2$. PXRD analysis of $[\text{Sm}(\text{C}(\text{Ph}_2\text{PNSiMe}_3)_2)(\text{NCy}_2)(\text{THF})]_4$ indicated that the main phase was amorphous with minor crystalline phases present. The crystalline phases proved to be mainly the decomposition products $\text{Ph}_2\text{P}(\text{O})\text{NH}_2$ and a possible iso-structural analogue of $[\text{N}(\text{Ph}_2\text{PCH}_3)(\text{Ph}_2\text{PNH}_2)][\text{Br}]\cdot\text{Ph}_2\text{P}(\text{O})\text{NH}_2$.

In conclusion the IR spectrum of $[\text{Sm}(\text{C}(\text{Ph}_2\text{PNSiMe}_3)_2)(\text{NCy}_2)(\text{THF})]_1$ indicated the possible production of the desired product but with the possible inclusion of excess $[\text{Sm}(\text{NCy}_2)_3\text{THF}] \cdot \text{C}_6\text{H}_5\text{CH}_3_1$ and the possible presence of a $[\text{HC}(\text{Ph}_2\text{PNSiMe}_3)_2]^-$ species. $[\text{Sm}(\text{C}(\text{Ph}_2\text{PNSiMe}_3)_2)(\text{NCy}_2)(\text{THF})]_2$ was characterised by both IR spectroscopy and SXR and it was concluded that the solid was mainly the moisture induced decomposition product of $\text{H}_2\text{C}(\text{Ph}_2\text{PNSiMe}_3)_2$, $\text{Ph}_2\text{P}(\text{O})\text{NH}_2$. The product $[\text{Sm}(\text{C}(\text{Ph}_2\text{PNSiMe}_3)_2)(\text{NCy}_2)(\text{THF})]_3$ was in good agreement with the IR data described in literature for the expected product, although the presence of $[\text{HC}(\text{Ph}_2\text{PNSiMe}_3)_2]^-$ could not be discounted. The IR spectrum of $[\text{Sm}(\text{C}(\text{Ph}_2\text{PNSiMe}_3)_2)(\text{NCy}_2)(\text{THF})]_4$ showed similarities to that of $[\text{Sm}(\text{C}(\text{Ph}_2\text{PNSiMe}_3)_2)(\text{NCy}_2)(\text{THF})]_3$ but it was concluded that the mono-anionic species was the prevalent component.

4.1.3.2. Characterisation of $[\text{Nd}(\text{C}(\text{Ph}_2\text{PN}i\text{Pr})_2)(\text{HC}(\text{Ph}_2\text{PN}i\text{Pr})_2)] \cdot 2\text{THF}$

The $[\text{Nd}(\text{C}(\text{Ph}_2\text{PN}i\text{Pr})_2)(\text{HC}(\text{Ph}_2\text{PN}i\text{Pr})_2)] \cdot 2\text{THF}$ complex was noted as being an initiator in lactide polymerisation and therefore was of interest in synthesis.⁴⁶ During this study the synthesis of this compound was attempted twice as described in Section 3.3.1.3.2, to yield two amorphous solids with negligible yields, namely $[\text{Nd}(\text{C}(\text{Ph}_2\text{PN}i\text{Pr})_2)(\text{HC}(\text{Ph}_2\text{PN}i\text{Pr})_2)] \cdot 2\text{THF}_1$ and $[\text{Nd}(\text{C}(\text{Ph}_2\text{PN}i\text{Pr})_2)(\text{HC}(\text{Ph}_2\text{PN}i\text{Pr})_2)] \cdot 2\text{THF}_2$. The syntheses were undergone using a methodology similar to the one published in literature by Buchard, A. and co-workers in 2009,⁴⁰ with some modifications. The main difference in the preparation procedure between the two attempts was that the starting reagent $\text{K}(\text{HC}(\text{Ph}_2\text{PN}i\text{Pr})_2)$ for the reaction undertaken to prepare $[\text{Nd}(\text{C}(\text{Ph}_2\text{PN}i\text{Pr})_2)(\text{HC}(\text{Ph}_2\text{PN}i\text{Pr})_2)] \cdot 2\text{THF}_1$ was prepared *in-situ* from $[\text{H}_2\text{C}(\text{Ph}_2\text{PNH}(i\text{Pr}))_2]\text{Br}_2_1$, which had been prepared previously as described in Section 3.3.1.1.1.1. Conversely the product $[\text{Nd}(\text{C}(\text{Ph}_2\text{PN}i\text{Pr})_2)(\text{HC}(\text{Ph}_2\text{PN}i\text{Pr})_2)] \cdot 2\text{THF}_2$ was produced using the pre-prepared $\text{K}(\text{HC}(\text{Ph}_2\text{PN}i\text{Pr})_2)_2$, which was synthesised as described in Section 3.3.1.1.1.2.

The presence of both $[\text{C}(\text{Ph}_2\text{PN}i\text{Pr})_2]^{2-}$ and $[\text{HC}(\text{Ph}_2\text{PN}i\text{Pr})_2]^-$ ligands in the compound is similar to other early and mid-lanthanide phosphorus(V)-stabilised carbenes for the $\text{H}_2\text{C}(\text{Ph}_2\text{PNSiMe}_3)_2$ starting reagent.⁹

4.1.3.2.1. Analysis by Infra-red spectroscopy

The most significant feature with the characterisation of this product using IR spectroscopy is that the compound contains both the ligands $[\text{C}(\text{Ph}_2\text{PNiPr})_2]^{2-}$ and $[\text{HC}(\text{Ph}_2\text{PNiPr})_2]^-$, which would be expected to have similar IR spectra. The bands typical for the vibrations of the P–Ph and –NiPr groups, along with any skeletal bands for the structure, are expected to remain almost unchanged for both anions in the spectrum of the expected complex. For the group P–Ph, bands in the regions of 1460–1400 cm^{-1} and 775–680 cm^{-1} are expected and these are diagnostic of the vibrations of this group. As for the –NiPr moiety, bands at about 975 cm^{-1} and 810 cm^{-1} are expected for the ν C–N + ν_{as} C–C and ν_{s} C–C vibrations respectively, along with bands in the regions of 1469–1345 cm^{-1} and 1180–1124 cm^{-1} , for the δ C–H and skeletal *i*Pr vibrations respectively.³⁶⁰ This would lead to the spectra of both anions having similar bands in significant portions of the spectra due to these many vibrations. The main difference between the spectra of these anions is expected to lie in the vibrations typical of the P^+-N^- and P–C–P bonds, namely the ν P^+-N^- and $\nu_{\text{as/s}}$ P–C–P vibrations. As described in Section 4.1.3.1.1, the changes in wavenumber for the bands in the IR spectra on deprotonation of these types of ligands from $[\text{H}_2\text{L}]$ to $[\text{HL}]^-$ to $[\text{L}]^{2-}$ can be tentatively related to the changes in the P–C and P–N bond lengths in the ligands, as described through XRD characterisation. As was the case with the compiled literature data for the P–C and P–N bond lengths in these types of compounds given in Section 4.1.3.1.1, the experimental bond lengths are listed in Table 4.10.

Table 4.10: Published XRD bond length data for the P-C and P-N bonds in relevant $\text{H}_2\text{C}(\text{Ph}_2\text{PNR})_2$ derivatives.

Structure	P–C, Å	P–N, Å
$\text{H}_2\text{C}(\text{Ph}_2\text{PNiPr})_2$	N/A	N/A
$\text{H}_2\text{C}(\text{Ph}_2\text{PNR})_2$ (R = 2,6(Me)-Ph-, -SiMe ₃ , -Mes, -P(O)(OPh) ₂ , -P(S)(OPh) ₂ , -Ad, 4(Me)-Ph-, -Ph) ^{7,9,36,41,42,118,122,178,188,191,313–321}	1.810–1.860	1.534–1.574
$[\text{HC}(\text{Ph}_2\text{PNiPr})_2]^-$ in $\text{Li}(\text{HC}(\text{Ph}_2\text{PNiPr})_2)(\text{THF})^{294}$	1.719	1.587

[HC(Ph ₂ PN <i>i</i> Pr) ₂] ⁻ in [Nd(C(Ph ₂ PN <i>i</i> Pr) ₂)(HC(Ph ₂ PN <i>i</i> Pr) ₂)]·2THF ⁴⁰	1.713	1.603
[C(Ph ₂ PN <i>i</i> Pr) ₂] ²⁻ in [Nd(C(Ph ₂ PN <i>i</i> Pr) ₂)(HC(Ph ₂ PN <i>i</i> Pr) ₂)]·2THF ⁴⁰	1.671	1.638

The bond length of the P⁺–N⁻ bond was shown to shift from the range of 1.534–1.574 Å for H₂C(Ph₂PNR)₂ compounds to 1.603 Å and 1.638 Å for the length of the analogous bonds in the [HC(Ph₂PN*i*Pr)₂]⁻ and [C(Ph₂PN*i*Pr)₂]²⁻ ligands of the published structure of [Nd(C(Ph₂PN*i*Pr)₂)(HC(Ph₂PN*i*Pr)₂)]·2THF.⁴⁰ In the case of both ligands the P⁺–N⁻ bond lengths are shorter than those typical for the P(V)–N and P(III)–N bonds, which are in the ranges of 1.676–1.754 Å and 1.646–1.704 Å respectively, as described in greater detail in Section 4.1.3.1.1.^{332–347} The two bond lengths lie close to the respective ranges of 1.601–1.613 Å for the [HL]⁻ anion and of 1.609–1.630 Å for the [L]²⁻ anion, as described for multiple H₂C(Ph₂PNSiMe₃)₂ derivative lanthanide complexes.^{7,9,36,41,42,118,122,178,188,191,313–321,323–331} Given this information the bands for the ν P⁺–N⁻ vibration are expected to lie in a similar region as described for these complexes in Section 4.1.3.1.1, namely in or about the region at 1110–1025 cm⁻¹, although for the [HC(Ph₂PN*i*Pr)₂]⁻ ligand the bands due to this vibration would be expected to lie in a range slightly higher than the previously given range, as described for K(HC(Ph₂PN*i*Pr)₂) in Section 4.1.1.1.2.1.

The analogous P–C–P bonds for the neutral ligand and its two anionic derivatives also experience a change in bond lengths with the formation of the complex. On transition from H₂C(Ph₂PNR)₂ to [HC(Ph₂PNR)₂]⁻ and [C(Ph₂PNR)₂]²⁻ lanthanide complexes, the P–C bond length shifts from the range of 1.810–1.860 Å to 1.724–1.747 Å and 1.637–1.700 Å respectively.^{7,9,36,41,42,118,122,178,188,191,313–321} In the published structure the P–C bond lengths for the two anionic ligands were noted to be 1.713 Å for the mono-anion and 1.671 Å for the di-anion, therefore falling in the same range as those for most other complexes.^{323–331} This similarity in bond lengths to the 1.669–1.757 Å range typical for simple P=C containing molecules would indicate that the IR bands for the desired compound should lie in the region typical for P=C bands, that is in the region of 1220–1150 cm⁻¹. This is in a region slightly higher than the region of 1110–1025 cm⁻¹, at which the ν P⁺–N⁻ vibration bands are expected for the di-anion. It should be noted that bands for complexes in this region are not typically found in published data and therefore

the $\nu_{\text{as}} \text{P}^+-\text{C}^{2-}-\text{P}^+$ vibrations cannot be used for structural determination. From this discussion it can be concluded that the most diagnostic feature in the spectra of the complexes obtained would be the assignment of the $\nu \text{P}^+-\text{N}^-$ vibration band in the region of $1110-1025 \text{ cm}^{-1}$. The discussion of the IR spectra of the products obtained in this study will be undertaken with this theoretical framework in mind.

The spectra of the two products obtained, $[\text{Nd}(\text{C}(\text{Ph}_2\text{PNiPr})_2)(\text{HC}(\text{Ph}_2\text{PNiPr})_2)] \cdot 2\text{THF}_1$ and $[\text{Nd}(\text{C}(\text{Ph}_2\text{PNiPr})_2)(\text{HC}(\text{Ph}_2\text{PNiPr})_2)] \cdot 2\text{THF}_2$, along with the IR spectrum of $\text{K}(\text{HC}(\text{Ph}_2\text{PNiPr})_2)_2$ are shown together in Figure 4.41. There was substantial similarity between the spectra of the products and the spectrum of the starting reagent, with the product $[\text{Nd}(\text{C}(\text{Ph}_2\text{PNiPr})_2)(\text{HC}(\text{Ph}_2\text{PNiPr})_2)] \cdot 2\text{THF}_2$ being more similar to the starting material than the product $[\text{Nd}(\text{C}(\text{Ph}_2\text{PNiPr})_2)(\text{HC}(\text{Ph}_2\text{PNiPr})_2)] \cdot 2\text{THF}_1$.

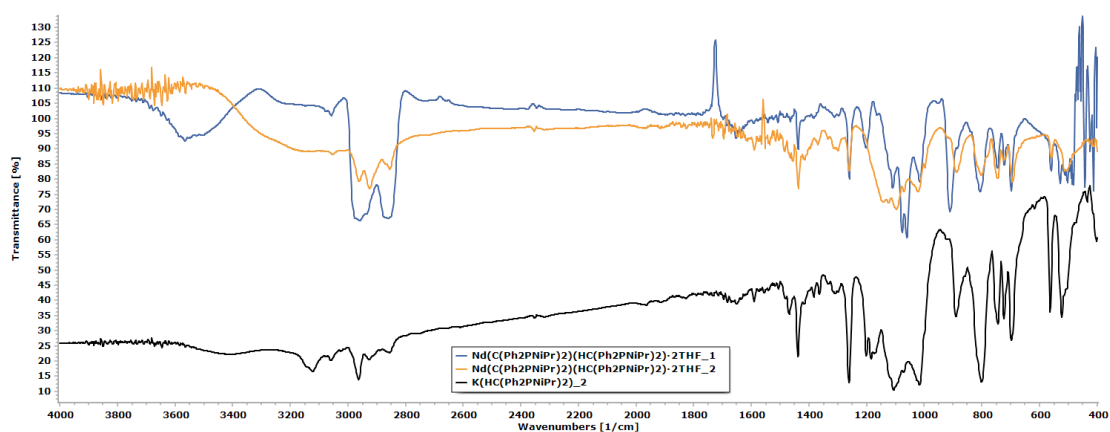


Figure 4.41: IR spectra of $[\text{Nd}(\text{C}(\text{Ph}_2\text{PNiPr})_2)(\text{HC}(\text{Ph}_2\text{PNiPr})_2)] \cdot 2\text{THF}_1$ (blue) and $[\text{Nd}(\text{C}(\text{Ph}_2\text{PNiPr})_2)(\text{HC}(\text{Ph}_2\text{PNiPr})_2)] \cdot 2\text{THF}_2$ (orange) and $\text{K}(\text{HC}(\text{Ph}_2\text{PNiPr})_2)_2$ (black).

For the two products $[\text{Nd}(\text{C}(\text{Ph}_2\text{PNiPr})_2)(\text{HC}(\text{Ph}_2\text{PNiPr})_2)] \cdot 2\text{THF}_1$ and $[\text{Nd}(\text{C}(\text{Ph}_2\text{PNiPr})_2)(\text{HC}(\text{Ph}_2\text{PNiPr})_2)] \cdot 2\text{THF}_2$, two bands were observed at 3564 cm^{-1} and 3188 cm^{-1} respectively. These were unexpected and they are typically assigned to the $\nu \text{O}-\text{H}$ and $\nu \text{N}-\text{H}$ vibrations. The former vibration could indicate the intrusion of water, while the latter vibration could indicate the protonation of the nitrogen in the P^+-N^- moiety. The associated band for the $\delta \text{O}-\text{H}$ vibrations at around 1620 cm^{-1} was not attested in the spectra of either of the products. The very weak bands at 1590 cm^{-1} attested in the spectra of both products and which were analogous to the band with a greater intensity in the spectrum of the $\text{K}(\text{HC}(\text{Ph}_2\text{PNiPr})_2)_2$, could indicate the presence of the $\delta \text{N}-\text{H}$ vibrations in the products. This would possibly support the presence of the

P–N–H moiety, although in diminished amounts as the bands were weak when compared with the same bands in the spectra of $\text{K}(\text{HC}(\text{Ph}_2\text{PNiPr})_2)_2$ and $[\text{H}_2\text{C}(\text{Ph}_2\text{PNH}(i\text{Pr}))_2]\text{Br}_2_1$, as given in Section 4.1.1.1.2.1 and Section 4.1.1.1.1.1 respectively.

The weak band at 3056 cm^{-1} and the strong bands at 1438 cm^{-1} , 747 cm^{-1} , 728 cm^{-1} and 693 cm^{-1} were observed for both product spectra and also for the spectrum of $\text{K}(\text{HC}(\text{Ph}_2\text{PNiPr})_2)_2$. The first band is typical of the aromatic $\nu\text{ C–H}$ vibrational mode, while the remaining bands are typical of the P–Ph vibrational modes for P–Ph groups, as previously discussed in this section. Analogues for these bands are also observed for the IR spectrum of dppm given in Appendix 5. These alone would be very indicative of the presence of a $\text{H}_2\text{C}(\text{Ph}_2\text{PNiPr})_2$ derivative in the products.

In the case of the spectra of both products several bands in the range of $2962\text{--}2852\text{ cm}^{-1}$, typically indicative of aliphatic $\nu\text{ C–H}$ vibrations, were observed. The presence of three bands in this region for the spectrum of $[\text{Nd}(\text{C}(\text{Ph}_2\text{PNiPr})_2)(\text{HC}(\text{Ph}_2\text{PNiPr})_2)]\cdot 2\text{THF}_2$ and only two strong bands for the spectrum of $[\text{Nd}(\text{C}(\text{Ph}_2\text{PNiPr})_2)(\text{HC}(\text{Ph}_2\text{PNiPr})_2)]\cdot 2\text{THF}_1$ indicated that the former contained more C–H bonds than the latter product. This could indicate that the product $[\text{Nd}(\text{C}(\text{Ph}_2\text{PNiPr})_2)(\text{HC}(\text{Ph}_2\text{PNiPr})_2)]\cdot 2\text{THF}_1$ underwent some deprotonation, while $[\text{Nd}(\text{C}(\text{Ph}_2\text{PNiPr})_2)(\text{HC}(\text{Ph}_2\text{PNiPr})_2)]\cdot 2\text{THF}_2$ showed less deprotonation. The problem with this analysis is that the presence of both $[\text{HC}(\text{Ph}_2\text{PNiPr})_2]^-$ and $[\text{C}(\text{Ph}_2\text{PNiPr})_2]^{2-}$ ligands were expected in the product and therefore these bands cannot be used to diagnose the presence of the carbene ligand.

Figure 4.42 shows a detail of the spectra of the two products and the starting reagent in the region of 1600 cm^{-1} to 400 cm^{-1} . As regards the bands representative of the $-\text{NiPr}$ moiety, the weak bands at 1314 cm^{-1} and 1297 cm^{-1} observed for both products were believed to be due to the $\delta\text{ C–H}$ vibrations for the iso-propyl group and analogous to bands in the same positions for the $\text{K}(\text{HC}(\text{Ph}_2\text{PNiPr})_2)_2$ spectrum. It was observed that the bands in the spectra of the products were shifted to slightly lower wavenumbers than is typically expected. The band observed at 888 cm^{-1} for the starting reagent $\text{K}(\text{HC}(\text{Ph}_2\text{PNiPr})_2)_2$ spectrum was also observed in the spectrum of the product $[\text{Nd}(\text{C}(\text{Ph}_2\text{PNiPr})_2)(\text{HC}(\text{Ph}_2\text{PNiPr})_2)]\cdot 2\text{THF}_2$. For the starting reagent this was previously assigned to either P–N–C or $\nu_{\text{as}}\text{ P–C–P}$ vibrations. The former vibrational mode could indicate the presence of the $-\text{NiPr}$ moiety. The band at 888 cm^{-1} was lost in the spectrum of $[\text{Nd}(\text{C}(\text{Ph}_2\text{PNiPr})_2)(\text{HC}(\text{Ph}_2\text{PNiPr})_2)]\cdot 2\text{THF}_1$, while a new strong band

at 910 cm^{-1} was observed in this spectrum. This could be a novel P–N–C mode of vibration which could indicate a different form of coordination about the nitrogen atom. This could be indicative of the carbene formation; however the original band would still be expected since both ligands should be present. The increase in wavenumber could be due to the constraints applied by coordination at the nitrogen atom, although further detail cannot be given. The shoulder at 997 cm^{-1} for both product spectra was indicative of the $\nu\text{ C–N} + \nu_{\text{as}}\text{ C–C}$ vibrations, further indicating the presence of the –NiPr group in these products.

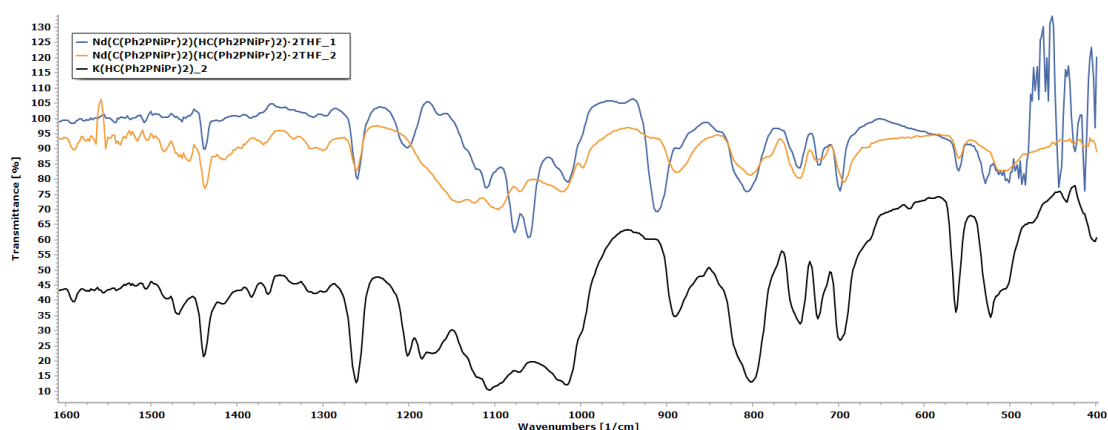


Figure 4.42: Details of IR spectra of $[\text{Nd}(\text{C}(\text{Ph}_2\text{PNiPr})_2)(\text{HC}(\text{Ph}_2\text{PNiPr})_2)]\cdot 2\text{THF}_1$ (blue) and $[\text{Nd}(\text{C}(\text{Ph}_2\text{PNiPr})_2)(\text{HC}(\text{Ph}_2\text{PNiPr})_2)]\cdot 2\text{THF}_2$ (orange) and $\text{K}(\text{HC}(\text{Ph}_2\text{PNiPr})_2)_2$ (black), in the region 1600 cm^{-1} to 400 cm^{-1} .

A strong band at 1261 cm^{-1} was observed for both the spectra of the products as well as the IR spectrum of $\text{K}(\text{HC}(\text{Ph}_2\text{PNiPr})_2)_2$. In the spectrum of the potassium salt this band was tentatively assigned to a possible $\nu\text{ P=N}$ vibrational mode or alternatively a possible $\nu\text{ C–N}$ vibration, as described in Section 4.1.1.1.2.1. The fact that this band did not change in the spectra of the products could indicate the expected presence of the $[\text{HC}(\text{Ph}_2\text{PNiPr})_2]^-$ ligand in the products or alternatively that this band was due to a skeletal feature present in the $\text{H}_2\text{C}(\text{Ph}_2\text{PNiPr})_2$ derivatives, such as the aforementioned $\nu\text{ C–N}$ vibration. No further information could be obtained from this data although bands in this region were observed for the spectra of $\text{H}_2\text{C}(\text{Ph}_2\text{PNSiMe}_3)_2$ derivatives and assigned to trimethylsilyl $\delta\text{ C–H}$ vibrations.

For the spectra of the products numerous bands were also noted in the region of 1110–1025 cm^{-1} , at which $\nu \text{P}^+-\text{N}^-$ vibration bands are expected for the di-anion. Bands in this region were also observed for the spectrum of the starting reagent $\text{K}(\text{HC}(\text{Ph}_2\text{PNiPr}_2)_2)_2$. In Section 4.1.1.1.2.1 the bands at 1109 cm^{-1} and 1015 cm^{-1} for the spectrum of $\text{K}(\text{HC}(\text{Ph}_2\text{PNiPr}_2)_2)_2$ were tentatively assigned to possible P–Ph vibrations or possibly other skeletal vibrations. In the region of 1110–1025 cm^{-1} , the bands in the spectrum of $[\text{Nd}(\text{C}(\text{Ph}_2\text{PNiPr}_2)_2)(\text{HC}(\text{Ph}_2\text{PNiPr}_2)_2)] \cdot 2\text{THF}_2$ were very similar to that of the starting reagent, with a number of weak bands at 1145 cm^{-1} , 1123 cm^{-1} and 1096 cm^{-1} . These bands could be due to the expected decrease in P–N bond order, although they lie at a higher wavenumber than typical, indicating a greater bond order than anticipated. For the spectrum of $[\text{Nd}(\text{C}(\text{Ph}_2\text{PNiPr}_2)_2)(\text{HC}(\text{Ph}_2\text{PNiPr}_2)_2)] \cdot 2\text{THF}_1$ two strong bands at 1076 cm^{-1} and 1060 cm^{-1} , which were clearly different from the bands present in this region for the $\text{K}(\text{HC}(\text{Ph}_2\text{PNiPr}_2)_2)_2$ spectrum, were observed. These could indicate the formation of a $\nu \text{P}^+-\text{N}^-$ bond band which due to a decrease in bond order due to deprotonation could have vibrational modes in this region, indicating the formation of the desired carbene. This decrease in bond order seemed to be stronger than that observed for the product $[\text{Nd}(\text{C}(\text{Ph}_2\text{PNiPr}_2)_2)(\text{HC}(\text{Ph}_2\text{PNiPr}_2)_2)] \cdot 2\text{THF}_2$.

In the spectrum of $\text{K}(\text{HC}(\text{Ph}_2\text{PNiPr}_2)_2)_2$ bands laying at a higher wavenumber than this region were observed at 1202 cm^{-1} , 1185 cm^{-1} and 1170 cm^{-1} and were previously assigned to $\nu \text{P}=\text{N}$ or $\nu \text{P}=\text{C}$ vibrations. In both product spectra most of these bands were lost, which could indicate a decrease in P–N bond order indicating deprotonation and the possible formation of the desired carbene. Again this is difficult to establish given that the desired compound also contained the initial $[\text{HC}(\text{Ph}_2\text{PNiPr}_2)_2]^-$ ligand. For the spectrum of $[\text{Nd}(\text{C}(\text{Ph}_2\text{PNiPr}_2)_2)(\text{HC}(\text{Ph}_2\text{PNiPr}_2)_2)] \cdot 2\text{THF}_1$ a band at 1203 cm^{-1} was observed. However, this could not be easily assigned, although it could be due to the presence of the $[\text{HC}(\text{Ph}_2\text{PNiPr}_2)_2]^-$ ligand or possible $\nu \text{P}=\text{C}$ vibrations. The lack of any bands in this region in the spectrum of the $[\text{Nd}(\text{C}(\text{Ph}_2\text{PNiPr}_2)_2)(\text{HC}(\text{Ph}_2\text{PNiPr}_2)_2)] \cdot 2\text{THF}_2$ complex indicated deprotonation but this was incongruent with the similarities in the IR spectra of this product and that of $\text{K}(\text{HC}(\text{Ph}_2\text{PNiPr}_2)_2)_2$ in the region $< 950 \text{cm}^{-1}$.

4.1.3.2.2. Analysis by Microscopy

The solids obtained from both the attempts undertaken to synthesise the complex $[\text{Nd}(\text{C}(\text{Ph}_2\text{PNiPr})_2)(\text{HC}(\text{Ph}_2\text{PNiPr})_2)] \cdot 2\text{THF}$ were analysed using polarised light microscopy. For both products the solids showed no extinction of plane polarised light which indicated the formation of amorphous solids. This was especially true for the product $[\text{Nd}(\text{C}(\text{Ph}_2\text{PNiPr})_2)(\text{HC}(\text{Ph}_2\text{PNiPr})_2)] \cdot 2\text{THF}_2$ which formed a brown residue.

4.1.3.2.3. Conclusion

In conclusion, the product $[\text{Nd}(\text{C}(\text{Ph}_2\text{PNiPr})_2)(\text{HC}(\text{Ph}_2\text{PNiPr})_2)] \cdot 2\text{THF}_1$ was more likely the desired carbene or a compound lacking the $[\text{HC}(\text{Ph}_2\text{PNiPr})_2]^-$ ligand. This was mainly concluded from the decrease in the number of aliphatic ν C–H bands, indicative of deprotonation. Another indicator was the possible shift of the $\text{K}(\text{HC}(\text{Ph}_2\text{PNiPr})_2)$ band located at 888 cm^{-1} to 910 cm^{-1} in the spectrum of the product indicating the presence of novel P–N–C vibrational modes. The two strong bands at 1076 cm^{-1} and 1060 cm^{-1} could also indicate the deprotonation indicating the possible formation of $\nu \text{ P}^+ \text{--} \text{N}^-$ bands due to the expected $[\text{C}(\text{Ph}_2\text{PNiPr})_2]^{2-}$ anion.

The IR spectrum for $[\text{Nd}(\text{C}(\text{Ph}_2\text{PNiPr})_2)(\text{HC}(\text{Ph}_2\text{PNiPr})_2)] \cdot 2\text{THF}_2$ exhibited a loss of bands in the region $1202\text{--}1170 \text{ cm}^{-1}$ in the spectrum of $\text{K}(\text{HC}(\text{Ph}_2\text{PNiPr})_2)$, indicative of the decrease in bond order for the P–N bond. However this spectrum also displayed bands which contradicted this assessment and showed a greater overall similarity to the spectrum of $\text{K}(\text{HC}(\text{Ph}_2\text{PNiPr})_2)$ as compared to the spectrum of $[\text{Nd}(\text{C}(\text{Ph}_2\text{PNiPr})_2)(\text{HC}(\text{Ph}_2\text{PNiPr})_2)] \cdot 2\text{THF}_1$. These differences could indicate that the ligand $[\text{HC}(\text{Ph}_2\text{PNiPr})_2]^-$ was more prevalent in $[\text{Nd}(\text{C}(\text{Ph}_2\text{PNiPr})_2)(\text{HC}(\text{Ph}_2\text{PNiPr})_2)] \cdot 2\text{THF}_2$ than in $[\text{Nd}(\text{C}(\text{Ph}_2\text{PNiPr})_2)(\text{HC}(\text{Ph}_2\text{PNiPr})_2)] \cdot 2\text{THF}_1$.

Therefore, it was inferred that two different products were obtained during synthesis. Furthermore the product $[\text{Nd}(\text{C}(\text{Ph}_2\text{PNiPr})_2)(\text{HC}(\text{Ph}_2\text{PNiPr})_2)] \cdot 2\text{THF}_1$, which was produced by a reaction starting with the preparation of the $\text{K}(\text{HC}(\text{Ph}_2\text{PNiPr})_2)$ *in-situ* from $[\text{H}_2\text{C}(\text{Ph}_2\text{PNH}(i\text{Pr}))_2]\text{Br}_2_1$, seemed to have more features indicating full deprotonation of the ligand than the product $[\text{Nd}(\text{C}(\text{Ph}_2\text{PNiPr})_2)(\text{HC}(\text{Ph}_2\text{PNiPr})_2)] \cdot 2\text{THF}_2$. This latter product was obtained from

$\text{K}(\text{HC}(\text{Ph}_2\text{PNiPr})_2)_2$, which was pre-prepared in a separate reaction. The reason for this difference is unknown and since NMR and XRD characterisation could not be undertaken, better data for characterisation of the two products was not obtained and characterisation was limited.

4.1.3.3. Characterisation of $[\text{Sm}_2(\text{C}(\text{Ph}_2\text{PS})_2)_2\text{I}_2\text{THF}_4]\cdot 4(\text{C}_6\text{H}_5\text{CH}_3)$

In this study several attempts were undertaken to synthesise the lanthanide carbene complex, $[\text{Sm}_2(\text{C}(\text{Ph}_2\text{PS})_2)_2\text{I}_2\text{THF}_4]$, using a methodology similar to the one published in literature by Cantat, T. and co-workers in 2005,⁸ with some modifications. The attempts undertaken were detailed out in Section 3.3.1.3.3, and in all cases the lithium salt $\text{Li}_2\text{C}(\text{Ph}_2\text{PS})_2$, which is the starting reagent for the production of the complex, was prepared *in situ* through the reaction between the $\text{H}_2\text{C}(\text{Ph}_2\text{PS})_2$ ligand and MeLi. The reaction between these two compounds and the synthesis of $\text{Li}_2\text{C}(\text{Ph}_2\text{PS})_2$ were observed in each case by the production of a slightly turbid yellow solution. This was in line with the observations published in literature.^{8,124} No characterisation of this yellow solution was undertaken in order not to lose any of the expected reagent and since the yellow solution obtained from the white suspension was clearly indicative of the consumption of the $\text{H}_2\text{C}(\text{Ph}_2\text{PS})_2$ in the mixture.

The reaction of the solution containing the lithium salt with the solid $\text{SmI}_3\cdot\text{THF}_{3.5}$, which was found to be difficult to dissolve in all reactions, yielded a solid which was expected to be the side product LiI. The expected $[\text{Sm}_2(\text{C}(\text{Ph}_2\text{PS})_2)_2\text{I}_2\text{THF}_4]$ complex would be dissolved in the remaining filtrate. This was always the case for all reactions, however the physical properties of the solid and the colour of the filtrate differed from one attempt to another, as described in Section 3.3.1.3.3. Several workup techniques were used to extract the expected product from the filtrates. In some cases work up on the first solid obtained was undertaken to yield other products. The resultant products were characterised by different techniques. The solids discussed in this section are given in Table 4.11 along with their respective yields, assuming that each solid is the desired compound. They are divided according to whether they were obtained from work up of the initial solid, expected to be LiI, or workup of products obtained from the initial filtrate. The solids produced during these processes varied physically from amorphous gelatinous materials to crystalline substances, as will be discussed in this section.

Table 4.11: Products collected from initial solid and filtrate workup respectively, including yields in brackets.

Reaction number	Initial solid/products from initial solid workup*	Products from initial filtrate/initial filtrate workup
1	_1a (93 %) (366 %)	_1b (Negligible)
		_1c (21.9 %)
2	_2a (78.7 %) (309 %)	_2b (32.7 %)
	_2a_1 (26.1 %) (102 %)	
	_2a_2 (18.2%)	
3	_3a (35.5 %) (139 %)	_3b_1 (30.1 %)
		_3b_2 (Negligible)
4	_4a (33.4 %) (132 %)	_4b (Negligible)
	_4a_1 (22.61 %) (89.3 %)	
	_4a_2 (Negligible)	

* A second yield is denoted for samples expected to be LiI and is calculated assuming that the product is dry unsolvated LiI.

4.1.3.3.1. Analysis by Infra-red spectroscopy

In all four reaction procedures the initial solids produced from the reaction of the $\text{Li}_2(\text{C}(\text{Ph}_2\text{PS})_2)$, prepared *in situ*, with $\text{SmI}_3 \cdot \text{THF}_{3.5}$, which were expected to be LiI, were analysed by IR spectroscopy. In all cases these solids, namely $[\text{Sm}_2(\text{C}(\text{Ph}_2\text{PS})_2)_2\text{I}_2\text{THF}_4] \cdot 4(\text{C}_6\text{H}_5\text{CH}_3)$ _1a, _2a, _3a and _4a showed IR spectra indicative of the starting reagent $\text{H}_2\text{C}(\text{Ph}_2\text{PS})_2$. IR spectra of these solids are given in Appendix 9. This indicated that the major mode of reaction in each case was possibly re-protonation of the $\text{Li}_2(\text{C}(\text{Ph}_2\text{PS})_2)$ through moisture intrusion. Further experimental work was undertaken on the two solids $[\text{Sm}_2(\text{C}(\text{Ph}_2\text{PS})_2)_2\text{I}_2\text{THF}_4] \cdot 4(\text{C}_6\text{H}_5\text{CH}_3)$ _2a and _4a, as the former was a pale yellow waxy solid and the latter was a very pale yellow residue. These contrasted with the white or pale yellow crystalline solids expected for both LiI and $\text{H}_2\text{C}(\text{Ph}_2\text{PS})_2$ as was the case for solids $[\text{Sm}_2(\text{C}(\text{Ph}_2\text{PS})_2)_2\text{I}_2\text{THF}_4] \cdot 4(\text{C}_6\text{H}_5\text{CH}_3)$ _1a and _3a.

The solid $[\text{Sm}_2(\text{C}(\text{Ph}_2\text{PS})_2)_2\text{I}_2\text{THF}_4] \cdot 4(\text{C}_6\text{H}_5\text{CH}_3)$ _2a was suspended in dry toluene after which filtration was undergone yielding the orange solid $[\text{Sm}_2(\text{C}(\text{Ph}_2\text{PS})_2)_2\text{I}_2\text{THF}_4] \cdot 4(\text{C}_6\text{H}_5\text{CH}_3)$ _2a_1 and a colourless filtrate which yielded the residue $[\text{Sm}_2(\text{C}(\text{Ph}_2\text{PS})_2)_2\text{I}_2\text{THF}_4] \cdot 4(\text{C}_6\text{H}_5\text{CH}_3)$ _2a_2 on removal of volatiles. The IR

spectrum of $[\text{Sm}_2(\text{C}(\text{Ph}_2\text{PS})_2)_2\text{I}_2\text{THF}_4]\cdot 4(\text{C}_6\text{H}_5\text{CH}_3)_2\text{a}_1$, in KBr, is given in Figure 4.43, together with the spectra of the two polymorphs of $\text{H}_2\text{C}(\text{Ph}_2\text{PS})_2$ (both collected in KBr) and the spectrum of $\text{SmI}_3\cdot\text{THF}_{3.5}_2$, collected in nujol. Unlike the previously discussed species the IR data of $[\text{Sm}_2(\text{C}(\text{Ph}_2\text{PS})_2)_2\text{I}_2\text{THF}_4]\cdot 4(\text{C}_6\text{H}_5\text{CH}_3)_2\text{a}_1$ showed noticeable differences which indicated the possible presence of other chemical species. The first noticeable bands in this spectrum were the bands at 3420 cm^{-1} and 1615 cm^{-1} . The former band is typical of water intrusion, as it is indicative of the $\nu\text{ O-H}$ vibrations. The latter band fell at a lower wavenumber than is typical for the band for the $\delta\text{ O-H}$ vibrations indicative of moisture intrusion. This band could be due to these vibrational modes although alternatively it could be due to the vibrational modes of multiple organic groups, such as aromatic $\nu\text{ C-C}$, aliphatic $\nu\text{ C=C}$ and amine $\delta\text{ N-H}$ vibrations, which all display bands in this region. Bands typical of P-Ph , $\nu\text{ P-C-P}$ and $\nu\text{ P=S}$ vibrations in the region $< 850\text{ cm}^{-1}$ were not observed in the spectrum of the solid, possibly indicating the loss of the ligand from the product. Loss of bands typical of the ligand in the region of $1250\text{--}850\text{ cm}^{-1}$ was also observed and this further confirmed the possible loss of the ligand.

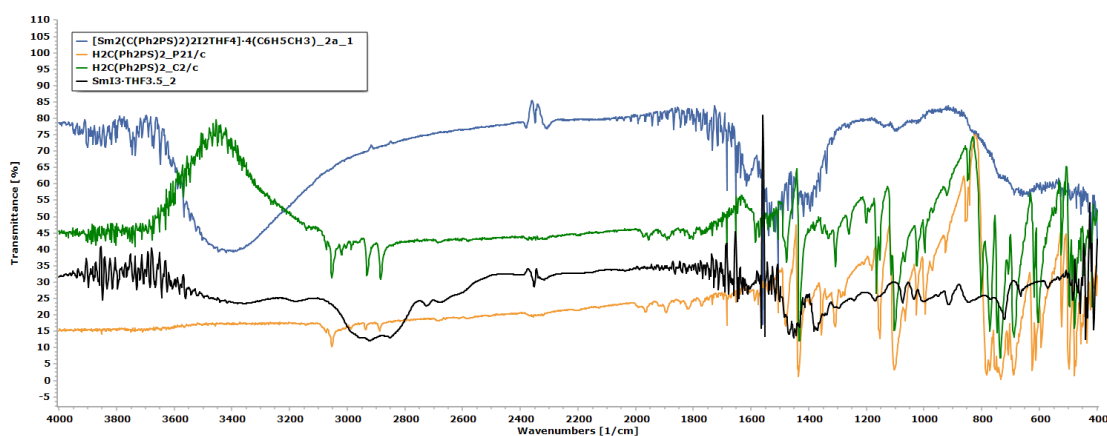


Figure 4.43: IR spectra of $[\text{Sm}_2(\text{C}(\text{Ph}_2\text{PS})_2)_2\text{I}_2\text{THF}_4]\cdot 4(\text{C}_6\text{H}_5\text{CH}_3)_2\text{a}_1$ (blue) and $\text{H}_2\text{C}(\text{Ph}_2\text{PS})_2\text{C}_2/c$ polymorph (green) and $\text{H}_2\text{C}(\text{Ph}_2\text{PS})_2\text{P}_21/c$ polymorph (orange) and $\text{SmI}_3\cdot\text{THF}_{3.5}_2$ (black).

Other bands of interest in the spectrum of $[\text{Sm}_2(\text{C}(\text{Ph}_2\text{PS})_2)_2\text{I}_2\text{THF}_4]\cdot 4(\text{C}_6\text{H}_5\text{CH}_3)_2\text{a}_1$ were grouped in two sets; the first being the two broad strong bands at 1520 cm^{-1} and 1402 cm^{-1} and the second set being the three weak bands at 1140 cm^{-1} , 1102 cm^{-1} and 1022 cm^{-1} . The only band which could be assigned as being analogous to bands in the spectra of either of the two $\text{H}_2\text{C}(\text{Ph}_2\text{PS})_2$

polymorphs was the weak band at 1102 cm^{-1} . However the lack of other IR bands of the two polymorphs would indicate that either the band was due to some other chemical species or that the ligand was present in very small amounts.

The two weak bands at 1140 cm^{-1} and 1022 cm^{-1} could tentatively indicate the presence of THF. These bands could be analogous to the 1184 cm^{-1} and 1070 cm^{-1} bands known for uncoordinated THF respectively. The band at 1140 cm^{-1} could most likely be attributed to either $\nu_{\text{as}}\text{ C-O-C}$ and $\nu_{\text{s}}\text{ C-O-C}$ vibrations of THF, which at this wavenumber could indicate solvation or very weak coordination. If this assignment was verified the band at 1022 cm^{-1} could be assigned to the corresponding $\nu_{\text{s}}\text{ C-O-C}$ or ring relaxation vibrations typical of THF, as described for other complexes in the current study. However, bands analogous to the un-coordinated THF band at 912 cm^{-1} decreased the probability of the presence of solvated or weakly coordinated THF in the solid. The strong bands at 1520 cm^{-1} and 1402 cm^{-1} could be due to multiple vibrations of various organic groups. However the lack of other bands to support the presence of any of these moieties means that any assignment would be speculative. The colour of the compound indicated the presence of Sm^{3+} and possibly iodine. However the presence of these elements could not be observed using the IR spectrum in the range studied and so definitive assignment of the presence of these elements in the solid could not be made.

The residue $[\text{Sm}_2(\text{C}(\text{Ph}_2\text{PS})_2)_2\text{I}_2\text{THF}_4]\cdot 4(\text{C}_6\text{H}_5\text{CH}_3)$ _2a_2 was also analysed by IR spectroscopy. Analysis of this data indicated that the major product was $\text{H}_2\text{C}(\text{Ph}_2\text{PS})_2$. The relevant IR spectrum is given in Appendix 9. Therefore, in this case the neutral ligand species remained in solution and was thus washed from the remaining solid.

The solid $[\text{Sm}_2(\text{C}(\text{Ph}_2\text{PS})_2)_2\text{I}_2\text{THF}_4]\cdot 4(\text{C}_6\text{H}_5\text{CH}_3)$ _4a was reacted with an excess of MeLi yielding a suspension. On filtration the solid $[\text{Sm}_2(\text{C}(\text{Ph}_2\text{PS})_2)_2\text{I}_2\text{THF}_4]\cdot 4(\text{C}_6\text{H}_5\text{CH}_3)$ _4a_1 was obtained along with a filtrate. The filtrate was layered with diethyl ether yielding a pale yellow gelatinous solid on filtration namely $[\text{Sm}_2(\text{C}(\text{Ph}_2\text{PS})_2)_2\text{I}_2\text{THF}_4]\cdot 4(\text{C}_6\text{H}_5\text{CH}_3)$ _4a_2. The IR spectrum for $[\text{Sm}_2(\text{C}(\text{Ph}_2\text{PS})_2)_2\text{I}_2\text{THF}_4]\cdot 4(\text{C}_6\text{H}_5\text{CH}_3)$ _4a_1 is also given in Appendix 9. As with the previously discussed initial solids, this solid was also mainly $\text{H}_2\text{C}(\text{Ph}_2\text{PS})_2$, despite the fact that LiI was expected as the main compound. In this case the major polymorph was likely *C2/c*.

The product $[\text{Sm}_2(\text{C}(\text{Ph}_2\text{PS})_2)_2\text{I}_2\text{THF}_4]\cdot 4(\text{C}_6\text{H}_5\text{CH}_3)$ _4a_2 was also analysed by IR spectroscopy and the spectrum obtained is given in Figure 4.44, along with the spectra of the $\text{H}_2\text{C}(\text{Ph}_2\text{PS})_2$ *P2₁/c* polymorph and the $\text{H}_2\text{C}(\text{Ph}_2\text{PS})_2$ *C2/c* polymorph. This

spectrum is discussed further as it showed noticeable differences from other products obtained from this reaction, indicating that different chemical species were possibly present. No bands indicative of moisture inclusion were observed, which indicated that the gelatinous nature of the solid was not due to the presence of water. The weak bands in the range of 3088–3029 cm^{-1} are typical of aromatic ν C–H vibrations, as was expected for the desired compound. The three strong bands at 2962 cm^{-1} , 2905 cm^{-1} and 2862 cm^{-1} are typical of methyl and methylene ν C–H vibrations, which would not be expected for the desired product but could be indicative of the presence of the mono-anionic derivative of $\text{H}_2\text{C}(\text{Ph}_2\text{PS})_2$ or of the toluene or the ether used in the preparation of this product. The bands at 728 cm^{-1} (medium), 705 cm^{-1} (shoulder) and 695 cm^{-1} (strong), along with the band at 1416 cm^{-1} were all indicative of P–Ph bands typical of $\text{H}_2\text{C}(\text{Ph}_2\text{PS})_2$ and its derivatives, thus indicating the presence of the ligand or one of its derivatives in the product. These could be analogous to the bands in the spectra of the ligand at 735 cm^{-1} , 708 cm^{-1} , 688 cm^{-1} and 1433 cm^{-1} respectively.

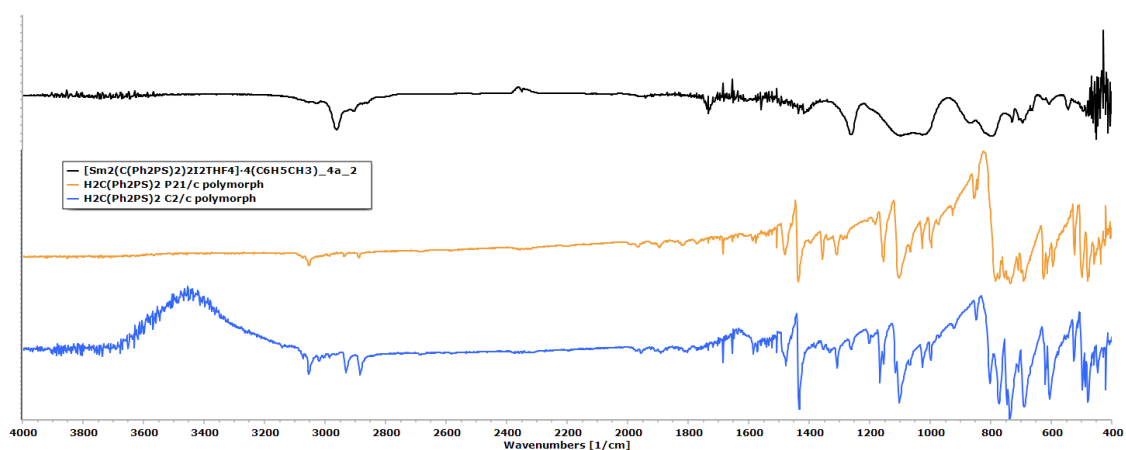


Figure 4.44: IR spectrum of $[\text{Sm}_2(\text{C}(\text{Ph}_2\text{PS})_2)_2\text{I}_2\text{THF}_4]\cdot 4(\text{C}_6\text{H}_5\text{CH}_3)$ _4a_2 (black), $\text{H}_2\text{C}(\text{Ph}_2\text{PS})_2$ P21/c polymorph (orange) and $\text{H}_2\text{C}(\text{Ph}_2\text{PS})_2$ C2/c polymorph (blue).

A unique band at 1732 cm^{-1} , observed in the spectrum of $[\text{Sm}_2(\text{C}(\text{Ph}_2\text{PS})_2)_2\text{I}_2\text{THF}_4]\cdot 4(\text{C}_6\text{H}_5\text{CH}_3)$ _4a_2, was not typical of any of the expected products or any of the reagents used. Strong bands in this region are typically due to the ν C=O vibrations of aldehydes, ketones and esters. However, no such compound was expected to form in the reactions used in the preparation of this complex. Therefore, this band was of interest because it could possibly indicate the formation of some by-product through an unknown route. The bands at 625 cm^{-1} and 607 cm^{-1} , which fell in the region $< 650 \text{ cm}^{-1}$ wherein most of the protonated ligand bands assigned to the ν P=S vibrations

are located, were observed in the spectrum of $[\text{Sm}_2(\text{C}(\text{Ph}_2\text{PS})_2)_2\text{I}_2\text{THF}_4] \cdot 4(\text{C}_6\text{H}_5\text{CH}_3)_{_4\text{a_}2}$. These bands could be assigned to these vibrations, although they were not directly analogous to the bands in this region observed in the spectra of the $\text{H}_2\text{C}(\text{Ph}_2\text{PS})_2$ $P_{21/c}$ and $C_{2/c}$ polymorphs. The lack of complete agreement of the bands in this range with those in the IR spectra of both polymorphs could possibly indicate the presence of another novel species containing $\nu \text{P}=\text{S}$ vibration bands. The bands in the spectra of the $\text{H}_2\text{C}(\text{Ph}_2\text{PS})_2$ ligands at 783 cm^{-1} and 772 cm^{-1} were lost in the spectrum of $[\text{Sm}_2(\text{C}(\text{Ph}_2\text{PS})_2)_2\text{I}_2\text{THF}_4] \cdot 4(\text{C}_6\text{H}_5\text{CH}_3)_{_4\text{a_}2}$ and since these bands were assigned to $\nu \text{P}-\text{CH}_2-\text{P}$ and $\nu \text{P}=\text{S}$ vibrations respectively this loss could indicate deprotonation and complexation. Another band was observed in the spectrum of the product at 868 cm^{-1} and this was possibly unique to $[\text{Sm}_2(\text{C}(\text{Ph}_2\text{PS})_2)_2\text{I}_2\text{THF}_4] \cdot 4(\text{C}_6\text{H}_5\text{CH}_3)_{_4\text{a_}2}$. This could possibly indicate the presence of $\nu_{\text{as}} \text{P}-\text{CH}^--\text{P}$ or $\nu_{\text{s}} \text{P}-\text{CH}^--\text{P}$ for a mono-anionic $\text{H}_2\text{C}(\text{Ph}_2\text{PS})_2$ derivative.

In these four attempts a number of solids were collected from work up of the resultant filtrates obtained on removal of the initial solids $[\text{Sm}_2(\text{C}(\text{Ph}_2\text{PS})_2)_2\text{I}_2\text{THF}_4] \cdot 4(\text{C}_6\text{H}_5\text{CH}_3)_{_1\text{a}, _2\text{a}, _3\text{a}}$ and $_4\text{a}$ (see Table 4.11). The solids $[\text{Sm}_2(\text{C}(\text{Ph}_2\text{PS})_2)_2\text{I}_2\text{THF}_4] \cdot 4(\text{C}_6\text{H}_5\text{CH}_3)_{_2\text{b}}$ and $_4\text{b}$ were obtained from the initial filtrate, the former by concentration and drowning out using diethyl ether and the latter through precipitation on standing for a week. In the case of the first and third reactions numerous solids were obtained throughout the respective work up procedures as described hereunder on discussion of the respective IR spectra.

The yellow paste $[\text{Sm}_2(\text{C}(\text{Ph}_2\text{PS})_2)_2\text{I}_2\text{THF}_4] \cdot 4(\text{C}_6\text{H}_5\text{CH}_3)_{_1\text{b}}$, produced after layering the first filtrate obtained during the first attempt with THF followed by the removal of volatiles, was analysed by IR spectroscopy and gave the spectrum shown in Figure 4.45 (for the region 1800 cm^{-1} to 400 cm^{-1}). The spectra for $\text{H}_2\text{C}(\text{Ph}_2\text{PS})_2_{_1}$ and $[\text{Sm}_2(\text{C}(\text{Ph}_2\text{PS})_2)_2\text{I}_2\text{THF}_4] \cdot 4(\text{C}_6\text{H}_5\text{CH}_3)_{_1\text{a}}$ are also shown in Figure 4.45. On comparison of these three spectra it was observed that most of the bands in the spectrum of $[\text{Sm}_2(\text{C}(\text{Ph}_2\text{PS})_2)_2\text{I}_2\text{THF}_4] \cdot 4(\text{C}_6\text{H}_5\text{CH}_3)_{_1\text{b}}$ were analogous to the bands of the other two spectra. The main differences were observed in the bands at 1458 cm^{-1} (strong), 1377 cm^{-1} (strong), 1292 cm^{-1} (weak), 1236 cm^{-1} (weak), 1186 cm^{-1} (medium), 1042 cm^{-1} (very strong), 914 cm^{-1} (very strong), 890 cm^{-1} (very strong), 645 cm^{-1} (medium) and 597 cm^{-1} (shoulder). The first two bands are typical of many $\delta \text{C}-\text{H}$ vibrations, although these were not analogous to the bands typical of the protonated ligand. These could therefore indicate the possible presence of a large amount of another

molecule containing these vibrations, such as toluene, diethyl ether and THF, which were all used in the reactions and work up procedures. The bands at 645 cm^{-1} and 597 cm^{-1} could be due to novel $\nu\text{ P}=\text{S}$ vibrations. However, these do not indicate deprotonation, as the formation of the decreased bond order species, P^+-S^- , should give rise to a decrease in wavenumber, which was not observed in this case.

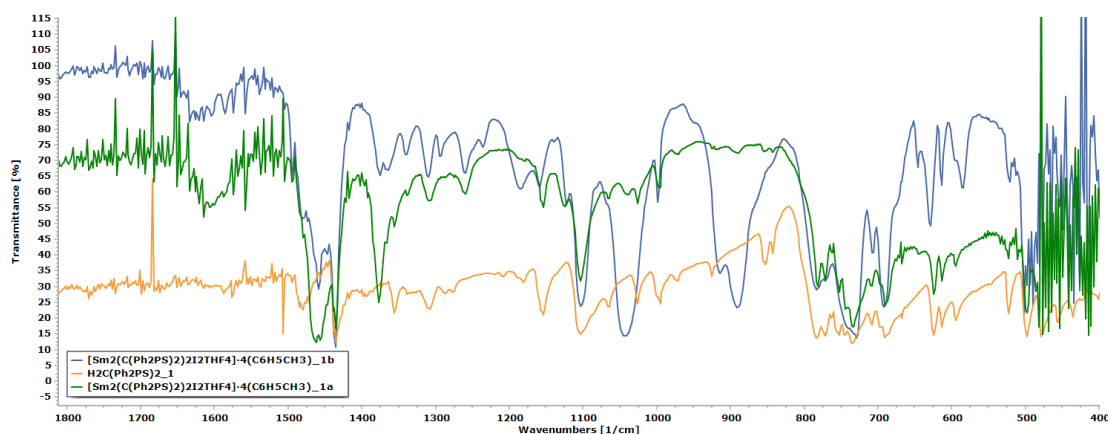


Figure 4.45: IR spectra of $[\text{Sm}_2(\text{C}(\text{Ph}_2\text{PS})_2)_2\text{I}_2\text{THF}_4]\cdot 4(\text{C}_6\text{H}_5\text{CH}_3)_1\text{b}$ (blue) and $\text{H}_2\text{C}(\text{Ph}_2\text{PS})_2_1$ (orange) and $[\text{Sm}_2(\text{C}(\text{Ph}_2\text{PS})_2)_2\text{I}_2\text{THF}_4]\cdot 4(\text{C}_6\text{H}_5\text{CH}_3)_1\text{a}$ (green), in the region 1800 cm^{-1} to 400 cm^{-1} .

The remaining bands were novel to this product and have been tentatively assigned to the $\nu\text{ P}-\text{C}-\text{P}$ vibrations for either the mono-anion or di-anion derivatives of $\text{H}_2\text{C}(\text{Ph}_2\text{PS})_2$. The bands at 1292 cm^{-1} , 1236 cm^{-1} and 1186 cm^{-1} fell in the range typical for the $\nu\text{ P}=\text{C}$ vibrations for $\text{P}=\text{C}$ containing organic molecules.^{99,348} For the desired product bands in this region are expected, given that the $\text{P}-\text{C}$ bond length in the complex $[\text{Sm}_2(\text{C}(\text{Ph}_2\text{PS})_2)_2\text{I}_2\text{THF}_4]\cdot 4(\text{C}_6\text{H}_5\text{CH}_3)$ falls in the same range of bond lengths for simple symmetric $\text{P}=\text{C}$ containing organic molecules and other phosphorus(V) stabilised lanthanide carbenes,^{323–331} as discussed in Section 4.1.3.1.1. However, it should be noted that for lanthanide carbenes of the $[\text{C}(\text{Ph}_2\text{PNR})_2]^{2-}$ analogues significant bands in this region were not reported in literature, which could be due to symmetric restraints on the bent $\text{P}=\text{C}=\text{P}$ moiety.

The strong bands at 1042 cm^{-1} , 914 cm^{-1} and 890 cm^{-1} could also be indicative of the presence of $\nu\text{ P}-\text{C}-\text{P}$ vibrations for the mono-anionic ligand, since these were located in a region between the expected regions for bands assigned to $\nu\text{ P}=\text{C}$ and $\nu\text{ P}-\text{CH}_2-\text{P}$ vibrations.^{99,348} This however is not in line with data for bond lengths. For mono-anionic derivative salts, $[\text{HC}(\text{Ph}_2\text{PS})_2]^-$, the $\text{P}-\text{C}$ bond lengths are in the range of $1.712\text{--}1.718\text{ \AA}$,^{108,303} which falls in the range for other mono-anions as discussed in

Section 4.1.3.1.1. These bond lengths also lie in the ranges typical of the P–C bond lengths for simple symmetric P=C containing organic molecules which as described above would indicate a higher wavenumber value for the ν P–CH–P vibrational modes than the wavenumbers of the three bands assigned in the current study.

On dissolution of $[\text{Sm}_2(\text{C}(\text{Ph}_2\text{PS})_2)_2\text{I}_2\text{THF}_4]\cdot 4(\text{C}_6\text{H}_5\text{CH}_3)$ _1b in toluene and precipitation by n-hexane the solid $[\text{Sm}_2(\text{C}(\text{Ph}_2\text{PS})_2)_2\text{I}_2\text{THF}_4]\cdot 4(\text{C}_6\text{H}_5\text{CH}_3)$ _1c was obtained. This solid gave a weak IR spectrum as given in Appendix 9 along with IR spectra of the starting reagents. This IR data clearly indicated that the major component of the solid was $\text{H}_2\text{C}(\text{Ph}_2\text{PS})_2$ indicating possible moisture induced decomposition of $[\text{Sm}_2(\text{C}(\text{Ph}_2\text{PS})_2)_2\text{I}_2\text{THF}_4]\cdot 4(\text{C}_6\text{H}_5\text{CH}_3)$ _1b.

The product precipitated from the initial filtrate for the reaction $[\text{Sm}_2(\text{C}(\text{Ph}_2\text{PS})_2)_2\text{I}_2\text{THF}_4]\cdot 4(\text{C}_6\text{H}_5\text{CH}_3)$ _2, namely $[\text{Sm}_2(\text{C}(\text{Ph}_2\text{PS})_2)_2\text{I}_2\text{THF}_4]\cdot 4(\text{C}_6\text{H}_5\text{CH}_3)$ _2b, was analysed by IR spectroscopy using a sample prepared in a nitrogen glove box in KBr. A detail in the range of 1600 cm^{-1} and 400 cm^{-1} of the spectrum obtained is given in Appendix 9, together with the spectra of the two polymorphs of $\text{H}_2\text{C}(\text{Ph}_2\text{PS})_2$ (in KBr) and the spectrum of $\text{SmI}_3\cdot\text{THF}_{3.5}$ _2 (in nujol). Two broad strong bands at 3433 cm^{-1} and 1616 cm^{-1} were observed in the spectrum of $[\text{Sm}_2(\text{C}(\text{Ph}_2\text{PS})_2)_2\text{I}_2\text{THF}_4]\cdot 4(\text{C}_6\text{H}_5\text{CH}_3)$ _2b. These bands could be assigned to the ν O–H and δ O–H vibrations of water included in the solid, either as a coordinated hydrate or as a solvate. These therefore indicated the presence of moisture in the sample. As with the solid $[\text{Sm}_2(\text{C}(\text{Ph}_2\text{PS})_2)_2\text{I}_2\text{THF}_4]\cdot 4(\text{C}_6\text{H}_5\text{CH}_3)$ _2a_2, a cursory look at the fingerprint region of $[\text{Sm}_2(\text{C}(\text{Ph}_2\text{PS})_2)_2\text{I}_2\text{THF}_4]\cdot 4(\text{C}_6\text{H}_5\text{CH}_3)$ _2b indicated that the major component of the solid was the neutral ligand precursor used in the reaction. No other bands were observed which could indicate the presence of other chemical species in the solid. The presence of the neutral ligand precursor for both $[\text{Sm}_2(\text{C}(\text{Ph}_2\text{PS})_2)_2\text{I}_2\text{THF}_4]\cdot 4(\text{C}_6\text{H}_5\text{CH}_3)$ _2a_2 and _2b indicated that the reaction did not yield the desired de-protonation or complexation.

For the third reaction as described in Section 3.3.1.3.3.5 the filtrate left after the removal of the solid $[\text{Sm}_2(\text{C}(\text{Ph}_2\text{PS})_2)_2\text{I}_2\text{THF}_4]\cdot 4(\text{C}_6\text{H}_5\text{CH}_3)$ _3a, again produced a suspension which on filtration yielded the solid $[\text{Sm}_2(\text{C}(\text{Ph}_2\text{PS})_2)_2\text{I}_2\text{THF}_4]\cdot 4(\text{C}_6\text{H}_5\text{CH}_3)$ _3b_1. After a week a small crop of crystals precipitated from the resultant filtrate and this was collected and labelled as $[\text{Sm}_2(\text{C}(\text{Ph}_2\text{PS})_2)_2\text{I}_2\text{THF}_4]\cdot 4(\text{C}_6\text{H}_5\text{CH}_3)$ _3b_2. The IR spectrum of the solid $[\text{Sm}_2(\text{C}(\text{Ph}_2\text{PS})_2)_2\text{I}_2\text{THF}_4]\cdot 4(\text{C}_6\text{H}_5\text{CH}_3)$ _3b_1 was found to be similar to that of the initial

product $[\text{Sm}_2(\text{C}(\text{Ph}_2\text{PS})_2)_2\text{I}_2\text{THF}_4]\cdot 4(\text{C}_6\text{H}_5\text{CH}_3)_3\text{a}$ and of the $\text{H}_2\text{C}(\text{Ph}_2\text{PS})_2$ *C2/c* polymorph, as given in Appendix 9. However, the IR spectrum of $[\text{Sm}_2(\text{C}(\text{Ph}_2\text{PS})_2)_2\text{I}_2\text{THF}_4]\cdot 4(\text{C}_6\text{H}_5\text{CH}_3)_3\text{b}_1$ also showed an increased moisture intrusion as compared to that of $[\text{Sm}_2(\text{C}(\text{Ph}_2\text{PS})_2)_2\text{I}_2\text{THF}_4]\cdot 4(\text{C}_6\text{H}_5\text{CH}_3)_3\text{a}$.

A detail of the IR spectrum of the crystalline solid precipitated from the final filtrate of this third attempt, namely $[\text{Sm}_2(\text{C}(\text{Ph}_2\text{PS})_2)_2\text{I}_2\text{THF}_4]\cdot 4(\text{C}_6\text{H}_5\text{CH}_3)_3\text{b}_2$, obtained in nujol, is given in Figure 4.46. Weak bands were observed at 1170 cm^{-1} , 1152 cm^{-1} , 1084 cm^{-1} , 1017 cm^{-1} , 935 cm^{-1} , 917 cm^{-1} , 890 cm^{-1} , 845 cm^{-1} , 799 cm^{-1} and 770 cm^{-1} . No bands typical of moisture were observed (range not shown in Figure 4.46) indicating that this solid was dry, which was a positive result. Given that these bands fell in the fingerprint region any number and types of molecular vibrations could be responsible for them and therefore assignment could only be given on the moieties assumed to be present.

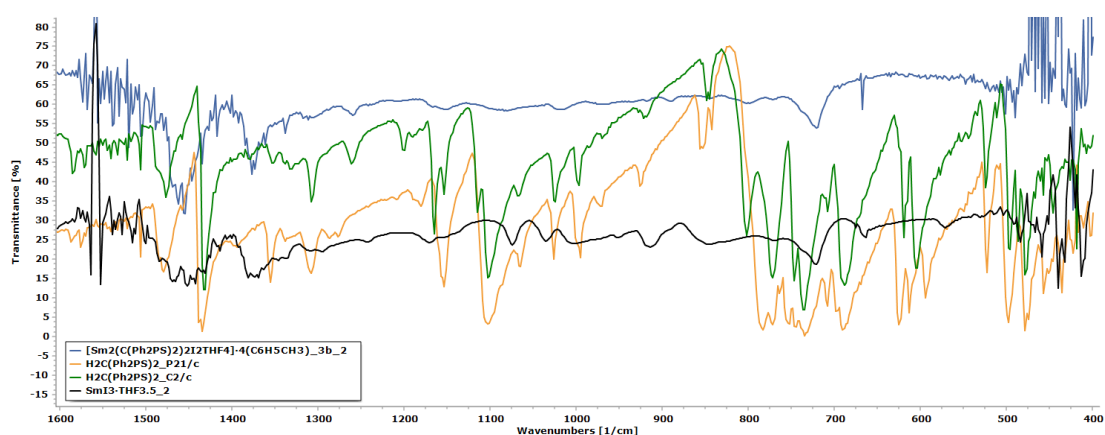


Figure 4.46: IR spectra of $[\text{Sm}_2(\text{C}(\text{Ph}_2\text{PS})_2)_2\text{I}_2\text{THF}_4]\cdot 4(\text{C}_6\text{H}_5\text{CH}_3)_3\text{b}_2$ (blue), $\text{H}_2\text{C}(\text{Ph}_2\text{PS})_2$ *C2/c* polymorph (orange) and $\text{H}_2\text{C}(\text{Ph}_2\text{PS})_2$ *P21/c* polymorph (green) and $\text{SmI}_3\cdot\text{THF}_{3.5}$ *2* (black), in the region 1600 cm^{-1} to 400 cm^{-1} .

Although the bands at 1152 cm^{-1} and 1084 cm^{-1} could be analogous to skeletal bands for the $\text{H}_2\text{C}(\text{Ph}_2\text{PS})_2$ ligand in this region, no other bands typical of this molecule and its derivatives, especially those typical of the P–Ph groups, were observed in the spectrum of the product. The bands at 1017 cm^{-1} and 890 cm^{-1} could be tentatively assigned to coordinated THF, although the latter could also be attributed to free THF along with the bands at 1170 cm^{-1} and 1084 cm^{-1} which could be analogous to the free THF bands at 1185 cm^{-1} and 1070 cm^{-1} respectively. It should be observed that, as shown in Figure 4.46, although THF was possibly present in the solid this was not the same species as that present in the $\text{SmI}_3\cdot\text{THF}_{3.5}$ salt, as the bands of coordinated THF in this

iodide did not agree with the data obtained in the spectrum of the product $[\text{Sm}_2(\text{C}(\text{Ph}_2\text{PS})_2)_2\text{I}_2\text{THF}_4] \cdot 4(\text{C}_6\text{H}_5\text{CH}_3)_3\text{b}_2$. The other bands listed beforehand could not be assigned with any certainty. Therefore, it was likely that the solid obtained was some type of THF containing solid which was highly soluble in toluene but did not seem to contain the $\text{H}_2\text{C}(\text{Ph}_2\text{PS})_2$ ligand or any of its derivatives. This could indicate that the product $[\text{Sm}_2(\text{C}(\text{Ph}_2\text{PS})_2)_2\text{I}_2\text{THF}_4] \cdot 4(\text{C}_6\text{H}_5\text{CH}_3)_3\text{b}_2$ could be a complex of Sm^{3+} , particularly containing THF, rather than a mixture of some of the starting reagents used.

Unfortunately the negligible amount of solid obtained from the first filtrate for the fourth attempt of this reaction, namely $[\text{Sm}_2(\text{C}(\text{Ph}_2\text{PS})_2)_2\text{I}_2\text{THF}_4] \cdot 4(\text{C}_6\text{H}_5\text{CH}_3)_4\text{b}$, meant that the IR spectrum of this solid could not be obtained.

4.1.3.3.2. Analysis by ^1H NMR spectroscopy

Only three samples from the attempts undertaken in this section were studied using ^1H NMR spectroscopy, namely $[\text{Sm}_2(\text{C}(\text{Ph}_2\text{PS})_2)_2\text{I}_2\text{THF}_4] \cdot 4(\text{C}_6\text{H}_5\text{CH}_3)_2\text{a}$, $[\text{Sm}_2(\text{C}(\text{Ph}_2\text{PS})_2)_2\text{I}_2\text{THF}_4] \cdot 4(\text{C}_6\text{H}_5\text{CH}_3)_2\text{b}$ and $[\text{Sm}_2(\text{C}(\text{Ph}_2\text{PS})_2)_2\text{I}_2\text{THF}_4] \cdot 4(\text{C}_6\text{H}_5\text{CH}_3)_3\text{b}_2$. The former two products were selected given that they represented two products from the initial solid and filtrate obtained in the same reaction. The ^1H NMR spectrum of $[\text{Sm}_2(\text{C}(\text{Ph}_2\text{PS})_2)_2\text{I}_2\text{THF}_4] \cdot 4(\text{C}_6\text{H}_5\text{CH}_3)_3\text{b}_2$ was undertaken due to its unique IR spectrum, possibly indicating the desired complexation product, and since it was clearly crystalline in nature. For the former two products samples were prepared using deuterated chloroform (CDCl_3), while the latter sample was prepared in benzene- d_6 . CDCl_3 was dried over P_2O_5 as a drying agent as described for chlorinated solvents in Appendix 2, while benzene- d_6 was dried over a sodium/benzophenone mixture as described in the aforementioned appendix. The mixtures were refluxed under argon overnight and collection was undertaken by application of a vacuum through a collection Schlenk tube set in a liquid nitrogen bath. Normal distillation was typically found to be less reliable for the collection of such small amounts of solvents. The spectra of these three compounds were initially compared with the ^1H NMR spectra of $\text{H}_2\text{C}(\text{Ph}_2\text{PS})_2$ in CDCl_3 and in benzene- d_6 .

The ^1H NMR spectra for the samples dissolved in CDCl_3 , namely $[\text{Sm}_2(\text{C}(\text{Ph}_2\text{PS})_2)_2\text{I}_2\text{THF}_4] \cdot 4(\text{C}_6\text{H}_5\text{CH}_3)_2\text{a}$ and $_2\text{b}$, are given in Appendix 9, together with the spectrum for $\text{H}_2\text{C}(\text{Ph}_2\text{PS})_2$ in CDCl_3 . In both the product spectra the same peaks

were observed. Three multiplets were observed at 7.82 ppm, 7.42 ppm and 7.34 ppm along with a triplet at 3.98 ppm ($J = 13.45$ Hz). These were in close agreement, in terms of both chemical shift and multiplicity, to the respective peaks observed for the $\text{H}_2\text{C}(\text{Ph}_2\text{PS})_2$ spectrum in CDCl_3 . The multiplets were assigned to the phenyl protons, o-H, p-H and m-H respectively while the triplet was assigned to the methylene protons, as described in Section 4.1.1.3.2. It was therefore inferred that all these spectra indicated the presence of $\text{H}_2\text{C}(\text{Ph}_2\text{PS})_2$. The triplet at 3.98 ppm in the spectra of the products clearly showed the presence of the fully protonated species, while the lack of broadening and shifts for all peaks clearly indicated the lack of complexation. This was in agreement with the IR data obtained for the product $[\text{Sm}_2(\text{C}(\text{Ph}_2\text{PS})_2)_2\text{I}_2\text{THF}_4] \cdot 4(\text{C}_6\text{H}_5\text{CH}_3)$ _2a and _2b, both of which indicated the presence of the free ligand. The hydrated species expected in the solid $[\text{Sm}_2(\text{C}(\text{Ph}_2\text{PS})_2)_2\text{I}_2\text{THF}_4] \cdot 4(\text{C}_6\text{H}_5\text{CH}_3)$ _2b was only observed in the NMR spectrum as a free water peak at 1.56 ppm with a higher relative intensity than the weak band observed in the spectrum of $[\text{Sm}_2(\text{C}(\text{Ph}_2\text{PS})_2)_2\text{I}_2\text{THF}_4] \cdot 4(\text{C}_6\text{H}_5\text{CH}_3)$ _2a. This could indicate that the major component of this product was either an inorganic hydrate or a hydrate of the neutral ligand. The presence of moisture in each sample could indicate the possible decomposition of the product on preparation of the ^1H NMR sample.

In each case a secondary group of peaks were observed in the spectra of both products, namely a quartet at 3.48 ppm and a triplet at 1.21 ppm with an integration values ratio of approximately 1:2. The chemical shifts were in agreement with literature values for diethyl ether as an impurity in CDCl_3 ,³⁶¹ although the integration values ratio for this impurity is expected to be 1:1.5 rather than 1:2. The two peaks could be indicative of the presence of large amounts of diethyl ether, although diethyl ether was not observed in the IR spectra of these two products. In both cases the integration of these values was independent of the values for the proton peaks of the $\text{H}_2\text{C}(\text{Ph}_2\text{PS})_2$, indicating that the amount of ether was not fixed to the amount of $\text{H}_2\text{C}(\text{Ph}_2\text{PS})_2$. This ether could be due to the MeLi reagent or for the latter product it could be due to the diethyl ether used in the precipitation procedure.

As given in Appendix 9 three peaks were observed in the ^1H NMR spectrum of $[\text{Sm}_2(\text{C}(\text{Ph}_2\text{PS})_2)_2\text{I}_2\text{THF}_4] \cdot 4(\text{C}_6\text{H}_5\text{CH}_3)$ _3b_2, namely the two multiplets at 7.89 ppm and 6.92 ppm and the triplet at 3.84 ppm. All these peaks were in complete agreement with the spectrum of $\text{H}_2\text{C}(\text{Ph}_2\text{PS})_2$ in benzene- d_6 . This agreement was also observed for the coupling constant of the peak at 3.84 ppm which was of 13.55 Hz, further indicating that the component present in the ^1H NMR sample for

$[\text{Sm}_2(\text{C}(\text{Ph}_2\text{PS})_2)_2\text{I}_2\text{THF}_4] \cdot 4(\text{C}_6\text{H}_5\text{CH}_3)$ _3b_2 was $\text{H}_2\text{C}(\text{Ph}_2\text{PS})_2$. This was not in agreement with the information obtained from the IR data for the product. However, it should be noted that the IR spectrum gave very weak bands and therefore the bands for this ligand might have been too weak to give significant information regarding the presence of this ligand. This free protonated ligand could be due to the presence of a novel crystalline form of the fully protonated ligand in the product or to the decomposition of the deprotonated derivative on preparation of the ^1H NMR sample.

4.1.3.3.3. Analysis by Microscopy

The solids obtained from the reactions undertaken to synthesise the complex $[\text{Sm}_2(\text{C}(\text{Ph}_2\text{PS})_2)_2\text{I}_2\text{THF}_4]$ were analysed using plane polarised light microscopy, in order to observe crystallinity and to observe any habits for the products obtained. In those cases where the characterisation of the product was established through IR and ^1H NMR spectroscopy analysis using this technique was not undertaken.

In all the reactions the first product deposited was expected to be the LiI side product. However, IR data indicated that in all cases this product contained $\text{H}_2\text{C}(\text{Ph}_2\text{PS})_2$, which was most likely mixed with some salts which were not noticeable in the IR data given the detection range used in the current study. Micrographs representing these products are given for $[\text{Sm}_2(\text{C}(\text{Ph}_2\text{PS})_2)_2\text{I}_2\text{THF}_4] \cdot 4(\text{C}_6\text{H}_5\text{CH}_3)$ _2a and $[\text{Sm}_2(\text{C}(\text{Ph}_2\text{PS})_2)_2\text{I}_2\text{THF}_4] \cdot 4(\text{C}_6\text{H}_5\text{CH}_3)$ _3a in Figures 4.47 and 4.48 respectively. In both cases powders were observed with little extinction of plane polarised light.

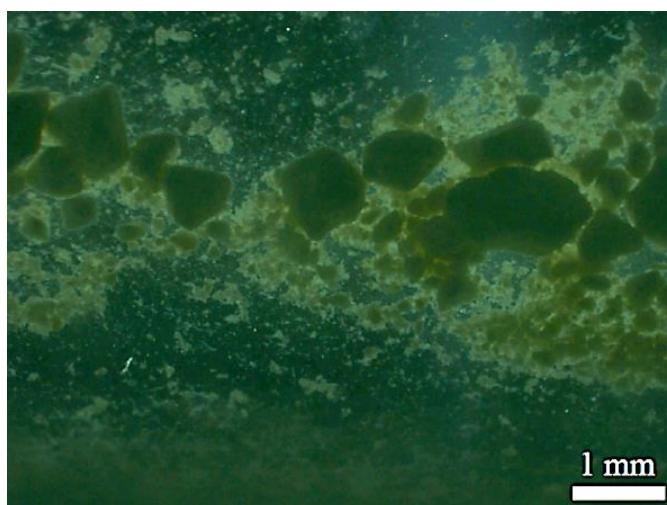


Figure 4.47: Micrograph of $[\text{Sm}_2(\text{C}(\text{Ph}_2\text{PS})_2)_2\text{I}_2\text{THF}_4] \cdot 4(\text{C}_6\text{H}_5\text{CH}_3)$ _2a.

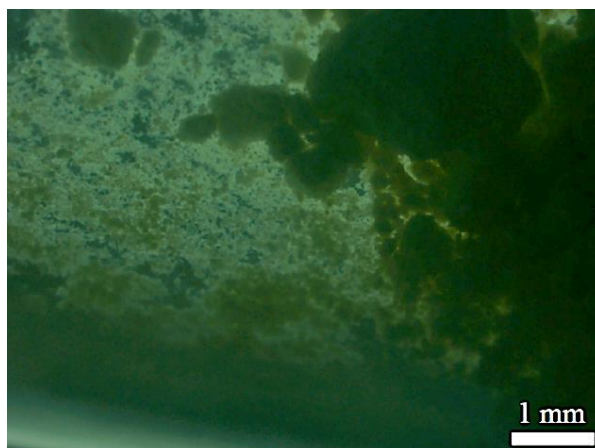


Figure 4.48: Micrograph of $[\text{Sm}_2(\text{C}(\text{Ph}_2\text{PS})_2)_2\text{I}_2\text{THF}_4]\cdot 4(\text{C}_6\text{H}_5\text{CH}_3)_3\text{a}$.

However, it was also observed that in both cases the products showed plane polarised light extinction dependent on the thickness of the solid particles, possibly indicating crystallinity. This possibly crystalline powder was typical for all products which were assumed to be a mixture of $\text{H}_2\text{C}(\text{Ph}_2\text{PS})_2$ and a number of unknown salts.

In the second and fourth attempts undertaken, the first product obtained was subjected to reactions and extraction techniques to try to extract the expected product. The products obtained namely $[\text{Sm}_2(\text{C}(\text{Ph}_2\text{PS})_2)_2\text{I}_2\text{THF}_4]\cdot 4(\text{C}_6\text{H}_5\text{CH}_3)_2\text{a}_2$ and $[\text{Sm}_2(\text{C}(\text{Ph}_2\text{PS})_2)_2\text{I}_2\text{THF}_4]\cdot 4(\text{C}_6\text{H}_5\text{CH}_3)_4\text{a}_2$ both appeared to be gelatinous solids to the naked eye. Micrographs for both these products, as given in Figures 4.49 and 4.50 respectively, showed that these masses contained crystalline particles. For the former the solid obtained seemed to be made up of multi-crystalline particles embedded in a thin film of an amorphous solid or a very viscous liquid. For the latter product small crystalline particles were observed to be embedded in a gelatinous mass.

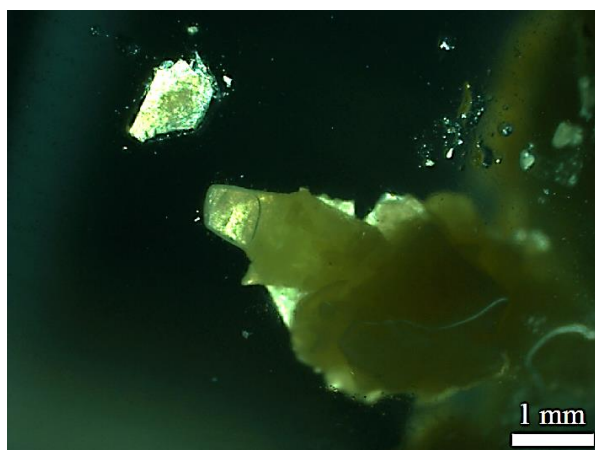


Figure 4.49: Micrograph of $[\text{Sm}_2(\text{C}(\text{Ph}_2\text{PS})_2)_2\text{I}_2\text{THF}_4]\cdot 4(\text{C}_6\text{H}_5\text{CH}_3)_2\text{a}_2$

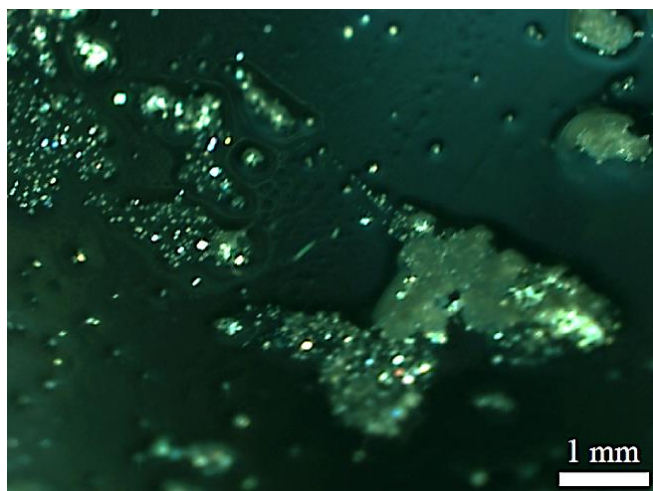


Figure 4.50: Micrograph of [Sm₂(C(Ph₂PS)₂)₂I₂THF₄]·4(C₆H₅CH₃)_{4a_2}

A number of solids obtained from the precipitation extracted from the first filtrate of the reactions and which were expected to contain the desired product were also analysed by microscopy. These were the products [Sm₂(C(Ph₂PS)₂)₂I₂THF₄]·4(C₆H₅CH₃)_{1b}, _{2b}, _{3b_1}, _{3b_2} and _{4b}. [Sm₂(C(Ph₂PS)₂)₂I₂THF₄]·4(C₆H₅CH₃)_{3b_1} and _{3b_2} are discussed separately below due to significantly different results obtained when compared to the other solids. For the products [Sm₂(C(Ph₂PS)₂)₂I₂THF₄]·4(C₆H₅CH₃)_{1b} and [Sm₂(C(Ph₂PS)₂)₂I₂THF₄]·4(C₆H₅CH₃)_{2b} the micrographs obtained under plane polarised light are given in Figures 4.51 and 4.52 respectively. In both cases the solid obtained was observed to be a pale yellow paste similar to the solid [Sm₂(C(Ph₂PS)₂)₂I₂THF₄]·4(C₆H₅CH₃)_{2a_2}, which was discussed earlier. In both cases crystallinity could not be concluded decisively, however the presence of small crystallites would indicate that the product [Sm₂(C(Ph₂PS)₂)₂I₂THF₄]·4(C₆H₅CH₃)_{2b} was more likely to be crystalline. It should be noted that both compounds could not be dismissed as being amorphous, given that plane polarised light extinction was not dependent on particle thickness. The micrograph in Figure 4.53 for the solid [Sm₂(C(Ph₂PS)₂)₂I₂THF₄]·4(C₆H₅CH₃)_{4b} showed similar properties to those described for [Sm₂(C(Ph₂PS)₂)₂I₂THF₄]·4(C₆H₅CH₃)_{2b}, although the solid was obtained in flakes which showed a lack of crystal habit and could be either amorphous or composed of multi crystalline solid particles.



Figure 4.51: Micrograph of $[\text{Sm}_2(\text{C}(\text{Ph}_2\text{PS})_2)_2\text{L}_2\text{THF}_4] \cdot 4(\text{C}_6\text{H}_5\text{CH}_3)_1\text{b}$.

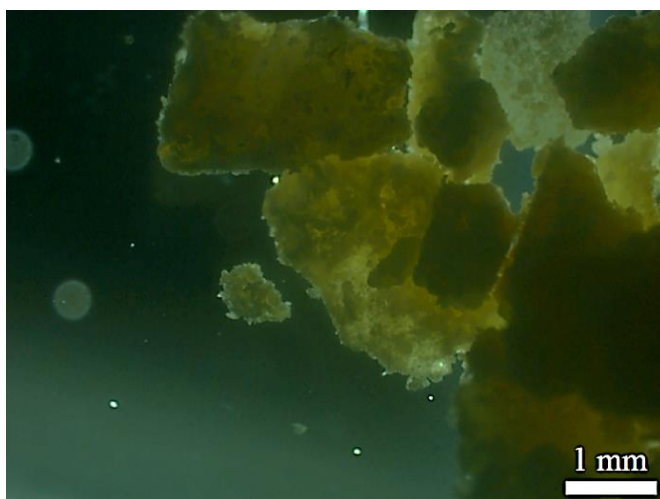


Figure 4.52: Micrograph of $[\text{Sm}_2(\text{C}(\text{Ph}_2\text{PS})_2)_2\text{L}_2\text{THF}_4] \cdot 4(\text{C}_6\text{H}_5\text{CH}_3)_2\text{b}$.

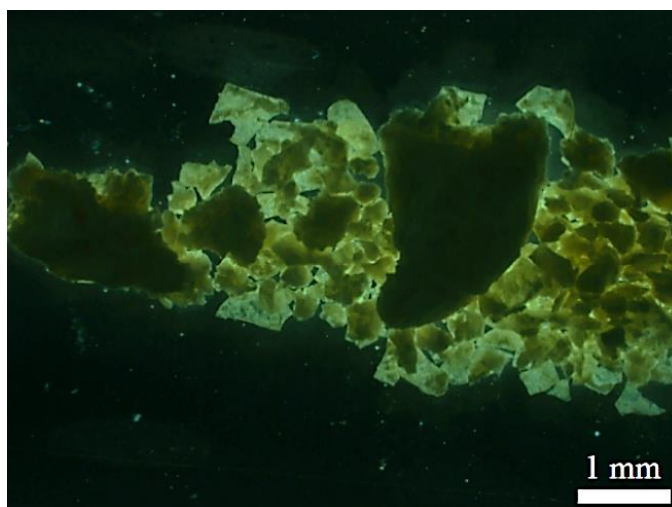


Figure 4.53: Micrograph of $[\text{Sm}_2(\text{C}(\text{Ph}_2\text{PS})_2)_2\text{L}_2\text{THF}_4] \cdot 4(\text{C}_6\text{H}_5\text{CH}_3)_4\text{b}$.

Unlike the other solids precipitated from the original filtrates and discussed above, the solid $[\text{Sm}_2(\text{C}(\text{Ph}_2\text{PS})_2)_2\text{I}_2\text{THF}_4]\cdot 4(\text{C}_6\text{H}_5\text{CH}_3)$ _3b_1 was found to be a white powder where crystallinity was not clear, as can be observed in Figure 4.54. The crystallinity could be indicated by the change in plane polarised light extinction related to the thickness of solid particles. This would corroborate the presence of the $\text{H}_2\text{C}(\text{Ph}_2\text{PS})_2$ $P2_1/c$ polymorph in this product as was inferred by the IR spectrum of this product.

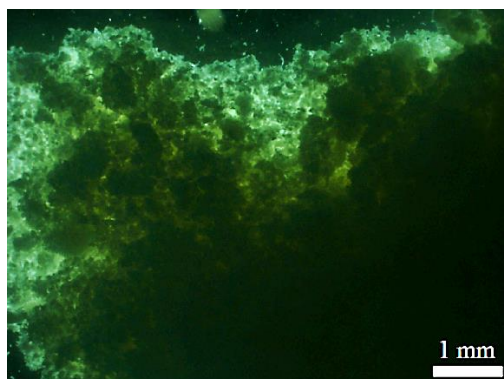


Figure 4.54: Micrograph of $[\text{Sm}_2(\text{C}(\text{Ph}_2\text{PS})_2)_2\text{I}_2\text{THF}_4]\cdot 4(\text{C}_6\text{H}_5\text{CH}_3)$ _3b_1.

A small crop of crystals was observed for the product $[\text{Sm}_2(\text{C}(\text{Ph}_2\text{PS})_2)_2\text{I}_2\text{THF}_4]\cdot 4(\text{C}_6\text{H}_5\text{CH}_3)$ _3b_2. The micrograph of this product is presented in Figure 4.55, along with a micrograph of the crystals of the $\text{H}_2\text{C}(\text{Ph}_2\text{PS})_2$ _1 ligand which showed some similarities in habit. $\text{H}_2\text{C}(\text{Ph}_2\text{PS})_2$ _1 was believed to be the $P2_1/c$ polymorph. The ^1H NMR data for the product $[\text{Sm}_2(\text{C}(\text{Ph}_2\text{PS})_2)_2\text{I}_2\text{THF}_4]\cdot 4(\text{C}_6\text{H}_5\text{CH}_3)$ _3b_2 had indicated that the $\text{H}_2\text{C}(\text{Ph}_2\text{PS})_2$ was present in this product. Therefore, the ^1H NMR data and the habit observed using microscopy were in agreement.

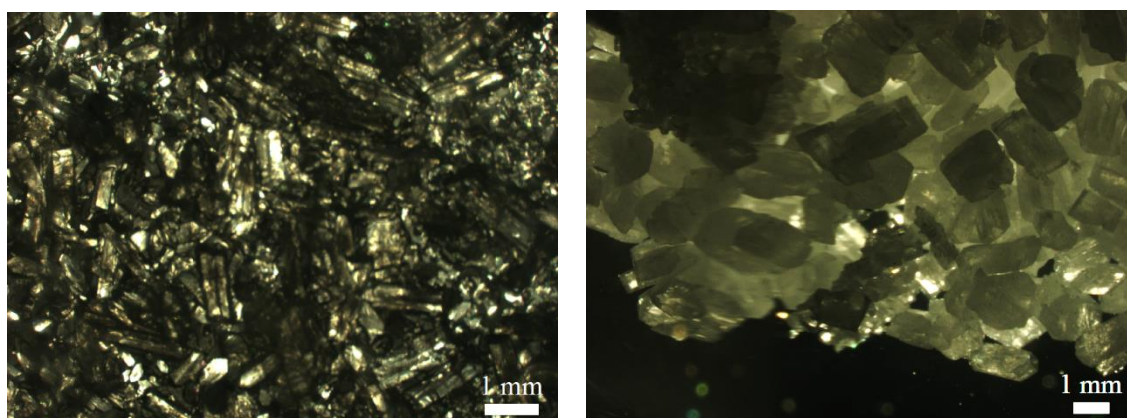


Figure 4.55: Micrographs for $[\text{Sm}_2(\text{C}(\text{Ph}_2\text{PS})_2)_2\text{I}_2\text{THF}_4]\cdot 4(\text{C}_6\text{H}_5\text{CH}_3)$ _3b_2 and $\text{H}_2\text{C}(\text{Ph}_2\text{PS})_2$ _1

Finally the solid $[\text{Sm}_2(\text{C}(\text{Ph}_2\text{PS})_2)_2\text{I}_2\text{THF}_4]\cdot 4(\text{C}_6\text{H}_5\text{CH}_3)$ _2a_1 which was the solid obtained on filtration which yielded the filtrate precipitating the product $[\text{Sm}_2(\text{C}(\text{Ph}_2\text{PS})_2)_2\text{I}_2\text{THF}_4]\cdot 4(\text{C}_6\text{H}_5\text{CH}_3)$ _2a_2 was also analysed by microscopy. The micrograph of $[\text{Sm}_2(\text{C}(\text{Ph}_2\text{PS})_2)_2\text{I}_2\text{THF}_4]\cdot 4(\text{C}_6\text{H}_5\text{CH}_3)$ _2a_1 is given in Figure 4.56. It was observed that the powder was possibly crystalline since it showed plane polarised light extinction dependent on the thickness of the solid particles. The orange colouration observed previously in Section 3.3.1.3.3.4 is also clearly visible in Figure 4.56.

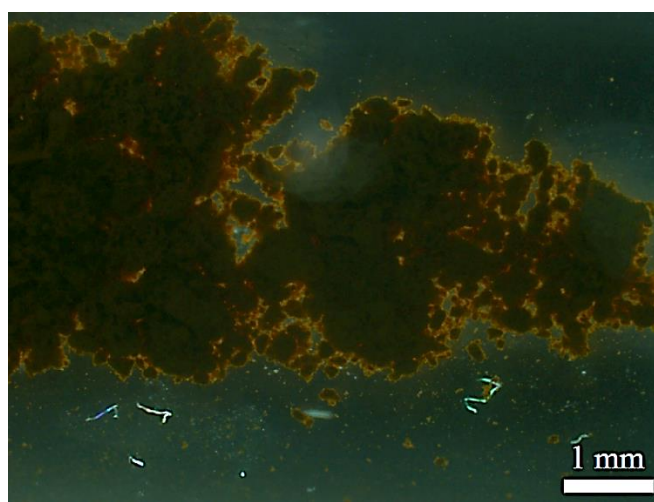


Figure 4.56: Micrograph for $[\text{Sm}_2(\text{C}(\text{Ph}_2\text{PS})_2)_2\text{I}_2\text{THF}_4]\cdot 4(\text{C}_6\text{H}_5\text{CH}_3)$ _2a_1.

4.1.3.3.4. Analysis by Powder X-ray diffraction

PXRD samples were prepared and sealed in 0.5 mm capillaries under dry nitrogen in a glove box. The determination of which products were likely candidates for PXRD studies was based primarily on the IR data and physical properties of the products. The solids which were observed as being mainly comprised of the $\text{H}_2\text{C}(\text{Ph}_2\text{PS})_2$ ligand were not characterised using this method, as this compound was already studied and in all probability the solids were a mixture containing numerous other compounds and any novel compounds would be problematic to structurally characterise from such PXRD data. Two samples were prepared for the products $[\text{Sm}_2(\text{C}(\text{Ph}_2\text{PS})_2)_2\text{I}_2\text{THF}_4]\cdot 4(\text{C}_6\text{H}_5\text{CH}_3)$ _2a_1 and _2b. Other products obtained in the attempts at producing $[\text{Sm}_2(\text{C}(\text{Ph}_2\text{PS})_2)_2\text{I}_2\text{THF}_4]\cdot 4(\text{C}_6\text{H}_5\text{CH}_3)$ which were of further interest were not analysed by PXRD mainly due to either a lack of sample or the fact that their physical characteristics impeded sample preparation.

For both $[\text{Sm}_2(\text{C}(\text{Ph}_2\text{PS})_2)_2\text{I}_2\text{THF}_4]\cdot 4(\text{C}_6\text{H}_5\text{CH}_3)_{2a_1}$ and $[\text{Sm}_2(\text{C}(\text{Ph}_2\text{PS})_2)_2\text{I}_2\text{THF}_4]\cdot 4(\text{C}_6\text{H}_5\text{CH}_3)_{2b}$ PXRD data was collected using Mo- $\text{K}\alpha_1$ radiation, with a Debye-Scherrer geometry, at room temperature. The PXRD pattern of $[\text{Sm}_2(\text{C}(\text{Ph}_2\text{PS})_2)_2\text{I}_2\text{THF}_4]\cdot 4(\text{C}_6\text{H}_5\text{CH}_3)_{2a_1}$ is given in Appendix 9. This PXRD pattern showed that the solid was amorphous and no evidence of a crystalline phase was observed. The IR data for this solid, as discussed in Section 4.1.3.3.1., indicated the presence of a heavily hydrated species which lacked bands typical of $[\text{C}(\text{Ph}_2\text{PS})_2]^{2-}$ species or its derivatives. This indicated that the solid was likely an inorganic species, such as the expected LiI, possibly containing THF. The presence of moisture in the solid could have caused the formation of an amorphous solid as the intrusion of moisture might not yield hydrates of a single stoichiometry. The presence of various hydrates in a single solid are less likely to give a crystalline product than a singular anhydrous or single hydrate compound, thus forming an amorphous solid. This was supported by the broad nature of the IR bands of the solid which were assigned to the ν O–H and δ O–H vibrations. The strong orange colour of the solid indicated the possible presence of Sm^{3+} but both the IR and PXRD data did not provide support for this presence.

Initial inspection of the PXRD pattern of $[\text{Sm}_2(\text{C}(\text{Ph}_2\text{PS})_2)_2\text{I}_2\text{THF}_4]\cdot 4(\text{C}_6\text{H}_5\text{CH}_3)_{2b}$ on the other hand indicated the possible presence of two crystalline phases, as given in Figure 4.57. The first phase, most likely comprised of the peaks observed in the orange range in Figure 4.57, was probably a high symmetry crystalline structure denoted by the presence of a few strong sharp peaks with large d-spacing differences between them. The second phase, most likely comprised of the peaks observed in the green range in Figure 4.57, was a minor phase noted as having multiple overlapping peaks or peaks with small d-spacing differences between each other, indicating the presence of a lower symmetry crystalline phase.

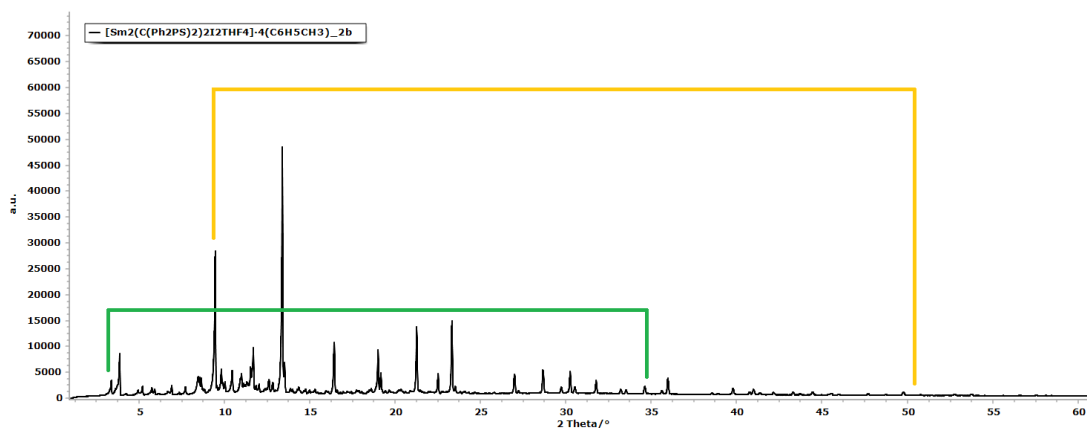


Figure 4.57: PXRD pattern of $[\text{Sm}_2(\text{C}(\text{Ph}_2\text{PS})_2)_2\text{I}_2\text{THF}_4] \cdot 4(\text{C}_6\text{H}_5\text{CH}_3)_2\text{b}$ with the range containing peaks most likely due to the major high symmetry phase noted in orange, while the range containing peaks most likely due to the minor lower symmetry phase noted in green.

Given that the salt metathesis reaction used in preparation of $[\text{Sm}_2(\text{C}(\text{Ph}_2\text{PS})_2)_2\text{I}_2\text{THF}_4] \cdot 4(\text{C}_6\text{H}_5\text{CH}_3)$ produces LiI, as discussed prior, the PXRD pattern of $[\text{Sm}_2(\text{C}(\text{Ph}_2\text{PS})_2)_2\text{I}_2\text{THF}_4] \cdot 4(\text{C}_6\text{H}_5\text{CH}_3)_2\text{b}$ was compared with PXRD data for various LiI containing species. Figure 4.58 shows that the major phase described for the $[\text{Sm}_2(\text{C}(\text{Ph}_2\text{PS})_2)_2\text{I}_2\text{THF}_4] \cdot 4(\text{C}_6\text{H}_5\text{CH}_3)_2\text{b}$ PXRD pattern proved to be analogous to the PXRD pattern of $\text{LiI} \cdot \text{H}_2\text{O}$.³⁶² The PXRD pattern of $\text{LiI} \cdot \text{H}_2\text{O}$ ($Pm-3m$) was calculated from published data, using Mercury software.^{297,362}

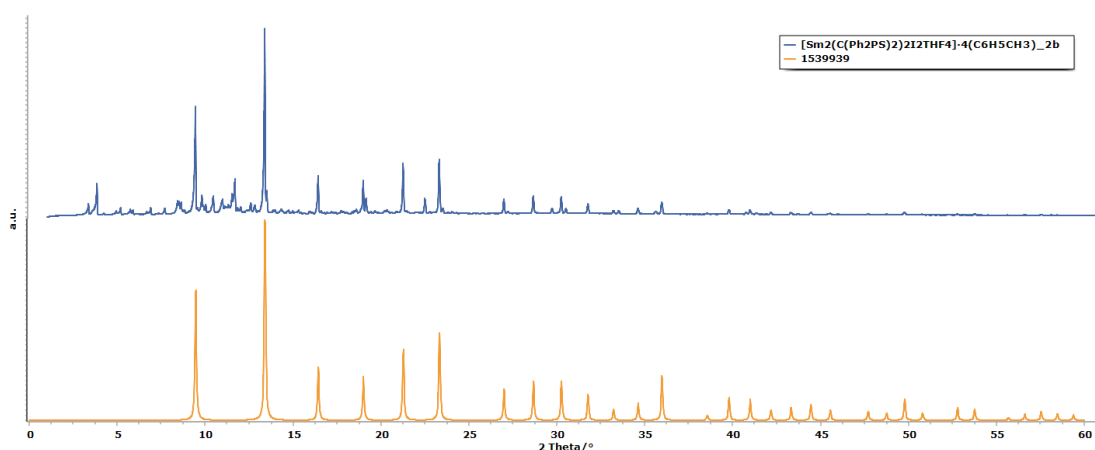


Figure 4.58: PXRD pattern of $[\text{Sm}_2(\text{C}(\text{Ph}_2\text{PS})_2)_2\text{I}_2\text{THF}_4] \cdot 4(\text{C}_6\text{H}_5\text{CH}_3)_2\text{b}$ (blue) and the calculated PXRD pattern of $\text{LiI} \cdot \text{H}_2\text{O}$ (orange).

The formation of LiI as a major phase of $[\text{Sm}_2(\text{C}(\text{Ph}_2\text{PS})_2)_2\text{I}_2\text{THF}_4] \cdot 4(\text{C}_6\text{H}_5\text{CH}_3)_2\text{b}$ indicated that a salt metathesis reaction did occur and therefore proved the occurrence of some reaction between $\text{SmI}_3 \cdot \text{THF}_{3.5}$ and $\text{Li}_2\text{C}(\text{Ph}_2\text{PS})_2$. The formation of the monohydrate of LiI corroborated the possibility of moisture intrusion either during the reaction or through one of the reagents. Moisture intrusion was observed in the IR spectra of both $[\text{Sm}_2(\text{C}(\text{Ph}_2\text{PS})_2)_2\text{I}_2\text{THF}_4] \cdot 4(\text{C}_6\text{H}_5\text{CH}_3)_2\text{a}_1$, as discussed prior, and of $[\text{Sm}_2(\text{C}(\text{Ph}_2\text{PS})_2)_2\text{I}_2\text{THF}_4] \cdot 4(\text{C}_6\text{H}_5\text{CH}_3)_2\text{b}$. Therefore, it was inferred that this intrusion occurred early in the reaction and that in the initial precipitate ($[\text{Sm}_2(\text{C}(\text{Ph}_2\text{PS})_2)_2\text{I}_2\text{THF}_4] \cdot 4(\text{C}_6\text{H}_5\text{CH}_3)_2\text{a}_1$) the solid formed was amorphous most likely due to the quick precipitation of the solid due to the presence of moisture. The LiI salt in the second solid ($[\text{Sm}_2(\text{C}(\text{Ph}_2\text{PS})_2)_2\text{I}_2\text{THF}_4] \cdot 4(\text{C}_6\text{H}_5\text{CH}_3)_2\text{b}$) precipitated out of the initial filtrate over a period of time and therefore the monohydrate was more likely to crystallise out rather than form an amorphous solid as noted for the first solid discussed.

The IR data for $[\text{Sm}_2(\text{C}(\text{Ph}_2\text{PS})_2)_2\text{I}_2\text{THF}_4] \cdot 4(\text{C}_6\text{H}_5\text{CH}_3)_2\text{b}$, as described in Section 4.1.3.3.1., also indicated the presence of free neutral ligand $\text{H}_2\text{C}(\text{Ph}_2\text{PS})_2$, which was not the case for the data for $[\text{Sm}_2(\text{C}(\text{Ph}_2\text{PS})_2)_2\text{I}_2\text{THF}_4] \cdot 4(\text{C}_6\text{H}_5\text{CH}_3)_2\text{a}_1$. Therefore it was expected that a PXRD pattern indicating the presence of this species in the solid would be observed in the PXRD pattern of $[\text{Sm}_2(\text{C}(\text{Ph}_2\text{PS})_2)_2\text{I}_2\text{THF}_4] \cdot 4(\text{C}_6\text{H}_5\text{CH}_3)_2\text{b}$ but not in that of $[\text{Sm}_2(\text{C}(\text{Ph}_2\text{PS})_2)_2\text{I}_2\text{THF}_4] \cdot 4(\text{C}_6\text{H}_5\text{CH}_3)_2\text{a}_1$.

Therefore the second phase containing the remaining peaks observed in the PXRD pattern of $[\text{Sm}_2(\text{C}(\text{Ph}_2\text{PS})_2)_2\text{I}_2\text{THF}_4] \cdot 4(\text{C}_6\text{H}_5\text{CH}_3)_2\text{b}$ and which were not assigned to the $\text{LiI} \cdot \text{H}_2\text{O}$ PXRD pattern, as given in Figure 4.58, could be due to $\text{H}_2\text{C}(\text{Ph}_2\text{PS})_2$. Comparison of this PXRD pattern with the PXRD patterns of the two known polymorphs of the neutral ligand indicated that the second phase was neither of these species. Comparison of this second phase with calculated PXRD patterns of the desired product,⁸ other samarium complexes of $[\text{C}(\text{Ph}_2\text{PS})_2]^{2-}$ species and its derivatives and other lithium salts of these ligand species, all of which could have been formed as by-products of the reaction or of other possible reactions, yielded no similarities with the experimental PXRD pattern.^{8,30,35,108,112} This therefore indicated that the second phase was due to a novel species, likely containing a $[\text{C}(\text{Ph}_2\text{PS})_2]^{2-}$ species or its derivatives, including the neutral ligand. Work on indexing an unit cell determination of this solid is ongoing.

4.1.3.3.5. Conclusion.

For a number of the solids obtained from the reactions undergone in the attempts to synthesise the lanthanide carbene complex $[\text{Sm}_2(\text{C}(\text{Ph}_2\text{PS})_2)_2\text{I}_2\text{THF}_4]$, the major component remained the free protonated ligand, $\text{H}_2\text{C}(\text{Ph}_2\text{PS})_2$, as inferred from both IR and ^1H NMR data. Comparison of the IR data obtained for these products to the data obtained and discussed in Section 4.1.1.3.1 on the polymorphs of this ligand indicated that both the $P2_1/c$ and $C2/c$ polymorphs of this ligand were observed to form on various occasions. This was especially true for the solids which were expected to be the LiI salt. Other solids, especially those precipitated from the final filtrate and which were expected to contain the desired product, gave IR spectra which indicated the presence of solids of an unknown composition, with only a few bands indicating the presence of the $\text{H}_2\text{C}(\text{Ph}_2\text{PS})_2$ ligand or its derivatives. The IR spectra of $[\text{Sm}_2(\text{C}(\text{Ph}_2\text{PS})_2)_2\text{I}_2\text{THF}_4] \cdot 4(\text{C}_6\text{H}_5\text{CH}_3)$ _1b and _4a_2 showed bands which could have indicated the presence of the mono and di-anionic derivatives of $\text{H}_2\text{C}(\text{Ph}_2\text{PS})_2$, thus indicating complexation.

The ^1H NMR data indicated the presence of free fully protonated $\text{H}_2\text{C}(\text{Ph}_2\text{PS})_2$ in the samples analysed by this technique. Therefore, the use of ^1H NMR was found to be problematic as it gave conflicting results with some of the respective IR data. This difference could be due to the re-protonation of the solids during sample preparation due to insufficiently dried deuterated solvents. The presence of coordinated Sm^{3+} in terms of peak broadening and shifts was also not observed in the samples studied.

Plane polarised microscopy indicated that many of the first products obtained from each synthesis attempt were possibly crystalline. In a number of cases this first product was subjected to reactions and extraction techniques to try to extract the expected product. The resultant products were typically pastes or gelatinous solids which clearly contained crystalline solids. Pastes which were possibly crystalline were also yielded from the precipitates obtained from the filtration of the original reaction mixture and obtained through layering. An exception was observed for reaction $[\text{Sm}_2(\text{C}(\text{Ph}_2\text{PS})_2)_2\text{I}_2\text{THF}_4] \cdot 4(\text{C}_6\text{H}_5\text{CH}_3)$ _3 which yielded a product that was clearly crystalline, namely $[\text{Sm}_2(\text{C}(\text{Ph}_2\text{PS})_2)_2\text{I}_2\text{THF}_4] \cdot 4(\text{C}_6\text{H}_5\text{CH}_3)$ _3b_2. However, this was identified in large parts to be the $\text{H}_2\text{C}(\text{Ph}_2\text{PS})_2$ ligand, as inferred through analysis by ^1H NMR and by inspection of the crystalline habit.

The PXRD data collected for the solids $[\text{Sm}_2(\text{C}(\text{Ph}_2\text{PS})_2)_2\text{I}_2\text{THF}_4] \cdot 4(\text{C}_6\text{H}_5\text{CH}_3)$ _2a_1 and $[\text{Sm}_2(\text{C}(\text{Ph}_2\text{PS})_2)_2\text{I}_2\text{THF}_4] \cdot 4(\text{C}_6\text{H}_5\text{CH}_3)$ _2b indicated that most likely both contained the LiI side product of the salt metathesis. In the case of the former this salt was obtained in an amorphous solid which may have also contained other inorganic species such as Sm^{3+} and which was significantly hydrated. In the case of $[\text{Sm}_2(\text{C}(\text{Ph}_2\text{PS})_2)_2\text{I}_2\text{THF}_4] \cdot 4(\text{C}_6\text{H}_5\text{CH}_3)$ _2b, which was obtained on precipitation of the initial filtration of the reaction mixture, crystalline $\text{LiI} \cdot \text{H}_2\text{O}$ was obtained along with at least one minor phase which seems to have been a lower symmetry crystalline phase. The presence of a hydrate of LiI also indicated that some moisture intrusion occurred either through the reaction or reagents. The novel second phase observed could be related to the presence of $\text{H}_2\text{C}(\text{Ph}_2\text{PS})_2$ (as described by IR data) or an $[\text{C}(\text{Ph}_2\text{PS})_2]^{2-}$ species or derivative. The presence of a derivative of this ligand was expected in this product given that the desired product is known to crystallise in the conditions in which this solid was obtained.

Overall the synthesis of the desired compound was found to be very difficult and its successful synthesis could not be proved from the IR, ^1H NMR and PXRD data obtained. This difficulty was most likely due to the intrusion of moisture or oxygen. This intrusion was observed for other compounds but not to the extent observed for this reaction.

4.1.3.4. Summary

This section addressed the characterisation of the products obtained from the attempts at synthesising lanthanide carbenes as described in Section 3.3.1.3. For each lanthanide carbene complex various attempts were undertaken either because the first product did not show the expected characteristics or to increase yield. All the carbene complexes were difficult to synthesise and characterise. For the products $[\text{Sm}(\text{C}(\text{Ph}_2\text{PNSiMe}_3)_2)(\text{NCy}_2)(\text{THF})]$ _1, _3 and _4 the possible formation of mono-anion derivatives was clear due to the presence of bands at $> 1110 \text{ cm}^{-1}$ but at a lower range than for the neutral ligand $\nu \text{ P=N}$ band at 1273 cm^{-1} . $[\text{Sm}(\text{C}(\text{Ph}_2\text{PNSiMe}_3)_2)(\text{NCy}_2)(\text{THF})]$ _1 indicated the possible presence of residual $[\text{Sm}(\text{NCy}_2)_3\text{THF}] \cdot \text{C}_6\text{H}_5\text{CH}_3$. The IR spectra of $[\text{Sm}(\text{C}(\text{Ph}_2\text{PNSiMe}_3)_2)(\text{NCy}_2)(\text{THF})]$ _3

and $_4$ showed certain similarities. $[\text{Sm}(\text{C}(\text{Ph}_2\text{PNSiMe}_3)_2)(\text{NCy}_2)(\text{THF})]_{_4}$ gave better quality data and showed that the mono-anionic species was the prevalent component. $[\text{Sm}(\text{C}(\text{Ph}_2\text{PNSiMe}_3)_2)(\text{NCy}_2)(\text{THF})]_{_2}$ had a significantly different IR spectrum than the other two products and this was determined to be composed of the neutral ligand decomposition product $\text{Ph}_2\text{P}(\text{O})\text{NH}_2$, by both IR and SXRD. PXRD analysis for $[\text{Sm}(\text{C}(\text{Ph}_2\text{PNSiMe}_3)_2)(\text{NCy}_2)(\text{THF})]_{_4}$ also showed the presence of decomposition products as minor components. For the two products obtained from separate reactions for the preparation of $[\text{Nd}(\text{C}(\text{Ph}_2\text{PNiPr})_2)(\text{HC}(\text{Ph}_2\text{PNiPr})_2)] \cdot 2\text{THF}$, dissimilar spectra were obtained with the spectrum of the product from the second reaction indicating a greater presence of the mono-anion as compared to the first product. Since both mono-anion and dianion were expected in the product the differences in the IR spectra of both anion species could not be used to conclusively characterise the desired compound. The differences in IR spectra of these two products $_1$ and $_2$ could however be due to the use of the $[\text{H}_2\text{C}(\text{Ph}_2\text{PNH}(i\text{Pr}))_2]\text{Br}_{_2_1}$ and $\text{K}(\text{HC}(\text{Ph}_2\text{PNiPr})_2)_{_2}$ as starting reagents respectively. Although all carbene complexes were difficult to synthesise and characterise the complex $[\text{Sm}_2(\text{C}(\text{Ph}_2\text{PS})_2)_2\text{I}_2\text{THF}_4] \cdot 4(\text{C}_6\text{H}_5\text{CH}_3)$ proved the most difficult to synthesise. Numerous species were obtained during the synthesis attempts of this compound and both IR and ^1H NMR data did not yield positive results in the characterisation of this compound. The products $[\text{Sm}_2(\text{C}(\text{Ph}_2\text{PS})_2)_2\text{I}_2\text{THF}_4] \cdot 4(\text{C}_6\text{H}_5\text{CH}_3)_{_1\text{b}}$ and $_4\text{a}_{_2}$ seemed to show IR spectra which most clearly indicated the possibility of the formation of the mono-anionic or dianionic derivatives although this data did not conclusively indicate the formation of the desired compound.

4.2. Lanthanide non-carbene di- $\lambda^5\sigma^4$ -phosphorane complexes

4.2.1. Ligands and ligand precursors

4.2.1.1. Characterisation of $\text{HN}(\text{Ph}_2\text{PO})_2$

In an attempt to synthesise $\text{HN}(\text{Ph}_2\text{PO})_2$, as described in Section 3.3.2.1.1, a single product was obtained, namely $\text{HN}(\text{Ph}_2\text{PO})_2\text{-1}$. This solid was obtained as a white crystalline solid and was characterised using IR and ^1H NMR spectroscopy and PXRD. The yield for $\text{HN}(\text{Ph}_2\text{PO})_2\text{-1}$ was of 82 %.

4.2.1.1.1. Analysis by Infra-red spectroscopy

The IR spectrum of $\text{HN}(\text{Ph}_2\text{PO})_2\text{-1}$ was collected using KBr pellet samples. These were compared to the spectrum of the starting reagent *N,N*-bis(diphenylphosphino)amine, ($\text{HN}(\text{Ph}_2\text{P})_2$), as shown in Figure 4.59.

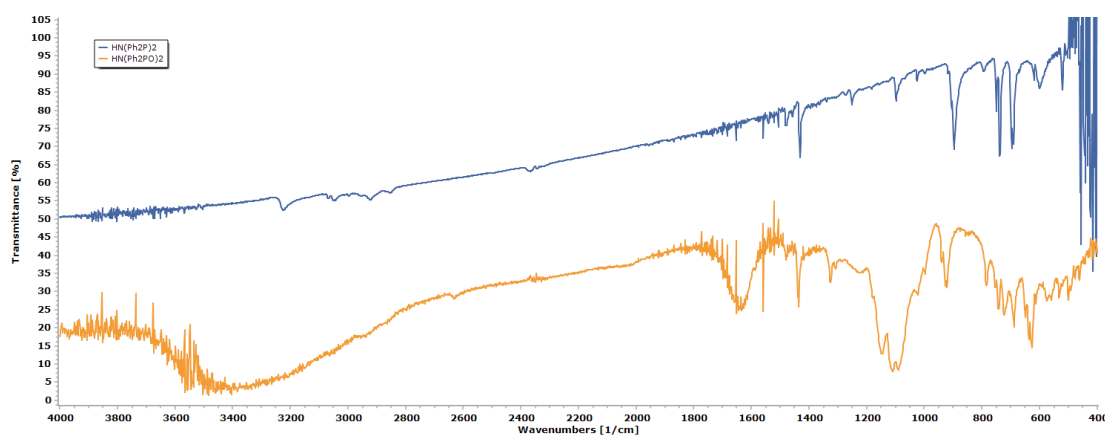


Figure 4.59: IR spectra of the starting reagent $\text{HN}(\text{Ph}_2\text{P})_2$ (blue) and the product $\text{HN}(\text{Ph}_2\text{PO})_2$ (orange).

IR spectroscopy indicated that the reaction was successful in the modification of the initial amine, as is clearly visible in Figure 4.59. The first noticeable features in the spectrum of the product were the bands at 3104 and 1645 cm^{-1} . These indicated the presence of ν O–H and δ O–H vibrations implying the presence of water. This water seems to be present in the sample, however it may not be water of crystallisation. This is inferred because of the broad nature of the bands, which is indicative of various modes of hydrogen bonding restricted vibrations.

A group of bands which were of interest in the IR spectrum of the oxide derivative were those of medium and weak intensities and observed at 1437 cm^{-1} , 754 cm^{-1} , 742 cm^{-1} , 740 cm^{-1} and 689 cm^{-1} . All these bands were believed to be due to numerous phosphorus to phenyl ring (P–Ph) vibrations and were clearly analogous to the $\text{HN}(\text{Ph}_2\text{P})_2$ bands at 1431 cm^{-1} , 750 cm^{-1} , 738 cm^{-1} , 697 cm^{-1} and 691 cm^{-1} . These bands are typical for all phenyl phosphine derivatives. The presence of these bands in the product was indicative of the retention of the phenyl phosphine groups as they were part of the backbone structure common to both the starting reagent and the product.

Another two groups of bands observed in both the IR spectrum of the product and that of the starting reagent were of interest, as these also indicated that the skeletal structure was common for both compounds in question and thus confirmed that this structure was maintained in the product. For the IR spectrum of the product the first of these groups of bands were the cluster of bands at 939 cm^{-1} , 928 cm^{-1} and 923 cm^{-1} , while the second group dealt with bands in the range 800–500 cm^{-1} namely the bands at 784 cm^{-1} , 649 cm^{-1} , 638 cm^{-1} , 625 cm^{-1} and 575 cm^{-1} . These groups have not been identified as pertaining to P–Ph vibrations as described prior. The cluster of bands at 939 cm^{-1} , 928 cm^{-1} and 923 cm^{-1} were believed to be analogous to the bands at 905 and 896 cm^{-1} for the starting reagent and the bands for both spectra were in the range expected for the asymmetric stretching vibration of the central P–NH–P (ν_{as} P–NH–P) skeletal moiety. The bands described in the range 800–500 cm^{-1} were considered to be due to the symmetric vibration ν_{s} P–NH–P and were believed to be analogous to the bands at 794 cm^{-1} , 600 cm^{-1} and 521 cm^{-1} present in the IR spectrum of $\text{HN}(\text{Ph}_2\text{P})_2$. The $\sim 30 \text{ cm}^{-1}$ shift to higher wavenumber values in the bands assigned to the ν_{as} P–NH–P was indicative of an increase in vibration stiffness of the P–N bond, typically due to increased bond order. However, it should be noted that ν P=N vibrations typically fall in the range 1425 to 1125 cm^{-1} . Therefore, the bond order can be tentatively described as < 2 . The numerous bands in the region 800–500 cm^{-1} could not be analysed in greater detail and therefore little structural information could be gathered from this region.

Finally, the most relevant bands in the spectrum of the product, with regards to the current discussion, were the shoulder at 1180 cm^{-1} and the very strong bands at 1148 cm^{-1} , 1110 cm^{-1} and 1089 cm^{-1} . These fall in the very low range of the region typical for the ν P=O vibrations, indicating the formation of the expected P=O bonds in the product. The low wavenumber values were interesting in that they indicated some diminished bond order. This could be complementary to the possible increased bond

order of the skeletal P–N bonds. Both orthophosphates and metaphosphates absorb in this region which typically contain P–O bonds of bond order 1 to 2, again indicating a decreased bond order in the P–O bond in the product.³⁴⁸

The assignment of the weak bands at 1325 cm⁻¹ and 1309 cm⁻¹ is more difficult since these fell in the middle range typical of the ν P=O and the ν P=N vibrations. All these band assignments are given in Figure 4.60 for clarity.

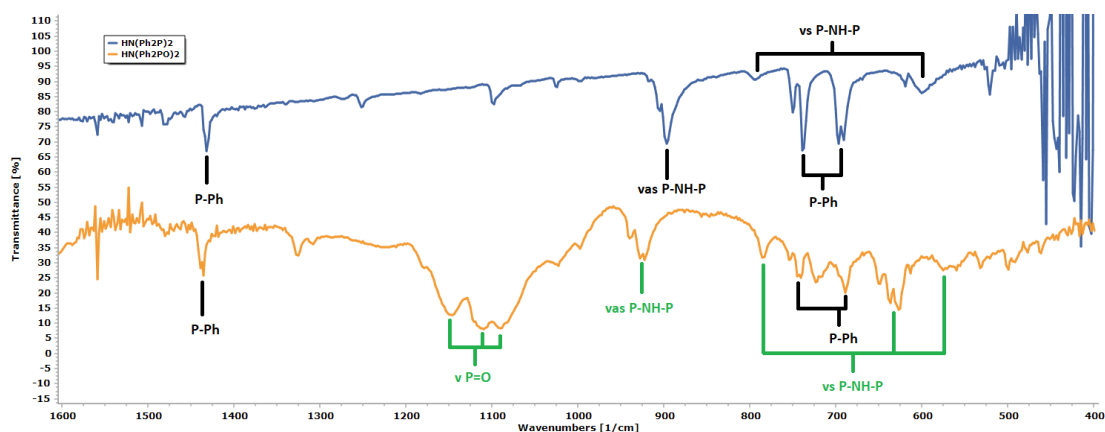


Figure 4.60: Assignment of bands in the IR spectrum of HN(Ph₂PO)₂_1, as described for the proposed amine tautomer and for the spectrum of the starting reagent.

IR spectral data for HN(Ph₂PO)₂ has been published previously by Gilson and Sisler, wherein the bands at 1330 cm⁻¹, 1310 cm⁻¹, 1190 cm⁻¹, 1120 cm⁻¹, 1110 cm⁻¹ and 935 cm⁻¹ were described.³⁶³ However, details regarding the intensities of these bands were not published. The bands at 1330 cm⁻¹, 1310 cm⁻¹ and 935 cm⁻¹ seem to be closely analogous to the bands at 1325 cm⁻¹ and 1309 cm⁻¹ obtained in this study, together with the cluster of bands around 928 cm⁻¹. The bands at 1120 cm⁻¹ and 1110 cm⁻¹ fall in the same range as the strong bands around 1148 cm⁻¹, 1110 cm⁻¹ and 1089 cm⁻¹ of the current study, while the published band at 1190 cm⁻¹ could only be related to the shoulder at 1180 cm⁻¹. In the publication by Gilson and Sisler the only band discussed in detail is the band at 935 cm⁻¹ which is described, as in the current discussion, to be indicative of the ν_{as} P–NH–P vibration.

The IR spectrum obtained in the current study can also be interpreted in the light of the structure previously published by Nöth in 1982, and given in Figure 4.61.²³⁶

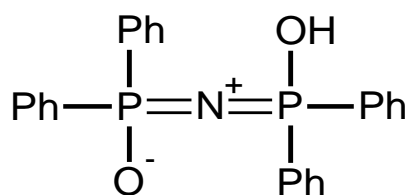


Figure 4.61: Molecular diagram of tautomer structure for $\text{HN}(\text{Ph}_2\text{PO})_2$ published by Nöth in 1982.

Taking this structure into consideration different band assignments could be given to the IR data obtained in the current study. The band at 3104 cm^{-1} , given in Figure 4.59, could be either due to the expected $\nu \text{ O-H}$ vibration or due to an overlap of these expected vibrations with $\nu \text{ O-H}$ vibrations arising from moisture intrusion. The bands at 1437 cm^{-1} , 754 cm^{-1} , 742 cm^{-1} , 740 cm^{-1} and 689 cm^{-1} could still be assigned to P-Ph vibrations. The assignment of the bands at 1325 cm^{-1} and 1309 cm^{-1} remained problematic because of the fact that they could be attributed to both $\nu \text{ P=O}$ and the $\nu \text{ P=N}$ vibrations and also because of their weak intensities. The major differences between the two tautomers arose in the assignment of the bands at 1180 cm^{-1} , 1148 cm^{-1} , 1110 cm^{-1} , 1089 cm^{-1} , the cluster at around 928 cm^{-1} , and the bands in the range $800\text{--}500 \text{ cm}^{-1}$ which were not assigned to P-Ph vibrations. A tentative assignment could be attempted to fit the IR data with the published structure.

As discussed previously, the bands in the range $1180\text{--}1080 \text{ cm}^{-1}$ could be attributed to either $\nu \text{ P=O}$ or $\nu \text{ P=N}$ vibrations. In this region it is also possible to assign bands to higher bond order $\nu \text{ P}^+\text{-O}^-$ vibrations, typical of orthophosphate and metaphosphate ions. The bands clustered around 928 cm^{-1} were tentatively attributed to the bending $\delta \text{ P-O-H}$, if the P-N bonds are of a higher bonding order, thus putting their vibrational modes in the range $1180\text{--}1080 \text{ cm}^{-1}$, as described prior. The bands in the range $800\text{--}500 \text{ cm}^{-1}$ and which were not assigned to P-Ph vibrations could not be easily assigned to the published structure. These band assignments in the fingerprint region are given in Figure 4.62 for clarity.

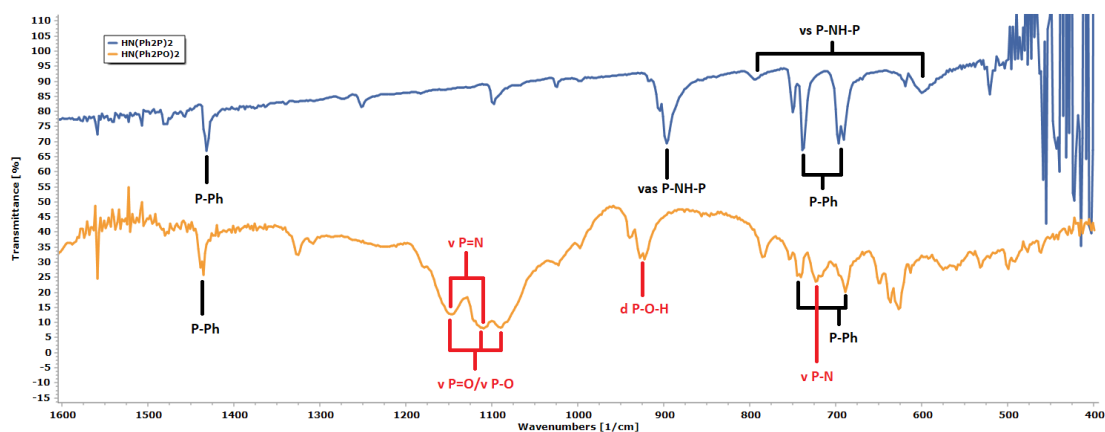


Figure 4.62: Assignment of bands in the $\text{HN}(\text{Ph}_2\text{PO})_2$ product, as described for the tautomer proposed by Nöth in 1982 and for the spectrum of the starting reagent.

Therefore, the analytical band which could be mainly used to tentatively distinguish between the two possible tautomers was the cluster around 928 cm^{-1} . This cluster not only occurred in the expected range but it also held significant intensity and structure similarities to the analogous band in the starting reagent. This indicated that the same skeletal structure (P-NH-P) is found in both the reagent and the product and therefore a previously uncharacterised structure was obtained rather than the published tautomer structure. The bands in the region $1180\text{--}1080\text{ cm}^{-1}$ could be tentatively described for both structures of the product and therefore do not allow for a better characterisation of the structure.

4.2.1.1.2. Analysis by ^1H NMR spectroscopy

The compound was also characterised by ^1H NMR Spectroscopy. Previous work on this compound published ^1H NMR data that only detailed out the presence of aromatic proton peaks, namely a multiplet at $7.80\text{--}7.65\text{ ppm}$ (8H) and another multiplet at $7.48\text{--}7.27\text{ ppm}$ (12H).³² The 2:3 ratio of the integration values for the two multiplets indicate either a meta versus ortho/para or an ortho versus meta/para split. Data regarding peaks due to the proton of the P-NH-P or $\text{O}^-\text{P}=\text{N}^+=\text{P-OH}$ is not given in literature and therefore no comparison could be undergone.

In the current work, the spectrum obtained contained three peaks in the typical aromatic ring proton region, namely at 7.83 ppm (8H), 7.41 ppm (4H) and 7.32 ppm (8H), as shown in Figure 4.63. The integration values indicated a similar separation of the aromatic proton peaks as published prior. The triplet at 7.41 ppm was indicative of the

symmetric para protons of the aromatic rings. This was further confirmed by the integration value for this triplet. The fact that this peak was obtained as a triplet was indicative that the aromatic rings in the compounds have clear reflection symmetry, orthogonal to the plane of the aromatic ring running parallel to the para protons. Therefore, the doublet of doublets at 7.83 ppm and the multiplet at 7.32 ppm were believed to be due to the ortho and meta aromatic protons respectively. The integration values substantiated this idea, however they gave no indication as to which peak represented which protons. Coupling data for the doublet of doublets at 7.83 ppm indicated a proton with two distinct NMR active neighbours. Two coupling constants were confirmed for this peak, namely $J_1 = 7.75$ Hz and $J_2 = 12.67$ Hz, as given in Figure 4.64. The latter of these is typical of the $^3J_{HP}$ constants of the ortho aromatic protons vicinal to the phosphorus centers of various di- $\lambda^5\sigma^4$ -phosphorane compounds which are analogous to $\text{HN}(\text{Ph}_2\text{PO})_2$.^{364,365} These J values indicate that the ortho aromatic protons were the most deshielded which is a typical effect of electron withdrawing groups.

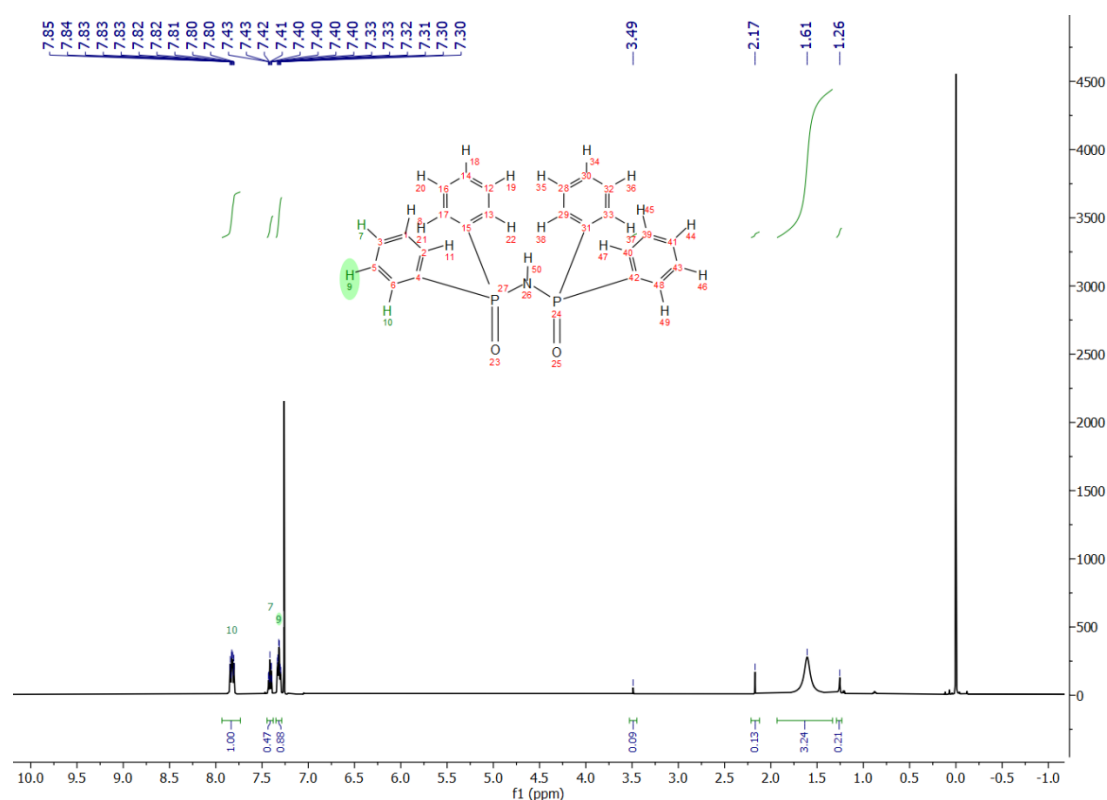


Figure 4.63: ^1H NMR spectrum of $\text{HN}(\text{Ph}_2\text{PO})_2_1$.

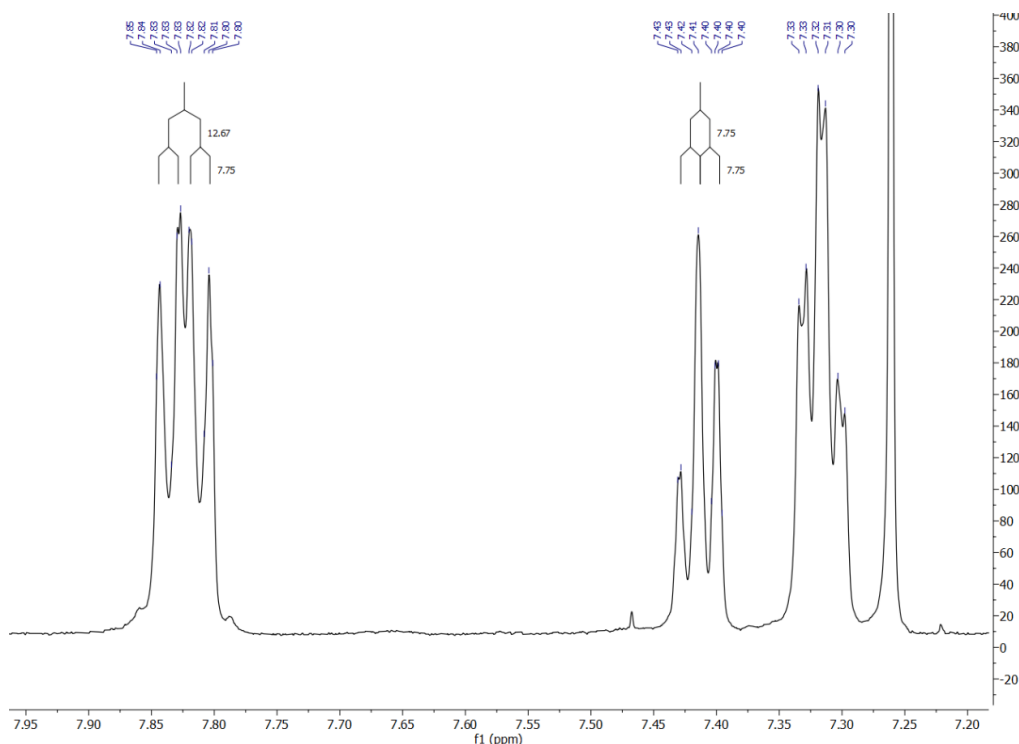


Figure 4.64: ^1H NMR spectrum of $\text{HN}(\text{Ph}_2\text{PO})_2_1$ showing multiplet structures for the peaks believed to be due to the ortho and para protons.

This deshielding of the ortho and para aromatic protons is known for many aromatic P(V) derivatives. This occurs since the P(V) centre tends to act as a weak inductive electron withdrawing group and a stronger mesomeric electron withdrawing group causing deshielding of ortho and para protons on the aromatic rings.³⁶⁶ The mesomeric electron withdrawing property in such compounds could be due to either $\text{C}(\text{p}\pi)\text{--P}(\text{d}\pi)$ bonding or negative hyperconjugation of the type $\text{C}(\text{p}\pi)\rightarrow\text{P}(\sigma^*)$.³⁶⁶ Therefore, the structure of the deshielding of the aromatic protons in the product was indicative of the formation of a P–O bond, however information on the bond order cannot be obtained from this data.

The assignment of the expected amine proton was more problematic. It is known that alcohol and amine protons fall in similar ranges in ^1H NMR spectroscopy. A number of ^1H NMR spectra were obtained for the same solid obtained from different trials of the same reaction and in one sample only was a singular peak obtained as a singlet at 4.39 ppm. This was the only case in which the various ^1H NMR spectra gave a peak which fell in the expected range and the peak had an integration value which was as expected in relation to the values obtained for the aromatic protons. This was also in agreement with previously published data.³⁶⁷ The only issue was the singlet nature of the

peak, as a triplet was expected in this case, but this could have been due to the quadrupolar nature of the amine nitrogen. The same triplet would have been expected in the tautomer containing an alcohol group. Nonetheless the expected N–H or O–H proton peak could not be used to determine structural information on the compound in question. Minor impurity peaks for water (1.61 ppm), acetone (2.17 ppm) and grease (1.26 ppm) were noted in the spectrum.

4.2.1.1.3. Analysis by Melting point determination.

The melting point of the solid obtained was recorded as being in the range 274.1 - 276.1 °C. This was higher than the melting point provided in literature, which is of 268 - 269 °C.^{278,363} The higher melting point of the solid obtained during synthesis could have been indicative of a polymorph other than that obtained in literature, with stronger intermolecular interactions.

4.2.1.1.4. Analysis by Powder X-ray diffraction

PXRD data for the product HN(Ph₂PO)₂_1 was collected using Cu-K_{α1} radiation. The raw data was indexed and Pawley refinement undertaken using DASH 3.4.1. This gave a viable unit cell with parameters and relevant statistics given in Table 4.12.

Table 4.12: Cell parameters and statistics for unit cell obtained through indexing and Pawley refinement of HN(Ph₂PO)₂_1.

Space group	<i>P2</i>
<i>a</i>	17.808(4) Å
<i>b</i>	6.068(2) Å
<i>c</i>	11.466(1) Å
β	119.43°
<i>V</i>	1079.1 Å ³
<i>R</i> _{wp}	2.72
<i>R</i> _{exp}	1.47
χ^2	3.00

Structure solution and refinement were undertaken using TOPAS6.1. Structure solution was undergone through simulated annealing. Unit cell parameters for the refined structure are given in Table 4.13. The unit cell obtained through structure solution is given in Figure 4.65.

Table 4.13: Unit cell parameters for the structure solution of HN(Ph₂PO)₂_1.

Space group	<i>P</i> 2
<i>a</i>	17.816 Å
<i>b</i>	6.068 Å
<i>c</i>	11.471 Å
β	119.45°
<i>V</i>	1079.9 Å ³

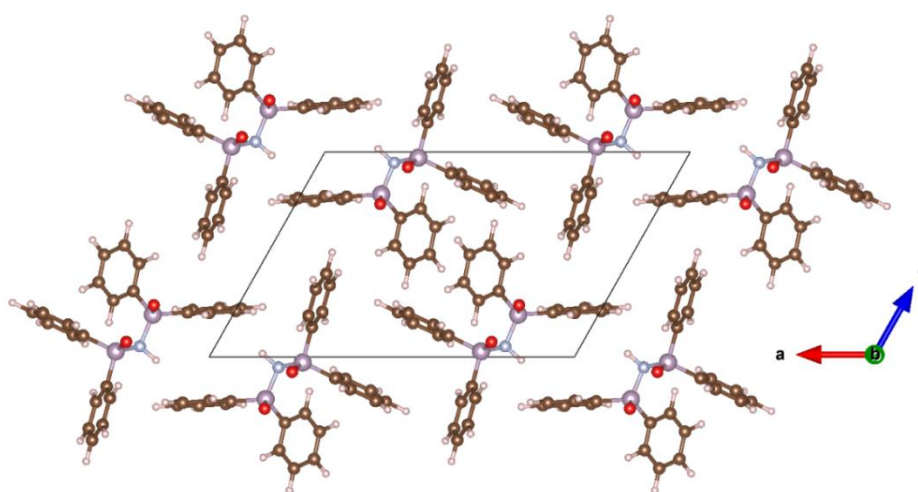


Figure 4.65: Completed unit cell for the crystal structure obtained for HN(Ph₂PO)₂_1.

This compound was characterised through SXRD data by Nöth in 1982.²³⁶ In that study a different crystalline form was found, containing the tautomer described in Figure 4.61. Given the formation of different tautomers between the study performed by Nöth and the current study, it was evident that the crystal structures would be different. This makes the structure identified in this study and labelled as HN(Ph₂PO)₂_1 the first crystal and molecular structure for this tautomer of HN(Ph₂PO)₂ known to the author. This also indicates that the first IR band assignment given previously fully supports this structure.

The first evident structural characteristic observed in this structure was the clear significant impact of the phenyl groups on packing. Viewing the unit cell along the *b* axis, as shown in Figure 4.65, clearly illustrates that the molecules are significantly affected by the intermolecular interactions of these phenyl rings, which appear to be more significant than the intermolecular interactions of the O=P–N(H)–P=O moiety. The packing structure can be easily described as parallel chains in the direction of the *a* axis, in which the molecules are bound together by two alternating synthons as given in Figure 4.66. In this figure the first synthon is shown enclosed in green, wherein this important synthon is formed through short contact interactions between the amine N–H and the phenyl para C–H group. The second synthon is shown enclosed in red, wherein the main interactions are short contact interactions between the phenyl para C–H proton and geminal ortho and meta phenyl carbons. This could indicate the formation of a C–H--- π Ph interaction maintaining this synthon. In the *b* axis contacts are minimal and occur mainly through the P=O--- π Ph interactions.

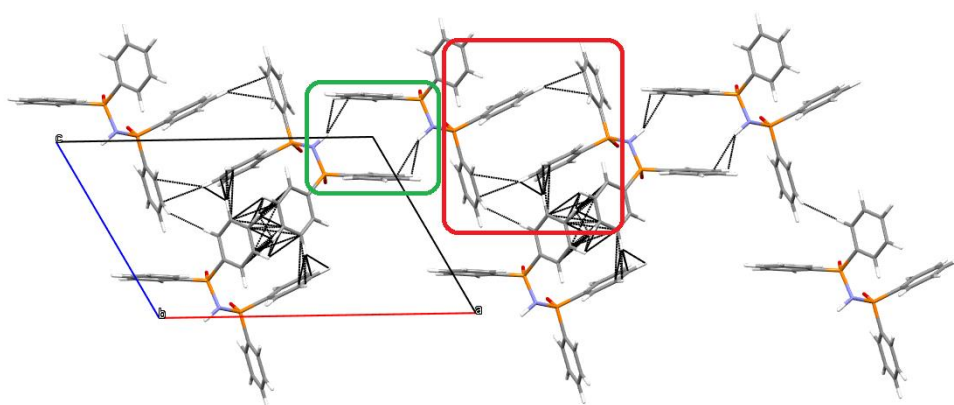


Figure 4.66: Packing structure for HN(Ph₂PO)₂_1 crystals, with major synthons shown in sections enclosed in green and red.

Another structural feature of interest is the near eclipsed structure about the phosphorus centres obtained for the non-backbone groups. Typically structures of compounds having a general formula of HN(R₂PY)₂ (where Y = O/S/Se) fall qualitatively in two distinct categories as regards molecular structure conformations.^{217–221,236,368–373} These are described here as staggered and eclipsed conformations, with Newman projection diagrams as given in Figure 4.67a and b and structures as shown in Figure 4.68a and b respectively. Only the structure of HN(*i*Pr₂PO)₂ deviates from this by forming a staggered structure wherein the O atoms are found in gauche conformation rather than

the anti-conformation described for the remainder of the staggered conformations observed in literature and described here.²²⁰ In the case of the structure obtained in this study an eclipsed conformation was obtained, similar to that given in Figure 4.68b. However, it is the oxygen atoms that are eclipsed rather than the expected phenyl and oxygen groups. This eclipsing is given in Figure 4.69. The formation of this structure is unknown to the author and suggests that the interactions of the phenyl and amine moieties, generally considered weak, seem to have a greater impact in packing in the crystal structure obtained in this study.

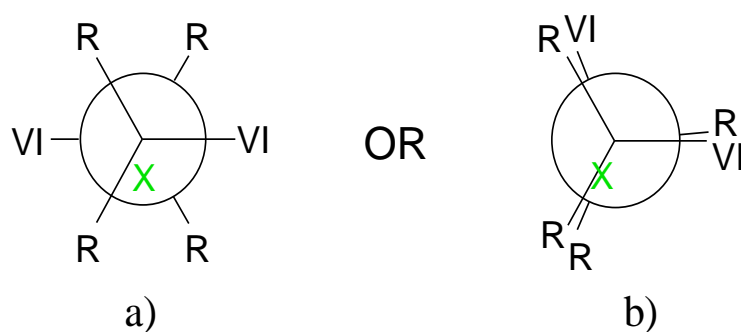


Figure 4.67: Newman Diagrams of a) staggered and b) eclipsed conformations typical of $\text{HN}(\text{R}_2\text{P}(\text{VI}))_2$ (where VI = O/S/Se), green X represents the position of the central nitrogen in the structure.

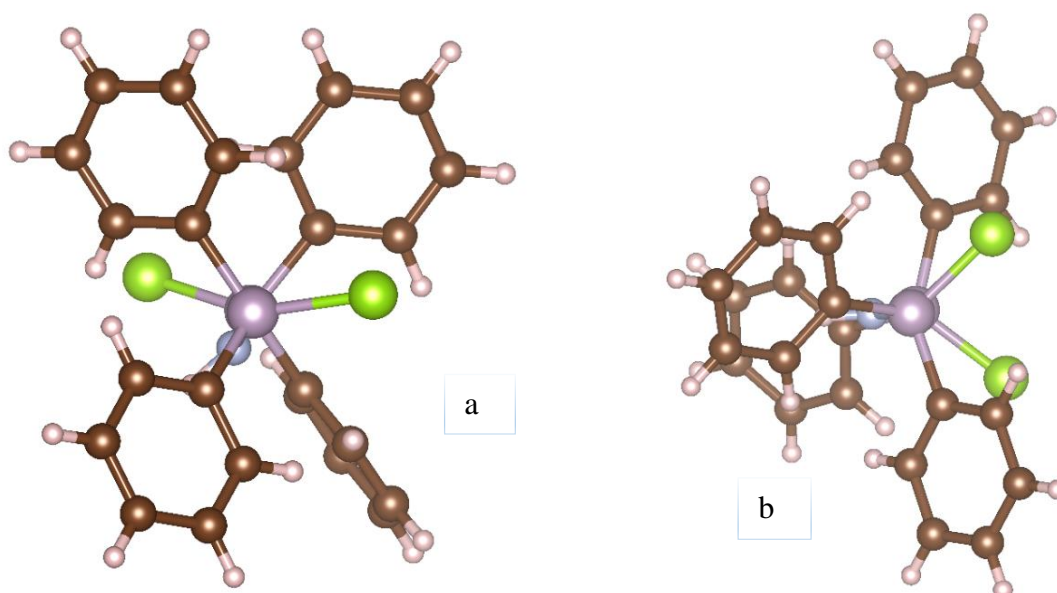


Figure 4.68: Example for crystalline structures in a) staggered and b) eclipsed conformations for polymorphs of $\text{HN}(\text{Ph}_2\text{PSe})_2$.

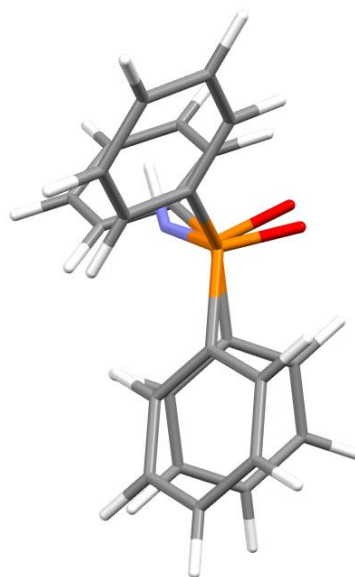


Figure 4.69: Eclipsed conformation observed for the molecular structure of $\text{HN}(\text{Ph}_2\text{PO})_2_1$.

4.2.1.1.5. Conclusion

The synthesis of the desired product in $\text{HN}(\text{R}_2\text{PO})_2_1$ was confirmed using IR and ^1H NMR spectroscopy. The discussion above ensued by comparing results obtained from the characterisation of this product to previously published data. This product was also characterised using PXRD, which yielded a crystal structure which was not previously published. The product was crystallised as an amine tautomer of the previously identified alcoholic tautomer, the structure of which was solved through SXRD data and previously published. This crystalline product also showed packing through two main synthons which was not expected given the presence of $\text{P}=\text{O}$ and $\text{N}-\text{H}$ groups which are believed to form Hydrogen bonding easily.

4.2.1.2. Characterisation of $\text{HN}(\text{Ph}_2\text{PS})_2$

Bis(diphenylthiophosphinoyl)imine, $\text{HN}(\text{Ph}_2\text{PS})_2$, was prepared as described in Section 3.3.2.1.2., using a method derived from that published by Wang and co-workers in 1978.²⁷⁸ The product obtained was a colourless crystalline solid with a yield of 69%.

4.2.1.2.1. Analysis by Infra-red spectroscopy

The product $\text{HN}(\text{Ph}_2\text{PS})_2_1$ was analysed by IR spectroscopy. The IR of the product is given in Figure 4.70, along with the spectrum of the starting reagent, $\text{HN}(\text{Ph}_2\text{P})_2$. It was noticed that the reagent band at 3225 cm^{-1} , which is assigned to the ν N–H vibration in $\text{HN}(\text{Ph}_2\text{P})_2$, was lost in the spectrum of the product. This was unexpected, although it was possible that this band might be obscured by the broader band at 3030 cm^{-1} in the spectrum of the product. This broad band was most likely due to ν O–H vibrations of any water present in the sample. However, the expected δ O–H vibration band for water at about 1620 cm^{-1} was not observed. This broad band also obscured the bands typical of the aromatic ν C–H vibrations. The major differences expected between the IR spectra of the starting reagent and that of the expected product should lie in the bands typically assigned to the ν P–N–P and ν P=S vibrations.

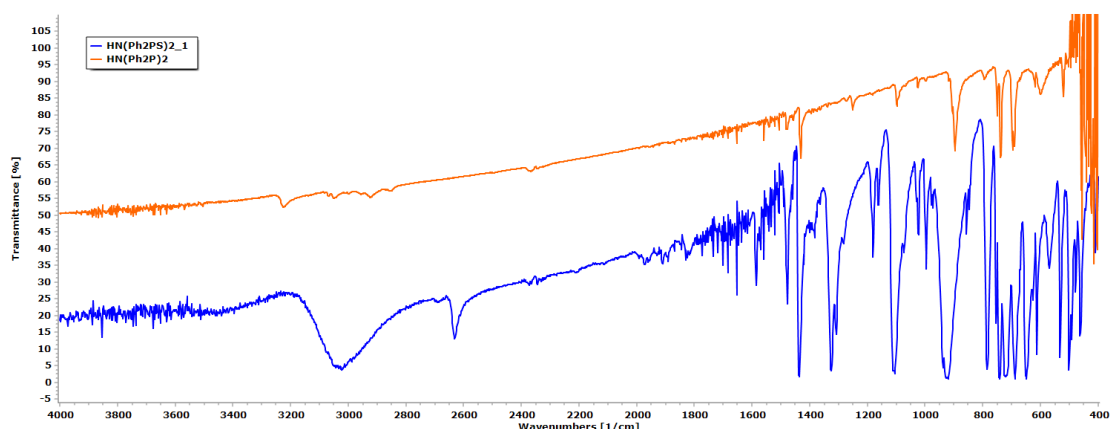


Figure 4.70: IR spectra of $\text{HN}(\text{Ph}_2\text{PS})_2_1$ (blue) and $\text{HN}(\text{Ph}_2\text{P})_2$ (orange).

A detailed discussion of IR data regarding this compound was published by McQuillan and Oxtan in 1977 and therefore comparison with this data was undertaken as discussed hereunder.³⁷⁴ The experimental bands at 937 cm^{-1} and 924 cm^{-1} for the product spectrum, as given in Figure 4.71, were clearly assigned to the ν_{as} P–N–P vibrations and these were shifted from the band due to the same vibrations in the spectrum of the $\text{HN}(\text{Ph}_2\text{P})_2$ reagent, at 896 cm^{-1} . This was confirmed in the publication mentioned above, with regards to similar bands observed at 935 cm^{-1} and 922 cm^{-1} respectively. The increase in wavenumber is a trait of shifting from a $\lambda^3\sigma^3$ to a $\lambda^5\sigma^4$ phosphorane as described in greater detail in Section 4.2.1.1.1, with reference to the IR data of

HN(Ph₂PO)₂1. A number of bands in the experimental IR spectrum fell in the region typical of bands associated with the ν_s P–N–P, ν P=S and P–Ph vibrations, namely at wavenumbers lower than 800 cm⁻¹. The bands falling between 754 cm⁻¹ and 688 cm⁻¹ were believed to be due to the P–Ph vibrations, as was the case for similar and analogous bands in the spectrum of the HN(Ph₂P)₂ reagent and therefore were not considered in detail.

The remaining bands could not be assigned specifically to either ν_s P–N–P or ν P=S vibrations. However, when compared to the spectra of the analogous H₂C(Ph₂PS)₂ it could be speculated that the bands that fall at a wavenumber lower than 660 cm⁻¹ can be assigned to ν P=S vibrations. The previously published data indicates that the band at 785 cm⁻¹ could be assigned to the ν_s P–N–P vibration while the bands at 648 cm⁻¹ and 627 cm⁻¹ could be assigned to the ν P=S vibrations. The latter inference is in agreement with the observations in Section 4.1.1.3.1 for the analogous H₂C(Ph₂PS)₂. These proposed assignments are given in Figure 4.71.

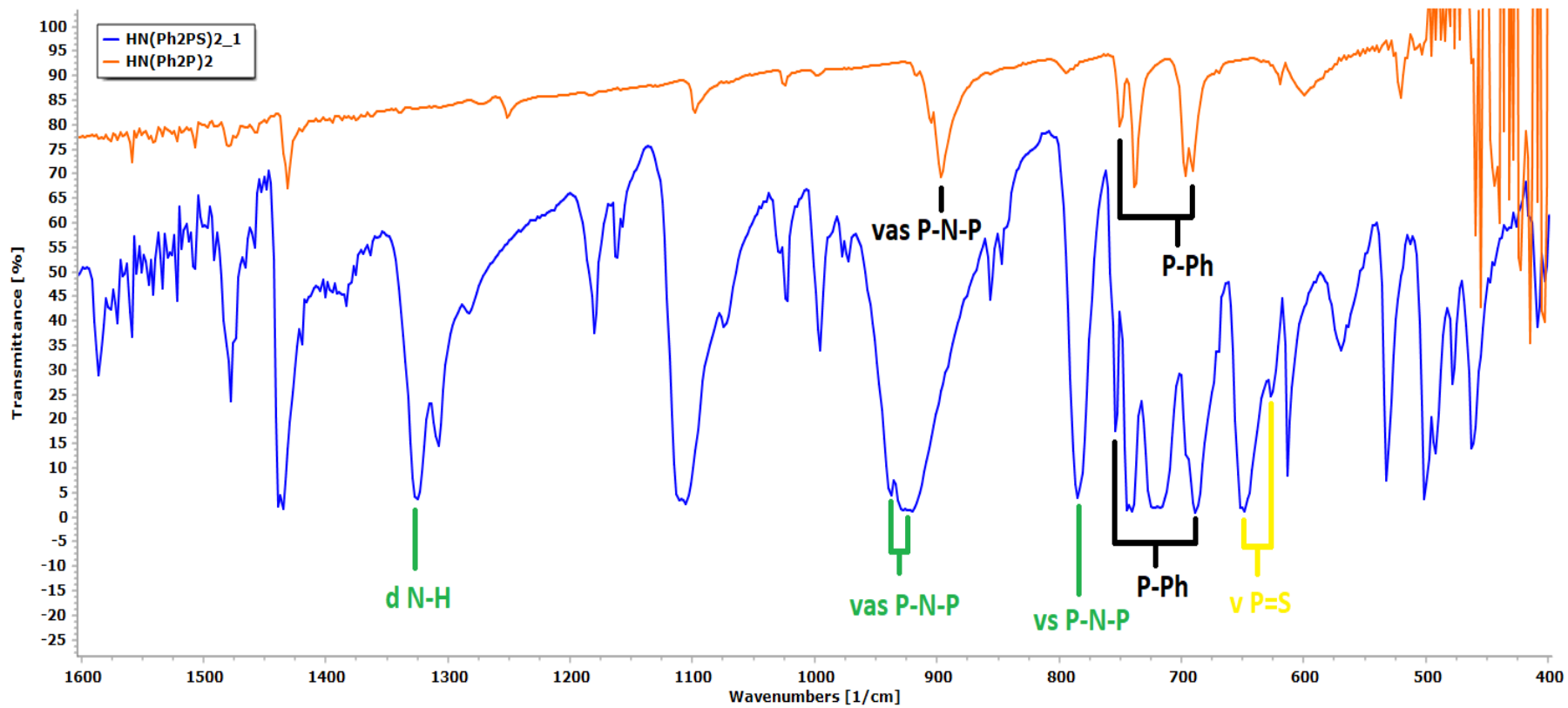


Figure 4.71: Details of IR spectra of HN(Ph₂PS)_{2_1} (blue) and HN(Ph₂P)₂ (orange) in the range 1600-400 cm⁻¹ with tentative assignments.

4.2.1.2.2. Analysis by ^1H NMR spectroscopy

The ^1H NMR spectrum obtained for the product $\text{HN}(\text{Ph}_2\text{PS})_2_1$, is given in Figure 4.72. This spectrum was similar to what was expected and to the spectrum of the product $\text{HN}(\text{Ph}_2\text{PO})_2_1$ as described in Figure 4.63 in Section 4.2.1.1.2.

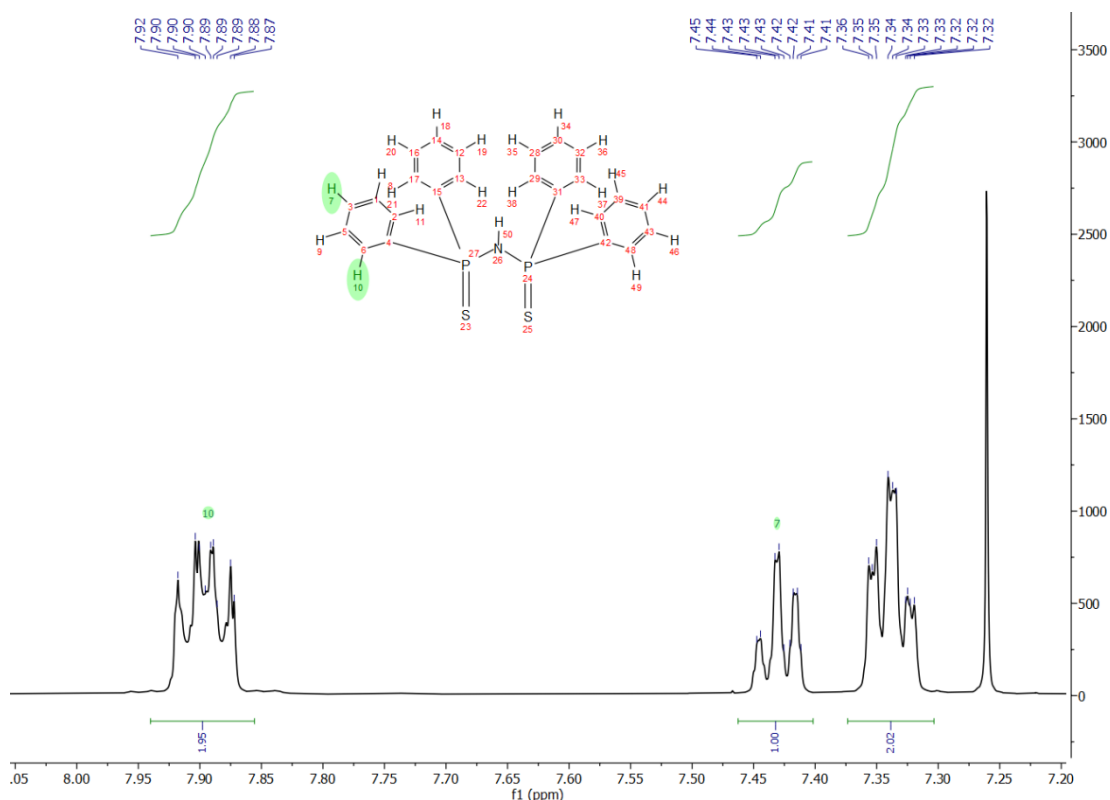


Figure 4.72: ^1H NMR spectrum of $\text{HN}(\text{Ph}_2\text{PS})_2_1$ showing the peaks in the aromatic region.

The ^1H NMR data in the current work gave the expected three peaks which are typically found in the aromatic ring proton region, namely at 7.89 ppm, 7.43 ppm and 7.34 ppm, with respective integration value data of 1.95:1.00:2.02. This ratio was in line with the expected proton ratio of 8:4:8 for the desired compound. Given the integration values the triplet at 7.43 ppm was assigned to the para aromatic protons. The coupling constant of 7.48 Hz for the same peak supported this assignment with the coupling being $^3J_{\text{HH}}$ between the para and meta protons. The two remaining peaks could be described as the ortho and meta proton peaks respectively. The doublet of doublets at 7.89 ppm indicated a proton with two distinct NMR active neighbours and this was corroborated by the two distinct coupling constants, $J_1 = 6.94$ Hz and $J_2 = 12.59$ Hz. The latter of these was typical of the $^3J_{\text{HP}}$ constants of the ortho aromatic protons vicinal to the phosphorus

centers of various di- $\lambda^5\sigma^4$ -phosphorane compounds, which are analogous to $\text{HN}(\text{Ph}_2\text{PS})_2$.^{364,365} This led to the doublet of triplets at 7.34 ppm being assigned to the meta aromatic protons, with coupling constants of $J_1 = 3.43$ Hz and $J_2 = 7.59$ Hz.

This deshielding of the ortho and para aromatic protons is known for many aromatic P(V) derivatives. This occurs since the P(V) centre tends to act as a weak inductive electron withdrawing group and a stronger mesomeric electron withdrawing group causing deshielding of ortho and para protons on the aromatic rings.³⁶⁶ The mesomeric electron withdrawing property in such compounds may be due to either $\text{C}(\text{p}_\pi)\text{-P}(\text{d}_\pi)$ bonding or negative hyperconjugation of the type $\text{C}(\text{p}_\pi)\rightarrow\text{P}(\sigma^*)$.³⁶⁶ Therefore, the structure of the deshielding of the aromatic protons in the product was indicative of the formation of a P=S bond, however information on the bond order cannot be obtained from this data.

The assignment of the expected amine proton in the product $\text{HN}(\text{Ph}_2\text{PS})_2\text{-1}$ proved to be problematic, as was the case with $\text{HN}(\text{Ph}_2\text{PO})_2\text{-1}$. Two peaks were observed in the typical amine proton region, however neither yielded the desired integration values. Both were singlets, although they do not show the broadening typical of N-H proton peaks effected by the quadrupole of the nitrogen atom.

4.2.1.2.3. Analysis by Powder X-ray diffraction

Given the lack of heavy metal components, Powder X-ray diffraction data for $\text{HN}(\text{Ph}_2\text{PS})_2\text{-1}$ was collected using a $\text{Cu-K}_{\alpha 1}$ source. The diffraction pattern was compared to previously published data obtained from ConQuest,²²⁵ for the structure of $\text{HN}(\text{Ph}_2\text{PS})_2$ published by Husebye and Maartmann-Moe in 1983.²²² This comparison is shown in Figure 4.73. The close similarity between the 2θ and intensity values clearly indicated that the crystalline product obtained in the current study was the same as that published and therefore the compound synthesised was most likely identical. This conformity between the experimental and literature data clearly indicated that the desired product was not only obtained but also that it was produced in the same crystalline form as that published previously in *P-1*.

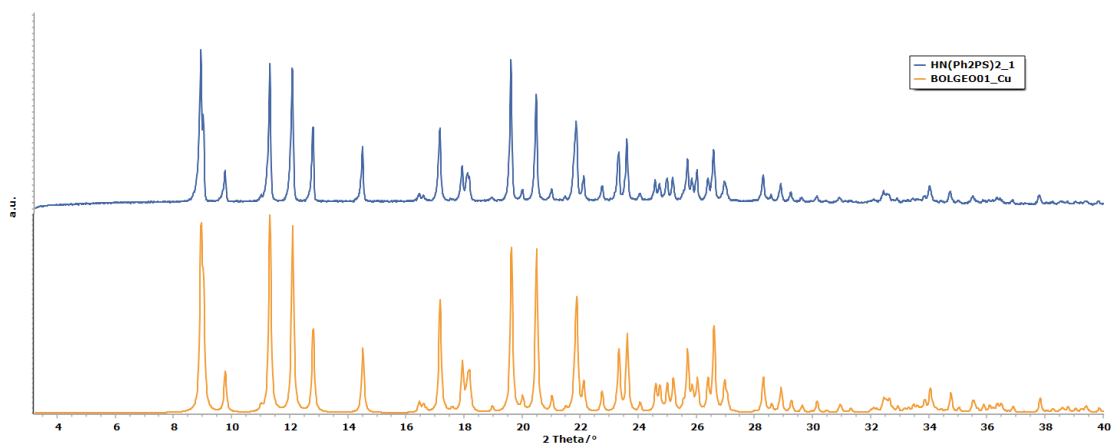


Figure 4.73: PXRD patterns of HN(Ph₂PS)₂_1 (blue) and the same product published in literature by Husebye and Maartmann-Moe (orange).

4.2.1.2.4. Conclusion

The IR spectrum for the product HN(Ph₂PS)₂_1 was in agreement with previously published data, indicating that the structure was of the amine tautomer rather than a sulphide tautomer. Therefore, this indicated that the desired product was obtained. The data obtained from the PXRD pattern was also conclusive in determining that the desired compound was obtained in the product HN(Ph₂PS)₂_1. ¹H NMR data indicated the formation of the desired compound with the aromatic protons shielding and coupling constants' pattern indicative of the oxidation of the P(III) in the starting reagent to the P(V) in the product. With regards to all the data obtained the preparation of HN(Ph₂PS)₂ was undergone favourably.

4.2.1.3. Characterisation of O((Et₂N)₂PO)₂

A number of attempts were undertaken to synthesise this compound and the one that yielded the best results was described in Section 3.3.2.1.3. Two physically distinct products were obtained, namely a colourless crystalline precipitate believed to be the expected side product Et₂NH₂Cl and a wine coloured liquid believed to be the desired product and labelled O((Et₂N)₂PO)₂_1. The yield of O((Et₂N)₂PO)₂_1 was 75 %.

4.2.1.3.1. Analysis by Infra-red spectroscopy

The synthesis of $O((Et_2N)_2PO)_2_1$ was fairly simple, as described in Section 3.3.2.1.3.2. However numerous solids and liquids were obtained during the workup procedure and all of these were analysed using IR spectroscopy. During the synthesis of $O((Et_2N)_2PO)_2_1$ a colourless crystalline solid mass was initially obtained. This was determined to be mainly composed of the expected side-product Et_2NH_2Cl , as described in Appendix 10. This indicated that the expected reaction, or a similar reaction occurred.

The final product obtained from the workup, $O((Et_2N)_2PO)_2_1$, was a wine coloured liquid. This was analysed by IR spectroscopy and the IR spectrum obtained was compared with the spectra of the starting reagents, as given in Figure 4.74.

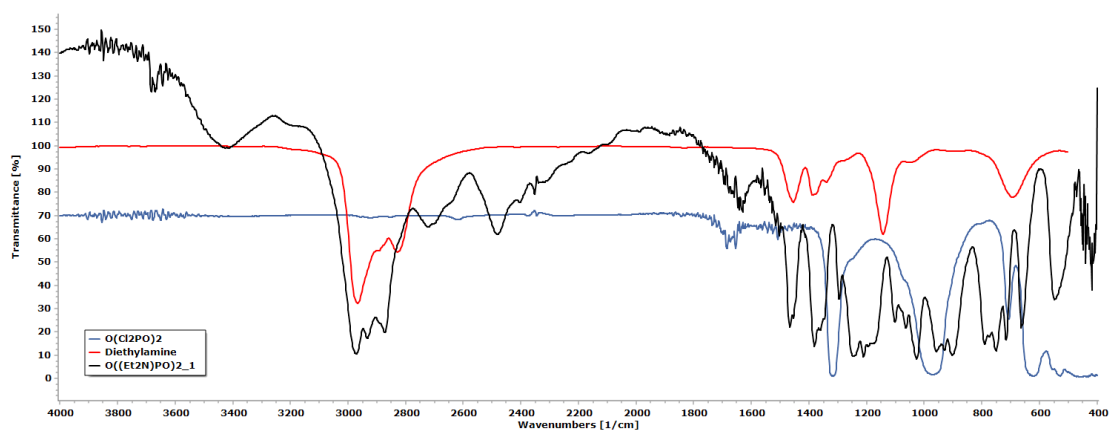


Figure 4.74: IR spectra of $O(Cl_2PO)_2$ (blue), diethylamine (red) and $O((Et_2N)_2PO)_2_1$ (black).

The first noticeable bands obtained in the IR spectrum of the $O((Et_2N)_2PO)_2_1$ were clearly the bands at 3425 cm^{-1} , 2722 cm^{-1} , 2481 cm^{-1} and 2404 cm^{-1} . The first band listed was analogous to the $\nu\text{ N-H}$ band in the spectrum of the diethylamine and the bands at 2481 cm^{-1} and 2404 cm^{-1} were analogous to the combination bands typical of the Et_2NH_2Cl side product. The second band could be analogous to the broad band at 2810 cm^{-1} in the spectrum of the salt, which was very broad and possibly composed of two bands. These bands strongly indicated that the liquid contained the salt Et_2NH_2Cl . The other bands in the spectrum of $O((Et_2N)_2PO)_2_1$ could not be conclusively assigned to Et_2NH_2Cl and were indicative of the presence of another compound. The resultant spectrum was composed of overlaps of the spectra of the salt and this compound.

The three bands at 2972 cm^{-1} , 2931 cm^{-1} and 2873 cm^{-1} were clearly indicative of methyl and methylene groups in the sample, either due to the $\text{Et}_2\text{NH}_2\text{Cl}$ salt or the ethyl groups expected for the desired product. The bands at wavenumbers lower than 1800 cm^{-1} indicated that the compound or mixture of compounds was more complex than the organic ammonium salt by-product. The broad band at 1632 cm^{-1} could not be assigned specifically to any moiety expected and may be due to water inclusion. The first two bands that could be easily assigned were those at 1466 cm^{-1} and 1381 cm^{-1} , which were assigned to δ C–H of the methyl and methylene groups, either from the salt by-product or the desired product.

The strong bands at 1294 cm^{-1} , 1240 cm^{-1} and 1211 cm^{-1} all fell in the expected range for the typical ν P=O vibration. These indicated that the compound or at least one of the compounds was a pyrophosphoryl derivative. In the case of all these bands a decrease in wavenumber was observed from the analogous ν P=O band in the spectrum of the $\text{O}(\text{Cl}_2\text{PO})_2$ starting reagent. This was an expected shift, as it is known that the electronegativity of substituents causes a proportional shift in the ν P=O band.³⁷⁵ This indicated that with the decreasing electronegativity of the substituents, from Cl to N, the bond order of the P=O decreased, thus favouring the P^+-O^- structure. Thus the pyrophosphoryl derivative was most likely the expected amine derivative.

The bands in the two regions 1064-902 cm^{-1} and 790-662 cm^{-1} all fell in the range expected for the two vibrational modes ν_{as} P–O–P and ν_{s} P–O–P respectively. However, these do not give any detail that can be used to describe the structure of the product. The two strong bands at 1175 cm^{-1} and 1102 cm^{-1} could be indicative of the ν C–N vibration, indicating the presence of the Et_2N moiety in the new compound.

As described above the IR spectrum of $\text{O}(\text{Et}_2\text{N})_2\text{PO}_2$ contained bands indicative of the presence of $\text{Et}_2\text{NH}_2\text{Cl}$. Therefore, the spectrum of $\text{O}(\text{Et}_2\text{N})_2\text{PO}_2$ in the range 1900-400 cm^{-1} was compared in more detail with the spectrum of $\text{Et}_2\text{NH}_2\text{Cl}$ in the same range, as given in Figure 4.75. This comparison corroborated the fact that the bands observed in the spectrum of $\text{O}(\text{Et}_2\text{N})_2\text{PO}_2$, at 1175 cm^{-1} , 1064 cm^{-1} , 930 cm^{-1} , 790 cm^{-1} and 662 cm^{-1} could all have been bands due to $\text{Et}_2\text{NH}_2\text{Cl}$ impurities.

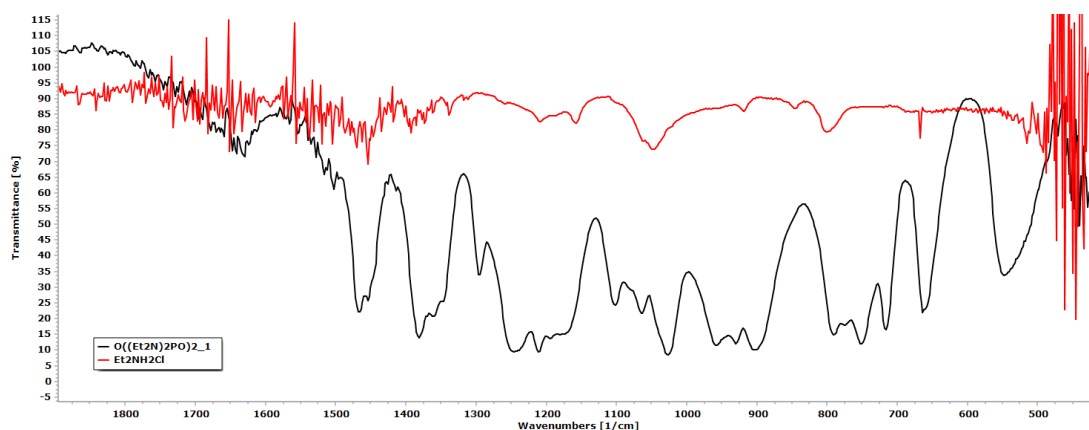


Figure 4.75: IR spectra of $O((Et_2N)_2PO)_2_1$ (black) and Et_2NH_2Cl (red), in the range $1900-400\text{ cm}^{-1}$.

Given that a number of IR bands in the spectrum of $O((Et_2N)_2PO)_2_1$ indicated the presence of Et_2NH_2Cl and that data obtained from the 1H NMR and ^{31}P NMR spectroscopy, as discussed in Sections 4.2.1.3.2 and 4.2.1.3.3 respectively, indicated the presence of multiple compounds in the crude product $O((Et_2N)_2PO)_2_1$, it was decided to purify a sample of this product by column chromatography. IR spectra for all fractions collected were obtained and it was inferred that the main fraction of interest was $O((Et_2N)_2PO)_2_1_f13$. The IR spectrum of this fraction was compared to the IR spectrum of the crude $O((Et_2N)_2PO)_2_1$, as shown in Figure 4.76.

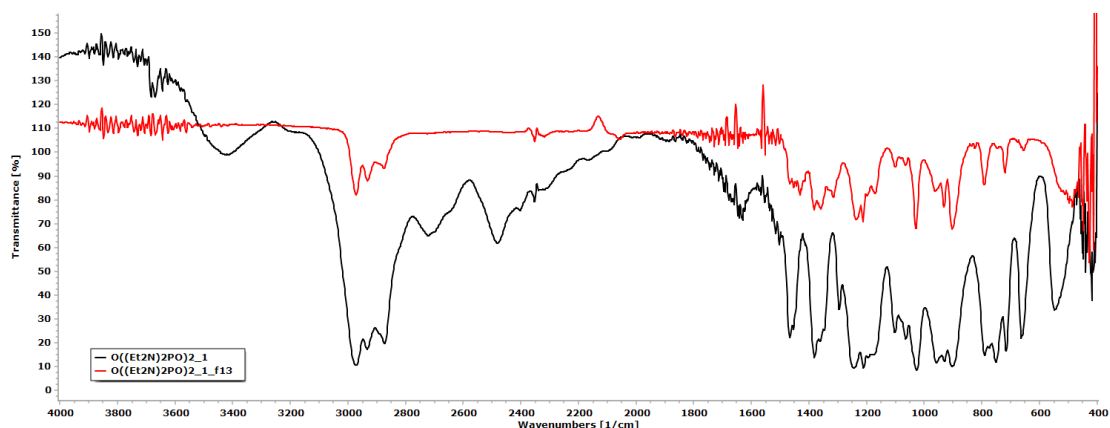


Figure 4.76: IR spectra of $O((Et_2N)_2PO)_2_1$ (black) and $O((Et_2N)_2PO)_2_1_f13$ (red).

The first change shown in Figure 4.76 was the loss of the $O((Et_2N)_2PO)_2_1$ bands at 3425 cm^{-1} , 2722 cm^{-1} , 2481 cm^{-1} and 2404 cm^{-1} in the spectrum of the purified sample. All of these have been previously assigned to the side product Et_2NH_2Cl and therefore it seems that the purification from this salt by column chromatography was more successful

than the multiple filtrations undertaken in the workup procedure. The band at 1632 cm^{-1} was also lost, which may indicate drying of the sample. A more detailed discussion is necessary on the bands found in the region below 1600 cm^{-1} .

The changes observed in the spectrum of $\text{O}((\text{Et}_2\text{N})_2\text{PO})_2_1_{\text{f13}}$ as compared to that of $\text{O}((\text{Et}_2\text{N})_2\text{PO})_2_1$ and which could not be described by the removal of $\text{Et}_2\text{NH}_2\text{Cl}$ were mainly the following. The bands at 1466 cm^{-1} and 1175 cm^{-1} in the IR spectrum of $\text{O}((\text{Et}_2\text{N})_2\text{PO})_2_1$ were both shifted to lower wavenumbers of 1432 cm^{-1} and 1170 cm^{-1} in the spectrum of $\text{O}((\text{Et}_2\text{N})_2\text{PO})_2_1_{\text{f13}}$. New bands were observed in the spectrum of $\text{O}((\text{Et}_2\text{N})_2\text{PO})_2_1_{\text{f13}}$, the first in the increased prominence of the shoulder at 1360 cm^{-1} and the second being a new weak to medium intensity band at 1315 cm^{-1} . There was a consistent decrease in intensity of the common bands at 1102 cm^{-1} (m to w), 1064 cm^{-1} (w to w), 958 cm^{-1} (s to m) and 930 cm^{-1} (s to m) in the spectrum of $\text{O}((\text{Et}_2\text{N})_2\text{PO})_2_1_{\text{f13}}$, whilst the bands at 1294 cm^{-1} and 751 cm^{-1} were lost entirely.

In the spectrum of $\text{O}((\text{Et}_2\text{N})_2\text{PO})_2_1_{\text{f13}}$ the bands at 1432 cm^{-1} , 1381 cm^{-1} and 1360 cm^{-1} were believed to be due to the methyl and methylene δ C–H vibrations. The band at 1432 cm^{-1} seemed to be shifted from the crude sample's band position at 1466 cm^{-1} . However, a small shoulder at the latter wavenumber was still visible in the spectrum of $\text{O}((\text{Et}_2\text{N})_2\text{PO})_2_1_{\text{f13}}$. The bands at 1381 cm^{-1} and 1360 cm^{-1} were present in both spectra, however the intensities of the two bands were found to be more similar in the case of the purified liquid than in the case of the crude product.

A definitive reason for the diminishment of the intensity of the $\text{O}((\text{Et}_2\text{N})_2\text{PO})_2_1_{\text{f13}}$ spectrum bands at 1102 cm^{-1} , 1064 cm^{-1} , 958 cm^{-1} and 930 cm^{-1} could not be determined. The band at 1102 cm^{-1} remained un-assigned and therefore its discussion is difficult. The other three bands, together with the stronger bands at 1027 cm^{-1} and 902 cm^{-1} which were un-effected by the purification process, fall in the range typical of the ν_{as} P–O–P vibrations. It is observed that these bands fell in the fingerprint region, which typically contains many bands of different moieties, such as the expected ν C–N, ν C–C and ω C–H vibrations, and therefore the assignment is not definitive. The diminished intensity of the bands at 1102 cm^{-1} , 1064 cm^{-1} , 958 cm^{-1} and 930 cm^{-1} could be due to the alkane vibrational modes. The bands at 1102 cm^{-1} , 1064 cm^{-1} and 1027 cm^{-1} could all be due to the ν C–N vibration, while bands at 958 cm^{-1} , 930 cm^{-1} and 902 cm^{-1} can also be due to P–N–C vibrations (including ν_{as} P–N) typically found in this region.^{99,376} These both indicated the possible formation of the desired compound.

If more than one of these bands are due to the ν_{as} P–O–P vibration it might be indicative of multiple species in the samples $\text{O}((\text{Et}_2\text{N})_2\text{PO})_2_1$ and $\text{O}((\text{Et}_2\text{N})_2\text{PO})_2_1_{f13}$. The first possibility, especially for the two major bands at 1027 cm^{-1} and 902 cm^{-1} , was that the multiple bands were due to two or more symmetrically distinct modes of the ν_{as} P–O–P vibration.

Another possibility was that there could be chemical differences between the two P–O bonds in the P–O–P skeleton. This is further substantiated by the fact that the bands at 1102 cm^{-1} , 1064 cm^{-1} and 1027 cm^{-1} lie at higher wavenumbers than the ν_{as} P–O–P vibration in $\text{O}(\text{Cl}_2\text{PO})_2$, while the bands at 958 cm^{-1} , 930 cm^{-1} and 902 cm^{-1} lie at lower wavenumbers. This splitting of the singular band in the starting reagent could indicate that the resonance structures $\text{P}=\text{O}=\text{P} \leftrightarrow \text{P}=\text{O}-\text{P}$ could give two separate spectra demarcating two distinct P–O bond orders, possible due to the resonance of the ylide structure $\text{P}=\text{O} \leftrightarrow \text{P}^+-\text{O}^-$ of the attached P=O. This is not typical of normal resonance structures in which a singular band is expected, since the resonance structures are not long lasting enough to be treated as being chemically distinct. This could imply that the substitution of the Cl with the amine substituent causes the resonance structures to become more long lasting rather than intermediate, even though within a single resonance stabilised form. This was possibly the effect of the change in the electronegativity of the substituent on the P atom and the change in the negative hyperconjugation ability of the new substituent as compared to that of the initial Cl. A second possibility for this bond order distinction in the two P–O bonds of the P–O–P vibration group could be that the compound obtained was asymmetric about the central O of the pyrophosphoryl group. This possibility would indicate that the compound obtained in $\text{O}((\text{Et}_2\text{N})_2\text{PO})_2_1$ and $\text{O}((\text{Et}_2\text{N})_2\text{PO})_2_1_{f13}$ was not the desired product but an asymmetric analogue.

The bands found in the $\text{O}((\text{Et}_2\text{N})_2\text{PO})_2_1_{f13}$ spectrum in the region 1315 cm^{-1} to 1175 cm^{-1} could be discussed in relation to the ν P=O band visible in the spectrum of $\text{O}(\text{Cl}_2\text{PO})_2$ at 1315 cm^{-1} . The presence of the medium intensity band at 1315 cm^{-1} in the spectrum of $\text{O}((\text{Et}_2\text{N})_2\text{PO})_2_1_{f13}$, which was not visible in the spectrum of the crude $\text{O}((\text{Et}_2\text{N})_2\text{PO})_2_1$, was problematic as it may indicate the reformation of the starting reagent. However, it should be noted that given the reactivity of this compound further studies must be carried out to determine whether this is possible. This change was accompanied by the loss of the sharp band at 1294 cm^{-1} present in the spectrum of the crude product, which could indicate that some reaction and structural change occurred during the purification by chromatography. The bands at 1240 cm^{-1} and 1211 cm^{-1}

remained strong in the spectra of the purified product and it is fairly reasonable to assume that these were due to the ν P=O vibration of this product, as described prior for the crude product. If both these were due to ν P=O vibrations, it may be indicative of two distinct P–O bonds as discussed in the previous paragraph.

The band at 1175 cm^{-1} showed a decrease in intensity, however it was still present. Apart from falling in the lower range for the ν P=O vibrations it was more likely that this band was due to the expected ν C–N vibration, which is given at 1048 cm^{-1} in the spectrum of diethylamine. This increase in wavenumber could be due to an increase in C–N stiffness similar to that observed for the $\text{Et}_2\text{NH}_2\text{Cl}$ spectrum.

The range between 850 cm^{-1} to 400 cm^{-1} was expected to contain bands for the ν_s P–O–P, ν P–N and ρ C–H vibrations. In this region the bands at 790 cm^{-1} , 717 cm^{-1} and 662 cm^{-1} were common in both the $\text{O}((\text{Et}_2\text{N})_2\text{PO})_2_1$ and the $\text{O}((\text{Et}_2\text{N})_2\text{PO})_2_1_{f13}$ spectra, while a singular band at 751 cm^{-1} was lost on purification. No new bands were observed for the purified product, as compared to the crude. All these bands fell in the range typical for the ν_s P–O–P. The band at 790 cm^{-1} was initially thought to be analogous to that present in the IR spectrum of the $\text{Et}_2\text{NH}_2\text{Cl}$ impurity. This however remained in the spectrum of the purified compound and therefore could be due to all the aforementioned vibrational modes. The band at 717 cm^{-1} fell in the same region as the ν_s P–O–P band of $\text{O}(\text{Cl}_2\text{PO})_2$, which is found at 708 cm^{-1} and the ρ C–H vibration of diethylamine. If this band was analogous to the former vibration for $\text{O}(\text{Cl}_2\text{PO})_2$ it was indicative that the change in substituent at the P atom has little effect on this vibrational mode. The possibility that this band was due to the ν P–N mode is still equally likely. The same can be said for the band at 662 cm^{-1} , although if this band was due to the ν_s P–O–P vibration it would indicate a decrease in stiffness of the P–O–P bonds. The only conclusion that can be obtained in this region would be that the band at 790 cm^{-1} was more likely to be due to ν P–N vibrational mode if the shift in the wavenumber for the ν_s P–O–P and ρ C–H bands from the reagent spectrum to the product spectrum was small. If one of these bands was indicative of the ν P–N vibrational modes this would support the formation of the desired compound or similar analogues.

4.2.1.3.2. Analysis by ^1H NMR spectroscopy

In the preparation of the compound $\text{O}((\text{Et}_2\text{N})_2\text{PO})_2\text{1}$ a colourless crystalline solid was obtained prior to the extraction of the liquid $\text{O}((\text{Et}_2\text{N})_2\text{PO})_2\text{1}$. This solid was also analysed by ^1H NMR which confirmed that it was the $\text{Et}_2\text{NH}_2\text{Cl}$ salt, as described in Appendix 10. No more analysis was undertaken on this product given that it was a known side product.

The crude wine coloured liquid product, $\text{O}((\text{Et}_2\text{N})_2\text{PO})_2\text{1}$, was analysed by ^1H NMR spectroscopy using CDCl_3 . The full ^1H NMR spectrum of this product is given in Appendix 11. The region with relevant peaks is shown in Figure 4.77. Peaks were observed at 3.16 ppm, 3.07 ppm, 2.95 ppm, 1.39 ppm, and 1.13 ppm. Alongside these peaks a broad singlet was also observed in the spectrum at 9.90 ppm. The first two peaks in the region given in Figure 4.77 (3.16 and 3.07 ppm) resemble a broad doublet centred around 3.11 ppm. The remaining peaks all seem to be non-symmetric triplets with the peak around 1.13 ppm also being possibly a multiplet. Data regarding these peaks is given in Table 4.14 for clear presentation.

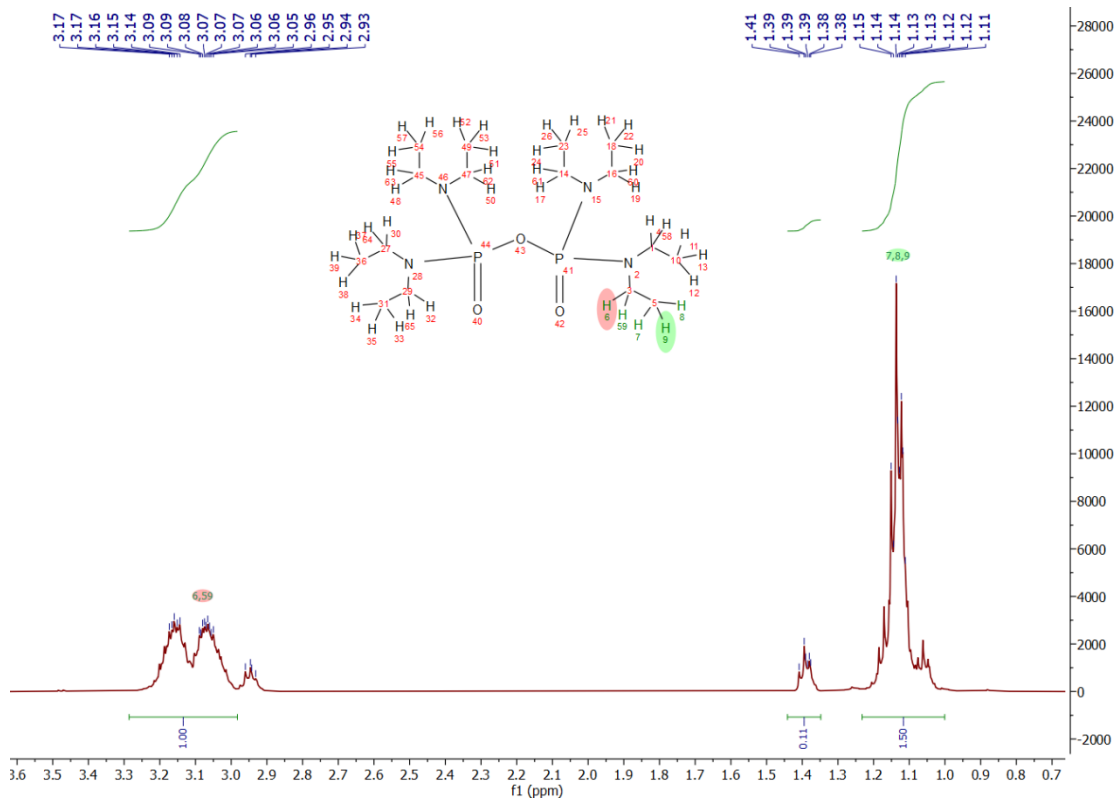


Figure 4.77: ^1H NMR spectrum of $\text{O}((\text{Et}_2\text{N})_2\text{PO})_2\text{1}$.

Table 4.14: ^1H NMR experimental data for proton peaks of $\text{O}((\text{Et}_2\text{N})_2\text{PO})_2_1$ in CDCl_3 .

^1H NMR experimental data for proton peaks of $\text{O}((\text{Et}_2\text{N})_2\text{PO})_2_1$ in CDCl_3			
ppm	Multiplicity	Integration	Coupling
9.90	broad singlet	0.12	N/A
3.16	broad multiplets	4.39	N/A
3.07	broad multiplets	4.52	N/A
OR			
3.11	broad doublet	8.90	$J = 43.11 \text{ Hz}$
AND			
2.95	triplet	0.68	$J = 7.25 \text{ Hz}$
1.39	triplet	1.00	$J = 7.38 \text{ Hz}$
1.13	triplet or multiplet	13.8	$J = 7.15 \text{ Hz}$

The presence of the singlet at 9.90 ppm indicated possible contamination of the product with dissolved $\text{Et}_2\text{NH}_2\text{Cl}$. The peaks at 2.95 and 1.39 ppm, could be due to either the presence of $\text{Et}_2\text{NH}_2\text{Cl}$ or diethylamine reagent.

Therefore, the peaks of interest in the discussion of the spectrum of the crude $\text{O}((\text{Et}_2\text{N})_2\text{PO})_2_1$ were mainly those at 3.16 ppm, 3.07 ppm and 1.13 ppm. The triplet or multiplet peak at 1.13 ppm remained in the region typical of the methyl proton peaks for both the diethylamine starting reagent and the $\text{Et}_2\text{NH}_2\text{Cl}$. However, there was also the possibility that the peak at 1.13 ppm could be due to the methyl groups present in the expected product. This is because the protons in the methyl group are the least effected by the highly electronegative N atom present in the reagent and the two expected products. If this was the case the triplet nature of the peak would confirm that this is the methyl group adjacent to the methylene of the ethyl groups expected in the product.

In the expected product $\text{O}((\text{Et}_2\text{N})_2\text{PO})_2$ the expected proton ratio is 2:3 (methylene to methyl proton). Therefore, if this was the case the peaks indicative of the methylene protons in the spectrum should agree with this ratio. The integration value ratio for the three peaks, 3.16 ppm, 3.07 ppm and 1.13 ppm, was however 1:1.03:3.05. This indicated

that the two peaks at 3.16 ppm and 3.07 ppm were indeed the doublet peaks for a single peak at 3.11 ppm. Thus the integration value ratio of the peaks at 3.11 ppm and 1.13 ppm was of 1:1.5 or 2:3 and this was in agreement with the expected values. Although this data indicated that these two peaks (3.11 ppm and 1.13 ppm) could indeed be due to the methylene and methyl protons of the ethyl group the expected quartet at 3.11 ppm was not observed and the presence of the ethyl group does not in itself confirm the formation of the desired product.

Further analysis of the doublet at 3.11 ppm was therefore important. In the context of an ethyl group the methylene is expected as a quartet in the spectrum, downfield to the methyl proton triplet due to the electronegative nitrogen atom bound to the methylene group. The downfield shift as compared to the methyl triplet was found to be as expected, however the peak assigned to the methylene was found to be a broad doublet. The doublet nature of the peak at 3.11 ppm could be explained by the presence of the $\frac{1}{2}$ spin P atom bound to the N atom. The formation of a P–N bond should have created a vicinal P to H relationship. This was found to be in agreement with the observed data. The coupling constant of 43.11 Hz is considered to be very high for the $^3J_{HH}$ for vicinal protons on organic skeletons. The high value observed is however in the region typical for $^3J_{HP}$ coupling, which is usually in the range of 40–45 Hz.^{99,249} The doublet nature of the peak was in agreement with the presence of a single P atom on the N atom bound to the methylene group. The broad nature of the peaks could also be due to the presence of the quadrupole of the N atom, which in the case of the P–N–C–H system is integral to the coupling electron system. This doublet therefore could be conclusive of the formation of the desired product in a crude form in O((Et₂N)₂PO)₂_1 or at least the formation of a P–N containing product as the major component of the crude product.

As described in Section 3.3.2.1.3.2, the crude product O((Et₂N)₂PO)₂_1 was purified using column chromatography, to yield numerous fractions. Fraction O((Et₂N)₂PO)₂_1_f13 was analysed by ¹H NMR spectroscopy, with the spectrum obtained given in Appendix 11. The region with relevant peaks is shown in Figure 4.78. Although not shown in this spectrum no peaks above 8.00 ppm were observed, indicating that any organic ammonium salt by-product was removed through column chromatography.

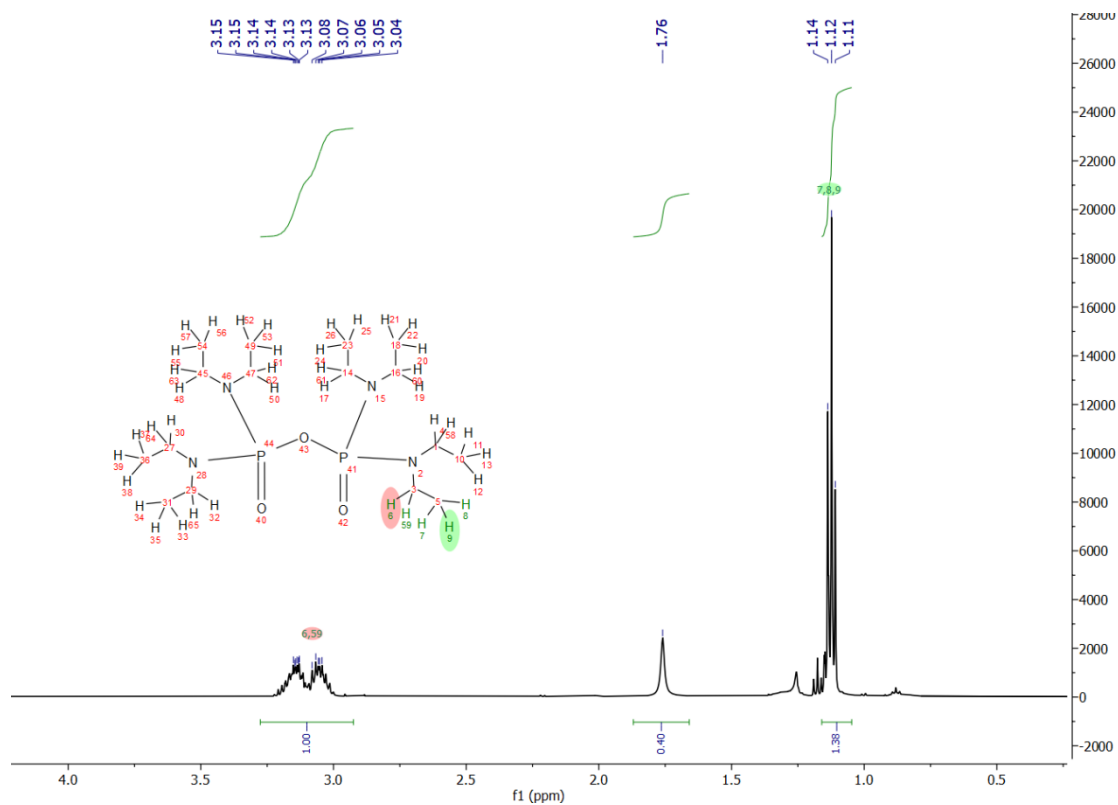


Figure 4.78: Detail of ^1H NMR spectrum of $\text{O}((\text{Et}_2\text{N})_2\text{PO})_2_1_{\text{f13}}$ showing peaks of main interest and integration values.

The data for $\text{O}((\text{Et}_2\text{N})_2\text{PO})_2_1_{\text{f13}}$ was found to be very similar to the expected data, as given in Figure 4.78. As was the case for the $\text{O}((\text{Et}_2\text{N})_2\text{PO})_2_1$, a broad doublet at 3.10 ppm and a triplet at 1.12 ppm were clearly visible in the spectrum of $\text{O}((\text{Et}_2\text{N})_2\text{PO})_2_1_{\text{f13}}$. The triplet was observed to be better defined in the spectrum of $\text{O}((\text{Et}_2\text{N})_2\text{PO})_2_1_{\text{f13}}$, when compared to that of $\text{O}((\text{Et}_2\text{N})_2\text{PO})_2_1$, where the peak appeared to be a multiplet. This indicated that the sample $\text{O}((\text{Et}_2\text{N})_2\text{PO})_2_1_{\text{f13}}$ contained less impurities which might have given peaks which overlapped with this peak. Furthermore, the loss of a number of smaller unassigned and by-product or reagent assigned peaks was a general observation for the entirety of the $\text{O}((\text{Et}_2\text{N})_2\text{PO})_2_1_{\text{f13}}$ spectrum. The coupling constant for the broad doublet at 3.10 ppm was however found to be 40.11 Hz, rather than the 43.11 Hz of the doublet in $\text{O}((\text{Et}_2\text{N})_2\text{PO})_2_1$. All this information therefore showed that the major component of $\text{O}((\text{Et}_2\text{N})_2\text{PO})_2_1_{\text{f13}}$ seemed to have been the same as that of the $\text{O}((\text{Et}_2\text{N})_2\text{PO})_2_1$, with several of the peaks indicating impurities being lost. However, it was noted that the integration value ratio of the peaks assigned to the methylene and methyl protons was not the expected 1:1.5 but rather 1:1.37, this being slightly smaller than expected.

The only major issue that was clearly visible in the spectrum of the $\text{O}((\text{Et}_2\text{N})_2\text{PO})_2_1_{\text{f13}}$ was the singlet at 1.76 ppm. This peak could not be assigned to any of the protons expected in the desired product. The nature of the singlet indicated that the protons detected were not coupled and could be isolated. An integration value of 0.40 for this peak indicated that the number of protons was approximately equal to half the amount of methylene protons present in the product. This is similar in ratio to the organic ammonium salt, however the high upfield shift of the peak from the respective NH_2^+ peak of $\text{Et}_2\text{NH}_2\text{Cl}$ indicated that this was not due to the presence of this salt. This peak falls in the range typical of many organic groups, including aliphatic skeletons, protons geminal to N atoms, amine and alcoholic protons and alkyne protons. Given the nature of the reaction and workup the most likely protons to be present at this position were either protons geminal to N atoms and amine or alcoholic protons. All this may therefore indicate the presence of either a small amine or alcoholic impurity in the product at higher concentrations than desired or possibly the presence of protons on the N atoms in the P–N moieties in the product, which would make it a cationic species.

Therefore, through the interpretation of the ^1H NMR spectroscopy data for $\text{O}((\text{Et}_2\text{N})_2\text{PO})_2_1$ it can be speculated that the product obtained was the crude form of a compound containing the P– NEt_2 moiety. The ^1H NMR data for $\text{O}((\text{Et}_2\text{N})_2\text{PO})_2_1_{\text{f13}}$ indicated that the liquid chromatography was successful in further purifying this crude product but with the inclusion of a single impurity of unknown composition.

4.2.1.3.3. Analysis by ^{31}P NMR spectroscopy

The discussion of ^{31}P NMR data is restricted to the spectra obtained for the products $\text{O}((\text{Et}_2\text{N})_2\text{PO})_2_1$ and $\text{O}((\text{Et}_2\text{N})_2\text{PO})_2_1_{\text{f13}}$. An initial proton decoupled ($^{31}\text{P}\{^1\text{H}\}$ NMR) spectrum was obtained for the crude $\text{O}((\text{Et}_2\text{N})_2\text{PO})_2_1$, as given in Figure 4.79. The spectrum yielded two major peaks of interest, at 27.41 ppm and 8.45 ppm. Other peaks, some of which may have been coupled, were also observed. The two major peaks most likely describe two distinct compounds containing either a single P atom or numerous magnetically equivalent P atoms. Given the symmetric nature of the compound $\text{O}((\text{Et}_2\text{N})_2\text{PO})_2$ the two phosphorus atoms should be equivalent, and therefore either of these peaks could be indicative of this product. The other peaks observed would indicate the presence of minor non-symmetric PPTC derivatives.

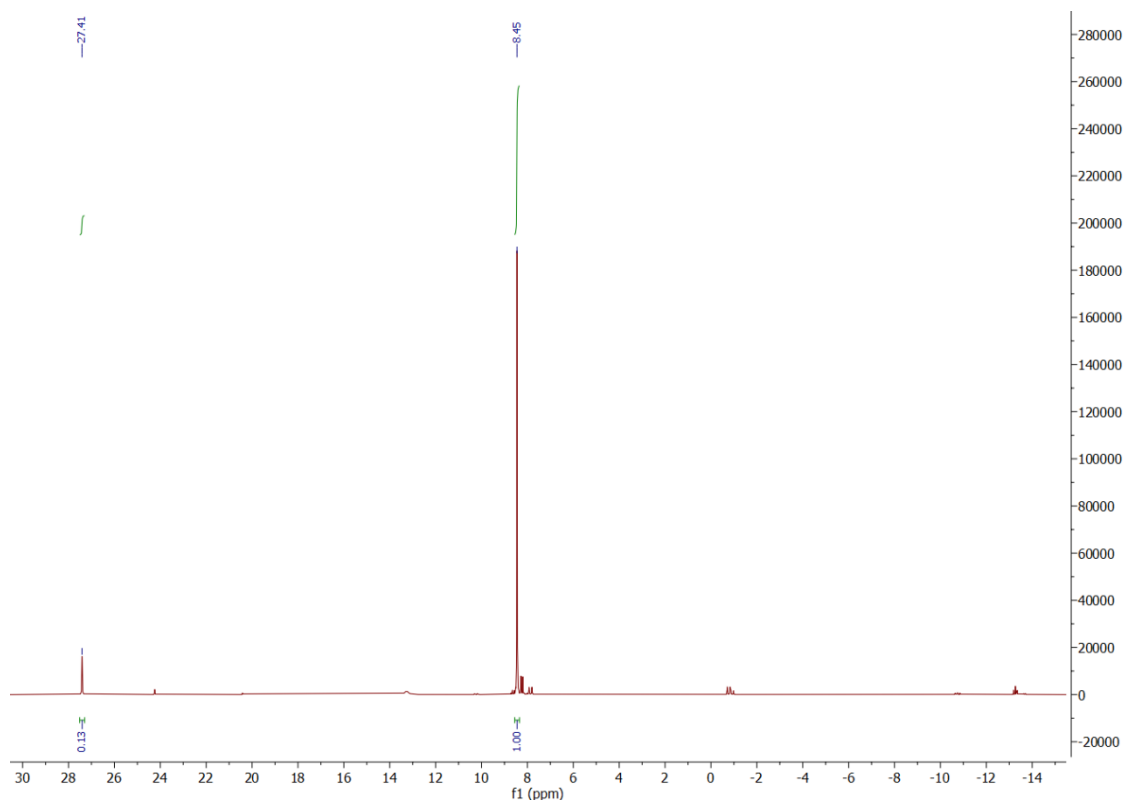


Figure 4.79: $^{31}\text{P}\{^1\text{H}\}$ NMR spectrum of $\text{O}((\text{Et}_2\text{N})_2\text{PO})_2_1$.

First of all it should be noted that the peak expected for the starting reagent PPTC is a singlet at -9.53 ppm, as given in the Appendix 4. Therefore, the lack of this peak in the spectrum of $\text{O}((\text{Et}_2\text{N})_2\text{PO})_2_1$ was indicative of the full consumption of the PPTC during reaction. This was expected due to the high reactivity of this compound. The main issue in this analysis was to determine whether the desired product was obtained.

Phosphorus follows the same rules as protons in NMR spectroscopy and therefore the data from $^{31}\text{P}\{^1\text{H}\}$ NMR spectroscopy can be treated similarly to that from ^1H NMR spectroscopy. The first noticeable difference between the spectra of PPTC and that of $\text{O}((\text{Et}_2\text{N})_2\text{PO})_2_1$ is the downfield shift of the majority of the peaks in the spectrum of the $\text{O}((\text{Et}_2\text{N})_2\text{PO})_2_1$ crude mixture, including the two major peaks, when compared to the position of the peak assigned to PPTC phosphorus.

This downfield shift from the PPTC peak to the $\text{O}((\text{Et}_2\text{N})_2\text{PO})_2_1$ peaks was indicative of compounds where the P atom is deshielded, either by electronic or magnetic means, as compared to the PPTC. In the case of $\lambda^3\sigma^3$ -phosphanes of the type PR_3 the presence of increased electronegative R groups causes such a downfield shift. However, this is not the case for $\text{O}=\text{PR}_3$ groups. In the case of the reaction under study the expected structural change is depicted in Figure 4.80. The pyrophosphoryl system (given in red)

remains unchanged and therefore the chemical shift in the ^{31}P NMR spectrum is not affected by the pyrophosphoryl group but rather by the replacement of the Cl atoms with amine groups, depicted in green in Figure 4.80.

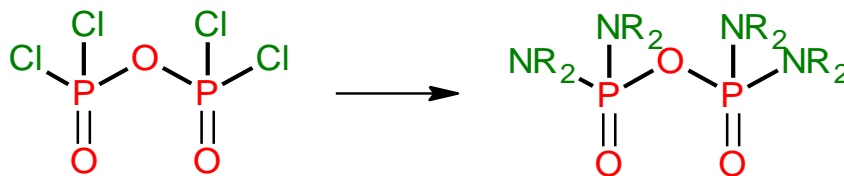


Figure 4.80: Expected structure change on formation of $\text{O}((\text{Et}_2\text{N})_2\text{PO})_2_1$ from PPTC, pyrophosphoryl moiety (red) and the changed groups (green).

In both compounds the phosphorus is present as a $\lambda^5\sigma^4$ -phosphorane and therefore the discussion of the chemical shifts obtained must be through data available for such structures. Although slightly, chlorine is typically regarded as being more electronegative than nitrogen, therefore one would expect an upfield shift from the -9.53 ppm peak for PPTC to the peak expected for $\text{O}((\text{Et}_2\text{N})_2\text{PO})_2_1$. This however was not the case with the experimental data, but the downfield shift as observed in the experimental data was in line with literature data.^{99,249,377} For example, for typical phosphoryl compounds ($\text{O}=\text{PY}_3$), of which pyrophosphoryl compounds are a specific sub-set, a downfield shift is observed between chemical shifts of $\text{O}=\text{PX}_3$ ($\text{X} = \text{halide}$) as compared to those of $\text{O}=\text{P}(\text{NR}_2)_3$.²⁸² If the pyrophosphoryl moiety is not affected by the reaction and therefore its effect on the chemical shift change is non-existent or minimal, the experimental chemical shift change is in line with the published trends.

In the case of $\text{O}=\text{PCl}_3$, with a chemical shift in the range 2 to 3.5 ppm in CDCl_3 ,^{378,379} the chemical shift falls in the region typical for $\text{O}=\text{P}(\text{OR})_3$ compounds. In describing these effects, the $\text{P}=\text{O}$ bond will not be regarded as a typical double bond but as the effect of negative hyperconjugation on the basic bond P^+-O^- . Phosphoryl halides have chemical shifts typically upfield of other phosphoryl compounds which have substituents that are less electronegative than the halides. This arises from the ability of halides to form π -back bonds to the phosphorus centre. This back bonding decreases the positive charge about the phosphorus in the P^+-O^- moiety and thus increases electron density about the phosphorus centre, which causes shielding and therefore an upfield shift.³⁷⁷

For other phosphoryl compounds the substituents have various effects on the electron density around the phosphorus of the P^+-O^- moiety. Both an increase in electronegativity of substituents and the capability of P–Y bonds to minimise negative hyperconjugation on the P^+-O^- moiety would cause a downfield shift of the compound as compared to halide analogues. The nitrogen of the amine substituents is only slightly less electronegative than the halide chlorine. Therefore, on this basis alone one would expect similar chemical shift values. Based on the notion that the chloride has a greater π -back donation than the amine nitrogen, the downfield shift attested in the chemical shifts observed in the spectrum of $O((Et_2N)_2PO)_2_1$ is in line with what was expected.²⁴⁹ Therefore, from the basis of this data it can be assumed that the chlorine atoms of the PPTC were in fact substituted by non-halide substituents. Both major peaks obtained in the experimental data, 27.41 ppm and 8.45 ppm, fell in the range typical of $O=P(NR_2)_3$ as was expected. These same peaks also fell in the typical range for $O=P(OR)_3$ or $O=P(OR)_{3-n}(OH)_n$.²⁸² This was expected given that the expected product contains the P–O–P bond system. These peaks could however also indicate the formation of a pyrophosphoric acid derivative, as peaks due to these compounds also fall in the same range.

Given that the 1H NMR spectrum of $O((Et_2N)_2PO)_2_1$ gave a doublet with a coupling constant of 43.11 Hz, which was believed to be due to the $^3J_{HP}$ between the methylene protons of the diethylamine moiety and the phosphorus centres, non-decoupled ^{31}P NMR was attempted to identify this same coupling constant. The ^{31}P NMR of $O((Et_2N)_2PO)_2_1$ is given in Appendix 11. Many of the minor peaks, including that at 27.41 ppm, revealed multiplets, while the main peak was observed to have shifted slightly to 8.50 ppm from the 8.45 ppm position of the original $^{31}P\{^1H\}$ NMR. This was observed to form either a quartet or a septet. Unfortunately, the coupling constant obtained for the quartet was of 10.77 Hz. None of the other peaks revealed a coupling constant approximating the 40-45 Hz expected. Further information from the coupling could not be obtained.

A $^{31}P\{^1H\}$ NMR spectrum in $CDCl_3$ for $O((Et_2N)_2PO)_2_1_{f13}$ was obtained as given in Figure 4.81, showing two singlet peaks at 9.38 ppm and -11.03 ppm. Therefore, the $O((Et_2N)_2PO)_2_1$ peak at 27.41 ppm was lost, which together with the IR spectrum obtained for $O((Et_2N)_2PO)_2_1_{f13}$ indicated that this was related to an impurity which was removed by column chromatography. The peak at 8.45 ppm for $O((Et_2N)_2PO)_2_1$ was shifted slightly downfield to 9.38 ppm for $O((Et_2N)_2PO)_2_1_{f13}$.

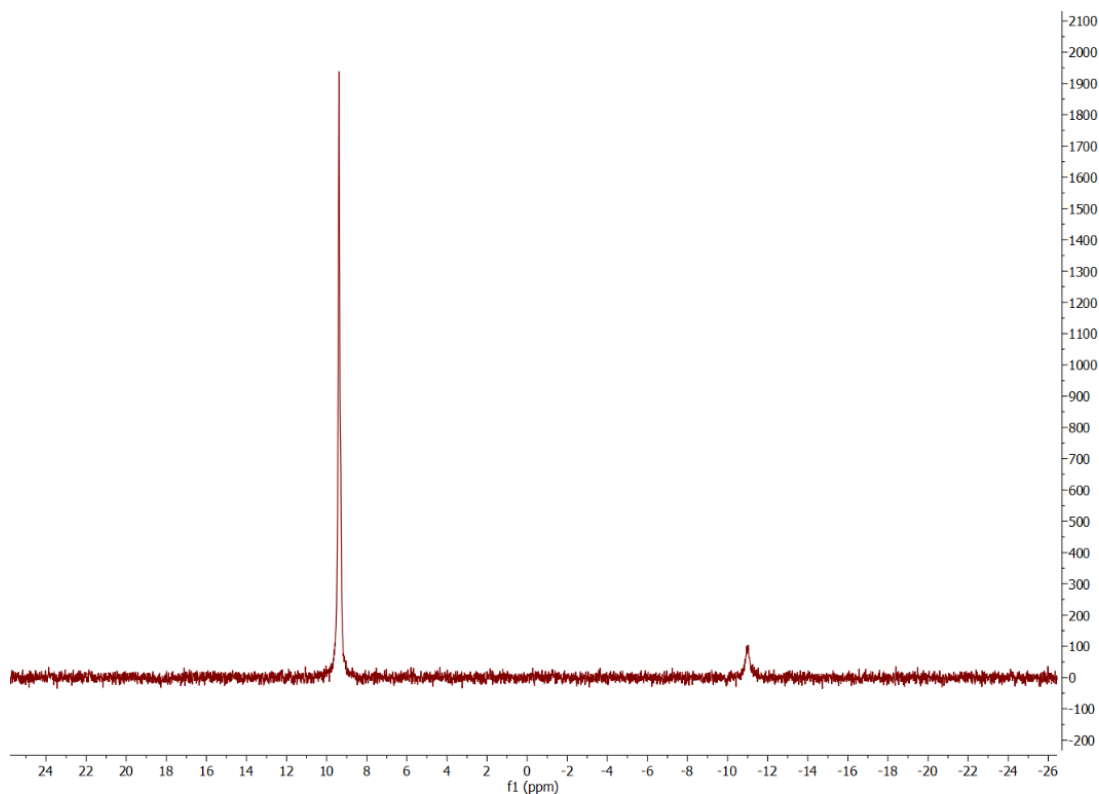


Figure 4.81: $^{31}\text{P}\{^1\text{H}\}$ NMR spectrum of $\text{O}((\text{Et}_2\text{N})_2\text{PO})_2_1_{\text{f13}}$.

The $^{31}\text{P}\{^1\text{H}\}$ NMR spectrum of $\text{O}((\text{Et}_2\text{N})_2\text{PO})_2_1_{\text{f13}}$ confirmed that the column chromatography technique proved effective in separating the numerous products obtained in the crude $\text{O}((\text{Et}_2\text{N})_2\text{PO})_2_1$. The reason for the shift from 8.45 ppm in the $\text{O}((\text{Et}_2\text{N})_2\text{PO})_2_1$ spectrum to 9.38 ppm for the $\text{O}((\text{Et}_2\text{N})_2\text{PO})_2_1_{\text{f13}}$ spectrum is not known. The purification procedure seems to have obtained a single phosphorus species which was most likely the same as that which produced the peak at 8.45 ppm in the spectrum of the crude product.

Given that it was inferred that the peak at 9.38 ppm for $\text{O}((\text{Et}_2\text{N})_2\text{PO})_2_1_{\text{f13}}$ was analogous to the peak at 8.45 ppm for $\text{O}((\text{Et}_2\text{N})_2\text{PO})_2_1$, a coupled ^{31}P NMR spectrum for $\text{O}((\text{Et}_2\text{N})_2\text{PO})_2_1_{\text{f13}}$ was obtained. The coupled ^{31}P NMR spectrum of $\text{O}((\text{Et}_2\text{N})_2\text{PO})_2_1_{\text{f13}}$ is given in Appendix 11, where it can be observed that the peak at 9.30 ppm showed no coupling. Various attempts at obtaining better detail did not yield coupling. This was problematic and could indicate the decomposition of the compound obtained in $\text{O}((\text{Et}_2\text{N})_2\text{PO})_2_1$. This is in disagreement with the data inferred from the IR spectra, described in Section 4.2.1.3.1.

4.2.1.3.4. Analysis by Gas Chromatography Mass Spectroscopy (GC-MS)

From the data discussed previously, the two compounds $O((Et_2N)_2PO)_2_1$ and $O((Et_2N)_2PO)_2_1_{f13}$ were considered likely to contain the desired product. In order to further clarify this, both samples in chloroform, were analysed by GC-MS. The gas chromatograph of $O((Et_2N)_2PO)_2_1$ is given in Figure 4.82. This clearly showed the presence of a large number of compounds. The major peak was obtained at 10.89 minutes and the mass spectrum of this fraction is shown in Figure 4.83. In the mass spectrum obtained for the 10.89 minutes' fraction the peak at 398.26 m/z, having a relative abundance of 1.15%, was the one with the highest m/z value. This was in very good agreement with the expected molecular mass of the $O((Et_2N)_2PO)_2$, namely 398.51 gmol^{-1} .

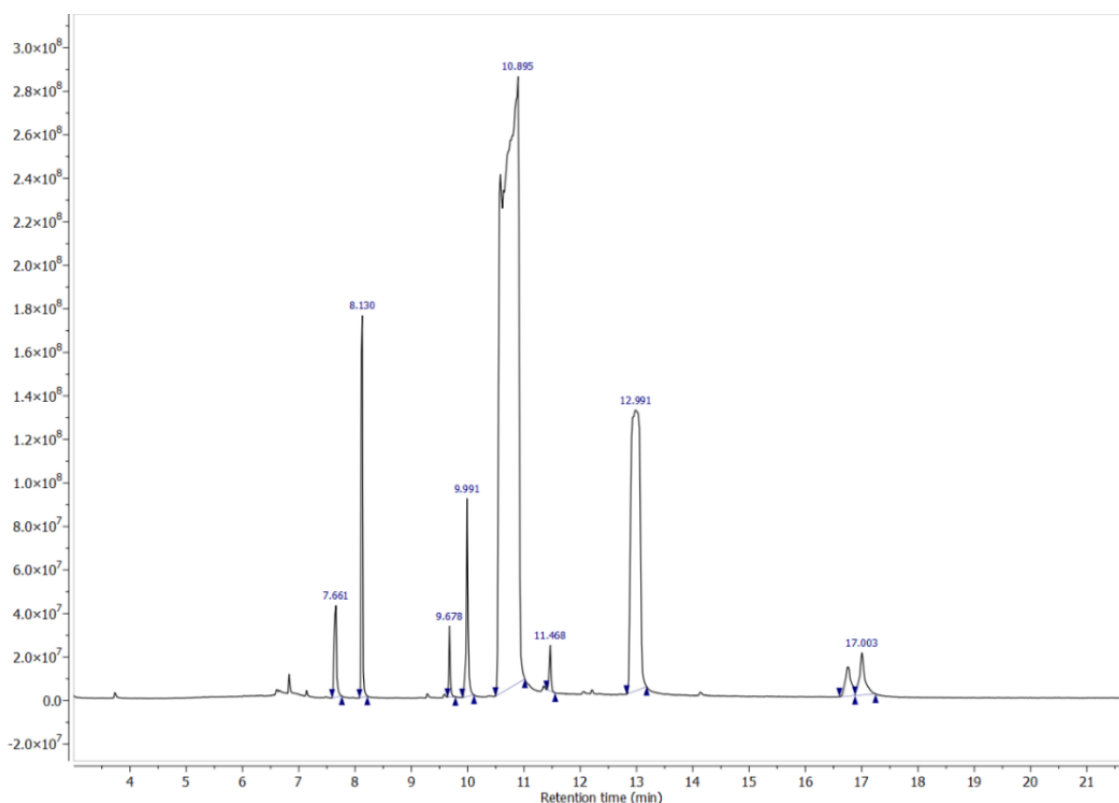


Figure 4.82: Gas chromatograph of $O((Et_2N)_2PO)_2_1$.

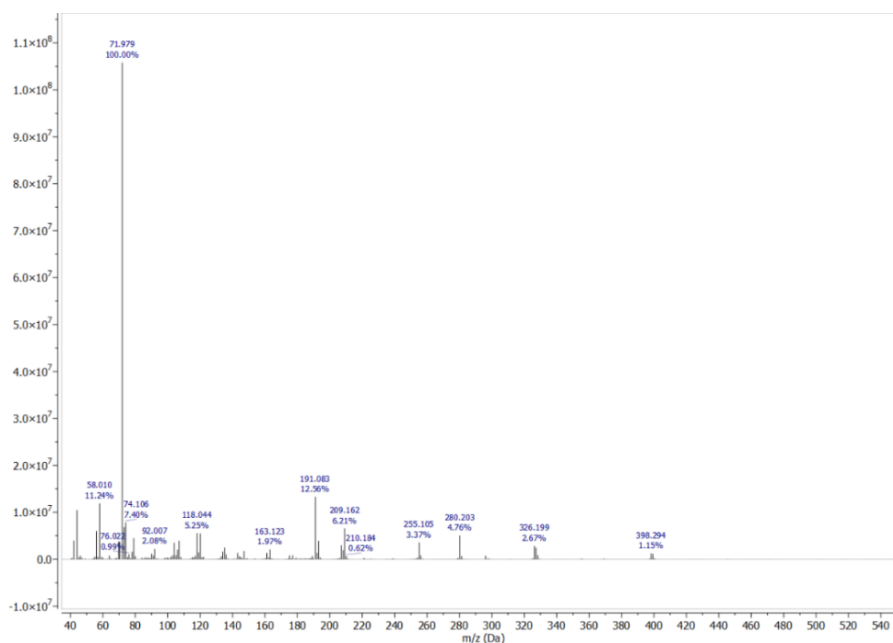


Figure 4.83: Mass spectrum of the 10.89 minute fraction of O((Et₂N)₂PO)_{2_1}.

The peak with a 100% relative abundance in the mass spectrum of the 10.89 minutes' fraction was given at 71.99 m/z. This was believed to be due to the [Et₂N]⁺ fragment with an expected value of 72.14 m/z. This would suggest that this fragmentation is the most typical in the fraction, indicating that the compounds therein have a large amount of diethylamine moieties and that fragmentation occurred at the P–N bonds. The second largest band, at 12.5% relative abundance, was observed at 191.09 m/z, which was assigned to the expected [(Et₂N)₂PO]⁺ fragment, with a theorised m/z value of 191.28 m/z. The expected complementary fragment [(Et₂N)₂PO₂]⁺ at about 207.23 m/z was not observed, although a peak at 209.15 m/z was observed. The two peaks at 280.23 m/z and 326.18 m/z could also be tentatively assigned to the [O((Et₂N)₂PO)((N)₂PO)]⁺ fragment (expected, 281.51 m/z) and the [O((Et₂N)₂PO)((Et₂N)PO)]⁺ fragment (expected, 326.37 m/z). All of this data would indicate that the main compound present in the fraction at 10.89 minutes for O((Et₂N)₂PO)_{2_1} could be the desired product.

The product O((Et₂N)₂PO)_{2_1_f13} was also analysed by GC-MS with the gas chromatograph given in Figure 4.84. In Figure 4.84 only two peaks were obtained namely at 10.56 minutes and 12.88 minutes. Although not exact, these two peaks seem to be analogous to the O((Et₂N)₂PO)_{2_1} peaks at 10.89 minutes and 12.99 minutes. The mass spectrum of the 10.59 minutes fraction is given in Figure 4.85, along with the mass spectrum of the 10.89 minute fraction of O((Et₂N)₂PO)_{2_1}. It was observed that both fractions gave mass spectra with similar m/z and relative abundancy values. Again the

highest m/z value obtained was of 398.30 m/z, which compares well with the expected value of 398.51 g mol^{-1} . Also the peak at 72.05 m/z was retained as the major peak and this was believed to be analogous to the expected peak of $[\text{Et}_2\text{N}]^+$ at 72.14 m/z. All the remaining peaks are also in agreement with the data for the 10.89 minute fraction for $\text{O}((\text{Et}_2\text{N})_2\text{PO})_2_1$ and therefore the same assignment and conclusions apply.

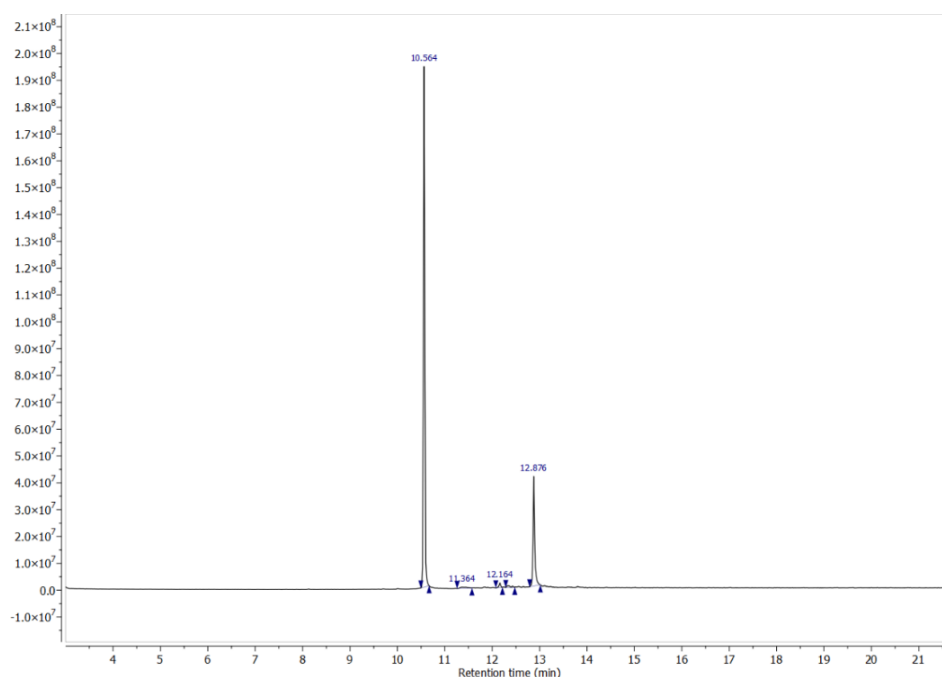


Figure 4.84: Gas chromatograph of $\text{O}((\text{Et}_2\text{N})_2\text{PO})_2_1_{\text{f13}}$.

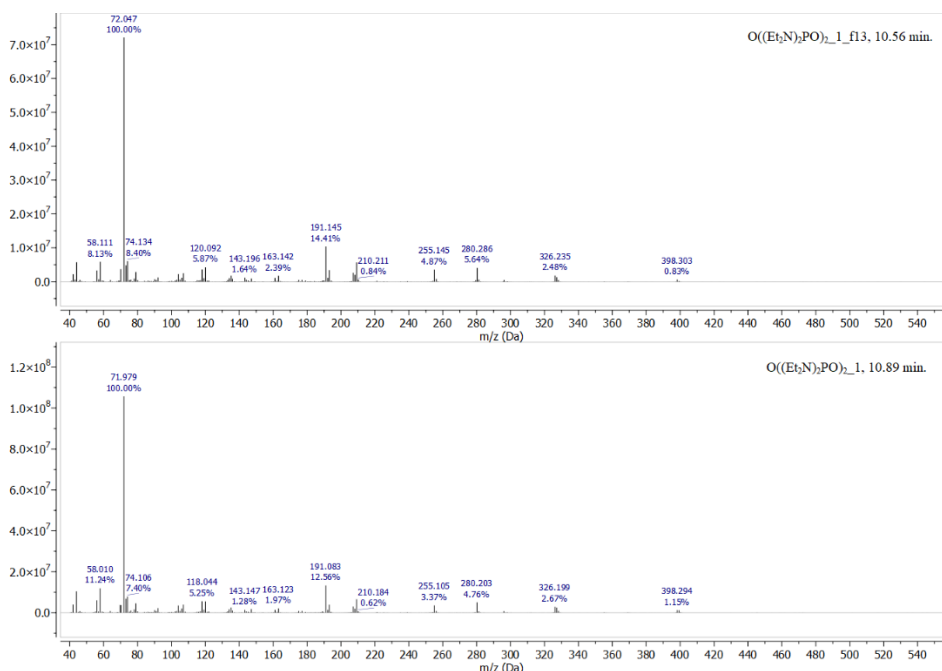


Figure 4.85: Mass spectrum of the 10.56 minute fraction of $\text{O}((\text{Et}_2\text{N})_2\text{PO})_2_1_{\text{f13}}$ (above) and the 10.89 minute fraction of $\text{O}((\text{Et}_2\text{N})_2\text{PO})_2_1$ (below).

4.2.1.3.5. Analysis by Single crystal X-ray diffraction

Freezing of the viscous liquids $O((Et_2N)_2PO)_2_1$ and $O((Et_2N)_2PO)_2_1_{f13}$ gave amorphous solids and therefore no structural data could be collected from these. $O((Et_2N)_2PO)_2_1_{f13}$ produced a small crop of colourless single crystals after standing in storage. Crystals were collected under oil and mounted in oil. Data was collected using a STOE Stadivari diffractometer with a microfocus Cu- $K_{\alpha 1}$ source. Structure solution was undertaken using the ShelXT Intrinsic phasing method and refined using the ShelXL least squares method.^{380,381} The crystallographic data obtained after structure solution and refinement is given in Table 4.15, while the molecular structure and unit cell are given in Figure 4.86 and Figure 4.87. The full set of data is presented in Appendix 12.

Table 4.15: Crystal data for $O((Et_2N)_2PO)_2_1_{f13}$.

Identification code	$O((Et_2N)_2PO)_2_1_{f13}$
Empirical formula	$C_{32}H_{84}N_{12}O_{20}P_4Ca_2$
Formula weight/ $gmol^{-1}$	1161.15
Crystal system	monoclinic
Space group	$P2_1/n$
$a/\text{\AA}$	10.6249(7)
$b/\text{\AA}$	15.5774(12)
$c/\text{\AA}$	17.0925(10)
$\alpha/^\circ$	90
$\beta/^\circ$	96.707(5)
$\gamma/^\circ$	90
Volume/ \AA^3	2809.6(3)
Z	2

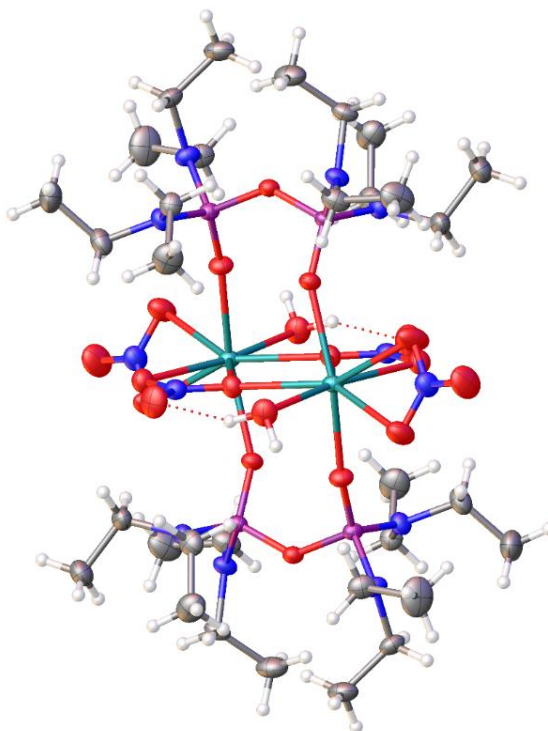


Figure 4.86: Molecular structure obtained for O((Et₂N)₂PO)₂_1_f13.

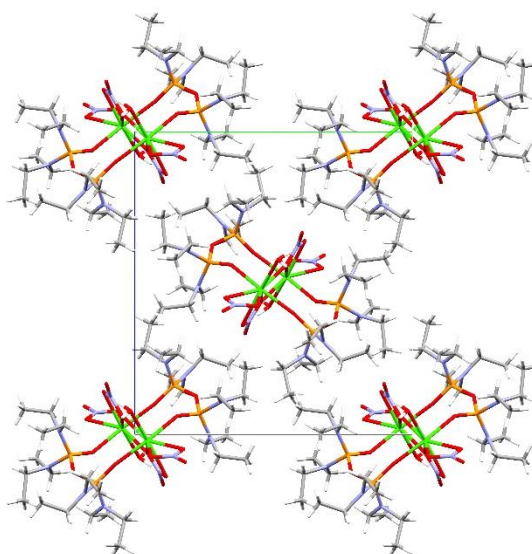


Figure 4.87: Unit cell for O((Et₂N)₂PO)₂_1_f13, as viewed along the *a*-axis.

The compound obtained was not the simple ligand desired but appeared to be a calcium complex of this ligand. The full formula of the compound was $\text{Ca}_2(\text{O}((\text{Et}_2\text{N})_2\text{PO})_2)_2(\text{NO}_3)_4(\text{H}_2\text{O})_2$. Although this solid proved the formation of the $\text{O}((\text{Et}_2\text{N})_2\text{PO})_2$ ligand it appeared that this ligand had complexed itself with $\text{Ca}(\text{NO}_3)_2$. This was unexpected and a clear derivation of the nitrate is unknown. The IR and GC-

MS data did not indicate the presence of nitrate which would be expected for this complex. This could indicate that this complex was in fact a minor component of the product O((Et₂N)₂PO)₂_1_f13 with the expected product O((Et₂N)₂PO)₂ being the major component in the viscous liquid obtained. Given that such crystallisation was not observed for the crude product O((Et₂N)₂PO)₂_1 it was believed that the possible intrusion of Ca(NO₃)₂ occurred during column chromatography. One probability was that some of the silica gel used was previously treated with dilute nitric acid and distilled water as an activation method and this introduced Ca(NO₃)₂ as an impurity in the silica gel due to reaction of CaO impurity with the nitric acid. The presence of water coordinating with the Ca²⁺ centres further indicated that this complex was a minor product since IR bands due to moisture were not observed in the IR spectrum of the bulk liquid O((Et₂N)₂PO)₂_1_f13.

No other complexes of the compound O((Et₂N)₂PO)₂ have been reported in literature making this an early example of this ligand's complexation ability. Given the structural similarities of O((Et₂N)₂PO)₂ and the more widely studied O((Me₂N)₂PO)₂ a similarity in the structure of their complexes was expected. However, this was not the case. O((Me₂N)₂PO)₂ is known to complex with divalent transition metals and magnesium to form simple chelation complexes of the structures [M(O((Me₂N)₂PO)₂)₃][ClO₄] M = Mg²⁺, Cu²⁺ or Co²⁺ and [Cu(O((Me₂N)₂PO)₂)₂(ClO₄)₂].^{208,209}

Ca₂(O((Et₂N)₂PO)₂)₂(NO₃)₄(H₂O)₂ contains Ca²⁺ centres with a CN of 8, which is typical for Ca²⁺. Two O((Et₂N)₂PO)₂ are bonded through a singular P=O group each at the axial positions. This monodentate bonding causes the O((Et₂N)₂PO)₂ to act as a bridging ligand. The nitrate and aqua ligands are bound in the equatorial positions. Therefore, Ca₂(O((Et₂N)₂PO)₂)₂(NO₃)₄(H₂O)₂ is an example of a complex in which a di-N-substituted pyrophosphoramidate compound acts as a bridging ligand, along with two of the complexed nitrates. This bridging behaviour was probably due to the presence of these nitrate anions which remained coordinated. Similar structures may not have been reported, as previous work on complexation of O((Me₂N)₂PO)₂ dealt mainly with perchlorate starting reagents.

Packing of these complexes is shown in Figure 4.88 to be mainly due to the packing of the ethyl moieties in relation to one another. Along the *a*-axis neighbouring complexes are bound by intermolecular hydrogen bonding of the type N–O---H–O in the synthon shown in Figure 4.88, incorporating the aqua ligand and the non-bridging nitrate

anion. This same aqua ligand forms a similar intramolecular hydrogen bonding motif with the bridging nitrate although this does not seem to affect the intramolecular structure.

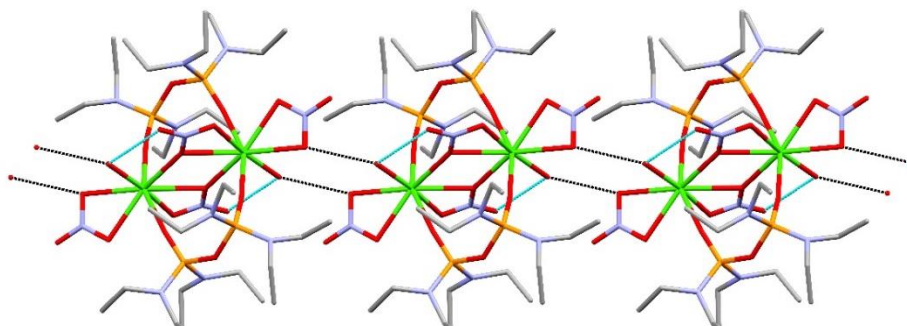


Figure 4.88: Intermolecular (black) and intramolecular (blue) N–O---H–O hydrogen bonding that created the packing chains for O((Et₂N)₂PO)_{2_1_f13} along the *a*-axis, viewed along the *c*-axis.

4.2.1.3.6. Conclusion

The crude product, O((Et₂N)₂PO)_{2_1}, contained numerous phosphorus containing compounds, as described in the interpretation of the respective ³¹P NMR and ³¹P{¹H} NMR spectra. The presence of numerous compounds was further supported by the GC-MS data. O((Et₂N)₂PO)_{2_1_f13} was most likely the desired product. ³¹P NMR data indicated that at least 2 phosphorus containing compounds were present in the product O((Et₂N)₂PO)_{2_1_f13}, one of which was the major component. This 2 component system was also observed in the GC-MS data for the same product. The major component for both O((Et₂N)₂PO)_{2_1} and O((Et₂N)₂PO)_{2_1_f13} seemed to be the same compound as described by the ³¹P NMR and GC-MS data. ¹H NMR, ³¹P NMR and GC-MS data for O((Et₂N)₂PO)_{2_1_f13} inferred that this major component was in fact O((Et₂N)₂PO)₂. The product in O((Et₂N)₂PO)_{2_1_f13}, was cleaner than that in O((Et₂N)₂PO)_{2_1}. IR data for both O((Et₂N)₂PO)_{2_1} and O((Et₂N)₂PO)_{2_1_f13} also indicated the superior purification of O((Et₂N)₂PO)_{2_1_f13} and in both cases most bands were indicative of the formation of the desired compound. Single crystals obtained from O((Et₂N)₂PO)_{2_1_f13} indicated that a Ca²⁺ complex formed as a minor component of the product after column chromatography. This complex Ca₂(O((Et₂N)₂PO)₂)₂(NO₃)₄(H₂O)₂ proved novel and an early example of complexation for the O((Et₂N)₂PO)₂.

4.2.1.4. Characterisation of O((iPrNH)₂PO)₂

Numerous products were obtained in the attempts undertaken to synthesise this compound, as given in Section 3.3.2.1.4. In each case solids which were typically colourless or very pale yellow and which were either crystalline or amorphous in nature were obtained. The products formed throughout the procedure, as described in Section 3.3.2.1.4, and discussed hereunder were labelled as O((iPrNH)₂PO)_{2_1_a}, O((iPrNH)₂PO)_{2_1_b}, O((iPrNH)₂PO)_{2_1_b1}, O((iPrNH)₂PO)_{2_1_c1} and its various column chromatography fractions and O((iPrNH)₂PO)_{2_1_c2}. The respective yield for O((iPrNH)₂PO)_{2_1_b} was 40.6 %, while the yields for the remaining products were not calculated due to the small amounts obtained.

4.2.1.4.1. Analysis by Infra-red spectroscopy

The first solid obtained through the reaction described in Section 3.3.2.1.4., namely O((iPrNH)₂PO)_{2_1_a}, was characterised by IR spectroscopy. This indicated that this product was mainly the expected side product *i*PrNH₃Cl.³⁸² The IR spectra for the remaining O((iPrNH)₂PO)_{2_1} products (except for the chromatography fractions discussed further on) are shown in Figure 4.89. These spectra were similar to each other, indicating the formation of the same mixture of compounds within each sample obtained. The first bands of interest were the numerous bands which indicated the presence of the *i*PrNH₃Cl salt. The organic ammonium combination bands in the range 2800–1800 cm⁻¹, the bands at 1637 cm⁻¹, 1527 cm⁻¹ and 1396 cm⁻¹ in the range for δ C–H vibrations, the band at 804 cm⁻¹ believed to be due to ω N–H vibration and the bands at 1229 cm⁻¹ and 952 cm⁻¹, believed to be analogous to the 1218 cm⁻¹ and 939 cm⁻¹ bands of the salt, were all observed in these products and were believed to be due to the presence of the *i*PrNH₃Cl salt.³⁸² In the case of all these bands it was observed that in the spectra of the crystalline products O((iPrNH)₂PO)_{2_1_b1} and O((iPrNH)₂PO)_{2_1_c2} these bands were less noticeable, indicating the loss of the salt on obtaining the crystalline products rather than the residue products.

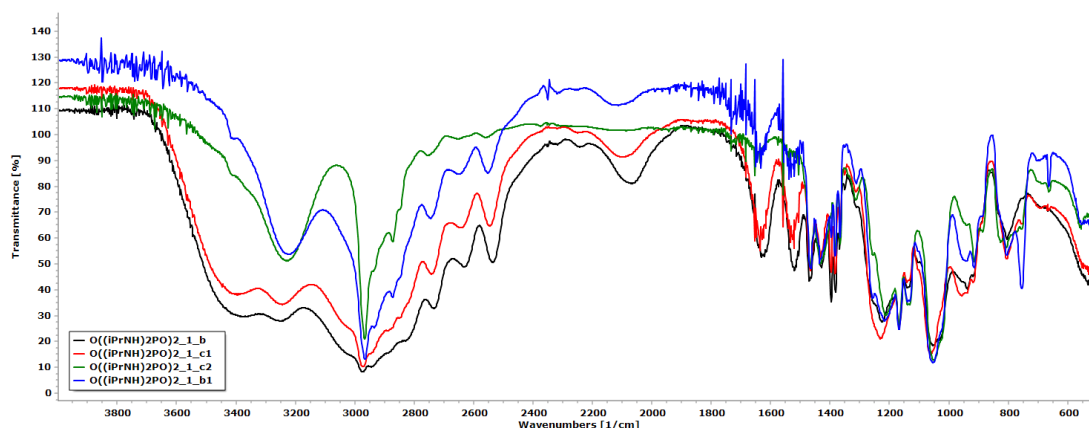


Figure 4.89: IR spectra of $O((iPrNH)_2PO)_2_1_b$ (black), $O((iPrNH)_2PO)_2_1_c1$ (red) and $O((iPrNH)_2PO)_2_1_c2$ (green) and $O((iPrNH)_2PO)_2_1_b1$ (blue).

The two bands observed in the IR spectra of all $O((iPrNH)_2PO)_2_1$ products, at 3400 cm^{-1} and approximately 3252 cm^{-1} are believed to be due to two distinct ν N–H vibrations, given that other bands typical of water intrusion were not present. The decreased intensity of the band at 3400 cm^{-1} in products $O((iPrNH)_2PO)_2_1_b1$ and $O((iPrNH)_2PO)_2_1_c2$ indicated that this was likely due to the salt by-product.³⁸² In the cases of the residues $O((iPrNH)_2PO)_2_1_b$ and $O((iPrNH)_2PO)_2_1_c1$ these bands were broad and strong bands, while in the crystalline $O((iPrNH)_2PO)_2_1_b1$ and $O((iPrNH)_2PO)_2_1_c2$ the band at 3400 cm^{-1} was greatly diminished but also sharpened. The bands at 1466 cm^{-1} , 1432 cm^{-1} , 1396 cm^{-1} , 1382 cm^{-1} and 1367 cm^{-1} in all the spectra of the $O((iPrNH)_2PO)_2_1$ products, accounting for minor variations were assigned to isopropyl δ C–H vibrations.

In the case of all the IR spectra for the $O((iPrNH)_2PO)_2_1$ products the bands at 1167 cm^{-1} and 1136 cm^{-1} were assigned to the ν C–N vibrations. This indicated that if these were due to the presence of the desired product the formation of P–N bonds did not affect the stiffness of the C–N bonds. The shoulder at 1257 cm^{-1} and the strong band at around 1229 cm^{-1} could be tentatively assigned in all $O((iPrNH)_2PO)_2_1$ spectra to the ν P=O vibration, as they fell in the same range attributed to these vibrations. This shift to lower wavenumbers from the PPTC value of 1316 cm^{-1} , was expected on preparation of the desired product. This shift was due to the slight decrease in the electronegativity of the substituents about the phosphorus centres on the formation of the desired product, leading to a decrease in bond order of the P=O bond to the P^+-O^- moiety.⁹⁹ This would lead to a shift of the ν P=O band to lower wavenumbers as shown by the two bands at 1257 cm^{-1} and 1229 cm^{-1} .

The bands at 1055 cm⁻¹ and 914 cm⁻¹ and the shoulders at 1026 cm⁻¹ and 886 cm⁻¹ could be possibly due to ν_{as} P–O–P vibrations. The two band pairs could indicate that at least two distinct modes of ν_{as} P–O–P vibration are present in the product. These two modes would be due to increased P–O–P bond stiffness (for the 1055 cm⁻¹ and 1026 cm⁻¹ bands) and decreased P–O–P bond stiffness (for the 914 cm⁻¹ and 886 cm⁻¹ bands), given in relation to the band for PPTC. The formation of these two bands could have multiple explanations. The formation of distinct structures P–O=P \leftrightarrow P=O–P may have occurred, however the mechanism for this is unknown. Secondly this could indicate the formation of an asymmetric product indicating the production of an unknown and undesired product. A third possible explanation could be crystallographic rather than chemical. In the case of the formation of the desired product numerous intermolecular bonding modes are possible, especially about the P=O and the N–H moieties, which could cause different shifts in the IR bands of these moieties. Alternatively all four bands could be due to P–N–C vibrations, including ν P–N vibrations, which are typically also found in this region and which could indicate the formation of the desired compound or another similar species containing the P–N–C group. The bands at 1055 cm⁻¹ and 1026 cm⁻¹ also fell in the range typical for the ν C–N and ρ P–N–H vibrations, again yielding the same general conclusion. Therefore although these bands could be attributed to vibrations of either the P–O–P, P–N–C or P–N–H moieties expected for the desired product definitive assignment was not possible and a full description of the structure from the IR data could not be undertaken.

The band at 750 cm⁻¹ for O((*i*PrNH)₂PO)_{2_1_b1}, O((*i*PrNH)₂PO)_{2_1_c1} and O((*i*PrNH)₂PO)_{2_1_c2} could be assigned to either ν_{s} P–O–P or ν P–N vibrations. Therefore, in all O((*i*PrNH)₂PO)_{2_1} cases it is believed that the desired compound or a compound very similar to the desired product was obtained.

Given that a number of IR bands in the spectra of the O((*i*PrNH)₂PO)_{2_1} products indicated the presence of the *i*PrNH₃Cl salt and that data obtained from the ¹H NMR and ³¹P NMR spectroscopy, as discussed in Sections 4.2.1.4.2 and 4.2.1.4.3 respectively, indicated the presence of multiple compounds in the crude O((*i*PrNH)₂PO)_{2_1} products, it was decided to purify a sample of O((*i*PrNH)₂PO)_{2_1_c1} by column chromatography.

Figure 4.90 shows the IR spectra for the residues obtained from the column chromatography. As expected the bands typical of the *i*PrNH₃Cl salt were not present in these spectra. For all these IR spectra bands assigned to ν O–H and δ O–H vibrations were observed. This was expected given that the eluents used in this chromatography

were not dried prior to use. Most bands remained unchanged from the spectrum of $O((iPrNH)_2PO)_2_1_c1$ and therefore only significant changes are discussed hereunder. In all cases the band at 1229 cm^{-1} shifted to the range $1222\text{--}1204\text{ cm}^{-1}$, as was observed for the $O((iPrNH)_2PO)_2_1_c2$ spectrum. The fractions that showed most purification were the final fractions, namely $O((iPrNH)_2PO)_2_1_c1_f10$ and $O((iPrNH)_2PO)_2_1_c1_f15$. In both of these spectra the band at 957 cm^{-1} present in the other fractions was lost indicating that this band was indeed due to some impurity and not due to $\nu_{as}\text{ P-O-P}$ or P-N-C vibrations. The band at 916 cm^{-1} was typical of the given product and this could be due to the $\nu_{as}\text{ P-O-P}$ or P-N-C vibrations. For these spectra it was observed that the band at about 800 cm^{-1} , which could be due to either $iPrNH_3Cl$ or PPTC, was lost or significantly diminished. On the contrary the band around 771 cm^{-1} , which could be due to $\nu_s\text{ P-O-P}$ or $\nu\text{ P-N}$ vibrations, became increasingly prominent, and was present in increasing intensity for $O((iPrNH)_2PO)_2_1_c1_f10$ and $O((iPrNH)_2PO)_2_1_c1_f15$. This could be analogous to the band at 750 cm^{-1} for $O((iPrNH)_2PO)_2_1_b1$.

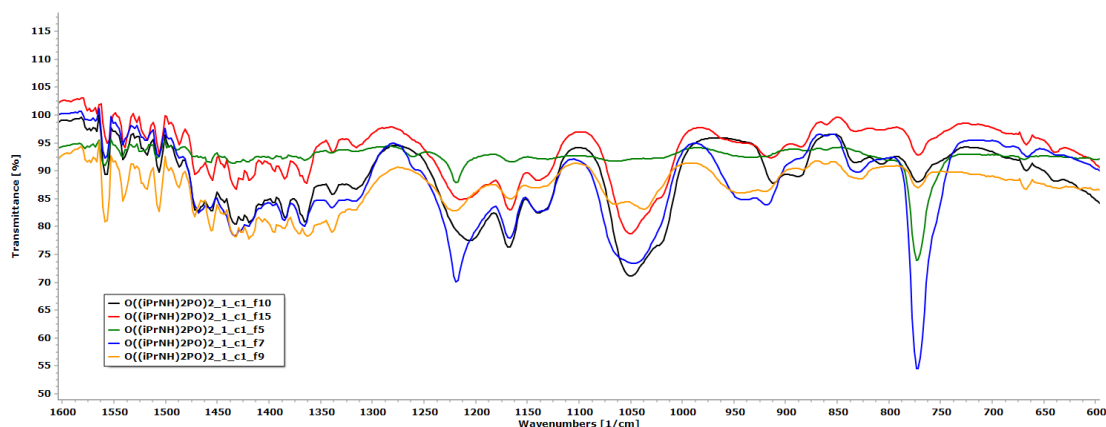


Figure 4.90: IR spectra of column chromatography fractions obtained from $O((iPrNH)_2PO)_2_1_c1$.

4.2.1.4.2. Analysis by ^1H NMR spectroscopy

Products obtained from the reaction undertaken to synthesise $O((iPrNH)_2PO)_2$ were analysed by ^1H NMR spectroscopy. The spectra of $O((iPrNH)_2PO)_2_1_b$ and $O((iPrNH)_2PO)_2_1_b1$ were obtained with very unexpected results. The ^1H NMR spectrum of $O((iPrNH)_2PO)_2_1_b$ is given in Figure 4.91, along with the spectrum of $iPrNH_3Cl$. The similarity in the major peaks would indicate that the major component of $O((iPrNH)_2PO)_2_1_b$ was the $iPrNH_3Cl$ salt, in contrast to the data obtained from IR spectra. The peak at 1.15 ppm however also indicated the presence of a secondary isopropyl methyl proton species possibly from the desired product.

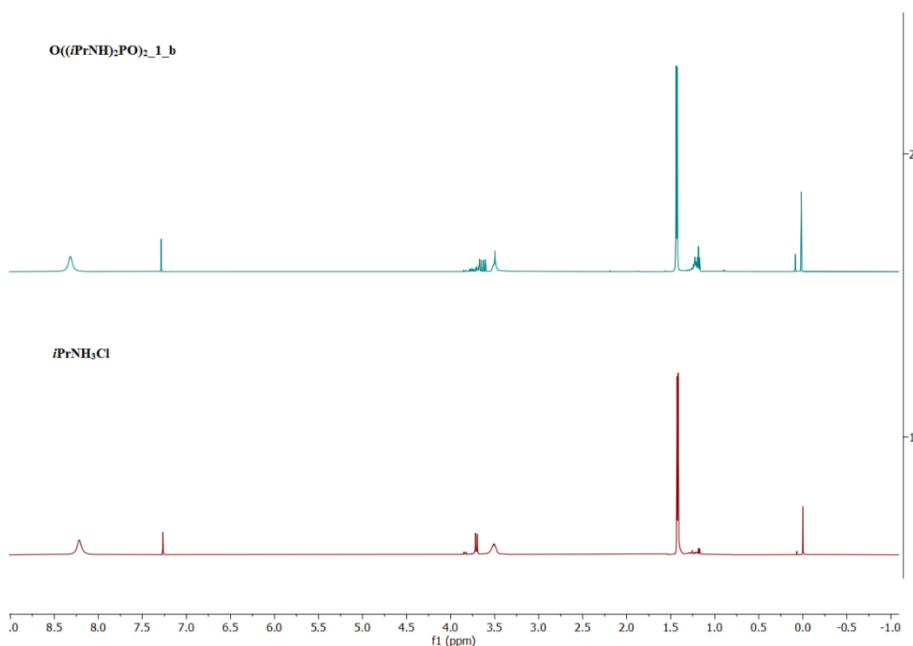


Figure 4.91: ^1H NMR spectra of $\text{O}((i\text{PrNH})_2\text{PO})_2_1_b$ (blue) and $i\text{PrNH}_3\text{Cl}$ (red).

The ^1H NMR spectrum of $\text{O}((i\text{PrNH})_2\text{PO})_2_1_b1$ is given in Figure 4.92. The peak data is given in Table 4.16. It was clear that $i\text{PrNH}_3\text{Cl}$ salt was a significant component of the solid product, as indicated by the peaks at 8.31 ppm, 3.64 ppm and 1.39 ppm. A detailed discussion of the remaining peaks given in Table 4.17 is given hereunder.

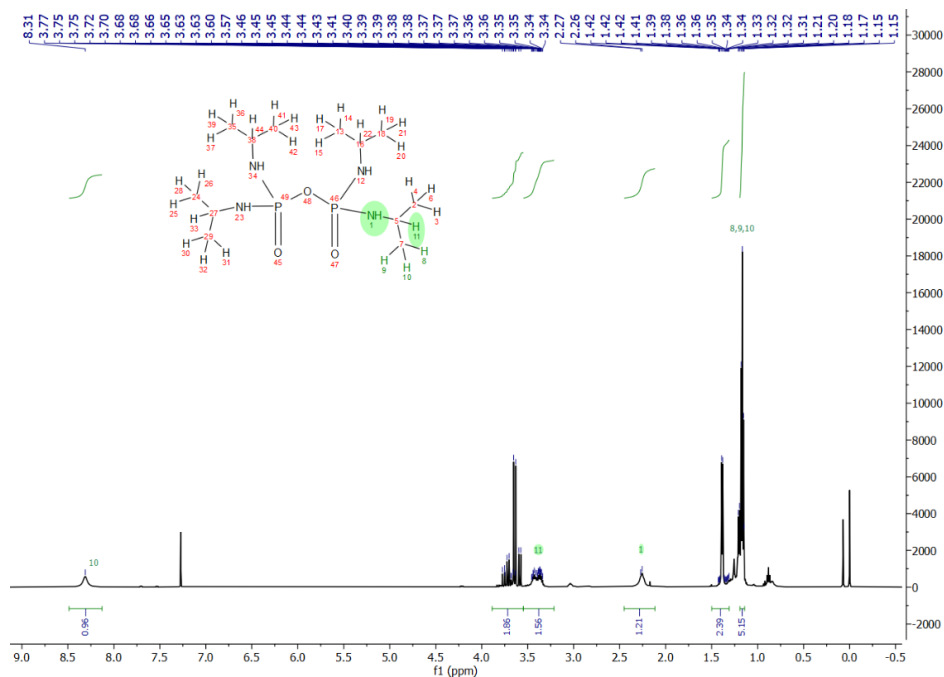


Figure 4.92: ^1H NMR spectrum of $\text{O}((i\text{PrNH})_2\text{PO})_2_1_b1$.

Table 4.16: ^1H NMR experimental data and assignment for proton peaks of $\text{O}((i\text{PrNH})_2\text{PO})_2_1_{b1}$ in CDCl_3 .

^1H NMR experimental data and assignment for proton peaks of $\text{O}((i\text{PrNH})_2\text{PO})_2_1_{b1}$ in CDCl_3				
ppm	Multiplicity	Integration	Coupling	Assignment
8.31	singlet	1.00	N/A	NH_3^+ (amine salt)
3.64	triplet of doublets	1.17	N/A	CH (Iso-propyl, amine salt)
3.40	multiplet	1.00	N/A	CH (Iso-propyl, product)
2.26	broad singlet	1.17	N/A	NH (product)
1.39	doublet	2.39	$J = 6.50 \text{ Hz}$	CH_3 (Iso-propyl, amine salt)
1.14	triplet	6.15	$J = 6.20 \text{ Hz}$	CH_3 (Iso-propyl, product)

Three main peaks of interest were noted, namely the multiplet at 3.40 ppm, the broad singlet at 2.26 ppm and the triplet at 1.14 ppm, assigned to the iso-propyl C–H, N–H moiety and the iso-propyl methyl protons respectively. This was confirmed by the 1:1.17:6.15 (CH:NH:CH₃) integration value ratio indicating the presence of the *iPrNH*–group. The iso-propyl C–H and methyl peaks were both shifted downfield from the analogous peaks for *iPrNH*₂, which are found at 3.10 ppm and 1.06 ppm respectively. These shifts indicated loss of electron density around the amine nitrogen and its proton, which could be due to the formation of the P–N bond wherein the more electronegative N could lose electron density through negative hyperconjugation effects; although this cannot be described with certainty. The same downfield shift, but with a greater intensity, was observed from the *iPrNH*₂ peak at 1.11 ppm, to the $\text{O}((i\text{PrNH})_2\text{PO})_2_1_{b1}$ peak at 2.26 ppm. This peak did not show coupling which could be assigned to the nitrogen atom to which the phosphorus and proton are bound.

A major issue in this NMR spectrum was that the peak at 1.14 ppm was a triplet rather than the expected doublet. This would indicate the presence of two coupling protons which is not possible for the iso-propyl moiety. The reason why a triplet was

obtained in the spectrum of O((iPrNH)₂PO)₂_1_b1 for the peak at 1.14 ppm, rather than the expected doublet, is unknown. The remaining minor peaks in the region 1.5-0.5 ppm of the spectrum of O((iPrNH)₂PO)₂_1_b1 were indicative of the presence of impurities possibly containing similar iso-propyl methyl proton species which could not be described further. This data indicated that in both O((iPrNH)₂PO)₂_1_b and O((iPrNH)₂PO)₂_1_b1, the *i*PrNH₃Cl salt and other products were obtained, with O((iPrNH)₂PO)₂_1_b1 containing a higher amount of the said other products. Further impurity peaks were noted for silicone grease (0.07 ppm) and in a number of peaks in the region 4.0-3.5 ppm. The latter peaks were likely due to other phosphorus containing organic species and similar peaks in this region were noted for most spectra discussed in this section.

The product O((iPrNH)₂PO)₂_1_c1 gave a spectrum similar to that obtained for O((iPrNH)₂PO)₂_1_b1, with the details given in Table 4.17.

Table 4.17: ¹H NMR experimental data and assignment for proton peaks of O((iPrNH)₂PO)₂_1_c1 in CDCl₃.

¹H NMR experimental data and assignment for proton peaks of O((iPrNH)₂PO)₂_1_c1 in CDCl₃				
ppm	Multiplicity	Integration	Coupling	Assignment
8.27	broad singlet	1.60	N/A	NH ₃ ⁺ (amine salt)
3.44	triplet	1.00	N/A	CH (Iso-propyl, amine salt)
3.36	multiplet	0.75	N/A	CH (Iso-propyl, product)
2.38	broad triplet	0.36	N/A	NH (product)
1.39	doublet	3.43	J = 6.50 Hz	CH ₃ (Iso-propyl, amine salt)
1.17	triplet	4.93	J = 6.20 Hz	CH ₃ (Iso-propyl, product)

The major difference in the O((iPrNH)₂PO)₂_1_c1 spectrum when compared to the spectrum of O((iPrNH)₂PO)₂_1_b1 is that the broad triplet assigned to the NH of the product was found in lesser amounts, with only a 0.36 integration value as opposed to the

expected 1. Apart from this, it is clearly visible that as with the spectrum of $O((iPrNH)_2PO)_2_1_b1$ both the same major products and the by-product ammonium salt were present in this product.

The spectrum for $O((iPrNH)_2PO)_2_1_c2$, as given in Figure 4.93, did not have the typical NH_3^+ (amine salt) peak at around 8.20 ppm, which indicated that the salt by-product was not present. Although the spectrum contained all the expected peaks for the protons of groups CH (iso-propyl, product) and CH_3 (iso-propyl, product), it also showed a number of broad peaks in the region 3.20–1.40 ppm. In previous products a singular peak at about 2.35 ppm was typically assigned to the N–H of the desired product, and although a peak at 2.22 ppm was obtained in this case, the other peaks in this region could indicate the formation of a mixture of N–H containing products. Integration data would indicate that both the peak at 2.22 ppm and that at 2.99 ppm could be related to the triplet which remained typical of the iso-propyl methyl group (with an approximate integration ratio of 1:6 in both cases).

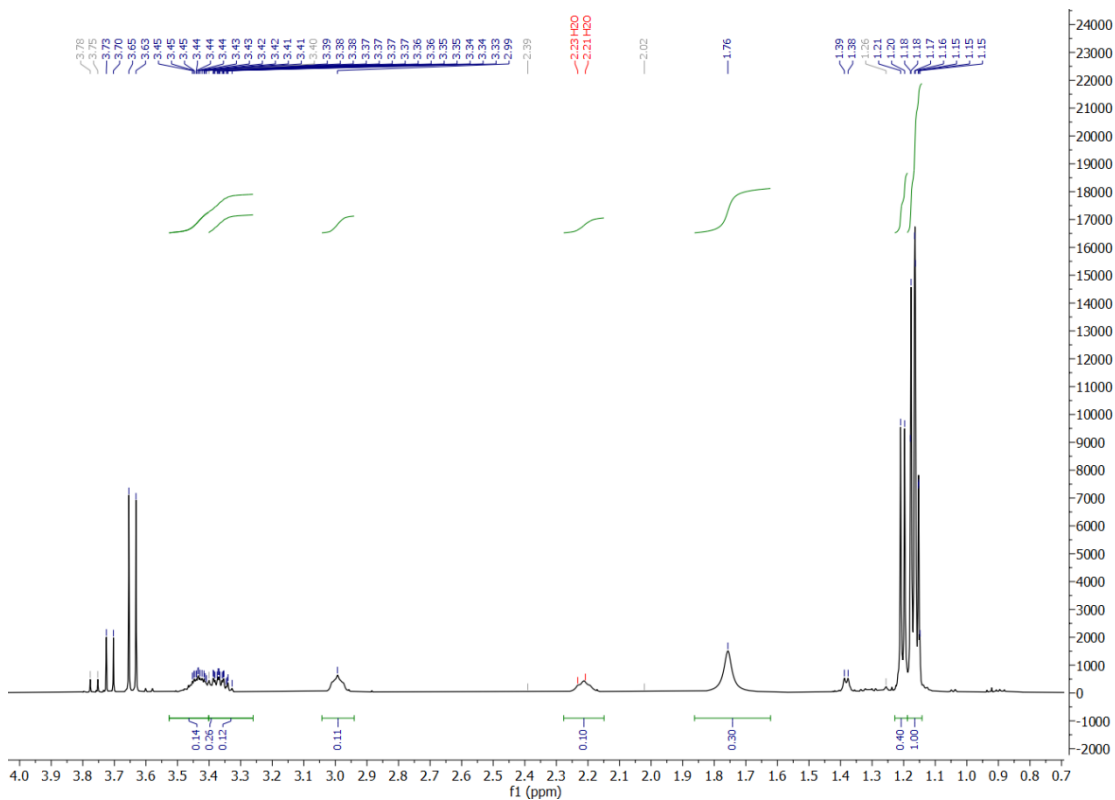


Figure 4.93: 1H NMR spectrum of $O((iPrNH)_2PO)_2_1_c2$.

As described in Section 3.3.2.1.4.2, a sample of $O((iPrNH)_2PO)_2_1_c1$ was purified by column chromatography and this yielded numerous fractions. The 1H NMR spectra of fractions which gave the most interesting results are given in Figure 4.94. These

spectra did not show the peak at about 8.27 ppm and therefore it was possible that the salt was removed early on in the chromatography process. The peaks visible in these fractions are given in Table 4.18, for ease of comparison, where blank cells indicate that no analogous peak was observed for the fraction. In all cases the peaks assigned to the product iso-propyl CH and CH₃ protons were present. However, only the spectrum of the fraction O((iPrNH)₂PO)₂_1_c1_f10 retained the same peak assigned to the expected product N–H peak. All other fractions had bands either at 1.75 ppm or 1.61 ppm, which could indicate the presence of numerous N–H species, similar to the expected P–N–H moiety. Therefore, from this data it was concluded that the product O((iPrNH)₂PO)₂_1_c1_f10 was the product of interest in the original product O((iPrNH)₂PO)₂_1_c1. Given the chemical shift assigned to the product N–H was at 2.29 ppm in this product, it is inferred that it is the same major product as that obtained in O((iPrNH)₂PO)₂_1_b1 but purified further. The integration values of the peaks assigned to product protons for O((iPrNH)₂PO)₂_1_c1_f10 further corroborated the production of a *i*PrNH– group. The ratio of integration values for CH:NH:CH₃ was of 1.00:0.96:6.28 which is in agreement with the ratio of integration values for the expected moiety. The triplet coupling for the CH₃ group remains however problematic to explain.

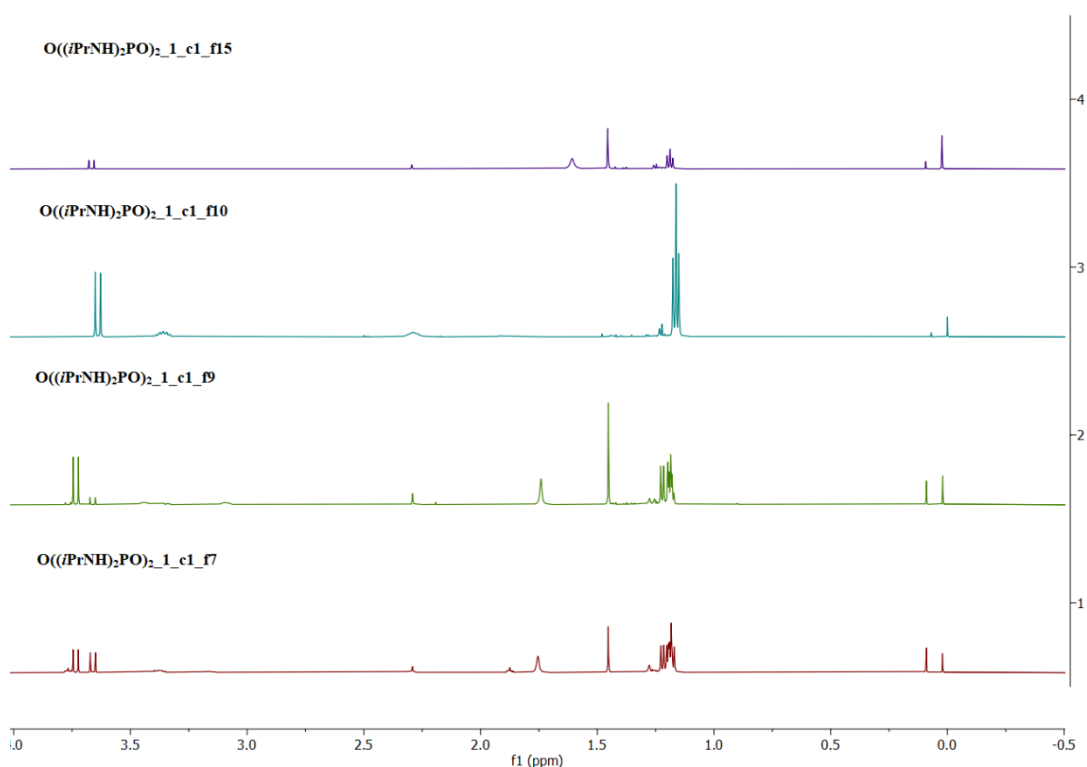


Figure 4.94: ¹H NMR of fractions f7, f9, f10 and f15 of O((iPrNH)₂PO)₂_1_c1.

Table 4.18: Comparison of analogous peaks in the spectra of the chromatography fractions f7, f9, f10 and f15 of O((iPrNH)₂PO)₂_1_c1

_c1	Assign.	_c1_f7	_c1_f9	_c1_f10	_c1_f15
8.27 (bs)	NH ₃ ⁺ (amine salt)				
3.44 (t)	CH (Iso-propyl, amine salt)	3.44 (m)	3.44 (m)		
3.36 (m)	CH (Iso-propyl, product)	3.37 (m)	3.37 (m)	3.37 (m)	3.37 (m)
2.38 (bt)	NH (product)			2.29 (bt)	
	NH (product)	1.75 (s)	1.75 (s)		
	NH (product)				1.61 (s)
1.39 (d)	CH ₃ (Iso-propyl, amine salt)	1.44 (s)	1.44 (s)	1.44 (s)	1.44 (s)
	N/A	1.22 (d)	1.22 (d)		
1.17 (t)	CH ₃ (Iso-propyl, product)	1.19 (t)	1.19 (t)	1.16 (t)	1.16 (t)

4.2.1.4.3. Analysis by ³¹P NMR spectroscopy

The products from reaction O((iPrNH)₂PO)₂_1 that showed the possibility of containing the desired product following analysis by ¹H NMR spectroscopy were analysed using ³¹P{¹H} NMR spectroscopy. The spectra of O((iPrNH)₂PO)₂_1_b and O((iPrNH)₂PO)₂_1_b1 are given together in Figure 4.95. Numerous peaks were observed indicating that numerous phosphorus containing species were present. This was in agreement with previous IR and ¹H NMR data, which showed the presence of possible impurities. It could be qualitatively inferred that the product O((iPrNH)₂PO)₂_1_b1 showed a decrease in the intensity of numerous peaks, indicating that for both O((iPrNH)₂PO)₂_1_b and O((iPrNH)₂PO)₂_1_b1 the main product obtained and retained in the crystalline O((iPrNH)₂PO)₂_1_b1 was the phosphorus species indicated by the peak at 14.33 ppm. Since O((iPrNH)₂PO)₂_1_b1 was crystalline in nature it was believed that this species was most likely the main product of the reaction.

The majority of the peaks were found to be downfield from the PPTC peak at -9.52 ppm. These downfield shifts from the PPTC peak were indicative of a compound where the P atom is deshielded either by electronic or magnetic means. This type of deshielding was to be expected if the desired product was obtained, given that usually phosphoryl compounds of the structure $\text{O}=\text{P}(\text{NR}_2)_3$ and $\text{O}=\text{P}(\text{OR})_3$, especially the former, are known to give peaks downfield of those of the phosphoryl halides.^{282,249} This arises from the ability of halides to form π -back bonds to the phosphorus centre, which are stronger than those for amine nitrogen and oxygen. In describing these effects the $\text{P}=\text{O}$ bond will not be regarded as a typical double bond but as the effect of negative hyperconjugation on the basic bond P^+-O^- . This back bonding decreases the positive charge about the phosphorus in the P^+-O^- moiety, increasing electron density about the phosphorus centre, which causes shielding and therefore an upfield shift.³⁷⁷ This could therefore indicate that one of the species present was the desired product.

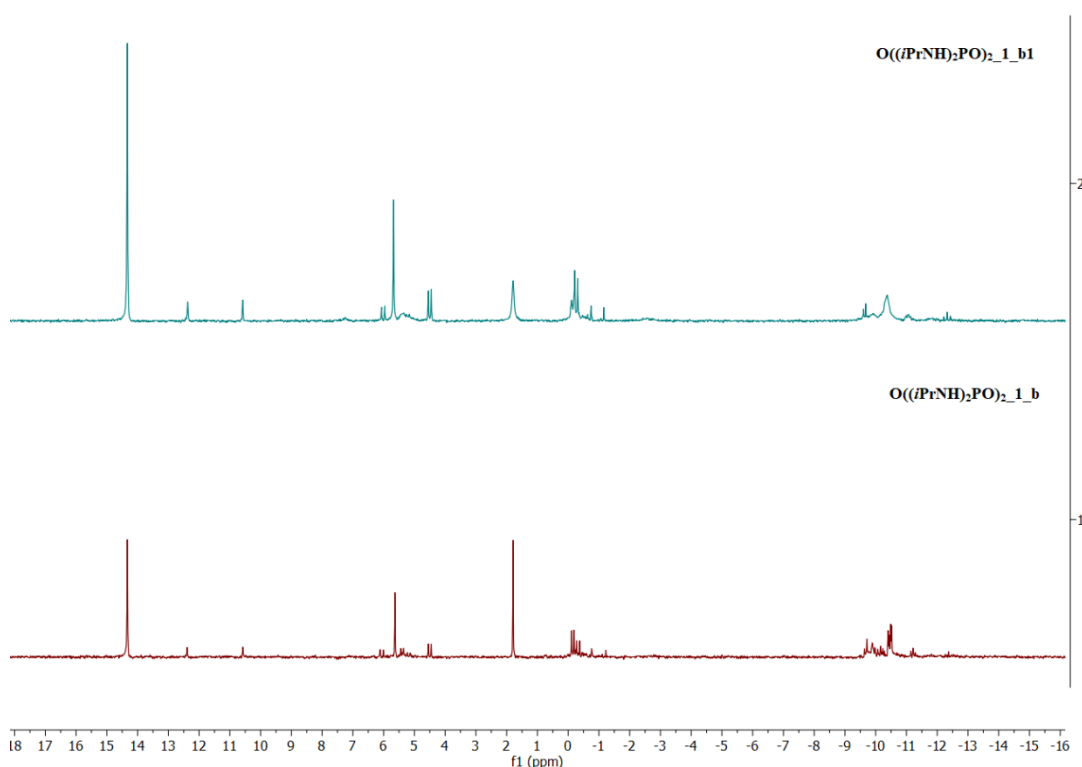


Figure 4.95: $^{31}\text{P}\{^1\text{H}\}$ NMR spectra of $\text{O}((i\text{PrNH})_2\text{PO})_2_1_b$ (red) and $\text{O}((i\text{PrNH})_2\text{PO})_2_1_b1$ (blue).

The product $\text{O}((i\text{PrNH})_2\text{PO})_2_1_c1$ was also analysed to yield the spectrum given in Figure 4.96, which was very similar to the spectra of $\text{O}((i\text{PrNH})_2\text{PO})_2_1_b$ and $\text{O}((i\text{PrNH})_2\text{PO})_2_1_b1$. Therefore, it seems that the same phosphorus species were obtained for $\text{O}((i\text{PrNH})_2\text{PO})_2_1_c1$. This trend was also observed for the

chromatography fractions obtained from $O((iPrNH)_2PO)_2_1_c1$ and for the crystalline $O((iPrNH)_2PO)_2_1_c2$. Given these similarities the peak data for all the spectra of the $O((iPrNH)_2PO)_2_1$ products is given in Table 4.19 for ease of comparison. The rows relay analogous peaks for the various products, with the relative intensity of the peak compared to others in the same spectrum given in brackets.

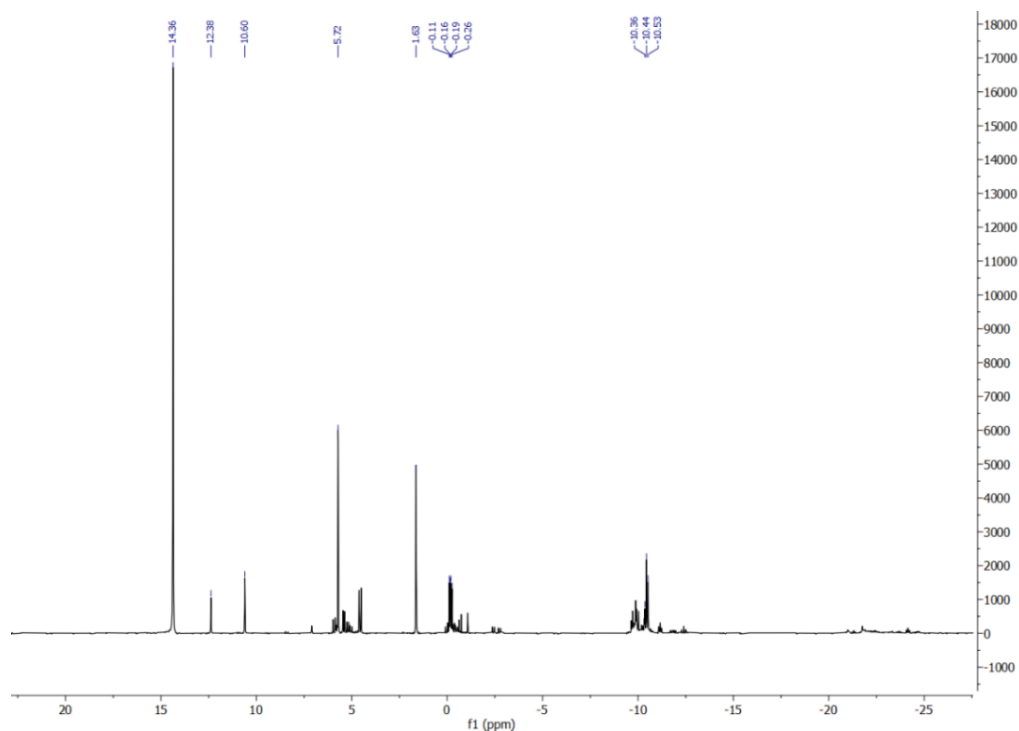


Figure 4.96: $^{31}P\{^1H\}$ NMR spectrum of $O((iPrNH)_2PO)_2_1_c1$.

The $^{31}P\{^1H\}$ NMR data for these compounds, as summarised in Table 4.19, shows the presence of two major phosphorus containing products in the products obtained from the synthesis reactions. The compound yielding the peak at 12.38-12.29 ppm was present in most of the products and believed to be the unexpected side product $(iPrNH)_3PO$ (detailed characterisation data of this compound is given in Appendix 13 and was collected from a failed attempt at preparing $O((iPrNH)_2PO)_2$).³⁸³ For the products obtained from the reaction $O((iPrNH)_2PO)_2_1$, the only phosphorus species common to all products was the one which gave the peak at 14.38-14.27 ppm. This was the only species which was separated in the column chromatography fraction, $O((iPrNH)_2PO)_2_1_c1_f10$. The major species observed through the presence of these peaks at 14.38-14.27 ppm could therefore be the desired compound.

It should be stated that coupled ^{31}P NMR spectra did not yield information on proton to phosphorus coupling which could be used to describe these products further.

Table 4.19: $^{31}\text{P}\{^1\text{H}\}$ NMR peak data for the various products obtained during the attempts to synthesise $\text{O}((i\text{PrNH})_2\text{PO})_2$, giving the analogous peaks for each row and the relative intensities of the peaks in brackets.

_b	_b1	_c1	_c1_f7	_c1_f9	_c1_f10	_c1_f15	_c2
14.38 (1)	14.33 (1)	14.36 (1)	14.27 (2)	14.32 (3)	14.33 (1)	14.34 (1)	14.32 (2)
12.39 (7)	12.37 (7)	12.38 (7)					12.32 (4)
10.58 (6)	10.58 (6)	10.6 (4)	10.52 (3)	10.58 (2)			10.61 (3)
5.63 (3)	5.68 (2)	5.72 (2)	6.07 (1)	5.92 (1)		5.81 (3)	5.77 (1)
	4.55 (5)						
1.79 (2)	1.79 (4)	1.63 (3)					
			-0.56 (4)	-0.53 (4)			
-0.14 (4)	-0.12 (3)	-0.18 (6)				-0.14 (2)	
-10.48 (5)	-10.36 (8)	-10.44 (5)					

4.2.1.4.4. Analysis by Gas chromatography Mass spectroscopy (GC-MS)

The products $\text{O}((i\text{PrNH})_2\text{PO})_2$ _1_b1 and $\text{O}((i\text{PrNH})_2\text{PO})_2$ _1_c1_f10 were analysed using GC-MS, following the interesting information obtained from the IR, ^1H NMR and ^{31}P NMR spectroscopy data.

This was especially the case with sample $\text{O}((i\text{PrNH})_2\text{PO})_2$ _1_c1_f10, given that both the ^1H NMR and $^{31}\text{P}\{^1\text{H}\}$ NMR spectra indicated the presence of a single compound. The gas chromatograph of this $\text{O}((i\text{PrNH})_2\text{PO})_2$ _1_c1_f10 fraction is given in Figure 4.97, showing the presence of two peaks, with the peak at 6.322 minutes being the clear major one. The mass spectrum of the component described by the peak at 7.244 minutes indicated that this impurity was $(i\text{PrNH})_3\text{PO}$ (details given in Appendix 13).³⁸³ The peak at 6.322 minutes was therefore likely to be due to the major chemical component. This indicated that although the ^{31}P NMR data for $\text{O}((i\text{PrNH})_2\text{PO})_2$ _1_c1_f10 showed the presence of a single phosphorus species, $(i\text{PrNH})_3\text{PO}$ could have also been present as a very minor component; as was the case for other chromatography fraction products analysed by ^{31}P NMR spectroscopy. All the peaks obtained from the mass spectrum of

the 6.322 minutes chromatography peak of $O((iPrNH)_2PO)_2_1_c1_f10$ are given in Figure 4.98. The peaks at 44.12 m/z, 58.11 m/z and a minor peak at 79.05 m/z can be assigned to the $[iPrH]^+$, $[iPrNH]^+$ and $[(NH)_2PO]^+$ fragments respectively.

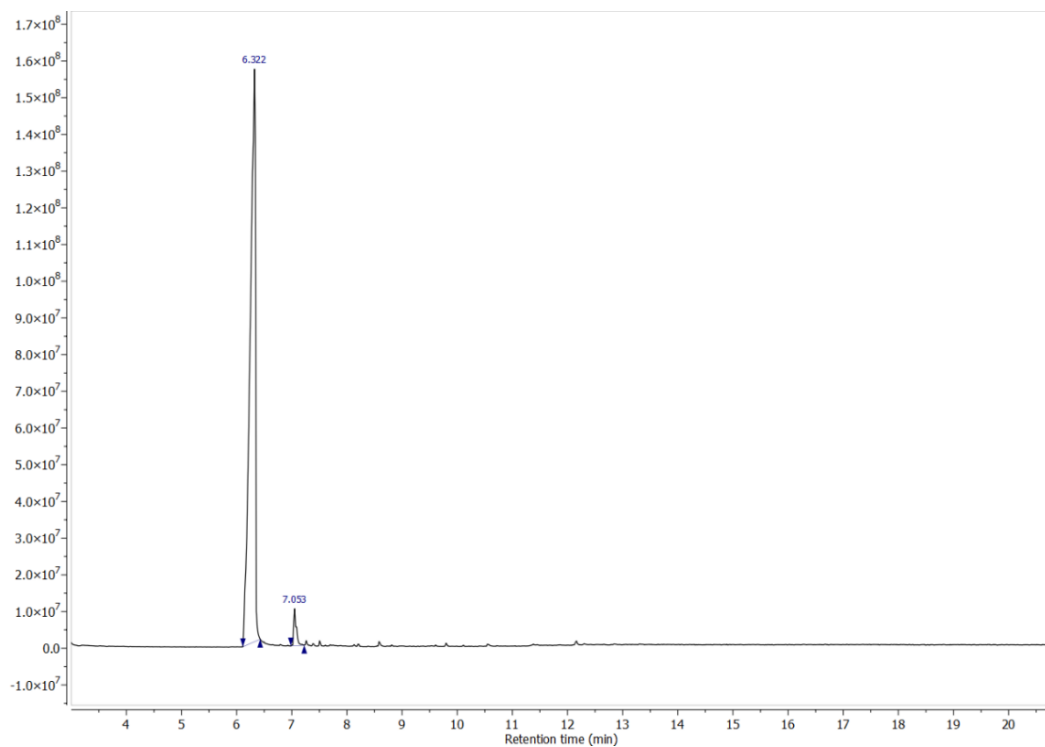


Figure 4.97: Gas chromatogram of $O((iPrNH)_2PO)_2_1_c1_f10$.

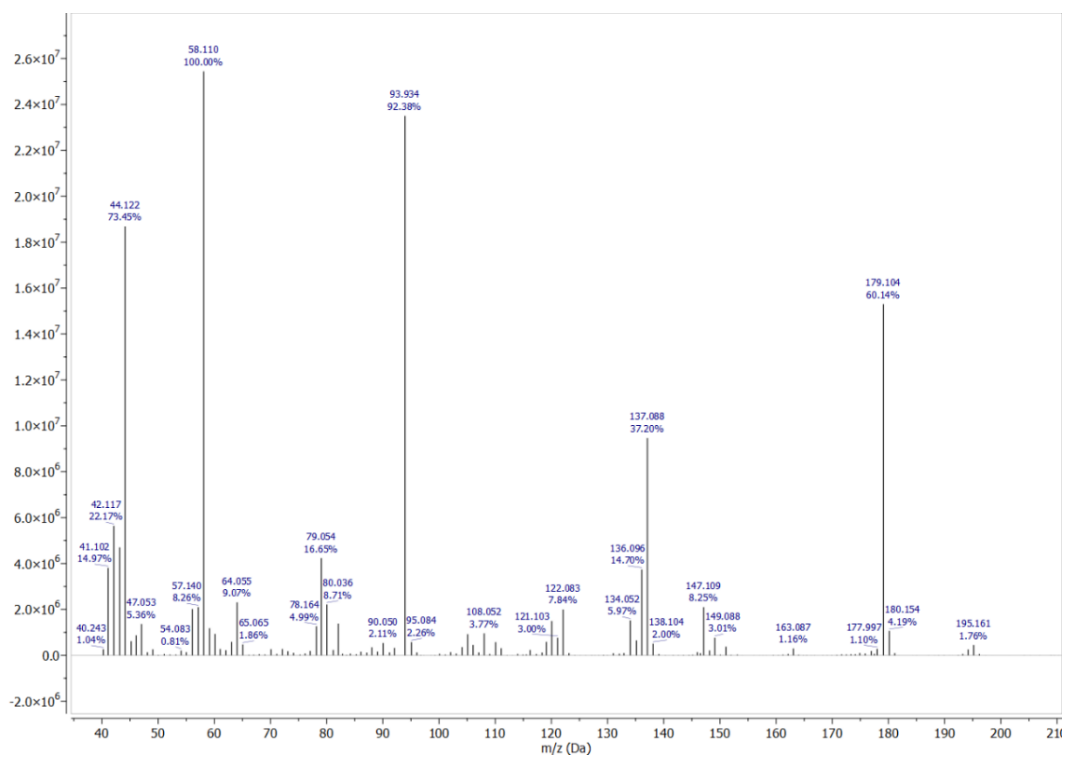


Figure 4.98: Mass spectrum of $O((iPrNH)_2PO)_2_1_c1_f10$.

The other major peaks were observed at 93.93 m/z, 137.1 m/z, 179.1 m/z and 195.1 m/z, with no peak obtained at higher m/z values. The peak at 179.1 m/z, which was believed to be due to a major fragment, could be due to the presence of the $[(iPrNH)_2PO_2]^+$ fragment which would indicate the presence of the desired compound as this would be representative of the fragmentation of the desired molecule along one of the P–O bonds of the P–O–P moiety. The complementary $[(iPrNH)_2PO]$ fragment was not observed. The fragment at 195.1 m/z did not reflect any known fragment for the expected compound but was observed to be related to the previous fragment as $195.1\text{ m/z} - 179.1\text{ m/z} = 16\text{ m/z}$, which could indicate that this was due to a rearrangement fragment $[(iPrNH)_2PO_3]^+$. The fragment at 137.1 m/z was found to be related to the fragment at 195.1 m/z by $195.1\text{ m/z} - 137.1\text{ m/z} = 58\text{ m/z}$ which would indicate another fragment $[(iPrNH)PO_3]^+$ wherein the initial rearrangement fragment loses the $[iPrNH]$ moiety. The final fragment at 93.93 m/z was easily described by the fragment $[PO_3H]^+$. This could be a derivative of the previously described fragments $[(iPrNH)_2PO_3]^+$ and $[(iPrNH)PO_3]^+$. The presence of the peaks at 93.93 m/z, 137.1 m/z and 195.1 m/z could indicate the presence of the pyrophosphoryl moiety. The presence of the $[PO_3]$ moiety in all three fragments along with the presence of the $[(NH)_2P]$ moiety in the fragments described for the peaks at 195.1 m/z and 79 m/z indicated that the $[PO_3]$ moiety was most likely obtained through rearrangement rather than the presence of a $[PO_3]$ containing product as this would require the formation of the $[PO_3N_2]$ containing compound, most likely a $\lambda^5\sigma^5$ -phosphorane, which are known but the route of formation of such a compound with the reagents used is unclear. It was observed that fragments related to the complementary $[(iPrNH)_2PO]^+$ fragment, expected given the presence of the $[(iPrNH)_2PO_2]^+$ fragment, were not observed.

These fragments observed for $O((iPrNH)_2PO)_2$ indicated the possibility of the formation of the desired compound although some important expected fragments and the M^+ peak were missing. The presence of the $[(iPrNH)_2PO_2]^+$ fragment could indicate that the main component of this product was in fact the desired compound $O((iPrNH)_2PO)_2$.

Analysis of the data for $O((iPrNH)_2PO)_2$ can be related directly to the data for $O((iPrNH)_2PO)_2$ and $(iPrNH)_3PO$. The gas chromatograph for $O((iPrNH)_2PO)_2$ is given in Figure 4.99 and this shows that the sample run contained multiple compounds which could have arose from both the reaction or the workup. This was also prevalent in the 1H NMR and ^{31}P NMR spectra of this compound

and therefore this result was expected. The two major peaks of interest that were analysed by MS are the ones at 6.618 minutes and 7.313 minutes. The MS peak data for both these peaks are given in Table 4.20, along with the MS peak data for the $(i\text{PrNH})_3\text{PO}$ and $\text{O}((i\text{PrNH})_2\text{PO})_2_1_c1_f10$ products. This data indicates that both of the compounds present in $\text{O}((i\text{PrNH})_2\text{PO})_2_1_c1_f10$ were found in $\text{O}((i\text{PrNH})_2\text{PO})_2_1_b1$. The other major peak at 12.181 minutes contained peaks for both $[i\text{PrH}]^+$ and $[i\text{PrNH}]^+$, but no significant structural data was obtained.

Table 4.20: Mass spectra peak data comparison for the $\text{O}((i\text{PrNH})_2\text{PO})_2_1_b1$ Gas chromatography peaks at 6.618 and 7.313 minutes and the peaks in the Mass spectra for $(i\text{PrNH})_3\text{PO}$ and $\text{O}((i\text{PrNH})_2\text{PO})_2_1_c1_f10$.

$(i\text{PrNH})_3\text{PO}$		$_1_b1$ (7.313 min.)		$_1_c1_f10$		$_1_b1$ (6.618 min.)	
m/z	%	m/z	%	m/z	%	m/z	%
44.11	32.35	44.13	47.70	44.12	73.45	44.12	74.03
58.01	100	58.11	100	58.11	100	58.08	96.56
79.02	62.68	79.04	59.95	79.05	16.65	79.01	18.66
				93.93	92.38	93.97	92.71
121.08	44.65	120.92	64.22				
				137.09	37.20	137.07	51.98
163.12	32.19	163.07	40.94				
				179.10	60.14	179.10	100
				195.16	1.76	195.16	5.24
206.16	12.67	206.13	16.01				
221.19	2.04	221.19	3.29				

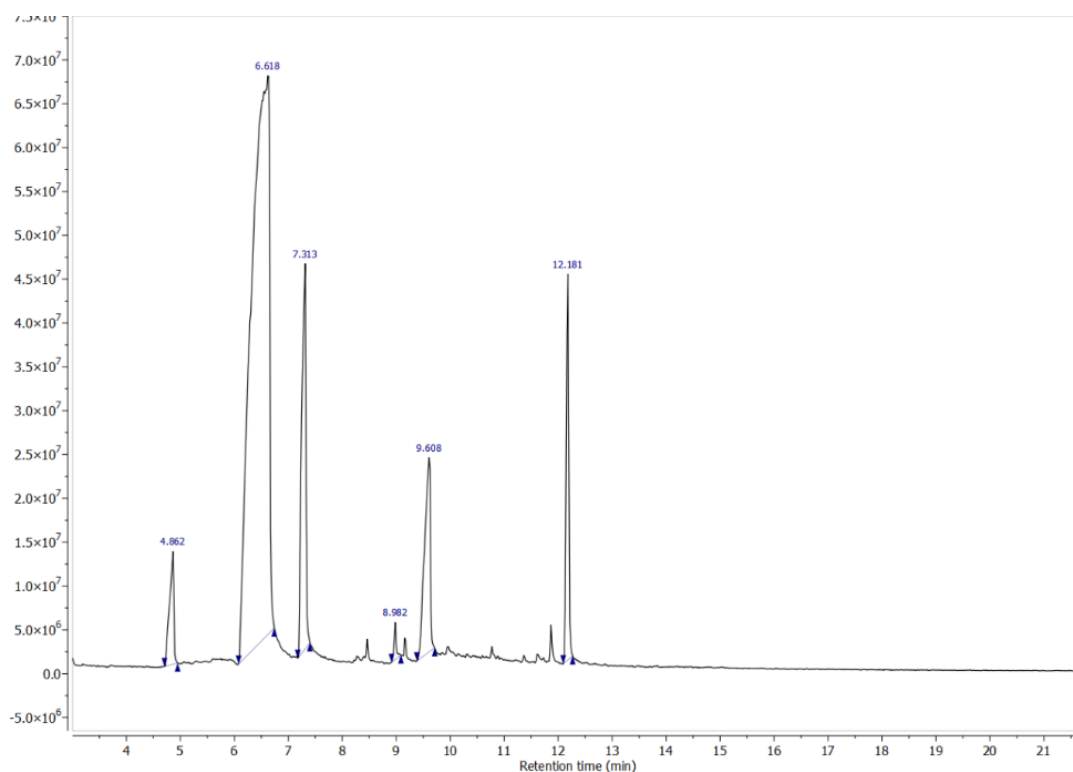
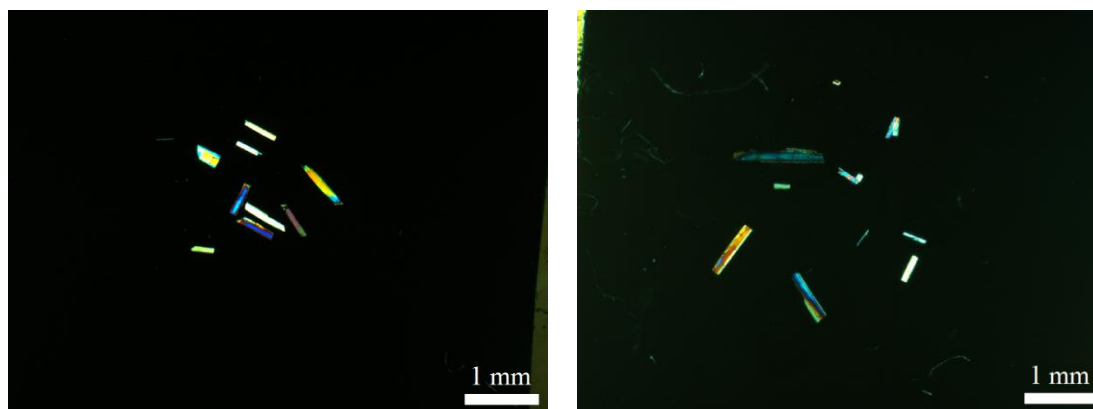


Figure 4.99: Gas chromatogram of O((iPrNH)₂PO)₂_1_b1.

4.2.1.4.5. Analysis by Microscopy

Solids obtained in the synthesis attempt of O((iPrNH)₂PO)₂ were checked under the microscope. Any crystalline samples were recorded and micrographs are given hereunder in Figure 4.100. The product O((iPrNH)₂PO)₂_1_b1 gave good quality needle like crystals while for O((iPrNH)₂PO)₂_1_c1 flat plates with a polygonal habit were collected. However the latter crystals were not of very good quality.



O((iPrNH)₂PO)₂_1_b1

O((iPrNH)₂PO)₂_1_c2

Figure 4.100: Micrographs of solids obtained for the O((iPrNH)₂PO)₂_1 reaction.

4.2.1.4.6. Analysis by Single crystal X-ray diffraction

Single crystals of O((iPrNH)₂PO)_{2_1_b1} were characterised by SXRD. The method used and the results obtained are discussed hereunder, along with a structural comparison to other previously structurally characterised pyrophosphoramides.

4.2.1.4.6.1 O((iPrNH)₂PO)_{2_1_b1}

Crystals were collected under oil and mounted in oil. Data was collected using Cu radiation on a STOE Stadivari diffractometer with a microfocus Cu-K_{α1} source. Structure solution was undertaken using the ShelXT Intrinsic phasing method and refined using the ShelXL least squares method.^{380,381} The crystallographic data obtained after structure solution and refinement is given in the report in Table 4.21, while the molecular structure and unit cell are given in Figure 4.101 and Figure 4.102 respectively. The full set of data is presented in Appendix 14.

Table 4.21: Crystal data for O((iPrNH)₂PO)_{2_1_b1}.

Identification code	O((iPrNH) ₂ PO) _{2_1_b1}
Empirical formula	C ₁₂ H ₃₂ N ₄ O ₃ P ₂
Formula weight/gmol ⁻¹	342.35
Crystal system	orthorhombic
Space group	<i>Pca</i> 2 ₁
<i>a</i> /Å	20.3379(4)
<i>b</i> /Å	5.04400(10)
<i>c</i> /Å	19.1488(5)
α /°	90
β /°	90
γ /°	90
Volume/Å ³	1964.37(8)
Z	4

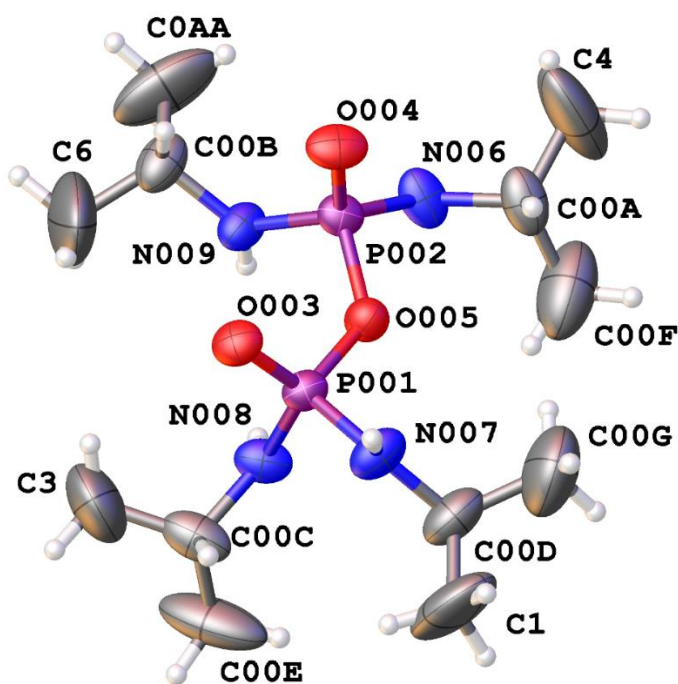


Figure 4.101: Molecular structure obtained for $O((iPrNH)_2PO)_2_1_b1$.

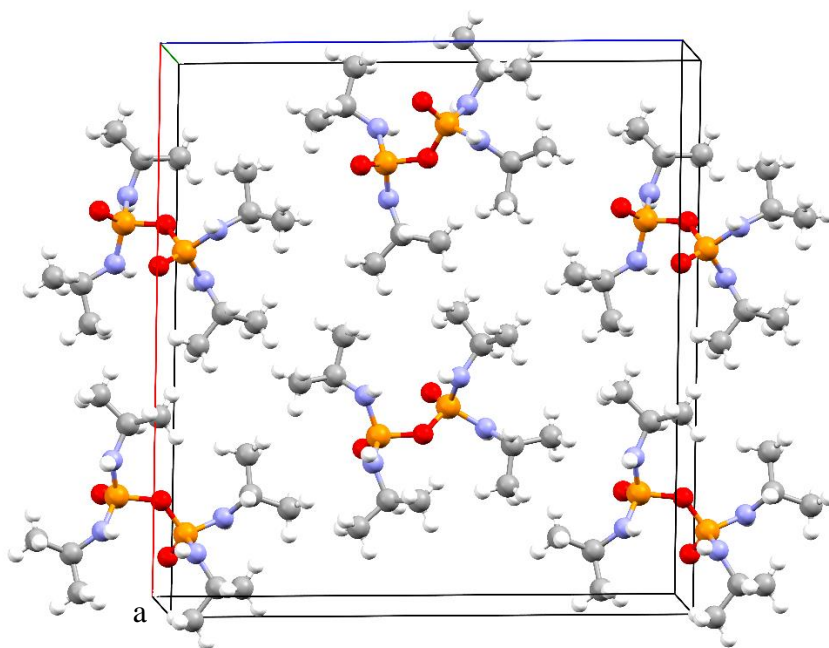


Figure 4.102: Unit cell for $O((iPrNH)_2PO)_2_1_b1$.

Viewed along the *b*-axis, as can be seen in Figure 4.102, the first notable structural characteristic was the isolation of the pyrophosphoryl and amine groups from each other by the iso-propyl groups. It seems that within the *a*-*c* plane the non-hydrogen bonding,

mainly Van der Waals interaction between the hydrophobic iso-propyl groups, were preferred. On the other hand, the intermolecular interactions between the pyrophosphoryl and amine moiety occurred along the *b* axis through the two hydrogen bonding motifs shown in detail in Figure 4.103. For each molecule in the column, both synthons were present involving both P=O and three of the N–H groups, leaving one of the iso-propyl amines uninvolved. The first synthon was a ring with a $R_2^1(8)$ graph set connecting one P=O group with two neighbouring N–H groups, as detailed in Figure 4.103 (left), which are bound to the two different phosphorus centres of the second molecule. The second synthon was a simple P=O---H–N interaction of the other P=O group of the first molecule with a neighbouring N–H group which is not part of the previously discussed synthon but which shares a phosphorus centre with one of the previously discussed amide groups as detailed in Figure 4.103 (right). Since these synthons were present only in the *b* axis this contributed to the small *b* axis length. The strict hydrogen bonding along the *b* axis repeated between each individual molecule and the isolation of each molecule through the bulky iso-propyl groups in the *a*-*c* plane caused the molecules to pack in columns along the *b* axis, with each molecule in the same column having the same symmetry and hydrogen bonding motifs.

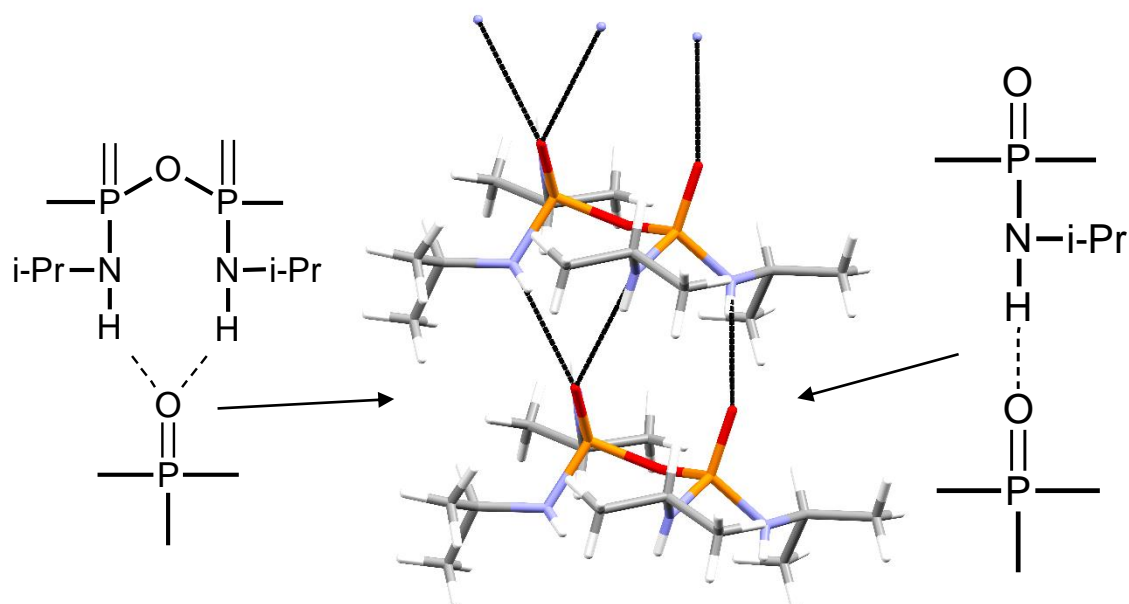


Figure 4.103: Hydrogen bonding synthons present in the structure of $O((iPrNH)_2PO)_2_1_b1$.

It was observed that on moving along the a axis each column was antiparallel in the b axis direction to its neighbours, with regards to the direction of the hydrogen bonding motifs, as given in Figure 4.104. This is described via a 2_1 screw axis along the b axis. Along the c axis the column remained parallel in terms of hydrogen bonding motifs but they were related to each other through the glide plane in the b - c plane along the c axis.

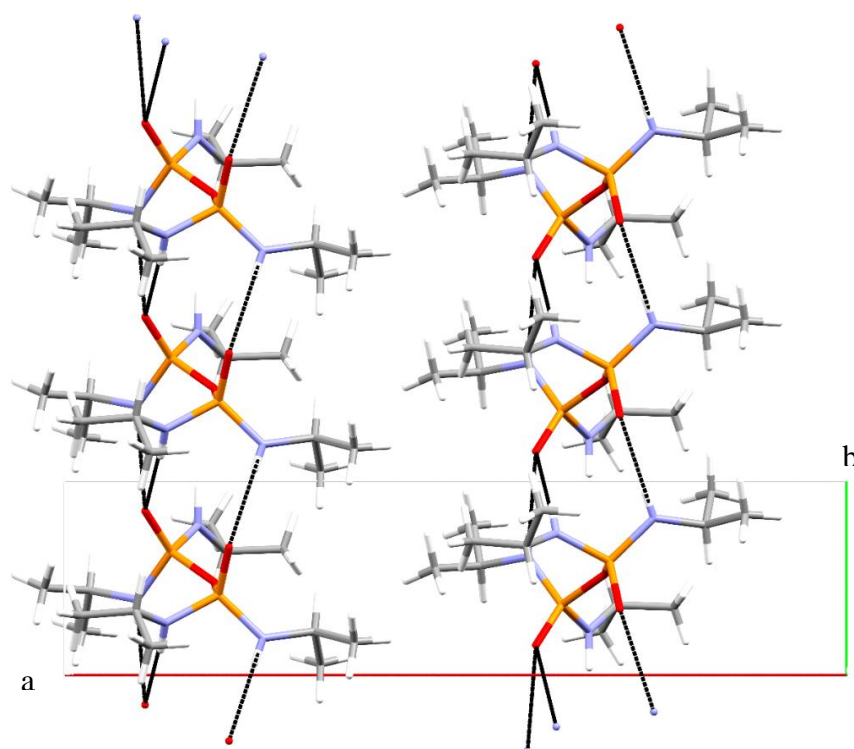


Figure 4.104: Antiparallel columns of $O((iPrNH)_2PO)_2$ along the a axis.

4.2.1.4.6.2 Structural Comparison of mono-N-substituted Pyrophosphoramides

Only a few pyrophosphoramides have been structurally characterised by XRD methods.^{33,207–214,384–386} It is known that most intermolecular motifs that build up the supramolecular structures which define crystal structures are due to the moieties within the molecule in question. Therefore, compounds with similar moieties and chemical structures may be expected to have similar intermolecular motifs and in turn similar crystal structures.^{387,388} In this regard the various previously structurally characterised and published pyrophosphoramides, along with the novel $O((iPrNH)_2PO)_2$ structure obtained from $O(iPrNH)_2PO)_2$ _1_b1, can be divided in five main groups dependent on their chemical structure, as described in Figure 4.105.

Pyrophosphoramides				
Di-N-substituted pyrophosphoramides			Mono-N-substituted pyrophosphoramides	
O((R ₂ N) ₂ PO) ₂ (Symmetric secondary amine derivatives)	O((R ¹ R ² N) ₂ PO) ₂ (Asymmetric secondary amine derivatives)	O((R ¹ (NR ²) ₂) ₂ PO) ₂ (N,N'-substituted diamine derivatives)	O((AlkylNH) ₂ PO) ₂ (Primary alkyl amine derivatives)	O((ArlyNH) ₂ PO) ₂ (Primary aryl amine derivatives)
O((Me ₂ N) ₂ PO) ₂ Liquid ^{201,202}	O((BzMeN) ₂ PO) ₂ C2/c ²¹⁴	O((C ₂ H ₄ (2,5- <i>i</i> PrPhN) ₂) ₂ PO) ₂ P2 ₁ /n ³⁸⁴	O((<i>t</i> BuNH) ₂ PO) ₂ P2 ₁ /c ³⁸⁶	O((2-MePhNH) ₂ PO) ₂ P2 ₁ /c ^{211,212}
		O((1,2-Cy(NaphN) ₂) ₂ PO) ₂ C2 ³⁸⁵	O((<i>i</i> PrNH) ₂ PO) ₂ Pca2 ₁ (current)	O((4-MePhNH) ₂ PO) ₂ Pccn ²¹⁴

Figure 4.105: Categorisation of pyrophosphoramides under discussion, including structures published from data obtained by SXR D for the solid products, along with the liquid O((Me₂N)₂PO)₂.

On comparison of the crystal structures of the compounds classified in each group given in Figure 4.105, it was noted that the most important molecular difference that affected the supramolecular structure was the presence of the N–H moiety. Its presence caused a significant difference between the structure of the mono-N-substituted pyrophosphoramides and the di-N-substituted pyrophosphoramides, which lack this moiety. The di-N-substituted pyrophosphoramides given in Figure 4.105 were shown to form crystalline structures wherein the pyrophosphoramide moieties did not interact with each other directly, due to a lack of the N–H moiety. Therefore in the di-N-substituted pyrophosphoramides the packing and supramolecular structures which influence the formation of the crystal structures are mostly dependent on the organic moieties of the compounds. In all three cases the modes of supramolecular arrangement are determined by and typical of the many organic groups present. It is interesting to note that there is a lack of Ph(π)---Ph(π) interactions, especially for O((BzMeN)₂PO)₂ and O((1,2-Cy(NaphN)₂)₂PO)₂.^{214,385} This may be due to these organic moieties being bound to the pyrophosphoramide group which in such conditions always takes on a staggered conformation along the P to P axis. This staggered conformation is most likely due to the lack of the amine N–H bonds which are present in the mono-N-substituted pyrophosphoramides. Therefore, since as described in Section 4.2.1.4.6.1. the structure of O((*i*PrNH)₂PO)₂_1_b1 is significantly influenced by P=O---H–N interactions no further comparison can be made to O((*i*PrNH)₂PO)₂.

The first noticeable difference when comparing $O((iPrNH)_2PO)_2$ to the previously published structures was that this solid crystallised in the orthorhombic space group $Pca2_1$. The only other compound that crystallised in this crystal system was $O((4-MePhNH)_2PO)_2$, crystallising in a $Pccn$ space group, while all the others crystallised in monoclinic space groups. Despite the chemical similarities of $O((iPrNH)_2PO)_2$ to $O((tBuNH)_2PO)_2$, it not only crystallised in a different spacegroup, namely $Pca2_1$, but also showed a different supramolecular motif.

For the previously described mono-N-substituted pyrophosphoramides all the polymorphs that crystallised in the monoclinic crystal system (including $O((tBuNH)_2PO)_2$) did so in a $P2_1/c$ space group. The $O((tBuNH)_2PO)_2$ and the two $O((2-MePhNH)_2PO)_2$ polymorphs all showed the same basic supramolecular motif,^{211,212,386} which on packing constructed the relevant crystal structures as shown in Figure 4.106. The basic supramolecular motif is given in Figure 4.107. This is composed of two hydrogen bonding synthons, shown in Figure 4.108. The first one is a ring synthon with a $R_2^2(8)$ graph set binding molecules through intermolecular hydrogen bonding, while the second consists of partially eclipsed conformations through intramolecular hydrogen bonding, as given in Figure 4.108. The second synthon constricts the molecules from taking on other conformations and therefore minimises the number of possible supramolecular structures available. These two synthons together create the same supramolecular structure for all of the above crystal structures, namely a chain like packing as given in Figure 4.107. This structure motif is repeated through translational symmetry to form infinite chains. The two molecules that form the actual supramolecular units are related to each other by the glide plane denoted in the $P2_1/c$ spacegroup.

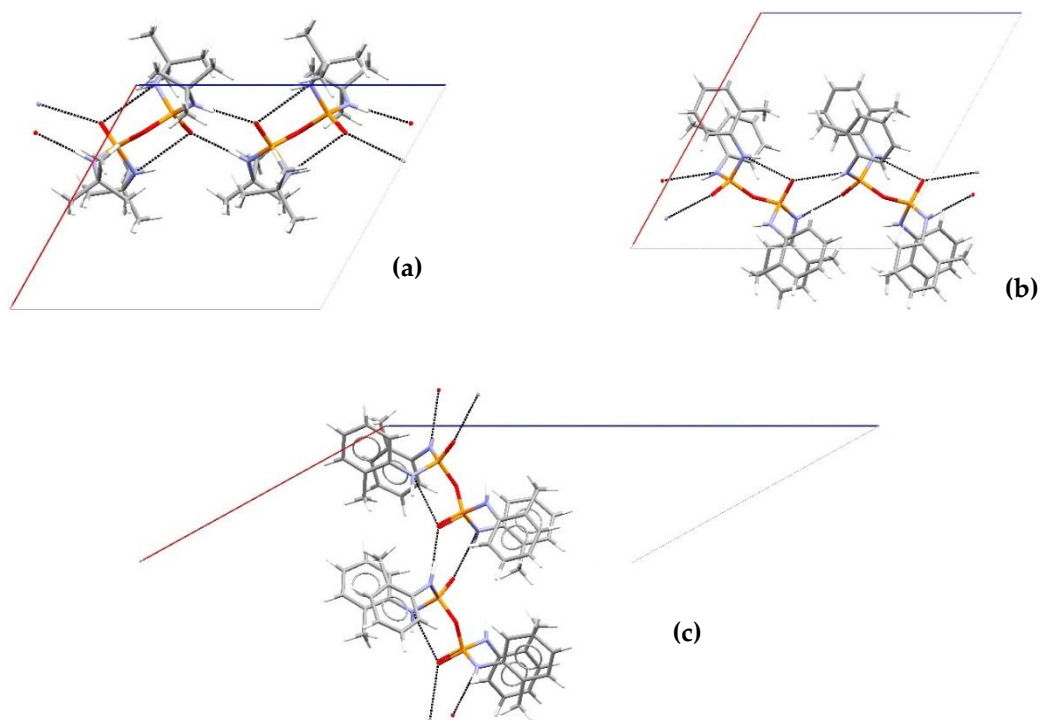


Figure 4.106: The hydrogen bonding motif common to all crystals having a $P2_1/c$ space group as described in the published structures: (a) $O((t\text{-BuNH})_2\text{PO})_2$; (b) $O((2\text{-MePhNH})_2\text{PO})_2$ published by Pourayoubi, M. et al.; (c) $O((2\text{-MePhNH})_2\text{PO})_2$ published by Cameron, S.T. et al.

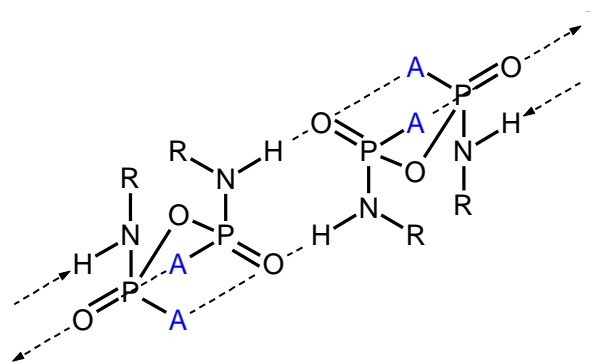


Figure 4.107: Basic unit for the supramolecular H-bonding motif that is common to all three mono-N-substituted pyrophosphoramidates that crystallise in a $P2_1/c$ space group, $A = (\text{R})\text{N-H}$.

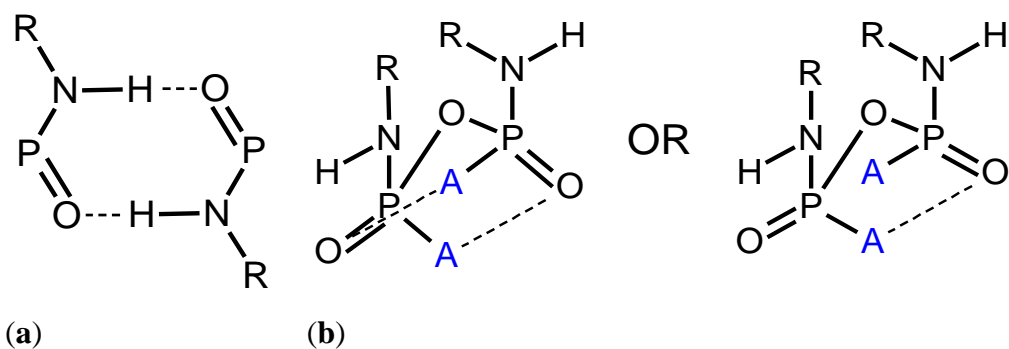


Figure 4.108: H-bonding synthons in $P2_1/c$ structures: (a) intermolecular ring synthon; (b) the two variants of the intramolecular synthon where A is the non-intermolecular bonding amine.

The formation of this hydrogen bonding motif seems to be independent of the nature of the organic substituent on the amide nitrogen, as it occurs for both the alkyl tert-butyl and aryl 2-methylphenyl analogues. The packing of these chains is, however, influenced by the organic substituents. The tert-butyl groups in $O((t\text{BuNH})_2\text{PO})_2$ do not interact, although they pack in a staggered formation resulting in the closest possible packing of the chains.³⁸⁶ The packing effects of the 2-methylphenyl groups are more complex than those of the tert-butyl groups giving rise to two polymorphs of this compound. For both polymorphs the 2-methylphenyl groups on the same phosphorus centre both stack antiparallel to each other through $\text{Ph}(\pi)\cdots\text{Ph}(\pi)$ interactions. The polymorph collected by Pourayoubi et al. showed closer packing between the chains.²¹² The chains are arranged by a square like motif composed of the $\text{Ph}(\pi)\cdots\text{H}-\text{C}(\text{meta})$ interactions which make up the vertices.³⁸⁷ In the polymorph described by Cameron et al. the main intermolecular interactions are the same stacking interactions as the intramolecular interactions described for both polymorphs.²¹¹

For the 4-methylphenyl derivative $O((4\text{-MePhNH})_2\text{PO})_2$, which crystallises in the orthorhombic *Pccn* spacegroup,²¹⁴ a different and unique supramolecular structure was recorded. This had a different internal conformation, due to a lack of intramolecular hydrogen bonding synthons, when compared to the other mono-N-substituted pyrophosphoramides, and therefore a different supramolecular motif was present. This contained a staggered internal conformation of the molecules along the P to P axis which was due to a lack of the intramolecular $\text{P}=\text{O}\cdots\text{H}-\text{N}$ bonding observed in the $P2_1/c$ structures. These staggered molecules are allowed to stack on top of each other to form the supramolecular motif given in Figure 4.109a. Since all the amines in this conformation are free from intramolecular bonding the ring synthon with graph set $R_2^2(12)$ given in Figure 4.109b is formed. Further $\text{N}-\text{H}\cdots\text{Ph}$ and $\text{P}=\text{O}\cdots\text{H}-\text{C}(\text{Ph}(\text{C}2))$ interactions are observed as shown in Figure 4.110. The $\text{N}-\text{H}\cdots\text{Ph}$ interactions are formed through the remaining amide moieties which do not interact in the $R_2^2(12)$ ring described prior and this additional set of interactions seems to stabilise the motif by increasing the packing efficiency and stopping this moiety from forming the previously mentioned intramolecular $\text{P}=\text{O}\cdots\text{H}-\text{N}$ bonding. The $\text{P}=\text{O}\cdots\text{H}-\text{C}(\text{Ph}(\text{C}2))$ interactions also seem to add stability by further aiding the $\text{P}=\text{O}$ oxygen atoms to obtain the orientation necessary for this synthon.^{250,387}

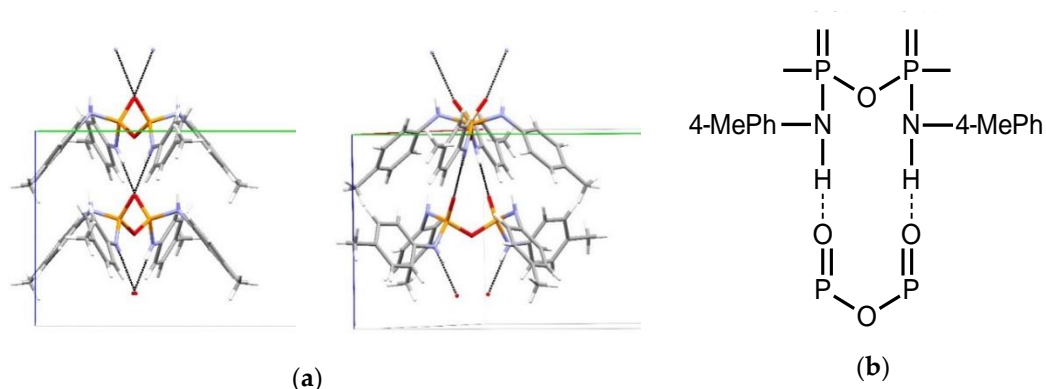


Figure 4.109: Hydrogen bonding motif for $O((4\text{-MePhNH})_2\text{PO})_2$ (a) as viewed along the a -axis, showing the complete repeatable moiety described for this structure (left) and offset to show the staggered conformation of the pyrophosphoramidate (right); (b) The ring synthon that is the base for the motif given in a simplified diagram.

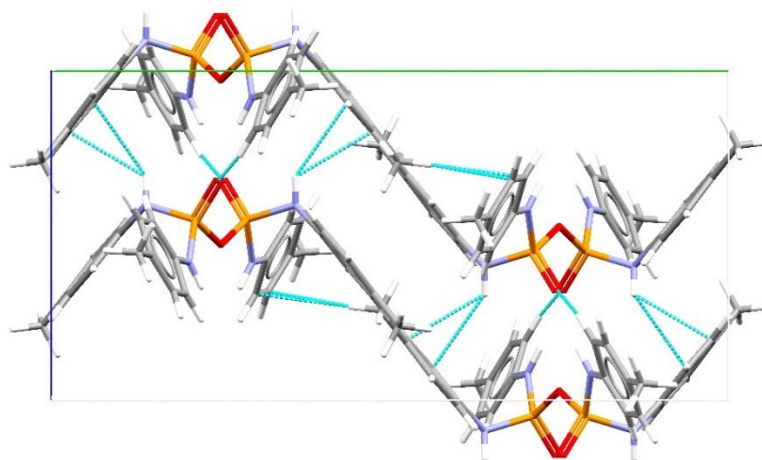


Figure 4.110: Intermolecular and intramolecular non-hydrogen bonding interactions in the structure of $O((4\text{-MePhNH})_2\text{PO})_2$.

The two molecules in the motif are related by a glide plane on the a - c plane along the c -axis. This motif can therefore theoretically form infinite chains along the c -axis. Neighbouring chains were noted to be anti-parallel to each other along the b -axis and related to each other by a second glide plane along the diagonal of the a - b plane. Chains neighbouring each other along the a -axis are parallel and related by translation. The main interaction responsible for arrangement in antiparallel chains is the $\text{Ph}(\pi)\cdots\text{H}-\text{C}(\text{para-methyl})$ interaction between the closely situated 4-methylphenyl groups bound to different molecules in different chains,²⁵⁰ as noted in Figure 4.110.²¹⁴ This guarantees the closest possible packing of the various phenyl groups in the molecule. The 4-methylphenyl groups are therefore mainly responsible for both the formation of a different hydrogen bonding motif and a different packing of the molecules in this structure compared to other pyrophosphoramidates.

On comparison with published cases it was concluded that the previously described crystal structure and supramolecular motif for $O((iPrNH)_2PO)_2$ 1_b1 and given in Figures 4.101 and 4.103 were unique. As this supramolecular motif was not attested in literature it was believed to be unique for the mono-N-substituted pyrophosphoramidate produced in this study and therefore novel. This motif was composed of two different hydrogen bonding intermolecular synthons of $P=O\cdots H-N$ interactions. Both these synthons were also found to be novel, increasing the number of intermolecular synthons known in crystal structures of mono-N-substituted pyrophosphoramidates. Therefore the strong impact of this type of hydrogen bonding on the supramolecular motifs in all previously published mono-N-substituted pyrophosphoramidates could be confirmed also for $O((iPrNH)_2PO)_2$. It should also be noted that a staggered internal conformation of the molecules along the P to P axis was noted, similar to that of analogue $O((4-MePhNH)_2PO)_2$. This could contribute to the difference in supramolecular structures as compared to other primary alkyl mono-N-substituted pyrophosphoramidates but does not explain the cause for the differences noted with all the previously described mono-N-substituted pyrophosphoramidates.

The cause of the formation of this different structure was difficult to determine. Chemical structure, synthesis method, crystallisation techniques, solvents used and the temperature during crystallisation and SXR data collection can all effect the crystal structure obtained. In the case of this novel structure the SXR data collection temperature fell in the same range used for other $P2_1/c$ crystallising compounds and therefore this was unlikely to be the cause of the structural difference.^{211,212,386} The synthesis and crystallisation approach used to produce this compound was different from those used to obtain the previously reported solids and therefore this could have been a factor influencing the formation of a novel supramolecular motif. Given the chemical similarities between the iso-propyl and tert-butyl moieties the difference in supramolecular motifs between the two was unexpected.

A summary for the structural comparison of the mono-N-substituted pyrophosphoramidates discussed above is given in Appendix 15.

4.2.1.4.7. Conclusion

Following the application of various characterisation techniques on the numerous products obtained from the reaction to synthesise the product $O((iPrNH)_2PO)_2$, the following conclusions were drawn up. The crystalline product labelled $O((iPrNH)_2PO)_2_{1_a}$ was found to be the expected $iPrNH_3Cl$ salt through IR and 1H NMR analysis. All other products were believed to contain derivatives of PPTC due to the presence of non-PPTC peaks in their respective $^{31}P\{^1H\}$ NMR spectra. These spectra indicated clearly that these derivatives were most likely amine, hydroxide or alkoxide derivatives, due to the downfield shifts observed in the peaks of the $^{31}P\{^1H\}$ NMR spectra as compared to the peak for PPTC.

IR, 1H NMR and $^{31}P\{^1H\}$ NMR data for $O((iPrNH)_2PO)_2_{1_b}$, $O((iPrNH)_2PO)_2_{1_b1}$, $O((iPrNH)_2PO)_2_{1_c1}$ and its various column chromatography fractions and $O((iPrNH)_2PO)_2_{1_c2}$, indicated the presence of multiple pyrophosphoryl derivatives, with the presence of a single major product throughout. GC-MS data indicated that the major product for the various $O((iPrNH)_2PO)_2_{1}$ products was likely the desired product or a very similar pyrophosphoramidate. However this technique could not definitively prove the formation of the desired compound. For most of these products $^{31}P\{^1H\}$ NMR and GC-MS data indicated that $(iPrNH)_3PO$ was also present as a minor component and side product of this reaction. The mechanism or decomposition route through which $(iPrNH)_3PO$ was formed from PPTC and the iso-propylamine reagents or the main product could not be deduced from the available data. SXR D characterisation of $O((iPrNH)_2PO)_2_{1_b1}$ clearly showed that the desired compound was obtained. Given the similarities between the IR, 1H NMR and $^{31}P\{^1H\}$ NMR data for the various products $O((iPrNH)_2PO)_2_{1_b}$, $O((iPrNH)_2PO)_2_{1_b1}$, $O((iPrNH)_2PO)_2_{1_c1}$ and its various column chromatography fractions and $O((iPrNH)_2PO)_2_{1_c2}$ and the final SXR D result for $O((iPrNH)_2PO)_2_{1_b1}$ it could be concluded that the major product was $O((iPrNH)_2PO)_2$. This indicated that the desired compound could be obtained through this reaction from which a pure crystalline product could be isolated.

This SXR D data analysis also produced the first solid state structure of $O((iPrNH)_2PO)_2$. A thorough structural comparison of $O((iPrNH)_2PO)_2_{1_b1}$ with other pyrophosphoramidates for which the crystal structures have been published previously was carried out. The $O((iPrNH)_2PO)_2$ obtained in the current work formed a novel supramolecular motif previously unattested for mono-N-substituted

pyrophosphoramides. This motif was composed of two different synthons with P=O---H-N interactions. Trends regarding the effects of the various organic moieties within the different compounds were difficult to describe due to the lack of systematic data. These novel structures, supramolecular motifs and synthons first described for mono-N-substituted pyrophosphoramides in O((iPrNH)₂PO)₂_1_b1 can also be of interest in possible polymorphism and co-crystallisation studies. This is important for mono-N-substituted pyrophosphoramides given their possible use as pesticides. The formation of different forms with different thermodynamic and kinetic stabilities can aid in complexation reactions and diminish decomposition on storage, a property of great importance for use in agriculture.^{270,389-391}

4.2.1.5. Summary

This section addressed the characterisation of the non-carbene di- $\lambda^5\sigma^4$ -phosphorane ligands and ligand precursors which were synthesised as described in Section 3.3.2.1, to be used in the synthesis of the lanthanide non-carbene di- $\lambda^5\sigma^4$ -phosphorane complexes. Synthesis of the neutral ligands and ligand precursors, HN(Ph₂PS)₂, HN(Ph₂PO)₂, O((Et₂N)₂PO)₂ and O((iPrNH)₂PO)₂ was fairly straightforward with the desired compounds obtained under inert conditions and characterised through IR, ¹H and ³¹P NMR spectroscopy and GC-MS. The ligands were found to be stable to air and moisture and synthesis was only undergone under inert conditions due to the use of the sensitive reagents. For HN(Ph₂PO)₂ and O((iPrNH)₂PO)₂ novel crystalline structures were observed. HN(Ph₂PO)₂ proved to form the amine tautomer on crystallisation in this study, unlike previous studies where an alcohol tautomer was collected on crystallisation. This proved to be the first time this tautomer was identified in the solid state. The ligand O((iPrNH)₂PO)₂ was characterised structurally for the first time although this compound is available commercially. This also showed a novel supramolecular motif and intermolecular synthons when compared to other previously described mono-N-substituted pyrophosphoramides. A novel Ca²⁺ complex of O((Et₂N)₂PO)₂ was formed unexpectedly. The compounds HN(Ph₂PS)₂, HN(Ph₂PO)₂ and O((Et₂N)₂PO)₂ were all used for complexation with lanthanide cations.

4.2.2. Complexation products

4.2.2.1. Characterisation of $[\text{Eu}(\text{N}(\text{Ph}_2\text{PO})_2)_3]$

In the current study two attempts at synthesising the previously known lanthanide complex $[\text{Eu}(\text{N}(\text{Ph}_2\text{PO})_2)_3]$ were undergone, as described in Section 3.3.2.2.1. The procedure used was as previously published by Pietraszkiewicz and co-workers in 2012, with a slight experimental variation.²⁴⁴ The two attempts undertaken in the current study also had a minor variation between them. Characterisation of these two products gave different results and therefore both products are discussed hereunder. The first synthesis gave the product labelled as $[\text{Eu}(\text{N}(\text{Ph}_2\text{PO})_2)_3]_1$ with a yield of 39%, whilst the second attempt gave the product labelled as $[\text{Eu}(\text{N}(\text{Ph}_2\text{PO})_2)_3]_2$ with a yield of 17%.

4.2.2.1.1. Analysis by Infra-red spectroscopy

The IR spectrum of the $[\text{Eu}(\text{N}(\text{Ph}_2\text{PO})_2)_3]_1$ product is given in Figure 4.111, along with the spectrum of the starting reagent $\text{HN}(\text{Ph}_2\text{PO})_2_1$. Significant differences were observed between the two spectra, with the first two differences being the presence of phenyl ν C–H bands in the typical region in the spectrum of the product in contrast to the lack of these bands in the spectrum of the ligand and the loss of the significant ν O–H and δ O–H bands in the spectrum of the product, when compared to that of the ligand.

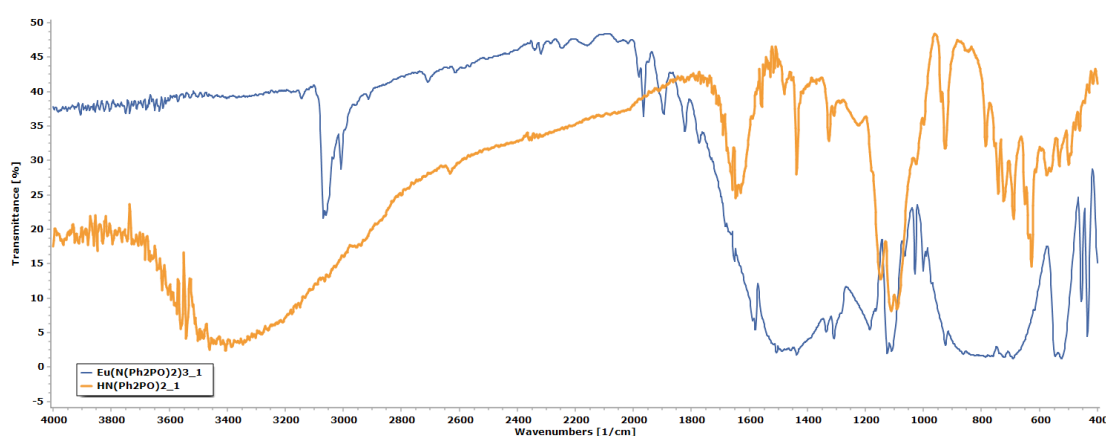


Figure 4.111: IR spectra of $[\text{Eu}(\text{N}(\text{Ph}_2\text{PO})_2)_3]_1$ (blue) and $\text{HN}(\text{Ph}_2\text{PO})_2_1$ (orange).

Other differences included the presence of very strong broad bands at 1467 cm^{-1} and 787 cm^{-1} in the spectrum of $[\text{Eu}(\text{N}(\text{Ph}_2\text{PO})_2)_3]_1$, together with strong to medium bands at 1336 cm^{-1} , 1309 cm^{-1} , 1184 cm^{-1} , 1028 cm^{-1} and 522 cm^{-1} , none of which were present in the spectrum of the ligand. The broad band at 1467 cm^{-1} was unexpected and fell in the very highest wavenumber region for $\nu\text{ P=N}$ or $\nu\text{ P=O}$ vibrations. This indicated a strong bond order of these two bonds which was unexpected for complexation. The broad band at 787 cm^{-1} fell in the higher wavenumber region for $\nu_s\text{ P-N-P}$ vibrations, although it was still in the range of bands assigned to this vibration in the IR spectrum of $\text{HN}(\text{Ph}_2\text{PO})_2_1$. The bands at 1336 cm^{-1} and 1309 cm^{-1} could be analogous to ligand bands at 1326 cm^{-1} and 1306 cm^{-1} , which were unassigned. The two bands at 1184 cm^{-1} and 1028 cm^{-1} showed no analogous bands in the spectrum of the ligand and could not be assigned. The strong band at 522 cm^{-1} was anomalous, although it fell in the region typical for bands of the $\delta\text{ P-O-H}$ vibrations, which could therefore indicate the presence of such a moiety. This group was however unexpected and could be indicative of the formation of another impurity. The strong band at 1124 cm^{-1} in the spectrum of $[\text{Eu}(\text{N}(\text{Ph}_2\text{PO})_2)_3]_1$ seemed to be analogous to the band at 1110 cm^{-1} in the spectrum of the ligand, showing little change in wavenumber. This band could be assigned to $\nu\text{ P=O}$ vibrations and therefore this was indicative of the lack of coordination of the metal ion with the oxygen of the P=O group, given that this structural change should have caused a decrease in bond order and wavenumber of the P=O bond.

The second product, $[\text{Eu}(\text{N}(\text{Ph}_2\text{PO})_2)_3]_2$, was also analysed by IR spectroscopy to yield a significantly different spectrum from both that observed for the starting reagent $\text{HN}(\text{Ph}_2\text{PO})_2_1$ and that observed for $[\text{Eu}(\text{N}(\text{Ph}_2\text{PO})_2)_3]_1$. A detail of this spectrum is given in Figure 4.112, along with that of the starting reagent. Any bands with wavenumbers $> 1600\text{ cm}^{-1}$ could not be identified due to the presence of very strong $\nu\text{ O-H}$ and $\delta\text{ O-H}$ bands, most likely due to the presence of water, and therefore the discussion hereunder deals with the bands falling in the wavenumber region of $1600\text{-}400\text{ cm}^{-1}$.

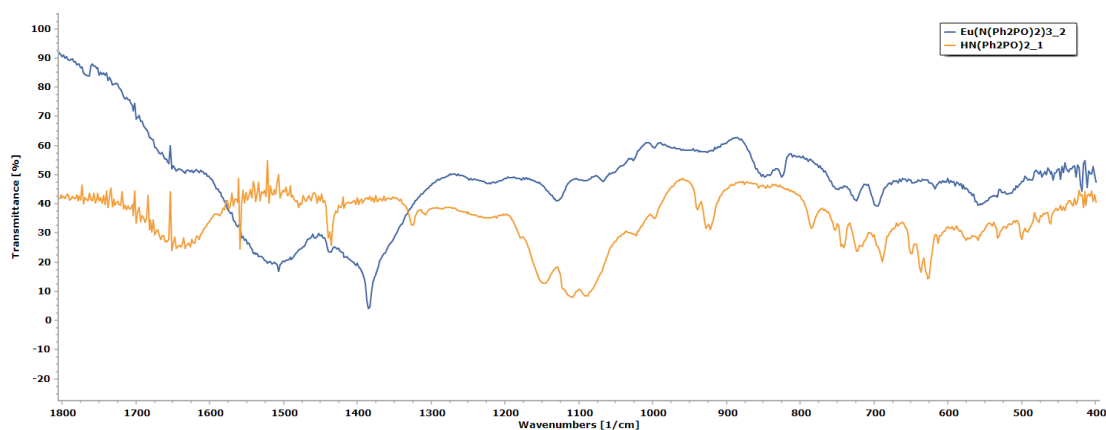


Figure 4.112: IR spectra of [Eu(N(Ph₂PO)₂)₃]₂ (blue) and HN(Ph₂PO)₂_1 (orange), in the range 1800cm⁻¹ to 400cm⁻¹.

First of all, the bands at 752 cm⁻¹, 725 cm⁻¹ and 697 cm⁻¹ observed in the spectrum of [Eu(N(Ph₂PO)₂)₃]₂ were believed to be analogous to the bands at 753 cm⁻¹, 742 cm⁻¹, 723 cm⁻¹ and 688 cm⁻¹ in the spectrum of the HN(Ph₂PO)₂_1 ligand, given that on comparison they fell in the same range and were of similar intensities and wavenumbers. These were assigned to the various P-Ph vibrations expected in this region for both samples and therefore indicated the presence of the ligand in the product. The bands at 784 cm⁻¹ and in the range of 649-626 cm⁻¹, which were assigned to the ν_s P-N-P vibrations in the spectrum of the ligand were lost in the spectrum of the [Eu(N(Ph₂PO)₂)₃]₂ product. This was also true for the bands at 1110 cm⁻¹ and 1090 cm⁻¹ assigned to the ν P=O vibrations.

New medium strength bands were observed at 849 cm⁻¹ and 826 cm⁻¹ in the spectrum of the product, which could indicate a decrease in bond order for the P-N-P bonds if these bands were considered to be analogous to the band at 925 cm⁻¹ in the spectrum of the reagent, which was assigned to the ν_{as} P-N-P vibrations. Such a change was not expected. Alternatively, if the expected deprotonation, along with coordination had occurred, these bands could be tentatively assigned to the ν_s P-N-P vibrations but with an increase in wavenumber from the aforementioned bands at 784 cm⁻¹ and in the range of 649-626 cm⁻¹ in the spectrum of the ligand, which were assigned to these vibrations. This increase in wavenumber for bands assigned to the same vibration modes from ligand to product would indicate an increase in bond order. However, these bands would fall in a range slightly higher than typical.

Two strong peaks were observed at 1515 cm^{-1} and 1384 cm^{-1} in the spectrum of the $[\text{Eu}(\text{N}(\text{Ph}_2\text{PO})_2)_3]_2$ product. These both fell in the higher range for the ν P=N or ν P=O vibrations, although in this case these were more likely to be for the ν P=N vibrations, which would indicate a significant bond order increase for this bond. The increase in wavenumber of the band of the ν P=N vibrations would be expected if the deprotonation expected for the reaction had occurred. If this was the case the loss of the band at 925 cm^{-1} , which was assigned to the ν_{as} P–N–P vibrations in the ligand, would be justified. The loss or diminished intensity of the bands assigned to the ν P=O vibrations in the ligand IR spectrum would also be indicative of deprotonation and coordination, as both these processes should decrease the bond order of the P=O bond. Unfortunately, an analogous band which could be tentatively assigned to the coordinated P=O bond was difficult to find, with the best fit being the bands at 1128 cm^{-1} , 849 cm^{-1} and 826 cm^{-1} in the spectrum of the product.

In addition to the assignment of the IR bands discussed prior the strong band at 1384 cm^{-1} and the medium intensity band at 826 cm^{-1} could also be related to the known IR spectrum of the salt metathesis by-product of the reaction used in the synthesis attempt of $[\text{Eu}(\text{N}(\text{Ph}_2\text{PO})_2)_3]_2$, namely KNO_3 .³⁹² Literature IR data for KNO_3 typically shows three bands attributable to the vibrations of the nitrate anion, namely at 1767 cm^{-1} (w), 1380 cm^{-1} (s) and 824 cm^{-1} (m) and thus the latter two bands may be present in the IR spectrum of the solid along with the bands of the desired product.

4.2.2.1.2. Analysis by ^1H NMR spectroscopy

A detail of the ^1H NMR spectrum of $[\text{Eu}(\text{N}(\text{Ph}_2\text{PO})_2)_3]_1$ is given in Figure 4.113, along with that of the starting reagent, $\text{HN}(\text{Ph}_2\text{PO})_2_1$. The three peaks typical of the aromatic rings were present in both spectra, with analogous and unchanged multiplet and coupling constants. The aromatic peaks were observed at 7.90 ppm, 7.43 ppm and 7.34 ppm in the spectrum of $[\text{Eu}(\text{N}(\text{Ph}_2\text{PO})_2)_3]_1$ and these were analogous in both chemical shift and multiplicity to the ligand peaks at 7.82 ppm (o-H), 7.41 ppm (p-H) and 7.32 ppm (m-H), respectively. In each case a slight downfield shift was observed; of about $\Delta\delta = -0.02$ ppm for the para and meta protons and $\Delta\delta = -0.07$ ppm for the ortho protons. This could indicate a slight increase in the electron withdrawing effect of the phosphorus centers. Other peaks in the region were indicative of impurities. The singlet at 4.38 ppm

(not shown in Figure 4.113) in the spectrum of $[\text{Eu}(\text{N}(\text{Ph}_2\text{PO})_2)_3]_1$ could indicate the presence of either an amine proton or an alcohol proton and thus was indicative of the lack of deprotonation on reaction. In all cases the lack of significant shifts and peak broadening indicated a lack of coordination to the paramagnetic Eu^{3+} ions.

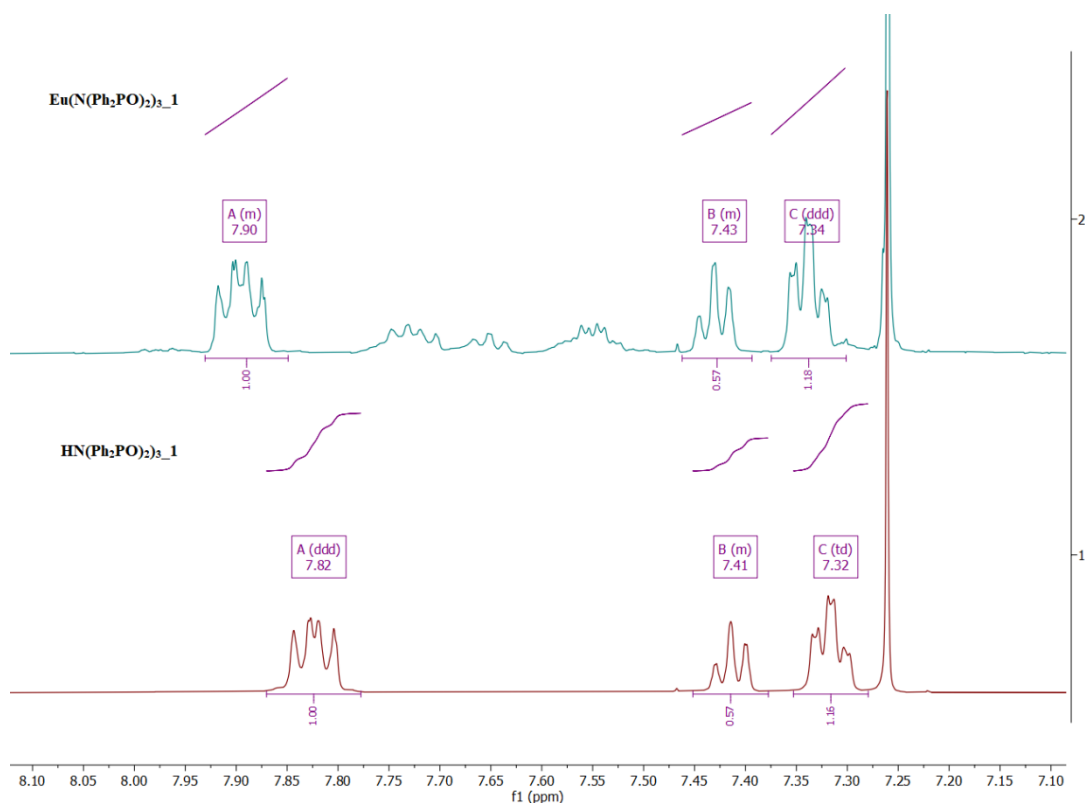


Figure 4.113: Detail of the aromatic region of the ^1H NMR spectra for $[\text{Eu}(\text{N}(\text{Ph}_2\text{PO})_2)_3]_1$ (blue) and $\text{HN}(\text{Ph}_2\text{PO})_2_1$ (red).

The $[\text{Eu}(\text{N}(\text{Ph}_2\text{PO})_2)_3]_2$ product was also characterised using ^1H NMR spectroscopy and its spectrum was observed to be significantly different from both the spectra of the reagent and that of the $[\text{Eu}(\text{N}(\text{Ph}_2\text{PO})_2)_3]_1$ product. As the spectra of $[\text{Eu}(\text{N}(\text{Ph}_2\text{PO})_2)_3]_1$ and $\text{HN}(\text{Ph}_2\text{PO})_2_1$ were very similar, the comparison of the data for $[\text{Eu}(\text{N}(\text{Ph}_2\text{PO})_2)_3]_2$ is only undertaken with regards to the spectrum of $\text{HN}(\text{Ph}_2\text{PO})_2_1$, as given in Figure 4.114.

The first observation in the spectrum of the product was that no singular peak could be described for the amine or alcohol peak, which would indicate the possibility of deprotonation. A detail of this spectrum in the aromatic region is given in Figure 4.114, together with that of the ligand. The peaks of interest for the $[\text{Eu}(\text{N}(\text{Ph}_2\text{PO})_2)_3]_2$

spectrum were those at 7.55 ppm, 7.24 ppm and 7.01 ppm in the aromatic region. All three peaks were in agreement with the literature values for the complex $[\text{Eu}(\text{N}(\text{Ph}_2\text{PO})_2)_3]$, given at 7.54 ppm, 7.21 ppm and 6.99 ppm respectively.

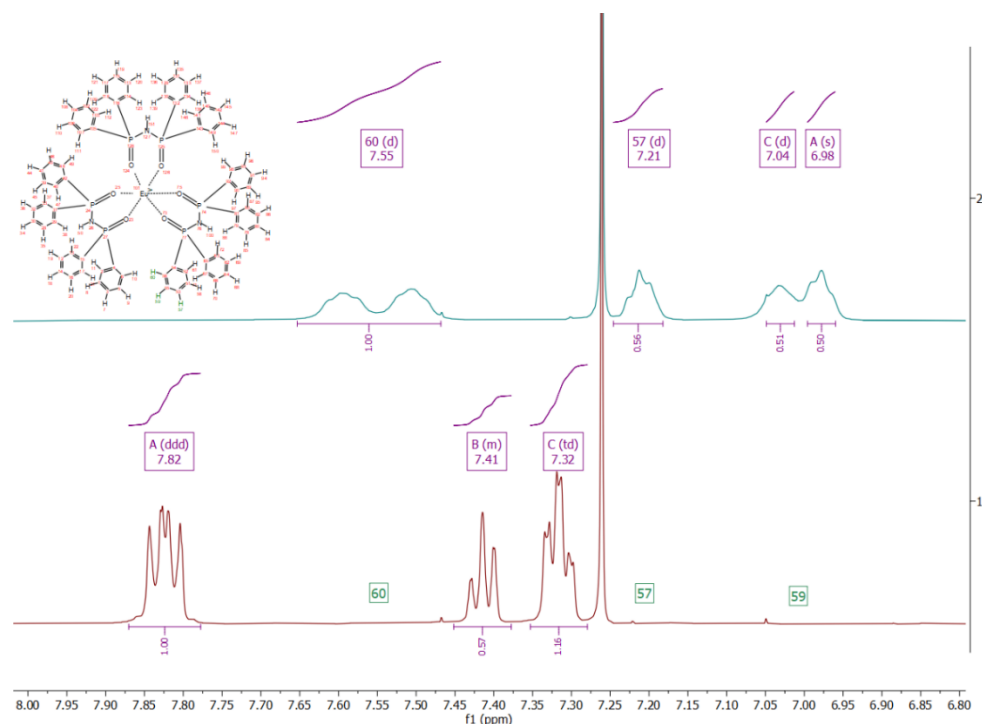


Figure 4.114: Detail of the aromatic region of the ^1H NMR spectra for $[\text{Eu}(\text{N}(\text{Ph}_2\text{PO})_2)_3]_2$ (blue) and $\text{HN}(\text{Ph}_2\text{PO})_2$ (red).

The main feature of interest in the spectrum of the product was the very clear broadening of the peaks assigned to the various aromatic peaks, which is typical of samples where paramagnetic ions are present. The integration values for the three peaks indicated a 2:1:2 proton ratio, as given in literature. The same ratio was present in the ligand, indicating that similar shielding effects were present in the phenyl protons of the product, as were observed in the ligand. Given that the broadening of the peaks did not allow for clear coupling constants to be observed no further assignment of these protons could be undertaken. The last feature of interest was the unexpected upfield shift of all the proton peaks. This was unexpected since coordination should increase the P^+-O^- nature of the $\text{P}=\text{O}$ bond and therefore increase the electron withdrawing effect of the phosphorus centres. Regardless the broadening and chemical shifts of the peaks were in agreement with published literature data and therefore indicated the presence of Eu^{3+} ions coordinated with the ligand.

4.2.2.1.3. Analysis by Powder X-ray diffraction

Both the products $[\text{Eu}(\text{N}(\text{Ph}_2\text{PO})_2)_3]_1$ and $[\text{Eu}(\text{N}(\text{Ph}_2\text{PO})_2)_3]_2$ were analysed by PXRD using $\text{Mo-K}\alpha_1$ radiation and the patterns obtained are discussed hereunder. The powder patterns for both these products were compared to the powder pattern of the reagent $\text{HN}(\text{Ph}_2\text{PO})_2_1$, which is described in Section 4.2.1.1.4. The pattern for $[\text{Eu}(\text{N}(\text{Ph}_2\text{PO})_2)_3]_1$ was initially thought to be different from that of the reagent used, however more detailed comparison with the calculated pattern for the previously published tautomer of $\text{HN}(\text{Ph}_2\text{PO})_2$, namely $\text{N}^+(\text{Ph}_2\text{PO}^-)(\text{Ph}_2\text{POH})$, showed that there were clear similarities. This crystal structure was published by Nöth (CCDC Refcode: BOLGIS)²³⁶ The experimental powder pattern for $[\text{Eu}(\text{N}(\text{Ph}_2\text{PO})_2)_3]_1$ and the powder pattern for BOLGIS calculated using Mercury software are given in Figure 4.115 and the similarity could be easily observed.²⁹⁷ This indicated that $[\text{Eu}(\text{N}(\text{Ph}_2\text{PO})_2)_3]_1$ was in fact $\text{N}^+(\text{Ph}_2\text{PO}^-)(\text{Ph}_2\text{POH})$.

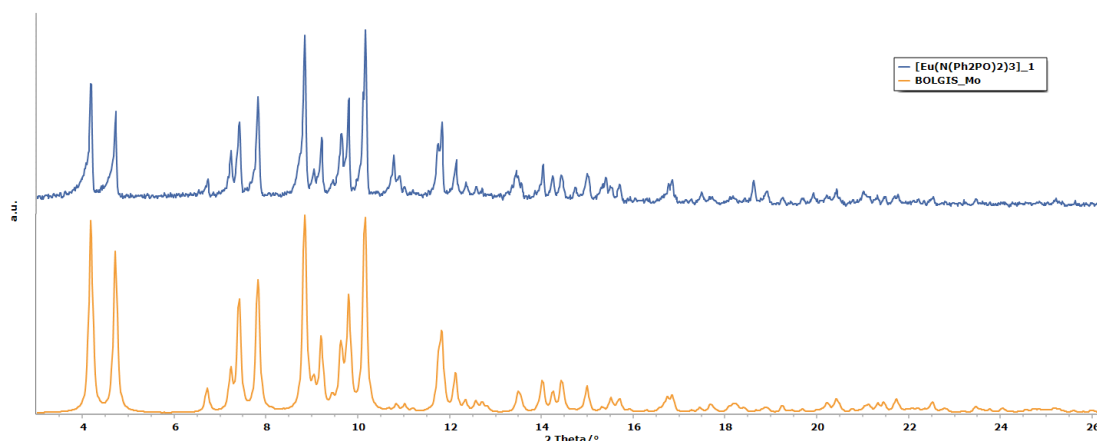


Figure 4.115: Powder patterns for $[\text{Eu}(\text{N}(\text{Ph}_2\text{PO})_2)_3]_1$ (blue) and BOLGIS (orange).

Given the close agreement between the ^1H NMR data obtained for the product $[\text{Eu}(\text{N}(\text{Ph}_2\text{PO})_2)_3]_2$ and the data described in literature for the desired compound, characterisation by PXRD was undertaken, to verify further whether this product had the expected structure. The powder pattern for $[\text{Eu}(\text{N}(\text{Ph}_2\text{PO})_2)_3]_2$ was compared to the patterns for the reagent and its tautomers, but there were no similarities. This same lack of similarity was also observed when the pattern of the product was compared to the calculated PXRD patterns for the two known crystallographic species of $[\text{Eu}(\text{N}(\text{Ph}_2\text{PO})_2)_3]$, namely $[\text{Eu}(\text{N}(\text{Ph}_2\text{PO})_2)_3]$ (CCDC Refcode ZAXDIN) and

[Eu(N(Ph₂PO)₂)₃]·0.67(H₂O) (CCDC Refcode: HIWDUM). There are large differences between the calculated powder patterns of these structures, and that of [Eu(N(Ph₂PO)₂)₃]₂ as shown in Figure 4.116.^{240,244}

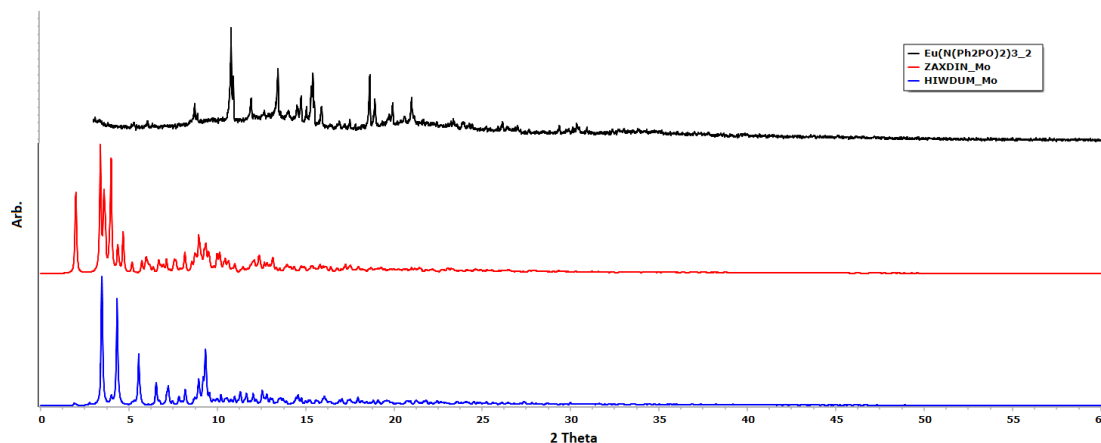


Figure 4.116: Powder patterns for [Eu(N(Ph₂PO)₂)₃]₂ (black) and ZAXDIN (red) and HIWDUN (blue).

Initial unit cell determination was attempted but no results were obtained. Further comparison work with possible products was undertaken. The powder pattern of [Eu(N(Ph₂PO)₂)₃]₂ was compared with the calculated powder pattern of the published anhydrous α -KNO₃ phase as shown in Figure 4.117.³⁹³ This comparison showed clearly that the major crystalline phase of the solid [Eu(N(Ph₂PO)₂)₃]₂ was this α -KNO₃ phase. A number of experimental powder pattern peaks, also shown in Figure 4.117, were observed at 5.25°, 6.05°, 11.91°, 14.00°, 14.53°, 15.89°, 20.59°, 23.38°, 23.90°, 23.95°, 26.13°, 27.62° and 27.65°. These peaks could not be attributed to the α -KNO₃ phase or the two [Eu(N(Ph₂PO)₂)₃] phases described prior. The presence of KNO₃ was considered a possibility on discussing the IR spectrum of the solid. However it was not expected to be the major crystalline phase of the solid given the clear presence of IR bands indicative of the desired product and the confirmation of the presence of the desired product in the ¹H NMR study. Therefore the unassigned peaks in the experimental powder pattern are most likely the desired product.

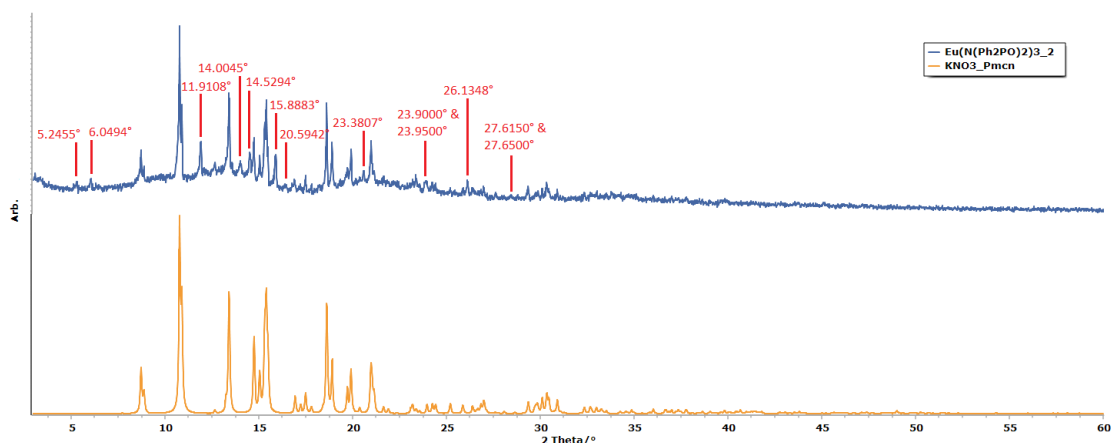


Figure 4.117: Powder patterns for [Eu(N(Ph₂PO)₂)₃]₂ (blue) and α -KNO₃ in a *Pmcn* space group (orange), the experimental peaks not attributable to this α -KNO₃ are labelled in red.

4.2.2.1.4. Conclusion

¹H NMR data for [Eu(N(Ph₂PO)₂)₃]₁ indicated that no complexation occurred in this product, although comparison of IR and PXRD data to similar data for the starting reagent HN(Ph₂PO)₂_1 indicated that some changes had occurred. The data obtained from the IR spectra and PXRD powder patterns led to the conclusion that the product [Eu(N(Ph₂PO)₂)₃]₁ was in fact the tautomer of HN(Ph₂PO)₂_3, N⁺(Ph₂PO⁻)(Ph₂POH), the structure of which was previously published by Nöth in 1982.²³⁶ The significant difference between the IR spectra of the two tautomers was interesting, especially with the presence of the strong bands at 1467 cm⁻¹ (ν P=N) and 522 cm⁻¹ (δ P-O-H) which could clearly characterise the tautomer published previously.

In the case of [Eu(N(Ph₂PO)₂)₃]₂ the ¹H NMR data obtained was in clear agreement with the published data, indicating the formation of the desired compound. Like the ¹H NMR data the IR data for this product also indicated the possible formation of the desired complex through a number of band shifts typical of the deprotonation of the free ligand. The IR data also indicated the possible presence of the side product KNO₃. The PXRD powder pattern for this product indicated that the crystallographic species obtained was dissimilar to the two previously published structures of [Eu(N(Ph₂PO)₂)₃]. Further comparison with literature data showed that the major crystalline phase of the solid was KNO₃ although this was unexpected given the IR and ¹H NMR results. A number of PXRD peaks did indicate the presence of a minor crystalline phase which could be a novel form of the complex although this data was not sufficient to undertake unit cell or structure determination.

4.2.2.2. Characterisation of $\text{HN}(\text{Ph}_2\text{PS})_2 + \text{Eu}(\text{ClO}_4)_3 \cdot n(\text{H}_2\text{O})$

During this study an attempt was made to synthesise the sulphide analogue of the $[\text{Eu}(\text{N}(\text{Ph}_2\text{PO})_2)_3]$ complex. Given that, as described in Section 3.3.2.2.2, the synthesis of a theoretical $[\text{Eu}(\text{N}(\text{Ph}_2\text{PS})_2)_3]$ complex could not be undertaken by wet chemistry techniques it was decided to attempt to produce this complex using a mechano-chemical method, as detailed out in the same section. This method involved the reaction of the free ligand, $\text{HN}(\text{Ph}_2\text{PS})_2$, with $\text{Eu}(\text{ClO}_4)_3 \cdot 6\text{H}_2\text{O}$. The perchlorate was used as a counter ion since this has a very low coordination ability. This reaction gave a brownish white powder, but its yield could not be calculated because of the nature of the reaction techniques. The desired structure for the unknown $\text{HN}(\text{Ph}_2\text{PS})_2$ analogue of the published compound $[\text{Eu}(\text{N}(\text{Ph}_2\text{PO})_2)_3]$ is given in Figure 4.118.

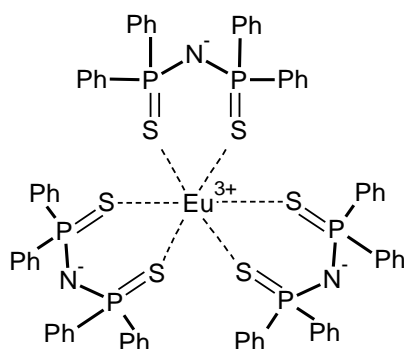


Figure 4.118: Molecular representation of the theoretical sulphide analogue of $[\text{Eu}(\text{N}(\text{Ph}_2\text{PO})_2)_3]$ – $[\text{Eu}(\text{N}(\text{Ph}_2\text{PS})_2)_3]$.

In the case of the product obtained in the current study, which was not produced by conventional reactions, the structure could be similar to that in Figure 4.118, but containing protonated amine moieties. Although the mode of coordination might have been impacted by the reaction technique, the coordination number should remain the same given that this is dependent on the ionic radius of the central cation.

4.2.2.2.1. Analysis by Infra-red spectroscopy

A detail of the IR spectrum of $\text{HN}(\text{Ph}_2\text{PS})_2 + \text{Eu}(\text{ClO}_4)_3 \cdot n(\text{H}_2\text{O})_1$ is given in Figure 4.119, along with the spectrum of the ligand reagent. It was very clear from the comparison of these two spectra that the two compounds were very similar to each other. No bands of interest were observed at wavenumbers higher than 1800 cm^{-1} and therefore

this region is not included in Figure 4.119. This lack of bands in this region was mainly due to the large band attributed to ν O–H vibrations, which was expected given that hydrated europium (III) perchlorate salt was used in the reaction.

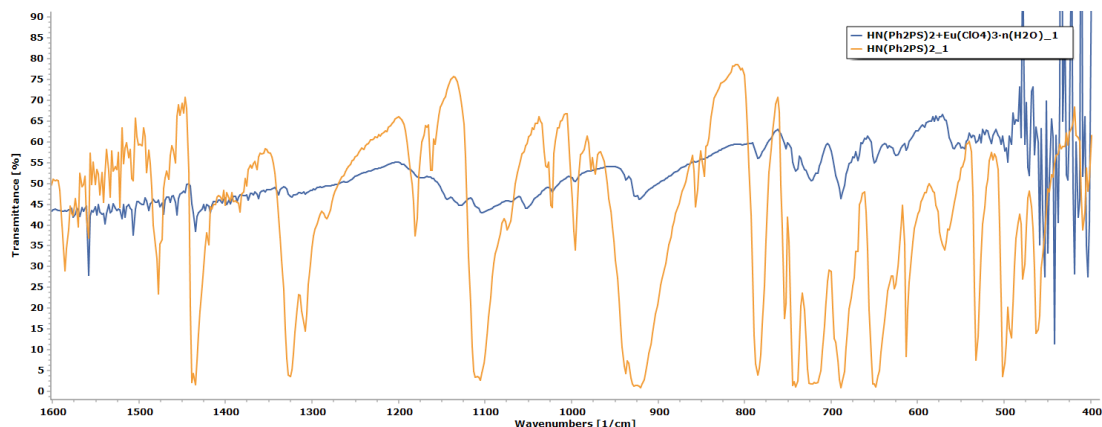


Figure 4.119: IR spectra, in the region 1600-400 cm^{-1} , for $\text{HN}(\text{Ph}_2\text{PS})_2+\text{Eu}(\text{ClO}_4)_3\cdot n(\text{H}_2\text{O})_1$ (blue) and $\text{HN}(\text{Ph}_2\text{PS})_2_1$ (orange).

The major bands in the spectrum of the product at 1325 cm^{-1} , 1102 cm^{-1} , 921 cm^{-1} and all the bands at wavenumbers below 800 cm^{-1} were in clear agreement with the analogous bands for the spectrum of the free ligand. This lack of change in wavenumbers and intensities from the bands in the spectrum of the ligand to those in the spectrum of the product and more specifically the lack of change in the bands at 1102 cm^{-1} and 784 cm^{-1} , which were assigned in Section 4.2.1.2.1 to the ν_{as} P–N–P and ν_{s} P–N–P vibrations, was a clear indication that the ligand remained protonated in the product mixture. The only bands which differed between the spectrum of the product and that of the ligand were the bands at 1145 cm^{-1} , 1129 cm^{-1} and 1051 cm^{-1} in the spectrum of the product. Assignment of these bands was problematic as they all fell in the range typical of the ν_{as} P–N–P vibrations and the major ClO_4^- IR vibration. The possibility that any of these bands was due to the major ClO_4^- IR vibration would indicate the presence of either coordinated Eu^{3+} ions or the starting reagent salt. Further data from the IR spectra could not be obtained, given that minimal differences were observed between these spectra.

4.2.2.2.2. Analysis by ^1H NMR spectroscopy

As with the ^1H NMR spectrum of the ligand, the amine proton peak for $\text{HN}(\text{Ph}_2\text{PS})_2+\text{Eu}(\text{ClO}_4)_3\cdot n(\text{H}_2\text{O})_1$ could not be assigned with confidence. The main discussion hereunder deals with the aromatic region of the spectrum for $\text{HN}(\text{Ph}_2\text{PS})_2+\text{Eu}(\text{ClO}_4)_3\cdot n(\text{H}_2\text{O})_1$. Three very broad peaks at 7.90 ppm, 7.38 ppm and 7.14 ppm were noted in this region, as given in Figure 4.120, and these could be related to the three peaks known for the free ligand. The most distinct feature of these peaks was that they were broad, when compared to the peaks of the ligand. Broadening in ^1H NMR spectra is very typical of the presence of paramagnetic ions such as Eu^{3+} and the presence of this broadening could indicate the coordination of the ligand about ions of this species. This broadening was also observed in the published ^1H NMR data of the analogous $[\text{Eu}(\text{N}(\text{Ph}_2\text{PO})_2)_3]$ compound and was described therein as evidence of coordination.³² Similarly to the ^1H NMR spectrum of $\text{Eu}(\text{N}(\text{Ph}_2\text{PO})_2)_3$ as described in publication,³² slight shifts were observed for the peaks in the spectrum of the product when compared to the peaks in the spectrum of the ligand. The peak at 7.90 ppm was downfield of the ligand peak while the other two peaks were found upfield of the analogous peaks for the ligand spectrum. Unfortunately, the broadening made the application of the typical integration values and coupling constants in the assignment of peaks and structure determination ineffective.

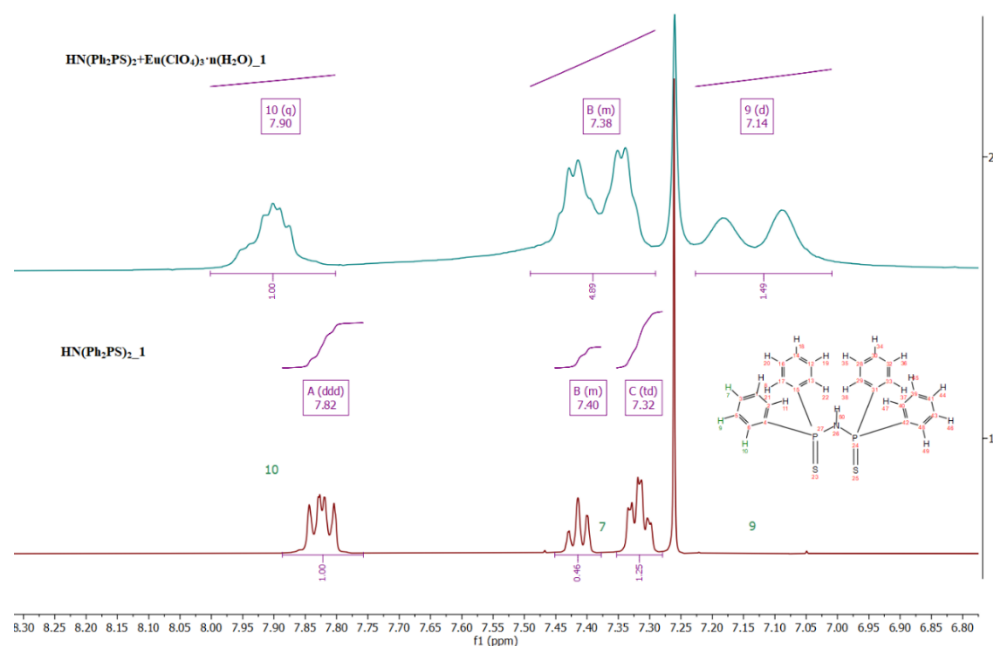


Figure 4.120: ^1H NMR spectra for $\text{HN}(\text{Ph}_2\text{PS})_2+\text{Eu}(\text{ClO}_4)_3\cdot n(\text{H}_2\text{O})_1$ (blue) and $\text{HN}(\text{Ph}_2\text{PS})_2_1$ (red).

4.2.2.2.3. Analysis by Microscopy and luminescence

The product $\text{HN}(\text{Ph}_2\text{PS})_2+\text{Eu}(\text{ClO}_4)_3\cdot n(\text{H}_2\text{O})_1$ was analysed under a polarised microscope and this clearly indicated crystallinity, as shown in Figure 4.121. During the microscopic analysis the sample was also subjected to the application of UV-Visible radiation at 254 nm, wherein a red luminescence was clearly visible in the sample, as shown in Figure 4.121. This is typical of the Eu^{3+} ion, be it free or coordinated and therefore the luminescence of the sample clearly indicated the presence of the Eu^{3+} ion in the solid, either as part of the mixture or part of a new product.

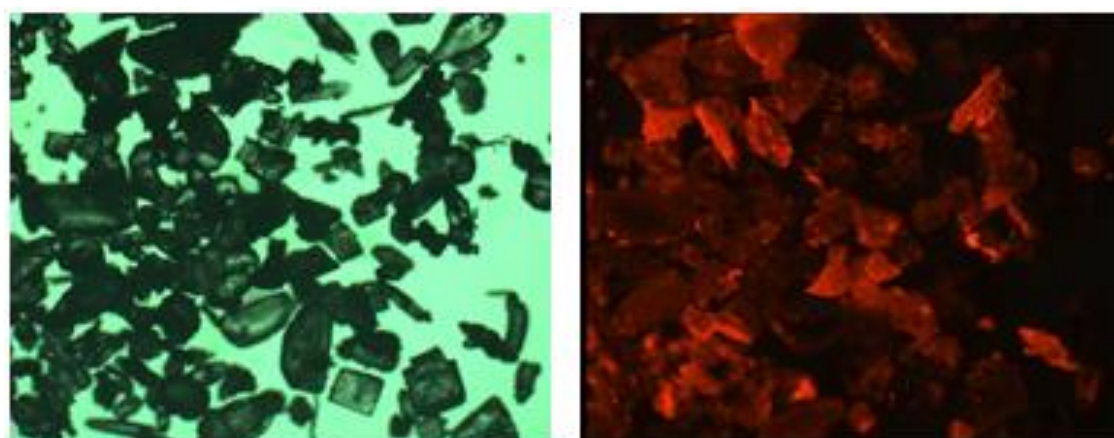


Figure 4.121: Micrographs of $\text{HN}(\text{Ph}_2\text{PS})_2+\text{Eu}(\text{ClO}_4)_3\cdot n(\text{H}_2\text{O})_1$ showing (left) particles with clear habit and (right) the same product under 254 nm UV-Visible radiation.

4.2.2.2.4. Analysis by Powder X-ray diffraction

The product $\text{HN}(\text{Ph}_2\text{PS})_2+\text{Eu}(\text{ClO}_4)_3\cdot n(\text{H}_2\text{O})_1$ was also analysed by PXRD, using $\text{Mo-K}_{\alpha 1}$ radiation, and the powder pattern obtained was compared to the calculated powder pattern of the ligand $\text{HN}(\text{Ph}_2\text{PS})_2$ (CCDC Refcode: BOLGEO01), as shown in Figure 4.122.²²² It was clear from this comparison that the compounds were dissimilar crystal species. The solid obtained was believed to be novel, as was expected given that IR and ^1H NMR data concluded that the product was most likely a complex which was previously unpublished. Structure solution from the data obtained proved difficult due to the small number of peaks and their overlap and is therefore still underway.

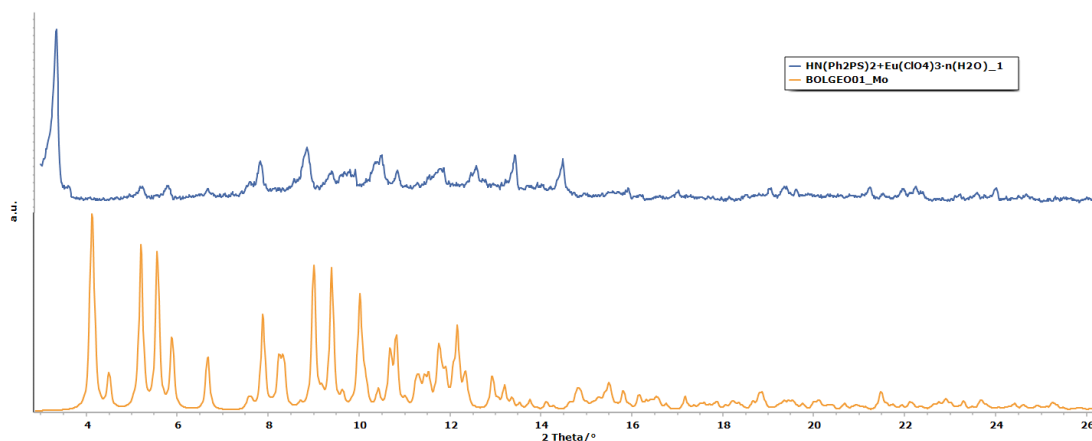


Figure 4.122: PXRD patterns for HN(Ph₂PS)₂+Eu(ClO₄)₃·n(H₂O)₁ (blue) and BOLGEO01 (orange).

4.2.2.2.5. Conclusion

Unfortunately, the IR spectrum of the product HN(Ph₂PS)₂+Eu(ClO₄)₃·n(H₂O)₁ did not give sufficient information to aid in the characterisation of this product, although relevant bands clearly showed that deprotonation did not occur. The ¹H NMR spectrum and the analysis by UV-visible light aided microscopy both indicated the possibility of coordination of the ligand, most likely protonated, to the Eu³⁺ cation. Characterisation was also undertaken using PXRD, which indicated that the crystalline species obtained was indeed new.

4.2.2.3. Characterisation of O((Et₂N)₂PO)₂+Nd(ClO₄)₃

As described in Section 3.3.2.2.3, during this study an initial attempt was made to produce a lanthanide complex using the ligand O((Et₂N)₂PO)₂, which was produced as described in Section 3.3.2.1.3. Characterisation of the various products (Section 4.2.1.3) yielded in the reactions undertaken in Section 3.3.2.1.3 indicated that O((Et₂N)₂PO)₂ was the major component of the product O((Et₂N)₂PO)₂_1. Thereby O((Et₂N)₂PO)₂_1 was reacted with Nd(ClO₄)₃, using a procedure that was adopted from methodologies used to produce complexes of analogous ligands with transition and actinide metal centres (as described in Section 3.3.2.2.3), yielding the very brown viscous liquid O((Et₂N)₂PO)₂+Nd(ClO₄)₃_1. The yield for O((Et₂N)₂PO)₂+Nd(ClO₄)₃_1 was of 33.94%.

4.2.2.3.1. Analysis by Infra-red spectroscopy

The IR spectrum of the product $\text{O}((\text{Et}_2\text{N})_2\text{PO})_2+\text{Nd}(\text{ClO}_4)_3_1$ is given in Figure 4.123, together with the IR spectra for the starting reagent $\text{O}((\text{Et}_2\text{N})_2\text{PO})_2_1$ and $\text{O}((\text{Et}_2\text{N})_2\text{PO})_2_1_{\text{f13}}$. The latter was a column fraction product which contained a purified $\text{O}((\text{Et}_2\text{N})_2\text{PO})_2$. As given in Figure 4.123 it was noticeable that the $\text{O}((\text{Et}_2\text{N})_2\text{PO})_2_1$ bands at 1360 cm^{-1} , 958 cm^{-1} and 930 cm^{-1} were diminished in transmittance in the spectrum of $\text{O}((\text{Et}_2\text{N})_2\text{PO})_2+\text{Nd}(\text{ClO}_4)_3_1$, while the bands at 1294 cm^{-1} and 750 cm^{-1} were both lost. This was in line with the changes observed in Section 4.2.1.3.1, between the IR spectra of the $\text{O}((\text{Et}_2\text{N})_2\text{PO})_2_1$ and $\text{O}((\text{Et}_2\text{N})_2\text{PO})_2_1_{\text{f13}}$, indicating that the product obtained from this reaction was purified similarly to the purification of $\text{O}((\text{Et}_2\text{N})_2\text{PO})_2_1$ by column chromatography. Therefore, the discussion hereunder will focus on the comparison between the spectra of $\text{O}((\text{Et}_2\text{N})_2\text{PO})_2_1_{\text{f13}}$ and $\text{O}((\text{Et}_2\text{N})_2\text{PO})_2+\text{Nd}(\text{ClO}_4)_3_1$.

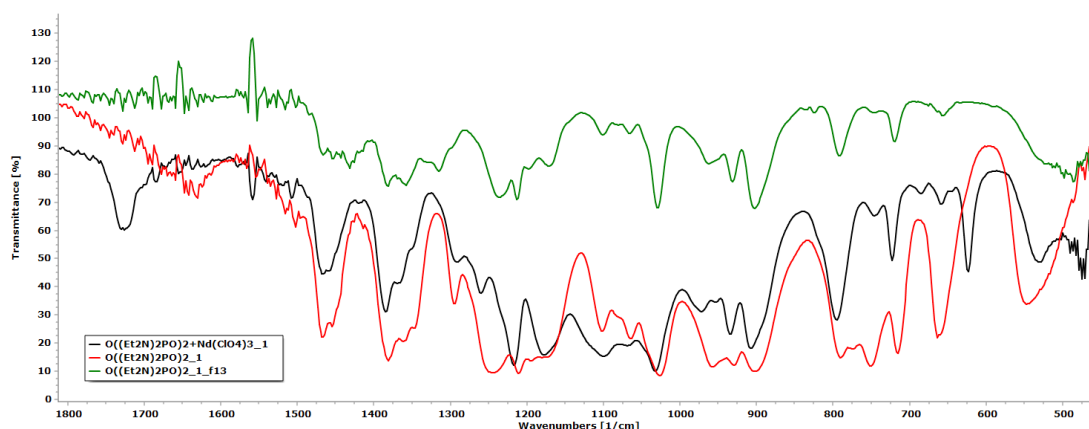


Figure 4.123: IR spectra of $\text{O}((\text{Et}_2\text{N})_2\text{PO})_2+\text{Nd}(\text{ClO}_4)_3_1$ (black), $\text{O}((\text{Et}_2\text{N})_2\text{PO})_2_1$ (red) and $\text{O}((\text{Et}_2\text{N})_2\text{PO})_2_1_{\text{f13}}$ (green).

The first band of interest in the spectrum of $\text{O}((\text{Et}_2\text{N})_2\text{PO})_2+\text{Nd}(\text{ClO}_4)_3_1$ was observed at 1732 cm^{-1} , which was the expected band for the $\nu\text{ C}=\text{O}$ vibration of acetone and thus indicating the presence of acetone in the product obtained. The lack of a decrease in wavenumber for this peak indicated that any acetone present in the sample was not coordinated to the Nd^{3+} ion.³⁰⁴ For the remainder of the spectrum the loss of the IR bands at 957 cm^{-1} , 751 cm^{-1} and 662 cm^{-1} indicated that the reaction and workup caused the purification of $\text{O}((\text{Et}_2\text{N})_2\text{PO})_2_1$ to a product similar to that obtained for $\text{O}((\text{Et}_2\text{N})_2\text{PO})_2_1_{\text{f13}}$, as described above.

For all bands at wavenumbers lower than 1145 cm^{-1} there was a near full agreement with the bands in the spectrum of $\text{O}((\text{Et}_2\text{N})_2\text{PO})_2_1_{\text{f13}}$, except for a strong broad band at 1101 cm^{-1} and the sharp medium band at 624 cm^{-1} . These two bands could be easily described as the bands of the perchlorate ion as shown in Figure 4.124, where the $\text{O}((\text{Et}_2\text{N})_2\text{PO})_2+\text{Nd}(\text{ClO}_4)_3_1$ spectrum is compared with that of the starting reagent $\text{Nd}(\text{ClO}_4)_3$. For the IR spectrum of $\text{Nd}(\text{ClO}_4)_3$ a strong band at 1116 cm^{-1} was present, indicating that the perchlorate was not coordinated or very weakly coordinated to the Nd^{3+} metal. The presence of this single band at 1101 cm^{-1} in the $\text{O}((\text{Et}_2\text{N})_2\text{PO})_2+\text{Nd}(\text{ClO}_4)_3_1$ spectrum was clearly analogous to the 1116 cm^{-1} band for the free perchlorates, indicating the presence of perchlorate in the mixture, but as an uncoordinated free species.³⁹⁴ The band at 624 cm^{-1} is also known for free perchlorates, although it is not typically used to describe coordination.

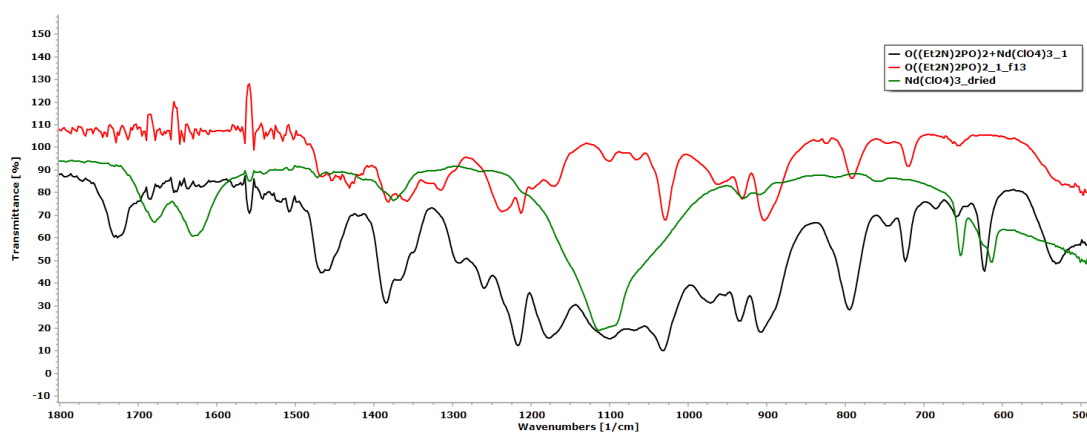


Figure 4.124: IR spectra of $\text{O}((\text{Et}_2\text{N})_2\text{PO})_2+\text{Nd}(\text{ClO}_4)_3_1$ (black), $\text{O}((\text{Et}_2\text{N})_2\text{PO})_2_1_{\text{f13}}$ (red) and $\text{Nd}(\text{ClO}_4)_3$ dried using 2,2-DMP (green).

The bands in the spectrum of $\text{O}((\text{Et}_2\text{N})_2\text{PO})_2+\text{Nd}(\text{ClO}_4)_3_1$ at 1294 cm^{-1} and 1261 cm^{-1} were too high in wavenumber to be due to coordinated perchlorate ions. The former was possibly a band retained from the $\text{O}((\text{Et}_2\text{N})_2\text{PO})_2_1$ compound while the latter could not be easily assigned. The $\text{O}((\text{Et}_2\text{N})_2\text{PO})_2_1$ band at 1211 cm^{-1} , assigned to $\nu\text{ P=O}$ vibrations, seems to have been retained although shifted to 1218 cm^{-1} . A small shift like this is not typical of coordination, wherein a greater shift is expected. The other band found at 1240 cm^{-1} in the $\text{O}((\text{Et}_2\text{N})_2\text{PO})_2_1_{\text{f13}}$ IR spectrum, which was also tentatively assigned to $\nu\text{ P=O}$ vibration, was apparently lost in the spectrum of $\text{O}((\text{Et}_2\text{N})_2\text{PO})_2+\text{Nd}(\text{ClO}_4)_3_1$. This could indicate coordination. On coordination a decrease in wavenumber of the $\nu\text{ P=O}$ band was expected, however such a shift was not

noticed in the spectrum of the $\text{O}((\text{Et}_2\text{N})_2\text{PO})_2+\text{Nd}(\text{ClO}_4)_3_1$. No more detail could be inferred from the data obtained for the IR spectrum of $\text{O}((\text{Et}_2\text{N})_2\text{PO})_2+\text{Nd}(\text{ClO}_4)_3_1$. The possibility of coordination was only supported by the loss of the ligand band at 1240 cm^{-1} , whose analogue in the spectrum of $\text{O}((\text{Et}_2\text{N})_2\text{PO})_2+\text{Nd}(\text{ClO}_4)_3_1$ was not identified.

4.2.2.3.2. Analysis by ^1H NMR spectroscopy

Analysis by ^1H NMR spectroscopy was attempted to aid in the characterisation of the product $\text{O}((\text{Et}_2\text{N})_2\text{PO})_2+\text{Nd}(\text{ClO}_4)_3_1$. The spectrum of $\text{O}((\text{Et}_2\text{N})_2\text{PO})_2+\text{Nd}(\text{ClO}_4)_3_1$ is given in Figure 4.125. Numerous peaks were observed throughout the typical organic proton region.

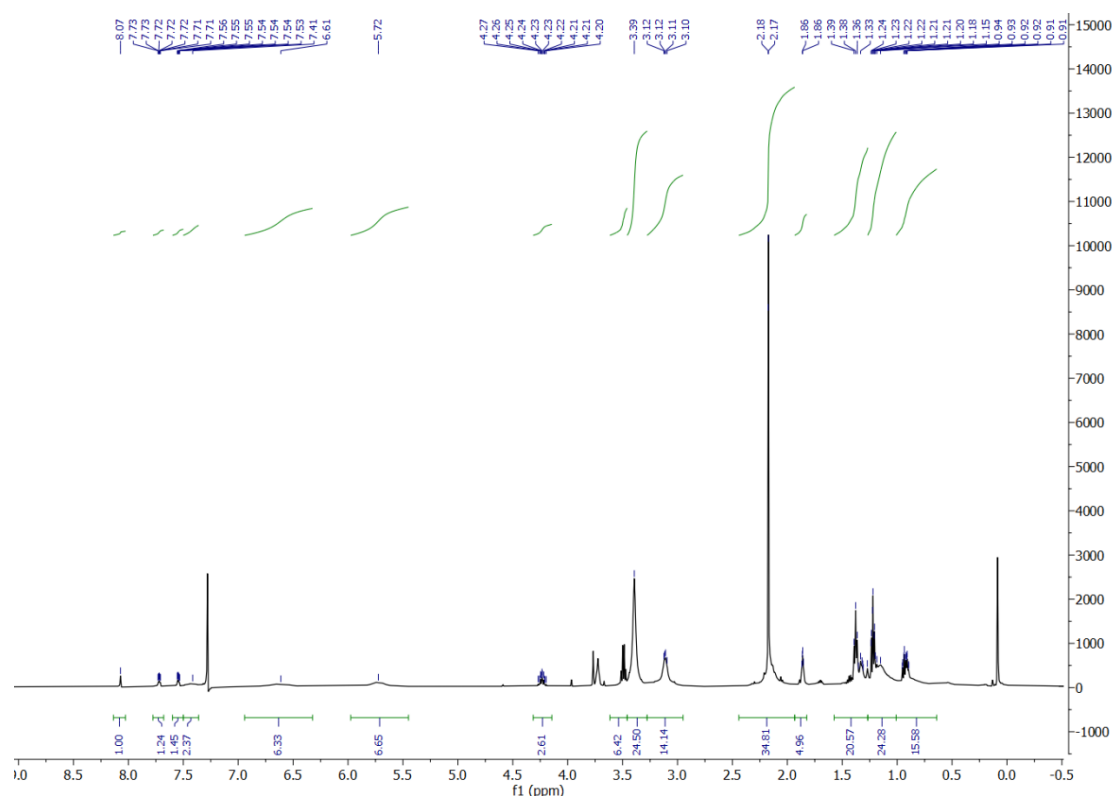


Figure 4.125: ^1H NMR spectrum of $\text{O}((\text{Et}_2\text{N})_2\text{PO})_2+\text{Nd}(\text{ClO}_4)_3_1$ in CDCl_3 .

The presence of these numerous peaks could indicate the presence of multiple components. The peaks at 2.17 ppm and 3.39 ppm were likely due to remaining acetone and methanol (methyl proton) peaks in CDCl_3 ,³⁶¹ although the alcohol peak at 1.09 ppm for methanol was not noticed. The broad peak at 1.14 ppm could however correspond to

this proton species, although this could not be supported by integration values due to overlap with the triplet at 1.22 ppm. These two compounds are products of the 2,2-DMP hydration, which was expected in this reaction. The peaks for 2,2-DMP (equal intensity singlets at 3.19 Hz and 1.33 Hz) and water (1.56 Hz) were not clearly visible, indicating that both were fully consumed. For the remaining product peaks the multiplet structures and the given integration values do not yield valuable information on the structure of the product. The peaks closest to the values for peaks obtained in the O((Et₂N)₂PO)₂_1_f13 ¹H NMR spectrum were those at 1.22 ppm or 1.38 ppm, 1.86 ppm and 3.11 ppm, corresponding to the O((Et₂N)₂PO)₂_1_f13 peaks at 1.12 ppm, 1.76 ppm and 3.10 ppm. These peaks were also the major peaks barring methanol and acetone peaks. A clear downfield shift for the ligand peak at 1.12 ppm to either 1.22 ppm or 1.38 ppm and the formation of a singlet at 3.11 ppm as compared to the broad doublet at 3.10 ppm for the ligand could indicate coordination with the paramagnetic Nd³⁺ centre. Such downfield shifts are known for Nd³⁺ complexes obtained from Nd(ClO₄)₃, although both downfield and upfield shifts can occur depending on solution conditions and individual proton conformation within the dipolar field of the paramagnetic lanthanide centres.^{395,396} If a significant downfield shift for the ligand peak at 3.10 ppm occurred this could overlap with the peak at 3.39 ppm attributed to methanol. In all cases however these peaks do not have integration values which are in agreement with the expected values.

Both the triplet described earlier at 1.22 ppm and the quartet at 3.48 ppm had coupling constants of 7.04 Hz.³⁶¹ This could be indicative of the presence of diethyl ether in the sample, possibly introduced during the workup. The multiplet at 0.92 ppm could be due to the presence of a minor alkane impurity.³⁶¹ The remaining unassigned peaks were the four peaks with chemical shifts > 7.26 ppm and the two broad peaks at 6.61 ppm and 5.72 ppm. The four former peaks were possibly due to minor aromatic impurities. The two broad peaks could not be assigned to any expected species. These peaks could be due to shifts of other peaks not typically observed in this region. This along with the broadening of these peaks could be due to interactions with the Nd³⁺. These peaks could be due to methylene and methyl groups of the ligand which occupy different general positions within the dipolar magnetic field of the lanthanide centre in the complex.³⁹⁶ This causes protons which are chemical-shift equivalent in the spectrum of the ligand to experience different shielding and therefore become non-equivalent in the spectrum of the complex.³⁹⁷

Therefore, apart from the possibility of a mixture of components as described above, the incidence of numerous peaks in the spectrum of $O((Et_2N)_2PO)_2+Nd(ClO_4)_3_1$ might be due to the effect of the presence of either coordinated or dissolved paramagnetic Nd^{3+} .

4.2.2.3.3. Analysis by ^{31}P NMR spectroscopy

The product $O((Et_2N)_2PO)_2+Nd(ClO_4)_3_1$ was also analysed by $^{31}P\{^1H\}$ NMR spectroscopy, with the spectrum obtained given in Figure 4.126. It was clear that two major peaks were obtained, at 86.34 ppm and 9.71 ppm. In both cases the peaks were found to be fairly broadened as compared to other $^{31}P\{^1H\}$ NMR spectra in general. The peak at 9.71 ppm seems to be analogous to the peaks at 8.45 ppm and 9.34 ppm for the spectra of $O((Et_2N)_2PO)_2_1$ and $O((Et_2N)_2PO)_2_1_{f13}$ respectively, which could indicate the presence of the main component of these two products in $O((Et_2N)_2PO)_2+Nd(ClO_4)_3_1$. The peak at 86.34 ppm was not observed in the spectra for the $O((Et_2N)_2PO)_2_1$ products and does not fall in the range typical of amine and alkoxide phosphoryl compounds. If the ligand coordinated to the Nd^{3+} ion through the $P=O$ bond a loss of bond order to a bond better represented as P^+-O^- would cause the ligand peak at 9.71 ppm to shift downfield.^{249,377} This shift would explain the peak at 86.34 ppm. The presence of this peak could therefore be indicative of the coordination of the ligand. The broadening of the two bands was also indicative of complexation since this is a typical effect of the presence of coordinated paramagnetic ions in NMR spectra.³⁹⁸ The integration values seem to indicate a 1.2:1 ratio for the 86.34 ppm and 9.71 ppm peaks. This would indicate that if symmetric coordination did occur the ratio of free and coordinated ligand could tentatively be approximately 1:1. Given the initial ligand to metal ratio of the reaction mixture, the complex could contain a 3:1 ligand to metal stoichiometry.

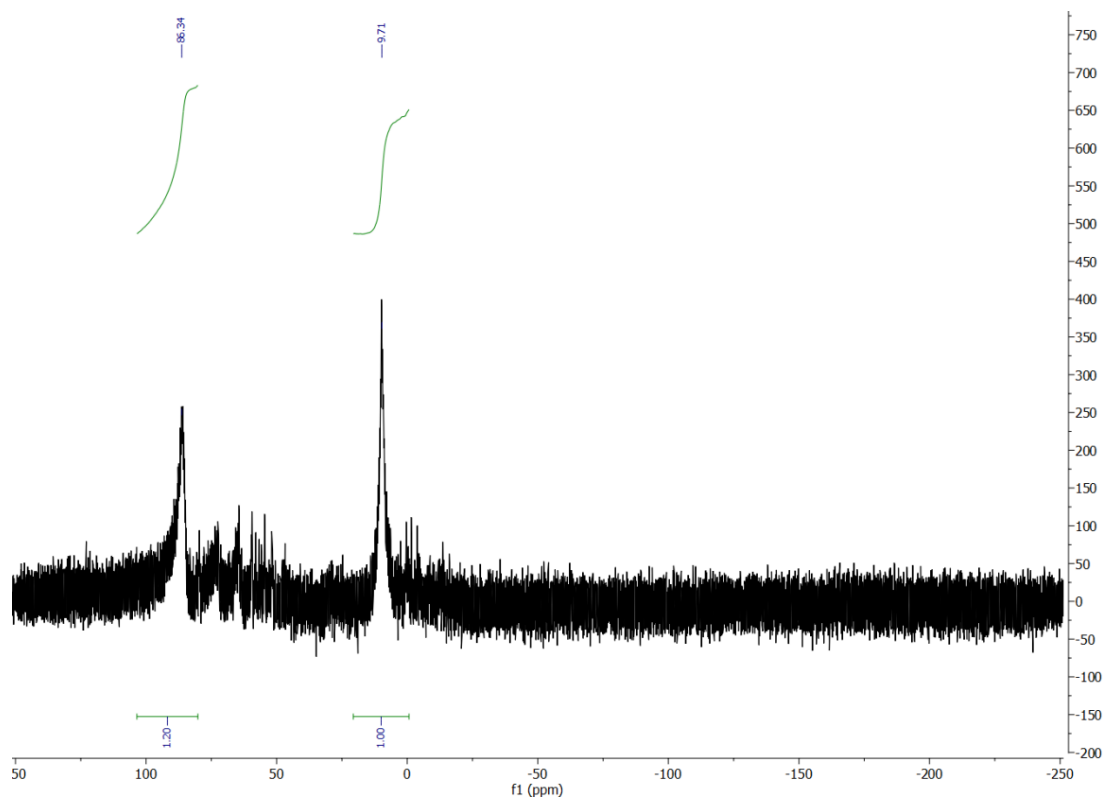


Figure 4.126: $^{31}\text{P}\{^1\text{H}\}$ NMR spectrum of $\text{O}((\text{Et}_2\text{N})_2\text{PO})_2+\text{Nd}(\text{ClO}_4)_3_1$ in CDCl_3 .

4.2.2.3.4. Analysis by Gas Chromatography Mass Spectroscopy (GC-MS)

The gas chromatography of $\text{O}((\text{Et}_2\text{N})_2\text{PO})_2+\text{Nd}(\text{ClO}_4)_3_1$ showed the presence of a mixture of two compounds, as given in Figure 4.127. This is in agreement with the data obtained from the analysis by $^{31}\text{P}\{^1\text{H}\}$ NMR. As shown in Figure 4.128, the mass spectrum of the GC peak at 10.60 minutes for $\text{O}((\text{Et}_2\text{N})_2\text{PO})_2+\text{Nd}(\text{ClO}_4)_3_1$ was nearly identical to the mass spectra of the GC fractions at 10.90 minutes and 10.56 minutes for $\text{O}((\text{Et}_2\text{N})_2\text{PO})_2_1$ and $\text{O}((\text{Et}_2\text{N})_2\text{PO})_2_1_{\text{f13}}$ respectively. This is in line with the data from the IR and ^{31}P NMR spectra which indicated that the major product found in both $\text{O}((\text{Et}_2\text{N})_2\text{PO})_2_1$ and $\text{O}((\text{Et}_2\text{N})_2\text{PO})_2_1_{\text{f13}}$ was also present in $\text{O}((\text{Et}_2\text{N})_2\text{PO})_2+\text{Nd}(\text{ClO}_4)_3_1$.

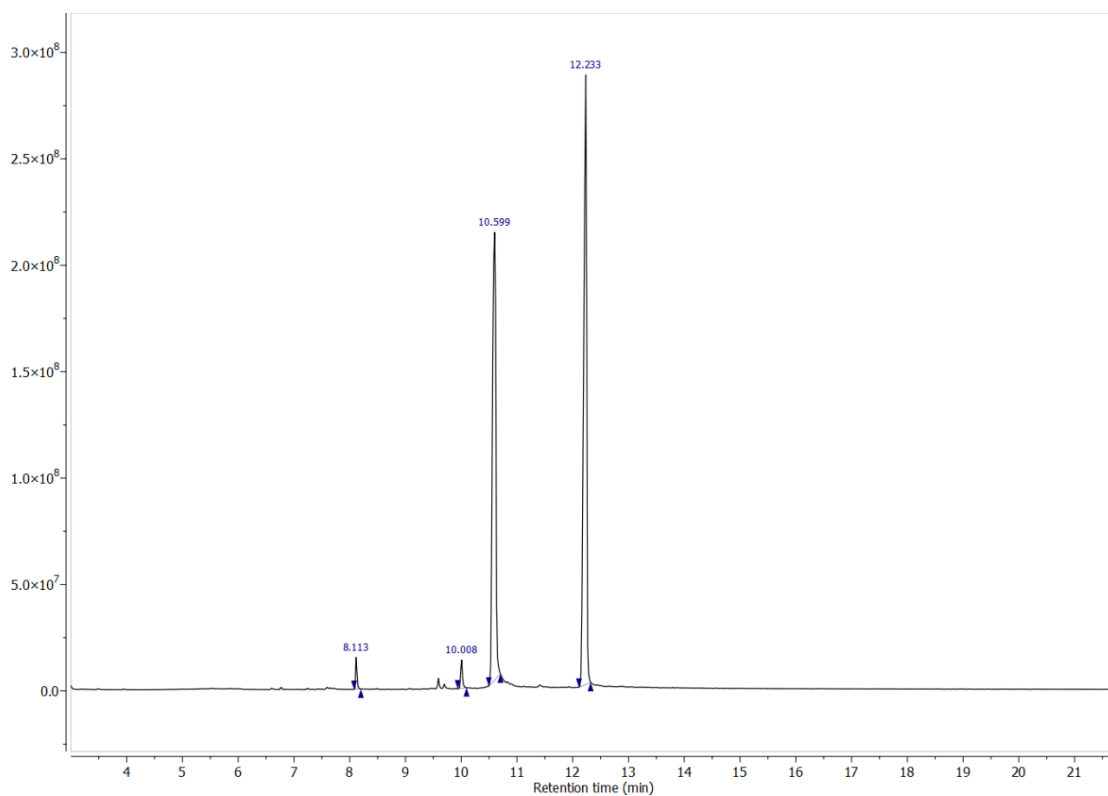


Figure 4.127: Gas chromatography of $O((Et_2N)_2PO)_2+Nd(ClO_4)_3_1$.



Figure 4.128: Comparison of the Mass spectra of $O((Et_2N)_2PO)_2_1$ (GC peak at 10.90 min.), $O((Et_2N)_2PO)_2_1_{f13}$ (GC peak at 10.56 min.) and $O((Et_2N)_2PO)_2_1$ (GC peak at 10.60 min.).

The MS data for the GC peak of $O((Et_2N)_2PO)_2+Nd(ClO_4)_3_1$ at 12.23 minutes, as given in Figure 4.129, was initially compared to that of the GC peaks at 12.99 minutes and 12.89 minutes for the gas chromatographs of $O((Et_2N)_2PO)_2_1$ and $O((Et_2N)_2PO)_2_1_{f13}$ respectively. This peak however gave MS data which was too dissimilar to the other two spectra, leading to the conclusion that this peak represented a different product than that found in the two ligand products. The peaks which could be easily described for the MS data for the GC peak of $O((Et_2N)_2PO)_2+Nd(ClO_4)_3_1$ at 12.23 minutes, were the fairly large bands at 43.11 m/z, 57.10 m/z and 71.12 m/z. These were tentatively assigned to the fragments $[EtN]^+$, $[EtNCH_2]^+$ and $[Et_2N-1]^+$. None of these peaks were observed in the GC-MS data of the ligand products. The peak at 279.21 m/z was found to be the highest significant peak for the mass spectrum. This could be tentatively assigned to the $[O((Et_2N)_2PO)((N)_2PO)-3]^+$ fragment or even to the theoretical $[LNdO]^{2+}$ fragment (where $L = O((Et_2N)_2PO)_2$). If the latter assignment is true this would support the occurrence of complexation. The main peak at 149.01 m/z could be assigned to the fragment $[Nd+5]^+$ as opposed to the expected 144 m/z for the $[Nd]^+$ fragment. Given these peaks, a peak at either 160 m/z or 165 m/z would be expected for the peak $[NdO]^+$ or $[Nd+5+O]^+$ fragment.³⁹⁹ Typically fragments of the $[Ln]^+$ or $[LnO]^+$ mass are found in mass spectra of free lanthanide ions which could indicate the presence of Nd^{3+} , although with a greater possibility of this being uncoordinated.³⁹⁹ Finally the band at 83.12 m/z could be indicative of the presence of the $[ClO_3]^-$ fragment, possibly indicating the presence of perchlorate, either coordinated to the Nd^{3+} ion or to any complex formed. The band at 99 m/z for the $[ClO_4]^-$ ion was not observed. The other bands could not be assigned with any certainty.

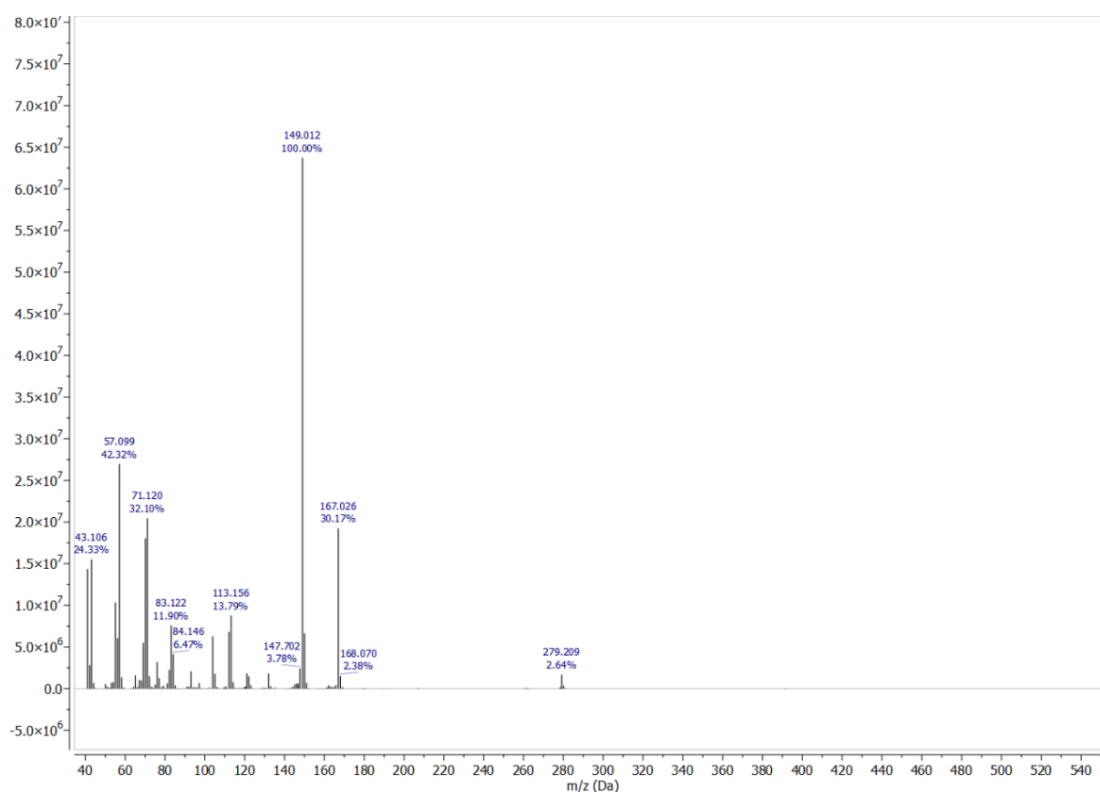


Figure 4.129: Mass spectra of the $O((Et_2N)_2PO)_2+Nd(ClO_4)_3_1$ (GC peak at 12.23 minutes).

4.2.2.3.5. Analysis by Hot stage microscopy

An attempt was made to crystallise any products in $O((Et_2N)_2PO)_2+Nd(ClO_4)_3_1$ from the viscous liquid obtained, through cooling. This was attempted since crystallisation from chloroform solution by cooling and prolonged evaporation at room temperature proved futile. The liquid became visibly more viscous at around 0.0 °C. Dendritic crystallites started to form at around -40.0 °C, with growth stopping at -79.9 °C. This could be attributed to either crystallisation or to the freezing of CO_2 on the sample. Between -75.0 °C and -77.4 °C a crack formed through the sample, indicating that an amorphous solid had formed at around this temperature.

4.2.2.3.6. Analysis by Microscopy

Throughout the reaction, workup and analysis the product $O((Et_2N)_2PO)_2+Nd(ClO_4)_3_1$ remained a thick viscous liquid with a dark brown colour. A small crop of long plate like single crystals, which were clear and either colourless or very faint brown, were however obtained from remaining GC-MS sample after the $CDCl_3$

solvent was evaporated at 6 to 8 °C in a refrigerator. These were collected and micrographs taken. Although crystallinity was evident, as given in Figure 4.130, many of the crystals were observed as having no clear habit.

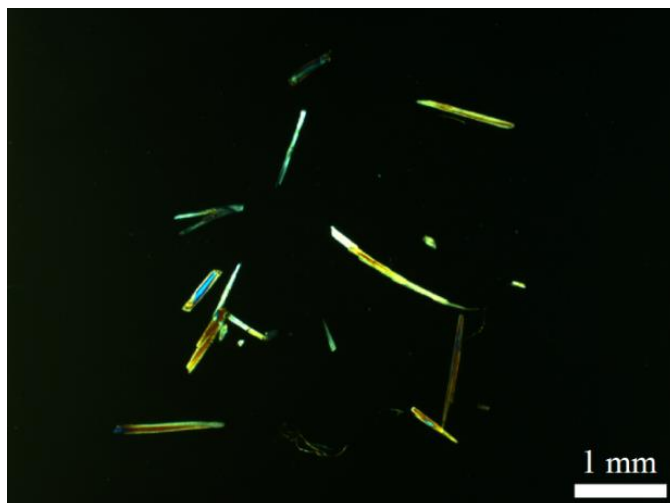


Figure 4.130: Micrograph of crystals obtained from the viscous liquid $O((Et_2N)_2PO)_2+Nd(ClO_4)_3_1$.

4.2.2.3.7. Conclusion

Following the application of various characterisation techniques on the product $O((Et_2N)_2PO)_2+Nd(ClO_4)_3_1$, the following conclusions were drawn up.

The IR spectrum indicated that the reaction and workup most likely served to purify the ligand $O((Et_2N)_2PO)_2_1$, to yield the same product obtained in $O((Et_2N)_2PO)_2_1_{f13}$. The 1H NMR spectrum indicated the presence of multiple components, including acetone and methanol from the 2,2-DMP hydration reaction. However the numerous peaks, with unclear integration value relations spanning the entire typical proton region, could also indicate the presence of the paramagnetic Nd^{3+} cation. This was further corroborated by the broadening of the two peaks in the $^{31}P\{^1H\}$ NMR spectrum of $O((Et_2N)_2PO)_2+Nd(ClO_4)_3_1$. The $^{31}P\{^1H\}$ NMR spectrum also yielded a peak at 86.34 ppm, which could indicate coordination of the ligand with Nd^{3+} . GC-MS data indicated the presence of two components in $O((Et_2N)_2PO)_2+Nd(ClO_4)_3_1$. The first was clearly identified as the ligand (purified form of $O((Et_2N)_2PO)_2_1$) and the other compound contained fragments which were not similar to those of the ligand and somewhat difficult to assign. In each case the data indicated the presence of the Nd^{3+} in the product but the coordination of the lanthanide with the ligand could not be definitively concluded. A small crop of crystals was obtained from the solution used for GC-MS.

4.2.2.4. Summary

This section addressed the characterisation of the non-carbene di- $\lambda^5\sigma^4$ -phosphorane lanthanide complexes which were synthesised as described in Section 3.3.2.2. For some complexations numerous attempts were undertaken either because the first product did not show the expected characteristics or to increase yield. Complexation of $[\text{N}(\text{Ph}_2\text{PO})_2]^-$ with Eu^{3+} was achieved under normal laboratory conditions and shown by ^1H NMR spectroscopy in solution, to yield the complex $[\text{Eu}(\text{N}(\text{Ph}_2\text{PO})_2)_3]$. However PXRD data indicated that the solid contained the side product KNO_3 as the major phase with a possible novel crystalline form of this complex as the minor phase. Complexation of $[\text{N}(\text{Ph}_2\text{PS})_2]^-$ with Eu^{3+} on the other hand proved difficult using normal laboratory conditions although complexation of $\text{HN}(\text{Ph}_2\text{PS})_2$ with Eu^{3+} through grinding yielded a novel crystalline solid. Complexation of $\text{O}((\text{Et}_2\text{N})_2\text{PO})_2$ with Nd^{3+} under moisture free conditions yielded mainly a brown viscous liquid, which was unexpected. Single crystals were formed from this liquid however the composition of this solid is unknown. Most spectroscopic data did not yield significant evidence of complexation for this Nd^{3+} complex but ^{31}P NMR clearly supported such complexation, possibly indicating a complex which could have a 3:1 ligand to metal stoichiometry.

4.3. Co-Crystallisation

Characterisation for co-crystals was undertaken using solid state sample analysis, mainly IR and Raman spectroscopy and XRD techniques. Characterisation via dissolved samples typical in chemical analysis cannot give data regarding co-crystallisation as the unique properties of co-crystals are due to the solid state structure rather than simply molecular. As described in the Section 3.3.3 co-crystallisation was mainly undergone for the complex $[\text{Sm}(\text{C}(\text{Ph}_2\text{PNSiMe}_3)_2)(\text{NCy}_2)(\text{THF})]$.

4.3.1. Characterisation of co-crystallisation products of $[\text{Sm}(\text{C}(\text{Ph}_2\text{PNSiMe}_3)_2)(\text{NCy}_2)(\text{THF})] \cdot 0.5(\text{C}_6\text{H}_5\text{CH}_3)$

In co-crystallisation the objective is typically to introduce two or more components into a singular crystal structure. This is undertaken as the resultant product usually has different physical characteristics from the separate components and in this study the increased stability of lanthanide carbene complexes is being investigated. Normally, and as is the case in the discussion hereunder, co-crystallisation deals with molecular species which are typically bound together using intermolecular interactions in defined synthons.

In this study co-crystallisation was attempted and undertaken as described in Section 3.3.3.1, by grinding the $[\text{Sm}(\text{C}(\text{Ph}_2\text{PNSiMe}_3)_2)(\text{NCy}_2)(\text{THF})]_3$ and $[\text{Sm}(\text{C}(\text{Ph}_2\text{PNSiMe}_3)_2)(\text{NCy}_2)(\text{THF})]_4$ products and a co-former in a 1:1 molar ratio. Three co-formers were used in this study, namely biphenyl, 4,4'-bipyridine and 4,4'-oxydianiline. As described in Section 3.3.3.1 these were selected to maximise the number of available intermolecular bonds. Analysis of the co-crystallisation products of $[\text{Sm}(\text{C}(\text{Ph}_2\text{PNSiMe}_3)_2)(\text{NCy}_2)(\text{THF})]_3$ by IR spectroscopy, as shown in Figure 4.131, indicated that there was likely full decomposition or loss of the inorganic co-former. This was indicated by the loss of most bands distinctive of $[\text{Sm}(\text{C}(\text{Ph}_2\text{PNSiMe}_3)_2)(\text{NCy}_2)(\text{THF})]_3$ and the appearance of only four major bands at around 1260 cm^{-1} , 1103 cm^{-1} , 1018 cm^{-1} and 800 cm^{-1} which were undiagnostic of any species expected in the mixture. Therefore these products will not be discussed further.

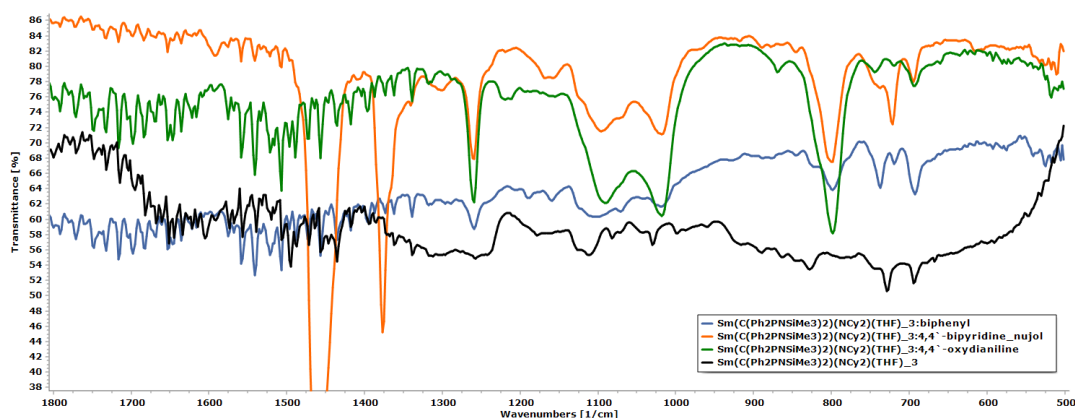


Figure 4.131: IR spectra of $[\text{Sm}(\text{C}(\text{Ph}_2\text{PNSiMe}_3)_2)(\text{NCy}_2)(\text{THF})]_3$:biphenyl (blue), $[\text{Sm}(\text{C}(\text{Ph}_2\text{PNSiMe}_3)_2)(\text{NCy}_2)(\text{THF})]_3$:4,4'-bipyridine in nujol (orange), $[\text{Sm}(\text{C}(\text{Ph}_2\text{PNSiMe}_3)_2)(\text{NCy}_2)(\text{THF})]_3$:4,4'-oxydianiline (green) and $[\text{Sm}(\text{C}(\text{Ph}_2\text{PNSiMe}_3)_2)(\text{NCy}_2)(\text{THF})]_3$ (black).

4.3.1.1. Analysis by Infra-red spectroscopy

Unlike the IR spectra for the co-crystal products for the solid $[\text{Sm}(\text{C}(\text{Ph}_2\text{PNSiMe}_3)_2)(\text{NCy}_2)(\text{THF})]_3$ the IR spectra for the co-crystal products for the solid $[\text{Sm}(\text{C}(\text{Ph}_2\text{PNSiMe}_3)_2)(\text{NCy}_2)(\text{THF})]_4$ were dissimilar to each other, as shown in Figure 4.132 and are best discussed separately. In each case bands from both the solid $[\text{Sm}(\text{C}(\text{Ph}_2\text{PNSiMe}_3)_2)(\text{NCy}_2)(\text{THF})]_4$ and from the respective co-formers were noticeable.

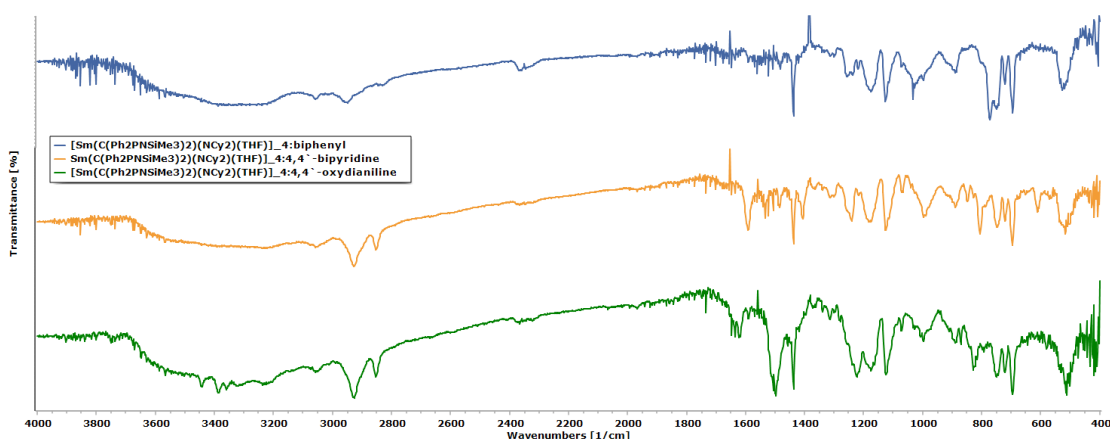


Figure 4.132: IR spectra of $[\text{Sm}(\text{C}(\text{Ph}_2\text{PNSiMe}_3)_2)(\text{NCy}_2)(\text{THF})]_4$:biphenyl (blue), $[\text{Sm}(\text{C}(\text{Ph}_2\text{PNSiMe}_3)_2)(\text{NCy}_2)(\text{THF})]_4$:4,4'-bipyridine (orange) and $[\text{Sm}(\text{C}(\text{Ph}_2\text{PNSiMe}_3)_2)(\text{NCy}_2)(\text{THF})]_4$:4,4'-oxydianiline (green).

The IR spectrum of the first co-crystal product $[\text{Sm}(\text{C}(\text{Ph}_2\text{PNSiMe}_3)_2)(\text{NCy}_2)(\text{THF})]_4$:biphenyl was initially compared to both the IR spectra of $[\text{Sm}(\text{C}(\text{Ph}_2\text{PNSiMe}_3)_2)(\text{NCy}_2)(\text{THF})]_4$ and the co-former biphenyl, as shown in Figure 4.133. The first noticeable difference was the loss of a number of bands found in the spectrum of the $[\text{Sm}(\text{C}(\text{Ph}_2\text{PNSiMe}_3)_2)(\text{NCy}_2)(\text{THF})]_4$ product. The bands attributed to the trimethylsilyl δ C–H vibrations at 1253 cm^{-1} and 1240 cm^{-1} diminished to reveal bands at 1256 cm^{-1} and 1238 cm^{-1} , while the bands possibly attributed to the ρ $\text{CH}_3 + \nu$ Si–C vibrations at 847 cm^{-1} and 828 cm^{-1} were completely lost. This was complementary to the loss of the bands at 997 cm^{-1} , 920 cm^{-1} and 788 cm^{-1} , as the former band was assigned to the ν $\text{P}^+ - \text{CH}^- - \text{P}^+$ vibration while the latter band was tentatively assigned to a unique P–Ph vibration, both typical of the $[\text{HC}(\text{Ph}_2\text{PNSiMe}_3)_2]^-$ species. The band at 920 cm^{-1} was initially assigned to the ν P–N vibrations for the decomposition by-product $\text{Ph}_2\text{P}(\text{O})\text{NH}_2$. The loss of this band indicated that this could also be due to the

ν $P^+-CH^--P^+$ vibration for the $[HC(Ph_2PNSiMe_3)_2]^-$ species, while the band at 890 cm^{-1} previously assigned to this vibration could be due to the ν $P-N$ vibration for $Ph_2P(O)NH_2$. The discrimination between these two bands was not possible prior in Section 4.1.3.1.1. since the analogous band for $Ph_2P(O)NH_2$ in this region was very strong encompassing a range of wavenumbers.

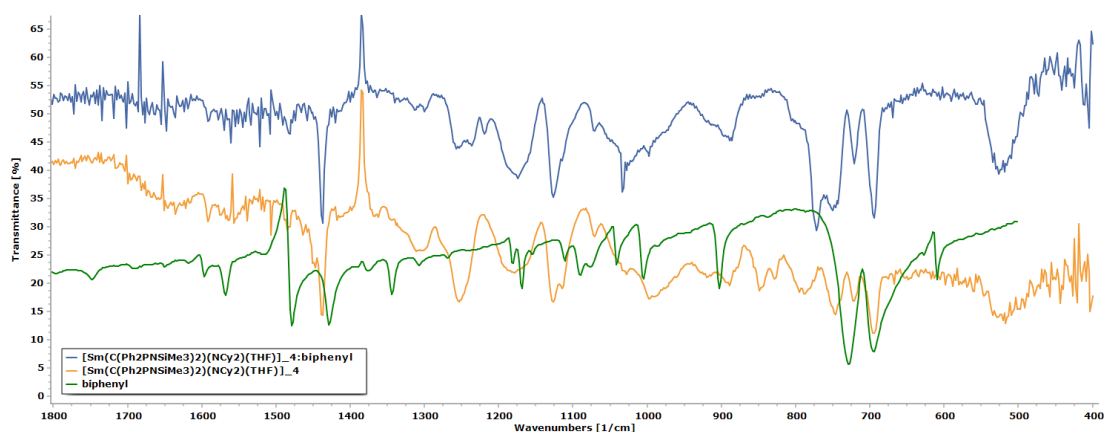


Figure 4.133: IR spectra of $[Sm(C(Ph_2PNSiMe_3)_2)(NCy_2)(THF)]_4$:biphenyl (blue), $[Sm(C(Ph_2PNSiMe_3)_2)(NCy_2)(THF)]_4$ (orange) and biphenyl (green) in the region $1800\text{-}400\text{ cm}^{-1}$.

The remaining major bands in the spectrum of the co-crystal product were observed to be analogous to other bands observed in the IR spectrum of the $[Sm(C(Ph_2PNSiMe_3)_2)(NCy_2)(THF)]_4$ product. These were observed at 1173 cm^{-1} , 1127 cm^{-1} , 1113 cm^{-1} and 887 cm^{-1} which were analogous to the $[Sm(C(Ph_2PNSiMe_3)_2)(NCy_2)(THF)]_4$ bands at 1180 cm^{-1} , 1127 cm^{-1} , 1115 cm^{-1} and 890 cm^{-1} . These bands could be due to multiple vibrational modes for the $[HC(Ph_2PNSiMe_3)_2]^-$ species, however all these bands could also be due to vibrations known for $Ph_2P(O)NH_2$. This indicated that both $Ph_2P(O)NH_2$ and $[HC(Ph_2PNSiMe_3)_2]^-$ were present in $[Sm(C(Ph_2PNSiMe_3)_2)(NCy_2)(THF)]_4$ and/or that some decomposition occurred during the co-crystallisation procedure. This co-crystallisation attempt, unlike the other two $[Sm(C(Ph_2PNSiMe_3)_2)(NCy_2)(THF)]_4$ co-crystallisation attempts, formed a yellow paste on grinding. This could be due to different processes. The first possible process could be the melting of the biphenyl which has a low melting point of $69.2\text{ }^\circ\text{C}$. The second possibility could be the formation of $HN(SiMe_3)_2$, which is a volatile liquid by-product of the decomposition of $H_2C(Ph_2PNSiMe_3)_2$, as described in Section 4.1.3.1.4. The former should not affect the inorganic co-former while the latter could be supported by the IR data. If the latter was the case this would be expected in all the

co-crystallisation attempts. However, this was not visible in the IR data of the other two co-crystallisation products. Therefore, if this was the case the biphenyl could have aided this decomposition of the original complex through an unknown process.

Bands typical of the biphenyl co-former were not observed in the spectrum, which was unexpected. Bands in the range 1500–1400 cm^{-1} , due to the presence of phenyl ν C=C vibrations are typical of all three compounds expected to be present in the product but the bands expected for the biphenyl were not observed. The only two bands of diagnostic interest in this spectrum were the band at 1238 cm^{-1} and the strong band at 772 cm^{-1} . The band at 1238 cm^{-1} which was described prior could be due to retained trimethylsilyl containing species. However, it had no distinct relation to the bands in this region of the organic co-former or the two main components of $[\text{Sm}(\text{C}(\text{Ph}_2\text{PNSiMe}_3)_2)(\text{NCy}_2)(\text{THF})]_4$. The band at 772 cm^{-1} did not have a strict analogue in either the spectrum of $[\text{Sm}(\text{C}(\text{Ph}_2\text{PNSiMe}_3)_2)(\text{NCy}_2)(\text{THF})]_4$ or $\text{Ph}_2\text{P}(\text{O})\text{NH}_2$, which is interesting. This band was in a region typical for both ν P–N and ν P–O–C(aliphatic) vibrations. Therefore, this band could be indicative of the formation of a compound containing these groups. The ν P–N vibration was more likely, but this would not be the expected vibration for $\text{Ph}_2\text{P}(\text{O})\text{NH}_2$ and therefore was more likely due to some other species possibly obtained from the $[\text{HC}(\text{Ph}_2\text{PNSiMe}_3)_2]^-$ species on grinding. The band at 1027 cm^{-1} was still visible indicating that the coordinated THF, possibly in a $\text{Sm}(\text{NCy}_2)(\text{THF})$ moiety, was still present. This could indicate that although decomposition of the main ligand may have occurred a samarium species was still present.

The IR data for $[\text{Sm}(\text{C}(\text{Ph}_2\text{PNSiMe}_3)_2)(\text{NCy}_2)(\text{THF})]_4:4,4'$ -bipyridine yielded more favourable results than that for $[\text{Sm}(\text{C}(\text{Ph}_2\text{PNSiMe}_3)_2)(\text{NCy}_2)(\text{THF})]_4$:biphenyl. The spectrum of this co-crystallisation product is given in Figure 4.134, along with the spectra for $[\text{Sm}(\text{C}(\text{Ph}_2\text{PNSiMe}_3)_2)(\text{NCy}_2)(\text{THF})]_4$ and 4,4'-bipyridine. It was immediately observed that although some changes occurred for the bands typical of the trimethylsilyl and the ν P⁺–CH–P⁺ vibrations of the inorganic co-former, most of the bands observed for $[\text{Sm}(\text{C}(\text{Ph}_2\text{PNSiMe}_3)_2)(\text{NCy}_2)(\text{THF})]_4$ were still present. This indicated that although some decomposition may have occurred it was not to the same extent as that for $[\text{Sm}(\text{C}(\text{Ph}_2\text{PNSiMe}_3)_2)(\text{NCy}_2)(\text{THF})]_4$:biphenyl.

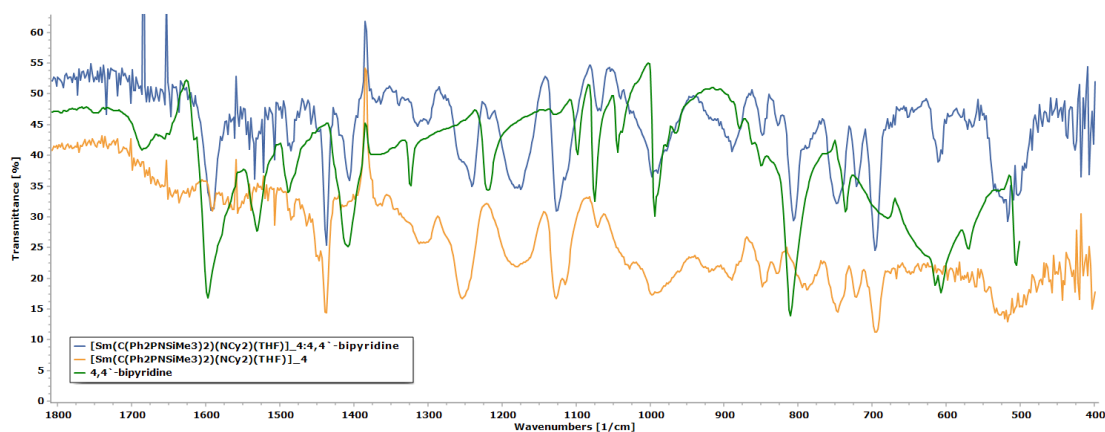


Figure 4.134: IR spectra of $[\text{Sm}(\text{C}(\text{Ph}_2\text{PNSiMe}_3)_2)(\text{NCy}_2)(\text{THF})]_4:4,4'$ -bipyridine (blue), $[\text{Sm}(\text{C}(\text{Ph}_2\text{PNSiMe}_3)_2)(\text{NCy}_2)(\text{THF})]_4$ (orange) and 4,4'-bipyridine (green) in the region 1800-400 cm^{-1} .

The bands typical of the trimethylsilyl moiety, namely 1253 cm^{-1} , 1240 cm^{-1} , 847 cm^{-1} and 828 cm^{-1} and the bands typical of the $\nu \text{P}^+-\text{CH}^--\text{P}^+$ vibration namely 998 cm^{-1} , 920 cm^{-1} , 890 cm^{-1} , 847 cm^{-1} and 828 cm^{-1} , with their clear overlap, were still visible in the IR spectrum of the co-crystal product. All of these bands indicated that the $[\text{HC}(\text{Ph}_2\text{PNSiMe}_3)_2]^-$ group was still present. Changes were only observed in the diminished intensity of the band at 1253 cm^{-1} , especially in relation to the band at 1240 cm^{-1} . The latter had a greater relative intensity in the co-crystal IR spectrum when compared to its intensity in the spectrum of $[\text{Sm}(\text{C}(\text{Ph}_2\text{PNSiMe}_3)_2)(\text{NCy}_2)(\text{THF})]_4$.

Bands typical of the co-former 4,4'-bipyridine were also clearly visible. The visible bands were mainly the strongest intensity analogous bands for the organic co-former in the spectrum of the co-crystallisation product namely at 1592 cm^{-1} , 1532 cm^{-1} , 1486 cm^{-1} , 1406 cm^{-1} , 1217 cm^{-1} , 1069 cm^{-1} , 994 cm^{-1} , 806 cm^{-1} and 610 cm^{-1} . The main changes from the analogous bands in the 4,4'-bipyridine spectrum to those listed for the co-crystallisation product were a decrease in the intensity for the band at 1217 cm^{-1} and the overlap of the band at 994 cm^{-1} with the $[\text{Sm}(\text{C}(\text{Ph}_2\text{PNSiMe}_3)_2)(\text{NCy}_2)(\text{THF})]_4$ band at 998 cm^{-1} . All the bands in the range 1217–610 cm^{-1} can be attributed to aromatic C–H vibrations and therefore specific changes were not expected on co-crystallisation unless strong C–H $\cdots \pi$ interactions were formed, which are rarely given in IR data.⁴⁰⁰ This was in fact the case as very little change was observed in the $[\text{Sm}(\text{C}(\text{Ph}_2\text{PNSiMe}_3)_2)(\text{NCy}_2)(\text{THF})]_4:4,4'$ -bipyridine IR data for these bands on comparison with the IR spectrum of the 4,4'-bipyridine. Changes on co-crystallisation of bands attributed to the 4,4'-bipyridine would be expected for the bands in the range 1592–1409 cm^{-1} , which related to the $\nu \text{C}=\text{C}$ and $\nu \text{C}=\text{N}$ vibrations of

the co-former. Any X–H --- Ph, Ph(π) --- Ph(π) and N --- H–A, interactions with 4,4'-bipyridine should show changes in the bands in this range, as is also typical for complexation with 4,4'-bipyridine. On complexation with 4,4'-bipyridine bands in this region typically experience an increase in wavenumber indicating increased bond stiffness.^{400,401} Unexpectedly the bands in the co-crystals showed a slight decrease in wavenumber (approximately 0 to -5 cm⁻¹) from the wavenumber of the analogous bands in the spectrum of 4,4'-bipyridine. π --- π and π --- Mⁿ⁺ interactions may cause this decrease in wavenumber. However, any interaction with the pyridine nitrogen (N --- H–A or π --- N(Pyridine)) should have caused an increase in wavenumber.

Therefore it was concluded that the solid obtained was most likely a mixture between the solid [Sm(C(Ph₂PNSiMe₃)₂)(NCy₂)(THF)]₄ and the co-former 4,4'-bipyridine. No major shifts were observed for the bands analogous to those in the spectra of both co-formers, indicating a lack of intermolecular interactions. Some changes were observed for the bands in the region of 1592–1409 cm⁻¹ but the slight decrease in wavenumbers could not definitively prove the presence of new intermolecular interactions.

The IR spectrum of [Sm(C(Ph₂PNSiMe₃)₂)(NCy₂)(THF)]₄:4,4'-oxydianiline is given in Figure 4.135, along with the IR spectra of [Sm(C(Ph₂PNSiMe₃)₂)(NCy₂)(THF)]₄ and 4,4'-oxydianiline. On initial comparison similar changes were observed for the IR spectrum of [Sm(C(Ph₂PNSiMe₃)₂)(NCy₂)(THF)]₄:4,4'-oxydianiline as were observed for the spectrum of [Sm(C(Ph₂PNSiMe₃)₂)(NCy₂)(THF)]₄:biphenyl, indicating some level of [HC(Ph₂PNSiMe₃)₂]⁻ decomposition.

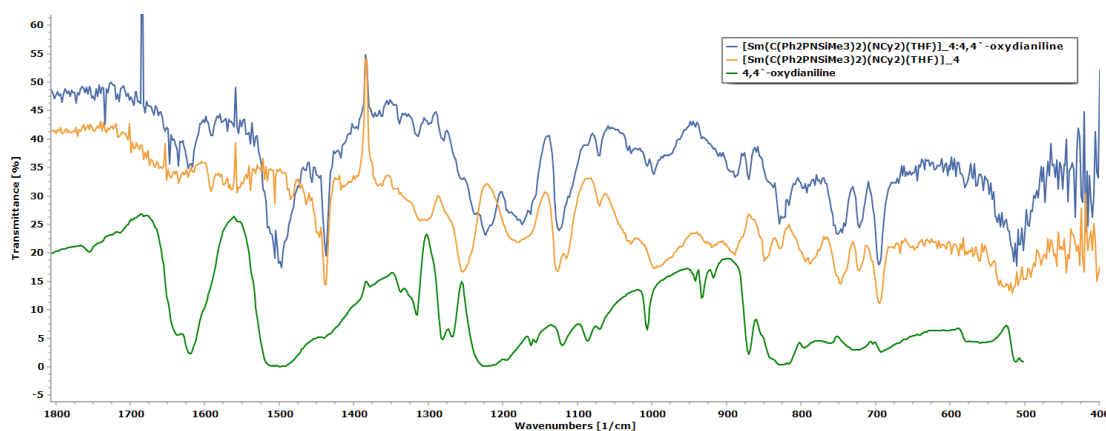


Figure 4.135: IR spectra of [Sm(C(Ph₂PNSiMe₃)₂)(NCy₂)(THF)]₄:4,4'-oxydianiline (blue), [Sm(C(Ph₂PNSiMe₃)₂)(NCy₂)(THF)]₄ (orange) and 4,4'-oxydianiline (green) in the region 1800-400 cm⁻¹.

The δ C–H trimethylsilyl bands at 1253 cm^{-1} and 1240 cm^{-1} were lost, giving a shoulder at 1255 cm^{-1} . The intensity of this shoulder was drastically diminished from that of the analogous bands in the spectrum of $[\text{Sm}(\text{C}(\text{Ph}_2\text{PNSiMe}_3)_2)(\text{NCy}_2)(\text{THF})]_4$ but the extent of the band loss was effected by significant overlap with the strong band at 1222 cm^{-1} in the spectrum of the co-crystal. Again the two bands in the spectrum of $[\text{Sm}(\text{C}(\text{Ph}_2\text{PNSiMe}_3)_2)(\text{NCy}_2)(\text{THF})]_4$ at 847 cm^{-1} and 828 cm^{-1} were overlapped with the stronger co-crystal band at 826 cm^{-1} , analogous to the band at 829 cm^{-1} for the organic co-former. This left a single shoulder at 843 cm^{-1} , which could be analogous to the band in the spectrum of the complex at 847 cm^{-1} and so the loss of these bands by chemical processes could not be concluded definitively. Therefore, although some decomposition was suspected this overlap with strong co-former bands made this analysis difficult.

The diminished intensity of the $[\text{Sm}(\text{C}(\text{Ph}_2\text{PNSiMe}_3)_2)(\text{NCy}_2)(\text{THF})]_4$ bands at 997 cm^{-1} and 920 cm^{-1} , previously assigned to the $[\text{HC}(\text{Ph}_2\text{PNSiMe}_3)_2]^-$ species ν $\text{P}^+\text{--CH}^-\text{--P}^+$ vibrations, further attested to some possible decomposition. This decomposition was also supported by the loss of the P–Ph band at 787 cm^{-1} . However, the remaining strong band at 998 cm^{-1} in the spectrum of the co-crystal product indicated the presence of the $[\text{HC}(\text{Ph}_2\text{PNSiMe}_3)_2]^-$ species, as the organic co-former band that could overlap in this region was visible as a sharp and distinct band at 1007 cm^{-1} , which was unchanged from the analogous band in the 4,4'-oxydianiline IR spectrum. Therefore, although some decomposition was likely the $[\text{HC}(\text{Ph}_2\text{PNSiMe}_3)_2]^-$ species was still the major component.

Numerous strong bands analogous to the bands observed for the IR spectrum of the 4,4'-oxydianiline co-former were visible in the spectrum of the co-crystallisation product. The sharp bands at 3444 cm^{-1} , 3387 cm^{-1} and 3359 cm^{-1} observed in the spectrum of the co-former were also visible with no changes in the IR spectrum of $[\text{Sm}(\text{C}(\text{Ph}_2\text{PNSiMe}_3)_2)(\text{NCy}_2)(\text{THF})]_4$:4,4'-oxydianiline. This indicated that the amine moiety of 4,4'-oxydianiline was left unaffected by the grinding procedure. The same was true for the bands at 1639 cm^{-1} and 1500 cm^{-1} assigned to the organic co-former δ N–H vibrations. This indicated that the 4,4'-oxydianiline did not form new N–H \cdots B and N \cdots H–A intermolecular interactions during the grinding procedure and that no protonation or deprotonation occurred in the organic co-former. This was supported by the fact that other changes expected along with the protonation or deprotonation of the 4,4'-oxydianiline amines groups, such as the reformation of the $\text{H}_2\text{C}(\text{Ph}_2\text{PNSiMe}_3)_2$

species or the formation of hydration decomposition products of this ligand, were not observed in the IR data.

The previously discussed band at 1222 cm^{-1} was analogous to the band at 1225 cm^{-1} of the organic co-former, attributed to the $\nu\text{ C-O-C}$ vibration of this compound.⁴⁰² The minor difference between the wavenumbers of these two analogous bands indicated that the ether oxygen of the 4,4'-oxydianiline did not form any intermolecular interactions. Therefore, the possible O --- H-A intermolecular interactions posited in Section 3.3.3.1, were unlikely to be present in the co-crystallisation product. The same was true for the co-crystal bands at 871 cm^{-1} and 826 cm^{-1} which were likely due to skeletal vibration bands of the organic co-former, analogous to the co-former bands at 870 cm^{-1} and 826 cm^{-1} .

The loss of the 4,4'-oxydianiline bands at 1282 cm^{-1} and 1268 cm^{-1} , attributed to the $\nu\text{ C-N}$ vibrations, was observed to be the main difference between the IR data of 4,4'-oxydianiline and $[\text{Sm}(\text{C}(\text{Ph}_2\text{PNSiMe}_3)_2)(\text{NCy}_2)(\text{THF})]_4:4,4'$ -oxydianiline. Given the intensity of these bands in the spectrum of the organic co-former it was unlikely that they would be lost in the co-crystal IR spectrum through overlap with the stronger band at 1222 cm^{-1} and the trimethylsilyl bands at 1253 cm^{-1} and 1240 cm^{-1} for $[\text{Sm}(\text{C}(\text{Ph}_2\text{PNSiMe}_3)_2)(\text{NCy}_2)(\text{THF})]_4$. Therefore, it was possible that the C-N bonds in the 4,4'-oxydianiline could have been effected by the co-crystallisation procedure. Unfortunately, no analogous shifted bands in the IR spectrum of the product were observed and therefore any correlation between this difference and any chemical and structural changes could not be described. The lack of these bands could indicate a shift overlapping with the strong band at 1222 cm^{-1} but this would indicate a decrease in bond stiffness of the C-N bond. Such a change in this bond should have been accompanied with other changes in the bands due to 4,4'-oxydianiline which were not manifested in the spectrum of the co-crystallisation product. Therefore, the remaining IR data could not provide information as to why any changes in the $\nu\text{ C-N}$ vibration may have occurred. Furthermore, it could not provide information on the importance of this difference in determining any structural changes in 4,4'-oxydianiline between the co-former and the co-crystallisation product.

4.3.1.2. Analysis by Powder X-ray diffraction

In all cases the co-crystal PXRD data was collected using Mo- $K_{\alpha 1}$ radiation to avoid absorption problems due to the expected presence of Sm^{3+} . PXRD data, using Cu- $K_{\alpha 1}$ radiation, was also collected for the organic co-formers biphenyl, 4,4'-bipyridine and 4,4'-oxydianiline, to verify their composition and the crystal structure present. The biphenyl proved to be the polymorph typically described in literature for this compound.^{403,404} The 4,4'-bipyridine proved to be the anhydrous polymorph previously described by Candana and co-workers in 1999.⁴⁰⁵ The 4,4'-oxydianiline used proved to be the same polymorph described by Chetkina and co-workers in 1991.^{406,407} Comparison of the respective experimental and calculated powder patterns of these co-formers is given in Appendix 16. In order to compare the co-former and co-crystal powder patterns the powder patterns calculated from literature data of the respective co-former phases, calculated assuming a Mo- $K_{\alpha 1}$ source, are used in this section.

Samples for all three co-crystallisations attempted were prepared for analysis by PXRD, using 0.5 mm capillaries for all three. In each case the capillaries were prepared under inert condition in a nitrogen filled glovebox. PXRD data was collected using Mo- $K_{\alpha 1}$ radiation for samples of $[\text{Sm}(\text{C}(\text{Ph}_2\text{PNSiMe}_3)_2)(\text{NCy}_2)(\text{THF})]_4$:biphenyl, $[\text{Sm}(\text{C}(\text{Ph}_2\text{PNSiMe}_3)_2)(\text{NCy}_2)(\text{THF})]_4$:4,4'-bipyridine and $[\text{Sm}(\text{C}(\text{Ph}_2\text{PNSiMe}_3)_2)(\text{NCy}_2)(\text{THF})]_4$:4,4'-oxydianiline.

On initial inspection all solids contained a major amorphous phase and while the former contained little crystalline peaks the latter two showed significant minor crystalline phases. Given that the starting inorganic co-former common to each co-crystallisation product was also amorphous and contained minor crystalline phases composed of the decomposition products $\text{Ph}_2\text{P}(\text{O})\text{NH}_2$ in $P2_12_12_1$ and possibly $[\text{N}(\text{Ph}_2\text{PCH}_3)(\text{Ph}_2\text{PNH}_2)][\text{Br}] \cdot \text{Ph}_2\text{P}(\text{O})\text{NH}_2$ or a similar iso-structural compound, the powder patterns of the co-crystals were compared to that of $[\text{Sm}(\text{C}(\text{Ph}_2\text{PNSiMe}_3)_2)(\text{NCy}_2)(\text{THF})]_4$ as given in Figures 4.136 and 4.137, for $[\text{Sm}(\text{C}(\text{Ph}_2\text{PNSiMe}_3)_2)(\text{NCy}_2)(\text{THF})]_4$:biphenyl and $[\text{Sm}(\text{C}(\text{Ph}_2\text{PNSiMe}_3)_2)(\text{NCy}_2)(\text{THF})]_4$:4,4'-bipyridine and $[\text{Sm}(\text{C}(\text{Ph}_2\text{PNSiMe}_3)_2)(\text{NCy}_2)(\text{THF})]_4$:4,4'-oxydianiline respectively.

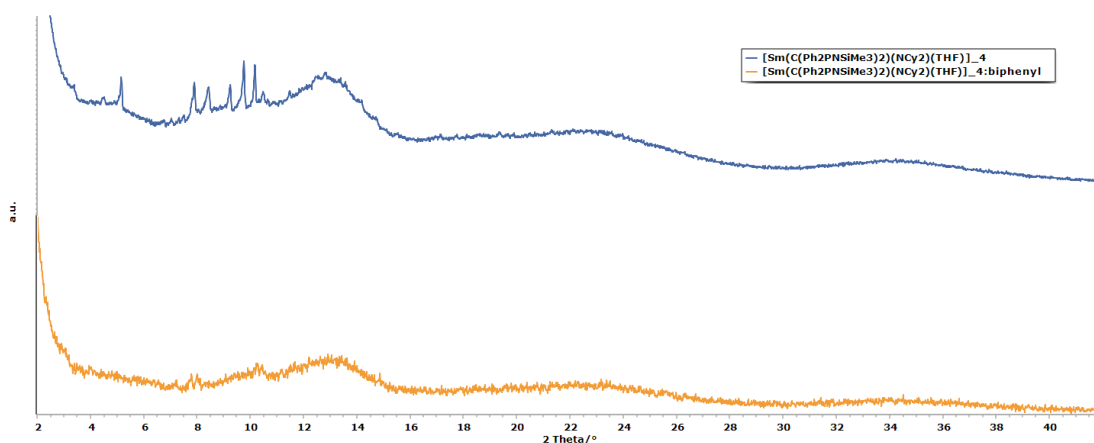


Figure 4.136: PXRD patterns of $[\text{Sm}(\text{C}(\text{Ph}_2\text{PNSiMe}_3)_2)(\text{NCy}_2)(\text{THF})]_4$ (blue) and $[\text{Sm}(\text{C}(\text{Ph}_2\text{PNSiMe}_3)_2)(\text{NCy}_2)(\text{THF})]_4$:biphenyl (orange).

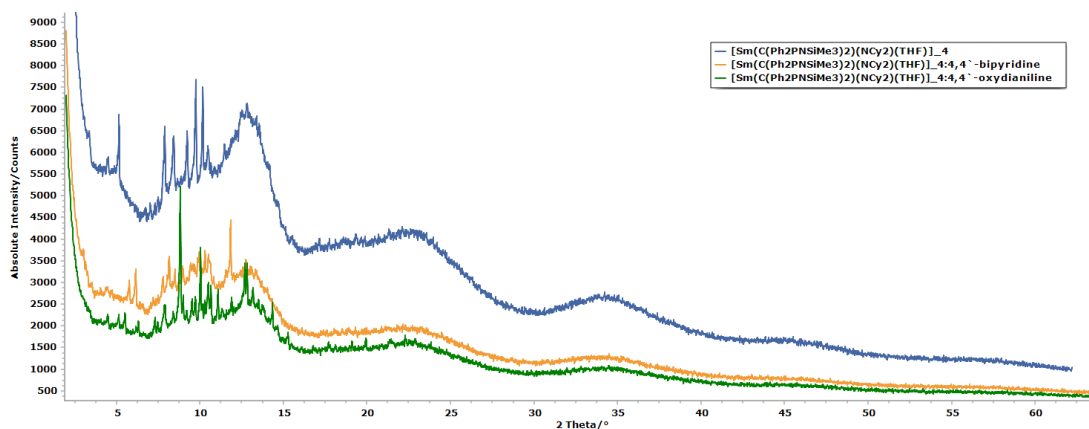


Figure 4.137: PXRD patterns of $[\text{Sm}(\text{C}(\text{Ph}_2\text{PNSiMe}_3)_2)(\text{NCy}_2)(\text{THF})]_4$ (blue), $[\text{Sm}(\text{C}(\text{Ph}_2\text{PNSiMe}_3)_2)(\text{NCy}_2)(\text{THF})]_4$:4,4'-bipyridine (orange) and $[\text{Sm}(\text{C}(\text{Ph}_2\text{PNSiMe}_3)_2)(\text{NCy}_2)(\text{THF})]_4$:4,4'-oxydianiline (green).

Initial comparison of the three co-crystallisation products' powder patterns with that of the inorganic co-former showed a very similar profile for the amorphous phase present in each. Therefore, this indicated that the amorphous phase present in the co-crystallisation products was most likely due to the same chemical component as present in $[\text{Sm}(\text{C}(\text{Ph}_2\text{PNSiMe}_3)_2)(\text{NCy}_2)(\text{THF})]_4$. However, it was clearly visible that the majority of the crystalline peaks for all patterns were unique. This indicated that the possible decomposition products in $[\text{Sm}(\text{C}(\text{Ph}_2\text{PNSiMe}_3)_2)(\text{NCy}_2)(\text{THF})]_4$ were either lost or decreased in concentration on grinding, or underwent a phase transition to an amorphous phase which could not be detected in the experimental data. Given the remaining differences detailed discussion of the co-crystallisation powder patterns is given hereunder.

The experimental powder pattern of $[\text{Sm}(\text{C}(\text{Ph}_2\text{PNSiMe}_3)_2(\text{NCy}_2)(\text{THF}))_4\text{:biphenyl}]$ was compared in Figure 4.138 to the calculated powder pattern of biphenyl used in this study, which is identified in the CSD as BIPHEN04.^{297,403,404} The calculated powder pattern was obtained using Mercury software.²⁹⁷ Only four crystalline peaks were clearly observed, namely at 7.79° , 8.02° , 10.26° and 10.44° . No peaks analogous to the peaks known for the powder pattern for the biphenyl co-former used were observed. The loss of co-former peaks was unexpected given that no new crystalline phase was formed as typical of co-crystallisation. This could indicate that the biphenyl was either lost on grinding or that it underwent a phase transition to an amorphous phase that could not be discerned from the PXRD data. Although the former was unlikely the IR data also showed a lack of bands attributable to the biphenyl indicating that the organic co-former was lost. The formation of an amorphous biphenyl could also cause changes in the IR spectrum, making the assignment of bands in the IR difficult and resulting in the apparent loss of biphenyl. During the grinding procedure a yellow paste was formed which became a powder after drying. IR data indicated that the formation of this paste could be due to the decomposition of the inorganic co-former. However, the PXRD could also indicate that the low melting point organic co-former underwent a phase transition to an amorphous phase. This paste formation could have also aided in the phase changes of other crystalline phases, such as the decomposition by-products present, to amorphous phases which would explain the increase in decomposition observed in IR and the lack of decomposition product crystalline phases observed in the PXRD pattern of $[\text{Sm}(\text{C}(\text{Ph}_2\text{PNSiMe}_3)_2(\text{NCy}_2)(\text{THF}))_4\text{:biphenyl}]$.

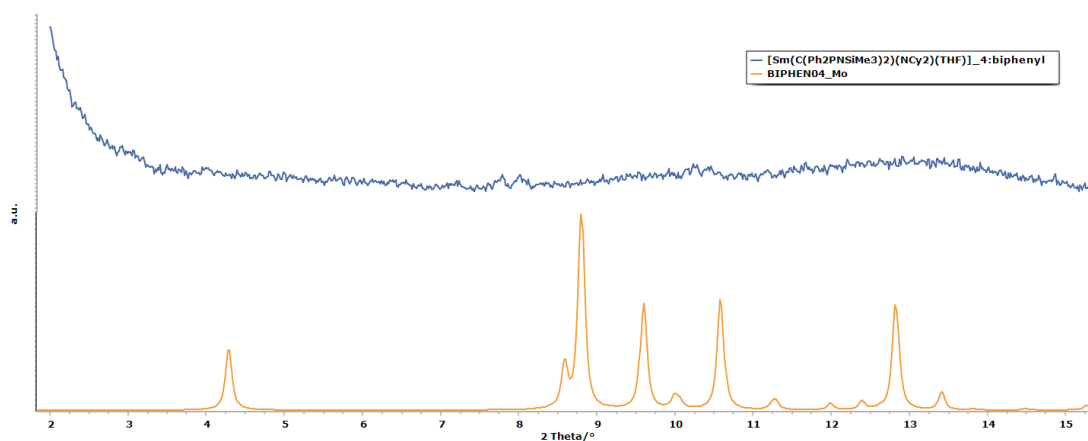


Figure 4.138: Experimental PXRD pattern of $[\text{Sm}(\text{C}(\text{Ph}_2\text{PNSiMe}_3)_2(\text{NCy}_2)(\text{THF}))_4\text{:biphenyl}]$ (blue) and calculated PXRD pattern of the biphenyl form, published in the CSD as BIPHEN04 (orange).

Of the four crystalline peaks the peak at 7.79° could be analogous to a medium intensity peak at 7.78° for the pattern of the decomposition product $\text{Ph}_2\text{P}(\text{O})\text{NH}_2$ in $P2_12_12_1$ present in $[\text{Sm}(\text{C}(\text{Ph}_2\text{PNSiMe}_3)_2)(\text{NCy}_2)(\text{THF})]_4$. This could indicate the presence of this decomposition product however this was not verified due to the lack of other peaks for this phase. The remaining crystalline peaks could not be assigned to any other known phase and the lack of further peaks meant that no further information could be obtained. The paucity of novel crystalline peaks indicated that co-crystallisation was unlikely.

The experimental powder pattern of $[\text{Sm}(\text{C}(\text{Ph}_2\text{PNSiMe}_3)_2)(\text{NCy}_2)(\text{THF})]_4:4,4'$ -bipyridine was compared with the calculated powder pattern of anhydrous $4,4'$ -bipyridine in the $P-1$ spacegroup as shown in Figure 4.139. The calculated powder pattern was obtained using Mercury software.²⁹⁷ This clearly indicated that the main crystalline phase of the product was in fact this anhydrous $4,4'$ -bipyridine. Therefore, co-crystallisation was unlikely to have occurred. This corroborated the IR data for this product in which only small changes were observed and no indication of co-crystallisation was observed. Two very minor peaks at 4.45° and 7.79° could have been analogous to peaks in the pattern of the inorganic co-former and could indicate the presence of $[\text{N}(\text{Ph}_2\text{PCH}_3)(\text{Ph}_2\text{PNH}_2)][\text{Br}] \cdot \text{Ph}_2\text{P}(\text{O})\text{NH}_2$ or a similar iso-structural compound as a very minor phase. Two small peaks at 8.05 and 9.46 could not be assigned to any expected products but no further information could be obtained from these.

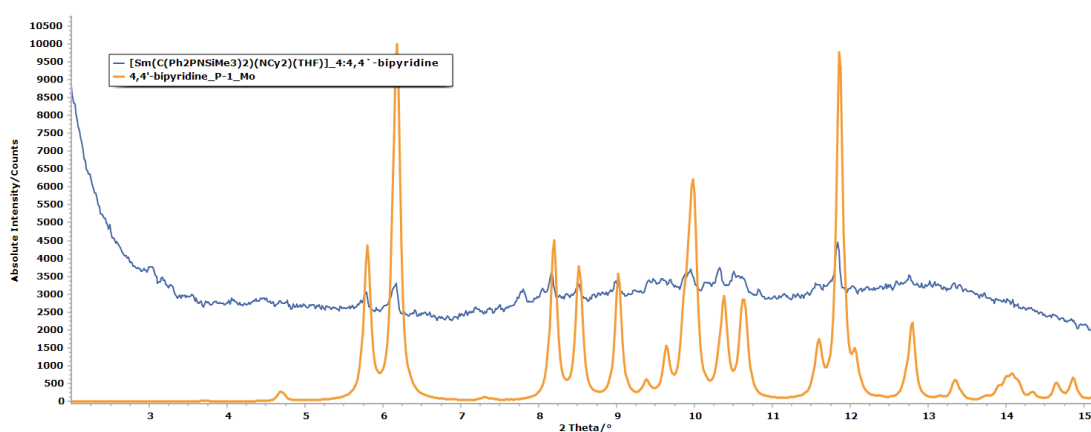


Figure 4.139: Experimental PXRD pattern of $[\text{Sm}(\text{C}(\text{Ph}_2\text{PNSiMe}_3)_2)(\text{NCy}_2)(\text{THF})]_4:4,4'$ -bipyridine (blue) and calculated PXRD pattern of $4,4'$ -bipyridine in $P-1$ unit cell (orange).

The experimental powder pattern of $[\text{Sm}(\text{C}(\text{Ph}_2\text{PNSiMe}_3)_2(\text{NCy}_2)(\text{THF}))_4:4,4\text{-oxydianiline}]$ was compared in Figure 4.140 to the calculated powder pattern of 4,4'-oxydianiline for the polymorph used in this study which is identified in the CSD as SUCVER.^{406,407} The calculated powder pattern was obtained using Mercury software.²⁹⁷ This showed that the major crystalline phase in the solid was the un-altered 4,4'-oxydianiline co-former used, as the majority of crystalline peaks for the product pattern were analogous to the strongest peaks for the pattern of the co-former. This was in line with the IR data collected which indicated that co-crystallisation was unlikely. A number of minor peaks, namely 4.5° , 5.13° , 8.42° , 9.22° and 9.73° , could not be attributed to the co-former. The peak at 8.42° could be attributed to the $\text{Ph}_2\text{P}(\text{O})\text{NH}_2$ in $P2_12_12_1$ while those at 4.5° and 9.73° could be attributed to possibly $[\text{N}(\text{Ph}_2\text{PCH}_3)(\text{Ph}_2\text{PNH}_2)][\text{Br}] \cdot \text{Ph}_2\text{P}(\text{O})\text{NH}_2$ or a similar iso-structural compound. No other peaks for these two phases could be observed so the presence of any of the decomposition products could not be confirmed. The presence of decomposition would however corroborate minor changes observed in the IR spectrum of the product. The peaks at 5.13° and 9.22° could not be assigned to any expected products but no further information could be obtained from these.

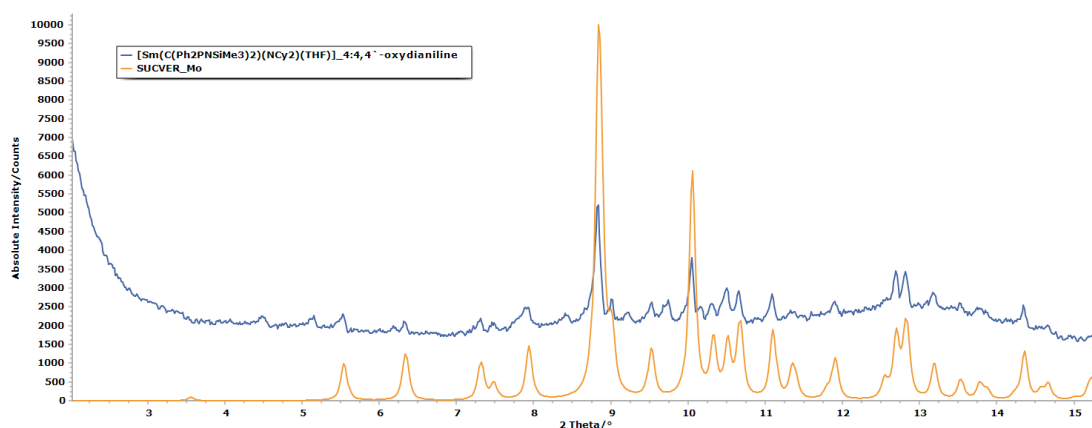


Figure 4.140: Experimental PXRD pattern of $[\text{Sm}(\text{C}(\text{Ph}_2\text{PNSiMe}_3)_2(\text{NCy}_2)(\text{THF}))_4:4,4\text{-oxydianiline}]$ (blue) and calculated PXRD pattern of the $P2_12_12_1$ polymorph of 4,4'-oxydianiline, published in the CSD as SUCVER (orange).

4.3.1.3. Analysis by Raman spectroscopy

Raman data was collected for all the organic co-formers used in this study and all three co-crystallisation products of $[\text{Sm}(\text{C}(\text{Ph}_2\text{PNSiMe}_3)_2)(\text{NCy}_2)(\text{THF})]_4$ using the samples sealed in 0.5 mm capillaries used for PXRD analysis. Data was collected using a 532 nm laser and a 500 nm grating using different exposure times. All organic co-formers yielded good Raman spectra while significant peak broadening and other interference was observed for all three $[\text{Sm}(\text{C}(\text{Ph}_2\text{PNSiMe}_3)_2)(\text{NCy}_2)(\text{THF})]_4$ containing products. This interference could be due to the low crystallinity of the samples as observed in Section 4.3.1.2. and the presence of a lanthanide which undergoes fluorescence under the conditions used. This latter feature indicated the presence of samarium (Sm^{3+}) in all three solids,⁴⁰⁸ which could not be described using the other analytical techniques used.

The best quality co-crystallisation Raman spectrum was obtained for $[\text{Sm}(\text{C}(\text{Ph}_2\text{PNSiMe}_3)_2)(\text{NCy}_2)(\text{THF})]_4$:biphenyl. This showed three broad peaks at 1598 cm^{-1} , 1318 cm^{-1} and 1171 cm^{-1} possibly analogous to the biphenyl peaks at 1614 cm^{-1} and 1597 cm^{-1} , 1283 cm^{-1} and 1008 cm^{-1} , thus indicating the presence of the biphenyl. This was in contrast to the IR and PXRD data wherein the presence of this co-former could not be confirmed. This assignment is however tentative given the quality of the data. A small sharp peak in the Raman spectrum of $[\text{Sm}(\text{C}(\text{Ph}_2\text{PNSiMe}_3)_2)(\text{NCy}_2)(\text{THF})]_4$:4,4'-bipyridine was observed at 1006 cm^{-1} indicating the presence of 4,4'-bipyridine on comparison with the Raman spectrum of this co-former. The Raman spectrum of $[\text{Sm}(\text{C}(\text{Ph}_2\text{PNSiMe}_3)_2)(\text{NCy}_2)(\text{THF})]_4$:4,4'-oxydianiline did not yield any peaks which could further characterise the product. All Raman spectra and comparisons are given in Appendix 17.

4.3.1.4. Analysis by Single crystal X-ray diffraction

Small samples of $[\text{Sm}(\text{C}(\text{Ph}_2\text{PNSiMe}_3)_2)(\text{NCy}_2)(\text{THF})]_4$:biphenyl, $[\text{Sm}(\text{C}(\text{Ph}_2\text{PNSiMe}_3)_2)(\text{NCy}_2)(\text{THF})]_4$:4,4'-bipyridine and $[\text{Sm}(\text{C}(\text{Ph}_2\text{PNSiMe}_3)_2)(\text{NCy}_2)(\text{THF})]_4$:4,4'-oxydianiline were dissolved in dry toluene to try to obtain single crystals from the co-crystallisation attempts. $[\text{Sm}(\text{C}(\text{Ph}_2\text{PNSiMe}_3)_2)(\text{NCy}_2)(\text{THF})]_4$:4,4'-oxydianiline yielded crystal microbundles

which could not be analysed by SXRD while $[\text{Sm}(\text{C}(\text{Ph}_2\text{PNSiMe}_3)_2)(\text{NCy}_2)(\text{THF})]_4$:biphenyl yielded only an amorphous precipitate and therefore no attempts at analysis were made.

$[\text{Sm}(\text{C}(\text{Ph}_2\text{PNSiMe}_3)_2)(\text{NCy}_2)(\text{THF})]_4$:4,4'-bipyridine yielded a number of small single crystals, one of which was collected for analysis. Data was collected using a STOE Stadivari diffractometer with a microfocus Mo- $K_{\alpha 1}$ source, at 293 K. Unit cell and space group determination was undertaken using X-Area and structure solution was undergone using Olex2.^{351,352} This yielded a previously uncharacterised compound $[\text{N}(\text{Ph}_2\text{PCH}_3)(\text{Ph}_2\text{PNH}_2)][\text{Cl}]\cdot\text{Ph}_2\text{P}(\text{O})\text{NH}_2$, the structure of which is given in Figure 4.141. Available crystallographic data is given in Appendix 18. This compound is iso-structural to the previously published $[\text{N}(\text{Ph}_2\text{PCH}_3)(\text{Ph}_2\text{PNH}_2)][\text{Br}]\cdot\text{Ph}_2\text{P}(\text{O})\text{NH}_2$ also given in Figure 4.141.³⁵⁹ The compound reported in literature was produced through moisture induced decomposition of $\text{H}_2\text{C}(\text{Ph}_2\text{PNSiMe}_3)_2$ on reaction with $[\text{NEt}_4]_2[\text{Re}(\text{CO})_3\text{Br}_3]$. The decomposition mechanism described by Hagenbach and co-workers is different than that described in Section 4.1.3.1.4. and as described by Aguiar and Beisler and by Schlecht and co-workers.^{295,350} This therefore indicates that two separate mechanisms of decomposition may occur in different conditions, which are difficult to distinguish due to the formation of $\text{Ph}_2\text{P}(\text{O})\text{NH}_2$ in both.

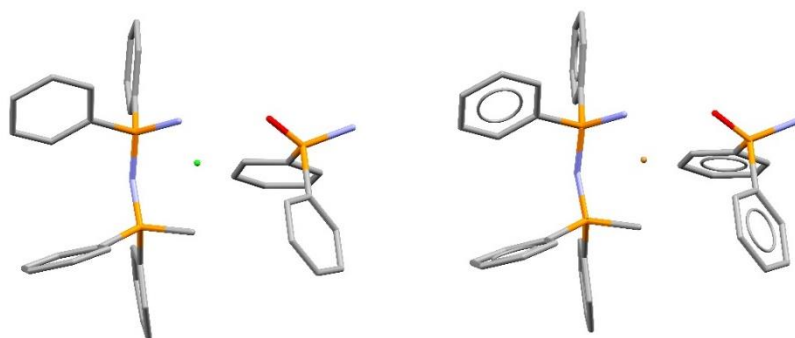


Figure 4.141: Structures of the iso-structural $[\text{N}(\text{Ph}_2\text{PCH}_3)(\text{Ph}_2\text{PNH}_2)][\text{Cl}]\cdot\text{Ph}_2\text{P}(\text{O})\text{NH}_2$ (left) and $[\text{N}(\text{Ph}_2\text{PCH}_3)(\text{Ph}_2\text{PNH}_2)][\text{Br}]\cdot\text{Ph}_2\text{P}(\text{O})\text{NH}_2$ (right).

This product was believed to be present in the inorganic co-former $[\text{Sm}(\text{C}(\text{Ph}_2\text{PNSiMe}_3)_2)(\text{NCy}_2)(\text{THF})]_4$, since as described in Section 4.1.3.1.5. a crystalline phase was observed in the PXRD pattern of $[\text{Sm}(\text{C}(\text{Ph}_2\text{PNSiMe}_3)_2)(\text{NCy}_2)(\text{THF})]_4$ which indicated the possible presence of $[\text{N}(\text{Ph}_2\text{PCH}_3)(\text{Ph}_2\text{PNH}_2)][\text{Br}]\cdot\text{Ph}_2\text{P}(\text{O})\text{NH}_2$. This was described as unlikely given the

lack of the possible presence of bromide and the lack of support from the IR data. However, given that $[\text{N}(\text{Ph}_2\text{PCH}_3)(\text{Ph}_2\text{PNH}_2)][\text{Cl}]\cdot\text{Ph}_2\text{P}(\text{O})\text{NH}_2$ and $[\text{N}(\text{Ph}_2\text{PCH}_3)(\text{Ph}_2\text{PNH}_2)][\text{Br}]\cdot\text{Ph}_2\text{P}(\text{O})\text{NH}_2$ are iso-structural it was clear that this assignment indicated the presence of $[\text{N}(\text{Ph}_2\text{PCH}_3)(\text{Ph}_2\text{PNH}_2)][\text{Cl}]\cdot\text{Ph}_2\text{P}(\text{O})\text{NH}_2$ in the inorganic co-former. Therefore, it seems likely that this decomposition product was present as a minor component of $[\text{Sm}(\text{C}(\text{Ph}_2\text{PNSiMe}_3)_2)(\text{NCy}_2)(\text{THF})]_4$ as described in Section 4.1.3.1.5. and crystallised separately from all other components in the product $[\text{Sm}(\text{C}(\text{Ph}_2\text{PNSiMe}_3)_2)(\text{NCy}_2)(\text{THF})]_4:4,4'$ -bipyridine. The PXRD data of $[\text{Sm}(\text{C}(\text{Ph}_2\text{PNSiMe}_3)_2)(\text{NCy}_2)(\text{THF})]_4:4,4'$ -bipyridine did not indicate the presence of this component showing that this compound was again a minor phase in the solid.

4.3.1.5. Conclusion

The IR spectra for all co-crystallisation products gave limited information that could be used to characterise the samples and determine co-crystallisation. In all cases for the $[\text{Sm}(\text{C}(\text{Ph}_2\text{PNSiMe}_3)_2)(\text{NCy}_2)(\text{THF})]_3$ co-crystals the IR spectra indicated complete loss of the inorganic co-former possibly through the thermal effects of the grinding procedure. These spectra proved similar and could not provide data to characterise the inorganic composition of the solids.

In all cases regarding $[\text{Sm}(\text{C}(\text{Ph}_2\text{PNSiMe}_3)_2)(\text{NCy}_2)(\text{THF})]_4$ co-crystallisation the formation of co-crystals could not be definitively determined from the IR data. Mixtures of both respective co-formers were clearly present for the products $[\text{Sm}(\text{C}(\text{Ph}_2\text{PNSiMe}_3)_2)(\text{NCy}_2)(\text{THF})]_4:4,4'$ -bipyridine and $[\text{Sm}(\text{C}(\text{Ph}_2\text{PNSiMe}_3)_2)(\text{NCy}_2)(\text{THF})]_4:4,4'$ -oxydianiline. However, in both cases some intermolecular bonding was concluded from the IR spectra. For the former the $\nu \text{C}=\text{N}$ and the $\nu \text{C}=\text{C}$ bands for the organic co-former showed slight changes which could indicate some intermolecular interactions between $4,4'$ -bipyridine and $[\text{Sm}(\text{C}(\text{Ph}_2\text{PNSiMe}_3)_2)(\text{NCy}_2)(\text{THF})]_4$. The only interesting change in the $[\text{Sm}(\text{C}(\text{Ph}_2\text{PNSiMe}_3)_2)(\text{NCy}_2)(\text{THF})]_4:4,4'$ -oxydianiline IR spectrum was that observed for the $\nu \text{C}-\text{N}$ bands of $4,4'$ -oxydianiline but given the lack of the expected analogous bands and the lack of shifts for all other organic co-former bands a proper description of this change could not be provided. The IR spectrum for $[\text{Sm}(\text{C}(\text{Ph}_2\text{PNSiMe}_3)_2)(\text{NCy}_2)(\text{THF})]_4$:biphenyl showed few biphenyl bands and therefore little information could be obtained and the formation of co-crystals was

unlikely. In all cases there seemed to be the possible decomposition of the $[\text{Sm}(\text{C}(\text{Ph}_2\text{PNSiMe}_3)_2)(\text{NCy}_2)(\text{THF})]_4$. This was concluded from changes to the intensity of bands previously assigned to the trimethylsilyl and the $\text{P}^+-\text{CH}^--\text{P}^+$ groups of $[\text{Sm}(\text{C}(\text{Ph}_2\text{PNSiMe}_3)_2)(\text{NCy}_2)(\text{THF})]_4$. The process for this decomposition was unknown and the extent of the decomposition was not the same for all the cases. The extent of decomposition was shown to increase from the co-crystal products of 4,4'-bipyridine to 4,4'-oxydianiline to biphenyl. The IR data showed a lack of conclusive evidence towards co-crystal formation with the biphenyl co-crystallisation product showing the least potential for novel intermolecular interaction formation as compared to the attempts with 4,4'-bipyridine and 4,4'-oxydianiline.

PXRD data was collected for the co-crystallisation products of $[\text{Sm}(\text{C}(\text{Ph}_2\text{PNSiMe}_3)_2)(\text{NCy}_2)(\text{THF})]_4$. In all three cases the major phase was an amorphous phase with the same profile for each product and similar to the profile obtained from the powder pattern of $[\text{Sm}(\text{C}(\text{Ph}_2\text{PNSiMe}_3)_2)(\text{NCy}_2)(\text{THF})]_4$. This indicated that the main phase remained the same major component as described for the inorganic co-former. Minor crystalline phases were observed for each of the three co-crystallisation attempts to varying degrees. The data for $[\text{Sm}(\text{C}(\text{Ph}_2\text{PNSiMe}_3)_2)(\text{NCy}_2)(\text{THF})]_4$:4,4'-bipyridine and $[\text{Sm}(\text{C}(\text{Ph}_2\text{PNSiMe}_3)_2)(\text{NCy}_2)(\text{THF})]_4$:4,4'-oxydianiline showed that the organic co-formers were present as the major crystalline phase, indicating that co-crystallisation was unlikely. Data for $[\text{Sm}(\text{C}(\text{Ph}_2\text{PNSiMe}_3)_2)(\text{NCy}_2)(\text{THF})]_4$:biphenyl did not indicate the presence of the co-former or co-crystal formation, which was unexpected, but this was inline with the IR data for the same product. In all cases peaks relating to the decomposition products were observed. However, the intensity of respective peaks was diminished in all co-crystallisation patterns when compared to analogous peaks in the pattern of $[\text{Sm}(\text{C}(\text{Ph}_2\text{PNSiMe}_3)_2)(\text{NCy}_2)(\text{THF})]_4$. This could be due to the grinding procedure.

Raman data for the co-crystallisation attempts of $[\text{Sm}(\text{C}(\text{Ph}_2\text{PNSiMe}_3)_2)(\text{NCy}_2)(\text{THF})]_4$ confirmed the presence of samarium in the solids. However no further structural data could be obtained from these spectra. SXRD could only be undertaken for a single crystal from the $[\text{Sm}(\text{C}(\text{Ph}_2\text{PNSiMe}_3)_2)(\text{NCy}_2)(\text{THF})]_4$:4,4'-bipyridine crystallisation and this showed the presence of the decomposition product $[\text{N}(\text{Ph}_2\text{PCH}_3)(\text{Ph}_2\text{PNH}_2)][\text{Cl}]\cdot\text{Ph}_2\text{P}(\text{O})\text{NH}_2$ believed to be present from the inorganic co-former.

4.3.2. Summary

Stabilisation attempts for the lanthanide carbene complex $[\text{Sm}(\text{C}(\text{Ph}_2\text{PNSiMe}_3)_2)(\text{NCy}_2)(\text{THF})]$ or a methanide samarium complex of $[\text{HC}(\text{Ph}_2\text{PNSiMe}_3)_2]^-$ were undergone through co-crystallisation as described in Section 3.3.3.1. Only $[\text{Sm}(\text{C}(\text{Ph}_2\text{PNSiMe}_3)_2)(\text{NCy}_2)(\text{THF})]_4$ gave products which could be characterised properly. The IR data for $[\text{Sm}(\text{C}(\text{Ph}_2\text{PNSiMe}_3)_2)(\text{NCy}_2)(\text{THF})]_4$ co-crystal products showed the likely formation of mixtures with the organic co-formers used. The 4,4'-bipyridine and 4,4'-oxydianiline co-crystal products may have formed some novel intermolecular interactions but the data available could not provide a clear conclusion. In all three cases some decomposition of the inorganic co-former was observed. This was most evident for the product of the co-crystallisation with biphenyl while for the other two products decomposition was low.

PXRD data for the $[\text{Sm}(\text{C}(\text{Ph}_2\text{PNSiMe}_3)_2)(\text{NCy}_2)(\text{THF})]_4$ co-crystallisation products did not yield enough data for complete unit cell and structure determination. In all cases the major phase was an amorphous phase which was common to all three products of $[\text{Sm}(\text{C}(\text{Ph}_2\text{PNSiMe}_3)_2)(\text{NCy}_2)(\text{THF})]_4$. This indicated that it was due to the inorganic co-formers used. In all cases minor crystalline phases were obtained. For the co-crystallisation products obtained from $[\text{Sm}(\text{C}(\text{Ph}_2\text{PNSiMe}_3)_2)(\text{NCy}_2)(\text{THF})]_4$ the organic co-formers proved to be the major crystalline phases for 4,4'-bipyridine and 4,4'-oxydianiline while the biphenyl phase was not observed. The remaining peaks were believed to be due to mainly decomposition products. Raman data for $[\text{Sm}(\text{C}(\text{Ph}_2\text{PNSiMe}_3)_2)(\text{NCy}_2)(\text{THF})]_4$ co-crystallisation products indicated the presence of samarium in the inorganic co-former. SXRD data from $[\text{Sm}(\text{C}(\text{Ph}_2\text{PNSiMe}_3)_2)(\text{NCy}_2)(\text{THF})]_4$:4,4'-bipyridine indicated that only a minor decomposition product crystallised out during the study.

5. CONCLUSIONS AND FURTHER WORK

As expressed in literature most of the compounds described in this study, and more specifically the compounds discussed in the lanthanide carbene study, were only stable under inert conditions. Therefore throughout this study inert conditions were required both during the synthesis procedures and for the storage of compounds, both purchased and synthesised. In the majority of the study this was undertaken by using Schlenk line techniques using argon as the inert atmosphere. Thus constant purification of the argon was required. Purification from contaminant oxygen was the most problematic throughout the study. Notwithstanding the following conclusions were obtained from this study.

The ligand precursors $[\text{H}_2\text{C}(\text{Ph}_2\text{PNH}(i\text{Pr}))_2]\text{Br}_2$, $\text{H}_2\text{C}(\text{Ph}_2\text{PNSiMe}_3)_2$ and $\text{H}_2\text{C}(\text{Ph}_2\text{PS})_2$ were synthesised and characterised using IR and ^1H NMR spectroscopy. The desired compounds were clearly confirmed by these analytical techniques. IR and PXRD data indicated that both the $P2_1/n$ and the $C2/c$ polymorphs of $\text{H}_2\text{C}(\text{Ph}_2\text{PS})_2$, previously recorded in literature, were formed through the same reaction. An in depth discussion of the differences in IR spectra of the two polymorphs was given. The characterisation of $\text{K}[\text{HC}(\text{Ph}_2\text{PN}i\text{Pr})_2]$ through IR and ^1H NMR data indicated the possible formation of a compound with the expected properties, likely the desired compound. PXRD data showed that a novel structure was obtained, with further work on structure solution underway.

A number of lanthanide iodide THF solvate salts along with $[\text{Sm}(\text{NCy}_2)_3\text{THF}]\cdot\text{C}_6\text{H}_5\text{CH}_3$ were synthesised as lanthanide starting reagents for the lanthanide carbene complexes. Re-crystallisation of the crude iodides through Soxhlet extraction yielded the desired crystalline phase and it is believed that this is necessary to prepare the specific $\text{LnI}_3\text{THF}_{3.5}$ stoichiometry, although the crude was also used for synthesis. The synthesis of the non-iodide starting reagent $[\text{Sm}(\text{NCy}_2)_3\text{THF}]\cdot\text{C}_6\text{H}_5\text{CH}_3$ was found to be more problematic given the greater reactivity of the product and the reagents with which it was prepared. PXRD data for $[\text{Sm}(\text{NCy}_2)_3\text{THF}]\cdot\text{C}_6\text{H}_5\text{CH}_3$ indicated the formation of an amorphous solid, which was unexpected and this could indicate the formation of other similar compounds.

During this study attempts to synthesise the three lanthanide carbene complexes $[\text{Sm}(\text{C}(\text{Ph}_2\text{PNSiMe}_3)_2)(\text{NCy}_2)(\text{THF})]$, $[\text{Nd}(\text{C}(\text{Ph}_2\text{PN}i\text{Pr})_2)(\text{HC}(\text{Ph}_2\text{PN}i\text{Pr})_2)]\cdot 2\text{THF}$ and $[\text{Sm}_2(\text{C}(\text{Ph}_2\text{PS})_2)_2]\text{I}_2\text{THF}_4\cdot 4(\text{C}_6\text{H}_5\text{CH}_3)$ were made. Further to the required use of inert

atmosphere the starting reagents and ligands for these synthesis may have contained impurities thus decreasing the ability of preparing the desired complexes. Characterisation of these complexes was mainly undertaken by IR spectroscopy applying the following theoretical background. The formation of Ln–C or Ln=C bonds could not be observed directly so analysis was undertaken using the changes expected and recorded in literature. For iminophosphorano compounds the shift in the band due to the ν P=N vibration on deprotonation to the region 1110–1025 cm^{-1} was the most useful diagnostic feature, backed by both IR and XRD literature data. The shifts expected for the ν P–C–P vibrations for both iminophosphorano and thiophosphorane were found to be more complicated to describe for the di-anionic species and therefore their use in the determination of the deprotonation and complexation could not yield valuable information. The changes observed for ν P–C–P vibrations were more diagnostic in describing the formation of mono-anionic analogues than the respective changes for the ν P=N vibrations. However it was observed that the use of all these previously mentioned changes in IR could only tentatively discriminate between the mono-anion and di-anion species. Changes in the bands presumed to be due to the ν P=S vibrations could not be used in attempts to describe mono-anion or di-anion species since changes were not observed to be strong or of a singular increase or decrease in wavenumber.

For the complex $[\text{Sm}(\text{C}(\text{Ph}_2\text{PNSiMe}_3)_2)(\text{NCy}_2)(\text{THF})]$ the products $[\text{Sm}(\text{C}(\text{Ph}_2\text{PNSiMe}_3)_2)(\text{NCy}_2)(\text{THF})]_3$ and $[\text{Sm}(\text{C}(\text{Ph}_2\text{PNSiMe}_3)_2)(\text{NCy}_2)(\text{THF})]_4$ had the best IR spectra on comparison with literature data, while $[\text{Sm}(\text{C}(\text{Ph}_2\text{PNSiMe}_3)_2)(\text{NCy}_2)(\text{THF})]_1$ indicated the possible presence of residual $[\text{Sm}(\text{NCy}_2)_3\text{THF}] \cdot \text{C}_6\text{H}_5\text{CH}_3$. All three products showed the possible presence of the mono-anionic derivative as a main component. SXRD and IR data of $[\text{Sm}(\text{C}(\text{Ph}_2\text{PNSiMe}_3)_2)(\text{NCy}_2)(\text{THF})]_2$ indicated that $\text{Ph}_2\text{P}(\text{O})\text{NH}_2$ was the main product showing full moisture induced decomposition. A tentative complete mechanism for this decomposition was also proposed. The presence of both mono-anion and dianion ligands in the product $[\text{Nd}(\text{C}(\text{Ph}_2\text{PNiPr})_2)(\text{HC}(\text{Ph}_2\text{PNiPr})_2)] \cdot 2\text{THF}$ made characterisation by IR spectroscopy inconclusive in terms of composition. For this complex two different IR spectra for the two products $_1$ and $_2$ were obtained which could be due to the use of the $[\text{H}_2\text{C}(\text{Ph}_2\text{PNH}(i\text{Pr}))_2]\text{Br}_2_1$ and $\text{K}(\text{HC}(\text{Ph}_2\text{PNiPr})_2)_2$ as starting reagents respectively. Although all carbene complexes were difficult to synthesise and characterise the complex $[\text{Sm}_2(\text{C}(\text{Ph}_2\text{PS})_2)_2\text{I}_2\text{THF}_4] \cdot 4(\text{C}_6\text{H}_5\text{CH}_3)$ proved the most difficult to synthesise with numerous species produced as described using IR, ^1H NMR

and PXRD techniques. Salt metathesis was shown to have occurred through the formation of LiI by-products. However, the characterisation of the desired complex yielded no definitive results. In all cases the detailed discussion of analytical data showed the high moisture sensitivity of both products and reagents used throughout this section of the study.

The main study regarding the stabilisation of lanthanide carbenes was undertaken using co-crystallisation. This technique was preferred as it is a green chemical method, easy to implement, both in the current study and in the industrial sphere and versatile. Six co-crystallisation products of the complex $[\text{Sm}(\text{C}(\text{Ph}_2\text{PNSiMe}_3)_2)(\text{NCy}_2)(\text{THF})]$ or its methanide analogue were prepared through a grinding procedure, using three organic co-formers, under dry nitrogen in an attempt to prepare them under inert conditions while using a solvent-free technique. The IR spectra of the co-crystallisation products from $[\text{Sm}(\text{C}(\text{Ph}_2\text{PNSiMe}_3)_2)(\text{NCy}_2)(\text{THF})]$ indicated a complete loss of the inorganic co-former structure.

For the $[\text{Sm}(\text{C}(\text{Ph}_2\text{PNSiMe}_3)_2)(\text{NCy}_2)(\text{THF})]$ co-crystallisation products some decomposition was noted throughout. This was especially visible for the biphenyl co-crystal product but not prominent for the other two products. The 4,4'-bipyridine and 4,4'-oxydianiline co-crystallisation products showed clear signs of mixture formation with possible indications of novel intermolecular interactions forming, especially with the former compound. For $[\text{Sm}(\text{C}(\text{Ph}_2\text{PNSiMe}_3)_2)(\text{NCy}_2)(\text{THF})]$ and its co-crystallisation products the presence of Sm^{3+} was indicated by Raman. PXRD data for the $[\text{Sm}(\text{C}(\text{Ph}_2\text{PNSiMe}_3)_2)(\text{NCy}_2)(\text{THF})]$ co-crystallisation products did not yield further information on the possibility of the formation of a single phase as the major phase proved to be amorphous. Therefore in all cases co-crystallisation was unlikely.

In general the lanthanide carbenes were difficult to synthesise and store. IR and PXRD data for all co-crystallisation attempts indicated that this was difficult to achieve. Therefore, the usefulness of this approach in stabilising these compounds seems limited from this study. Both these features limit the use of these complexes in different synthetic fields both in research and industry.

The synthesis of lanthanide non-carbene di- $\lambda^5\sigma^4$ -phosphorane complexes proved to give mixed results. Synthesis of the neutral ligands and ligand precursors, $\text{HN}(\text{Ph}_2\text{PS})_2$, $\text{HN}(\text{Ph}_2\text{PO})_2$, $\text{O}((\text{Et}_2\text{N})_2\text{PO})_2$ and $\text{O}((i\text{PrNH})_2\text{PO})_2$ was fairly straightforward with the desired compounds obtained under inert conditions and characterised through IR, ^1H and ^{31}P NMR spectroscopy and GC-MS. To the knowledge of the author the first crystal

structure for $O((iPrNH)_2PO)_2$ was determined. This was also shown to contain supramolecular motifs and hydrogen bonding synthons which were unique to its crystal structure as compared to those found in the structures of previously published mono-N-substituted pyrophosphoramides. This study also indicated that $(iPrNH)_3PO$ was a major side product for the formation of $O((iPrNH)_2PO)_2$ through the method used. $HN(Ph_2PO)_2$ was crystallised in a novel amine tautomer structure whereas previously only the structure of the alcoholic tautomer was published for the solid state. The ligands were found to be stable to air and moisture and synthesis was only undergone under inert conditions due to the use of the sensitive reagents. Complexation of $[N(Ph_2PO)_2]^-$ with Eu^{3+} was easily achieved under normal laboratory conditions and analysed by 1H NMR spectroscopy in solution. PXRD data indicated that the major phase collected was the by-product KNO_3 , while the novel minor crystalline phase observed could have been due to the desired compound. Complexation of $[N(Ph_2PS)_2]^-$ with Eu^{3+} on the other hand proved difficult using normal laboratory conditions although complexation of $HN(Ph_2PS)_2$ with Eu^{3+} through grinding yielded a novel crystalline solid. Complexation of $O((Et_2N)_2PO)_2$ with Nd^{3+} under moisture free conditions yielded mainly a brown viscous liquid, which was unexpected. However, ^{31}P NMR data indicated that a possible complex of $O((Et_2N)_2PO)_2$ with Nd^{3+} was produced. Data regarding the Ln–N and Ln–O bonding analogous to the Ln=C bonding of carbenes was not obtained.

A number of novel crystalline products were obtained throughout this study and identified and characterised through both SXRD and PXRD. These are listed below.

- $O((iPrNH)_2PO)_2$ _1_b1 – characterised using SXRD, first reported crystal structure of $O((iPrNH)_2PO)_2$.
- $HN(Ph_2PO)_2$ – characterised using PXRD, novel tautomer.
- $HN(Ph_2PS)_2 + Eu(ClO_4)_3 \cdot n(H_2O)$ _1 – novel PXRD pattern.
- $K[HC(Ph_2PNiPr)_2]$ _2 – novel PXRD pattern,.
- $O((Et_2N)_2PO)_2$ _1_f13 – single crystals believed to be an impurity were found to be the novel compound $Ca_2(O((Et_2N)_2PO)_2)_2(NO_3)_4(H_2O)_2$.

Future work with regards to the characterisation of the possibly novel crystalline solids is required. Detailed studies into the polymorphism of lanthanide carbenes could also be of interest for further work. Further work on the stabilisation of air and moisture sensitive compounds using co-crystallisation, given that this is a solid state technique and therefore solvent free, is interesting but the current results indicated that this was difficult to achieve. Its use in stabilisation seems limited and further studies are required on a greater variety of compounds to give definitive data on the effect of co-crystallisation on moisture and air sensitive compound stabilisation.

Published Work:

"Exploring the Structural Chemistry of Pyrophosphoramides: N,N',N'',N'''-Tetraisopropylpyrophosphoramidate", D. Micallef, L. Vella-Zarb, U. Baisch, *Chemistry*, 2021, 3, 149-163.

"Di- μ -nitrate-bis(μ -octaethyl pyrophosphoramidate)bis[aquadinitratocalcium(II)]" D. Micallef, U. Baisch, *Acta Crystallogr. Sect. E Crystallogr. Commun.*, 2021, 77, 795-798.

"Structural studies on isoelectronic analogues of pyrophosphoramides" D. Micallef, L. Vella-Zarb, U. Baisch, *Cryst. Growth & Design*, 2021, in preparation.

REFERENCES

- (1) Cotton, F. A.; Wilkinson, G. *Advanced Inorganic Chemistry*, 4th Ed.; John Wiley & Sons: New York, 1980, pp 981–983, 995, 1199–1200, 71–72, 1265–1267.
- (2) Cotton, S. Scandium, Yttrium, and the Lanthanides. In *Comprehensive Coordination Chemistry II*; McCleverty, J. A., Meyer, T. J., Parkin, G. F., Eds.; Elsevier: New York, 2005; Vol. 3, pp 1–3, 93–188, 108, 191–192, 347–348.
- (3) Wells, W. H.; Wells, V. L. The Lanthanides , Rare Earth Elements. In *Patty's Toxicology*; Bingham, E., Cofrancesco, B., Eds.; John Wiley & Sons, Inc., 2012; Vol. 1, pp 817–840.
- (4) Hirano, S.; Suzuki, K. T. Exposure , Metabolism , and Toxicity of Rare Earths and Related Compounds. *Environ. Health Perspect.* **1996**, *104*, 85–95.
- (5) Wilkinson, G.; Birmingham, J. M. CYCLOPENTADIENYL COMPOUNDS OF Sc, Y, La, Ce AND SOME LANTHANIDE ELEMENTS. *J. Am. Chem. Soc.* **1954**, *76*, 6210–6210.
- (6) Edelmann, F. T. Lanthanides and Actinides: Annual Survey of Their Organometallic Chemistry Covering the Year 2013. *Coord. Chem. Rev.* **2015**, *284*, 124–205.
- (7) Aparna, K.; Ferguson, M.; Cavell, R. G. A Monomeric Samarium Bis (Iminophosphorano) Chelate Complex with a Sm=C Bond. *J. Am. Chem. Soc.* **2000**, *122*, 726–727.
- (8) Cantat, T.; Jaroschik, F.; Nief, F.; Ricard, L.; Mézailles, N.; Le Floch, P. New Mono- and Bis-Carbene Samarium Complexes: Synthesis, X-Ray Crystal Structures and Reactivity. *Chem. Commun.* **2005**, *0*, 5178.
- (9) Wooles, A. J.; Mills, D. P.; Lewis, W.; Blake, A. J.; Liddle, S. T. Lanthanide Tri-Benzyl Complexes: Structural Variations and Useful Precursors to Phosphorus-Stabilised Lanthanide Carbenes. *Dalt. Trans.* **2010**, *39*, 329–336.
- (10) Gregson, M.; Lu, E.; McMaster, J.; Lewis, W.; Blake, A. J.; Liddle, S. T. A Cerium(IV)-Carbon Multiple Bond. *Angew. Chemie Int. Ed. English* **2013**, *52*, 13016–13019.
- (11) Bonnet, F.; Jones, C. E.; Semlali, S.; Bria, M.; Roussel, P.; Visseaux, M.; Arnold, P. L. Tuning the Catalytic Properties of Rare Earth Borohydrides for the Polymerisation of Isoprene. *Dalt. Trans.* **2013**, *42*, 790–801.
- (12) Buchard, A.; Platel, R. H.; Auffrant, A.; Le Goff, X. F.; Floch, P. Le; Williams, C. K. Iminophosphorane Neodymium(III) Complexes as Efficient Initiators for Lactide Polymerization. *Organometallics* **2010**, *29*, 2892–2900.
- (13) Rogosnitzky, M.; Branch, S. Gadolinium-Based Contrast Agent Toxicity: A Review of Known and Proposed Mechanisms. *BioMetals* **2016**, *29*, 365–376.
- (14) Binnemans, K.; Tom, P.; Blanpain, B.; Gerven, T. Van; Yang, Y.; Walton, A.; Buchert, M. Recycling of Rare Earths : A Critical Review. *J. Clean. Prod.* **2013**, *51*, 1–22.
- (15) Wayda, A. L.; Atwood, J. L.; Hunter, W. E. Homoleptic Organolanthanoid Hydrocarbyls. The Synthesis and X-Ray Crystal Structure of Tris[o-((Dimethylamino)Methyl)Phenyl]Lutetium. *Organometallics* **1984**, *3*, 939–941.

- (16) Hillesheim, N. S.; Elfferding, M.; Linder, T.; Sundermeyer, J. Neuartige Cyclopentadienyl-N-Silylphosphazen-Komplexe Der Seltenerdmetalle Yttrium Und Lutetium. *Zeitschrift für Anorg. und Allg. Chemie* **2010**, *636*, 1776–1782.
- (17) Deacon, G. B.; Forsyth, C. M. A Half-Sandwich Perfluoroorganoytterbium(II) Complex from a Simple Redox Transmetalation/Ligand Exchange Synthesis. *Organometallics* **2003**, *22*, 1349–1352.
- (18) Marsh, J. K. Separation of the Lanthanons with the Aid of Ethylenediamine-NNN'N'-Tetra-Acetic Acid. *J. Chem. Soc.* **1950**, 1819–1823.
- (19) Atkins, P.; Overton, T.; Rourke, J.; Weller, M.; Armstrong, F. *Shriver and Atkins' Inorganic Chemistry*, 5th Ed.; Oxford University Press: Oxford, 2010, pp 50, 581, 587, 586–587, 534–535, 514–515.
- (20) Crabtree, R. H. *The Organometallic Chemistry of the Transition Metals*, 4th Ed.; John Wiley & Sons, Inc.: Hoboken, NJ, USA, 2005, pp 140–145, 481–483.
- (21) Bunzli, J. C. G. Benefiting from the Unique Properties of Lanthanide Ions. *Acc. Chem. Res.* **2006**, *39*, 53–61.
- (22) Schumann, H. Organolanthanoid Compounds**. *Angew. Chemie Int. Ed. English* **1984**, *23*, 474–493.
- (23) Bunzli, J. G.; Eliseeva, S. V. Basics of Lanthanide Photophysics. In *Lanthanide luminescence Photophysical, Analytical and Biological aspects.*; Hanninen, P., Harma, H., Eds.; Springer-Verlag Berlin Heidelberg, 2011; pp 1–45.
- (24) Li, F. Y.; Xu, L.; Gao, G. G.; Fan, L. H.; Bi, B. Unusual Magnetic Behavior of a 2D Citrate-Bridged Dysprosium(III) Coordination Polymer. *Eur. J. Inorg. Chem.* **2007**, *2007*, 3405–3409.
- (25) Luan, F.; Yan, P.; Zhu, J.; Liu, T.; Zou, X.; Li, G. A Salen-Type Dy₄ Single-Molecule Magnet with an Enhanced Energy Barrier and Its Analogues. *Dalt. Trans.* **2015**, *44*, 4046–4053.
- (26) Florini, N.; Faglioni, F.; Zucchi, C.; Caglioti, L.; Pályi, G. Aqueous-Phase Quantitative NMR Determination of Amino Acid Enantiomer Ratio by ¹³C-NMR Using Chiral Neodymium Shift Reagent. *Amino Acids* **2010**, *38*, 1343–1350.
- (27) Turov, A. V.; Bondarenko, S. P.; Tkachuk, A. A.; Khilya, V. P. Conformational Mobility of Substituted 2-Methoxychalcones under the Action of Lanthanide Shift Reagents. *Russ. J. Org. Chem.* **2005**, *41*, 47–53.
- (28) Carney, C. E.; Tran, A. D.; Wang, J.; Schabel, M. C.; Sherry, A. D.; Woods, M. Towards the Rational Design of MRI Contrast Agents: δ-Substitution of Lanthanide(III) NB-DOTA-Tetraamide Chelates Influences but Does Not Control Coordination Geometry. *Chem. - A Eur. J.* **2011**, *17*, 10372–10378.
- (29) Aime, S.; Cabella, C.; Colombatto, S.; Crich, S. G.; Gianolio, E.; Maggioni, F. Insights into the Use of Paramagnetic Gd(III) Complexes in MR-Molecular Imaging Investigations. *J. Magn. Reson. Imaging* **2002**, *16*, 394–406.
- (30) Cantat, T.; Ricard, L.; Le Floch, P.; Mezailles, N. Phosphorus-Stabilized Geminal Dianions. *Organometallics* **2006**, *25*, 4965–4976.
- (31) Liddle, S. T.; Mills, D. P.; Wooles, A. J. Early Metal Bis(Phosphorus-Stabilised)Carbene Chemistry. *Chem. Soc. Rev.* **2011**, *40*, 2164–2176.

- (32) Magennis, S. W.; Parsons, S.; Pikramenou, Z. Assembly of Hydrophobic Shells and Shields around Lanthanides. *Chem. - A Eur. J.* **2002**, *8*, 5761–5771.
- (33) Joesten, M. D. The Donor Properties of Pyrophosphate Derivatives. V. Complexes of MoOCl_3 , UO_2^{2+} , and Th^{4+} with Octamethylpyrophosphoramidate. *J. Inorg. Nucl. Chem.* **1967**, *6*, 1598–1599.
- (34) Appel, R.; Ruppert, I. Darstellung Silylierter Alkylen-Bisimino-phosphorane Und Ihre Cyclisierung Mit Phosphor(V)-Fluoriden. *Zeitschrift für Anorg. und Allg. Chemie* **1974**, *406*, 131–144.
- (35) Carmalt, C. J.; Cowley, A. H.; Decken, A.; Lawson, Y. G.; Norman, N. C. Bis(Diphenylphosphino)Methane Disulfide. *Acta Crystallogr. Sect. C Cryst. Struct. Commun.* **1996**, *52*, 931–933.
- (36) Demange, M.; Boubekur, L.; Auffrant, A.; Mezailles, N.; Ricard, L.; Le Goff, X.; Le Floch, P. A New and Convenient Approach towards Bis(Iminophosphoranyl)Methane Ligands and Their Dicationic, Cationic, Anionic and Dianionic Derivatives. *New J. Chem.* **2006**, *30*, 1745–1754.
- (37) Fluck, E.; Goldmann, F. L. Kenntnis Der Imido-Diphosphonsäuren Und Ihrer Derivate, II Imido-Tetraphenyldiphosphinsäure Und Ihr Trichlorid. *Chem. Ber.* **1963**, *11*, 3091–3093.
- (38) Nöth, H.; Fluck, E. Röntgenstrukturuntersuchungen an Verbindungen Mit P—NH—P-Gerüst. *Zeitschrift für Naturforsch. - Sect. B J. Chem. Sci.* **1984**, *39*, 744–753.
- (39) Bannister, R. D.; Levason, W.; Reid, G.; Zhang, W. Diphosphine Dioxide Complexes of Lanthanum and Lutetium – The Effects of Ligand Architecture and Counter-Anion. *Polyhedron* **2017**, *133*, 264–269.
- (40) Buchard, A.; Auffrant, A.; Ricard, L.; Le Goff, X.-F. F.; Platel, R. H.; Williams, C. K.; Le Floch, P. First Neodymium(III) Alkyl-Carbene Complex Based on Bis(Iminophosphoranyl) Ligands. *Dalt. Trans.* **2009**, *3*, 10219–10222.
- (41) Mills, D. P.; Wooles, A. J.; McMaster, J.; Lewis, W.; Blake, A. J.; Liddle, S. T. Heteroleptic $[\text{M}(\text{CH}_2\text{C}_6\text{H}_5)_2(\text{I})(\text{THF})_3]$ Complexes (M = Y or Er): Remarkably Stable Precursors to Yttrium and Erbium T-Shaped Carbenes. *Organometallics* **2009**, *28*, 6771–6776.
- (42) Gregson, M.; Chilton, N. F.; Ariciu, A.-M.; Tuna, F.; Crowe, I. F.; Lewis, W.; Blake, A. J.; Collison, D.; McInnes, E. J. L.; Winpenny, R. E. P.; et al. A Monometallic Lanthanide Bis(Methanediide) Single Molecule Magnet with a Large Energy Barrier and Complex Spin Relaxation Behaviour. *Chem. Sci.* **2016**, *7*, 155–165.
- (43) Mills, D. P.; Soutar, L.; Lewis, W.; Blake, A. J.; Liddle, S. T. Regioselective C–H Activation and Sequential C–C and C–O Bond Formation Reactions of Aryl Ketones Promoted by an Yttrium Carbene. *J. Am. Chem. Soc.* **2010**, *132*, 14379–14381.
- (44) Mills, D. P.; Soutar, L.; Cooper, O. J.; Lewis, W.; Blake, A. J.; Liddle, S. T. Reactivity of the Yttrium Alkyl Carbene Complex $[\text{Y}(\text{BIPM})(\text{CH}_2\text{C}_6\text{H}_5)(\text{THF})]$ (BIPM = $\{\text{C}(\text{PPh}_2\text{NSiMe}_3)_2\}^2$): From Insertions, Substitutions, and Additions to Nontypical Transformations. *Organometallics* **2013**, *32*, 1251–1264.

- (45) Mills, D. P.; Lewis, W.; Blake, A. J.; Liddle, S. T. Reactivity Studies of a T-Shaped Yttrium Carbene: C–F and C–O Bond Activation and C=C Bond Formation Promoted by [Y(BIPM)(I)(THF)₂] (BIPM = C(PPh₂NSiMe₃)₂). *Organometallics* **2013**, *32*, 1239–1250.
- (46) Buchard, A.; Platel, R. H.; Auffrant, A.; Le Goff, X. F.; Floch, P. Le; Williams, C. K. Iminophosphorane Neodymium(III) Complexes as Efficient Initiators for Lactide Polymerization. *Organometallics* **2010**, *29*, 2892–2900.
- (47) Birmingham, J. M.; Wilkinson, G. The Cyclopentadienides of Scandium, Yttrium and Some Rare Earth Elements. *J. Am. Chem. Soc.* **1956**, *78*, 42–44.
- (48) Hanusa, T. P. Group 1s and 2s Metals. In *Comprehensive Coordination Chemistry II*; McCleverty, J. A., Meyer, T. J., Parkin, G. F., Eds.; Elsevier: New York, 2005; pp 3–4.
- (49) Schumann, H.; Albrecht, I.; Loebel, J.; Hahn, E.; Hossain, M. B.; Van der Helm, D. Organometallic Compounds of the Lanthanides. 36. Bis(Pentamethylcyclopentadienyl) Halide and Alkyl Derivatives of the Lanthanides. *Organometallics* **1986**, *5*, 1296–1304.
- (50) Liddle, S. T. Lanthanides: Organometallic Chemistry. In *Encyclopedia of Inorganic and Bioinorganic Chemistry*; Scott, R. A., Ed.; John Wiley & Sons, Inc., 2012.
- (51) Evans, W. J.; Davis, B. L. Chemistry of Tris(Pentamethylcyclopentadienyl) f-Element Complexes, (C₅Me₅)₃M. *Chem. Rev.* **2002**, *102*, 2119–2136.
- (52) Evans, W. J.; Seibel, C. A.; Ziller, J. W. Unsolvated Lanthanide Metallocene Cations [(C₅Me₅)₂Ln][BPh₄]: Multiple Syntheses, Structural Characterization, and Reactivity Including the Formation of (C₅Me₅)₃Nd. *J. Am. Chem. Soc.* **1998**, *120*, 6745–6752.
- (53) Evans, W. J.; Perotti, J. M.; Kozimor, S. A.; Champagne, T. M.; Davis, B. L.; Nyce, G. W.; Fujimoto, C. H.; Clark, R. D.; Johnston, M. A.; Ziller, J. W. Synthesis and Comparative η¹-Alkyl and Sterically Induced Reduction Reactivity of (C₅Me₅)₃Ln Complexes of La, Ce, Pr, Nd, and Sm. *Organometallics* **2005**, *24*, 3916–3931.
- (54) Edelmann, F. T. Lanthanides and Actinides: Annual Survey of Their Organometallic Chemistry Covering the Year 2010. *Coord. Chem. Rev.* **2012**, *256*, 2641–2740.
- (55) MacDonald, M. R.; Bates, J. E.; Ziller, J. W.; Furche, F.; Evans, W. J. Completing the Series of +2 Ions for the Lanthanide Elements: Synthesis of Molecular Complexes of Pr²⁺, Gd²⁺, Tb²⁺, and Lu²⁺. *J. Am. Chem. Soc.* **2013**, *135*, 9857–9868.
- (56) Shima, T.; Hou, Z. Selective Ammonolysis of Half-Sandwich Rare-Earth Metal Dialkyl and Polyhydride Complexes: Synthesis of Polyamido Rare-Earth Complexes Having Novel Structures†. *Dalt. Trans.* **2010**, *39*, 6858–6863.
- (57) Xu, L.; Wang, Y.-C.; Zhang, W.-X.; Xi, Z. Half-Sandwich Bis(Propiolamidinate) Rare-Earth Metal Complexes: Synthesis, Structure and Dissociation of the Cyclopentadienyl Ligand via Competition with an Amidinate. *Dalt. Trans.* **2013**, *42*, 16466–16469.

- (58) Harder, S.; Naglav, D.; Ruspic, C.; Wickleder, C.; Adlung, M.; Hermes, W.; Eul, M.; Poettgen, R.; Rego, D. B.; Poineau, F.; et al. Physical Properties of Superbulky Lanthanide Metallocenes: Synthesis and Extraordinary Luminescence of [EuII(CpBIG)₂] (CpBIG=(4-NBu-C₆H₄)₅-Cyclopentadienyl). *Chem. - A Eur. J.* **2013**, *19*, 12272–12280.
- (59) Jian, Z.; Zhao, W.; Liu, X.; Chen, X.; Tang, T.; Cui, D. Synthesis of Linked Half Sandwich Rare-Earth Metal Chlorido and Borohydrido Complexes and Their Catalytic Behavior towards MMA Polymerization†. *Dalt. Trans.* **2010**, *39*, 6871–6876.
- (60) Jian, Z.; Cui, D.; Hou, Z.; Li, X. Living Catalyzed-Chain-Growth Polymerization and Block Copolymerization of Isoprene by Rare-Earth Metal Allyl Precursors Bearing a Constrained-Geometry-Conformation Ligand. *Chem. Commun.* **2010**, *46*, 3022–3024.
- (61) Cotton, F. A.; Schwotzer, W. Sm(η⁶-C₆Me₆)(η²-AlCl₄)₃: The First Structure of a Rare Earth Complex with a Neutral π-Ligand. *J. Am. Chem. Soc.* **1986**, *696*, 4657–4658.
- (62) Brennan, J. G.; Cloke, G. N.; Sameh, A. A.; Zalkin, A. Synthesis of Bis(η-1,3,5-Tri-*t*-Butylbenzene) Sandwich Complexes of Yttrium(0) and Gadolinium(0); the X-Ray Crystal Structure. *J. Chem. Soc. Chem. Commun.* **1987**, *1987*, 1668–1669.
- (63) Lee, H. S.; Niemeyer, M. Homoleptic Heavy Alkaline Earth and Europium Triazenides. *Inorg. Chem.* **2010**, *49*, 730–735.
- (64) Heitmann, D.; Jones, C.; Mills, D. P.; Stasch, A. Low Coordinate Lanthanide(II) Complexes Supported by Bulky Guanidinato and Amidinato Ligands. *Dalt. Trans.* **2010**, *39*, 1877.
- (65) Basalov, I. V.; Lyubov, D. M.; Fukin, G. K.; Cherkasov, A. V.; Trifonov, A. A. Reactivity of Ytterbium(II) Hydride. Redox Reactions: Ytterbium(II) vs Hydrido Ligand. Metathesis of the Yb-H Bond. *Organometallics* **2013**, *32*, 1507–1516.
- (66) Yuan, Y.; Chen, Y.; Li, G.; Xia, W. Synthesis and Structural Features of Boratabenzene Rare-Earth Metal Alkyl Complexes. *Organometallics* **2010**, *29*, 3722–3728.
- (67) Yin, H.; Lewis, A. J.; Carroll, P.; Schelter, E. J. Electrophilic Ln(III) Cations Protected by C-F → Ln Interactions and Their Coordination Chemistry with Weak σ- And π-Donors. *Inorg. Chem.* **2013**, *52*, 8234–8243.
- (68) Brunelli, M.; Poggio, S.; Pedretti, U.; Lugli, G. The Synthesis and Nuclear Magnetic Resonance Investigation of the Structure and Chemical Dynamics of New Anionic Tetra-Allyl Complexes of Lanthanide Ions. *Inorganica Chim. Acta* **1987**, *131*, 281–285.
- (69) Carpentier, J. F.; Guillaume, S. M.; Kirillov, E.; Sarazin, Y. Discrete Allyl Complexes of Group 3 Metals and Lanthanides. *Comptes Rendus Chim.* **2010**, *13*, 608–625.
- (70) Cui, P.; Spaniol, T. P.; Okuda, J. Heterometallic Potassium Rare-Earth-Metal Allyl and Hydrido Complexes Stabilized by a Dianionic (NNNN)-Type Macrocyclic Ancillary Ligand. *Organometallics* **2013**, *32*, 1176–1182.

- (71) Cui, P.; Spaniol, T. P.; Maron, L.; Okuda, J. Dehydrogenation of Amine-Borane $\text{Me}_2\text{NH}\cdot\text{BH}_3$ Catalyzed by a Lanthanum-Hydride Complex. *Chem. - A Eur. J.* **2013**, *19*, 13437–13444.
- (72) Robert, D.; Abinet, E.; Spaniol, T. P.; Okuda, J. Cationic Allyl Complexes of the Rare-Earth Metals: Synthesis, Structural Characterization, and 1,3-Butadiene Polymerization Catalysis. *Chem. - A Eur. J.* **2009**, *15*, 11937–11947.
- (73) Schumann, H.; Muller, J.; Bruncks, N.; Lauke, H.; Pickardt, J.; Schwarz, H.; Eckart, K. Organometallic Compounds of the Lanthanides. 17. Tris[(Tetramethyl ethylenediamine)Lithium] Hexamethyl Derivatives of the Rare Earths. *Organometallics* **1984**, *3*, 69–74.
- (74) Schumann, H.; Lauke, H.; Hahn, E.; Pickardt, J. Metallorganische Verbindungen Der Lanthanoiden XVIII*. Synthese Und Struktur von Tris[(1,2-Dimethoxyethan)Lithium]Hexamethyllutetat(III). *J. Organomet. Chem.* **1984**, *263*, 29–35.
- (75) Hitchcock, P. B.; Lappert, M. F.; Smith, R. G.; Bartlett, R. a.; Power, P. P. Synthesis and Structural Characterisation of the First Neutral Homoleptic Lanthanide Metal(III) Alkyls: $[\text{LnR}_3]$ [Ln = La or Sm, R = $\text{CH}(\text{SiMe}_3)_2$]. *J. Chem. Soc. Chem. Commun.* **1988**, *3*, 1007–1009.
- (76) Guttenberger, C.; Amberger, H.-D. Zur Elektronenstruktur Metallorganischer Komplexe Der F-Elemente XLIII Züchtung Größerer Tris(Bis(Trimethylsilyl) Methyl) Lanthanid-Einkristalle Für Optische Und Magnetochemische Untersuchungen. *J. Organomet. Chem.* **1997**, *545–546*, 601–606.
- (77) Reddmann, H.; Guttenberger, C.; Amberger, H.-D. Zur Elektronenstruktur Metallorganischer Komplexe Der F-Elemente IL. Erstmalige Aufklärung Der Elektronenstruktur Eines Metallorganischen σ -Komplexes Der f-Elemente: Tris (Bis(Trimethylsilyl) Methyl) Erbium (III). *J. Organomet. Chem.* **2000**, *602*, 65–71.
- (78) Oliver, T.; Sundermeyer, J. Homoleptic Rare Earth Triaryl Complexes. WO2013017281 A1, 2013.
- (79) Cole, M. L.; Deacon, G. B.; Forsyth, C. M.; Junk, P. C.; Konstas, K.; Wang, J. Steric Modulation of Coordination Number and Reactivity in the Synthesis of Lanthanoid(III) Formamidinates. *Chem. - A Eur. J.* **2007**, *13*, 8092–8110.
- (80) Saliu, K. O.; Cheng, J.; McDonald, R.; Ferguson, M. J.; Takats, J. Reactions of Scorpionate-Anchored Yttrium and Lutetium Dialkyls with Terminal Alkynes: From Bimetallic Complexes with Bridging Enynediyl Ligands to Monomeric Terminal Dialkynyl Complexes. *Organometallics* **2010**, *29*, 4950–4965.
- (81) Burns, C. J.; Andersen, R. A. Preparation of the First η^2 -Olefin Complex of a 4f-Transition Metal, $(\text{Me}_5\text{C}_5)_2\text{Yb}(\mu^2\text{-C}_2\text{H}_4)\text{Pt}(\text{PPh}_3)_2$. *J. Am. Chem. Soc.* **1987**, *109*, 915–917.
- (82) Eaborn, C.; Hitchcock, P. B.; Izod, K.; Lu, Z.-R.; Smith, J. D. Alkyl Derivatives of Europium(+2) and Ytterbium(+2). Crystal Structures of $\text{Eu}[\text{C}(\text{SiMe}_3)_3]_2$, $\text{Yb}[\text{C}(\text{SiMe}_3)_2(\text{SiMe}_2\text{CH}=\text{CH}_2)]\text{I.OEt}_2$ and $\text{Yb}[\text{C}(\text{SiMe}_3)_2(\text{SiMe}_2\text{OMe})]\text{I.OEt}_2$. *Organometallics* **1996**, *15*, 4783–4790.
- (83) Burns, C. J.; Andersen, R. A. Preparation of the First Molecular η^2 -Acetylene Complex of a 4f Transition Metal, $(\text{Me}_5\text{C}_5)_2\text{Yb}(\eta^2\text{-MeC}\equiv\text{CMe})$. *J. Am. Chem. Soc.* **1987**, *109*, 916–917.

- (84) Bourissou, D.; Guerret, O.; Gabbai, F. P.; Bertrand, G.; Gabbai, F. P.; Bertrand, G. Stable Carbenes. *Chem. Rev.* **2000**, *100*, 39–91.
- (85) Pauling, L. The Structure of Singlet Carbene Molecules. *J. Chem. Soc. Chem. Commun.* **1980**, *0*, 688.
- (86) Schoeller, W. W. When Is a Singlet Carbene Linear? *J. Chem. Soc. Chem. Commun.* **1980**, *0*, 124.
- (87) Öfele, K. 1,3-Dimethyl-4-Imidazolinylyden-(2)-Pentacarbonylchrom Ein Neuer Übergangsmetall-Carben-Komplex. *J. Organomet. Chem.* **1968**, *12*, P42–P43.
- (88) Arduengo, A. J.; Kline, M.; Harlow, R. L. A Stable Crystalline Carbene. *J. Am. Chem. Soc.* **1991**, *113*, 361–363.
- (89) Arduengo, A. J.; Tamm, M.; McLain, S. J.; Calabrese, J. C.; Davidson, F.; Marshall, W. J. Carbene-Lanthanide Complexes. *J. Am. Chem. Soc.* **1994**, *116*, 7927–7928.
- (90) Dixon, D. A.; Arduengo, A. J. Electronic Structure of a Stable Nucleophilic Carbene. *J. Phys. Chem.* **1991**, *95*, 4180–4182.
- (91) Arduengo, A. J.; Dixon, D. A. Electron Distribution in a Stable Carbene. *J. Am. Chem. Soc.* **1994**, *116*, 6812–6822.
- (92) Arduengo III, A. J.; Bock, H.; Chen, H.; Denk, M.; Dixon, D. A.; Green, J. C.; Herrmann, W. a; Jones, N. L.; Wagner, M.; West, R. Photoelectron Spectroscopy of a Carbene/Silylene/Germylene Series. *J. Am. Chem. Soc.* **1994**, *116*, 6641–6649.
- (93) Boehme, C.; Frenking, G. Electronic Structure of Stable Carbenes, Silylenes, and Germylenes. *J. Am. Chem. Soc.* **1996**, *118*, 2039–2046.
- (94) Heinemann, C.; Müller, T.; Apeloig, Y.; Schwarz, H. On the Question of Stability, Conjugation, and “Aromaticity” in Imidazol-2-Ylidenes and Their Silicon Analogs †. *J. Am. Chem. Soc.* **1996**, *118*, 2023–2038.
- (95) Herrmann, W. A.; Koecher, C. N-Heterocyclic Carbenes. *Angew. Chemie Int. Ed. English* **1997**, *36*, 2167–2187.
- (96) Alder, R. W.; Allen, P. R.; Murray, M.; Orpen, A. G. Bis(Diisopropylamino)Carbene. *Angew. Chemie Int. Ed. English* **1996**, *35*, 1121–1123.
- (97) Heuclin, H.; Fustier-Boutignon, M.; Ho, S. Y.; Goff, X.-F. Le; Carencio, S.; So, C.; Mézailles, N. Synthesis of Phosphorus(V)-Stabilized Geminal Dianions. The Cases of Mixed P=X/P→BH₃ (X = S, O) and P=S/SiMe₃ Derivatives. *Organometallics* **2013**, *32*, 498–508.
- (98) Cantat, T.; Mézailles, N.; Auffrant, A.; Le Floch, P. Bis-Phosphorus Stabilised Carbene Complexes. *Dalt. Trans.* **2008**, *0*, 1957–1972.
- (99) Corbridge, D. E. C. *Phosphorus Chemistry, Biochemistry and Technology*, 6th Ed.; CRC Press, Taylor & Francis Group: Boca Raton, FL, USA, 2013, pp 79, 81, 1344–1346.
- (100) Izod, K.; Rayner, D. G.; El-Hamruni, S. M.; Harrington, R. W.; Baisch, U. Stabilization of a Diphosphagermylene through Pπ-Pπ Interactions with a Trigonal-Planar Phosphorus Center. *Angew. Chemie Int. Ed. English* **2014**, *53*, 3636–3640.

- (101) Baceiredo, A.; Bertrand, G.; Sicard, G. Synthesis of the First α -Diazophosphines. Phosphorous-Carbon Multiple-Bond Character of Phosphinocarbenes. *J. Am. Chem. Soc.* **1985**, *107*, 4781–4783.
- (102) Soleilhavoup, M.; Alcaraz, G.; Reau, R.; Bachredo, A.; Bertrand, G. Phosphanlycarbenes: From Unstable Intermediates to X-Ray Characterized Compounds. *Phosphorus. Sulfur. Silicon Relat. Elem.* **1993**, *76*, 49–52.
- (103) Römer, B.; Gatev, G. G.; Zhong, M.; Brauman, J. I. α -Stabilization By Silyl and Phosphino Substitution. *J. Am. Chem. Soc.* **1998**, *120*, 2919–2924.
- (104) Dixon, D. A.; Dobbs, K. D.; Arduengo III, A. J.; Bertrand, G. Electronic Structure of λ^5 -Phosphaacetylene and Corresponding Triplet Methylenes. *J. Am. Chem. Soc.* **1991**, *113*, 8782–8785.
- (105) Leysens, T.; Peeters, D. Negative Hyperconjugation in Phosphorus Stabilized Carbanions. *J. Org. Chem.* **2008**, *73*, 2725–2730.
- (106) Dobado, J. A.; Martinez-Garcia, H.; Molina Molina, J.; Sundberg, M. R. Chemical Bonding in Hypervalent Molecules Revised. 3.† Application of the Atoms in Molecules Theory to Y_3X-CH_2 ($X = N, P, \text{ or } As; Y = H \text{ or } F$) and H_2X-CH_2 ($X = O, S, \text{ or } Se$) Ylides. *J. Am. Chem. Soc.* **2000**, *122*, 1144–1149.
- (107) Heuclin, H.; Grounstein, D.; Le Goff, X.-F.; Le Floch, P.; Mezailles, N. Phosphorus Stabilized Carbene Complexes: Bisphosphonate Dianion Synthesis, Reactivity and DFT Studies of O~C~O Zirconium(IV) Complexes. *Dalt. Trans.* **2010**, *39*, 492–499.
- (108) Leung, W. P.; Wan, C. L.; Mak, T. C. W. Synthesis and Structure of Magnesium and Group 13 Metal Bis(Thiophosphinoyl)Methanediide Complexes. *Organometallics* **2010**, *29*, 1622–1628.
- (109) Orzechowski, L.; Harder, S. Syntheses, Structures, and Reactivity of Barium Carbene Complexes with Chelating Bis-Iminophosphorano Arms. *Organometallics* **2007**, *26*, 5501–5506.
- (110) Orzechowski, L.; Harder, S. Isolation of an Intermediate in the Catalytic Trimerization of Isocyanates by a Monomeric Calcium Carbene with Chelating Iminophosphorane Substituents. *Organometallics* **2007**, *26*, 2144–2148.
- (111) Cowley, A. H.; Gabbai, F. P.; Carrano, C. J.; Mokry, L. M.; Bond, M. R.; Bertrand, G. Reactivity of a Phosphanlycarbene (λ^5 -Phosphaacetylene) with Lewis Acids: X-Ray Crystal Structures of the First Carbene-Gallane Complex and C-Gallyl-Substituted Phosphorus Ylide. *Angew. Chemie Int. Ed. English* **1994**, *33*, 578–580.
- (112) Thirumoorthi, R.; Chivers, T.; Vargas-Baca, I. Experimental and Theoretical Investigations of Tellurium(IV) Methanediides and Their Insertion Products with Sulfur and Iodine. *Organometallics* **2012**, *31*, 627–636.
- (113) El-Hellani, A.; Monot, J.; Tang, S.; Guillot, R.; Bour, C.; Gandon, V. Relationship between Gallium Pyramidalization in $L\cdot GaCl_3$ Complexes and the Electronic Ligand Properties. *Inorg. Chem.* **2013**, *52*, 11493–11502.
- (114) Petz, W.; Dehnicke, K.; Holzmann, N.; Frenking, G.; Neumüller, B. The Reaction of $BeCl_2$ with Carbodiphosphorane $C(PPh_3)_2$; Experimental and Theoretical Studies. *Zeitschrift für Anorg. und Allg. Chemie* **2011**, *637*, 1702–1710.

- (115) Wooles, A. J.; Cooper, O. J.; McMaster, J.; Lewis, W.; Blake, A. J.; Liddle, S. T. Synthesis and Characterization of Dysprosium and Lanthanum Bis(Iminophosphorano)Methanide and -Methanediide Complexes. *Organometallics* **2010**, *29*, 2315–2321.
- (116) Al-Benna, S.; Sarsfield, M. J.; Thornton-Pett, M.; Ormsby, D. L.; Maddox, P. J.; Brès, P.; Bochmann, M. Sterically Hindered Iminophosphorane Complexes of Vanadium, Iron, Cobalt and Nickel: A Synthetic, Structural and Catalytic Study †. *J. Chem. Soc. Dalton Trans.* **2000**, *0*, 4247–4257.
- (117) Southern, J. M.; O’Neil, I. A. Preparation and Reactions of Iminophosphoranes and Their Synthetic Applications in the Aza-Wittig Reaction. In *Organophosphorus Reagents A Practical Approach in Chemistry*; Murphy, P. J., Ed.; Oxford University Press: Oxford, 2004; pp 140, 143, 153, 196.
- (118) Imhoff, P.; Asselt, R. Van; Elsevier, C. J.; Vrieze, K.; Goubitz, K.; Van Malssen, K. F.; Stam, C. H. SYNTHESIS, STRUCTURE AND REACTIVITY OF BIS(N-ARYL-IMINOPHOSPHORANYL)METHANES. X-RAY CRYSTAL STRUCTURES OF (4-CH₃-C₆H₄-N=PPh₂)₂CH₂ AND (4-NO₂-C₆H₄-N=PPh₂)₂CH₂. *Phosphorus. Sulfur. Silicon Relat. Elem.* **1990**, *47*, 401–415.
- (119) Horner, L.; Oediger, H. Phosphinimino-Verbindungen Aus Phosphindihalogeniden Und Primären Aminem. *Justus Liebigs Ann. Chem.* **1959**, *627*, 142–162.
- (120) Zimmer, H.; Singh, G. Synthesis of Some Triphenylphosphinalkylimines and Mono- and Dialkylaminotriphenylphosphonium Halides. *J. Org. Chem.* **1963**, *28*, 483–486.
- (121) Klemp, C.; Buchard, A.; Houdard, R.; Auffrant, A.; Mezailles, N.; Le Goff, X. F.; Ricard, L.; Saussine, L.; Magna, L.; Le Floch, P. Chromium (III)-Bis(Iminophosphoranyl)Methanido Complexes: Synthesis, X-Ray Crystal Structures and Catalytic Ethylene Oligomerization. *New J. Chem.* **2009**, *33*, 1748–1752.
- (122) Ong, C. M.; Stephan, D. W. Lithiations of Bis-Diphenyl-N-Trimethylsilylphosphiniminomethane: An X-Ray Structure of a 1,1-Dilithiomethane Derivative. *J. Am. Chem. Soc.* **1999**, *121*, 2939–2940.
- (123) Cantat, T.; Jaroschik, F.; Ricard, L.; Le Floch, P.; Nief, F.; Mézailles, N. Thulium Alkylidene Complexes: Synthesis, X-Ray Structures, and Reactivity. *Organometallics* **2006**, *25*, 1329–1332.
- (124) Cantat, T.; Mezailles, N.; Ricard, L.; Jean, Y.; Le Floch, P. A Bis(Thiophosphinoyl)Methanediide Palladium Complex: Coordinated Dianion or Nucleophilic Carbene Complex? *Angew. Chemie Int. Ed. English* **2004**, *43*, 6382–6385.
- (125) Errington, R. J. *Advanced Practical Inorganic and Metalorganic Chemistry*, 1st Ed.; Blackie Academic & Professional: London, 1997, pp 123.
- (126) Narayan, S.; Muldoon, J.; Finn, M. G.; Fokin, V. V.; Kolb, H. C.; Sharpless, K. B. “On Water”: Unique Reactivity of Organic Compounds in Aqueous Suspension. *Angew. Chemie Int. Ed. English* **2005**, *44*, 3275–3279.
- (127) Mioduski, T.; Gumiński, C.; Zeng, D. IUPAC-NIST Solubility Data Series. 87. Rare Earth Metal Chlorides in Water and Aqueous Systems. Part 1. Scandium Group (Sc, Y, La). *J. Phys. Chem. Ref. Data* **2008**, *37*, 1765–1853.

- (128) Mioduski, T.; Gumiński, C.; Zeng, D. IUPAC-NIST Solubility Data Series. 87. Rare Earth Metal Chlorides in Water and Aqueous Systems. Part 3. Heavy Lanthanides (Gd–Lu). *J. Phys. Chem. Ref. Data* **2009**, *38*, 925.
- (129) Mioduski, T.; Gumiński, C.; Zeng, D. IUPAC-NIST Solubility Data Series. 87. Rare Earth Metal Chlorides in Water and Aqueous Systems. Part 2. Light Lanthanides (Ce–Eu). *J. Phys. Chem. Ref. Data* **2009**, *38*, 441–562.
- (130) Mioduski, T.; Gumiński, C.; Zeng, D. IUPAC-NIST Solubility Data Series. 100. Rare Earth Metal Fluorides in Water and Aqueous Systems. Part 1. Scandium Group (Sc, Y, La). *J. Phys. Chem. Ref. Data* **2014**, *43*, 013105.
- (131) Mioduski, T.; Gumiński, C.; Zeng, D. IUPAC-NIST Solubility Data Series. 100. Rare Earth Metal Fluorides in Water and Aqueous Systems. Part 2. Light Lanthanides (Ce–Eu). *J. Phys. Chem. Ref. Data* **2015**, *44*, 013102.
- (132) Mioduski, T.; Salomon, M. *Scandium, Yttrium, Lanthanum and Lanthanide Halides in Nonaqueous Solvents* 22; Kertes, A. S., Ed.; IUPAC Secretariat: Oxford, 1985, pp 1–396.
- (133) Miyamoto, H.; Miyamoto, R.; Gumiński, C.; Salomon, M.; Balarew, C.; Zagnit'ko, E. V.; Eyseltova, J.; Counioux, J.-J. IUPAC-NIST Solubility Data Series. 85. Transition and 12–14 Main Group Metals, Lanthanide, Actinide, and Ammonium Halates. *J. Phys. Chem. Ref. Data* **2008**, *37*, 933.
- (134) Abbasi, A.; Risberg, E. D.; Eriksson, L.; Mink, J.; Persson, I.; Sandstrom, M.; Sidorov, Y. V.; Skripkin, M. Y.; Ullstrom, A. S. Crystallographic and Vibrational Spectroscopic Studies of Octakis(DMSO)Lanthanoid(III) Iodides. *Inorg. Chem.* **2007**, *46*, 7731–7741.
- (135) Semenova, L. I.; Skelton, B. W.; White, A. H. Structural Systematics of Rare Earth Complexes. VIII The Rare Earth(III) Nitrate/Dimethyl Sulfoxide Adducts [(DMSO)_nLn(O₂NO)₃]. *Aust. J. Chem.* **1996**, *49*, 997–1004.
- (136) Nolan, S. P.; Stern, D.; Marks, T. J. Organo-f-Element Thermochemistry. Absolute Metal-Ligand Bond Disruption Enthalpies in Bis(Pentamethylcyclopentadienyl)Samarium Hydrocarbyl, Hydride, Dialkylamide, Alkoxide, Halide, Thiolate, and Phosphide Complexes. Implications for Organolanthanide Bonding. *J. Am. Chem. Soc.* **1989**, *111*, 7844–7853.
- (137) Izod, K.; Liddle, S. T.; Clegg, W. A Convenient Route to Lanthanide Triiodide THF Solvates. Crystal Structures of LnI₃(THF)₄ [Ln = Pr] and LnI₃(THF)_{3.5} [Ln = Nd, Gd, Y]. *Inorg. Chem.* **2004**, *43*, 214–218.
- (138) Taylor, M. D.; Carter, C. P. Preparation of Anhydrous Lanthanide Halides, Especially Iodides. *J. Inorg. Nucl. Chem.* **1962**, *24*, 387–391.
- (139) Taylor, M. D. Preparation of Anhydrous Lanthanide Halides. *Chem. Rev.* **1961**, *62*, 503–511.
- (140) Young, R. C.; Hastings, J. L. Reaction of Lanthanum Oxide with Ammonium Iodide. *J. Am. Chem. Soc.* **1937**, *59*, 765–766.
- (141) Barnhart, D. M.; Frankcom, T. M.; Gordon, P. L.; Sauer, N. N.; Thompson, J. A.; Watkin, J. G. Dissolution of Lanthanide and Actinide Metals Using Iodine and 2-Propanol. Synthesis and X-Ray Crystal Structures of LnI₃(HO-*i*-Pr)₄ (Ln = La, Ce) and Th₂I₄(O-*i*-Pr)₄(HO-*i*-Pr)₂. *Inorg. Chem.* **1995**, *34*, 4862–4867.

- (142) Burin, M. E.; Fukin, G. K.; Bochkarev, M. N. Complexes of Neodymium and Dysprosium Triiodides with Amines. Molecular Structures $\{\text{Dy}[\text{Me}_2\text{N}(\text{CH}_2)_3\text{NH}_2]_8\}_3\text{I}_3$, $\text{NdI}_3(\text{Pr}^i\text{NH}_2)_4$, and $\text{NdI}_3(\text{Pr}^i\text{NH}_2)_5$ complexes*. *Russ. Chem. Bull.* **2007**, *56*, 1736–1741.
- (143) Brown, J. L.; Davis, B. L.; Scott, B. L.; Gaunt, A. J. Early-Lanthanide(III) Acetonitrile-Solvento Adducts with Iodide and Noncoordinating Anions. *Inorg. Chem.* **2015**, *54*, 11958–11968.
- (144) Girard, P.; Namy, J. .; Kagan, H. . Divalent Lanthanide Derivatives in Organic Synthesis. 1. Mild Preparation of SmI_2 and YbI_2 and Their Use as Reducing or Coupling Agents. *J. Am. Chem. Soc.* **1980**, *102*, 2693–2698.
- (145) Watson, P. L.; Tulip, T. H.; Williams, I. Defluorination of Perfluoroolefins by Divalent Lanthanoid Reagents: Activating Carbon-Fluorine Bonds. *Organometallics* **1990**, *9*, 1999–2009.
- (146) Bochkarev, M. N.; Fedushkin, I. L.; Fagin, A. A.; Petrovskaya, T. V.; Ziller, J. W.; Broomhall-dillard, R. N. R.; Evans, W. J. Synthesis and Structure of the First Molecular Thulium(II) Complex: $[\text{TmI}_2(\text{MeOCH}_2\text{CH}_2\text{OMe})_3]$. *Angew. Chemie Int. Ed. English* **1997**, *36*, 133–135.
- (147) Bochkarev, M. N.; Fagin, A. A. A New Route to Neodymium(II) and Dysprosium(II) Iodides. *Chem. - A Eur. J.* **1999**, *5*, 2990–2992.
- (148) Bochkarev, M. N.; Khoroshenkov, G. V.; Burin, M. E.; Kuzyaev, D. M.; Fagin, A. A.; Maleev, A. A.; Fukin, G. K.; Baranov, E. V. Letters to the Editor Complexes of Lanthanide (II) Diiodides with Isopropylamine. *Russ. Chem. Bull. Int. Ed.* **2006**, *55*, 588–590.
- (149) Emge, T. J.; Kornienko, A.; Brennan, J. G. Trans Influence in a Mer-Octahedral Triiodidolanthanide: Triiodidotris(Tetrahydrofuran- κ -O)Ytterbium(III). *Acta Crystallogr. Sect. C Cryst. Struct. Commun.* **2009**, *65*, m422–m425.
- (150) Hazin, P. N.; Huffman, J. C.; Bruno, J. W. Synthetic and Structural Studies of Pentamethylcyclopentadienyl Complexes of Lanthanum and Cerium. *Organometallics* **1987**, *6*, 23–27.
- (151) Balashova, T. V.; Kusyaev, D. M.; Kulikova, T. I.; Kuznetsova, O. N.; Edelmann, F. T.; Gießmann, S.; Blaurock, S.; Bochkarev, M. N. Use of Neodymium Diiodide in the Synthesis of Organosilicon, -Germanium and -Tin Compounds. *Zeitschrift fur Anorg. und Allg. Chemie* **2007**, *633*, 256–260.
- (152) Khoroshenkov, G. V.; Fagin, A. A.; Bochkarev, M. N.; Dechert, S.; Schumann, H. Reactions of Neodymium(II), Dysprosium(II), and Thulium(II) Diiodides with Cyclopentadiene. Molecular Structures of Complexes $\text{CpTmI}_2(\text{THF})_3$ and $[\text{NdI}_2(\text{THF})_5]^+[\text{NdI}_4(\text{THF})_2]^-$. *Russ. Chem. Bull. Int. Ed.* **2003**, *52*, 1715–1719.
- (153) Xie, Z.; Chiu, K.; Wu, B.; Mak, T. C. W. Autoionization of SmI_3 in Tetrahydrofuran. X-Ray Crystal Structure of the Ionic Complex $[\text{SmI}_2(\text{THF})_5][\text{SmI}_4(\text{THF})_2]$. *Inorg. Chem.* **1996**, *35*, 5957–5958.
- (154) Bochkarev, M. N.; Petrov, B. I.; Fedyushkin, I. L.; Petrovskaya, T. V.; Nevodchikov, V. I.; Patrikeeva, N. B.; Zakharov, L. N.; Struchkov, Y. T. Anionic Bipyridyl Complexes of Lanthanides. Structure of $[\text{Yb}(\text{Bipy})_3][\text{Li}(\text{THF})_4]$. *Russ. Chem. Bull.* **1997**, *46*, 371–373.

- (155) Kuehl, C. J.; Simpson, C. K.; John, K. D.; Sattelberger, A. P.; Carlson, C. N.; Hanusa, T. P. Monomeric F-Element Chemistry with Sterically Encumbered Allyl Ligands. *J. Organomet. Chem.* **2003**, *683*, 149–154.
- (156) Yatabe, T.; Nakai, H.; Nozaki, K.; Yamamura, T.; Isobe, K. Photofunctionalization of a Pentamethylcyclopentadienyl Ligand with the N-Phenylcarbazolyl Group to Prepare a Highly Luminescent Tb³⁺ Complex Having a Fast Radiation Rate. *Organometallics* **2010**, *29*, 2390–2393.
- (157) Niemeyer, M. Trans -Diodopentakis(Tetrahydrofuran)Ytterbium(III) Tetraiodo-Trans-Bis(Tetrahydrofuran)Ytterbium(III). *Acta Crystallogr. Sect. E Crystallogr. Commun.* **2001**, *57*, m363–m364.
- (158) Giesbrecht, G. R.; Gordon, J. C.; Clark, D. L.; Scott, B. L. Auto-Ionization in Lutetium Iodide Complexes : Effect of the Ionic Radius on Lanthanide – Iodide Binding. *Inorg. Chem.* **2004**, *43*, 1065–1070.
- (159) Anfang, S.; Karl, M.; Faza, N.; Massa, W.; Magull, J.; Dehnicke, K. Synthese Und Kristallstrukturen Der Seltenerd-Komplexe [LaI₂(THF)₅]⁺I₃⁻, [SmCl₃(THF)₄], [ErCl₂(THF)₅]⁺[ErCl₄(THF)₂]⁻. *Zeitschrift fur Anorg. und Allg. Chemie* **1997**, *632*, 1425–1432.
- (160) Shannon, R. D. Revised Effective Ionic Radii and Systematic Studies of Interatomic Distances in Halides and Chalcogenides. *Acta Crystallogr. Sect. A Found. Adv.* **1976**, *32*, 751–767.
- (161) Piers, W. E.; Emslie, D. J. H. Non-Cyclopentadienyl Ancillaries in Organogroup 3 Metal Chemistry: A Fine Balance in Ligand Design. *Coord. Chem. Rev.* **2002**, *233–234*, 131–155.
- (162) Minhas, R. K.; Ma, Y.; Song, J.-I.; Gambarotta, S. Synthesis, Reactivity, and Stability of Di- and Trivalent Samarium Amides. *Inorg. Chem.* **1996**, *35*, 1866–1873.
- (163) Liddle, S. T.; McMaster, J.; Green, C.; Arnold, P. L.; Green, J. C. Synthesis and Structural Characterisation of an Yttrium-Alkyl-Alkylidene. *Chem. Commun.* **2008**, *78*, 1747–1749.
- (164) Lappert, M. F.; Pearce, R. Stable Silylmethyl and Neopentyl Complexes of Scandium(III) and Yttrium(III). *J. Chem. Soc. Chem. Commun.* **1973**, No. 126, 126.
- (165) Schumann, H.; Glanz, M.; Winterfeld, J.; Hemling, H.; Kuhn, N.; Kratz, T. Organolanthanoid-Carbene-Adducts. *Angew. Chemie Int. Ed. English* **1994**, *669*, 12–13.
- (166) Schumann, H.; Glanza, M.; Winterfeld, J.; Hemling, H.; Kuhn, N.; Jratz, T. Carben-Addukte Des Zweiwertigen Samariums Und Ytterbiums. *Chem. Ber.* **1994**, *127*, 2369–2372.
- (167) Herrmann, W. A.; Munck, F. C.; Artus, G. R. J.; Runte, O.; Anwender, R. 1,3-Dimethylimidazolin-2-Ylidene Carbene Donor Ligation in Lanthanide Silylamide Complexes. *Organometallics* **1997**, *16*, 682–688.
- (168) Arnold, P. L.; Mungur, S. A.; Blake, A. J.; Wilson, C. Anionic Amido N-Heterocyclic Carbenes: Synthesis of Covalently Tethered Lanthanide-Carbene Complexes. *Angew. Chemie Int. Ed. English* **2003**, *42*, 5981–5984.

- (169) Liddle, S. T.; Arnold, P. L. Synthesis of Heteroleptic Cerium(III) Anionic Amido-Tethered N-Heterocyclic Carbene Complexes. *Organometallics* **2005**, *24*, 2597–2605.
- (170) Fegler, W.; Spaniol, T. P.; Okuda, J. Trimethylsilylmethyl Complexes of the Rare-Earth Metals with Sterically Hindered N-Heterocyclic Carbene Ligands: Adduct Formation and C–H Bond Activation. *Dalt. Trans.* **2010**, *39*, 6774–6779.
- (171) Long, S.; Wang, B.; Xie, H.; Yao, C.; Wu, C.; Cui, D. Rare-Earth Metal Alkyl Complexes Bearing an Alkoxy N-Heterocyclic Carbene Ligand: Synthesis, Characterization, Catalysis for Isoprene Polymerization. *New J. Chem.* **2015**, *39*, 7682–7687.
- (172) Yao, H.; Zhang, J.; Zhang, Y.; Sun, H.; Shen, Q. Synthesis of Cationic N-Heterocyclic Carbene Lanthanide Bromide and the Influence of N-Heterocyclic Carbene and Lanthanide Metals. *Organometallics* **2010**, *29*, 5841–5846.
- (173) Simler, T.; Feuerstein, T. J.; Roesky, P. W.; Yadav, R.; Gamer, M. T. Access to Divalent Lanthanide NHC Complexes by Redox-Transmetalation from Silver and CO₂ Insertion Reactions†. *Chem. Commun.* **2019**, *55*, 222–225.
- (174) Lv, K.; Cui, D. CCC-Pincer Bis(Carbene) Lanthanide Dibromides. Catalysis on Highly Cis-1,4-Selective Polymerization of Isoprene and Active Species. *Organometallics* **2010**, *29*, 2987–2993.
- (175) Glanz, M.; Dechert, S.; Schumann, H.; Wolff, D.; Wolff, D.; Springer, J. Der Einfluß Der Koordinationssphäre von Samarocenen Auf Die Synthese von Flüssigkristallinen Polymethacrylaten. *Zeitschrift für Anorg. und Allg. Chemie* **2000**, *626*, 2467–2477.
- (176) Yao, C.; Wu, C.; Wang, B.; Cui, D. Copolymerization of Ethylene with 1-Hexene and 1-Octene Catalyzed by Fluorenyl N-Heterocyclic Carbene Ligated Rare-Earth Metal Precursors. *Organometallics* **2013**, *32*, 2204–2209.
- (177) Giesbrecht, G. R.; Gordon, J. C. Lanthanide Alkylidene and Imido Complexes. *Dalt. Trans.* **2004**, *0*, 2387–2393.
- (178) Schumann, H.; Müller, J. Metallorganische Verbindungen Der Lanthaniden. VI. Neutrale Und Anionische Alkyliden-Komplexe von Erbium Und Lutetium. *J. Organomet. Chem.* **1979**, *169*, C1–C4.
- (179) Dietrich, H. M.; Toernoos, K. W.; Anwander, R. “Ionic Carbenes”: Synthesis, Structural Characterization, and Reactivity of Rare-Earth Metal Methylidene Complexes. *J. Am. Chem. Soc.* **2006**, *4*, 9298–9299.
- (180) Zimmermann, M.; Takats, J.; Kiel, G.; Törnroos, K. W.; Anwander, R. Ln(III) Methyl and Methylidene Complexes Stabilized by a Bulky Hydrotris(Pyrazolyl)Borate Ligand. *Chem. Commun.* **2008**, *0*, 612–614.
- (181) Venugopal, A.; Kamps, I.; Bojer, D.; Berger, R. J. F.; Mix, A.; Willner, A.; Neumann, B.; Stammler, H.-G.; Mitzel, N. W. Neutral Ligand Induced Methane Elimination from Rare-Earth Metal Tetramethylaluminates up to the Six-Coordinate Carbide State. *Dalt. Trans.* **2009**, *0*, 5755.
- (182) Li, S.; Wang, M.; Liu, B.; Li, L.; Cheng, J.; Wu, C.; Liu, D.; Liu, J.; Cui, D. Lutetium-Methanediide-Alkyl Complexes: Synthesis and Chemistry. *Chem. - A Eur. J.* **2014**, *20*, 15493–15498.

- (183) Litlabø, R.; Zimmermann, M.; Saliu, K.; Takats, J.; Törnroos, K. W.; Anwander, R. A Rare-Earth Metal Variant of the Tebbe Reagent. *Angew. Chemie Int. Ed. English* **2008**, *47*, 9560–9564.
- (184) Scott, J.; Fan, H.; Wicker, B. F.; Fout, A. R.; Baik, M. H.; Mindiola, D. J. Lewis Acid Stabilized Methylidene and Oxoscandium Complexes. *J. Am. Chem. Soc.* **2008**, *130*, 14438–14439.
- (185) Bojer, D.; Neumann, B.; Stammler, H.-G.; Mitzel, N. W. Subtle Size Effects in C-H Activation Reactions of Lanthanum and Praseodymium Tetramethylaluminates by Neutral Trinitrogen Bases. *Eur. J. Inorg. Chem.* **2011**, *2011*, 3791–3796.
- (186) Cavell, R. G.; Babu, R. P. K.; Aparna, K.; McDonald, R. Early Transition Metal and Lanthanide Bis(Iminophosphorano)Methandiide Complexes; “pincer” and Bridging Bis(Phosphorus) Metal Carbenes. *J. Organomet. Chem.* **2001**, *617–618*, 158–169.
- (187) Marshall, G.; Wooles, A.; Mills, D.; Lewis, W.; Blake, A.; Liddle, S. Synthesis and Characterisation of Lanthanide N-Trimethylsilyl and -Mesityl Functionalised Bis(Iminophosphorano)Methanides and -Methanediides. *Inorganics* **2013**, *1*, 46–69.
- (188) Mills, D. P.; Cooper, O. J.; McMaster, J.; Lewis, W.; Liddle, S. T. Synthesis and Reactivity of the Yttrium-Alkyl-Carbene Complex [Y(BIPM)(CH₂C₆H₅)(THF)] (BIPM = {C(PPh₂NSiMe₃)₂}). *Dalt. Trans.* **2009**, No. 23, 4547–4555.
- (189) Groom, C. R.; Bruno, I. J.; Lightfoot, M. P.; Ward, S. C. The Cambridge Structural Database. *Acta Crystallogr. Sect. B Struct. Sci. Cryst. Eng. Mater.* **2016**, *72*, 171–179.
- (190) Liddle, S. T.; Mills, D. P.; Gardner, B. M.; McMaster, J.; Jones, C.; Woodul, W. D. A Heterobimetallic Gallyl Complex Containing an Unsupported Ga-Y Bond. *Inorg. Chem.* **2009**, *48*, 3520–3522.
- (191) Wooles, A. J.; Gregson, M.; Cooper, O. J.; Middleton-Gear, A.; Mills, D. P.; Lewis, W.; Blake, A. J.; Liddle, S. T. Group 1 Bis(Iminophosphorano)Methanides, Part 1: N-Alkyl and Silyl Derivatives of the Sterically Demanding Methanes H₂C(PPh₂NR)₂ (R = Adamantyl and Trimethylsilyl). *Organometallics* **2011**, *30*, 5314–5325.
- (192) Wooles, A. J.; Gregson, M.; Robinson, S.; Cooper, O. J.; Mills, D. P.; Lewis, W.; Blake, A. J.; Liddle, S. T. Group 1 Bis(Iminophosphorano)Methanides, Part 2 : N-Aryl Derivatives of the Sterically Demanding Methanes H₂C(PPh₂NR)₂ (R = 2,4,6-Trimethylphenyl or 2,6-Diisopropylphenyl). *Organometallics* **2011**, *30*, 5326–5337.
- (193) Ortu, F.; Gregson, M.; Wooles, A. J.; Mills, D. P.; Liddle, S. T. Yttrium Methanide and Methanediide Bis(Silyl)Amide Complexes. *Organometallics* **2017**, *36*, 4584–4591.
- (194) Gregson, M.; Lu, E.; Mills, D. P.; Tuna, F.; McInnes, E. J. L.; Hennig, C.; Scheinost, A. C.; McMaster, J.; Lewis, W.; Blake, A. J.; et al. The Inverse-Trans-Influence in Tetravalent Lanthanide and Actinide Bis(Carbene) Complexes. *Nat. Commun.* **2017**, *8*, 1–11.
- (195) Zhu, Q.; Zhu, J.; Zhu, C. Recent Progress in the Chemistry of Lanthanide-Ligand Multiple Bonds. *Tetrahedron Lett.* **2018**, *59*, 514–520.

- (196) Ge, S.; Zhao, J.; Ferguson, M. J.; Ma, G.; Cavell, R. G. Rare Carbon-Bridged Bimetallic Lanthanide (Nd or Sm) and Tl(I) Geminal Carbon Derivatives of a Bis (Iminophosphorano)Methanediide. *Organometallics* **2020**, *39*, 478–486.
- (197) Fustier, M.; Le Goff, X. F.; Le Floch, P.; Mézailles, N. Nucleophilic Scandium Carbene Complexes. *J. Am. Chem. Soc.* **2010**, *132*, 13108–13110.
- (198) Fustier, M.; Le Goff, X. F.; Lutz, M.; Slootweg, J. C.; Mézailles, N. Scandium Carbene Complexes: Synthesis of Mixed Alkyl, Amido, and Phosphido Derivatives. *Organometallics* **2015**, *34*, 63–72.
- (199) Goehring, M.; Niedenzu, K. Diphosphorsäure-Tetrakis-Dimethylamid. *Angew. Chemie* **1956**, *68*, 1956.
- (200) Wang, G. C.; Sung, H. H. Y.; Williams, I. D.; Leung, W. H. Tetravalent Titanium, Zirconium, and Cerium Oxo and Peroxo Complexes Containing an Imidodiphosphate Ligand. *Inorg. Chem.* **2012**, *51*, 3640–3647.
- (201) Lickerish, L. A. STUDIES ON COMMERCIAL OCTAMETHYLPYROPHOSPHOR-AMIDE (SCHRADAN) V.*-Insecticidal Comparisons of the Two Main Constituents. *J. Sci. Food Agric.* **1953**, *4*, 24–28.
- (202) Rediske, J. H.; Lawrence, W. H. Octamethylpyrophosphoramidate (OMPA) As a Systemic Animal Repellent for Douglas-Fir Seedlings. *For. Sci.* **1964**, *10*, 93–103.
- (203) Tsuyuki, H.; Stahmann, M. A.; Casida, J. E. Preparation, Purification, Isomerisation and Biological Properties of Octamethyl Pyrophosphoramidate N-Oxide. *J. Agric. Food Chem.* **1955**, *3*, 922–932.
- (204) Saito, T. Selective Toxicity of Systemic Insecticides. In *Experimental approaches to pesticide metabolism, degradation, and mode of action*; Gunther, F.A., Eds.; Residue Reviews; Springer-Verlag: New York, 1967; Vol. 25, pp 175–186.
- (205) Agriculture & Environment Research Unit at the University of Hertfordshire. Pesticide Properties Database (PPDB) <https://sitem.herts.ac.uk/aeru/iupac/Reports/1678.htm> (accessed Oct 26, 2019).
- (206) Pianka, M. ORGANO-PHOSPHORUS COMPOUNDS. I. Interaction of Organic Phosphorohalogenides with Solid Alkalis: A New Synthesis of Schradan. *J. Appl. Chem.* **1956**, *5*, 109–120.
- (207) du Preez, J. G. H.; Sadie, F. G. HEXAMETHYLPHOSPHORAMIDE AND OCTAMETHYLPYROPHOSPHORAMIDE COMPLEXES OF TETRAVALENT METAL CHLORIDES. *J. South African Chem. Inst.* **1966**, *19*, 73–84.
- (208) Joesten, M. D.; Hussain, M. S.; Lenhert, P. G. Structure Studies of Pyrophosphate Chelate Rings. I. The Crystal Structures of Tris-Octamethylpyrophosphoramidate Complexes of Cobalt (II), Magnesium (II) and Copper (II) Perchlorates. *Inorg. Chem.* **1970**, *9*, 151–161.
- (209) Hussain, M. S.; Joesten, M. D.; Lenhert, P. G. Structure Studies of Pyrophosphate Chelate Rings. II. The Crystal Structure of Bis(Perchlorato)Bis(Octamethylpyrophosphoramidate)Copper(II). *Inorg. Chem.* **1970**, *9*, 162–168.

- (210) Kepert, D. L.; Patrick, J. M.; White, A. H. Structure and Stereochemistry in *f*-Block Complexes of High Co-Ordination Number. Part 3.* The [M(Bidentate Ligand)₂(Unidentate Ligand)₄] System: Crystal Structures of Tetrakis(isothiocyanato)-bis(octamethylpyrophosphoramidate-OO⁻)uranium(IV) and Tetrachlorobis(octamethylpyrophosphoramidate-OO⁻)thorium(IV). *Dalt. Trans.* **1983**, 0, 559–566.
- (211) Cameron, T. S.; Cordes, R. E.; Jackman, F. A. Synthesis and Crystal Structure of μ -Oxo-Bis(Phosphenyl-Ortho-Toluidide). *Zeitschrift fur Naturforsch. - Sect. B J. Chem. Sci.* **1978**, 33, 728–730.
- (212) Pourayoubi, M.; Padělková, Z.; Rostami Chaijan, M.; Růžička, A. N,N',N'',N'''-Tetrakis(2-Methylphenyl)-Oxybis(Phosphonic Diamide): A Redetermination at 150 K with Mo K Radiation. *Acta Crystallogr. Sect. E Crystallogr. Commun.* **2011**, 67, 466–470.
- (213) Tarahhomi, A.; Pourayoubi, M.; Fejfarová, K.; Dusek, M. A Novel Amido-pyrophosphate MnII Chelate Complex with the Synthetic Ligand O{P(O)[NHC(CH₃)₃]₂}₂(L): [Mn(L)₂{OC(H)N(CH₃)₂}]₂Cl₂.2H₂O. *Acta Crystallogr. Sect. C Struct. Chem.* **2013**, 69, 225–229.
- (214) Tarahhomi, A.; Pourayoubi, M.; Golen, J. A.; Zargaran, P.; Elahi, B.; Rheingold, A. L.; Leyva Ramírez, M. A.; Mancilla Percino, T. Hirshfeld Surface Analysis of New Phosphoramidates. *Acta Crystallogr. Sect. B Struct. Sci. Cryst. Eng. Mater.* **2013**, 69, 260–270.
- (215) Merck; Sigma-Aldrich. Tetraisopropyl pyrophosphoramidate information page <https://www.sigmaaldrich.com/catalog/product/sigma/t1505?lang=en®ion=MT> (accessed Oct 26, 2019).
- (216) Schmidpeter, A.; Ebeling, J. Methyl-Imidodiphosphinsäuren, Ihre Trichloride Und Diamid-Chloride. *Chem. Ber.* **1968**, 101, 815–823.
- (217) Husebye, S.; Maartmann-Moe, K. A Planar, Four-Coordinate Se(II) Compound. The Preparation and Crystal Structure of Bis(Imidotetraphenyldithiophosphino-S,S')Selenium(II). *Acta Chem. Scand.* **1983**, A 37, 219–225.
- (218) Cupertino, D.; Keyte, R.; Slawin, A. M. Z.; Williams, D. J.; Woollins, J. D. Preparation and Single-Crystal Characterization of ⁱPr₂P(S)NHP(S)ⁱPr₂ and Homoleptic [ⁱPr₂P(S)NP(S)ⁱPr₂]⁻ Complexes of Zinc, Cadmium, and Nickel. *Inorg. Chem.* **1996**, 35, 2695–2697.
- (219) Cupertino, D. C.; Keyte, R. W.; Slawin, A. M. Z.; Woollins, J. D. Synthesis and Coordination Chemistry of Tetrabutylthioimidodiphosphinates. *Polyhedron* **1999**, 18, 707–716.
- (220) Cupertino, D.; Birdsall, D. J.; Slawin, A. M. Z.; Woollins, J. D. The Preparation and Coordination Chemistry of ⁱPr₂P(E)NHP(E')ⁱPr₂ (E, E' = Se; E = Se, E' = S; E = S, E' = O; E, E' = O). *Inorganica Chim. Acta* **1999**, 290, 1–7.
- (221) Silvestru, C.; Rosler, R.; Haiduc, I.; Cea-Olivares, R.; Espinosa-Perez, G. Crystal and Molecular Structure of Tetramethyldithioimidodiphosphinic Acid, (SPMe₂)₂NH, and Its Cobalt(II) Complex, Co[(SPMe₂)₂N]₂, Containing a Tetrahedral COS₄ Core. *Inorg. Chem.* **1995**, 34, 485–492.
- (222) Husebye, S.; Maartmann-Moe, K. The Crystal Structure of Imidotetraphenyldithiodiphosphinic Acid, a Compound with an N-H...S Hydrogen Bond. *Acta Chem. Scand.* **1983**, A 37, 439–441.

- (223) Slawin, Alexandra M Ward, Joanna Williams, David J Woollins, J. D. Interactions, X-Ray Structure of a Potassium-Sulfur Ladder Polymer with Strong K---Aryl Stabilising. *J. Chem. Soc. Chem. Commun.* **1994**, 5, 421–422.
- (224) Cupertino, D.; Keyte, R.; Slawin, A. M. Z.; Woollins, J. D.; Williams, D. J. THE PREPARATION AND CHARACTERIZATION OF $[M\{N(\text{Pr}^i_2\text{PS})_2\}_2]$ ($M = \text{Pt}$, Pd) AND $[\text{Pd}\{N(\text{Pr}^i_2\text{PS})_2\}\{\text{HN}(\text{Pr}^i_2\text{PS})_2\}]\text{Cl}$. *Polyhedron* **1996**, 15, 4441–4445.
- (225) Bruno, I. J.; Cole, J. C.; Edgington, P. R.; Macrae, C. F.; Pearson, J.; Taylor, R. New Software for Searching the Cambridge Structural Database and Visualizing Crystal Structures. *Acta Crystallogr. Sect. B Struct. Sci. Cryst. Eng. Mater.* **2002**, 58, 389–397.
- (226) N.W.Alcock; P.Moore; P.Williams. CCDC 722732: Experimental Crystal Structure Determination. 2011.
- (227) N.W.Alcock; P.Moore; P.Williams. CCDC 722733: Experimental Crystal Structure Determination. 2011.
- (228) Cheung, W.; Chiu, W.; Williams, I. D.; Leung, W. Ruthenium η^6 -Hexamethylbenzene Complexes Containing Dichalcogenoimidodiphosphate Ligands. *Eur. J. Inorg. Chem.* **2009**, 792–798.
- (229) Pernin, C. G.; Ibers, J. A. Soluble Yttrium Chalcogenides: Syntheses, Structures, and NMR Properties of $\text{Y}[\eta^3\text{-N}(\text{SPPPh}_2)_2]_3$ and $\text{Y}[\eta^2\text{-N}(\text{SePPh}_2)_2][\eta^3\text{-N}(\text{SePPh}_2)_2]$. *Inorg. Chem.* **2000**, 39, 1222–1226.
- (230) Gaunt, A. J.; Scott, B. L.; Neu, M. P. Homoleptic Uranium (III) Imidodiphosphinochalcogenides Including the First Structurally Characterised Molecular Trivalent Actinide–Se Bond. *Chem. Commun.* **2005**, 25, 3215–3217.
- (231) Ingram, K. I. M.; Tassell, M. J.; Gaunt, A. J.; Kaltsoyannis, N. Covalency in the f Element-Chalcogen Bond. Computational Studies of $\text{M}[(\text{NEPR}_2)_2]_3$ ($M = \text{La}$, Ce , Pr , Pm , Eu , U , Np , Pu , Am , Cm ; $E = \text{O}$, S , Se , Te ; $R = \text{H}$, ^iPr , Ph). *Inorg. Chem.* **2008**, 47, 7824–7833.
- (232) Pernin, C. G.; Ibers, J. A. Bis(Cyclopentadienyl)Yttrium Complexes of the Ligand $[\text{N}(\text{QPPH}_2)_2]^-$ ($Q = \text{S}$, Se): Synthesis, Structure, and NMR Properties of $\text{Cp}_2\text{Y}[\eta^3\text{-N}(\text{QPPH}_2)_2]$. *Inorg. Chem.* **1999**, 38, 5478–5483.
- (233) Sekar, P.; Ibers, J. A. Syntheses and Characterization of $\text{Cp}_2\text{Ce}[\eta^3\text{-N}(\text{QPPH}_2)_2]$ ($Q = \text{S}$, Se) and $\text{Cp}_2\text{Ce}[\eta^3\text{-N}(\text{SP}^i\text{Pr}_2)(\text{SePPh}_2)]$. *Inorganica Chim. Acta* **2006**, 359, 2751–2755.
- (234) Pernin, C. G.; Ibers, J. A. Syntheses, Structures, and Properties of the Bis(Cyclopentadienyl) Rare-Earth Imidodiphosphinochalcogenido Compounds $\text{Cp}_2\text{Ln}[\text{N}(\text{QPPH}_2)_2]$ ($\text{Ln} = \text{La}$, Gd , Er , or Yb for $Q = \text{Se}$; $\text{Ln} = \text{Yb}$ for $Q = \text{S}$). *Inorg. Chem.* **2000**, 39, 1216–1221.
- (235) Glover, P. B.; Bassett, A. P.; Nockemann, P.; Kariuki, B. M.; Deun, R. Van; Pikramenou, Z. Fully Fluorinated Imidodiphosphate Shells for Visible- and NIR-Emitting Lanthanides: Hitherto Unexpected Effects of Sensitizer Fluorination on Lanthanide Emission Properties. *Chem. - A Eur. J.* **2007**, 13, 6308–6320.
- (236) Nöth, H. Kristall- Und Molekülstruktur von „Imido-Tetraphenyl-Dithiophosphinsäure“ Und Imido-Tetraphenyl-Diphosphinsäure *Crystal. Zeitschrift für Naturforsch. B* **1982**, 37, 1491–1498.

- (237) Platzer, N.; Rudler, H.; Alvarez, C.; Barkaoui, L.; Denise, B.; Goasdoue, N.; Rager, M. N.; Vaissermann, J.; Daran, J. C. Praseodymium NMR-Shift Reagents for Carboxylic-Acids and Their Carboxylates - Synthesis, X-Ray Structure and Applications. *Bull. Soc. Chim. Fr.* **1995**, *132*, 95–113.
- (238) Bassett, A. P.; Van Deun, R.; Nockemann, P.; Glover, P. B.; Kariuki, B. M.; Van Hecke, K.; Van Meervelt, L.; Pikramenou, Z. Long-Lived near-Infrared Luminescent Lanthanide Complexes of Imidodiphosphinate “Shell” Ligands. *Inorg. Chem.* **2005**, *44*, 6140–6142.
- (239) Rodrigues, M. O.; da Luz, L. L.; Viana, B.; Silva, G. C. O.; Gatto, C. C.; Fontes, A. M.; Malta, M.; Weber, I. T.; Júnior, S. A. Controlling the Energy Transfer in Lanthanide-Organic Frameworks for White-Light Emitting Materials Production. *CrystEngComm* **2014**, *16*, 6914–6918.
- (240) Magennis, S. W.; Parsons, S.; Corval, A.; Derek, J.; Pikramenou, Z. Imidodiphosphinate Ligands as Antenna Units in Luminescent Lanthanide Complexes. *Chem. Commun.* **1999**, No. 1, 61–62.
- (241) Katkova, M. A.; Burin, M. E.; Logunov, A. A.; Ilichev, V. A.; Konev, A. N.; Fukin, G. K.; Bochkarev, M. N. Lanthanide Imidodiphosphinate Complexes Synthesis, Structure and New Aspects of Electroluminescent Properties. *Synth. Mater.* **2009**, *159*, 1398–1402.
- (242) Z.Pikramenou; S.Magennis; S.Parsons; D.Messenger. CCDC 279591: Experimental Crystal Structure Determination. 2005.
- (243) Zheng, W.; Li, S.; Li, C.; Zheng, Y.; You, X. Dramatic Improvement in Photostability of Luminescent Eu (III) Complexes with Tetraphenylimidodiphosphinate Ligand. *J. Lumin.* **2014**, *146*, 544–549.
- (244) Pietraszkiewicz, M.; Pietraszkiewicz, O.; Karpiuk, J.; Karpiuk, E.; Borowiak, T.; Dutkiewicz, G. Inorganica Chimica Acta The First Ternary Europium Tetraphenylimidodiphosphinate Complex: X-Ray Structure and Photoluminescent Properties. *Inorganica Chim. Acta* **2012**, *387*, 426–430.
- (245) Pietraszkiewicz, M.; Pietraszkiewicz, O.; Karpiuk, J.; Majka, A.; Dutkiewicz, G.; Borowiak, T.; Kaczmarek, A. M.; Deun, R. Van. Highly Photoluminescent Europium Tetraphenylimidodiphosphinate Ternary Complexes with Heteroaromatic Co-Ligands. Solution and Solid State Studies. *J. Lumin.* **2016**, *170*, 411–419.
- (246) Bock, H.; Heigel, E. Wechselwirkungen in Molekülkristallen, 157 [1, 2]. Mischkristallzüchtung Und Strukturbestimmungen von Tetra(3,4-Dimethylphenyl)-Imidodiphosphat-Salzen Mit Alkalikation-Verhältnissen $K^+/Rb^+(1:5)$ Und $Rb^+/Cs^+(1:1)$. *Zeitschrift für Naturforsch.* **2000**, *157*, 785–795.
- (247) Au-Yeung, K.-C.; So, Y.-M.; Wang, G.-C.; Sung, H. H.-Y.; Williams, I. D.; Leung, W.-H. Iodosylbenzene and Iodolbenzene Adducts of Cerium(IV) Complexes Bearing Chelating Oxygen Ligands. *Dalt. Trans.* **2016**, *45*, 5434–5438.
- (248) Wang, G.; Sung, H. H. Y.; Dai, F.; Chiu, W.; Wong, W.; Williams, I. D.; Leung, W. Heterometallic Cerium(IV) Perrhenate, Permanganate, and Molybdate Complexes Supported by the Imidodiphosphinate Ligand $[N(i-Pr_2PO)_2]^-$. *Inorg. Chem.* **2013**, *52*, 2556–2563.

- (249) Kuhl, O. *Phosphorus-31 NMR Spectroscopy*; Springer-Verlag Berlin Heidelberg: Berlin, 2008, pp 31–35.
- (250) Desiraju, G. R. Crystal Engineering: A Brief Overview. *J. Chem. Sci.* **2010**, *122*, 667–675.
- (251) Shan, N.; Zaworotko, M. J. The Role of Cocrystals in Pharmaceutical Science. *Drug Discov. Today* **2008**, *13*, 440–446.
- (252) Atkinson, M. B. J.; Mariappan, S. V. S.; Bučar, D.-K.; Baltrusaitis, J.; Friščić, T.; Sinada, N. G.; MacGillivray, L. R. Crystal Engineering Rescues a Solution Organic Synthesis in a Cocrystallization That Confirms the Configuration of a Molecular Ladder. *Proc. Natl. Acad. Sci. U. S. A.* **2011**, *108*, 10974–10979.
- (253) Braga, D.; Grepioni, F.; Desiraju, G. R. Crystal Engineering and Organometallic Architecture. *Chem. Rev.* **1998**, *98*, 1375–1406.
- (254) Braga, D.; Brammer, L.; Champness, N. R. New Trends in Crystal Engineering. *CrystEngComm* **2005**, *7*, 1–19.
- (255) Shee, N. K.; Naskar, J. P.; Drew, M. G. B.; Aliaga-Alcalde, N.; Datta, D. Stabilisation of True π -Electron– π -Electron Interactions in an Inorganic Cocrystal. *Inorganica Chim. Acta* **2015**, *427*, 97–102.
- (256) Taylor, P.; Trzesowska-kruszynska, A.; Kruszynski, R.; Bartczak, T. J. Coordination Sphere Geometry Changes of Lanthanoid (III) Nitrate Complexes with Hexamethylenetetramine. *J. Coord. Chem.* **2010**, *63*, 1013–1028.
- (257) Almarsson, O.; Zaworotko, M. J. Crystal Engineering of the Composition of Pharmaceutical Phases. Do Pharmaceutical Co-Crystals Represent a New Path to Improved Medicines? *Chem. Commun. (Camb)*. **2004**, No. 17, 1889–1896.
- (258) Aakeröy, C. B.; Fasulo, M. E.; Desper, J. Cocrystal or Salt: Does It Really Matter? *Mol. Pharm.* **2007**, *4*, 317–322.
- (259) Bak, A.; Gore, A.; Yanez, E.; Stanton, M.; Tufekcic, S.; Syed, R.; Akrami, A.; Rose, M.; Surapaneni, S.; Bostik, T.; et al. The Co-Crystal Approach to Improve the Exposure of a Water-Insoluble Compound: AMG 517 Sorbic Acid Co-Crystal Characterization and Pharmacokinetics. *J. Pharm. Sci.* **2008**, *97*, 3942–3956.
- (260) Myz, S. A.; Shakhtshneider, T. P.; Tumanov, N. A.; Boldyreva, E. V. Preparation and Studies of the Co-Crystals of Meloxicam with Carboxylic Acids. *Russ. Chem. Bull.* **2012**, *61*, 1798–1809.
- (261) Mirza, S.; Miroshnyk, I.; Heinamaki, J.; Yliruusi, J. Co-Crystals : An Emerging Approach for Enhancing Properties of Pharmaceutical Solids. *Dosis* **2008**, *24*, 90–96.
- (262) Fischer, W. M.; Taurinsch, A. Die Molekuelverbindungen von Oxy-Azokoerpern Mit Saure-Halogeniden. *Berichte der Dtsch. Chem. Gesellschaft (A B Ser.)* **1931**, *64*, 236–239.
- (263) Bach, A.; Lentz, D.; Luger, P.; Messerschmidt, M.; Olesch, C. Tetrafluorobutadiene and Experimental Determination of the Charge Density Of. *Angew. Chemie Int. Ed. English* **2002**, No. 2, 296–299.
- (264) Liu, P. H.; Li, L.; Webb, J. A.; Zhang, Y.; Goroff, N. S. Tetrabromobutatriene: Completing the Perhalocumulene Series. *Org. Lett.* **2004**, *6*, 2081–2083.
- (265) Pulham, C. R. Editorial. *CrystEngComm* **2014**, *16*, 5752.

- (266) Singhal, D.; Curatolo, W. Drug Polymorphism and Dosage Form Design: A Practical Perspective. *Adv. Drug Deliv. Rev.* **2004**, *56*, 335–347.
- (267) Pan, Q. Q.; Guo, P.; Duan, J.; Cheng, Q.; Li, H. Comparative Crystal Structure Determination of Griseofulvin: Powder X-Ray Diffraction versus Single Crystal X-Ray Diffraction. *Chinese Sci. Bull.* **2012**, *57*, 3867–3871.
- (268) Friscic, T.; Jones, W. Benefits of Cocrystallisation in Pharmaceutical Materials Science: An Update. *J. Pharm. Pharmacol.* **2010**, *62*, 1547–1559.
- (269) Landenberger, K. B.; Matzger, A. J. Cocrystal Engineering of a Prototype Energetic Material: Supramolecular Chemistry of 2,4,6-Trinitrotoluene. *Cryst. Growth Des.* **2010**, *10*, 5341–5347.
- (270) Haywood, A.; Mangan, M.; Grant, G.; Glass, B. Extemporaneous Isoniazid Mixture: Stability Implications. *J. Pharm. Pract. Res.* **2005**, *35*, 181–182.
- (271) Bhutani, H.; Singh, S.; Vir, S.; Bhutani, K. K.; Kumar, R.; Chakraborti, A. K.; Jindal, K. C. LC and LC-MS Study of Stress Decomposition Behaviour of Isoniazid and Establishment of Validated Stability-Indicating Assay Method. *J. Pharm. Biomed. Anal.* **2007**, *43*, 1213–1220.
- (272) Lemmerer, A.; Bernstein, J.; Kahlenberg, V. One-Pot Covalent and Supramolecular Synthesis of Pharmaceutical Co-Crystals Using the API Isoniazid: A Potential Supramolecular Reagent. *CrystEngComm* **2010**, *12*, 2856.
- (273) Sarcevic, I.; Orola, L.; Veidis, M. V.; Podjava, A.; Belyakov, S. Crystal and Molecular Structure and Stability of Isoniazid Cocrystals with Selected Carboxylic Acids. *Cryst. Growth Des.* **2013**, *13*, 1082–1090.
- (274) Spectragryph, 1.2.8.; Optical Spectroscopy Software; Friedrich Menges: Oberstdorf, Germany, 2016.
- (275) Shriver, D. F.; Drezzdon, M. A. *The Manipulation of Air-Sensitive Compounds*, 2nd Ed.; John Wiley & Sons: New York, 1986, pp 10, 83–84, 91.
- (276) Mueller, A.; Moehlen, M.; Neumueller, B.; Faza, N.; Massa, W.; Dehnicke, K. Crystal Structures of the Silylated Phosphaneimines $\text{Me}_3\text{SiNP}(\text{C-C}_6\text{H}_{11})_3$ and $(\text{Me}_3\text{SiNPPH}_2)_2\text{CH}_2$. *Zeitschrift fur Anorg. und Allg. Chemie* **1999**, *625*, 1748–1751.
- (277) Aparna, K.; Krishnamurthy, S. S.; Nethaji, M. Synthetic, Spectroscopic, and Structural Studies on Lanthanide Complexes of Diphosphazane Dioxide Ligands. *ZAAC - J. Inorg. Gen. Chem.* **1995**, *621*, 1913–1921.
- (278) Wang, F. T.; Najdzionek, J.; Louise, K. Synthesis and Reactivity in Inorganic and Metal-Organic Chemistry A Facile Synthesis of Imidotetraphenyldiphosphinic Acids. *Synth. React. Inorg. Met. Chem.* **1978**, *8*, 119–125.
- (279) Gaunt, A. J.; Reilly, S. D.; Enriquez, A. E.; Scott, B. L.; Ibers, J. A.; Sekar, P.; Ingram, K. I. M.; Kaltsoyannis, N.; Neu, M. P. Experimental and Theoretical Comparison of Actinide and Lanthanide Bonding in $\text{M}[\text{N}(\text{EPR}_2)_2]_3$ Complexes (M = U, Pu, La, Ce; E = S, Se, Te; R = Ph, IPr, H). *Inorg. Chem.* **2008**, *47*, 29–41.
- (280) Saito, T.; Yamaji, T.; Hayamizu, K.; Yanagisawa, M.; Yamamoto, O.; Matsuyama, S.; Wasada, N.; Someno, K.; Matsuyama, S.; Kinugasa, S.; Tanaba, K.; Tamura, T.; Tanabe, K.; Hiraishi, J. Spectral Database for Organic Compounds, SDBS https://sdb.sdb.aist.go.jp/sdb/cgi-bin/cre_index.cgi (accessed Apr 22, 2017).

- (281) Silverstein, R. M.; Webster, F. X.; Kiemle, D. J. *Spectrometric Identification of Organic Compounds*, 7th Ed.; John Wiley & Sons, Inc.: Hoboken, NJ, USA, 2005, pp 72–75, 73.
- (282) Dixon, K. R. Phosphorus to Bismuth. In *Multinuclear NMR*; Mason, J., Ed.; Plenum Press: New York, 1987; pp 396–398.
- (283) Mosely, M. E.; Stilbs, P. A Study of ^{14}N Relaxation and Nitrogen-Proton Spin Coupling in Nucleoside, Indole, and E-Caprolactam Systems through Fourier Transform Measurements of NH Proton Spin-Lattice Relaxation in the Rotating Frame. *Can. J. Chem.* **1978**, *56*, 1302–1305.
- (284) Lehn, J. M.; Franck-neunamm, M. Nuclear Spin—Spin Interactions. V. ^1H – ^{14}N Spin—Spin Coupling and Quadrupolar Relaxation in Quaternary Ammonium Salts. *J. Chem. Phys.* **1965**, *43*, 1421–1422.
- (285) Lehn, J. M.; Seher, R. Nuclear Spin-Spin Interactions. ^{14}N - ^1H Spin-Spin Coupling in Quaternary Enammonium Salts¹. *Chem. Commun.* **1966**, *0*, 847–849.
- (286) Suzuki, M.; Kubo, R. Theoretical Calculation of N.M.R. Spectral Line Shapes. *Mol. Phys. an Int. J. Interface Between Chem. Phys.* **1964**, *7*, 201–209.
- (287) Bullock, E.; Tuck, D. G.; Woodhouse, E. J.; Constants, C.; Shifts, S. I.; Salts, Q. A. Unusual SpinSpin Couplings in NMR Spectra of Alkyl Ammonium Salts. *J. Chem. Phys.* **1963**, *38*, 2318.
- (288) Goswami, B.; Feuerstein, T. J.; Yadav, R.; Kçppe, R.; Lebedkin, S.; Kappes, M. M.; Roesky, P. W. Enantiopure Calcium Iminophosphonamide Complexes: Synthesis, Photoluminescence, and Catalysis. *Chem. - A Eur. J.* **2020**, *27*, 4401–4411.
- (289) Feuerstein, T. J.; Goswami, B.; Rauthe, P.; Koppe, R.; Lebedkin, S.; Kappesbc, M. M.; Roesky, P. W. Alkali Metal Complexes of an Enantiopure Iminophosphonamide Ligand with Bright Delayed Fluorescence. *Chem. Sci.* **2019**, *10*, 4742–4749.
- (290) Nunez, M. G.; Farley, A. J. M.; Dixon, D. J. Bifunctional Iminophosphorane Organocatalysts for Enantioselective Synthesis: Application to the Ketimine Nitro-Mannich Reaction. *J. Am. Chem. Soc.* **2013**, *135*, 16348–16351.
- (291) Tang, J.; Dopke, J.; Verkade, J. G.; Synthesis of New Exceedingly Strong Non-Ionic Bases: $\text{RN}=\text{P}(\text{MeNCH}_2\text{CH}_2)_3\text{N}$. *J. Am. Chem. Soc.* **1993**, *115*, 5015–5020.
- (292) Holley, W. K.; Ryschkewitsch, G. E. SYNTHESIS AND CHARACTERIZATION OF THE FIRST BORANE ADDUCTS AND BORON CATIONS OF SOME N-ALKYL AND N-AMINOTRIPHENYLPHOSPHORANIMINES. *Phosphorus. Sulfur. Silicon Relat. Elem.* **1990**, *53*, 271–284.
- (293) Clegg, W.; Kleditzsch, S.; Mulvey, R. E.; Shaughnessy, P. O. Crystal Structure of a Heavier Alkali Metal Diisopropylamide Complex: A Discrete $(\text{KN})_2$ Ring Dimer with TMEDA Chelation and Short Intramolecular $\text{K}\cdots\text{H}(\text{C})$ Contacts. *J. Organomet. Chem.* **1998**, *558*, 193–196.
- (294) Normand, A. T.; Massard, A.; Richard, P.; Canovas, C.; Balan, C.; Picquet, M.; Auffrant, A.; Le Gendre, P. Titanium Imido Complexes Stabilised by Bis(Iminophosphoranyl)Methanide Ligands: The Influence of N-Substituents on Solution Dynamics and Reactivity†. *Dalt. Trans.* **2014**, *43*, 15098–15110.

- (295) Aguiar, A. M.; Beisler, J. The Cleavage of Methylenebis-(Diphenylphosphine) by Phenyl Azide. *J. Org. Chem.* **1964**, *29*, 1660–1662.
- (296) Hu, F.-H.; Wang, L.-S.; Cai, S.-F. Solubilities of Methylidiphenylphosphine Oxide in Selected Solvents. *J. Chem. Eng. Data* **2010**, *55*, 492–495.
- (297) Macrae, C. F.; Bruno, I. J.; Chisholm, J. a.; Edgington, P. R.; McCabe, P.; Pidcock, E.; Rodriguez-Monge, L.; Taylor, R.; Van De Streek, J.; Wood, P. A. Mercury CSD 2.0 - New Features for the Visualization and Investigation of Crystal Structures. *J. Appl. Crystallogr.* **2008**, *41*, 466–470.
- (298) NIST. Trimethylsilyl azide Spectroscopic Data <http://webbook.nist.gov/cgi/cbook.cgi?Name=trimethylsilyl+azide&Units=SI> (accessed Apr 29, 2017).
- (299) Ainscough, E. W.; Brodie, A. M. Sulphur-Ligand-Metal Complexes. Part 7. The Interaction of Some Diphosphine Dichalcogenides and Tetra-Alkylthiuram Disulphides with Halogens and Some First-Row Transition-Metal Salts. *J. Chem. Soc. Dalt. Trans.* **1977**, 565–570.
- (300) Apperley, D. C.; Bricklebank, N.; Hursthouse, M. B.; Light, M. E.; Coles, S. J. Vibrational, ³¹P NMR and Crystallographic Studies of Diiodine Adducts of Some Bidentate Tertiary Phosphine Sulfides. *Polyhedron* **2001**, *20*, 1907–1913.
- (301) Lobana, T. S.; Singh, G.; Nishioka, T. Copper-Sulfur Interactions: Synthesis and Structure of a Trigonal Planar Copper(I) Complex with Bis(Diphenylthiophosphinyl)Methane, [CuI(DppmS₂)]·MeCN. *J. Coord. Chem.* **2004**, *57*, 955–960.
- (302) Ainscough, E. W.; Brodie, A. M. Sulphur-Ligand-Metal Complexes. Part 8.1 Bis(Diphenylphosphino-Thioyl)Methane Complexes of Copper(I). *J. Chem. Soc. Dalt. Trans.* **1980**, 1042–1047.
- (303) Thirumoorthi, R.; Chivers, T. Alkali Metal, Magnesium, and Zinc Complexes of Bis(Chalcogenophosphinoyl)Methanide Ligands. *Eur. J. Inorg. Chem.* **2012**, *2012*, 3061–3069.
- (304) Greenwood, N. N. *Spectroscopic Properties of Inorganic and Organometallic Compounds*; Greenwood, N. N., Ed.; Spectroscopic Properties of Inorganic and Organometallic Compounds; The Royal Society of Chemistry: London, 1973; Vol. 6, pp 356–359.
- (305) Benner, L. S.; Root, C. A. Synthesis and Characterization of Trichlorotetrahydrofuraniron(III). *Inorg. Chem.* **1972**, *11*, 652–654.
- (306) Kilimov, A. P.; Svechnikova, M. A.; Shevchenko, V. I.; Smirnov, V. V.; Zotov, S. B.; Kvasnyuk-Mudryi, F. V. Infrared Spectra of Cyclic Ethers and Their Derivatives. *Chem. Heterocycl. Compd.* **1967**, *3*, 579–584.
- (307) Shurvell, H. F.; Southby, M. C. Infrared and Raman Spectra of Tetrahydrofuran Hydroperoxide. *Vib. Spectrosc.* **1997**, *15*, 137–146.
- (308) Hodgson, K. O.; Mares, F.; Starks, D. F.; Streitwieser, A. Lanthanide(III) Complexes with Cyclooctatetraene Dianion. Synthetic Chemistry, Characterization, and Physical Properties. *J. Am. Chem. Soc.* **1973**, *95*, 8650–8658.

- (309) Daly, S. R.; Girolami, G. S. Synthesis, Characterization, and Structures of Divalent Europium and Ytterbium N, N-Dimethylaminodiboranates. *Inorg. Chem.* **2010**, *49*, 4578–4585.
- (310) Gardner, J. M.; Abrahamsson, M.; Farnum, B. H.; Meyer, G. J. Visible Light Generation of Iodine Atoms and I–I Bonds: Sensitized I[•] Oxidation and I₃⁻ Photodissociation. *J. Am. Chem. Soc.* **2009**, *131*, 16206–16214.
- (311) Jung, S.-H.; Yeon, J.-W.; Yong, K.; Song, K. Determination of Triiodide Ion Concentration Using UV-Visible Spectrophotometry†. *Asian J. Chem.* **2014**, *26*, 3588–3594.
- (312) Withnall, R.; Dunkin, I. R.; Snaith, R. Thermal Decomposition of Lithium Amides: A Matrix Isolation Investigation. *Perkin Trans. II* **1994**, No. 9, 1973–1977.
- (313) Cooper, O. J.; Wooles, A. J.; McMaster, J.; Lewis, W.; Blake, A. J.; Liddle, S. T. A Monomeric Dilithio Methandiide with a Distorted Trans-Planar Four-Coordinate Carbon. *Angew. Chemie Int. Ed. English* **2010**, *49*, 5570–5573.
- (314) Hill, M. S.; Hitchcock, P. B.; Karagouni, S. M. A. Group 1 and 13 Complexes of Aryl-Substituted Bis(Phosphinimino)Methyls. *J. Organomet. Chem.* **2004**, *689*, 722–730.
- (315) Cadierno, V.; Josefina, D. Silver (I) Complexes of N-Thiophosphorylated Bis (Iminophosphorane) Ligands: From Monomers to Polymers †. *Dalt. Trans.* **2007**, *26*, 2760–2769.
- (316) Kasani, A.; Babu, R. P. K.; McDonald, R.; Cavell, R. G. [Ph₂P(NSiMe₃)₂CLi₂]: A Dilithium Dianionic Methanide Salt with an Unusual Li₄C₂ Cluster Structure. *Angew. Chemie Int. Ed. English* **1999**, *38*, 1483–1484.
- (317) Hull, K. L.; Noll, B. C.; Henderson, K. W. Structural Characterization and Dynamic Solution Behavior of the Disodio and Lithio-Sodio Geminal Organodimetallics [{{Ph₂P(Me₃Si)N}₂CNa₂}₂] and [{{Ph₂P(Me₃Si)N}₂CLiNa}₂]. *Organometallics* **2006**, *25*, 4072–4074.
- (318) Kamalesh Babu, R. P.; Aparna, K.; McDonald, R.; Cavell, R. G. Dimeric Bridged and Chelated Alkali Metal (Li and Na) Bis(Iminophosphorano)Methanide Complexes with Contrasting Structures. *Inorg. Chem.* **2000**, *39*, 4981–4984.
- (319) Gamer, M. T.; Roesky, P. W. Synthesis and Structure of Alkali Bis(Phosphinimino)Methanides. *ZAAC - J. Inorg. Gen. Chem.* **2001**, *627*, 877–881.
- (320) Leung, W.; So, C.; Wang, Z.; Wang, J.; Mak, T. C. W. Synthesis of Bisgermavinylidene and Its Reaction with Chalcogens. *Organometallics* **2003**, *22*, 4305–4311.
- (321) Babu, R. P. K.; Aparna, K.; McDonald, R.; Cavell, R. G. Monomeric Alkali Metal (Li, Na, K) Complexes of Bis(Iminophosphorano) Methanides. *Organometallics* **2001**, No. 14, 1451–1455.
- (322) Montejo, M.; Ureña, F. P.; Márquez, F.; Ignatyev, I. S.; González, J. J. L. Vibrational Spectrum of Chlorotrimethylsilane. *Spectrochim. Acta - Part A Mol. Biomol. Spectrosc.* **2005**, *62*, 293–301.

- (323) Schmidbaur, H.; Schier, A.; Neugebauer, D. Reindarstellung, NMR-Spektren Und Kristallstruktur von Triphenylphosphonium-Cyclobutylid, $(C_6H_5)_3P=C[CH_2]_2$. *Chem. Ber.* **1983**, *116*, 2173–2179.
- (324) Lichtenberg, C.; Hillesheim, N. S.; Elfferding, M.; Oelkers, B.; Sundermeyer, J. New Lithium Phosphonium Diylides: A Methylene and a Cyclopentadienyl Moiety as Ylidic Coordination Sites. *Organometallics* **2012**, *31*, 4259–4266.
- (325) Hariharan, P. S.; Mariyatra, M. B.; Mothi, E. M.; Neels, A.; Rosaire, G.; Anthonya, S. P. Polymorphism and Benzene Solvent Controlled Stimuli Responsive Reversible Fluorescence Switching in Triphenylphosphoniumfluorenylide Crystals. *New J. Chem.* **2017**, *41*, 4592–4598.
- (326) Aitken, R. A.; Boubalouta, Y.; Chang, D.; Cleghorn, L. P.; Gray, I. P.; Karodia, N.; Reid, E. J.; Slawin, A. M. Z. The Value of $^2J_{P-CO}$ as a Diagnostic Parameter for the Structure and Thermal Reactivity of Carbonyl-Stabilised Phosphonium Ylides. *Tetrahedron* **2017**, *73*, 6275–6285.
- (327) Schmidbaur, H.; Schier, A.; Frazpo, C. M. F.; Muller, G. Structural Correlations between the Tetraisopropylphosphonium Cation and Triisopropylphosphonium Isopropylide: An X-Ray Diffraction Study. *J. Am. Chem. Soc.* **1986**, *108*, 976–982.
- (328) Howells, M. A.; Howells, R. D.; Baenziger, N. C.; Burton, D. J. Crystal Structure of 2,2,3,3,4,4-Hexafluoro-(Triphenylphosphoran Ylidene) Cyclobutane. *J. Am. Chem. Soc.* **1973**, *95*, 5366–5370.
- (329) Castaneda, F.; Aliaga, C.; Bunton, C. A.; Garland, M. T.; Baggio, R. 3-(Triphenylphosphoranylidene)-Pentane-2,4-Dione and Diethyl 2-(Triphenylphosphoranylidene)-Malonate. *Acta Crystallogr. Sect. C Struct. Chem.* **2005**, *61*, 496–499.
- (330) Amman, H. L.; Wheeler, G. L.; Watts, P. H. The Structure of Triphenylphosphonium Cyclopentadienylide. An Evaluation of Ylene-Ylide Character from Structural Data. *J. Am. Chem. Soc.* **1973**, *95*, 6158–6163.
- (331) Schroder, F. G.; Sundermeyer, J. Fluorenylidene-Functionalized Lithium Phosphonium Di- and Triylides. *Organometallics* **2015**, *34*, 1017–1020.
- (332) Johnson, K. R. D.; Hayes, P. G. Yttrium and Scandium Complexes of a Bulky Bis(Phosphinimine) Carbazole Ligand. *Inorganica Chim. Acta* **2014**, *422*, 206–217.
- (333) Gruber, M.; Jones, P. G.; Schmutzler, R. PHOSPHORSUBSTITUIERTE N,N'-DIMETHYLTHIOHARNSTOFFVERBINDUNGEN. II. SYMMETRISCH BISPHOSPHORYLIERTE DERIVATE. *Phosphorus. Sulfur. Silicon Relat. Elem.* **1993**, *80*, 195–203.
- (334) Sariöz, Ö.; Öznergiz, S.; Saracoglu, H.; Buyukgungor, O. Aminophosphines Derived from N-Phenylpiperazine and N-Ethylpiperazine: Synthesis, Oxidation Reactions, and Molybdenum Complexes. *Heteroat. Chem.* **2011**, *22*, 679–686.
- (335) Gholivand, K.; Gholami, A.; Ebrahimi, A. A. V.; Abolghasemi, S. T.; Esrafil, M. D.; Fadaei, F. T.; Schenk, K. J. Triphenyltin(IV) Adducts of Diphosphoryl Ligands: Structural, Electronic and Energy Aspects from X-Ray Crystallography and Theoretical Calculations. *RSC Adv.* **2015**, *5*, 17482–17492.

- (336) Tao, Y.; Xu, L.; Zhang, Z.; Chen, R.; Li, H.; Xu, H.; Zheng, C.; Huang, W. Achieving Optimal Self-Adaptivity for Dynamic Tuning of Organic Semiconductors through Resonance Engineering. *J. Am. Chem. Soc.* **2016**, *138*, 9655–9662.
- (337) Sariöz, Ö.; Öznergiz, S. Crystal Structure , Spectroscopic Investigations and Quantum Chemical Computational Studies of N-Diphenylphosphino-4-Methylpiperidine Sulfide. *J. Mol. Struct.* **2014**, *1063*, 170–177.
- (338) Wada, A.; Yasuda, T.; Zhang, Q.; Yang, Y. S.; Takasu, I.; Enomoto, S.; Adachi, C. A Host Material Consisting of a Phosphinic Amide Directly Linked Donor–acceptor Structure for Efficient Blue Phosphorescent Organic Light-Emitting Diodes. *J. Mater. Chem. C* **2013**, *1*, 2404–2407.
- (339) Wang, Y.; Qian, P.; Su, J.; Li, Y.; Bi, M.; Zha, Z.; Wang, Z. Efficient Electrosynthesis of Phosphinic Amides via Oxidative Cross-Coupling between N–H/P–H. *Green Chem.* **2017**, *19*, 4769–4773.
- (340) Kempe, R.; Schareina, T. Crystal Structure of Diphenyl-2,2'-Dipyridylamidophosphane, C₂₂H₁₈N₃P. *Zeitschrift Für Krist. - New Cryst. Struct.* **2003**, *218*, 99–100.
- (341) Vyšvar, M.; Dastyh, D.; Taraba, J.; Nec, M. Inorganica Chimica Acta Synthesis and Characterization of New Imidophosphanes and Phosphine Oxides Containing 3,3,4,4-Tetramethylsuccinimidyl Group. *Inorganica Chim. Acta* **2009**, *362*, 4899–4905.
- (342) Ruiz, J.; Gonzalo, M. P.; Rosario, M. A Three-Component Reaction Involving Isocyanide, Phosphine and Ketenimine Functionalities. *Chem. Commun.* **2011**, *47*, 4270–4272.
- (343) Martin, D.; Tham, F. S.; Baceiredo, A.; Bertrand, G. Synthesis of Extended Polyphosphacumulenes. *Chem. - A Eur. J.* **2006**, *12*, 8444–8450.
- (344) Martin, D.; Gornitzka, H.; Baceiredo, A.; Bertrand, G. C-Phosphoniophosphaalkenes as Precursors of 1σ⁴,3σ²-Diphosphaallenes: Scope and Limitations. *Eur. J. Inorg. Chem.* **2005**, 2619–2624.
- (345) Ul-Haque, M.; Caughlan, C. N. Crystal and Molecular Structure of NN-Dimethyldiphenylphosphinamide. *Perkin Trans. II* **1976**, *111*, 1101–1104.
- (346) Davidowitz, B.; Modro, T. A.; Niven, M. L. PHOSPHORIC AMIDES. 9. CRYSTAL AND MOLECULAR STRUCTURES OF N-(DIPHENYLPHOSPHINOYL) ETHYLENIMINE AND ITS N-(β-CHLOROETHYL) PRECURSOR. *Phosphorus and Sulfur* **1985**, *22*, 255–263.
- (347) Darren Grice, I.; Jenkins, I. D.; Busfield, W. K.; Byriel, A.; Kennard, C. H. L. Diphenyl(1,1,3,3-Tetramethyl-2,3-Dihydro-1H-Isoindol-2-Yl)Phosphine Oxide. *Acta Crystallogr. Sect. E Crystallogr. Commun.* **2006**, *62*, 2329–2330.
- (348) Corbridge, D. E. C. Infra-Red Analysis of Phosphorus Compounds. *J. Appl. Chem.* **1956**, *6*, 456–465.
- (349) Clark, R. J. H.; Lewis, J.; Machin, D. J.; Nyholm, R. S. Complexes of Titanium Trichloride. *J. Chem. Soc.* **1963**, 379–387.
- (350) Schlecht, S.; Chitsaz, S.; Neumüller, B.; Dehnicke, K. Die Kristallstrukturen Des Diphenylphosphinsäureamids, Ph₂P(O)NH₂, Und Seines Cäsiumsalzes [Cs{Ph₂P(O)NH}]. *Zeitschrift für Naturforsch. B* **1998**, *53*, 17–22.

- (351) X-Area, 1.88.; Single Crystal Diffraction Software; Stoe&Cie: Darmstadt, Germany, 2002.
- (352) Dolomanov, O. V.; Bourhis, L. J.; Gildea, R. J.; Howard, J. A. K.; Puschmann, H. OLEX2: A Complete Structure Solution, Refinement and Analysis Program. *J. Appl. Cryst.* **2009**, *42*, 339–341.
- (353) Oliva, G.; Castellano, E. E.; Franco de Carvalho, L. R. The Structure of Diphenylphosphinamide. *Acta Crystallogr. Sect. B Struct. Sci.* **1981**, *37*, 474–475.
- (354) Wiberg, N.; Uhlenbrock, W. Notiz Zur Darstellung von Trimethylsilylamin. *Chem. Ber.* **1971**, *104*, 2643–2645.
- (355) Kuhner, S.; Hausen, H. D.; Weidlein, J. $\text{Br}_3\text{In}\cdot\text{NH}_2\text{Si}(\text{CH}_3)_3$ - a Stable Adduct of the Unstable Trimethylsilylamine Abstract. *Zeitschrift fur Anorg. und Allg. Chemie* **1998**, *624*, 13–14.
- (356) Pike, R. M. Chemistry of the Silylamines. V. Self-Condensation of $\text{R}_3\text{Si-NH}_2$ Type Silylamines. *Recl. des Trav. Chim. des Pays-Bas* **1962**, *81*, 28–32.
- (357) Bowser, J. R.; Williams, P. J.; Kurz, K. Cleavage of Silicon-Nitrogen Bonds by Acid Chlorides: An Unusual Synthetic Route to Amides. *J. Org. Chem.* **1983**, *48*, 4111–4113.
- (358) Jubb, J.; Berno, P.; Hao, S.; Gambarotta, S. Nonsolvated Li-Amide Clusters. Preparation and Crystal Structure of the Adduct $\{(\text{Meso-Octaethylcalix-[4-Pyrrole]Li}_4) \cdot (t\text{-BuLi})_2\}$ and of the Tetrameric $[(\text{Cyclohexyl})_2\text{NLi}]_4$. *Inorg. Chem.* **1995**, *34*, 3563–3566.
- (359) Hagenbach, A.; Athenstädt, S.; Daróczy, H. E.; Abram, U.; Alberto, R. Rhenium(I) and Technetium(I) Tricarbonyl Complexes with Phosphoraneimines. *Zeitschrift fur Anorg. und Allg. Chemie* **2004**, *630*, 2709–2716.
- (360) Hamada, Y.; Tsuboi, M.; Nakata, M.; Tasumi, M. INFRARED SPECTRUM OF ISOPROPYLAMINE. *Chem. Phys.* **1988**, *125*, 55–62.
- (361) Fulmer, G. R.; Miller, A. J. M.; Sherden, N. H.; Gottlieb, H. E.; Nudelman, A.; Stoltz, B. M.; Bercaw, J. E.; Goldberg, K. I. NMR Chemical Shifts of Trace Impurities: Common Laboratory Solvents, Organics, and Gases in Deuterated Solvents Relevant to the Organometallic Chemist. *Organometallics* **2010**, *29*, 2176–2179.
- (362) Weiss, E. Die Kristallstruktur Des Lithiumjodid-Monohydrats. *Zeitschrift Fur Anorg. Und Allg. Chemie* **1965**, *341*, 203–206.
- (363) Gilson, I. T.; Sisler, H. H. The Reaction of Diphenylchlorophosphine with Ammonia-Free Chloramine. *Inorg. Chem.* **1965**, *4*, 273–275.
- (364) Hilliard, C. R.; Bhuvanesh, N.; Gladysz, J. A.; Blümel, J. Synthesis, Purification, and Characterization of Phosphine Oxides and Their Hydrogen Peroxide Adducts. *Dalt. Trans.* **2012**, *41*, 1742–1754.
- (365) Xu, Y.; Su, Q.; Wanrong, D.; Peng, Z.; Delie, A. The Chan-Evans-Lam N-Arylation of Phosphonic/Phosphinic Amides. *Tetrahedron* **2017**, *73*, 4602–4609.
- (366) Modro, T. A. Substituent Effects of Phosphorus-Containing Groups on Aromatic Reactivity. Determination of Substituent Constants by ^{13}C Nuclear Magnetic Resonance Spectroscopy. *Can. J. Chem.* **1977**, *55*, 3681–3685.

- (367) Cai, X.-M.; Riener, K.; Herdtweck, E.; Pöthig, A.; Kühn, F. E. Rational Synthesis and Characterization of Dimolybdenum(II) Compounds Bearing Ferrocenyl-Containing Ligands toward Modulation of Electronic Coupling. *Inorg. Chem.* **2015**, *54*, 3272–3280.
- (368) Bhattacharyya, P.; Novosad, J.; Phillips, J.; Slawin, A. M.; Williamsa, D. J.; C, J. D. W. Bis(Bidentate) Complexes of Iminobis(Diphenylphosphine Chalcogenides) $[M(N(XPPh_2)_2-X,X'')]_2$ (X = S or Se; M = Ni, Pd or Pt). *Dalt. Trans.* **1995**, 1607–1613.
- (369) Copolovici, L.; Varga, R. A.; Lippolis, V.; Silvestru, C. Hydrogen Bis-(Tetra-Phenyl-Imido-Diphosinic Acid) Triiodide. *Acta Crystallogr. Sect. E Crystallogr. Commun.* **2007**, *63*, 3724–3734.
- (370) Silvestru, C.; Drake, J. E.; Yang, J.; Haiduc, I. Bis(Thiophosphinoyl)Amines and Their Neutral Cobalt(II) Complexes, Containing Stable Tetrahedral CoS_4 Cores. Crystal Structures of $NH(SPM_e_2)(SPP_h_2)$ and $[Co\{(SPM_e_2)(SPP_h_2)N\}_2]$. *J. Chem. Soc. Dalt. Trans.* **1998**, *50*, 73–78.
- (371) Birdsall, D. J.; Slawin, A. M. Z.; Woollins, J. D. The Preparation and Coordination Chemistry of $R_2P(S)NHP(S)R'_2$ (R and R' = i Pr, Ph, Et, OEt or OPh). *Polyhedron* **2001**, *20*, 125–134.
- (372) Necas, M.; Foreman, M. R. S. J.; Marek, J.; Derek Woollins, J.; Novosad, J. New Mixed-Donor Unsymmetrical P-N-P Ligands and Their Palladium(II) Complexes. *New J. Chem.* **2001**, *25*, 1256–1263.
- (373) Pernin, C. G.; Ibers, J. A. Two Tetrahydrofuran Solvates of $HN(SePPh_2)_2$. *Acta Crystallogr. Sect. C Cryst. Struct. Commun.* **2000**, *56*, 376–378.
- (374) McQuillan, G. P.; Oxtan, I. A. Vibrational Spectrum, Structure and Complex-Forming Reactions of “Imidobis(Diphenylphosphine Sulphide)”, $(Ph_2PS)_2NH$. *Inorganica Chim. Acta* **1977**, *75*, 69–75.
- (375) Larkin, P. IR and Raman Spectra-Structure Correlations: Characteristic Group Frequencies. In *IR and Raman Spectroscopy - Principles and Spectral Interpretation*; 2011; pp 73–115.
- (376) Gholivand, K.; Shariatnia, Z.; Orouzadeh, N. Phosphoramides: Synthesis, Spectroscopy, and X-Ray Crystallography. *Heteroat. Chem.* **2013**, *19*, 1–9.
- (377) Gorenstein, D. G. Phosphorus-31 Chemical Shifts: Principles and Empirical Observations. In *Phosphorous-31 NMR. Principles*; Academic Press: Orlando, 1984; pp 7–33.
- (378) Pretsch, E.; Buehlmann, P.; Badertscher, M. *Structure Determination of Organic Compounds*, 4th Ed.; Springer-Verlag Berlin Heidelberg: Heidelberg, 2009, pp 263–265.
- (379) Bezgubenko, L. V.; Pipko, S. E.; Shalimov, A. A.; Sinitza, A. D. Nucleophilic Catalysis of Phosphorus Trichloride Oxygen Oxidation. *Heteroat. Chem.* **2008**, *19*, 408–411.
- (380) Sheldrick, G. M. SHELXT - Integrated Space-Group and Crystal-Structure Determination. *Acta Crystallogr. Sect. A Found. Crystallogr.* **2015**, *71*, 3–8.
- (381) Sheldrick, G. M. Crystal Structure Refinement with SHELXL. *Acta Crystallogr. Sect. C Struct. Chem.* **2015**, *71*, 3–8.

- (382) NIST. Isopropyl amine hydrochloride Spectroscopic Data <https://webbook.nist.gov/cgi/cbook.cgi?ID=C15572562&Units=SI&Mask=80#I> R-Spec (accessed Dec 19, 2018).
- (383) Gupta, A. K.; Reddy, S. A. D.; Boomishankar, R. Facile Formation of Stable Tris(Imido)Phosphate Trianions as Their Tri- and Hexanuclear Pd(II) Complexes in Protic Solvents. *Inorganic Chem.* **2013**, *52*, 7608–7614.
- (384) Giffin, N. A.; Hendsbee, A. D.; Roemmele, T. L.; Lumsden, M. D.; Pye, C. C.; Masuda, J. D. Preparation of a Diphosphine with Persistent Phosphinyl Radical Character in Solution: Characterization, Reactivity with O₂, S₈, Se, Te, and P₄, and Electronic Structure Calculations. *Inorg. Chem.* **2012**, *51*, 11837–11850.
- (385) Yerramsetti, N.; Unruh, D. K.; Li, G. CCDC 1559159: Experimental Crystal Structure Determination. 2017.
- (386) Pourayoubi, M.; Tarahhomi, A.; Karimi Ahmadabad, F.; Fejfarová, K.; Lee, A. Van Der; Dušek, M. Two New XP(O)[NHC(CH₃)₃]₂ Phosphor-Amidates, with X = (CH₃)₂N and [(CH₃)₃CNH]₂P(O)(O). *Acta Crystallogr. Sect. C Cryst. Struct. Commun.* **2012**, *68*, 164–169.
- (387) Desiraju, G. R. Supramolecular Synthons in Crystal Engineering-A New Organic Synthesis. *Angew. Chemie Int. Ed.* **1995**, *34*, 2311–2327.
- (388) Desiraju, G. R. Designer Crystals: Intermolecular Interactions, Network Structures and Supramolecular Synthons. *Chem. Commun.* **1997**, No. 16, 1475–1482.
- (389) De Villiers, M. M.; van der Watt, J. G.; Lötter, A. P. Kinetic Study of the Solid-State Photolytic Degradation of Two Polymorphic Forms of Furosemide. *Int. J. Pharm.* **1992**, *88*, 275–283.
- (390) Foltz, M. F.; Coon, C. L.; Garcia, F.; Nicholas III, A. L. The Thermal Stability of the Polymorphs of Hexanitrohexaazaisowurtzitane. Part I. *Propellants, Explos. Pyrotech.* **1994**, *19*, 19–25.
- (391) Hilfiker, R.; Blatter, F.; Von Raumer, M. Relevance of Solid-State Properties for Pharmaceutical Products. In *Polymorphism in the Pharmaceutical Industry*; Hilfiker, R., Ed.; Wiley-VCH: Weinheim, 2006; pp 1–20.
- (392) Miller, F. A.; Wilkins, C. H. Infrared Spectra and Characteristic Frequencies of Inorganic Ions. *Anal. Chem.* **1952**, *24*, 1253–1294.
- (393) Nimmo, J. K.; Lucas, B. W. A Neutron Diffraction Determination of the Crystal Structure of α -Phase Potassium Nitrate at 25 °C and 100 °C. *J. Phys. Chem. C* **1973**, *6*, 201–211.
- (394) Wickenden, A. E.; Krause, R. A. Complexes of Nickel(II) with Acetonitrile. Coordination of Perchlorate. *Inorg. Chem.* **1965**, *4*, 404–407.
- (395) Birnbaum, E. R.; Moeller, T. Observations on the Rare Earths. LXXXI. Nuclear Magnetic Resonance and Calorimetric Studies of Complexes of the Tripositive Ions with Substituted Pyridine Molecules. *J. Am. Chem. Soc.* **1969**, *91*, 7274–7280.
- (396) Desreux, J. F. Nuclear Magnetic Resonance Spectroscopy of Lanthanide Complexes with a Tetraacetic Tetraaza Macrocycle. Unusual Conformational Properties. *Inorg. Chem.* **1980**, *19*, 1319–1324.

- (397) Aizawa, S. I.; Okano, M.; Kidani, T. Enantiomeric NMR Signal Separation Behavior and Mechanism of Samarium(III) and Neodymium(III) Complexes with (S,S)-Ethylenediamine-N,N'-Disuccinate. *Chirality* **2017**, *29*, 273–281.
- (398) Satterlee, J. D. Fundamental Concepts of NMR in Paramagnetic Systems Part II: Relaxation Effects. *Concepts Magn. Reson.* **1990**, *2*, 119–129.
- (399) Stewart, I. I.; Horlick, G. Electrospray Mass Spectra of Lanthanides. *Anal. Chem.* **1994**, *66*, 3983–3993.
- (400) Czylkowska, A. Synthesis and Some Properties of Light Lanthanide Complexes with 4,40-Bipyridine and Dibromoacetates. *J. Therm. Anal. Calorim.* **2013**, *114*, 989–995.
- (401) Mitchell, P. C. H. The Infrared Spectra of Complexes Containing Pyridine. *J. Inorg. Nucl. Chem.* **1961**, *21*, 382–384.
- (402) Dineshkumar, S.; Muthusamy, A.; Chitra, P.; Anand, S. Synthesis, Characterization, Optical and Electrical Properties of Thermally Stable Polyazomethines Derived from 4,4'-Oxydianiline. *J. Adhes. Sci. Technol.* **2015**, *29*, 2605–2621.
- (403) Charbonneau, G. P.; Delugeard, Y. Biphenyl: Three-Dimensional Data and New Refinement at 293 K. *Acta Crystallogr. Sect. B Struct. Crystallogr. Cryst. Chem.* **1977**, *33*, 1586–1588.
- (404) Charbonneau, B. Y. G.; Delugeard, Y. Structural Transition in Polyphenyls. III. Crystal Structure of Biphenyl at 110 K. *Acta Crystallogr.* **1976**, No. 1975, 1420–1423.
- (405) Candana, M. M.; Eroğlu, S.; Özbey, S.; Kendi, E.; Kantarci, Z. Structure and Conformation of 4,4'-Bipyridine. *Spectrosc. Lett.* **1999**, *32*, 35–45.
- (406) Chetkina, L. A.; Sobolev, A. N.; Bel'skii, V. K.; Serdyuk, L. E.; Kardash, I. E. CCDC 1263587: Experimental Crystal Structure Determination. *Krist.* **1991**, *36*, 902.
- (407) Lennartson, A.; Hedström, A.; Håkansson, M. Spontaneous Generation of Chirality in Simple Diaryl Ethers. *Chirality* **2015**, *27*, 425–429.
- (408) Koningstein, J. A.; Grunberg, P. Electronic Raman Spectra. VII. Raman Spectra of the Lanthanides. *Can. J. Chem.* **1971**, *49*, 2336–2344.
- (409) De Bruijn, T. J. W.; De Jong, W. A.; Van Den Berg, P. J. Thermal Decomposition of Aqueous Manganese Nitrate Solutions and Anhydrous Manganese Nitrate. Part 1. Mechanism. *Thermochim. Acta* **1981**, *45*, 265–278.
- (410) Coetzee, J. F. Purification of Acetonitrile and Tests for Impurities. Analytical Chemistry Division, Commission of Electroanalytical Chemistry: Pittsburgh 1966, pp 429–435.
- (411) Sigma-Aldrich, M. Pyrophosphoryl chloride information page <https://www.sigmaaldrich.com/catalog/product/sigma/p5142?lang=en®ion=MT> (accessed Oct 26, 2019).
- (412) Kemp, W. *NMR in Chemistry A Multinuclear Introduction*, 1st Ed.; MacMillan Education Ltd: London, 1986, pp 178.

- (413) Amirkhanov, V.; Ovchinnikov, V.; Legendziewicz, J.; Graczyk, A.; Hanuza, J.; Macalik, L. Spectroscopic Studies of Neodymium and Europium Phosphoro-Azo β -Diketonates. *Acta Phys. Pol. A* **1996**, *90*, 455–460.
- (414) Khorasani-Motlagh, M.; Noroozifar, M.; Niroomand, S.; Saffari, J. Archive of SID Synthesis and Spectroscopy Studies of New Neodymium (III) Complexes with Cyanamide Derivatives as N-Donor Ligand Archive of SID. *J. Iran. Chem. Soc.* **2010**, *7*, 807–813.
- (415) NIST. Diethylamine Spectroscopic Data
<https://webbook.nist.gov/cgi/cbook.cgi?ID=C109897&Units=SI&Mask=80#IR-Spec> (accessed Oct 30, 2018).

APPENDICES

APPENDIX 1: SCHLENK LINE TECHNIQUES

A-1.1. Argon Purification

A-1.1.1. Argon purification by means of moisture scavenger columns

Two columns were prepared in order to remove moisture contamination from the argon used as an inert atmosphere. The preparation and set up of these columns are given below. These columns were added to the Schlenk line between the Argon bottle and the Schlenk line to remove water contamination from the argon gas before the inert gas reached the Schlenk line.

A-1.1.1.1. 4 Å molecular sieve column

A 50 cm glass column was attached to the Schlenk line via a 10 ml Schlenk flask at the bottom of the column and closed at the top using an adapter with stopcock also attached to the line. This was purged thrice under argon and vacuum and afterwards flame dried under vacuum. A glass wool plug was added at the bottom of the column and the column was flame dried again. 4 Å molecular sieves were activated as described hereunder. The molecular sieves were heated at 250-300 °C overnight in a furnace in air after which the sieves were cooled under vacuum. In portions, the sieves were heated under argon using a Bunsen burner until a significant amount of condensation was obtained on the cooler parts of the flask and this condensation was removed under vacuum. This procedure was repeated multiple times until no more water condensation was obtained. Given the initial activation in the furnace this procedure was typically repeated around 2 to 3 times. The molecular sieves thus activated were transferred to the column prepared prior. This activation by Bunsen burner was repeated until the column was filled to the required length.

A-1.1.1.2. P₂O₅ column

A 50 cm glass column was attached to the Schlenk line via a 10 ml Schlenk flask at the bottom of the column and closed at the top using an adapter with stopcock also attached to the line. This was purged thrice under argon and vacuum and afterwards flame dried under vacuum. A glass wool plug was added at the bottom of the column and the column was flame dried once again. An equivolume mixture of P₂O₅ and glass Raschig rings was mixed under argon and transferred to the column prepared prior. The mixture was closed with another plug of glass wool at the top and closed under argon.

A-1.1.2. Argon purification by means of oxygen scavenger column

In order to remove reactive oxygen contamination from the argon used to supply an inert atmosphere for the reactions undertaken in this study it was decided that the gas should be passed through a column of oxygen scavenger. Shriver and Drezdson described manganese (II) oxide (MnO), which is a light green pyrophoric solid, as a well-established oxygen scavenger for inert gasses.²⁷⁵ Therefore the oxygen scavenger was prepared using the method described by the same authors.

A-1.1.2.1. Reagents used

The chemicals used in the procedure described in section A-1.1.2. were Mn(NO₃)₂·6H₂O (Analytical), Silica gel (Kieselgel 60), Nitric acid (1.5%) and Hydrogen gas (N/A).

A-1.1.2.2. Procedure and observations

The silica gel was activated by washing the solid with numerous portions of 1.5 % aqueous nitric acid alternating with an equal number of distilled water washings. The silica gel was then dried at 100 °C overnight and 53.387 g of this carrier were weighed and transferred to a 500 ml beaker. Stirring was undergone using a magnetic stirrer at 100 rpm. A slight excess of the Mn(NO₃)₂·6H₂O, 16.331 g, were weighed and dissolved in 43 ml of distilled water, yielding a pale orange solution. The

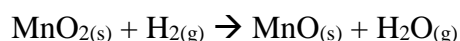
Mn(NO₃)₂·6H₂O solution was added to the stirred silica gel in 3 ml portions, which were added every 5 minutes. On addition of all the Mn(NO₃)₂·6H₂O solution a clumpy and wet light orange solid was obtained. A roughly equal volume of glass Raschig rings were mixed thoroughly with the mixture obtained. This mixture was allowed to stand in an oven at 150 °C overnight, yielding a black powder and releasing a brown gas as a side product.

A 50 cm glass column (~19 mm diameter) was attached to the Schlenk line via a 10 ml Schlenk tube connected at the bottom. The column was closed at the top using an adapter with a stop cock also attached to the Schlenk line. This set up was purged and flame dried under vacuum after which glass wool was introduced at the bottom of the column to act as a base for the solid mixture. The Mn(NO₃)₂·6H₂O/Silica gel/glass Raschig rings mixture was transferred to the column and the top of the mixture was closed with glass wool. The column was detached from the Schlenk line from the top and argon allowed to flow from the bottom upwards. The column was heated using a Bunsen burner until all the solid turned black. At intervals the column was cooled and shaken to decompose as much of the solid as possible. The black solid formed was MnO₂, obtained from the decomposition of the nitrate, as given in Scheme A-1.1.⁴⁰⁹



Scheme A-1.1: Thermal decomposition of Mn(NO₃)₂·6H₂O.

Subsequently the column was set up as given in Figure A-1.1 to introduce a hydrogen gas flow. The column was heated using a Bunsen burner until all the column changed colour to a pale green colour. This is the desired oxygen scavenger, MnO, embedded in the silica gel, produced through the redox reaction given in Scheme A-1.2.



Scheme A-1.2: Reduction of MnO₂ to MnO.

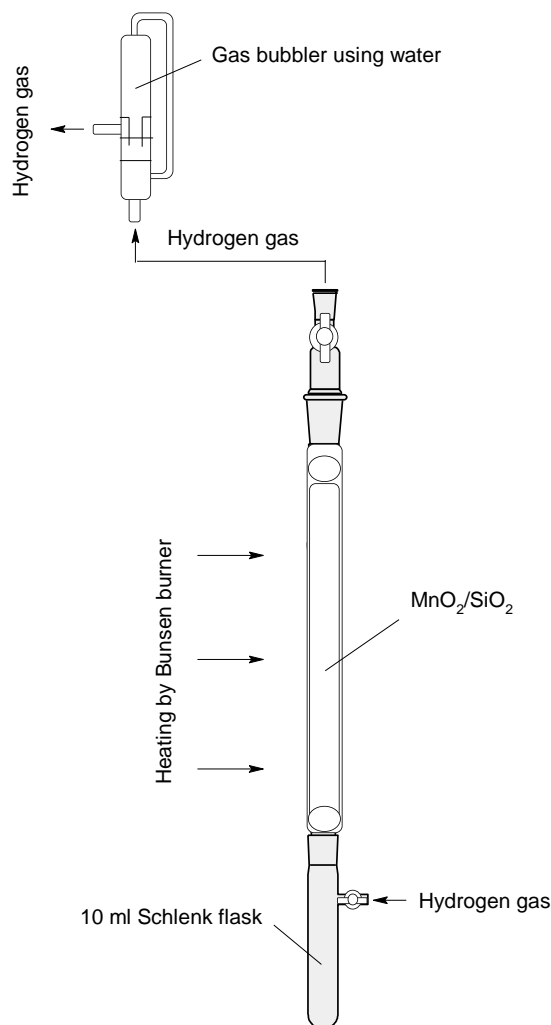


Figure A-1.1: Set up for the reduction of MnO_2 to MnO oxygen scavenger, diagram (left, drawn using ACD/ChemSketch software) and photograph (right).

This column was then set in line prior to the Schlenk line, after the 4 Å molecular sieve column and before the phosphorus pentoxide columns used to dry the argon stream, as shown in Figure A-1.2. Much of the column changed colour to a light brown/light green mixture which was expected giving a still active mixture of MnO and Mn_2O_3 .



Figure A-1.2: MnO column set in line in the path leading argon to the Schlenk line.

A-1.1.3. Argon purification by commercially available inert gas purifiers.

For certain reactions performed in this study it was observed that the purification column set ups prepared as described above were not sufficient to purify the argon to the desired quality for reasonable periods of time. This was especially true for the MnO oxygen scavenger columns which deactivated quickly. Therefore, for a number of reactions a new moisture and oxygen scavenger column set up was prepared to allow the undertaking of these more moisture and oxygen sensitive reactions. The reactions which were undergone while using this purification system are specified in the relevant methodology section.

A-1.1.3.1. Reagents/Materials used

The materials (and brands) used in the procedure described in Section A-1.1.3. were ZPure O₂/H₂O purifiers (Chromatography Research Supplies), P₂O₅ on inert carrier material (abcr) and 4 Å Molecular Sieves (N/A).

The gas purifiers, ZPure O₂/H₂O purifiers, were purchased already active from Chromatography Research Supplies. These purifiers are composed of a mixture of a number of oxides as given in Table A-1.1, which act as both moisture and oxygen scavengers. The chemical/physical processes that cause the desired effect is not published by the supplier.

Table A-1.1: Chemical composition of ZPure O₂/H₂O purifiers.

Component	Composition
Al ₂ O ₃	60–90 %
CuO	6–25 %
NiO	<1 %
Co ₃ O ₄	<1 %
SiO ₄ (Quartz)	<2 %

A-1.1.3.2. Procedure and observations

The moisture and oxygen scavenger column set up was prepared as given in Figure A-1.3. This set up contained four individual columns, namely a 4 Å molecular sieve column, a P₂O₅ column and two ZPure O₂/H₂O purifier columns. The 4 Å molecular sieve column was prepared as described in Section A-1.1.1. The P₂O₅ column was also prepared as described in Section A-1.1.2. However, rather than using reagent grade P₂O₅ as described prior, a granulated P₂O₅ on an inert carrier material having a chemical moisture indicator was purchased and used in order to allow for better gas flow and for better visible indication of the status of the moisture scavenger. These columns were attached to each other and the argon bottles and Schlenk line using mainly 3/16" ID Nalgene tubing.

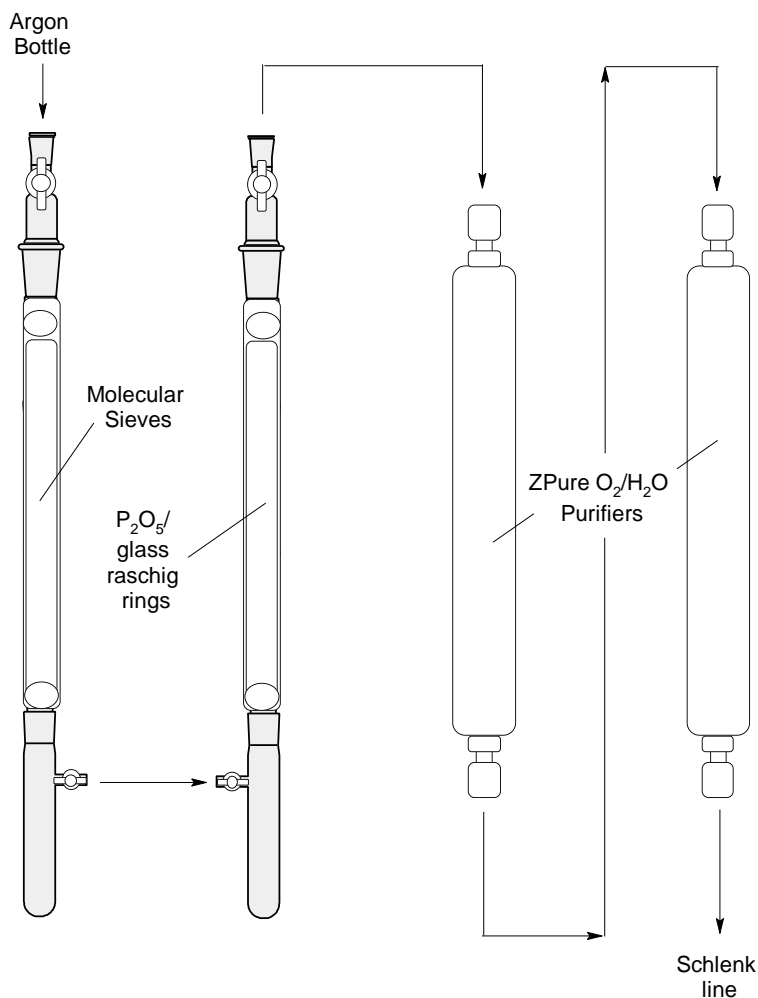


Figure A-1.3: Diagram of Set up of moisture and oxygen scavenger columns using purchased inert gas purifiers (drawn using ACD/ChemSketch software).

The argon was first passed through the columns of activated molecular sieves and granulated P_2O_5 to minimise the moisture impurity reaching the gas purifiers and thus reducing the introduction of moisture on set up and minimising the load on the purifiers during their use. The gas purifiers were attached individually starting from the attachment to the P_2O_5 column which was purged via strong argon flow for 5 minutes prior. This purging by strong argon flow was repeated on addition of tubing to the first gas purifier, on attachment of the second gas purifier and on attachment of this second gas purifier to the Schlenk line. The ZPure O_2/H_2O purifiers were installed with male compression fittings which could not be attached directly to the Nalgene tubing used throughout the remaining set up. Therefore, these gas purifiers were connected to the relevant pieces of Nalgene tubing using the set up shown in Figure A-1.4. The female barb connector and the PE tubing had an OD of $\frac{1}{4}$ '' while the brass fitting and compression fitting for the gas purifiers had an ID of $\frac{1}{4}$ ''.

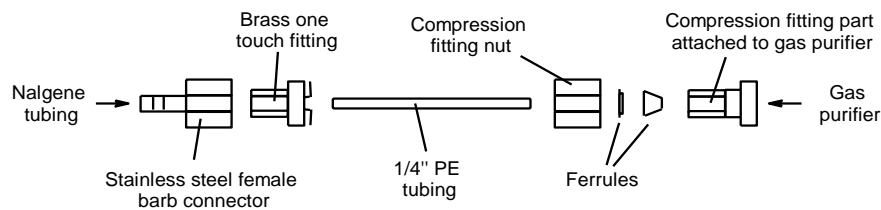


Figure A-1.4: Connection set up for connecting the gas purifiers to Nalgene tubing used throughout the set up.

A-1.2. Liquid transfer

Two main methods of liquid transfer were used in the study, namely cannula transfer and syringe transfer. Cannula transfer is a method in which a liquid is transferred via a cannula, under positive argon pressure. The set up necessary is given in Figure A-1.5. The technique was initiated by piercing through the suba seal meant for the reservoir flask using the blunt end of the cannula. The cannula was purged by passing argon through it when the suba seal is attached to the reservoir flask. The receiving flask was set up with the respective suba seal pierced with the bleed needle under argon flow. This suba seal was subsequently pierced using the needle point end of the cannula.

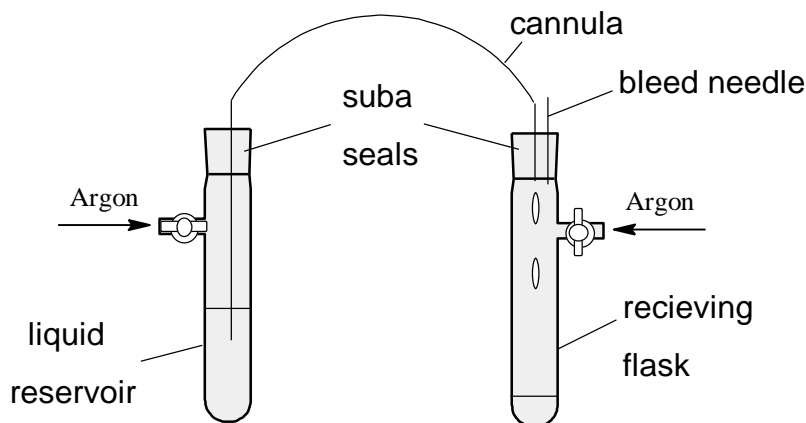


Figure A-1.5: Liquid transfer via cannula (drawn using ACD/ChemSketch software).

Transfer through positive argon pressure was obtained by placing the blunt end of the cannula in the liquid and closing the argon stopcock of the receiving flask. This forced the argon flow to push the liquid through the cannula to the receiving flask, wherein excess argon was pushed out through the bleed needle. Liquid transfer was stopped either by moving the blunt end of the cannula above the liquid or by opening the

argon flow from the stopcock of the receiving flask. Suba seals were reused until piercings no longer closed properly, while the cannulae were washed with acetone after use and dried at 150 °C overnight before reuse. The volume of liquid to be transferred was decided beforehand and the flasks were marked prior to drying. The position of the mark was determined by adding an equivalent volume of acetone to the receiving flask. In other cases the amount had to be estimated.

Liquid transfer via syringe was far more simple and straightforward to use. Glass syringes were used since they were easier to clean and since they could be dried as with other glassware. Syringes were purged by filling them with argon from a flask which was previously purged with argon and closed with a suba seal. The purging of each syringe was repeated between three to five times. These could then be stored, partially filled with argon, for small periods of time, by sticking the needle in clean rubber bungs. During liquid transfer excess liquid was initially extracted by the syringe and any bubbles were then removed by bending the needle in the seal and pushing the bubbles out. The volume of liquid in the syringe was then adjusted to the required amount by pushing out the extra liquid, with the needle still inserted in the seal. The liquid was then transferred through a suba seal to the receiving flask.

A-1.3. Filtration

Two methods of filtration have been employed in this study, namely the filtration tube technique and cannula filtration. The procedure for the filtration tube technique is presented in Figure A-1.6. The receiving flask-filtration tube set up was purged and the stopper/round bottomed flask was then replaced by the flask containing the relative suspension under argon. After the two parts were fitted together all stopcocks were closed and the set up flipped so that the suspension fell into the filtration tube by gravity. Filtration was induced by applying argon flow through all the inlets of the set up. A slight application of vacuum from the receiving flask was sometimes used to increase the filtration rate but this was not frequently done as there was the possibility that filtration would fail because of the infiltration of the solid into the sintered glass frit.

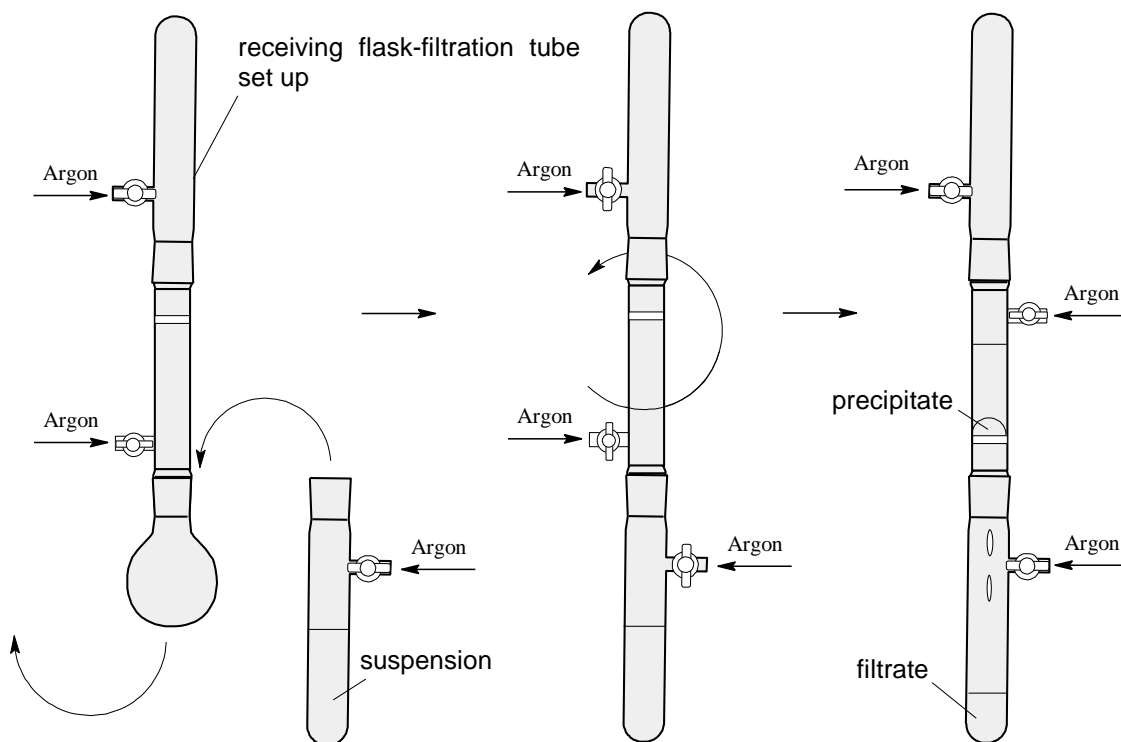


Figure A-1.6: Filtration using the filtration tube technique (drawn using ACD/ChemSketch software).

Cannula filtration is set up as given in Figure A-1.7; the set up being similar to that of cannula liquid transfer. The main difference is the inclusion and preparation of the filter paper head. The filter paper was prepared in a similar fashion to that of the preparation of fluted filter paper and it was affixed to the cannula using Teflon tape. The filtrate was pushed through the filter paper and the cannula through positive argon pressure, as described for cannula liquid transfer. The solid would then be left in the initial flask and normally vacuum was applied to remove trace amounts of filtrate.

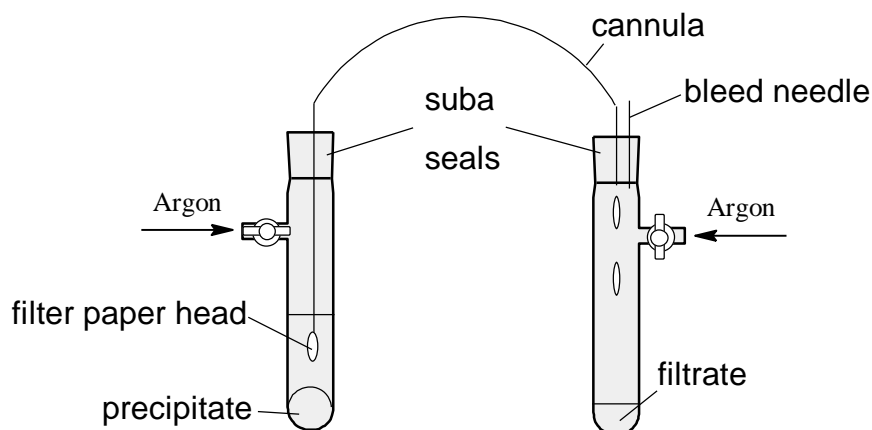


Figure A-1.7: Cannula filtration set up (drawn using ACD/ChemSketch software).

A-1.4. Ampoule preparation

Solid products prepared in the current study were usually stored in argon filled ampoules. These ampoules were prepared from glass test tubes having an external diameter of 16 mm and an internal diameter of 14 mm. The ampoules were prepared by forming a thin neck in the middle of the glass test tube, by heating the tube sufficiently to soften the glass so that it could be pulled to form the thin neck as shown in Figure A-1.8. These tubes were then flame dried in air, weighed and transferred to a freshly cleaned, purged and flame dried large, tube-like flask as shown in Figure A-1.9 (without the rubber band tied to the ampoule). These were then removed and reweighed and again purged once under argon. Afterwards these were removed and washed with 2 ml SOCl_3 each to dry them further. These washed test tubes were then set under vacuum for 8 hours, and the set up flame dried periodically, to remove the SOCl_3 . Finally, rubber bands were tied to the vials as given in Figure A-1.9 and then purged properly thrice under argon. The tubes were then filled with the solid by hanging them within the large tube, under argon flow. If a specific mass of product was required in a tube, the tube and its contents had to be weighed after each addition of the solid. Weighing was also undergone under argon flow. Afterwards the tubes were purged in the large tube flask and the open end sealed with Parafilm under argon. This film was then pierced by a bleed needle, and the neck was heated and pulled until the ampoule was formed by sealing the glass. An example of a finished ampoule is given in Figure A-1.10.

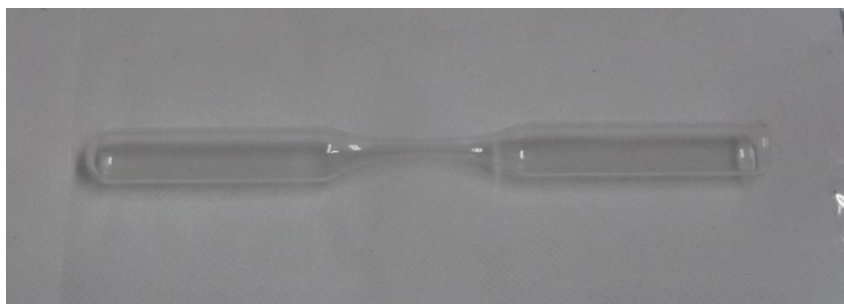


Figure A-1.8: Test tube formed for ampoule preparation.



Figure A-1.9: Large tube-like flask set up used to purge and fill ampoule tubes.

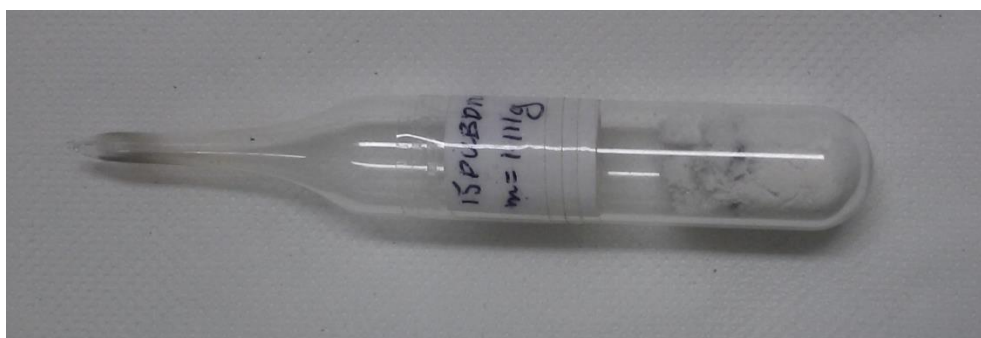


Figure A-1.10: Filled ampoule.

A-1.5. Weighing of compounds under argon

Since many solid reagents used in this study were air and moisture sensitive weighing the required amounts had to be undergone under an argon or nitrogen atmosphere. In order to do this a set up to allow the use of a table top mass balance under an argon atmosphere was necessary. In the current study weighing of solid reagents was therefore carried out using the set up given in Figure A-1.11.

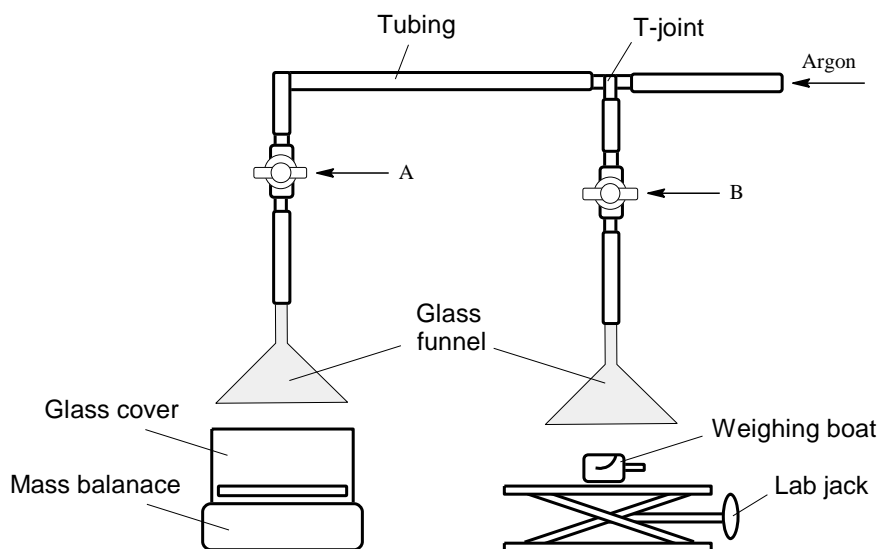


Figure A-1.11: Weighing set up used to weigh air and moisture sensitive compounds in inert conditions.

The solid to be weighed was transferred to a Schlenk tube of the required size which was attached to the Schlenk line through tubing long enough to reach the vicinity of the mass balance for easy handling and which was purged and dried properly to ensure proper working conditions. The set up shown in Figure A-1.11 was prepared with the argon coming from a single port of the Schlenk line through tubing which was long enough to allow easy manipulation of the set up and maintain a stable weight distribution to stop the set up from collapsing.

Throughout the procedure the argon flow from stopcock A was used to purge the volume over the mass balance from air to allow for inert measuring conditions while the flow from stopcock B was used to add solid in inert conditions and store said solid under argon during the procedure. In more detail, argon was allowed to flow over the mass balance for 10 minutes, through the stopcock A, to purge the volume above the mass balance enclosed by the glass cover. Stopcock A was closed and argon allowed to flow over the weighing boat for 5 minutes. Afterwards both mass balance and weighing boat were left under argon flow for 5 minutes simultaneously. Every time argon flow was stopped at stopcock A a plastic cover was used to close the glass cover from the top thus enclosing the volume above the mass balance for a minimum amount of time. This was considered a temporary measure and the time without argon flow from stopcock A was kept to a minimum.

Prior to weighing, the argon flow from stopcock A was stopped and the weighing boat was tared. The boat was transferred back to the argon flow from stopcock B and the mass balance set under argon flow, making sure that the tared value did not change. During weighing, the solid was transferred from the Schlenk tube containing the solid to the weighing boat under argon flow from the funnel attached to stopcock B. The weighing boat was then transferred to the mass balance and the weighing reading was taken without argon flow from stopcock A so as not to disturb the balance while argon flow from stopcock B was maintained during the weighing procedure. After measurement the weighing boat including the solid was placed under argon flow from stopcock B and the mass balance was allowed to reach the original tared value under argon flow from stopcock A. This procedure was repeated until the required mass was weighed.

If for any reason the tared value was not reached in between weighing procedures a new weighing boat was used, tared as described before and the solid transferred to it. Afterwards addition was continued as described prior. Finally, the solid was transferred to the required Schlenk tube or reaction mixture while the remaining solid was stored under argon until ampouling could be undertaken.

APPENDIX 2: DRYING OF SOLVENTS

In the case of the current study the solvent drying procedure was undergone by using the set up given in Figure A-2.1.

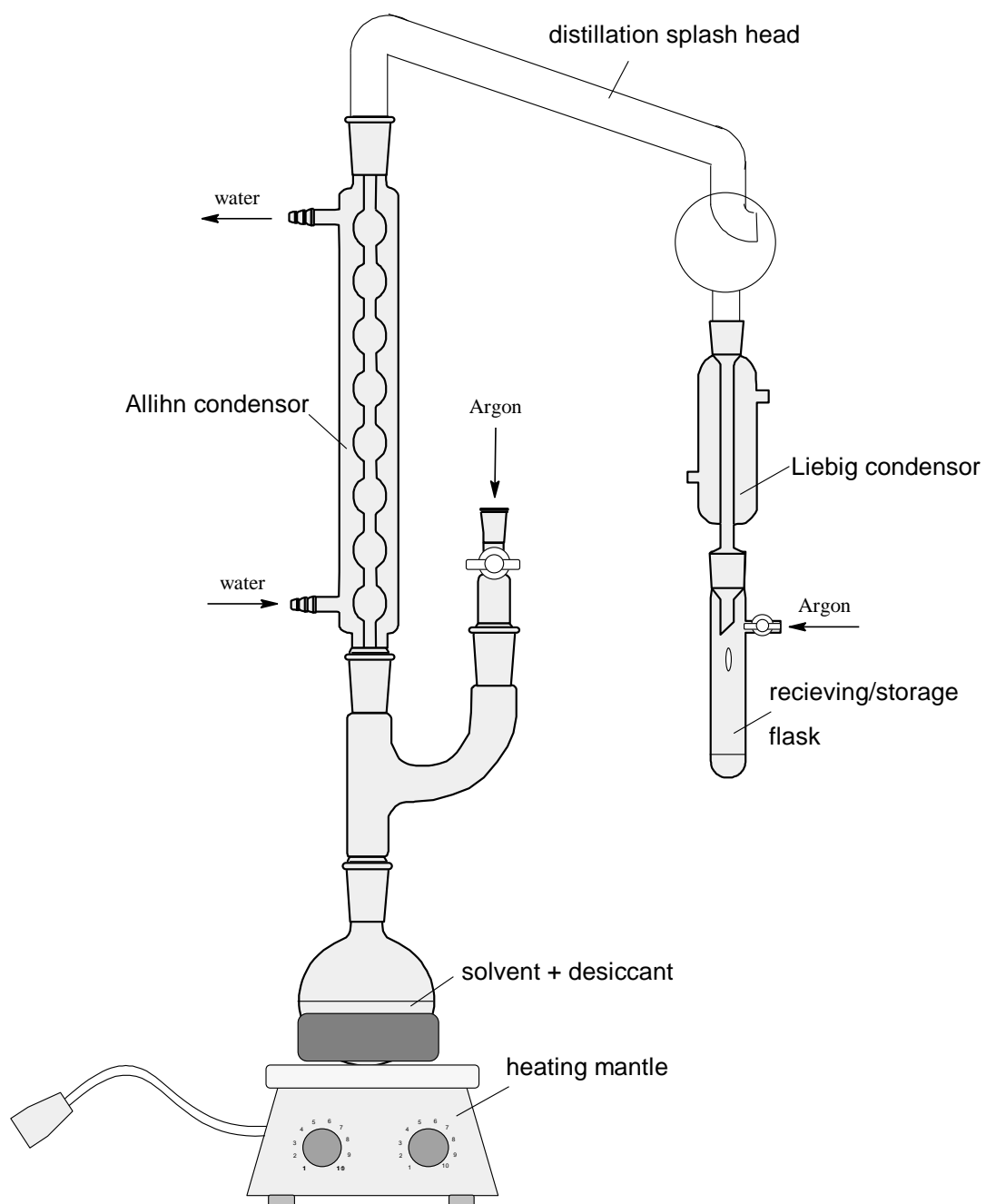


Figure A-2.1: Solvent drying still set up used throughout the study (drawn using ACD/ChemSketch software).

Before applying the drying procedure, all solvents had to be pre-dried using desiccants to remove large amounts of water. The procedures used for pre-drying differed depending on the solvent and its respective miscibility with water.

The two parts of the set up given in Figure A-2.1 namely, the solvent-desiccant still (500 ml round bottom flask, Claisen adapter and argon inlet) and the condensation-storage system (Allihn and Liebig condensers, distillation still head and receiving/storage flask) were purged separately. The relative desiccant, which was different from that used for the pre-drying, was added to the still, followed by the solvent. The solvent was degassed by freeze-pump-thaw degassing which was repeated three times over. Afterwards both parts of the set up were connected under argon flow, reflux established and the reflux left overnight. Subsequently water flow was transferred from the Allihn to the Liebig condenser to induce distillation of the solvent into the storage flask. Distillation was continued until about half the storage flask was filled. On completion of the process a desiccant was added to the freshly distilled solvent to maintain dry conditions. The choice of this desiccant was also dependent on the solvent. The solvent was finally degassed as described prior in this section.

The tables below outline the details of the procedures used to dry the solvents tetrahydrofuran (THF) – Table A-2.1, diethyl ether – Table A-2.2, petroleum ether 30-40, 40-60 °C and n-hexane – Table A-2.3, toluene – Table A-2.4, dichloromethane and chloroform – Table A-2.5 and acetonitrile – Table A-2.6.

Table A-2.1: Drying procedure for THF.

Tetrahydrofuran (THF) ^{125,275}	
Pre-drying	THF was mixed with anhydrous MgSO ₄ until no more clumping of the solid occurred. This mixture was filtered into a distillation flask within a simple distillation set up and then distilled over activated 4Å molecular sieves. The fraction obtained in the range of 64-66 °C was collected. This fraction was transferred to the solvent drying still.
Drying	THF was dried in the still set up over sodium as a desiccant and using benzophenone as an indicator. The ratio of solvent volume to the masses of sodium and benzophenone respectively was of 1L:2.5g:15g. On

	refluxing overnight a deep purple to black colour was obtained, indicating that the solvent was dry.
Storage	The distilled solvent was stored over activated 4Å molecular sieves and a clean copper film. The latter was used to decrease the amount of organic peroxides formed over time. The presence of peroxides was addressed further by testing the solvent for organic peroxides after distillation and by covering the flask with aluminium foil.

Table A-2.2: Drying procedure for Diethyl ether.

Diethyl ether ^{125,275}	
Pre-drying	Diethyl ether was mixed with anhydrous MgSO ₄ until no more clumping of the solid occurred. This was filtered and the ether dried over activated 4Å molecular sieves by stirring.
Drying	Diethyl ether was dried in the still set up over sodium as a desiccant and using benzophenone as an indicator. The ratio of solvent volume to the masses of sodium and benzophenone respectively was of 1L:2.5g:15g. On refluxing overnight a deep purple to black colour was obtained, indicating that the solvent was dry.
Storage	The distilled solvent was stored over activated 4Å molecular sieves and a clean copper film. The latter was used to decrease the amount of organic peroxides formed over time. The presence of peroxides was addressed further by testing the solvent for organic peroxides after distillation and by covering the flask with aluminium foil.

Table A-2.3: Drying procedure for petroleum ether 30-40, 40-60 °C and n-hexane.

Petroleum ether 30-40, 40-60 °C, and n-hexane ^{125,275}	
Pre-drying	The solvent was mixed with activated 4Å molecular sieves. This mixture was filtered into the solvent drying still.
Drying	The solvent was dried in the still set up over calcium hydride. The ratio of solvent volume to calcium hydride was of 1L:5g.
Storage	The distilled solvent was stored over a sodium film. If any excessive tarnishing of the sodium film was observed the solvent was re-distilled over more calcium hydride.

Table A-2.4: Drying procedure for Toluene.

Toluene ^{125,275}	
Pre-drying	Toluene was first washed thrice with an equivolume amount of conc. Sulphuric acid and then thrice with distilled water. The toluene was then washed thrice with 10gL ⁻¹ NaOH _(aq) and again thrice with distilled water. The toluene fraction was then mixed with anhydrous MgSO ₄ until no more clumping was present and then it was mixed with activated 4Å molecular sieves. This mixture was filtered into the solvent drying still.
Drying	Toluene was dried in the still set up over sodium as a desiccant and using benzophenone as an indicator. Tetraethylene glycol dimethyl ether was added as a stabiliser. The ratio of solvent volume with the masses of sodium and benzophenone and the volume of tetraethylene glycol dimethyl ether respectively was of 1L:2.5g:15g:8ml. On refluxing overnight a deep purple colour was obtained, indicating that the solvent was dry, as shown in Figure A-2.2.
Storage	The distilled solvent was stored over a sodium film. If any excessive tarnishing of the sodium film was observed the solvent was re-distilled over more sodium.



Figure A-2.2: Toluene being dried in still showing typical deep purple colour of Na/Benzophenone indicator indicating dryness

Table A-2.5: Drying procedure for dichloromethane and chloroform.

Dichloromethane and Chloroform ^{125,275} (same procedure used for both)	
Pre-drying	Dichloromethane or chloroform was mixed with activated 4Å molecular sieves. The resultant mixture was filtered into the solvent drying still.
Drying	Dichloromethane or chloroform was dried in the still set up over phosphorus pentoxide. The ratio of solvent volume to phosphorus pentoxide was of 1L:5g.
Storage	The distilled solvent was stored over activated 4Å molecular sieves.

Table A-2.6: Drying procedure for acetonitrile.

Acetonitrile ⁴¹⁰	
Pre-drying	Acetonitrile was mixed with activated 3Å molecular sieves. This mixture was filtered into a clean beaker and calcium hydride added to it in portions, until no more effervescence was observed.
Drying Part 1	Acetonitrile was dried in the still set up over phosphorus pentoxide as a desiccant. The ratio of solvent volume to the mass of phosphorus pentoxide was of 1L:5g. This was allowed to reflux overnight. This was therefore distilled over and used in the second part described hereunder.
Drying Part 2	Acetonitrile distilled from phosphorus pentoxide was transferred to a newly cleaned, purged and dried still set up and calcium hydride was added. The ratio of solvent volume to the mass of calcium hydride was of 1L:5g.
Storage	The distilled solvent was stored over activated 3Å molecular sieves. This is shown in Figure A-2.3.



Figure A-2.3: Dry Acetonitrile stored over 3Å molecular sieves.

APPENDIX 3: PREPARATION OF LITHIUM DICYCLOHEXYLAMIDE

A-3.1. Synthesis of LiNCy₂

This compound has been previously synthesised by Jubb and co-workers in 1995 and has the structure given in Figure A-3.1.³⁵⁸ The compound was prepared through a simple acid base reaction as given in Scheme A-3.1, wherein the desired product can be described as a salt. In the current study LiNCy₂ was also prepared using the procedure described by Jubb and co-workers with some modifications and characterised using IR.

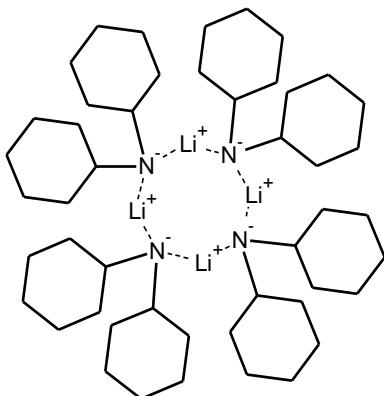
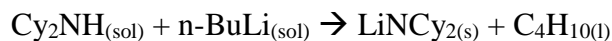


Figure A-3.1: Molecular diagram of LiNCy₂.



Scheme A-3.1: Synthesis of LiNCy₂.

A-3.1.1. Reagents used

The chemicals used in the procedures described in this section were Cy₂NH (97%), n-BuLi (2.5 moldm⁻¹) and n-hexane (dry).

A-3.1.2. Procedure for the two solids LiNCy₂_1 and LiNCy₂_2

A 100 ml Schlenk flask, with a Liebig condenser set up, was charged with 10 ml (50 mmol) Cy₂NH and 12 ml n-hexane to yield a clear solution. This was cooled to -78 °C and stirred with a magnetic stirrer. Glass syringes were used to add 20 ml (50 mmol) of 2.5 moldm⁻³ n-BuLi to the cooled solution. This was then allowed to warm up

to room temperature, at which point a white precipitate was formed. This mixture was then refluxed for 3 hours, filtered by cannula filtration and the resultant solid dried under vacuum. This white crystalline solid was collected as the final product. Yield LiNCy₂_1: 4.741 g, 40.51 %. Yield LiNCy₂_2: 8.370 g, 89.4 %.

A-3.1.5. Characterisation data

LiNCy₂_1, LiNCy₂_2 FT-IR (KBr, cm⁻¹): 3674 (s), 2924 (s), 2851 (s), 2665 (w), 2587 (w), 1455(s), 1363 (m), 1345 (m), 1301 (w), 1260 (m), 1236 (m), 1140 (s) 1094 (s/bs) 1026 (w), 985 (w), 946 (m), 916 (w), 888 (s), 849 (m), 791 (w).

A-3.2. Analysis by Infra-red spectroscopy

The IR spectra of the two solids obtained, namely LiNCy₂_1 and LiNCy₂_2, are given in Figure A-3.2, along with the spectrum of the Cy₂NH starting reagent. Comparison indicates that the two solids were likely the same chemical species. The broad band at around 3379 cm⁻¹ in the spectrum of Cy₂NH and which is associated with the ν N–H vibrations was lost in the spectra of both LiNCy₂_1 and LiNCy₂_2, indicating the expected deprotonation. Most of the bands in the fingerprint region in the spectra of the products, remained unchanged from the analogous bands in the spectrum of the starting reagent, thus indicating that the amine structure remained mostly unchanged.

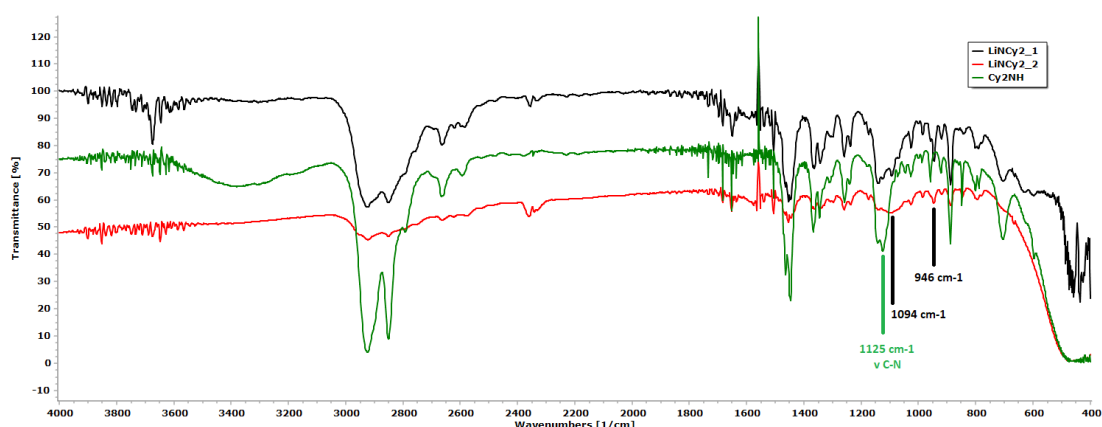


Figure A-3.2: IR spectra of LiNCy₂_1 (black), LiNCy₂_2 (red) and Cy₂NH (green).

The main changes in the skeletal region of the spectra of the products were the decrease in intensity of the C_2NH band at 1125 cm^{-1} , which was assigned to the $\nu\text{ C-N}$ vibrations of the amine, and the presence of new bands at 1094 cm^{-1} and 946 cm^{-1} . The band at 1094 cm^{-1} could be due to the new $\nu\text{ C-N}$ vibrations unique to the products. The band at 946 cm^{-1} could not be assigned. Therefore, the IR data did not yield any structural information. This was likely due to the fact that the solids produced were very moisture sensitive making IR data very difficult to obtain. The samples started to change from a white powder to a yellow residue during the analysis.

APPENDIX 4: PURIFICATION OF PYROPHOSPHORYL TETRACHLORIDE (PPTC)

A-4.1. Method

In the interest of synthesising ligands isoelectronic to the carbenes studied in this research, it was decided to look into structures containing the central moiety, P–O–P, where the phosphorus is pentavalent and four coordinate. Given the availability of pyrophosphoryl tetrachloride (PPTC) having the structure given in Figure A-4.1, it was decided to synthesise organic pyrophosphoryl compounds with the general structure given in Figure A-4.2, since PPTC could be used as a starting reagent for the production of these compounds.

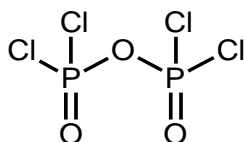


Figure A-4.1: Molecular diagram of pyrophosphoryl tetrachloride (PPTC).

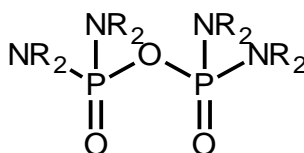


Figure A-4.2: General molecular diagram of organic pyrophosphoryl compounds derived from PPTC.

The PPTC available had a light dull orange/yellow colouration, which colour is indicative of contamination. This contamination was presumed to be a mixture of decomposition products. This decomposition is expected as the compound is moisture sensitive and should be stored under an inert atmosphere. Purification was undertaken using short path distillation as shown in Figure A-4.3.

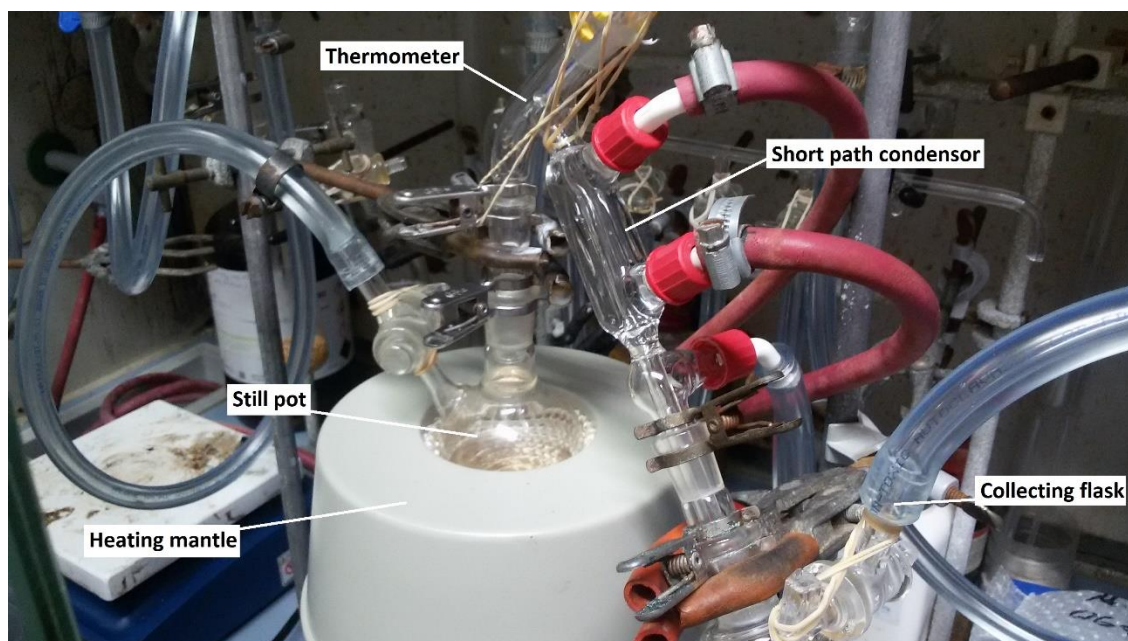


Figure A-4.3: Short path distillation used for the purification of PPTC.

The PPTC was transferred to the still pot and anti-bumping granules were added. The anti-bumping granules were found to be very useful since vigorous bumping was observed during the distillation. The collecting flask was placed in a liquid nitrogen bath and the distillation was performed under vacuum. Initially a solid was formed in the flask. This was believed to be ice and therefore it was removed by vacuum at room temperature. Afterwards the liquid nitrogen bath was re-set as before. Collection of the distillate, which was a clear colourless liquid, was obtained in the temperature range 52 – 54 °C. Distillation was discontinued before all the liquid in the still pot was removed, leaving only an orange liquid.

This procedure was repeated several times to purify all the available PPTC. In some cases, a fraction of liquid was also collected in the temperature range 60 – 80 °C. These latter fractions proved to have IR spectra which were similar to the expected product but not fully congruent with the literature data.⁴¹¹ Therefore, only the fractions collected at 52 – 54 °C and having IR spectra as given in literature were collected.⁴¹¹

These fractions were collected together in a cleaned amber glass bottle as shown in Figure A-4.4. In the aforementioned figure the bottle is shown being purged under argon and vacuum. Thus the liquid could be transferred to a flame dried argon filled bottle which could be easily used to extract the required volumes of the PPTC by syringe under argon using a set up similar to bottles containing in-built septa. Yield: 55.2 ml, 69 %.



Figure A-4.4: Purging of amber glass bottle to be used for the storage of PPTC.

A-4.2. Characterisation

The purified products were characterised using IR spectroscopy and examined for purity by ^{31}P $\{^1\text{H}\}$ NMR. The data collected from both these spectroscopic methods is given in Figures A-4.5 and A-4.6 respectively. The IR spectrum of PPTC was found to be in very good agreement with IR data published by suppliers of the chemical.⁴¹¹ The assignments of the bands were derived from the data published by Corbridge.^{99,348} No published data was found for the ^{31}P $\{^1\text{H}\}$ NMR of PPTC, however the spectrum obtained in the current study indicated the presence of a singular major component with a chemical shift value of -9.52 ppm. This is in the typical range of the phosphoryl halides of which PPTC is an example.³⁷⁷ The impurity peaks proved negligible in intensity.

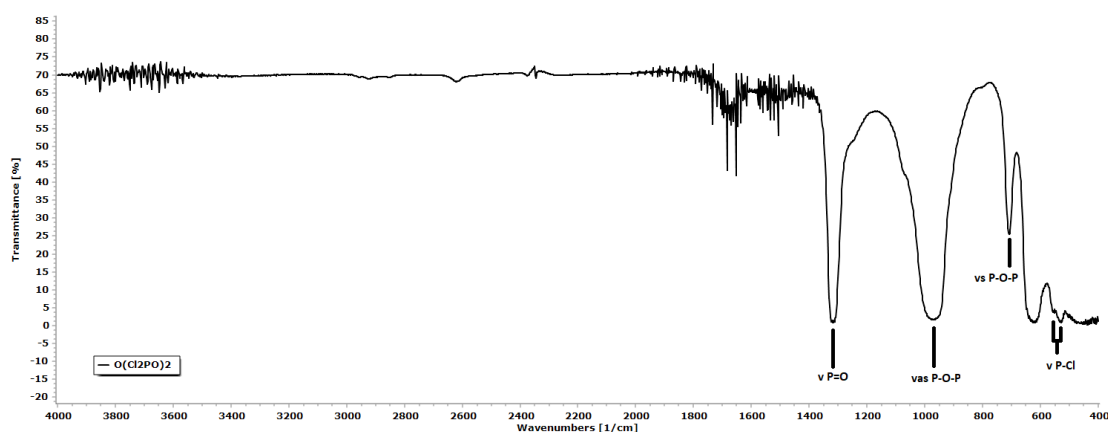


Figure A-4.5: IR Spectrum of the purified PPTC.

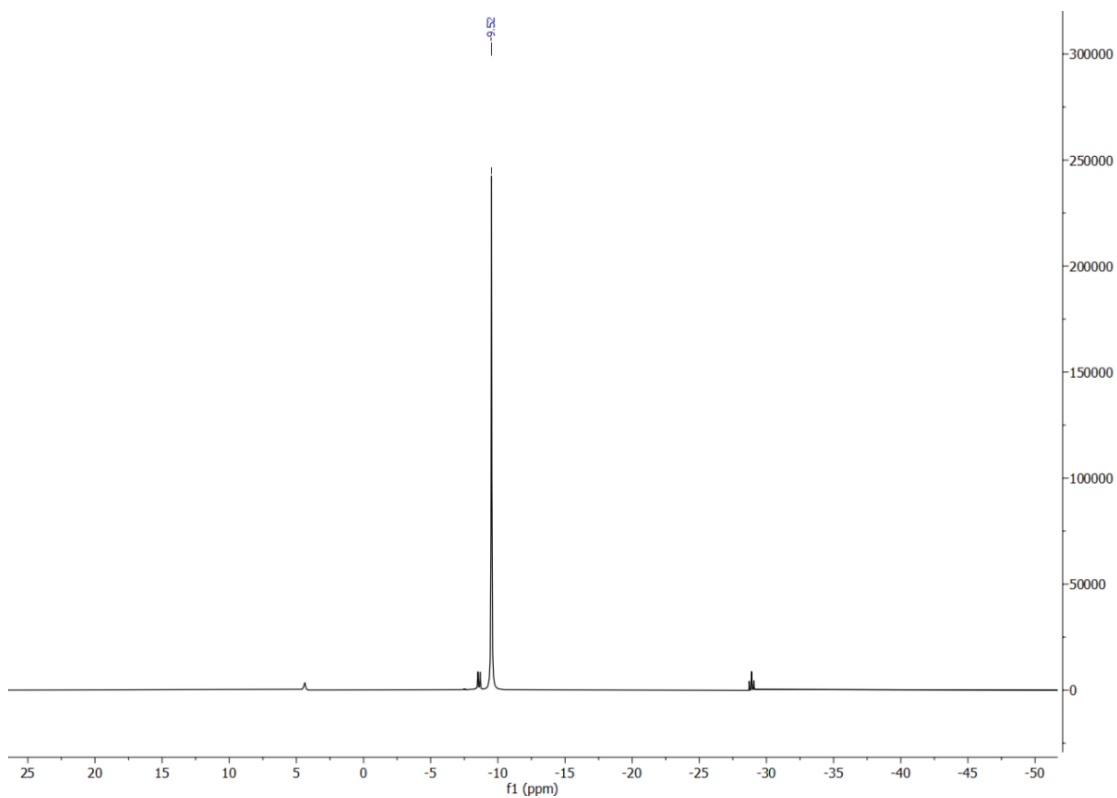


Figure A-4.6: $^{31}\text{P}\{^1\text{H}\}$ NMR spectrum of purified PPTC.

PPTC FT-IR (NaCl, cm^{-1}): 1315 (s), 969 (s), 709 (m), 624 (s), 530 (w). $^{31}\text{P}\{^1\text{H}\}$ NMR (CDCl_3): -9.52 ppm (s).

APPENDIX 5: CHARACTERISATION OF 1,1-BIS(DIPHENYLPHOSPHINO)METHANE (DPPM)

The main starting reagent used in the preparation of all the $\lambda_5\sigma_4$ -phosphorus carbene ligands synthesized in this study was 1,1-bis(diphenylphosphino)methane (dppm), as given in Figure A-5.1. The characterisation of the commercially obtained reagent was undergone by IR spectroscopy and ^1H NMR spectroscopy.

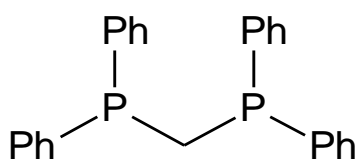


Figure A-5.1: Molecular diagram of dppm

A-5.1. Analysis by Infra-red spectroscopy

The IR spectrum of the purchased dppm was obtained in KBr disc and is presented in Figure A-5.2.

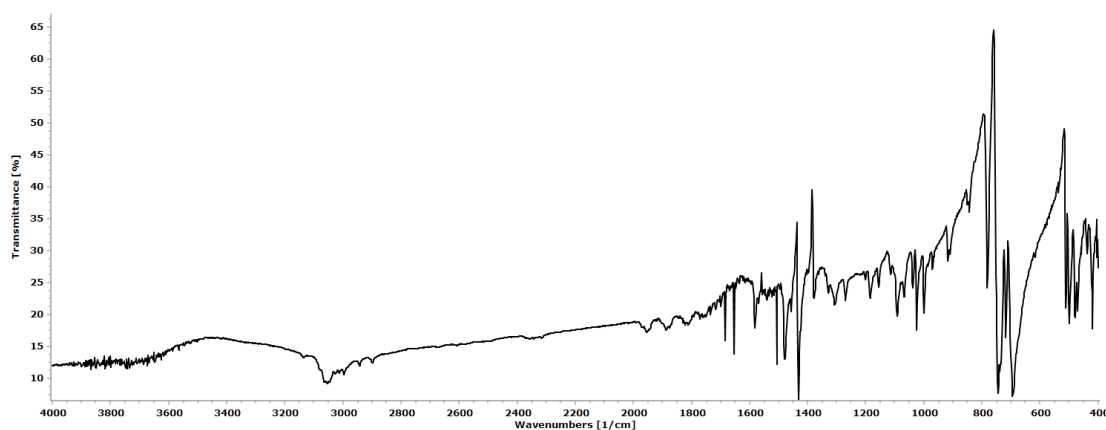


Figure A-5.2: IR spectrum of purchased dppm, in KBr disc.

The IR spectrum indicated that the solid was dry. It should be noted that after opening the container the solid was stored under argon to minimise the possibility of contamination by hydration. Assignments for the bands of the IR spectrum of dppm were not available in literature and therefore a tentative assignment of the bands in the IR spectrum in Figure A-5.2 was undertaken and the conclusions are presented in Table A-5.1.^{99,348}

Table A-5.1: Assignment of IR bands of dppm from spectrum in Figure A-5.2.

Wavenumber, cm ⁻¹	Transmittance	Description	Assignment
3054	9.1	w	v C–H(aromatic)
2996	10.5	w	v _{as} C–H(alkyl)
2942	11.9	w	v _s C–H(alkyl)
1954	17.6	w,b	Overtone bands
1886	~18.0	w,b	Overtone bands
1824	~18.0	w,b	Overtone bands
1581	18.3	w	v C=C(aromatic)
1479	13	m	P–Ph or δ CH ₂
1431	7.8	s	P–Ph
1376	21.6	m	N/A
1306	22.9	m	N/A
1296	22.3	m	N/A
1184	22.6	s	τ or ω CH ₂
1155	24.6	m	N/A
1091	19.9	s	P–Ph
1067	22.8	m	N/A
1022	22.3	m	N/A
998	20.9	s	P–Ph
969	27.2	w,sh	v _{as} P–CH ₂ –P or other P–CH ₂ –P vibration
918	29.8	m,b	v _{as} P–CH ₂ –P or other P–CH ₂ –P vibration
843	36.6	w	v _{as} P–CH ₂ –P or other P–CH ₂ –P vibration
786	24.7	s	v _{as} P–CH ₂ –P or v _s P–CH ₂ –P
744	7.8	s	P–Ph
717	~15.0	m	P–Ph, ρ CH ₂ or v _s P–CH ₂ –P
692	7.5	s	P–Ph

Where, w = weak, b = broad, m = medium, s = strong, sh = sharp, N/A = non-assigned.

Many of the non-assigned bands seem to be retained in the IR spectra of the dppm derivatives prepared in this study. This may be indicative of either skeletal dppm bands or some type of non-reactive impurity. The bands at 1306 cm^{-1} and 1296 cm^{-1} are thought to be due to oxide impurities, although the nature of these could not be determined.⁹⁹

A-5.2. Analysis by ^1H NMR spectroscopy

To further confirm the purity and composition of the dppm purchased, a sample of this reagent was analysed by ^1H NMR spectroscopy. The experimental spectrum is given in Figure A-5.3.

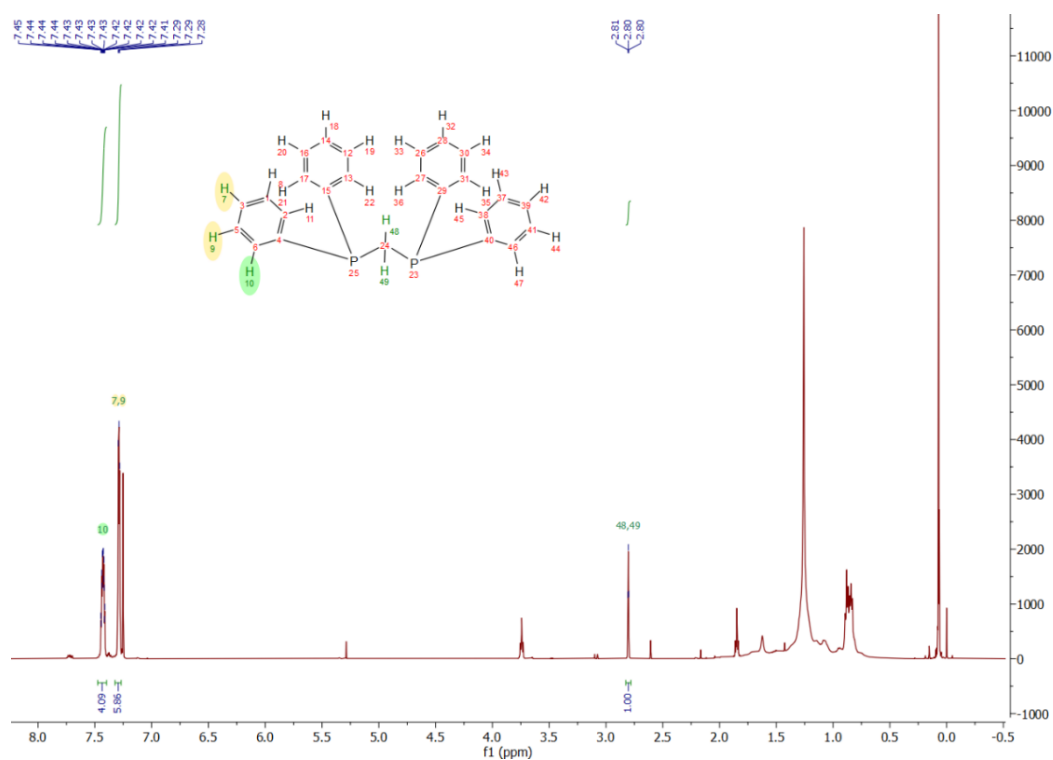


Figure A-5.3: Full ^1H NMR spectrum for dppm as purchased in CDCl_3 .

The spectrum was obtained in CDCl_3 as solvent, as characterised by the singlet at 7.25 ppm. The singlet at 1.6 ppm may be attributed to moisture within the solvent used as it was also visible in other spectra of samples prepared for analysis by ^1H NMR using this solvent. The same was true regarding the multiplets at 3.74 ppm and 1.85 ppm typical of THF and the singlet at 1.26 ppm and multiplet at 0.85 ppm typical of grease. The data obtained is presented in Table A-5.2, while Table A-5.3 lists the data set for the ^1H NMR spectrum of dppm found in literature.²⁸⁰

Table A-5.2: ^1H NMR experimental data for the purchased dppm.

^1H NMR experimental data for dppm in CDCl_3				
ppm	Assignment	Multiplicity	Integration	Calc. number of ^1H
7.43	o-H	multiplet	4.06	8.12
7.29	m/p-H	triplet	5.80	11.60
2.80	PCH_2P	triplet	1	2

Table A-5.3: ^1H NMR spectrum data for dppm obtained from literature.²⁸⁰

^1H NMR spectroscopy data for dppm in CDCl_3 , as given in literature			
ppm	Assignment	Multiplicity	Number of ^1H
7.43	o-H	multiplet	8
7.28	m/p-H	triplet	12
2.80	PCH_2P	triplet	2

From these tables it can be concluded that the compound analysed was indeed dppm and it did not contain significant amounts of impurities. The experimental and literature data were in good agreement with each other in terms of chemical shifts, assignment, multiplicity and the number of protons per peak. The only coupling constant given in literature for dppm is the $^2J_{\text{HP}}$ for the coupling between the methylene proton and phosphorus, with a value of 1.5 Hz. This was also in agreement with the $^2J_{\text{HP}}$ determined from experimental data, namely $^2J_{\text{HP}} = 1.5$ Hz. This is further shown in Figure A-5.4, which is a detail taken from the full spectrum presented in Figure A-5.3 above. This was in the expected range for the $^2J_{\text{HP}}$ coupling described in literature (0-50 Hz), albeit in the lower range.⁴¹²

The assignment of the experimental multiplets at 7.43 ppm and 7.29 ppm was undergone by comparison to the literature assignments as given in Table A-5.3. This was further corroborated by the ratio of 2:3 of the integration of the respective peaks.

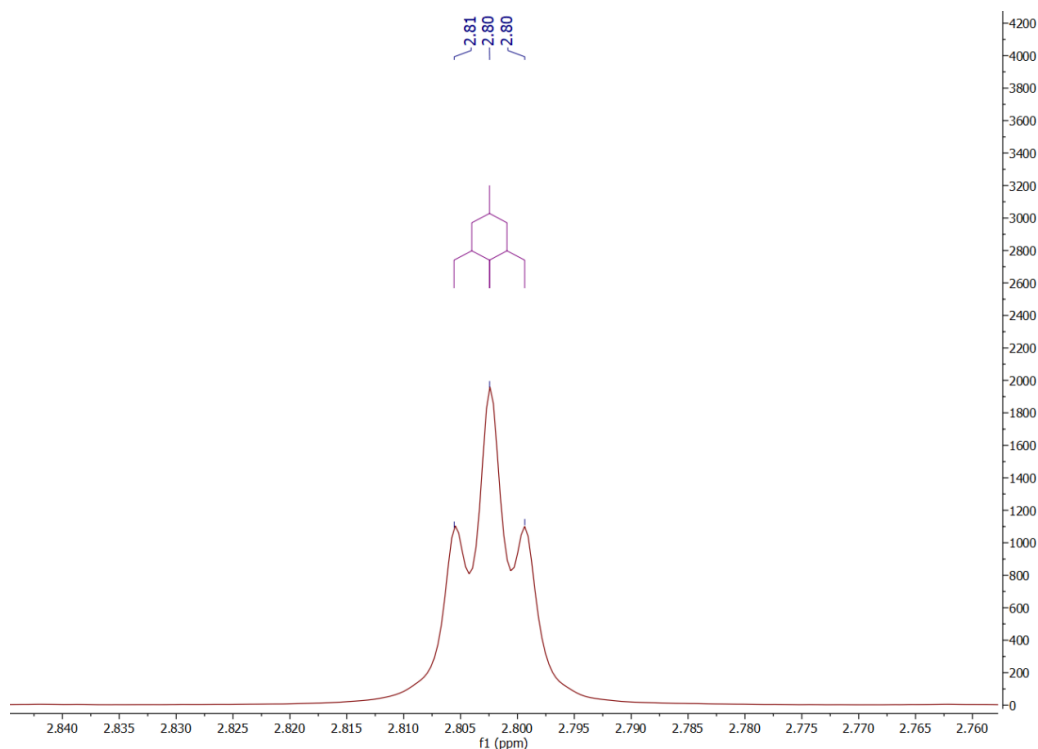


Figure A-5.4: Detail of dppm spectrum showing triplet assigned to the ^1H on PCH₂P.

Both experimental and literature data indicated that the phenyl protons were effected by the presence of the P(III) substituents, when compared to unsubstituted benzene. This indicated that the phosphorus centres acted as electron withdrawing groups, even though the electronegativity of phosphorus is slightly smaller than that of carbon and similar to that of hydrogen.²⁸¹ This effect seems to be entirely due to inductive effects, as conjugation effects of the phosphorus lone pair would cause an upfield shift of ortho and para proton peaks.²⁸¹ If the P(III) centres are inductively electron withdrawing there would be a downfield shift of the o-H while leaving the m/p-H unaffected since the induction effect is not long range. This also explains the presence of the triplet for the m/p-H as the chemical environment around these protons is unaffected by the P(III) and therefore they have the same chemical shift and are only coupled with the two o-H. This indicated that conjugation of the phenyl system and the phosphorus lone pair did not occur, as reported for compounds with similar P(III)–phenyl moieties.¹⁰⁰

The coupling constant for the m/p-H triplet was found to be of 3.2 Hz in the experimental spectrum, which was also in good agreement with the distances between the triplet peaks in the literature data. Coupling constants for the multiplet attributed to the increasingly deshielded o-H protons at around 7.43 ppm could not be properly described.

APPENDIX 6: EXPERIMENTAL DATA FOR $\text{H}_2\text{C}(\text{Ph}_2\text{PNSiMe}_3)_2$

Three batches of $\text{H}_2\text{C}(\text{Ph}_2\text{PNSiMe}_3)_2$ were prepared by following the Phospha-Staudinger method as described in Section 3.3.1.1.2. In all cases the desired product was obtained. This was confirmed by comparison of the characterisation data collected in this study with that published by Appel and Ruppert in 1974, as described in Section 4.1.1.2.³⁴

A-6.1. Analysis by Infra-red spectroscopy

The IR spectra of the two products, $\text{H}_2\text{C}(\text{Ph}_2\text{PNSiMe}_3)_2_1$ and $\text{H}_2\text{C}(\text{Ph}_2\text{PNSiMe}_3)_2_2$, were initially compared to the IR spectra of the two main reagents namely, dppm and trimethylsilyl azide.²⁹⁸ The comparison is presented in Figure A-6.1. The spectrum of $\text{H}_2\text{C}(\text{Ph}_2\text{PNSiMe}_3)_2_2$ was compared with the detailed IR data provided for $\text{H}_2\text{C}(\text{Ph}_2\text{PNSiMe}_3)_2$ by Appel and Ruppert in 1974 as given in Figure A-6.2.³⁴ This confirmed the nature of both aforementioned products. Comparison of the spectra of $\text{H}_2\text{C}(\text{Ph}_2\text{PNSiMe}_3)_2_1$ and $\text{H}_2\text{C}(\text{Ph}_2\text{PNSiMe}_3)_2_3$ as given in Figure A-6.3 showed that the latter compound had the same composition as the previous two products.

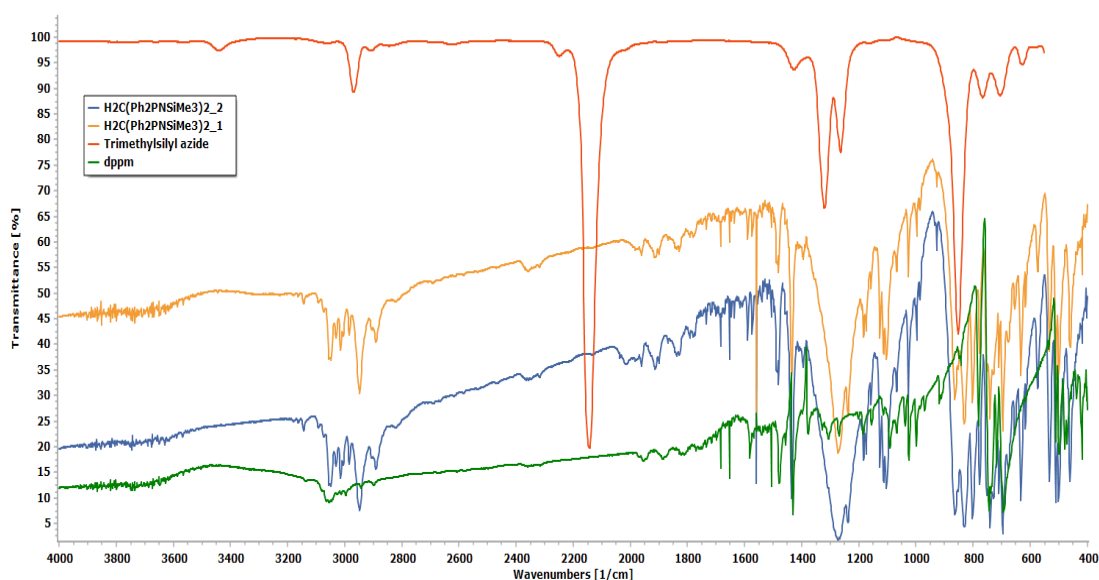


Figure A-6.1: IR spectra of $\text{H}_2\text{C}(\text{Ph}_2\text{PNSiMe}_3)_2_1$ (orange), $\text{H}_2\text{C}(\text{Ph}_2\text{PNSiMe}_3)_2_2$ (blue), trimethylsilyl azide (red) and dppm (green).

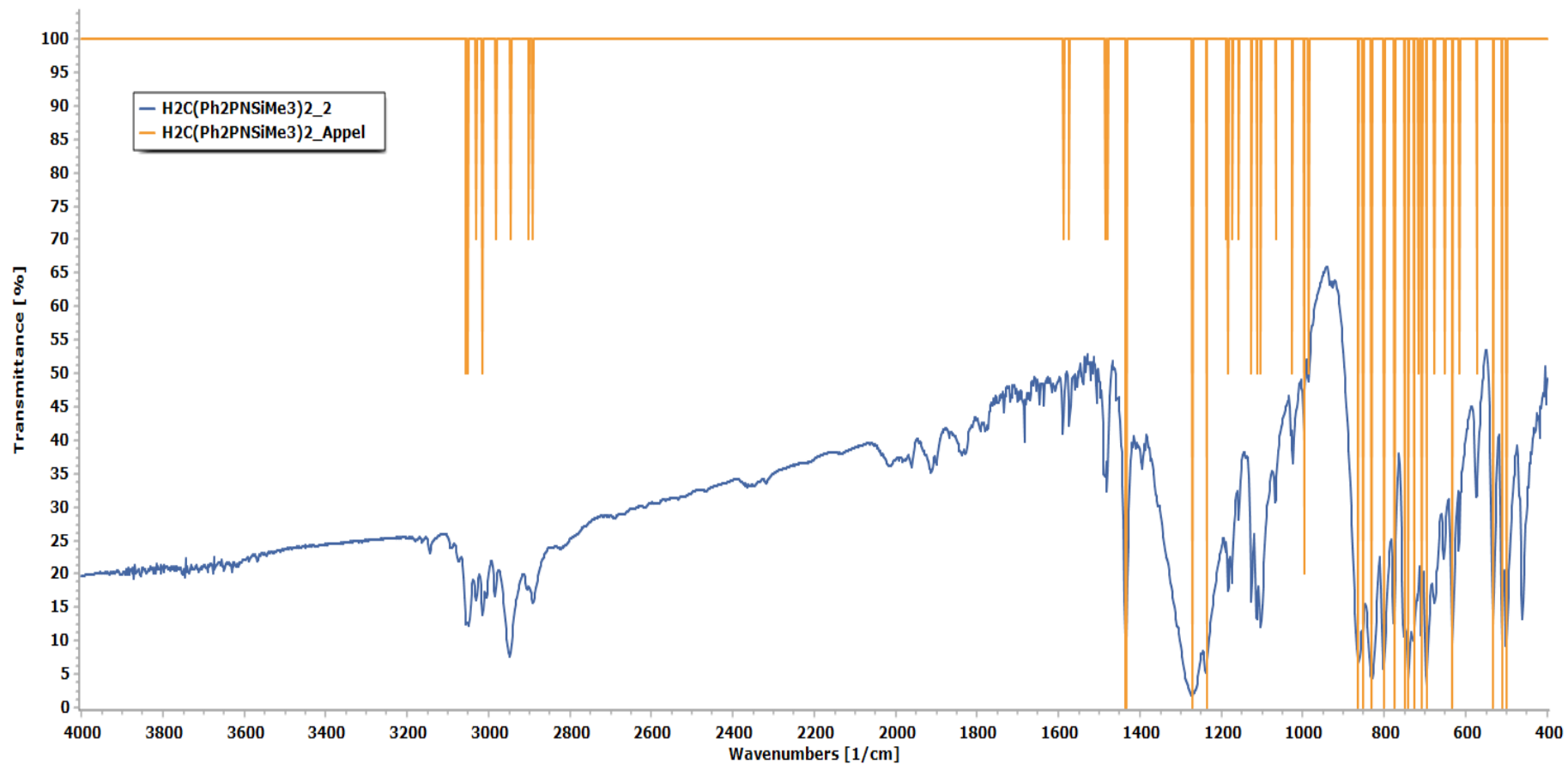


Figure A-6.2: IR spectra of $\text{H}_2\text{C}(\text{Ph}_2\text{PNSiMe}_3)_2$ (blue) with the literature data (orange).

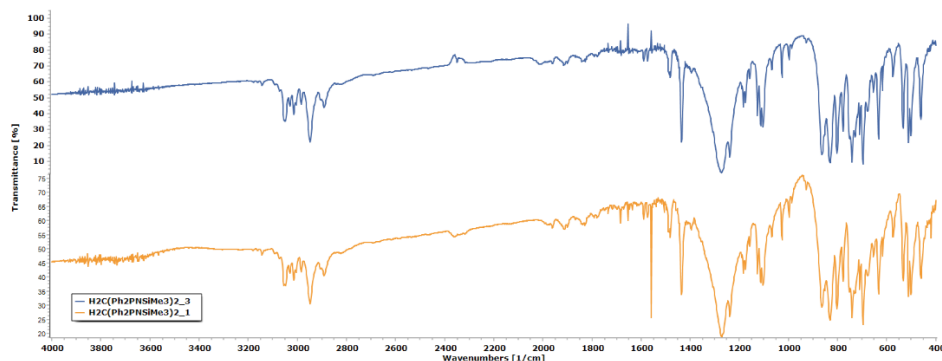


Figure A-6.3: IR spectra of $\text{H}_2\text{C}(\text{Ph}_2\text{PNSiMe}_3)_2_3$ (blue) and $\text{H}_2\text{C}(\text{Ph}_2\text{PNSiMe}_3)_2_1$ (orange).

A-6.2. Analysis by ^1H NMR spectroscopy

The ^1H NMR spectrum of $\text{H}_2\text{C}(\text{Ph}_2\text{PNSiMe}_3)_2_1$ was obtained in benzene- d_6 (C_6D_6) as a solvent. The full spectrum is given in Figure A-6.4. Apart from diagnostic peaks a number of impurity peaks were noted, namely the singlet at 2.11 ppm attributed to acetonitrile and the three doublets at 2.20 ppm, 1.54 ppm and 1.49 ppm possibly due to minor by-products. The first diagnostic feature of the spectrum was the triplet at 3.29 ppm, which is shown in more detail in Figure A-6.5. This was attributed to the methylene protons, PCH_2P .

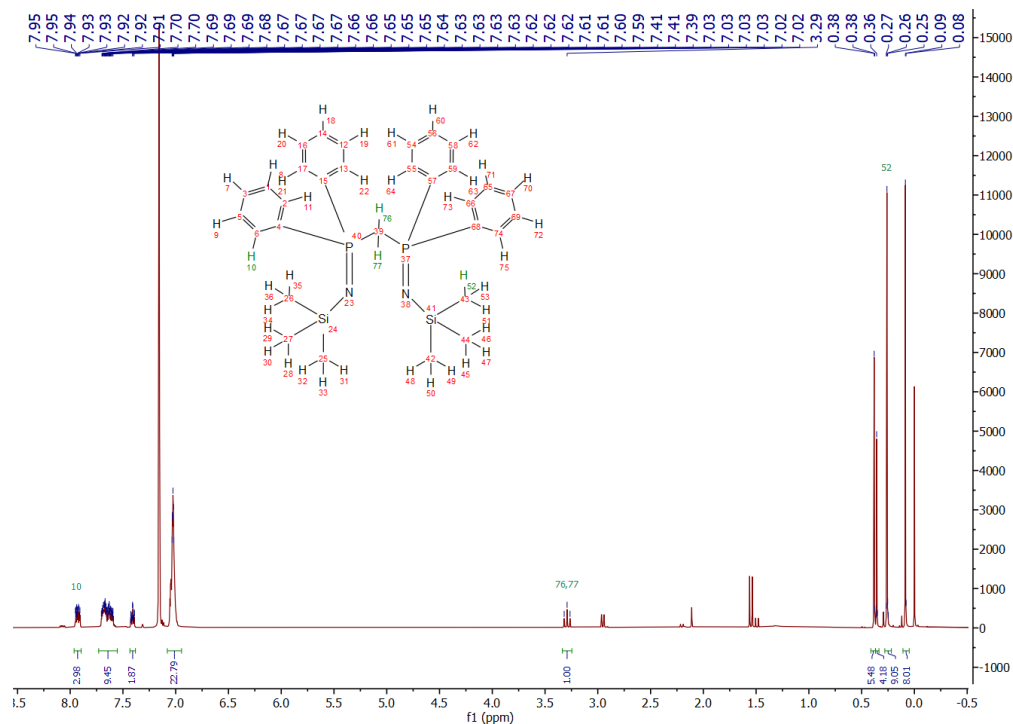


Figure A-6.4: Full ^1H NMR spectrum for $\text{H}_2\text{C}(\text{Ph}_2\text{PSiMe}_3)_2_1$ in C_6D_6 .

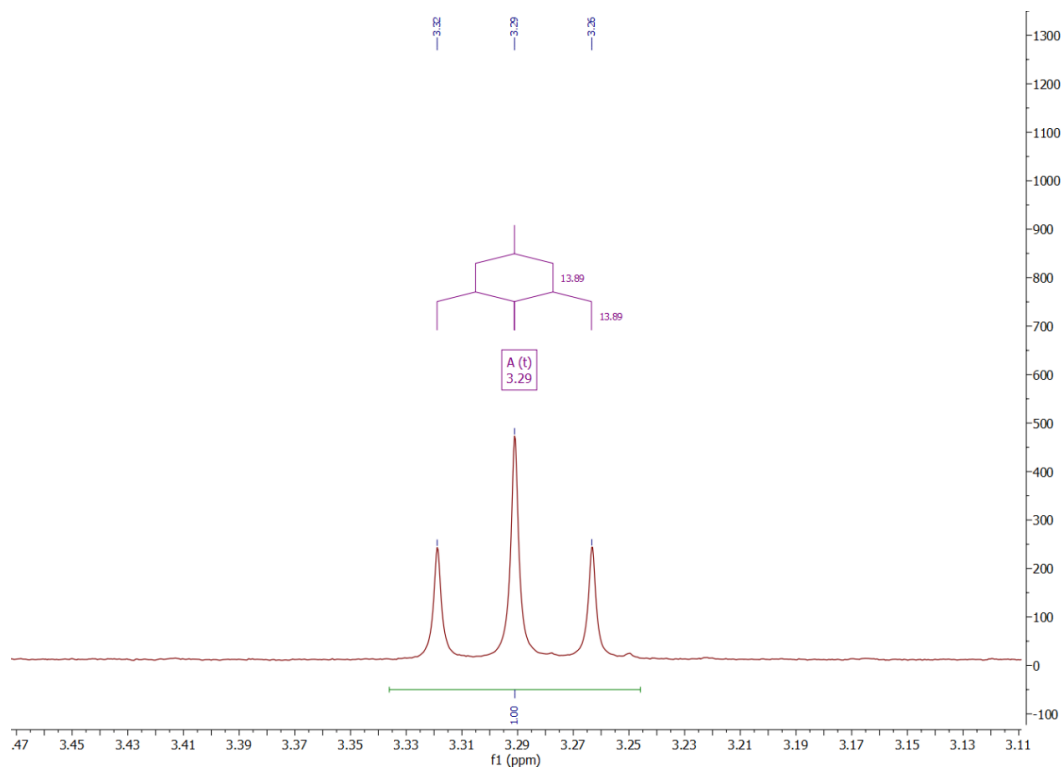


Figure A-6.5: Detail of triplet in ^1H NMR spectrum of $\text{H}_2\text{C}(\text{Ph}_2\text{PSiMe}_3)_2_1$ assigned to PCH_2P protons.

The multiplets attributed to the phenyl protons are given in Figure A-6.6, which shows a detail from the full spectrum obtained for $\text{H}_2\text{C}(\text{Ph}_2\text{PNSiMe}_3)_2_1$. Details of these peaks are given in Table A-6.1. The peaks around 7.41 ppm are given separately in Figure A-6.7, where the tentative coupling described in Table A-6.1 is shown.

Table A-6.1: Details of phenyl ring proton peaks for $\text{H}_2\text{C}(\text{Ph}_2\text{PNSiMe}_3)_2_1$.

^1H NMR experimental data for phenyl proton peaks of $\text{H}_2\text{C}(\text{Ph}_2\text{PNSiMe}_3)_2_1$ in C_6D_6				
Ppm	Multiplicity	Integration	Coupling	Calc. no. ^1H
7.93	multiplet, asymmetric	2.97	N/A	5.94
7.65	multiplet, asymmetric	9.43	N/A	18.86
7.41	triplet of doublets	1.81	$J_1 = 1.65 \text{ Hz (d)}$ $J_2 = 7.68 \text{ Hz (t)}$	3.62
7.03	multiplet, asymmetric	22.95	N/A	45.9

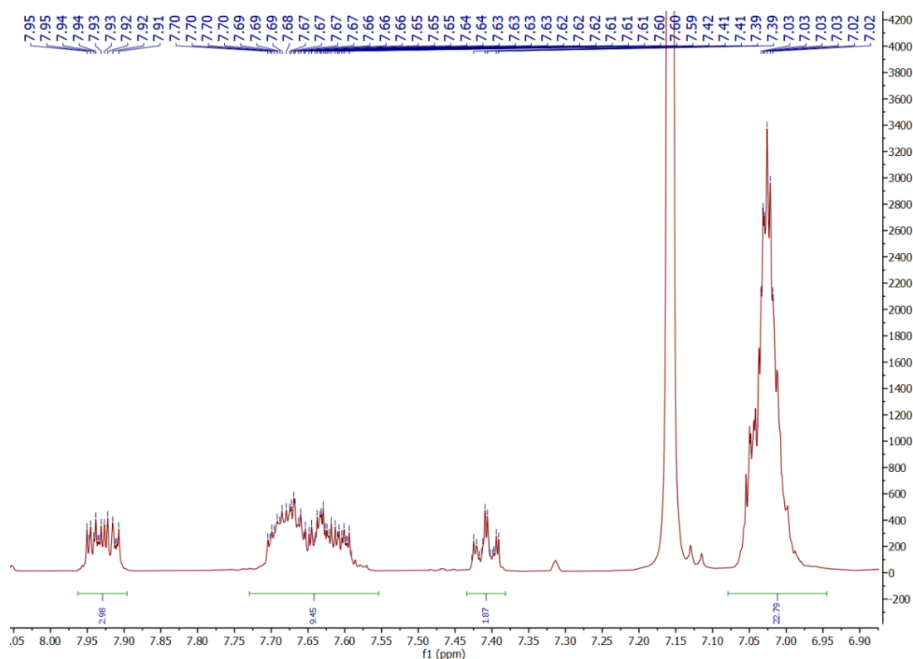


Figure A-6.6: Detail showing the peaks attributed to the phenyl protons of $\text{H}_2\text{C}(\text{Ph}_2\text{PSiMe}_3)_2_1$.

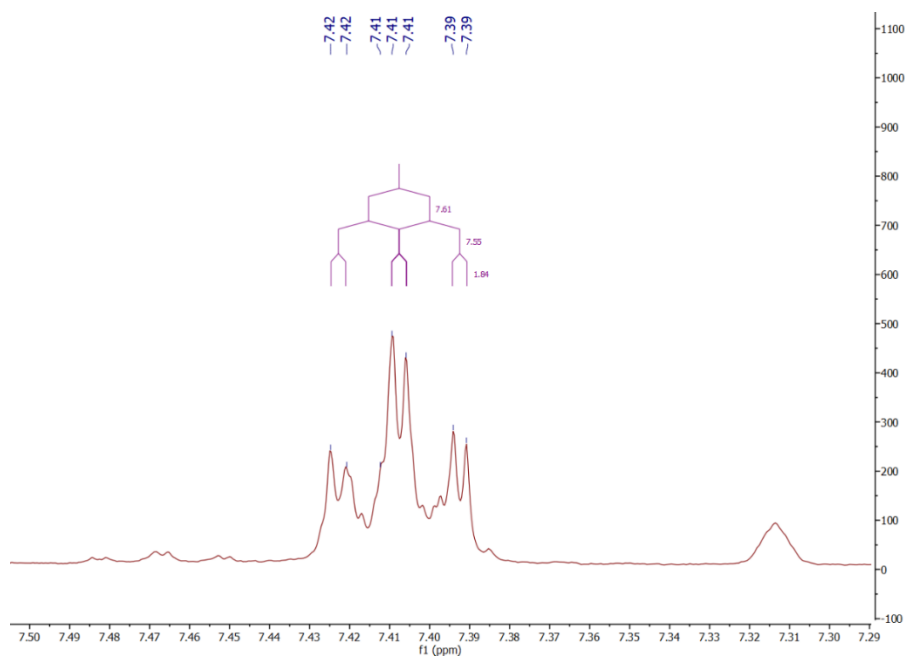


Figure A-6.7: Detail showing the peaks around 7.41 ppm for the spectrum of $\text{H}_2\text{C}(\text{Ph}_2\text{PSiMe}_3)_2_1$.

Four large singlets were observed in the range of 0.4 to 0.05 ppm of the spectrum obtained for $\text{H}_2\text{C}(\text{Ph}_2\text{PNSiMe}_3)_2_1$ and these are given in more detail in Figure A-6.8. The integration data for these peaks is given below in Table A-6.2. This data in Table A-6.2 may indicate that the singlet at 0.26 ppm is due to the protons of the trimethylsilyl groups as this yielded the closest calculated number of protons to the expected number of 18.

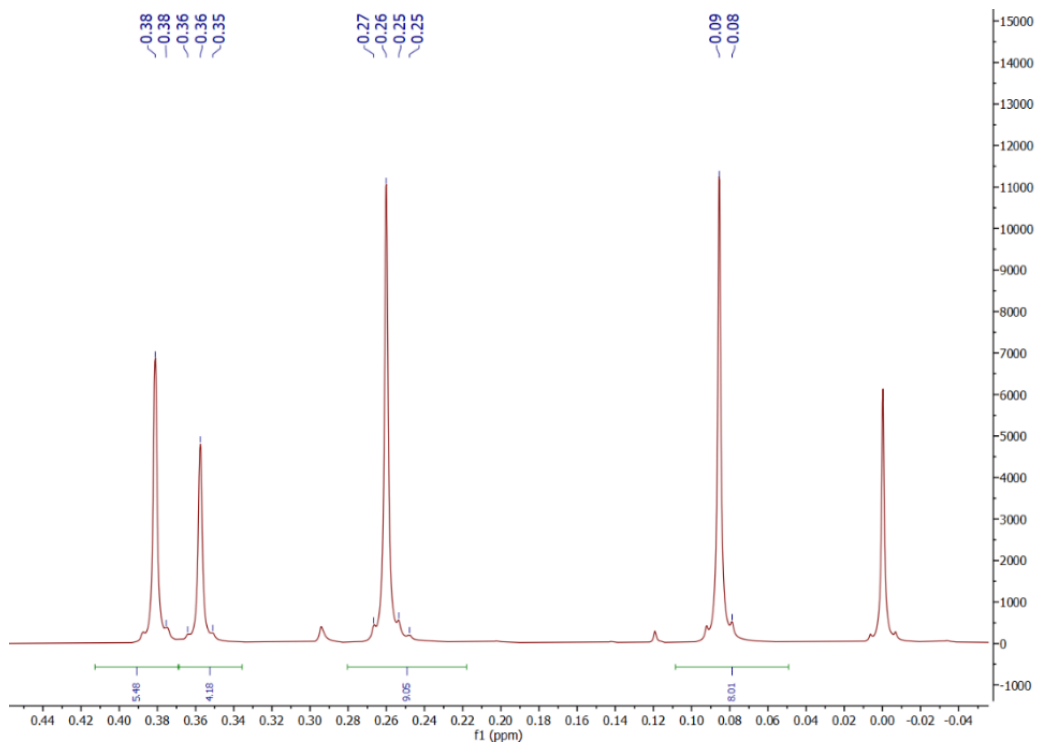


Figure A-6.8: Detail showing the range 0.4 to 0.05 ppm for the spectrum of $\text{H}_2\text{C}(\text{Ph}_2\text{PSiMe}_3)_2_1$.

Table A-6.2: Integration data for singlets in the region 0.4 to 0.05 ppm in the spectrum of $\text{H}_2\text{C}(\text{Ph}_2\text{PSiMe}_3)_2_1$.

Integration Data for singlets in the region 0.4 to 0.05ppm in the spectrum of $\text{H}_2\text{C}(\text{Ph}_2\text{PNSiMe}_3)_2_1$			
ppm	Integration	Calc. no. ^1H	Expected no. ^1H
0.38	5.56	11.12	18
0.35	4.20	8.40	18
0.26	9.09	18.18	18
0.09	8.05	16.1	18

APPENDIX 7: EXPERIMENTAL DATA FOR $\text{H}_2\text{C}(\text{Ph}_2\text{PS})_2$

A-7.1. Analysis by Infra-red spectroscopy

The IR spectrum of the product $\text{H}_2\text{C}(\text{Ph}_2\text{PS})_2_1$ was obtained and is presented in Figure A-7.1 hereunder, along with the spectrum obtained for the dppm starting reagent. The most likely bands that could be assigned to the diagnostic P=S vibration in the IR spectrum of product $\text{H}_2\text{C}(\text{Ph}_2\text{PS})_2_1$ are marked in yellow in Figure A-7.2.

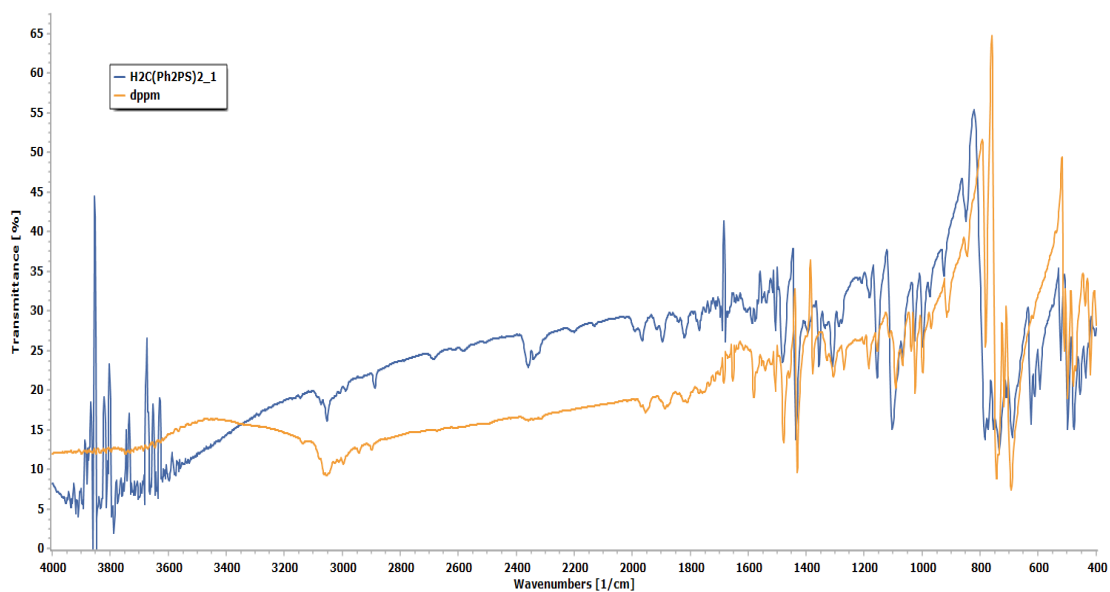


Figure A-7.1: IR spectrum of the $\text{H}_2\text{C}(\text{Ph}_2\text{PS})_2_1$ (blue) and dppm (orange).

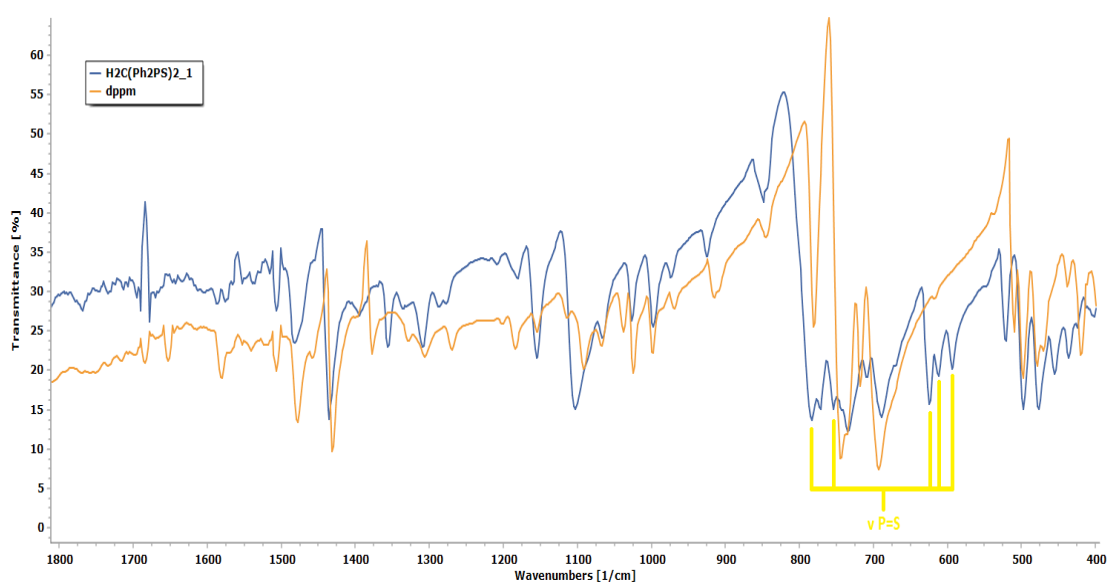


Figure A-7.2: Possible P=S vibration bands in the IR spectrum of $\text{H}_2\text{C}(\text{Ph}_2\text{PS})_2_1$.

The IR spectra of $\text{H}_2\text{C}(\text{Ph}_2\text{PS})_2_{2a}$ and $\text{H}_2\text{C}(\text{Ph}_2\text{PS})_2_{2b}$ are given in Figure A-7.3, while the spectra of $\text{H}_2\text{C}(\text{Ph}_2\text{PS})_2_{3a}$ and $\text{H}_2\text{C}(\text{Ph}_2\text{PS})_2_{3b}$ are given in Figure A-7.4. The bands of interest for each solid product lie in the fingerprint region, specifically between 805 and 590 cm^{-1} , wherein the bands due to $\nu\text{ P}=\text{S}$ and $\nu\text{ P}-\text{CH}_2-\text{P}$ are known to occur.

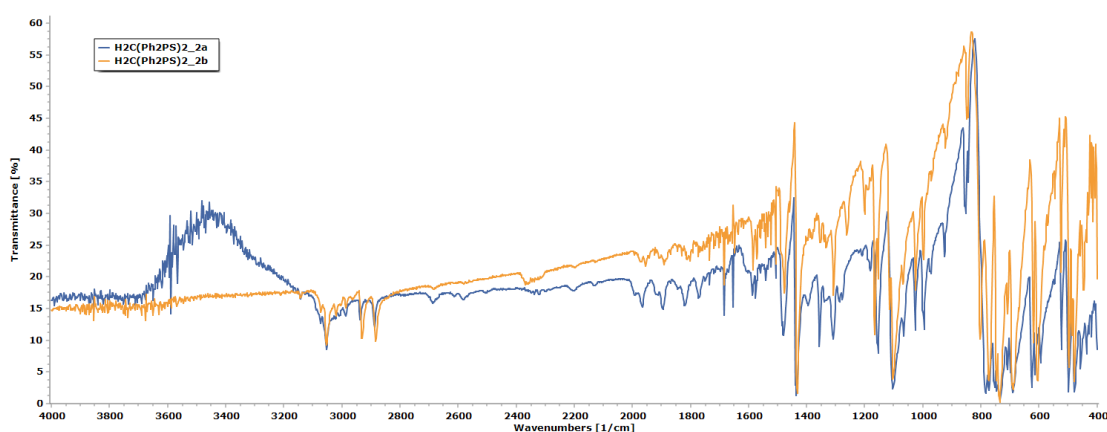


Figure A-7.3: IR spectra of $\text{H}_2\text{C}(\text{Ph}_2\text{PS})_2_{2a}$ (blue) and $\text{H}_2\text{C}(\text{Ph}_2\text{PS})_2_{2b}$ (orange).

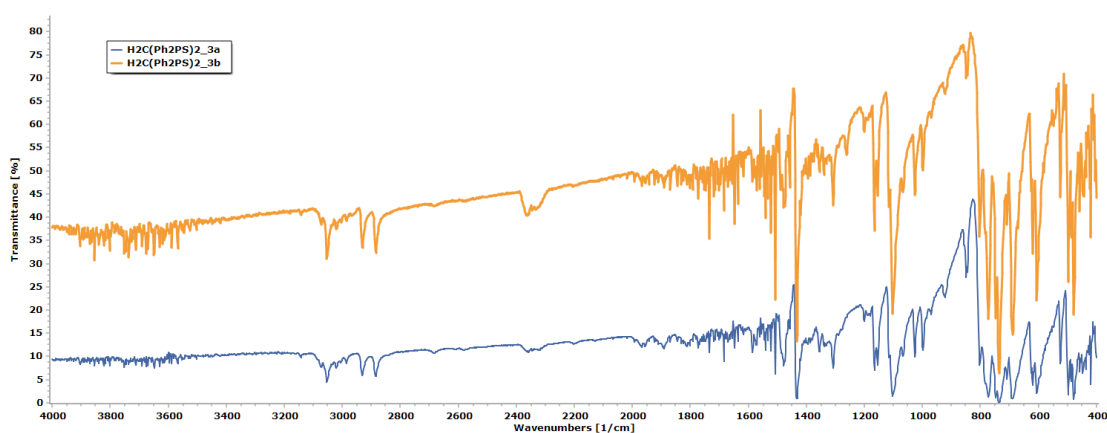


Figure A-7.4: IR spectra of $\text{H}_2\text{C}(\text{Ph}_2\text{PS})_2_{3a}$ (blue) and $\text{H}_2\text{C}(\text{Ph}_2\text{PS})_2_{3b}$ (orange).

A-7.2. Analysis by ^1H NMR spectroscopy

The ligand $\text{H}_2\text{C}(\text{Ph}_2\text{PS})_2_1$ in benzene- d_6 was analysed by ^1H NMR spectroscopy, with the spectrum obtained given in Figure A-7.5. The triplet at around 3.84 ppm, which is shown in more detail in Figure A-7.6. was attributed to the methylene protons (PCH_2P) in $\text{H}_2\text{C}(\text{Ph}_2\text{PS})_2_1$. The integration details of the peaks around 3.84, 6.92 and 7.89 ppm are given in Table A-7.1.

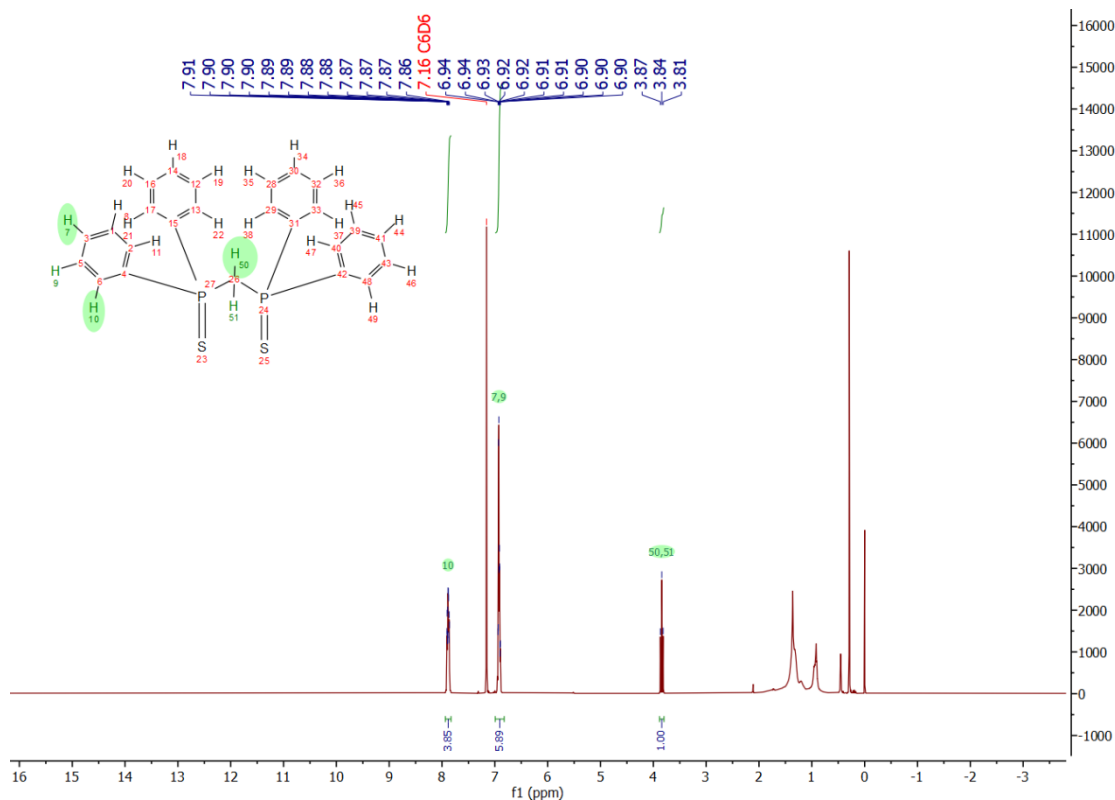


Figure A-7.5: ^1H NMR spectrum for $\text{H}_2\text{C}(\text{Ph}_2\text{PS})_2_1$ in C_6D_6 .

Table A-7.1: Integration details for the peaks assigned to PCH_2P , o-H and m/p-H respectively.

Integration details for the peaks assigned in $\text{H}_2\text{C}(\text{Ph}_2\text{PS})_2_1$				
Ppm	Assignment	Integration	Calc. no. ^1H	Expected no. ^1H
7.89	o-H	3.79	7.58	8
6.92	m/p-H	5.91	11.82	12
3.84	PCH_2P	1	2	2

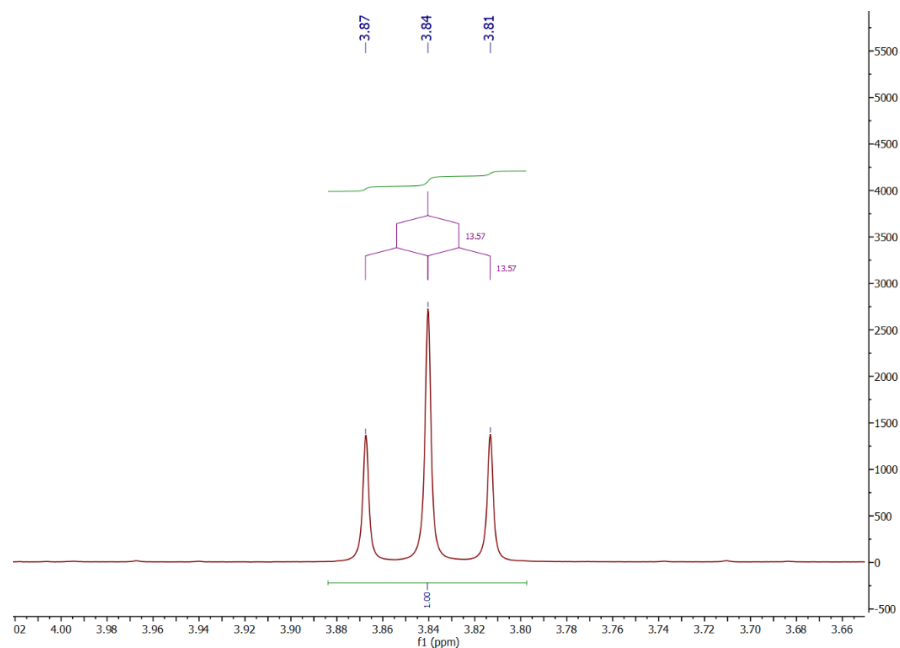


Figure A-7.6: Triplet at 3.84 ppm attributed to the PCH₂P protons.

The ¹H NMR spectra for the products H₂C(Ph₂PS)₂_2a, _2b, _3a and _3b in CDCl₃ are given in Figure A-7.7, along with the spectrum of H₂C(Ph₂PS)₂_1 in benzene-d₆. Details of the proton peaks in the ¹H NMR spectra for the products H₂C(Ph₂PS)₂_2a, _2b, _3a and _3b in CDCl₃ are given in Table A-7.2. In the CDCl₃ samples peaks for water (1.56 ppm) and silicone grease (0.07 ppm) impurities were observed, while in the benzene-d₆ sample the main impurities were grease (1.362 ppm and 0.918 ppm) and silicone grease (0.29 ppm).

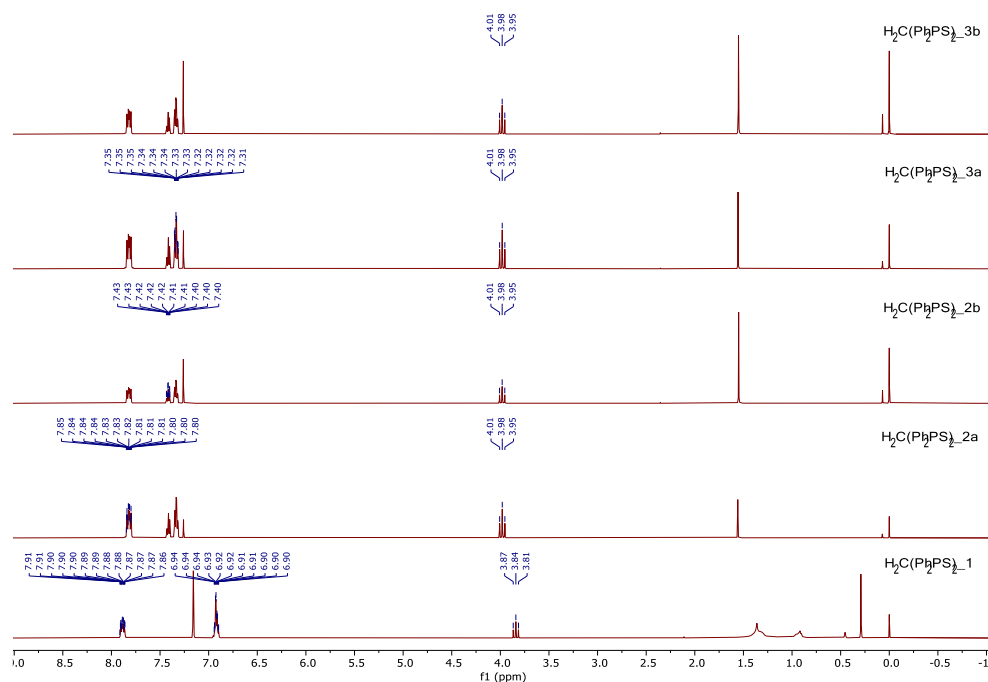


Figure A-7.7: ¹H NMR spectra of all the H₂C(Ph₂PS)₂ solids obtained in the study.

Table A-7.2: Details of proton peaks in spectra for H₂C(Ph₂PS)₂_2a, _2b, _3a and _3b in CDCl₃.

¹H NMR experimental data for phenyl proton peaks of H₂C(Ph₂PS)₂ in CDCl₃				
Ppm	Multiplicity	Integration	Coupling	Calc. no. ¹H
7.82	Doublet of doublets	2	J ₁ = 7.62 Hz J ₂ = 13.13 Hz	8
7.42	triplet	1	N/A	4
7.33	triplet	2	N/A	8
3.98	triplet	0.5	J = 13.43 Hz	2

A-7.3. Analysis by Microscopy

A micrograph of the crystals of H₂C(Ph₂PS)₂_1, obtained under polarised light, is given in Figure A-7.8.

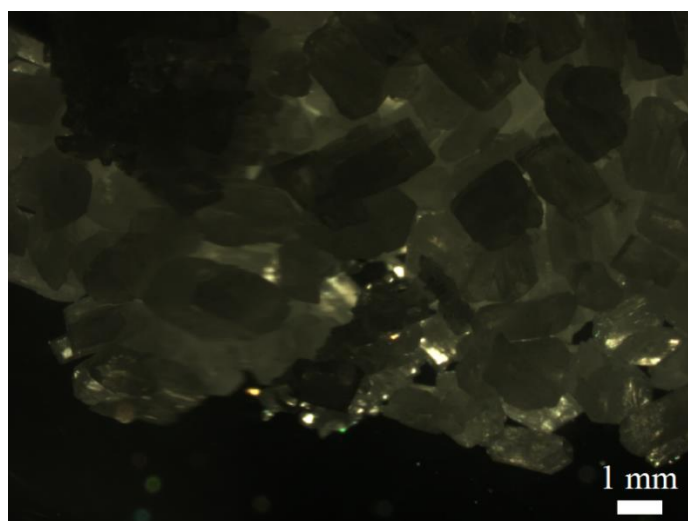


Figure A-7.8: Crystals of H₂C(Ph₂PS)₂_1 under polarised light.

A-7.4. Analysis by Powder X-ray diffraction

The experimental PXRD pattern for H₂C(Ph₂PS)₂_2b is given in Figure A-7.9 along with the calculated PXRD patterns of the two published polymorphs, namely the polymorph published by Carmalt in the space group *P2₁/n* and the polymorph in *C2/c* space group published by Thirumoorthi (both calculated in Mercury).^{35,297}

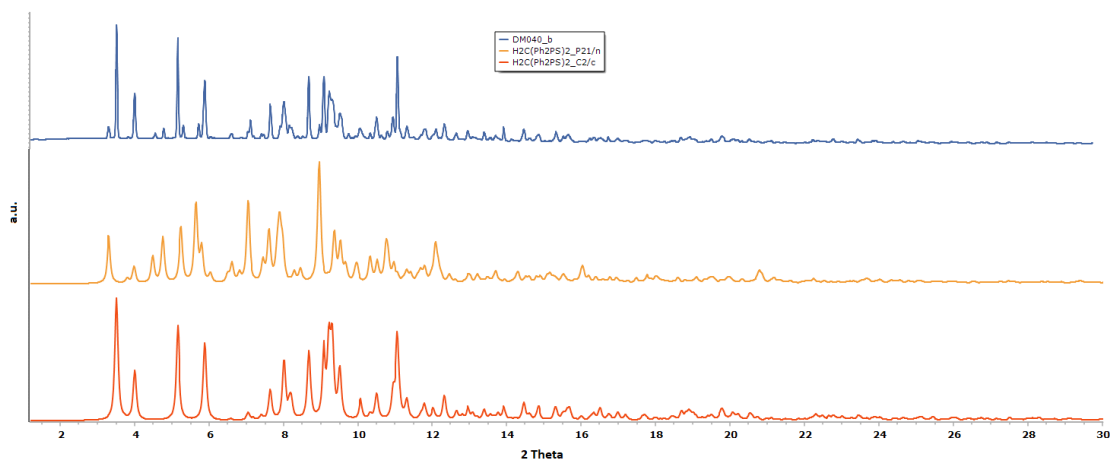


Figure A-7.9: PXRD patterns of H₂C(Ph₂PS)₂_2b (blue), P₂₁/n (orange) and C₂/c (red).

APPENDIX 8: EXPERIMENTAL DATA FOR $\text{LnI}_3(\text{THF})_{3.5}$ STARTING REAGENTS.

A-8.1. Characterisation of $\text{NdI}_3(\text{THF})_{3.5}$

A-8.1.1. Analysis by Infra-red spectroscopy

The spectra of $\text{NdI}_3(\text{THF})_{3.5_1}$, is given in Figure A-8.1. Samples for $\text{NdI}_3(\text{THF})_{3.5_1}$ were prepared in Nujol mull on salt windows. The peaks typical of the Nujol mull were visible as the broad band in the range $3000\text{-}2850\text{ cm}^{-1}$, the two strong bands at 1462 cm^{-1} and 1377 cm^{-1} , along with the shoulder at 1366 cm^{-1} and the distinct medium sized band at 723 cm^{-1} .²⁸⁰ The spectrum of $\text{NdI}_3(\text{THF})_{3.5_1}$ in Nujol mull in the wavenumber range $1800\text{-}400\text{ cm}^{-1}$ is given in Figure A-8.2, along with literature data for $\text{NdI}_3(\text{THF})_{3.5}$ (in Nujol Mull),¹³⁷ $\text{NdI}_3(\text{THF})_4$ (in KBr) and THF (liquid film) for comparison.^{151,280} In these cases bands, listed as weak, medium and strong in literature, are plotted at a transmittance of 70 %, 50 % and 0 % respectively, so as to provide better comparison.

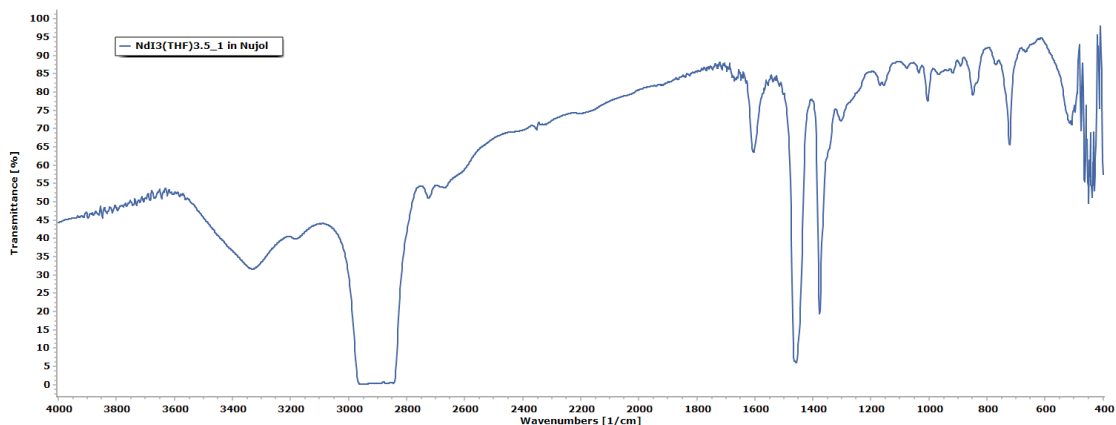


Figure A-8.1: IR spectra of $\text{NdI}_3(\text{THF})_{3.5_1}$ in Nujol (blue).

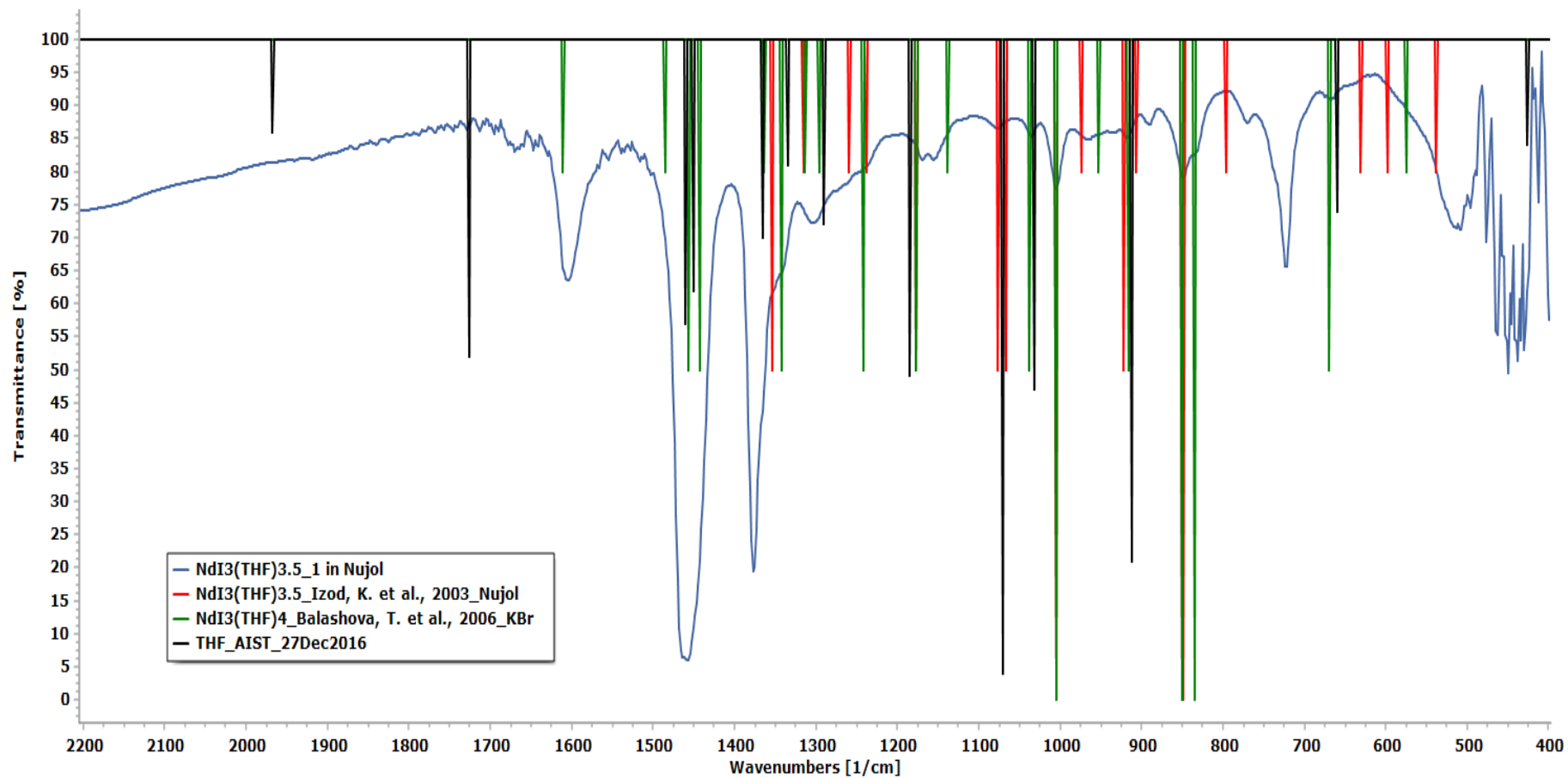


Figure A-8.2: IR spectra of NdI₃(THF)_{3.5_1} (blue), NdI₃(THF)_{3.5} (red), NdI₃(THF)₄ (green) and THF (black).

A-8.1.2. Analysis by UV-visible light spectroscopy

$\text{NdI}_3(\text{THF})_{3.5_1}$ was analysed qualitatively using UV-visible light spectroscopy. Sample solutions were prepared by heating and stirring small suspensions of the solids in THF. $\text{NdCl}_3 \cdot n\text{H}_2\text{O}$ was used as a reference to indicate the presence of the Nd^{3+} in a THF solution, since the absorption peaks of lanthanides are typically unaffected by ligands present and therefore unlikely to shift drastically between the iodides and the chloride.²³ A detail of the spectra of $\text{NdI}_3(\text{THF})_{3.5_1}$ (which had been left under vacuum at 140 °C but was not washed to remove excess iodine) and $\text{NdCl}_3 \cdot n\text{H}_2\text{O}$ in the wavelength range 500-900 nm is shown in Figure A-8.3.

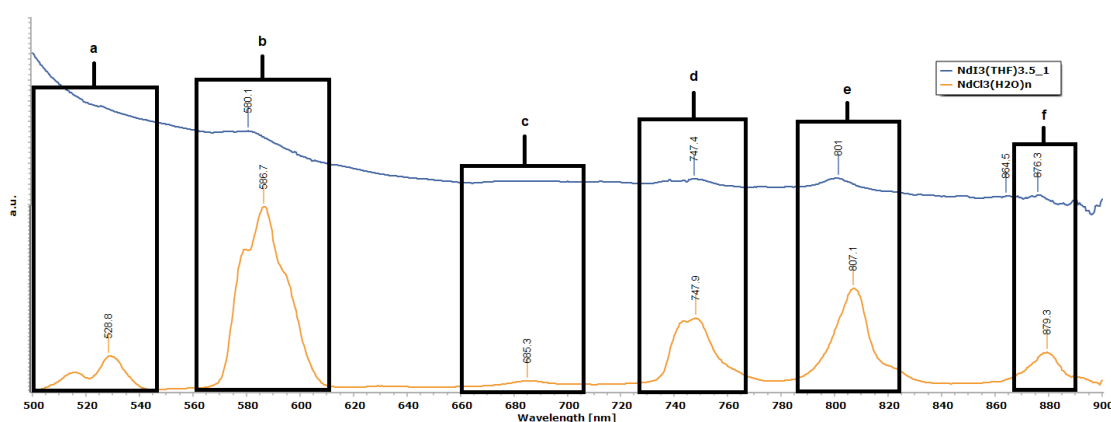


Figure A-8.3: UV-vis spectra of $\text{NdI}_3(\text{THF})_{3.5_1}$ (blue) and $\text{NdCl}_3 \cdot n\text{H}_2\text{O}$ (orange) in the range 400-900 nm.

The peaks labelled a to f are due to the neodymium (III) cation transitions as listed below:^{413,414}

- a - $^4\text{I}_{9/2}$ \rightarrow $^2\text{K}_{13/2}$, $^4\text{G}_{7/2}$, $^4\text{G}_{9/2}$
- b - $^4\text{I}_{9/2}$ \rightarrow $^4\text{G}_{5/2}$, $^2\text{G}_{7/2}$
- c - $^4\text{I}_{9/2}$ \rightarrow $^4\text{F}_{9/2}$
- d - $^4\text{I}_{9/2}$ \rightarrow $^4\text{F}_{3/2}$, $^4\text{S}_{3/2}$
- e - $^4\text{I}_{9/2}$ \rightarrow $^4\text{F}_{5/2}$, $^2\text{H}_{9/2}$
- f - $^4\text{I}_{9/2}$ \rightarrow $^4\text{F}_{3/2}$

The product $\text{NdI}_3(\text{THF})_{3.5_1}$ was analysed by UV-visible spectroscopy after vacuum removal of iodine and after the final washing of the solid with multiple portions of 40-60 °C petroleum ether and THF. The different spectra obtained are given in Figure A-8.4, with spectrum $\text{NdI}_3(\text{THF})_{3.5_1\text{a}}$ for the unwashed sample and spectrum $\text{NdI}_3(\text{THF})_{3.5_1\text{b}}$ for the washed sample.

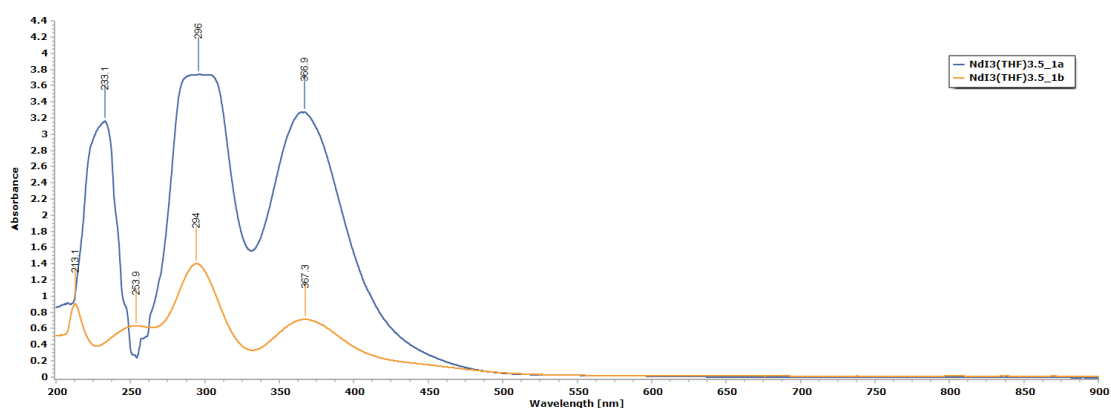


Figure A-8.4: UV-vis Spectra of $\text{NdI}_3(\text{THF})_{3.5_1a}$ (blue) and $\text{NdI}_3(\text{THF})_{3.5_1b}$ (orange)

A-8.2. Characterisation of $\text{SmI}_3(\text{THF})_{3.5}$

A-8.2.1. Analysis by Infra-red spectroscopy

The initial solid product from the $\text{SmI}_3(\text{THF})_{3.5}$ reaction was washed under solvent extraction in a filtration tube followed by elemental iodine removal under vacuum at 140 °C to yield the first product $\text{SmI}_3(\text{THF})_{3.5_1}$. A portion of this was then purified further by Soxhlet extraction to give the product $\text{SmI}_3(\text{THF})_{3.5_2}$. The IR spectra of the two solids, $\text{SmI}_3(\text{THF})_{3.5_1}$ and $\text{SmI}_3(\text{THF})_{3.5_2}$, in Nujol mull are given in Figure A-8.5.

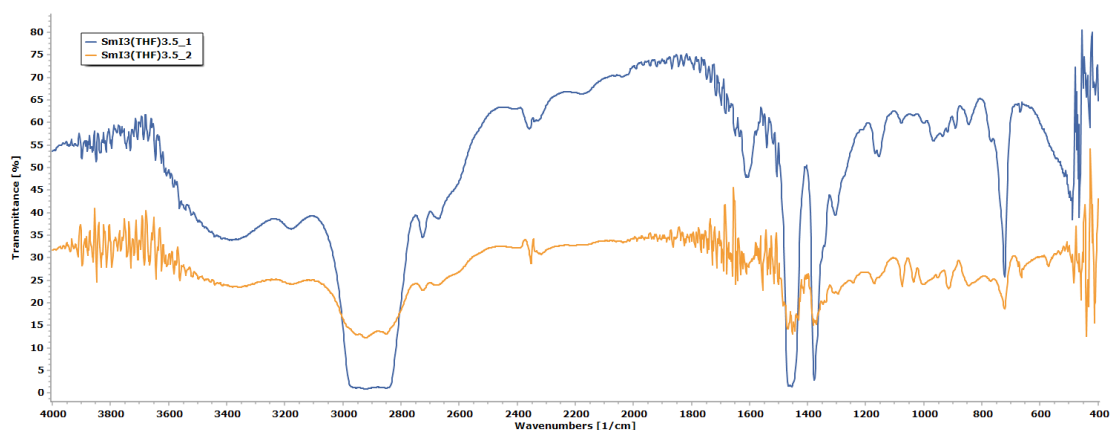


Figure A-8.5: IR Spectra of $\text{SmI}_3(\text{THF})_{3.5_1}$ (blue) and $\text{SmI}_3(\text{THF})_{3.5_2}$ (orange) in Nujol mull.

A detail of the spectra of $\text{SmI}_3(\text{THF})_{3.5_1}$ and $\text{SmI}_3(\text{THF})_{3.5_2}$ (in the region of 1800-400 cm^{-1}) along with the literature data for Nujol and for $\text{SmI}_3(\text{THF})_{3.5}$ are given in Figure A-8.6.¹³⁷ For the two spectra reproduced from published data, bands listed as

weak, medium and strong in literature, are plotted at a transmittance of 70 %, 50 % and 0 % respectively.^{137,280} For both experimental spectra the peaks typical of the Nujol were visible as the strong broad bands in the range 3000-2850 cm^{-1} , the two strong bands at 1462 cm^{-1} and 1377 cm^{-1} , along with the shoulder at 1366 cm^{-1} and the distinct medium sized band at 723 cm^{-1} .²⁸⁰

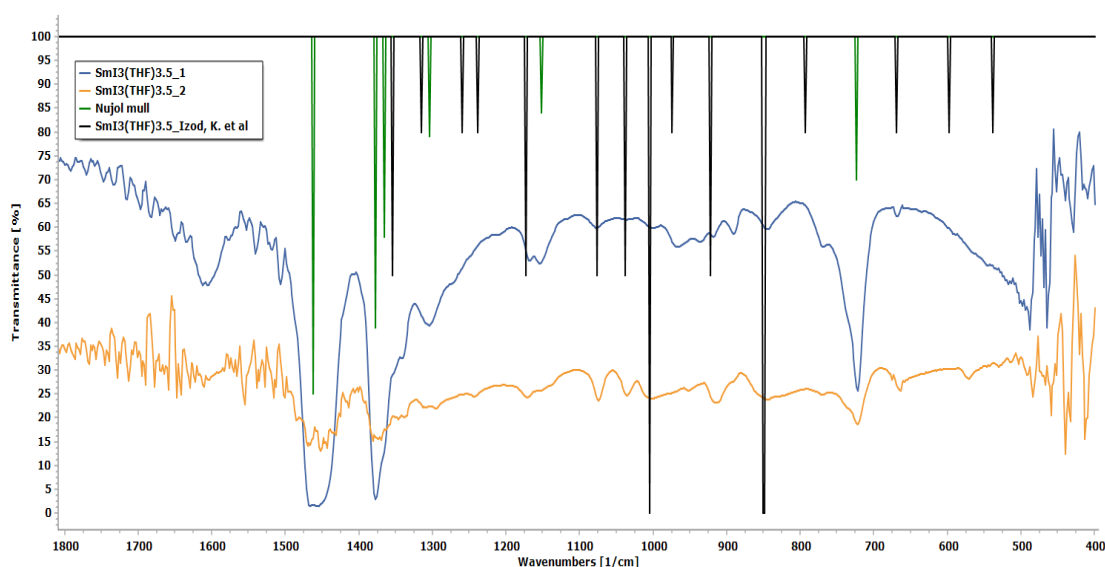


Figure A-8.6: IR spectra of SmI₃(THF)_{3.5_1} (blue) and SmI₃(THF)_{3.5_2} (orange), SmI₃(THF)_{3.5} in literature (black) and Nujol (green) in the region of 1800-400 cm^{-1} .

A-8.2.2. Analysis by Powder X-ray Diffraction

Both solids SmI₃(THF)_{3.5_1} and SmI₃(THF)_{3.5_2}, were observed under a microscope using plane polarised light. The solid SmI₃(THF)_{3.5_1} was likely to be amorphous as no extinction of plane polarised light was observed. In contrast the orange-yellow solid SmI₃(THF)_{3.5_2} was crystalline, as can be observed in Figure A-8.7. The crystalline solid SmI₃(THF)_{3.5_2} was characterised using PXRD. The solid was prepared in a 0.3 mm capillary, sealed under dry nitrogen, and data was collected at synchrotron radiation. The powder pattern of SmI₃(THF)_{3.5_2} is given in Figure A-8.8, together with the PXRD pattern of SmI₃(THF)_{3.5} calculated from the literature data, as obtained from Mercury software.^{137,297}

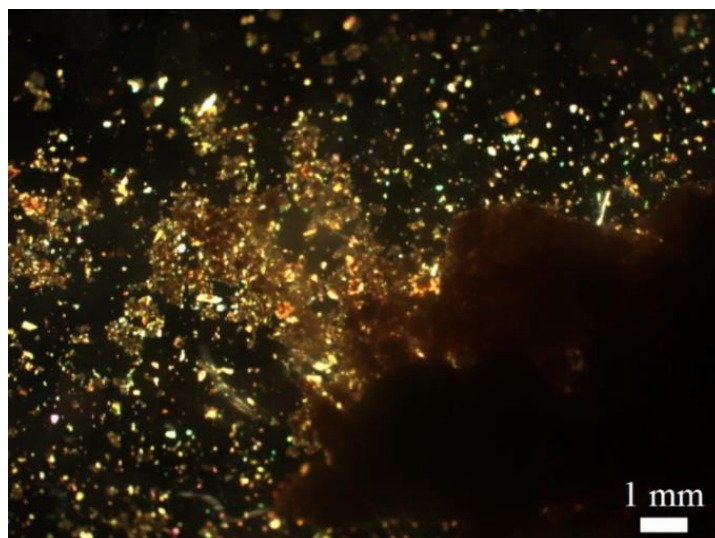


Figure A-8.7: Micrograph of $\text{SmI}_3(\text{THF})_{3.5_2}$.

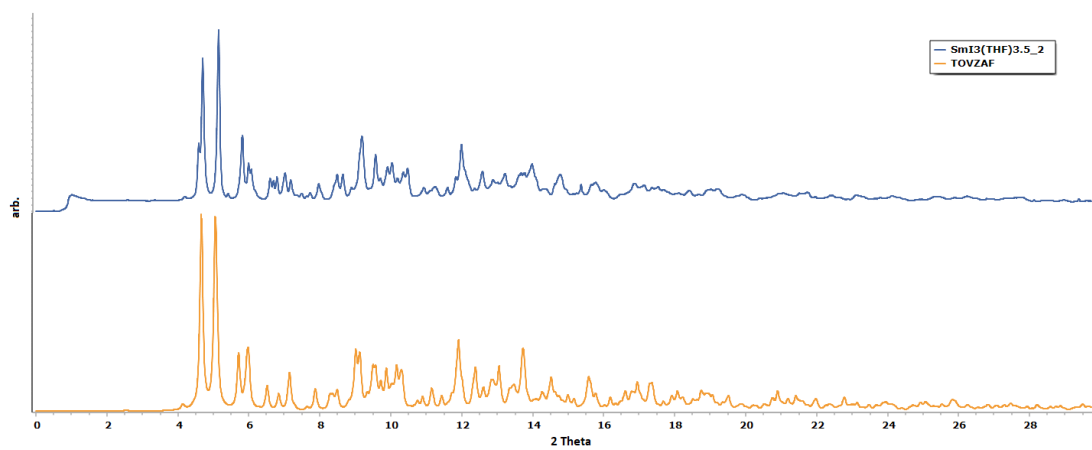


Figure A-8.8: PXRD patterns of $\text{SmI}_3(\text{THF})_{3.5_2}$ (blue) and calculated $\text{SmI}_3(\text{THF})_{3.5}$ literature data (orange).

APPENDIX 9: ADDITIONAL IR, NMR AND PXRD RESULTS FROM THE PREPARATION ATTEMPTS OF $[\text{Sm}_2(\text{C}(\text{Ph}_2\text{PS})_2)_2\text{I}_2\text{THF}_4]\cdot 4(\text{C}_6\text{H}_5\text{CH}_3)$.

A-9.1. IR spectroscopy

In all four preparation attempts for the complex $[\text{Sm}_2(\text{C}(\text{Ph}_2\text{PS})_2)_2\text{I}_2\text{THF}_4]\cdot 4(\text{C}_6\text{H}_5\text{CH}_3)$ numerous products were obtained and analysed by IR spectroscopy. Most of these yielded results which indicated moisture induced decomposition through the reformation of the neutral free ligand $\text{H}_2\text{C}(\text{Ph}_2\text{PS})_2$ rather than complexation. This IR data is presented hereunder in Figures A-9.1 to A-9.9 with the various spectra obtained compared to the IR spectra of the two $\text{H}_2\text{C}(\text{Ph}_2\text{PS})_2$ polymorphs and other starting reagents.

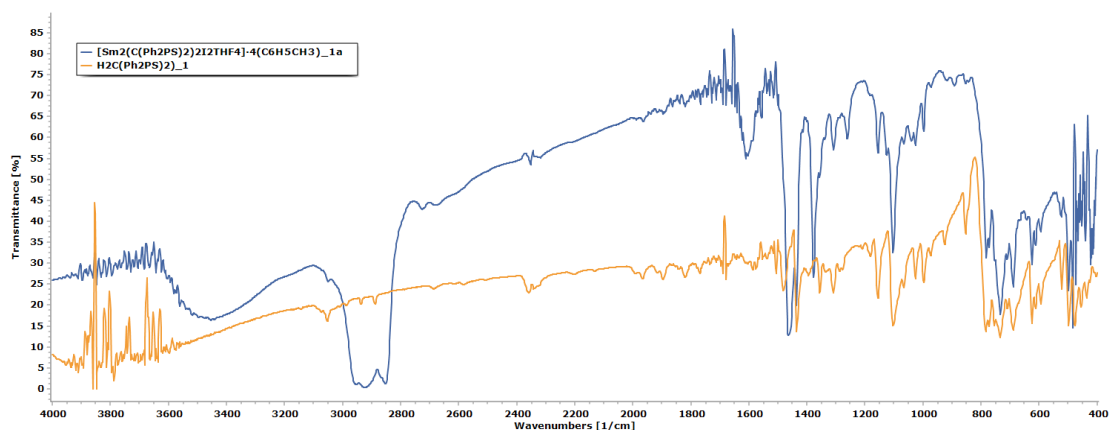


Figure A-9.1: IR spectra of $[\text{Sm}_2(\text{C}(\text{Ph}_2\text{PS})_2)_2\text{I}_2\text{THF}_4]\cdot 4(\text{C}_6\text{H}_5\text{CH}_3)_1\text{a}$ (blue) and $\text{H}_2\text{C}(\text{Ph}_2\text{PS})_2_1$ (orange).

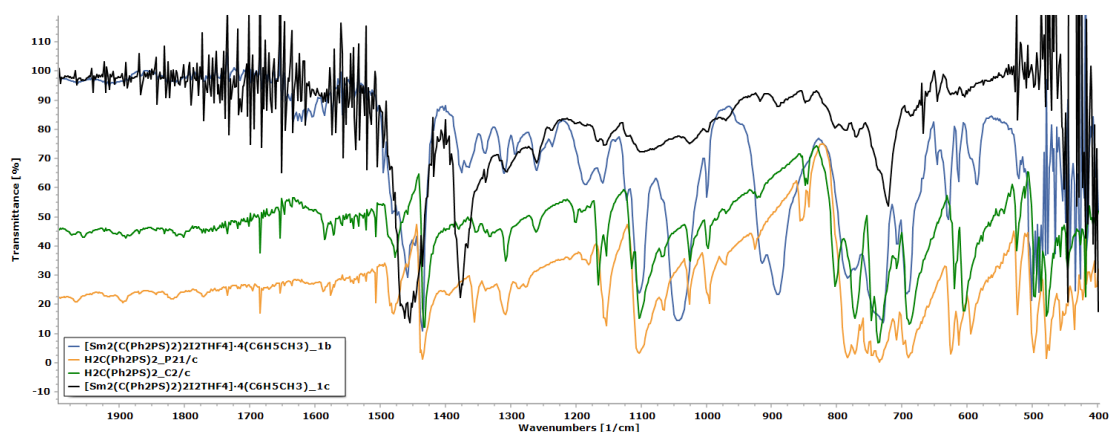


Figure A-9.2: IR spectra of $[\text{Sm}_2(\text{C}(\text{Ph}_2\text{PS})_2)_2\text{I}_2\text{THF}_4]\cdot 4(\text{C}_6\text{H}_5\text{CH}_3)_1\text{b}$ (blue) and $[\text{Sm}_2(\text{C}(\text{Ph}_2\text{PS})_2)_2\text{I}_2\text{THF}_4]\cdot 4(\text{C}_6\text{H}_5\text{CH}_3)_1\text{c}$ (black) and $\text{H}_2\text{C}(\text{Ph}_2\text{PS})_2_{P21/c}$ polymorph (green) and $\text{H}_2\text{C}(\text{Ph}_2\text{PS})_2_{C2/c}$ polymorph (orange), in the region 2000 cm⁻¹ to 400 cm⁻¹.

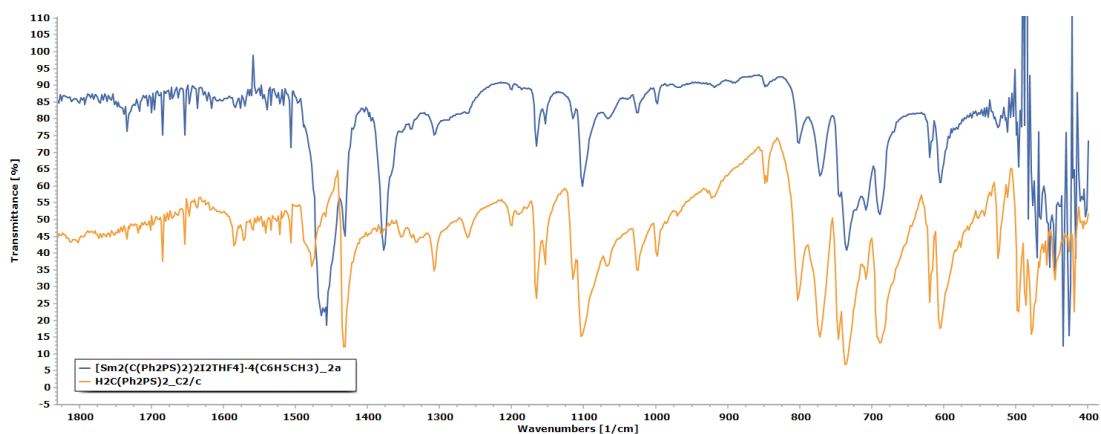


Figure A-9.3: IR spectra of [Sm₂(C(Ph₂PS)₂)₂I₂THF₄]-4(C₆H₅CH₃)_{2a} (blue) and H₂C(Ph₂PS)_{2_C2/c} polymorph (orange), in the region 1800 cm⁻¹ to 400 cm⁻¹.

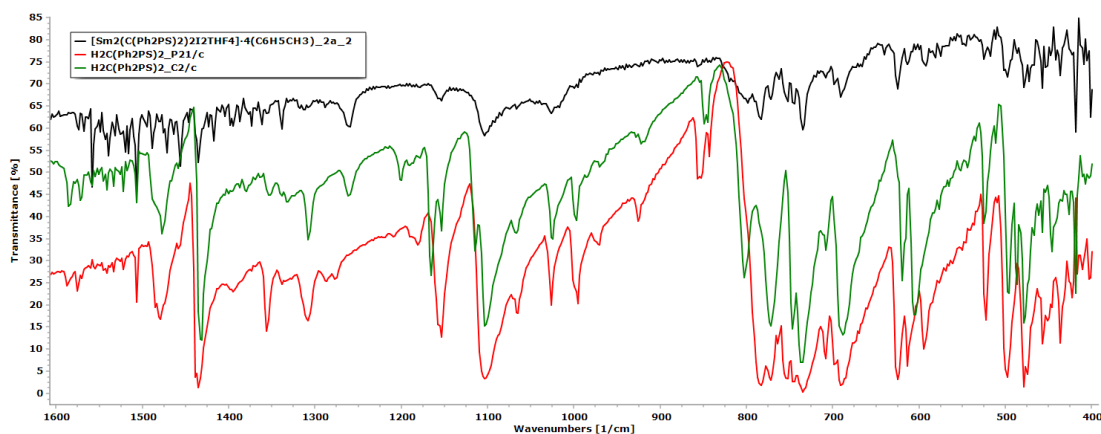


Figure A-9.4: IR spectra of [Sm₂(C(Ph₂PS)₂)₂I₂THF₄]-4(C₆H₅CH₃)_{2a_2} (black) and H₂C(Ph₂PS)_{2_C2/c} polymorph (green) and H₂C(Ph₂PS)_{2_P21/c} polymorph (red), in the region of 1600 to 400 cm⁻¹.

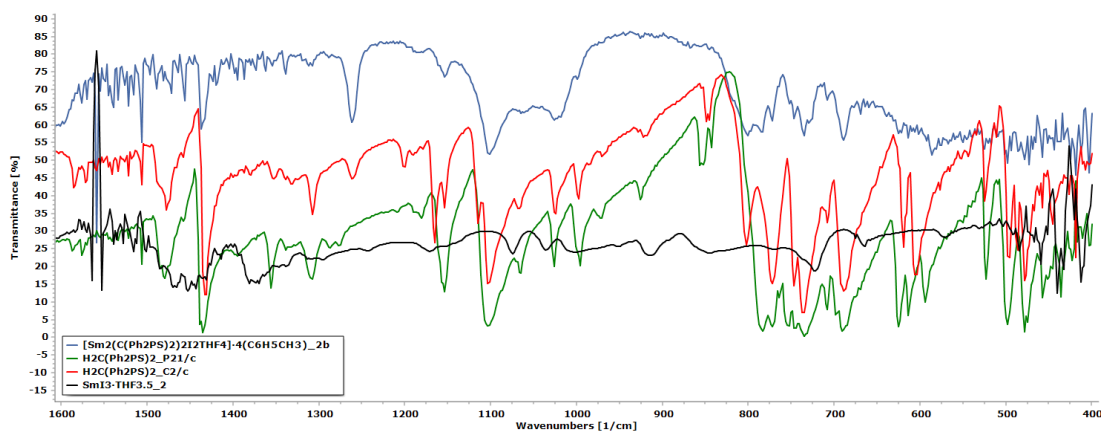


Figure A-9.5: IR spectra of [Sm₂(C(Ph₂PS)₂)₂I₂THF₄]-4(C₆H₅CH₃)_{2b} (blue) and H₂C(Ph₂PS)_{2_C2/c} polymorph (red) and H₂C(Ph₂PS)_{2_P21/c} polymorph (green) and SmI₃·THF_{3.5_2} (black), in the region 1600 cm⁻¹ to 400 cm⁻¹.

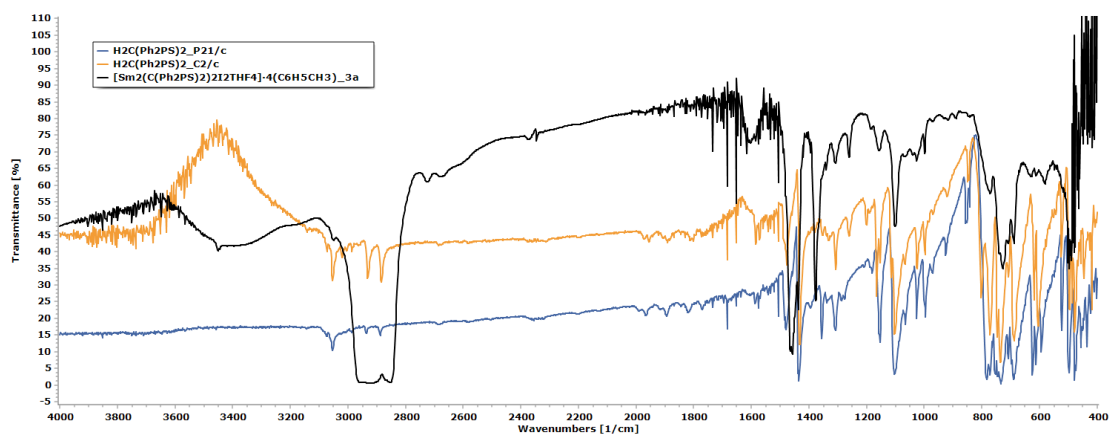


Figure A-9.6: IR spectra of $[\text{Sm}_2(\text{C}(\text{Ph}_2\text{PS})_2)_2\text{I}_2\text{THF}_4] \cdot 4(\text{C}_6\text{H}_5\text{CH}_3)_3\text{a}$ (black) and $\text{H}_2\text{C}(\text{Ph}_2\text{PS})_2_{\text{C}2/\text{c}}$ polymorph (orange) and $\text{H}_2\text{C}(\text{Ph}_2\text{PS})_2_{\text{P}21/\text{c}}$ polymorph (blue).

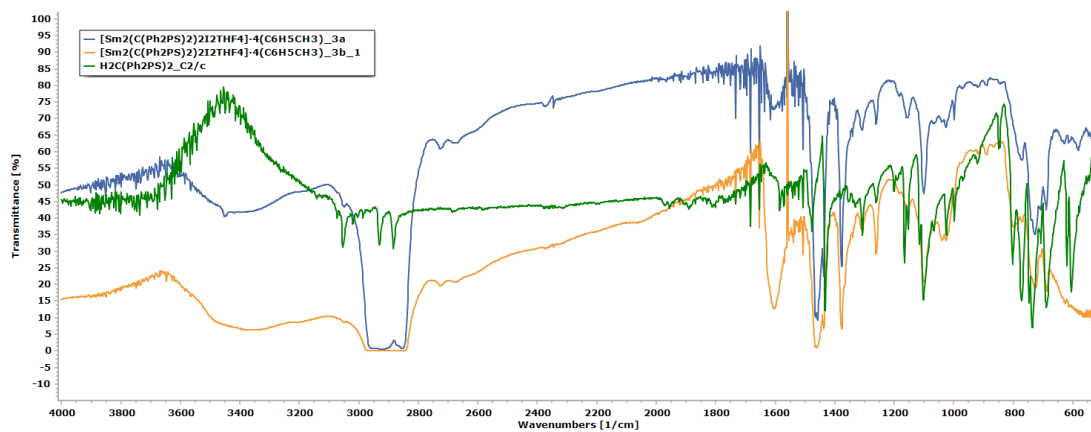


Figure A-9.7: IR spectra of $[\text{Sm}_2(\text{C}(\text{Ph}_2\text{PS})_2)_2\text{I}_2\text{THF}_4] \cdot 4(\text{C}_6\text{H}_5\text{CH}_3)_3\text{a}$ (blue) and $\text{H}_2\text{C}(\text{Ph}_2\text{PS})_2_{\text{C}2/\text{c}}$ polymorph (green) and $[\text{Sm}_2(\text{C}(\text{Ph}_2\text{PS})_2)_2\text{I}_2\text{THF}_4] \cdot 4(\text{C}_6\text{H}_5\text{CH}_3)_3\text{b}_1$ (orange).

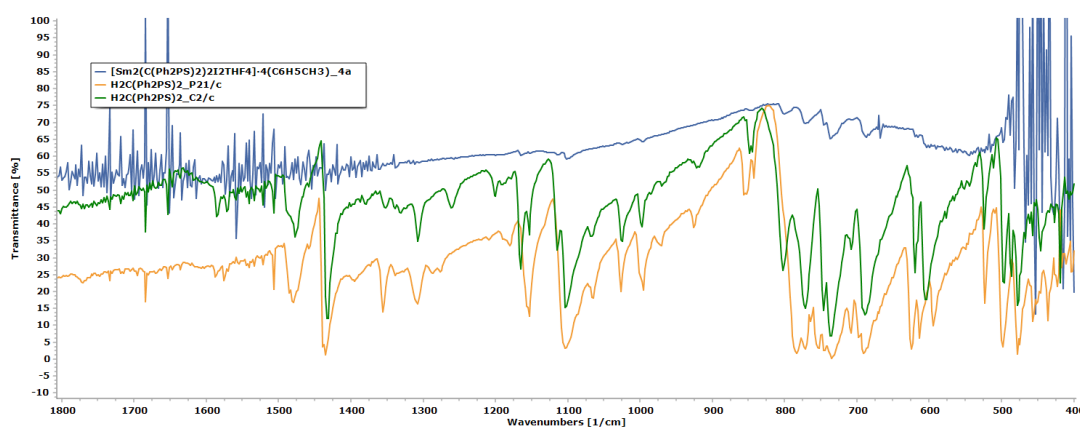


Figure A-9.8: IR spectra of $[\text{Sm}_2(\text{C}(\text{Ph}_2\text{PS})_2)_2\text{I}_2\text{THF}_4] \cdot 4(\text{C}_6\text{H}_5\text{CH}_3)_4\text{a}$ (blue) and $\text{H}_2\text{C}(\text{Ph}_2\text{PS})_2_{\text{C}2/\text{c}}$ polymorph (green) and $\text{H}_2\text{C}(\text{Ph}_2\text{PS})_2_{\text{P}21/\text{c}}$ polymorph (orange) in the region 1800 cm^{-1} to 400 cm^{-1} .

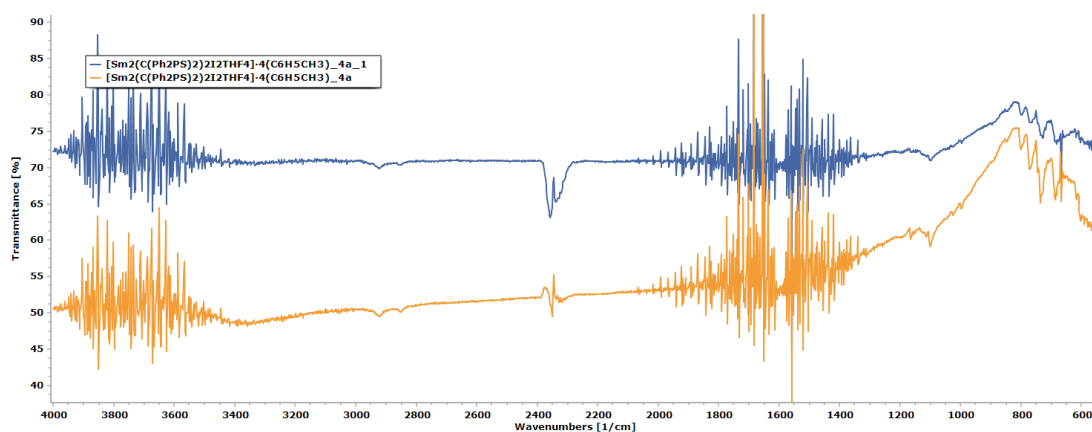


Figure A-9.9: IR spectra of $[\text{Sm}_2(\text{C}(\text{Ph}_2\text{PS})_2)_2\text{I}_2\text{THF}_4] \cdot 4(\text{C}_6\text{H}_5\text{CH}_3)_{4a_1}$ (blue) and $[\text{Sm}_2(\text{C}(\text{Ph}_2\text{PS})_2)_2\text{I}_2\text{THF}_4] \cdot 4(\text{C}_6\text{H}_5\text{CH}_3)_{4a}$ (orange).

A-9.2. NMR Spectroscopy

Only three products from the four preparation reactions for $[\text{Sm}_2(\text{C}(\text{Ph}_2\text{PS})_2)_2\text{I}_2\text{THF}_4] \cdot 4(\text{C}_6\text{H}_5\text{CH}_3)$ were analysed by ^1H NMR spectroscopy. These products were $[\text{Sm}_2(\text{C}(\text{Ph}_2\text{PS})_2)_2\text{I}_2\text{THF}_4] \cdot 4(\text{C}_6\text{H}_5\text{CH}_3)_{2a}$, $_{2b}$ and $_{3b_2}$. The ^1H NMR spectra of the former two in CDCl_3 are given in Figure A-9.10 along with the spectrum of $\text{H}_2\text{C}(\text{Ph}_2\text{PS})_2$ in the same solvent, while the ^1H NMR spectra of $[\text{Sm}_2(\text{C}(\text{Ph}_2\text{PS})_2)_2\text{I}_2\text{THF}_4] \cdot 4(\text{C}_6\text{H}_5\text{CH}_3)_{3b_2}$ and $\text{H}_2\text{C}(\text{Ph}_2\text{PS})_2$ in benzene- d_6 are given in Figure A-9.11. Discussion of these spectra is given in Section 4.1.3.3.2.

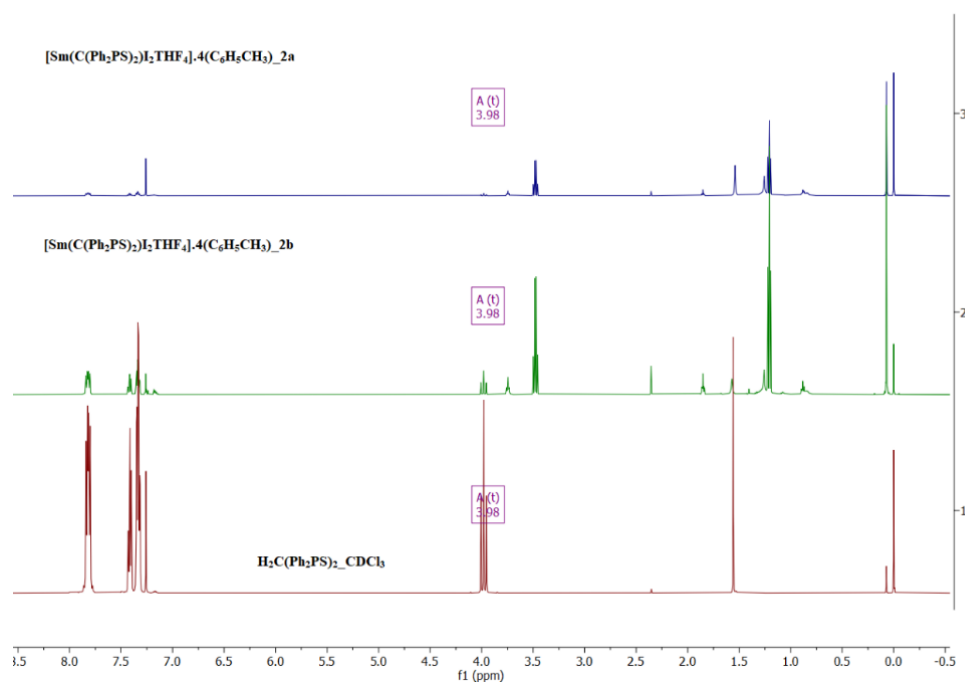


Figure A-9.10: ^1H NMR spectra of $[\text{Sm}_2(\text{C}(\text{Ph}_2\text{PS})_2)_2\text{I}_2\text{THF}_4] \cdot 4(\text{C}_6\text{H}_5\text{CH}_3)_{2a}$ (blue) and $[\text{Sm}_2(\text{C}(\text{Ph}_2\text{PS})_2)_2\text{I}_2\text{THF}_4] \cdot 4(\text{C}_6\text{H}_5\text{CH}_3)_{2b}$ (green) and $\text{H}_2\text{C}(\text{Ph}_2\text{PS})_2$ in CDCl_3 (red).

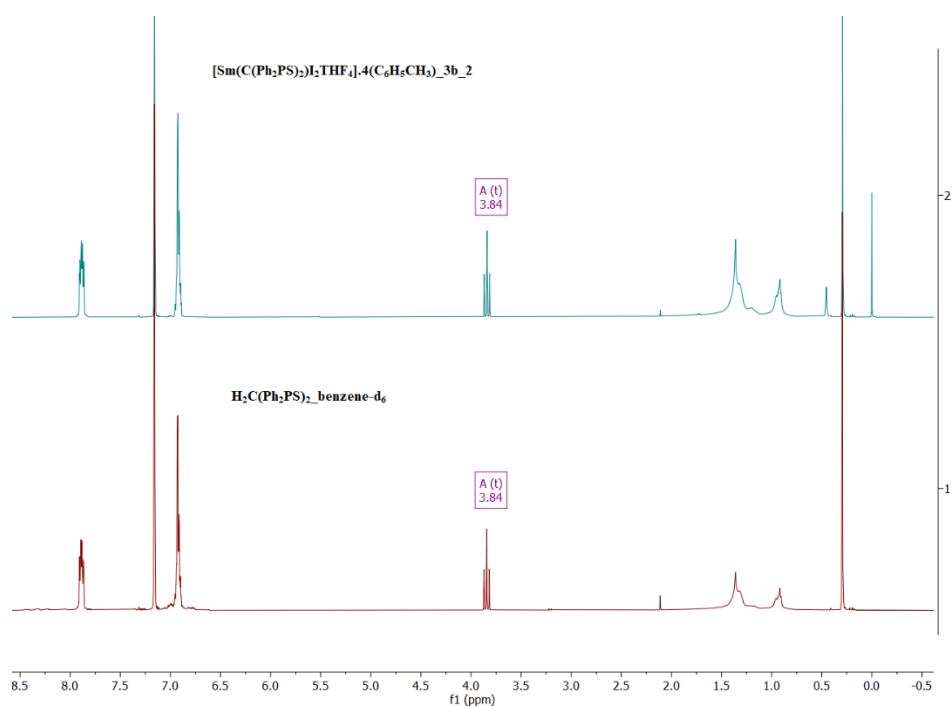


Figure A-9.11: ^1H NMR spectra of $[\text{Sm}_2(\text{C}(\text{Ph}_2\text{PS})_2)_2\text{I}_2\text{THF}_4]\cdot 4(\text{C}_6\text{H}_5\text{CH}_3)_{3b_2}$ (blue) and $\text{H}_2\text{C}(\text{Ph}_2\text{PS})_2$ in benzene- d_6 (red).

For samples in CDCl_3 impurity peaks were observed at 3.78 ppm and 1.85 ppm for THF, 3.48 ppm and 1.21 ppm for diethyl ether and at 0.07 ppm for silicone grease. For the sample in benzene- d_6 peaks at 1.36 ppm, 0.92 ppm and 0.29 ppm were due to grease and silicone grease as impurities.

A-9.3. Powder X-ray diffraction

$[\text{Sm}_2(\text{C}(\text{Ph}_2\text{PS})_2)_2\text{I}_2\text{THF}_4]\cdot 4(\text{C}_6\text{H}_5\text{CH}_3)_{2a_1}$ and $_{2b}$ were analysed by PXRD. Both diffraction patterns are discussed in Section 4.1.3.3.4. The diffraction pattern for the former is given in Figure A-9.12.

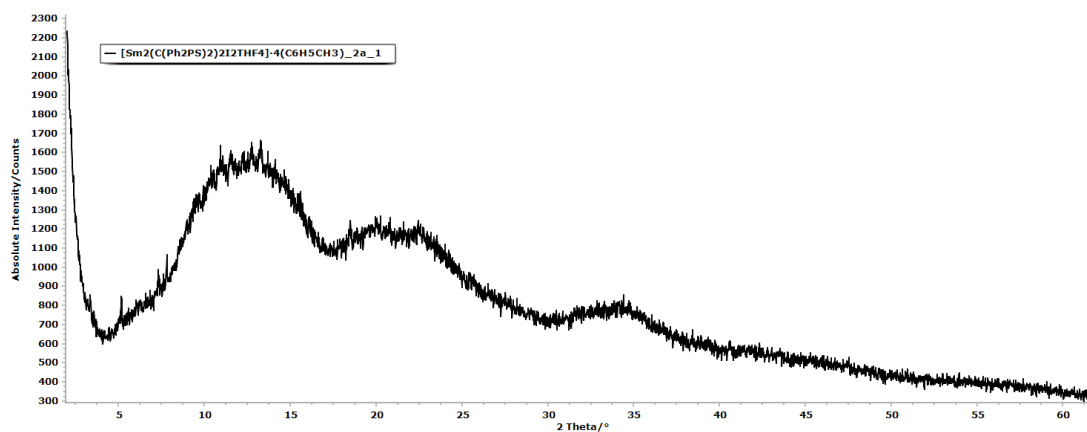


Figure A-9.12: PXRD pattern of $[\text{Sm}_2(\text{C}(\text{Ph}_2\text{PS})_2)_2\text{I}_2\text{THF}_4]\cdot 4(\text{C}_6\text{H}_5\text{CH}_3)_{2a_1}$.

APPENDIX 10: EXPERIMENTAL DATA FOR Et₂NH₂Cl

During the synthesis of O((Et₂N)₂PO)₂_1 a colourless crystalline solid mass was initially obtained. This was determined to be mainly composed of the expected side-product diethylammonium chloride (Et₂NH₂Cl), as characterised below. This brief characterisation is given since literature data was not available. This data was used in the discussion of the products O((Et₂N)₂PO)₂_1 and O((Et₂N)₂PO)₂_1_f13.

A-10.1. Characterisation of Et₂NH₂Cl

The Et₂NH₂Cl salt was analysed using ¹H NMR spectroscopy, in CDCl₃. This yielded the fairly clean spectrum given in Figure A-10.1, wherein three main peaks were observed, namely the singlet at 9.55 ppm, a quartet at 3.03 ppm and a triplet at 1.48 ppm.

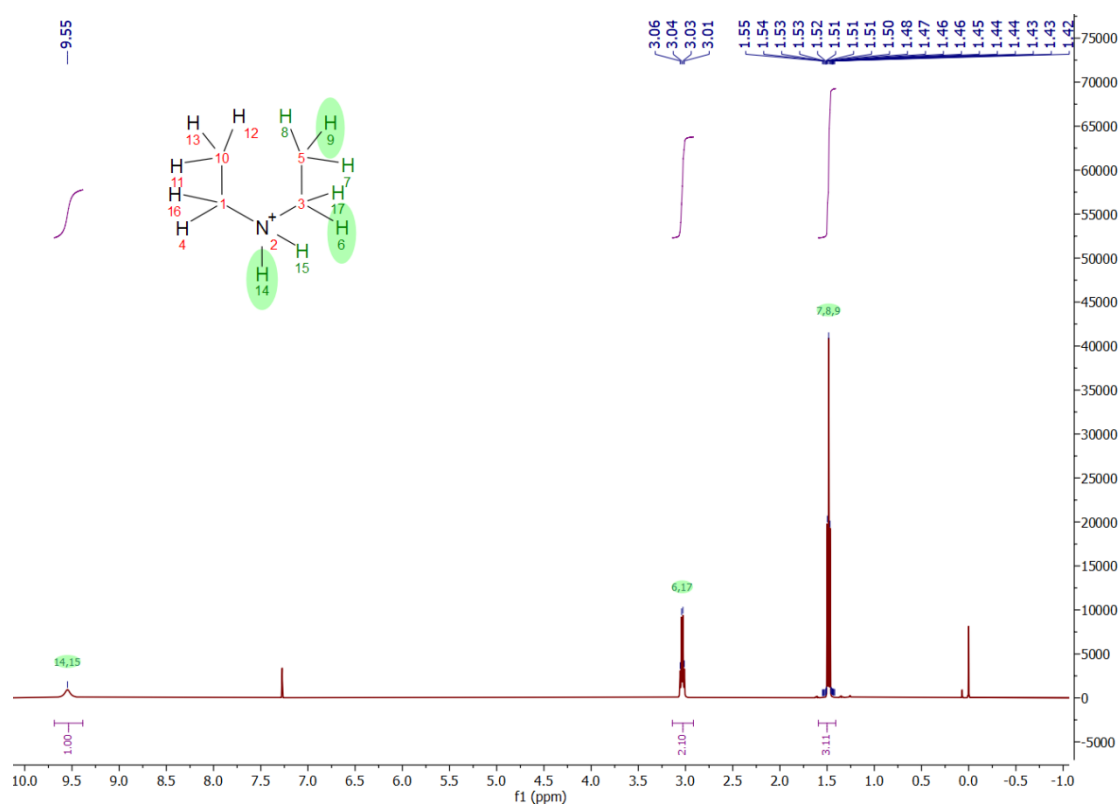


Figure A-10.1: ¹H NMR spectrum of Et₂NH₂Cl.

The quartet at 3.03 ppm and the triplet at 1.48 ppm, both having a coupling constant of 7.30 Hz, with an integration ratio of 2.10:3.11 respectively, were indicative of the presence of the methylene and methyl groups of the expected ethyl moieties.

Therefore, it was concluded that the methylene protons were deshielded when compared to the methyl protons, indicating that the methylene protons were vicinal to an electronegative atom or group. This is expected given that the methylene protons are closer to the nitrogen atom. However, the most important peak for characterisation was the broad singlet at 9.55 ppm. The protons related to this peak were highly deshielded, having a chemical shift higher than the typical (approximately 8.50 ppm) value for NH_n^+ ($n = 1 - 3$) in aliphatic ammonium salts. This value of 9.55 ppm was significantly downfield of the amine peak in diethylamine which typically occurs at 0.85 ppm. This downfield shift is due to the cationic charge centred on the ammonium nitrogen, which causes an increased electronegativity and deshielding of the ammonium protons. The broad nature of the peak is typical of such salts and is due to moderate to rapid proton exchange rates for the ammonium protons as well as the effect of the electron quadrupole moment on the ^{14}N atom. The integration ratio of 1:2.10 for this peak with respect to the methylene proton peak further confirmed the presence of the organic ammonium moiety as expected for $\text{Et}_2\text{NH}_2\text{Cl}$. Therefore, the three peaks were assigned as given in Table A-10.1.

Table A-10.1: ^1H NMR experimental data and assignment for proton peaks of $\text{Et}_2\text{NH}_2\text{Cl}$ in CDCl_3 .

^1H NMR experimental data and assignment for proton peaks of $\text{Et}_2\text{NH}_2\text{Cl}$ in CDCl_3				
ppm	Multiplicity	Integration	Coupling	Assignment
9.55	broad singlet	1.00	N/A	NH_2^+ (amine salt)
3.03	quartet	2.10	$J = 7.30 \text{ Hz}$	CH_2 (Ethyl)
1.48	triplet	3.11	$J = 7.30 \text{ Hz}$	CH_3 (Ethyl)

The IR spectrum of $\text{Et}_2\text{NH}_2\text{Cl}$ is given in Figure A-10.2, along with the spectrum of diethylamine (Et_2NH). The broad band in the range $3441\text{--}3173 \text{ cm}^{-1}$ was indicative of the ν N–H stretching vibrations. This band corroborated the presence of the organic ammonium species indicated by the peak at 9.55 ppm in the ^1H NMR spectrum of the solid. The bands at 2985 cm^{-1} and 2810 cm^{-1} were due to the presence of ν C–H of both methyl and methylene moieties, indicating the presence of the ethyl group of the diethylamine structure (Et_2N). The presence of these ethyl groups in $\text{Et}_2\text{NH}_2\text{Cl}$ was

further corroborated by the presence of bands at 1454 cm^{-1} and 1394 cm^{-1} , believed to be due to the bending vibration $\delta\text{ C-H}$ of the methyl and methylene groups respectively. The band at 1048 cm^{-1} was easily assigned to the $\nu\text{ C-N}$ stretching vibration, indicating the presence of the entire Et_2N group observed at a lower wavenumber when compared to the analogous band in the amine at 1143 cm^{-1} .⁴¹⁵ This was indicative of a change in the environment of the nitrogen atom, yielding weaker C–N bonds and could correspond to multiple chemical changes such as the protonation attested by the ^1H NMR data. The three bands at wavenumbers 2504 cm^{-1} , 2358 cm^{-1} and 2261 cm^{-1} were unusual and distinctive of combination bands typical of the organic ammonium salts of secondary amines.²⁸¹ This corroborated the ^1H NMR data in proving that the solid was $\text{Et}_2\text{NH}_2\text{Cl}$.

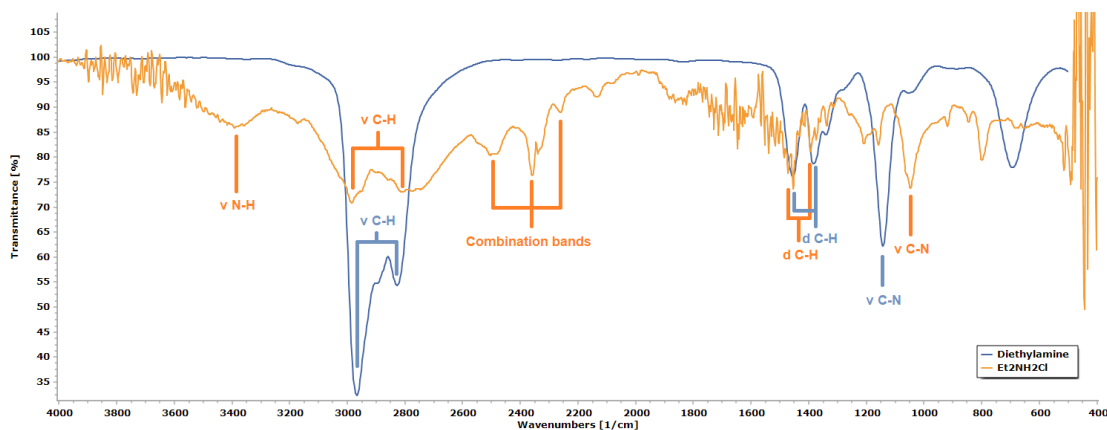


Figure A-10.2: IR spectra of diethylamine (blue) and diethylammonium chloride (orange).

APPENDIX 11: ADDITIONAL NMR RESULTS FOR O((Et₂N)₂PO)₂_1 AND O((Et₂N)₂PO)₂_1_f13.

A-11.1. ¹H NMR spectroscopy

¹H NMR spectra of liquid products collected from the reaction O((Et₂N)₂PO)₂_1 and its workup were obtained. The full spectra for O((Et₂N)₂PO)₂_1 and O((Et₂N)₂PO)₂_1_f13 are given in Figures A-11.1 and A-11.2 respectively.

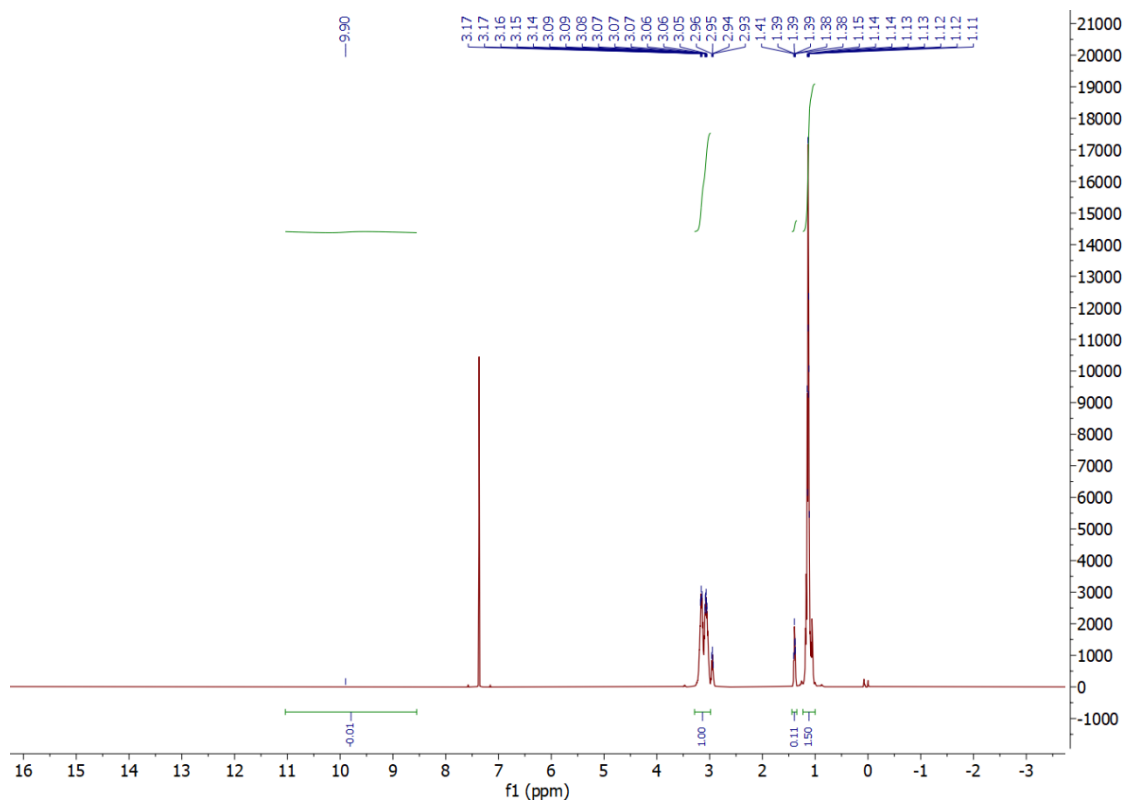


Figure A-11.1: ¹H NMR spectrum of O((Et₂N)₂PO)₂_1.

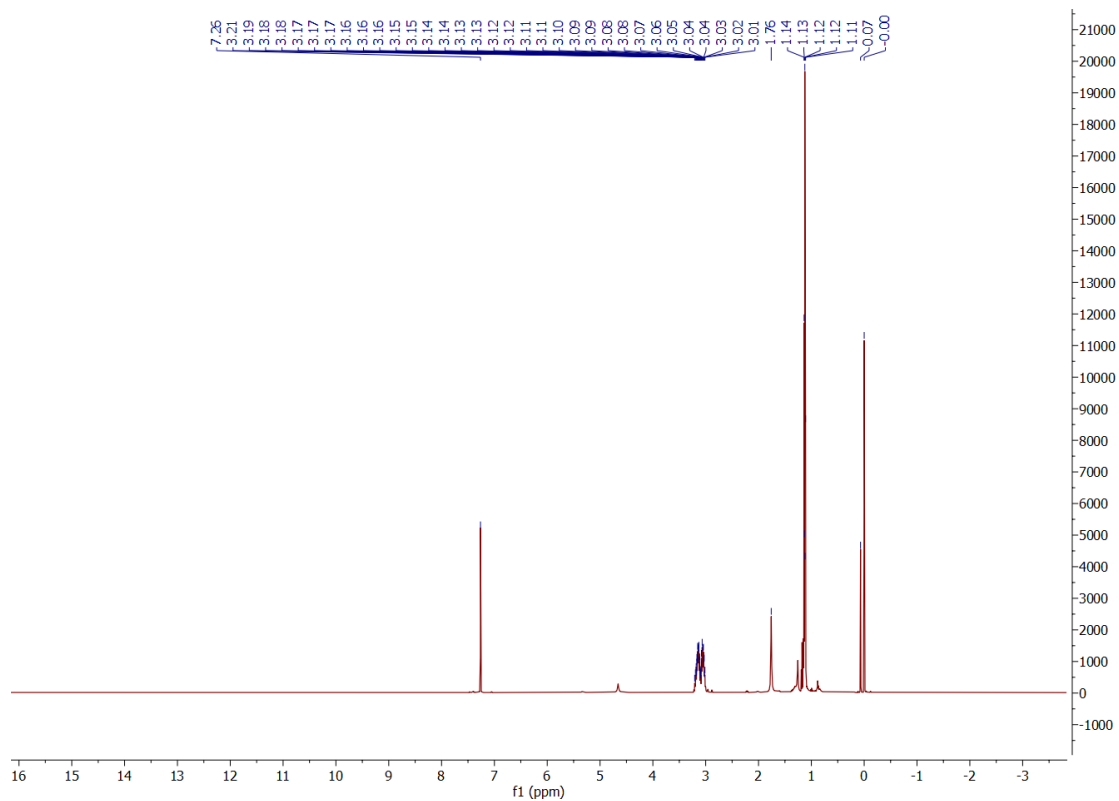


Figure A-11.2: ^1H NMR spectrum of $\text{O}((\text{Et}_2\text{N})_2\text{PO})_2_1_{\text{f13}}$.

A-11.2. ^{31}P NMR spectroscopy

As discussed in Section 4.2.1.3.3. both products $\text{O}((\text{Et}_2\text{N})_2\text{PO})_2_1$ and $\text{O}((\text{Et}_2\text{N})_2\text{PO})_2_1_{\text{f13}}$ were analysed using ^{31}P NMR spectroscopy. In addition to the spectra given in Section 4.2.1.3.3. other spectra, which were only briefly discussed or that did not yield further structural information were collected. These are given in Figures A-11.3, A-11.4 and A-11.5.

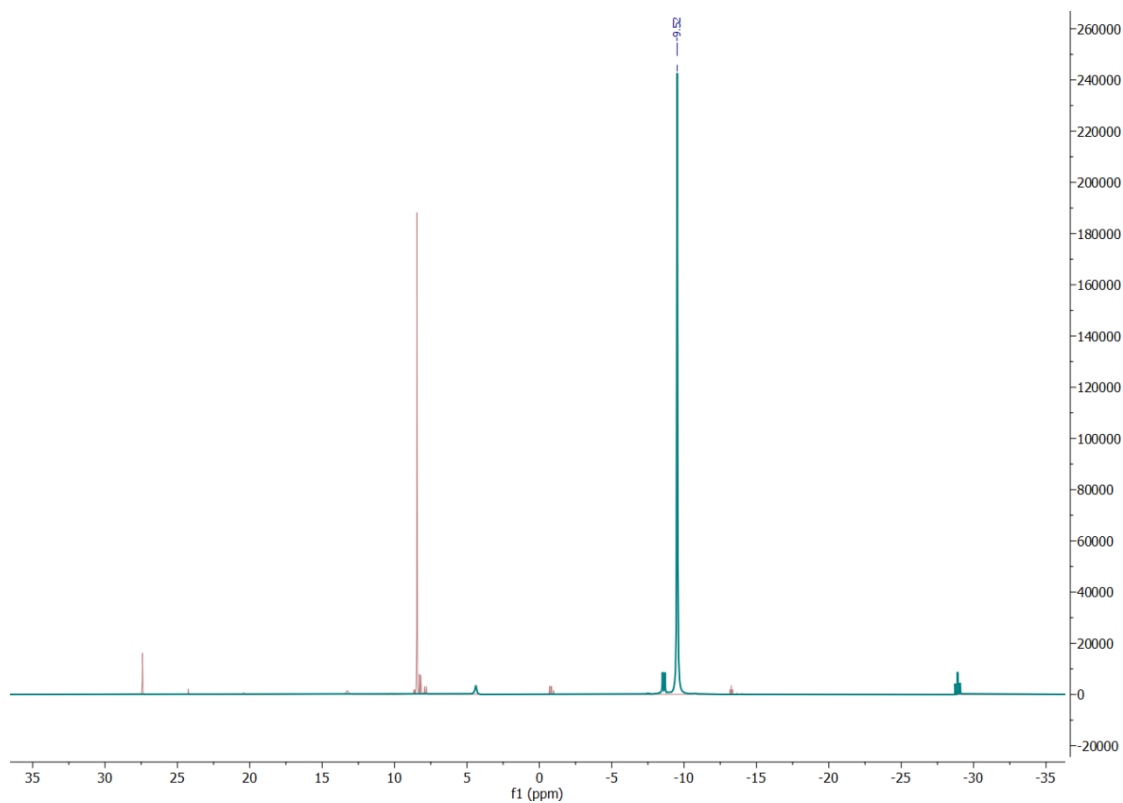


Figure A-11.3: $^{31}\text{P}\{^1\text{H}\}$ NMR spectra of PPTC (blue) and $\text{O}((\text{Et}_2\text{N})_2\text{PO})_2_1$ (light red).

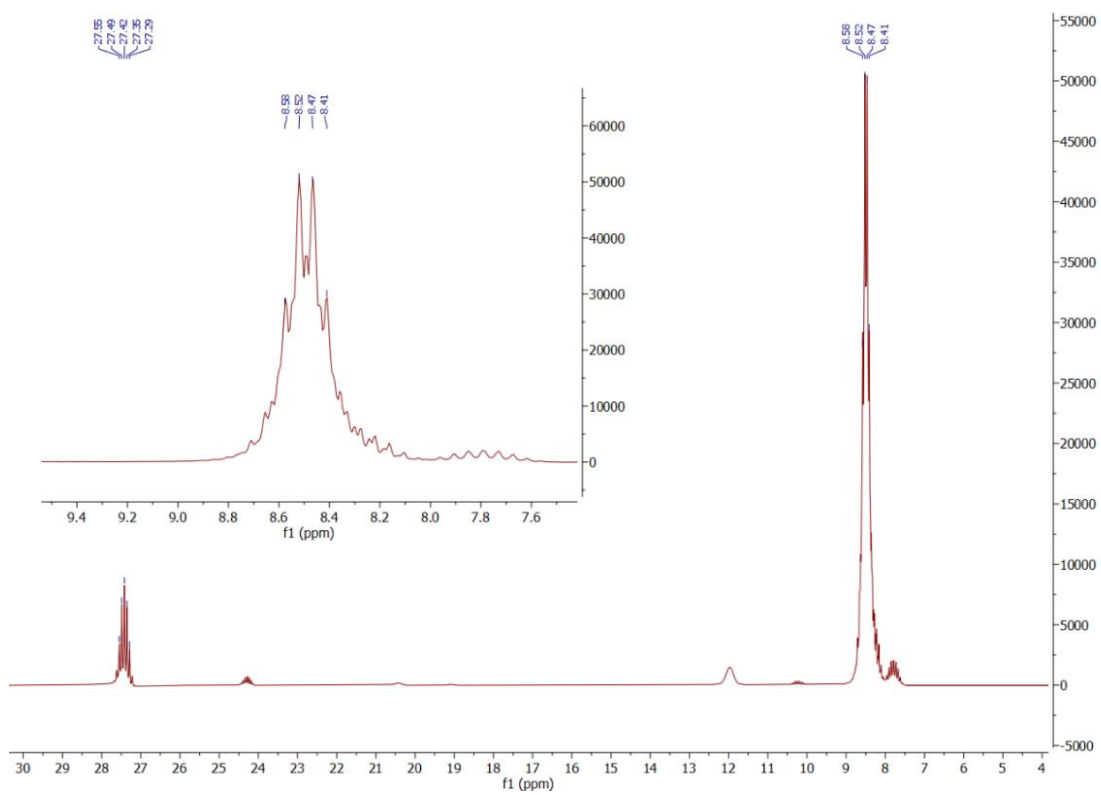


Figure A-11.4: ^{31}P NMR spectrum of $\text{O}((\text{Et}_2\text{N})_2\text{PO})_2_1$ with detail of peak at 8.50 ppm given in inset.

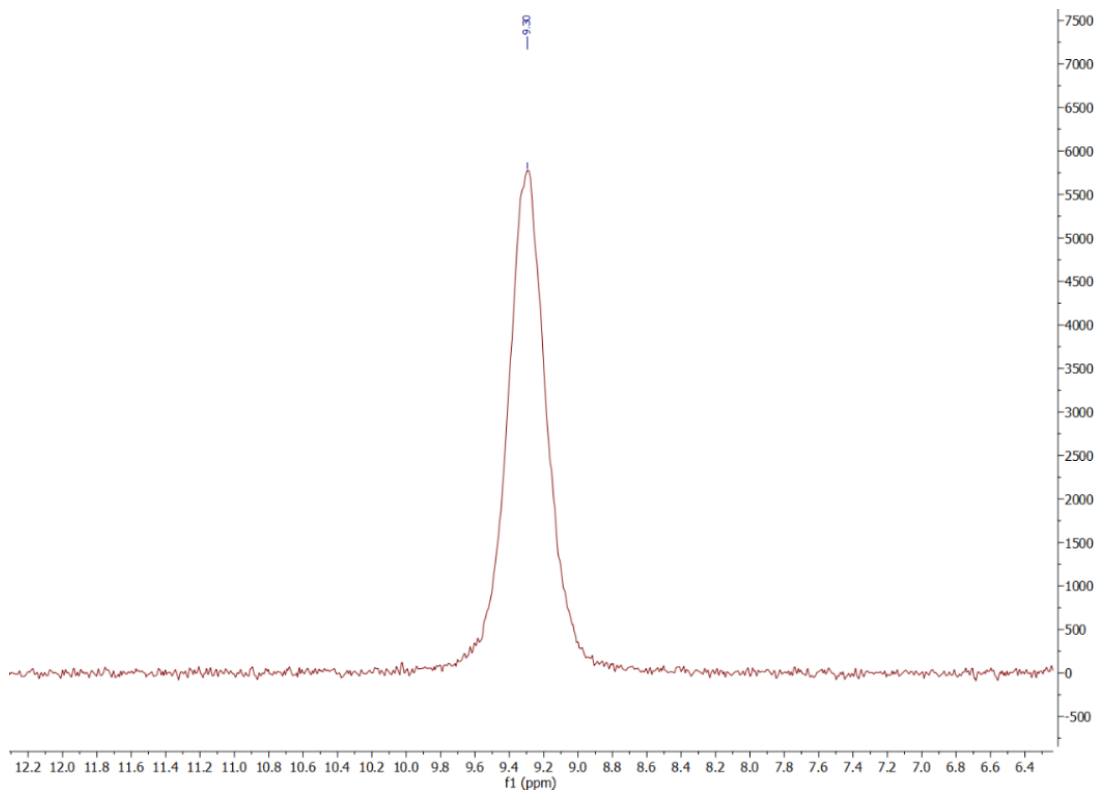


Figure A-11.5: Detail of ^{31}P NMR spectrum of $\text{O}((\text{Et}_2\text{N})_2\text{PO})_2_1_{\text{f13}}$.

APPENDIX 12: CRYSTALLOGRAPHIC DATA FOR PRODUCT

O((Et₂N)₂PO)₂_1_f13.

Hereunder is the data regarding the crystal structure of the single crystal obtained from O((Et₂N)₂PO)₂_1_f13.

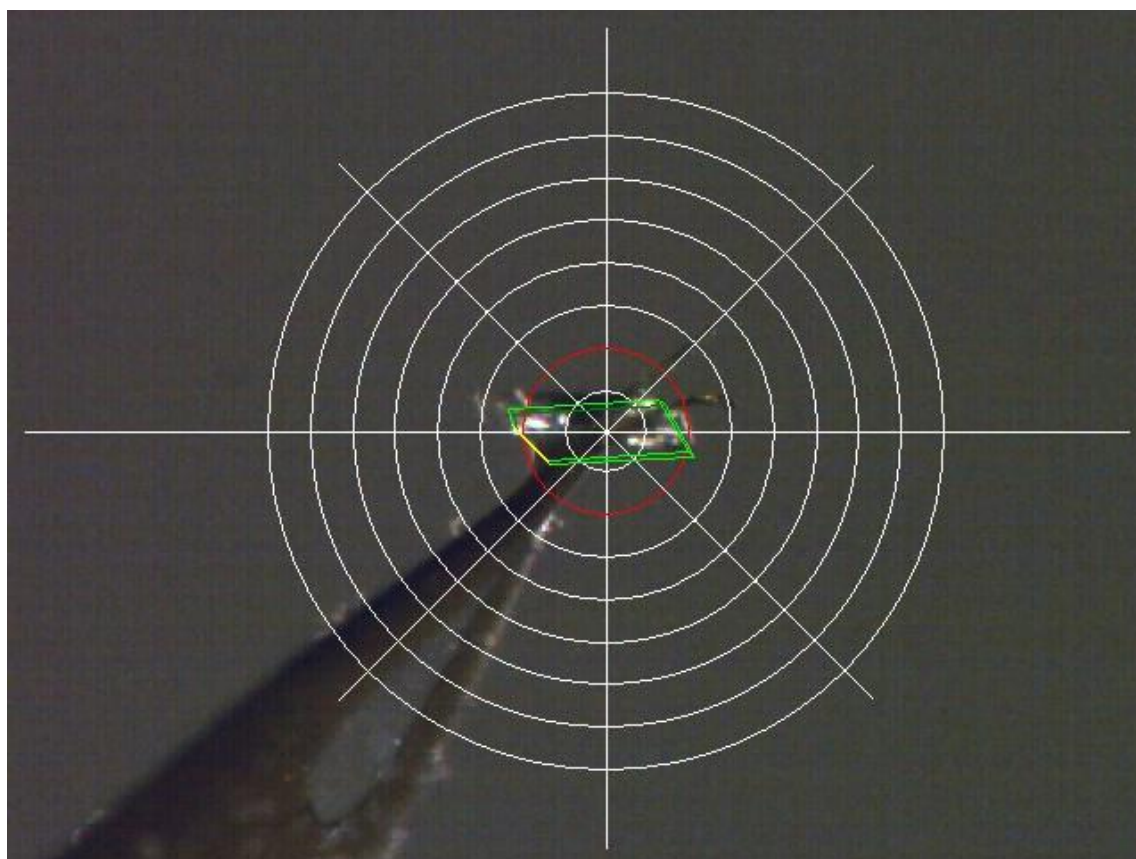


Figure A-12.1: Crystal used in structure determination of O((Et₂N)₂PO)₂_1_f13.

Table A-12.1: Crystal data and structure refinement for O((Et₂N)₂PO)₂_1_f13.

Identification code	O((Et ₂ NH) ₂ PO) ₂ _1_f13
Empirical formula	C ₃₂ H ₈₄ N ₁₂ O ₂₀ P ₄ Ca ₂
Formula weight	1161.15
Temperature/K	150(2)
Crystal system	monoclinic
Space group	<i>P</i> 2 ₁ / <i>n</i>
<i>a</i> /Å	10.6249(7)
<i>b</i> /Å	15.5774(12)
<i>c</i> /Å	17.0925(10)
<i>α</i> /°	90
<i>β</i> /°	96.707(5)

$\gamma/^\circ$	90
Volume/ \AA^3	2809.6(3)
Z	2
$\rho_{\text{calc}}/\text{cm}^3$	1.373
μ/mm^{-1}	3.503
F(000)	1240.0
Crystal size/ mm^3	$0.06 \times 0.22 \times 0.07$
Radiation	CuK α ($\lambda = 1.54186$)
2Θ range for data collection/ $^\circ$	7.702 to 131.288
Index ranges	$-12 \leq h \leq 9, -18 \leq k \leq 17, -20 \leq l \leq 15$
Reflections collected	27010
Independent reflections	4816 [$R_{\text{int}} = 0.0983, R_{\text{sigma}} = 0.0513$]
Data/restraints/parameters	4816/0/325
Goodness-of-fit on F^2	1.048
Final R indexes [$I \geq 2\sigma(I)$]	$R_1 = 0.0371, wR_2 = 0.1008$
Final R indexes [all data]	$R_1 = 0.0389, wR_2 = 0.1026$
Largest diff. peak/hole / $e \text{\AA}^{-3}$	0.45/-0.42

Table A-12.2: Fractional Atomic Coordinates ($\times 10^4$) and Equivalent Isotropic Displacement Parameters ($\text{\AA}^2 \times 10^3$) for $\text{O}((\text{Et}_2\text{N})_2\text{PO})_2_1_f13$. U_{eq} is defined as 1/3 of the trace of the orthogonalised U_{ij} tensor.

Atom	x	y	z	U(eq)
Ca1	6836.4(3)	5455.2(2)	4793.8(2)	19.00(12)
P002	4534.8(4)	2672.8(3)	4316.0(2)	18.23(13)
P003	6293.8(4)	3599.6(3)	3384.0(2)	18.61(13)
O004	3810.4(12)	3468.6(8)	4392.9(7)	22.7(3)
O005	5529.5(12)	4552.1(8)	5607.7(7)	24.5(3)
O006	5608.4(11)	2792.5(7)	3735.3(7)	20.5(3)
O007	6625.6(12)	4266.6(8)	3986.4(7)	25.4(3)
O008	8300.1(13)	4836.3(10)	5776.8(8)	33.6(3)
O009	4452.0(13)	3872.1(9)	6402.1(8)	29.5(3)
O00A	6496.5(14)	3972.7(11)	6667.2(9)	41.6(4)
O00B	9031.6(14)	5587.4(9)	4243.2(10)	38.0(4)
O00C	8096.2(14)	6752.1(10)	4509.9(11)	43.8(4)
N00D	5505.0(14)	4128.9(10)	6239.6(9)	24.2(3)
N00E	5315.4(14)	3878.7(10)	2622.4(9)	24.1(3)
N00F	3620.6(14)	1908.9(9)	3928.4(9)	23.4(3)
O00G	9937.1(15)	6814.2(11)	4080.4(11)	48.1(4)
N00H	7575.6(14)	3214.2(10)	3081.6(9)	25.0(3)
N00I	9042.7(15)	6397.0(11)	4276.7(10)	29.2(4)
N00J	5372.6(15)	2283.1(10)	5097.1(9)	24.3(3)
C00K	4176.9(19)	1093.7(12)	3708.6(12)	28.0(4)
C00L	7476.2(19)	2565.1(13)	2446.8(11)	28.4(4)
C00M	8816.1(18)	3306.9(14)	3558.9(12)	31.2(4)
C00N	4125.0(17)	3451.7(13)	2315.6(11)	26.7(4)

C00O	6738.4(19)	2432.6(14)	5306.0(12)	31.7(4)
C00P	5696(2)	4627.3(13)	2178.3(12)	33.8(5)
C00Q	2244.8(18)	2013.9(13)	3710.8(13)	31.9(4)
C00R	4636(2)	1965.0(13)	5724.3(12)	31.1(4)
C00S	4233(2)	994.6(14)	2831.6(13)	39.8(5)
C00T	7649(2)	1649.2(14)	2733.4(13)	38.0(5)
C00U	4689(2)	1003.9(13)	5832.9(13)	38.5(5)
C00V	2969(2)	4008.3(18)	2351.3(15)	45.7(6)
C00W	7569(2)	1708.4(17)	5074.0(14)	42.4(5)
C00X	1472(2)	1456.6(16)	4201.8(18)	49.6(6)
C00Y	9789(2)	3691(2)	3102.9(18)	57.7(7)
C00Z	5929(3)	4424.6(17)	1339.6(14)	49.1(6)

Table A-12.3: Anisotropic Displacement Parameters ($\text{\AA}^2 \times 10^3$) for O((Et₂N)₂PO)₂_1_f13. The Anisotropic displacement factor exponent takes the form: $-2\pi^2[h^2a^{*2}U_{11}+2hka^*b^*U_{12}+\dots]$.

Atom	U ₁₁	U ₂₂	U ₃₃	U ₂₃	U ₁₃	U ₁₂
Ca1	15.7(2)	17.64(19)	23.32(19)	-3.19(12)	1.03(14)	1.16(12)
P002	18.2(2)	15.3(2)	21.3(2)	-0.61(15)	2.31(17)	1.38(16)
P003	16.2(2)	18.3(2)	21.4(2)	-3.02(16)	2.36(17)	-0.19(16)
O004	22.9(6)	18.4(6)	27.1(6)	-1.2(5)	4.6(5)	3.2(5)
O005	21.4(6)	26.0(7)	25.5(6)	3.9(5)	0.5(5)	1.7(5)
O006	19.9(6)	18.2(6)	23.8(6)	-2.2(5)	3.9(5)	1.7(5)
O007	25.3(6)	23.0(6)	27.8(7)	-7.1(5)	2.5(5)	-1.7(5)
O008	20.5(6)	42.1(8)	37.3(7)	5.9(6)	-0.4(6)	5.7(6)
O009	28.1(7)	29.9(7)	31.0(7)	3.5(5)	5.8(6)	-0.7(6)
O00A	28.5(8)	58.6(10)	34.8(8)	10.4(7)	-8.7(6)	4.3(7)
O00B	31.9(8)	27.6(7)	56.3(9)	2.0(6)	13.2(7)	4.0(6)
O00C	28.7(8)	31.2(8)	75.6(11)	-3.3(7)	23.5(8)	1.0(6)
N00D	22.5(8)	24.5(8)	24.7(8)	-2.1(6)	-0.5(6)	2.0(6)
N00E	21.9(8)	22.1(7)	27.6(8)	2.8(6)	0.1(6)	-2.8(6)
N00F	18.8(7)	18.0(7)	32.9(8)	-1.9(6)	1.4(6)	0.2(6)
O00G	28.0(8)	46.2(9)	72.7(11)	10.6(8)	17.4(8)	-8.1(7)
N00H	18.3(8)	29.4(8)	27.5(8)	-7.3(6)	3.5(6)	0.4(6)
N00I	19.6(8)	32.1(9)	36.0(9)	3.3(7)	3.2(7)	-1.4(7)
N00J	25.5(8)	23.7(8)	23.5(7)	2.5(6)	1.8(6)	3.1(6)
C00K	27.6(10)	17.3(9)	37.8(10)	-3.7(7)	-1.2(8)	1.8(7)
C00L	26.0(9)	32.8(10)	27.4(9)	-8.4(8)	7.4(7)	0.7(8)
C00M	19.2(9)	36.4(11)	37.3(10)	-5.2(8)	0.5(8)	0.1(8)
C00N	21.3(9)	31.6(10)	26.0(9)	-0.2(7)	-2.2(7)	-2.6(8)
C00O	30(1)	34.7(11)	27.9(9)	1.5(8)	-6.9(8)	0.0(9)
C00P	39.7(12)	26.8(10)	33.7(11)	6.3(8)	-0.9(9)	-6.2(9)
C00Q	21.5(9)	27.1(10)	45.4(12)	-2.6(8)	-2.8(8)	0.8(8)
C00R	39.8(11)	27.4(10)	27.1(9)	5.5(7)	7.5(8)	6.7(9)
C00S	43.2(12)	34.5(11)	40.1(12)	-13.1(9)	-2.4(10)	7.7(10)
C00T	40.9(12)	32.1(11)	40.6(11)	-9.9(9)	3.7(10)	10.5(9)

C00U	47.9(13)	28.3(11)	40.0(11)	7.6(9)	8(1)	0.6(9)
C00V	26.4(11)	60.2(15)	49.4(13)	5.3(11)	-0.6(10)	10.8(10)
C00W	30.0(11)	56.4(14)	40.2(12)	1.5(10)	0.9(9)	10.7(10)
C00X	27.1(11)	45.1(14)	77.2(18)	0.2(12)	9.2(12)	-8.3(10)
C00Y	28.9(12)	79(2)	64.8(17)	8.7(14)	3.6(12)	-18.6(13)
C00Z	62.7(16)	47.2(14)	40.3(13)	10.9(10)	18.7(12)	-0.6(12)

Table A-12.4: Bond Lengths for O((Et₂N)₂PO)₂_1_f13.

Atom	Atom	Length/Å	Atom	Atom	Length/Å
Ca1	O004 ¹	2.3319(12)	O00A	N00D	1.234(2)
Ca1	O005 ¹	2.5272(13)	O00B	N00I	1.262(2)
Ca1	O005	2.5087(13)	O00C	N00I	1.253(2)
Ca1	O007	2.3045(13)	N00E	C00N	1.470(2)
Ca1	O008	2.3582(14)	N00E	C00P	1.473(2)
Ca1	O009 ¹	2.5489(14)	N00F	C00K	1.468(2)
Ca1	O00B	2.6232(15)	N00F	C00Q	1.475(2)
Ca1	O00C	2.5021(16)	O00G	N00I	1.230(2)
P002	O004	1.4732(13)	N00H	C00L	1.478(2)
P002	O006	1.6080(12)	N00H	C00M	1.474(2)
P002	N00F	1.6272(15)	N00J	C00O	1.472(3)
P002	N00J	1.6327(15)	N00J	C00R	1.484(2)
P003	O006	1.6043(13)	C00K	C00S	1.515(3)
P003	O007	1.4763(13)	C00L	C00T	1.513(3)
P003	N00E	1.6271(15)	C00M	C00Y	1.490(3)
P003	N00H	1.6269(15)	C00N	C00V	1.511(3)
O004	Ca1 ¹	2.3319(12)	C00O	C00W	1.513(3)
O005	Ca1 ¹	2.5273(13)	C00P	C00Z	1.516(3)
O005	N00D	1.268(2)	C00Q	C00X	1.514(3)
O009	Ca1 ¹	2.5489(14)	C00R	C00U	1.509(3)
O009	N00D	1.250(2)			

¹I-X, I-Y, I-Z

Table A-12.5: Bond Angles for O((Et₂N)₂PO)₂_1_f13.

Atom	Atom	Atom	Angle/°	Atom	Atom	Atom	Angle/°
O004 ¹	Ca ¹	O005	81.48(4)	O007	P003	N00E	116.63(8)
O004 ¹	Ca ¹	O005 ¹	79.17(4)	O007	P003	N00H	109.92(8)
O004 ¹	Ca ¹	O008	94.87(5)	N00H	P003	N00E	108.95(8)
O004 ¹	Ca ¹	O009 ¹	90.83(4)	P002	O004	Ca1 ¹	148.38(8)
O004 ¹	Ca ¹	O00B	119.59(5)	Ca1	O005	Ca1 ¹	116.70(5)
O004 ¹	Ca ¹	O00C	74.74(5)	N00D	O005	Ca1	146.25(11)
O005	Ca ¹	O005 ¹	63.30(5)	N00D	O005	Ca1 ¹	96.33(10)
O005 ¹	Ca ¹	O009 ¹	50.21(4)	P003	O006	P002	135.05(8)
O005	Ca ¹	O009 ¹	113.27(4)	P003	O007	Ca1	169.04(9)
O005	Ca ¹	O00B	144.67(5)	N00D	O009	Ca1 ¹	95.80(10)

O005 ¹	Ca ¹	O00B	143.21(5)	N00I	O00B	Ca1	93.79(11)
O007	Ca ¹	O004 ¹	156.89(5)	N00I	O00C	Ca1	99.94(11)
O007	Ca ¹	O005	81.96(4)	O009	N00D	O005	117.62(15)
O007	Ca ¹	O005 ₁	79.04(4)	O00A	N00D	Ca1 ¹	178.52(13)
O007	Ca ¹	O008	96.20(5)	C00N	N00E	P003	127.37(13)
O007	Ca ¹	O009 ¹	81.05(5)	C00N	N00E	C00P	116.76(15)
O007	Ca ¹	O00B	82.91(5)	C00P	N00E	P003	115.83(13)
O007	Ca ¹	O00C	123.32(5)	C00K	N00F	P002	119.85(12)
O008	Ca ¹	O005	74.77(5)	C00K	N00F	C00Q	116.63(15)
O008	Ca ¹	O005 ¹	138.07(5)	C00Q	N00F	P002	123.26(13)
O008	Ca ¹	O009 ¹	170.83(5)	C00L	N00H	P003	119.67(13)
O008	Ca ¹	O00B	75.39(5)	C00M	N00H	P003	121.04(13)
O008	Ca ¹	O00C	98.34(6)	C00M	N00H	C00L	117.13(15)
O009 ¹	Ca ¹	O00B	95.55(5)	O00C	N00I	O00B	116.87(16)
O00C	Ca ¹	O005 ¹	119.25(5)	O00G	N00I	O00B	121.25(17)
O00C	Ca ¹	O005	154.64(5)	O00G	N00I	O00C	121.88(17)
O00C	Ca ¹	O009 ¹	76.22(5)	C00O	N00J	P002	124.58(13)
O00C	Ca ¹	O00B	49.37(5)	C00O	N00J	C00R	117.76(15)
O004	P002	O006	111.91(7)	C00R	N00J	P002	115.56(13)
O004	P002	N00F	111.01(8)	N00F	C00K	C00S	113.88(16)
O004	P002	N00J	118.72(8)	N00H	C00L	C00T	114.33(16)
O006	P002	N00F	105.44(7)	N00H	C00M	C00Y	112.32(18)
O006	P002	N00J	100.92(7)	N00E	C00N	C00V	113.29(17)
N00F	P002	N00J	107.67(8)	N00J	C00O	C00W	114.02(17)
O006	P003	N00E	103.49(7)	N00E	C00P	C00Z	114.03(18)
O006	P003	N00H	105.26(7)	N00F	C00Q	C00X	112.47(17)
O007	P003	O006	111.86(7)	N00J	C00R	C00U	113.89(17)
O004 ¹	Ca ¹	O005	81.48(4)	O007	P003	N00E	116.63(8)
O004 ¹	Ca ¹	O005 ¹	79.17(4)	O007	P003	N00H	109.92(8)
O004 ¹	Ca ¹	O008	94.87(5)	N00H	P003	N00E	108.95(8)
O004 ¹	Ca ¹	O009 ¹	90.83(4)	P002	O004	Ca1 ¹	148.38(8)
O004 ¹	Ca ¹	O00B	119.59(5)	Ca ¹	O005	Ca1 ¹	116.70(5)
O004 ¹	Ca ¹	O00C	74.74(5)	N00D	O005	Ca1	146.25(11)
O005	Ca ¹	O005 ¹	63.30(5)	N00D	O005	Ca1 ¹	96.33(10)
O005 ¹	Ca ¹	O009 ¹	50.21(4)	P003	O006	P002	135.05(8)
O005	Ca ¹	O009 ¹	113.27(4)	P003	O007	Ca1	169.04(9)
O005	Ca ¹	O00B	144.67(5)	N00D	O009	Ca1 ¹	95.80(10)
O005 ¹	Ca ¹	O00B	143.21(5)	N00I	O00B	Ca1	93.79(11)
O007	Ca ¹	O004 ¹	156.89(5)	N00I	O00C	Ca1	99.94(11)
O007	Ca ¹	O005	81.96(4)	O009	N00D	O005	117.62(15)
O007	Ca ¹	O005 ¹	79.04(4)	O00A	N00D	Ca1 ¹	178.52(13)
O007	Ca ¹	O008	96.20(5)	C00N	N00E	P003	127.37(13)
O007	Ca ¹	O009 ¹	81.05(5)	C00N	N00E	C00P	116.76(15)
O007	Ca ¹	O00B	82.91(5)	C00P	N00E	P003	115.83(13)

¹1-X,1-Y,1-Z

Table A-12.6: Hydrogen Atom Coordinates ($\text{\AA}\times 10^4$) and Isotropic Displacement Parameters ($\text{\AA}^2\times 10^3$) for $\text{O}((\text{Et}_2\text{N})_2\text{PO})_2_1_f13$.

Atom	x	y	z	U(eq)
H00A	8884	4562	5565	50
H00B	7934	4440	6025	50
H00C	3684	625	3888	34
H00D	5029	1049	3979	34
H00E	8110	2689	2098	34
H00F	6650	2617	2142	34
H00G	9105	2747	3753	37
H00H	8721	3667	4011	37
H00I	4033	2932	2617	32
H00J	4171	3286	1773	32
H00K	6903	2519	5871	38
H00L	6973	2956	5052	38
H00M	6463	4869	2455	41
H00N	5038	5060	2166	41
H00O	2035	1869	3159	38
H00P	2020	2611	3778	38
H00Q	3758	2137	5598	37
H00R	4956	2237	6218	37
H00S	3395	1050	2557	60
H00T	4568	439	2728	60
H00U	4770	1432	2654	60
H00V	7485	1264	2295	57
H00W	7069	1532	3111	57
H00X	8502	1570	2976	57
H00Y	4315	729	5359	58
H	4229	846	6262	58
HA	5556	825	5946	58
H00Z	3033	4510	2033	69
HB	2917	4177	2887	69
HC	2223	3691	2157	69
H00	7432	1628	4514	64
HD	7359	1189	5333	64
HE	8443	1848	5229	64
H0AA	590	1507	4009	74
HF	1605	1640	4741	74
HG	1732	869	4166	74
H1AA	9959	3304	2691	87
HH	10555	3790	3448	87
HI	9480	4225	2876	87
H2AA	5159	4219	1050	74
HJ	6573	3992	1344	74
HK	6202	4935	1093	74

Experimental

Single crystals of $C_{32}H_{84}N_{12}O_{20}P_4Ca_2$ [**O((Et₂N)₂PO)₂_1_f13**] were [collected on prolonged storage of liquid product]. A suitable crystal was selected and [Collected in oil and frozen] on a diffractometer. The crystal was kept at 293(2) K during data collection. Using Olex2 [1], the structure was solved with the ShelXT [2] structure solution program using Intrinsic Phasing and refined with the ShelXL [3] refinement package using Least Squares minimisation.

1. Dolomanov, O.V., Bourhis, L.J., Gildea, R.J, Howard, J.A.K. & Puschmann, H. (2009), J. Appl. Cryst. 42, 339-341.
2. Sheldrick, G.M. (2015). Acta Cryst. A71, 3-8.
3. Sheldrick, G.M. (2015). Acta Cryst. C71, 3-8.

Crystal structure determination of [**O((Et₂N)₂PO)₂_1_f13**]

Crystal Data for $C_{32}H_{84}N_{12}O_{20}P_4Ca_2$ ($M = 1161.15$ g/mol): monoclinic, space group $P2_1/n$ (no. 14), $a = 10.6249(7)$ Å, $b = 15.5774(12)$ Å, $c = 17.0925(10)$ Å, $\beta = 96.707(5)^\circ$, $V = 2809.6(3)$ Å³, $Z = 4$, $T = 293(2)$ K, $\mu(\text{CuK}\alpha) = 3.503$ mm⁻¹, $D_{\text{calc}} = 1.373$ g/cm³, 27010 reflections measured ($7.702^\circ \leq 2\theta \leq 131.288^\circ$), 4816 unique ($R_{\text{int}} = 0.0983$, $R_{\text{sigma}} = 0.0513$) which were used in all calculations. The final R_1 was 0.0371 ($I > 2\sigma(I)$) and wR_2 was 0.1026 (all data).

Refinement model description

Number of restraints - 0, number of constraints - unknown.

Details:

1. Fixed Uiso

At 1.2 times of:

All C(H,H) groups

At 1.5 times of:

All C(H,H,H) groups, All O(H,H) groups

2.a Rotating group:

O008(H00A,H00B)

2.b Secondary CH₂ refined with riding coordinates:

C00K(H00C,H00D), C00L(H00E,H00F), C00M(H00G,H00H), C00N(H00I,H00J),

C00O(H00K,H00L), C00P(H00M,H00N), C00Q(H00O,H00P), C00R(H00Q,H00R)

2.c Idealised Me refined as rotating group:

C00S(H00S,H00T,H00U), C00T(H00V,H00W,H00X), C00U(H00Y,H,HA),

C00V(H00Z,HB,HC), C00W(H00,HD,HE), C00X(H0AA,HF,HG),

C00Y(H1AA,HH,HI), C00Z(H2AA,HJ,HK)

APPENDIX 13: EXPERIMENTAL DATA FOR $(i\text{PrNH})_3\text{PO}$

A failed attempt to prepare $\text{O}((i\text{PrNH})_2\text{PO})_2$ resulted in the production of $(i\text{PrNH})_3\text{PO}$. A detailed characterisation of this product is given hereunder as this species appears as an impurity in the attempts that yielded the desired product and therefore this data could be used for comparative purposes.

A-13.1. Synthesis of $(i\text{PrNH})_3\text{PO}$

A 100 ml Schlenk tube was charged with 5.8 ml (0.071 mol) iso-propyl amine. The amount of amine used was in excess of that required. This was cooled to $-78\text{ }^\circ\text{C}$ using a dry ice-acetone bath and stirred using a magnetic stirrer. When the required temperature was reached, 1 ml (0.007 mol) PPTC was added dropwise to the reaction solution using a glass syringe. The formation of white fumes was observed during the addition of the PPTC, however these dissipated soon afterwards. After addition of the PPTC the cooling bath was removed and the reaction mixture was allowed to react at room temperature overnight, with continuous stirring. This yielded a thick dull yellow paste. The solid was dissolved in a mixture of 5 ml distilled water and 6 ml chloroform to yield a two-layer system having a dull yellow chloroform phase and a clear aqueous phase which contained the expected ammonium salt by-product. Extraction was undertaken using chloroform to obtain a total of 25 ml chloroform solution of the dull yellow product. The solvent was removed under vacuum to yield a dull yellow paste. The paste was dissolved in a 3ml mixture of 1:2 by volume acetonitrile/methanol solution. This was left standing for 2 weeks to obtain a number of colourless crystals as the final product. FT-IR (KBr, cm^{-1}): 3400 (s), 3252 (bs), 2965 (s), 2933 (w), 2869 (w), 1462 (s), 1413 (s), 1379 (s), 1368 (s), 1309 (m), 1195 (sh), 1187 (sh), 1166 (s), 1139 (s), 1048 (s), 1016 (s), 909 (s), 890 (s), 752 (m). ^1H NMR (CDCl_3): 3.38 ppm (m, 1.00H, CH), 2.04 ppm (bs, 1.17H, NH), 1.14 ppm (d, $J = 6.60\text{ Hz}$, 6.15H, CH_3). $^{31}\text{P}\{^1\text{H}\}$ NMR (CDCl_3): 12.29 ppm. GC-MS (EI; 70 eV) m/z: 44.11, 58.01, 79, 121.1, 163.1, 206.2, 221.2 [$(i\text{PrNH})_3\text{PO}$] $^+$.

A-13.2. Characterisation of $(i\text{PrNH})_3\text{PO}$

Single crystals of the product of this reaction, shown in the micrograph in Figure A-13.1, were collected and analysed by SXRD. Crystals were mounted in oil. Data was collected using a STOE Stradivari diffractometer with a microfocus Mo- $K_{\alpha 1}$ source, at 293 K. Unit cell and space group determination was undertaken using X-Area and structure solution was undergone using Olex2.^{351,352} On unit cell determination an orthorhombic unit cell with parameters $a = 9.0574 \text{ \AA}$, $b = 18.1994 \text{ \AA}$, $c = 8.052 \text{ \AA}$ and where $\alpha = \beta = \gamma = 90^\circ$ with a space group $Pnma$ was obtained. Structure solution and refinement yielded a crystal structure for $(i\text{PrNH})_3\text{PO}$. This crystal structure was observed to be in agreement with the literature data for this compound as published by Gupta, A.K. and co-workers.³⁸³

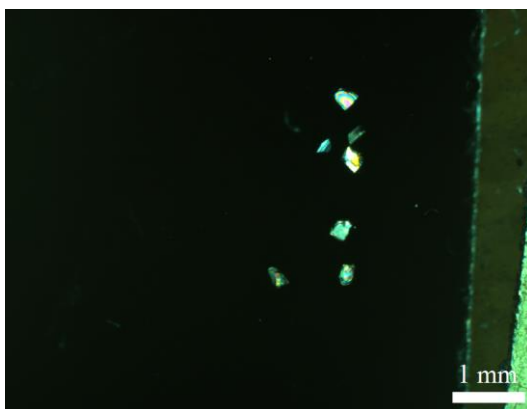


Figure A-13.1: Micrograph of $(i\text{PrNH})_3\text{PO}$.

This was confirmed through both ^{31}P NMR and GC-MS. The $^{31}\text{P}\{^1\text{H}\}$ NMR spectrum of $(i\text{PrNH})_3\text{PO}$ given in Figure A-13.2 gave a single peak at 12.29 ppm, while the gas chromatograph given in Figure A-13.3 gave only one significant peak at 7.244 minutes. The peak described by the $^{31}\text{P}\{^1\text{H}\}$ NMR spectrum at 12.29 ppm was found to be in agreement with the peak at 12.84 ppm described by Gupta, A.K. and co-workers for $(i\text{PrNH})_3\text{PO}$, further showing that the product obtained in the current study was $(i\text{PrNH})_3\text{PO}$.³⁸³ This was further confirmed through the MS data collected in the current study, and shown in Figure A-13.4, wherein the highest significant m/z value was at 221.2, which was indicative of the M^+ ion for $(i\text{PrNH})_3\text{PO}$, namely $[(i\text{PrNH})_3\text{PO}]^+$. The remaining significant peaks could all be assigned to viable and expected fragments. The peak at 44.11 m/z was assigned to the $[i\text{PrH}]^+$ fragment, the peak at 58.01 m/z to the

$[i\text{PrNH}]^+$ fragment, the peak at 79 m/z to the $[(\text{NH}_2)_2\text{PO}]^+$ fragment, the peak at 121.1 m/z to the $[(i\text{PrNH})(\text{NH}_2)_2\text{P}]^+$ fragment, the peak at 163.1 m/z to the $[(i\text{PrNH})_2\text{PO}]^+$ fragment and the peak at 206.2 m/z to the $[(i\text{PrNH})_2\text{PO} + i\text{Pr}]^+$ fragment.

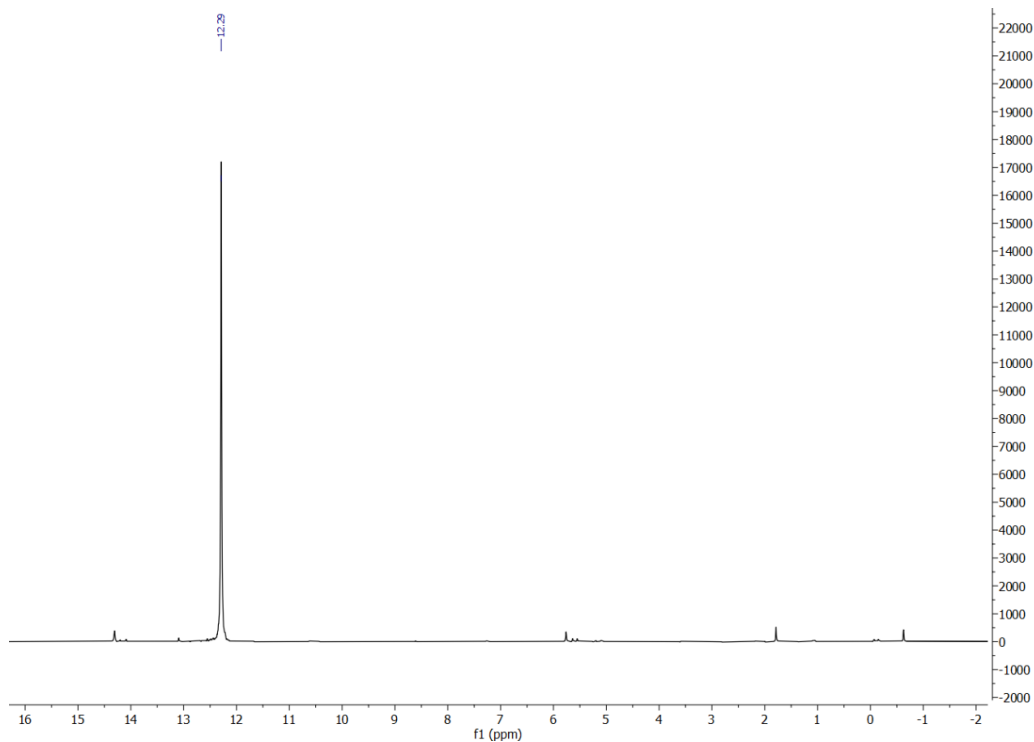


Figure A-13.2: $^{31}\text{P}\{^1\text{H}\}$ NMR spectra of $(i\text{PrNH})_3\text{PO}$.

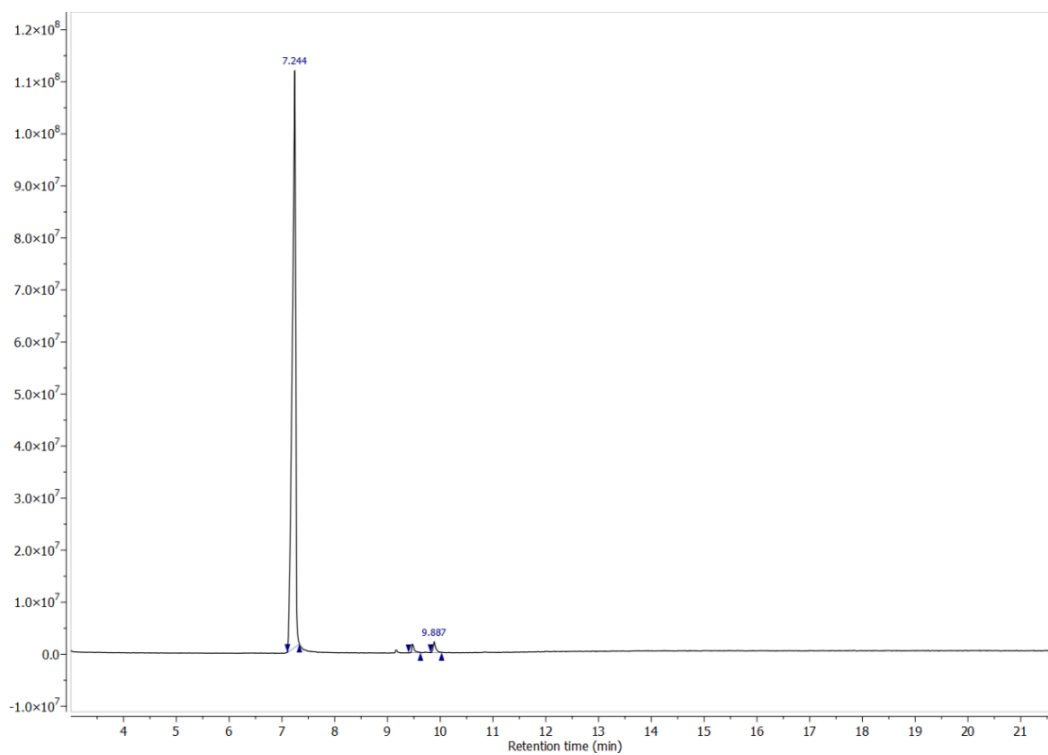


Figure A-13.3: Gas chromatograph of $(i\text{PrNH})_3\text{PO}$.

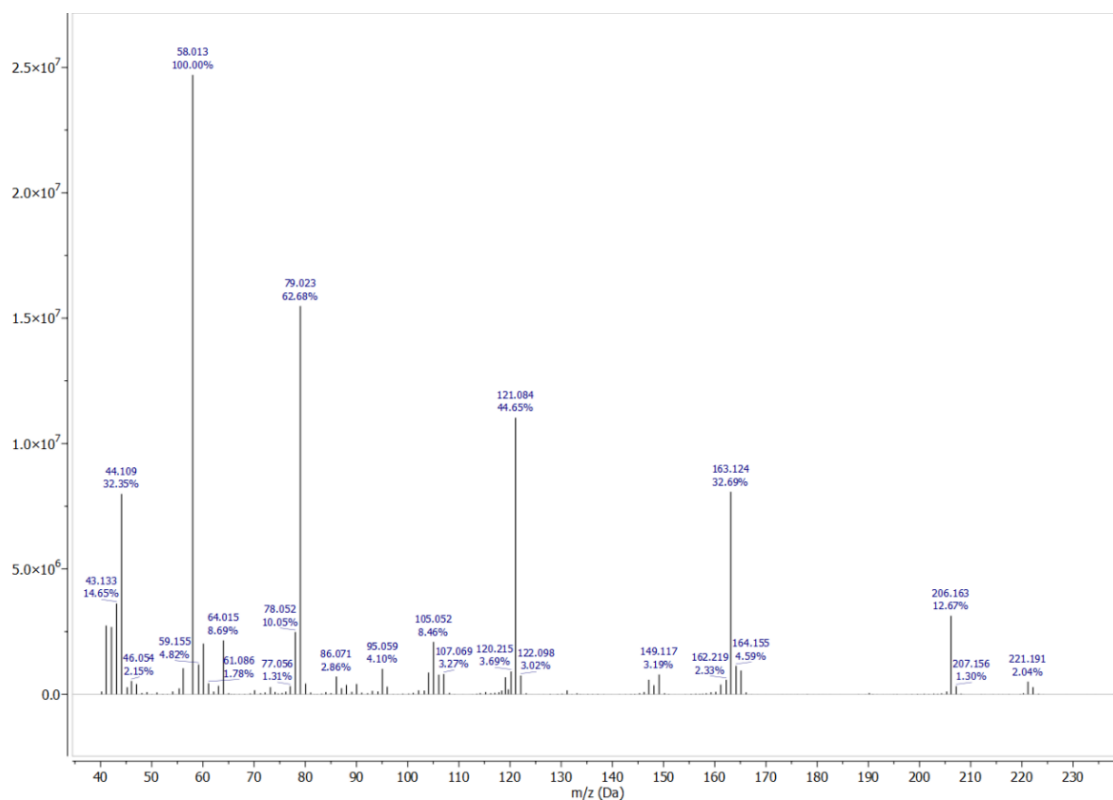


Figure A-13.4: Mass spectrum of (iPrNH)₃PO.

Further data was collected through ¹H NMR and IR spectroscopy which further supported the characterisation of this product as (iPrNH)₃PO. The ¹H NMR spectrum is given in Figure A-13.5 while the IR spectrum is given in Figure A-13.6. The assignment and descriptions of the peaks observed in the ¹H NMR spectrum are given in Table A-13.1 and these were in close agreement with the ¹H NMR data from literature.³⁸³ The IR spectrum given in Figure A-13.6 also shows assignments of the various bands.

Table A-13.1: ¹H NMR experimental data and assignment for proton peaks of (iPrNH)₃PO in CDCl₃:

¹H NMR experimental data and assignment for proton peaks of (iPrNH)₃PO in CDCl₃				
ppm	Multiplicity	Integration	Coupling	Assignment
3.38	multiplet	1.00	N/A	CH (Iso-propyl)
2.04	broad singlet	1.17	N/A	NH
1.14	doublet	6.15	J = 6.60 Hz	CH ₃ (Iso-propyl)

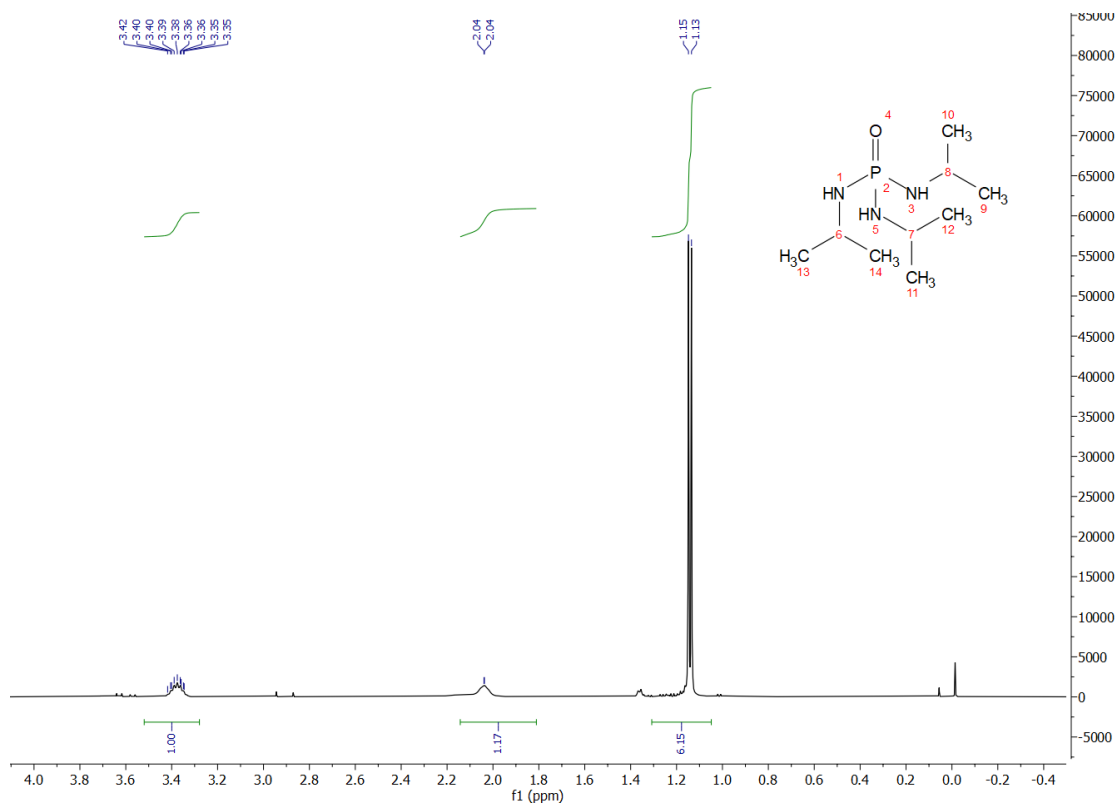


Figure A-13.5: 1H NMR spectrum of $(iPrNH)_3PO$.

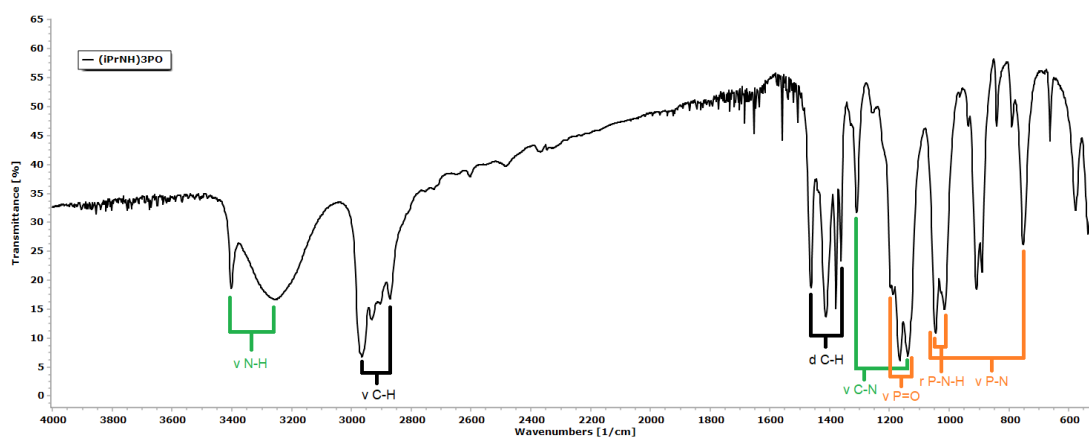


Figure A-13.6: IR spectra of $(iPrNH)_3PO$.

APPENDIX 14: CRYSTALLOGRAPHIC DATA FOR PRODUCT

O((iPrNH)₂PO)₂_1_b1.

Hereunder is the data regarding the crystal structure of the single crystal obtained from O((iPrNH)₂PO)₂_1_b1.

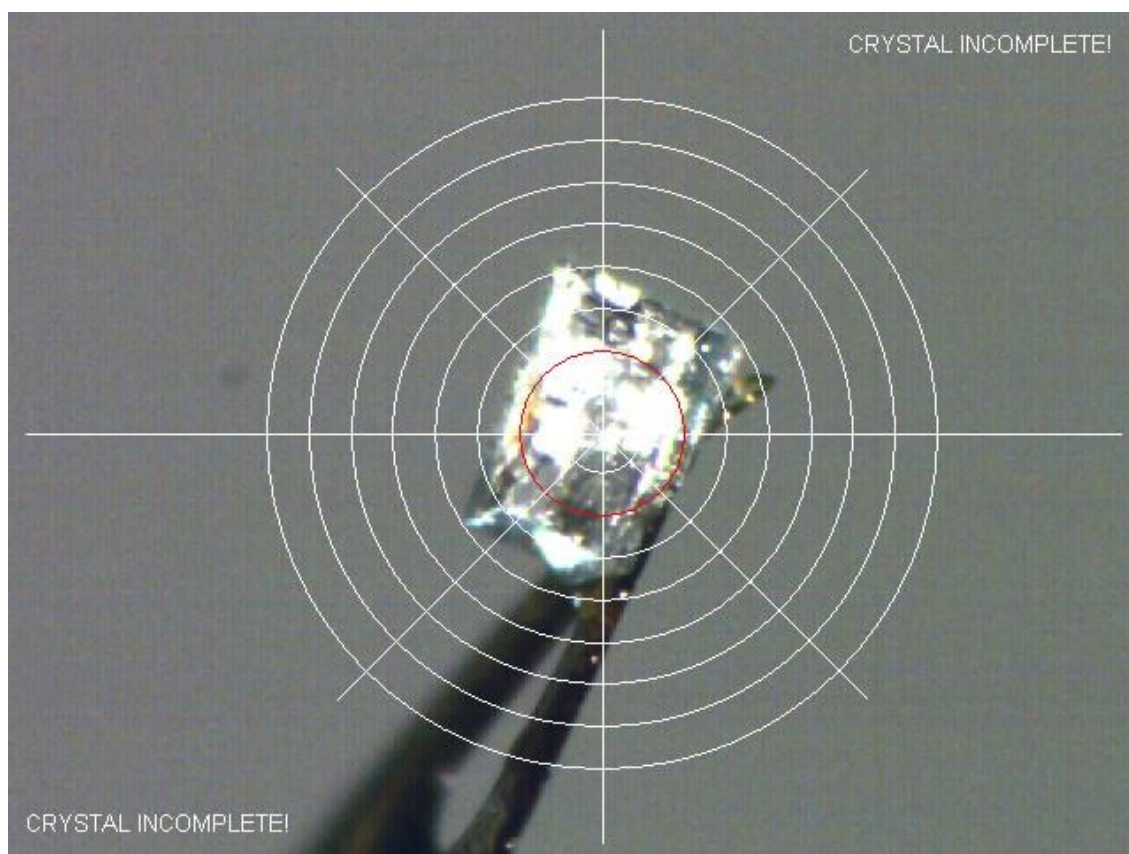


Figure A-14.1: Crystal used in structure determination of O((iPrNH)₂PO)₂_1_b1.

Table A-14.1: Crystal data and structure refinement for O((iPrNH)₂PO)₂_1_b1.

Identification code	O((iPrNH) ₂ PO) ₂ _1_b1
Empirical formula	C ₁₂ H ₃₂ N ₄ O ₃ P ₂
Formula weight	342.35
Temperature/K	293
Crystal system	orthorhombic
Space group	<i>Pca</i> 2 ₁
<i>a</i> /Å	20.3379(4)
<i>b</i> /Å	5.04400(10)
<i>c</i> /Å	19.1488(5)
α /°	90

$\beta/^\circ$	90
$\gamma/^\circ$	90
Volume/ \AA^3	1964.37(8)
Z	4
$\rho_{\text{calc}}/\text{g}/\text{cm}^3$	1.158
μ/mm^{-1}	2.131
F(000)	744.0
Crystal size/ mm^3	$0.8 \times 0.4 \times 0.02$
Radiation	CuK α ($\lambda = 1.54186$)
2Θ range for data collection/ $^\circ$	8.696 to 136.94
Index ranges	$-24 \leq h \leq 23, -3 \leq k \leq 6, -20 \leq l \leq 23$
Reflections collected	38282
Independent reflections	3317 [$R_{\text{int}} = 0.0617, R_{\text{sigma}} = 0.0292$]
Data/restraints/parameters	3317/1/214
Goodness-of-fit on F^2	1.045
Final R indexes [$I > 2\sigma(I)$]	$R_1 = 0.0411, wR_2 = 0.1087$
Final R indexes [all data]	$R_1 = 0.0417, wR_2 = 0.1092$
Largest diff. peak/hole / $e \text{\AA}^{-3}$	0.28/-0.24
Flack parameter	-0.01(3)

Table A-14.2: Fractional Atomic Coordinates ($\times 10^4$) and Equivalent Isotropic Displacement Parameters ($\text{\AA}^2 \times 10^3$) for O(*i*PrNH) $_2$ PO) $_2$ _1_b1. U_{eq} is defined as 1/3 of the trace of the orthogonalised U_{ij} tensor.

Atom	<i>x</i>	<i>y</i>	<i>z</i>	U_{eq}
P001	6360.1(4)	6372.4(14)	5384.6(5)	36.3(2)
P002	6969.9(4)	4128.7(14)	4136.5(5)	36.8(2)
O003	6028.8(13)	8460(4)	4977.2(14)	45.2(6)
O004	7103.0(15)	6597(5)	3751.3(16)	52.4(7)
O005	6913.5(11)	4796(5)	4965.8(14)	42.9(6)
N006	7537.9(15)	1902(6)	4121(2)	51.9(8)
N007	6704.8(19)	7720(7)	6058.2(18)	53.8(8)
N008	5922.4(18)	3903(6)	5678.8(19)	46.4(7)
N009	6288.9(16)	2676(7)	3922.4(17)	44.7(7)
C00A	8198.4(19)	2256(8)	4398(3)	63.1(13)
C00B	5907(2)	3307(9)	3310(3)	63.0(12)
C00C	5319(3)	4368(9)	6074(3)	67.7(14)
C00D	7058(3)	6396(12)	6625(3)	74.2(15)
C00E	5235(5)	2296(15)	6625(5)	138(4)
C00F	8274(5)	578(18)	5058(6)	140(4)
C00G	7793(5)	6490(30)	6541(7)	154(4)

C1	6866(6)	7720(30)	7311(4)	154(5)
C4	8706(4)	1720(30)	3861(7)	172(6)
C0AA	6091(8)	1494(19)	2712(4)	153(5)
C3	4738(3)	4500(30)	5604(6)	149(4)
C6	5197(5)	3080(40)	3483(8)	241(10)

Table A-14.3: Anisotropic Displacement Parameters ($\text{\AA}^2 \times 10^3$) for $\text{O}((i\text{PrNH})_2\text{PO})_2_1_b1$. The Anisotropic displacement factor exponent takes the form: $-2\pi^2[h^2a^{*2}U_{11}+2hka^*b^*U_{12}+\dots]$.

Atom	U_{11}	U_{22}	U_{33}	U_{23}	U_{13}	U_{12}
P001	47.0(4)	26.9(4)	35.0(4)	-0.1(3)	-1.1(4)	0.2(3)
P002	44.7(4)	24.0(4)	41.8(4)	-1.6(4)	3.0(3)	-5.4(3)
O003	57.6(14)	32.3(12)	45.7(14)	5.7(10)	-0.7(11)	5.0(10)
O004	77.8(18)	29.6(13)	49.8(16)	2.9(11)	9.6(13)	-13.4(12)
O005	43.8(12)	44.0(13)	40.8(13)	-2.3(11)	-0.1(9)	4.2(9)
N006	45.6(16)	27.9(14)	82(2)	-14.0(17)	4.8(17)	-4.3(12)
N007	78(2)	38.5(18)	45.1(18)	-2.4(13)	-14.3(15)	-1.4(14)
N008	66(2)	25.0(15)	48.5(17)	-2.8(13)	13.5(15)	-1.4(12)
N009	54.6(17)	32.4(16)	47.0(18)	4.7(13)	-9.1(12)	-8.5(12)
C00A	43.6(19)	43(2)	103(4)	-17(2)	-2(2)	-2.3(15)
C00B	72(3)	50(2)	67(3)	13(2)	-23(2)	-7.2(19)
C00C	81(3)	41(2)	82(3)	1(2)	37(3)	1.0(18)
C00D	100(4)	71(3)	52(3)	5(2)	-25(3)	2(3)
C00E	191(9)	81(4)	142(7)	38(5)	113(7)	24(5)
C00F	114(6)	119(6)	186(10)	35(6)	-70(7)	-9(5)
C00G	105(6)	210(12)	148(9)	13(8)	-55(6)	24(7)
C1	201(10)	215(12)	47(4)	-13(5)	-38(5)	58(9)
C4	58(4)	255(14)	204(12)	-103(11)	41(5)	-18(5)
C0AA	283(14)	108(6)	66(4)	-20(4)	-54(7)	-2(7)
C3	57(4)	235(12)	154(9)	6(8)	18(4)	-5(5)
C6	65(5)	460(30)	195(14)	92(17)	-36(6)	33(10)

Table A-14.4: Bond Lengths for $\text{O}((i\text{PrNH})_2\text{PO})_2_1_b1$.

Atom	Atom	Length/ \AA	Atom	Atom	Length/ \AA
P001	O003	1.474(2)	N008	C00C	1.462(6)
P001	O005	1.594(3)	N009	C00B	1.443(6)
P001	N007	1.618(3)	C00A	C00F	1.528(11)
P001	N008	1.631(3)	C00A	C4	1.482(9)
P002	O004	1.472(3)	C00B	C0AA	1.513(11)
P002	O005	1.627(3)	C00B	C6	1.485(12)

P002	N006	1.611(3)	C00C	C00E	1.494(8)
P002	N009	1.620(3)	C00C	C3	1.486(11)
N006	C00A	1.456(5)	C00D	C00G	1.503(11)
N007	C00D	1.463(6)	C00D	C1	1.524(11)

Table A-14.5: Bond Angles for O((iPrNH)₂PO)₂_1_b1.

Atom	Atom	Atom	Angle/°	Atom	Atom	Atom	Angle/°
O003	P001	O005	114.38(16)	C00C	N008	P001	121.0(3)
O003	P001	N007	108.66(17)	C00B	N009	P002	124.5(3)
O003	P001	N008	118.62(17)	N006	C00A	C00F	109.1(5)
O005	P001	N007	107.73(18)	N006	C00A	C4	111.5(6)
O005	P001	N008	100.26(16)	C4	C00A	C00F	113.8(8)
N007	P001	N008	106.4(2)	N009	C00B	C0AA	110.4(5)
O004	P002	O005	109.09(16)	N009	C00B	C6	109.0(6)
O004	P002	N006	116.64(19)	C6	C00B	C0AA	111.3(10)
O004	P002	N009	114.40(18)	N008	C00C	C00E	110.4(5)
N006	P002	O005	102.28(19)	N008	C00C	C3	111.1(5)
N006	P002	N009	107.03(17)	C3	C00C	C00E	111.6(7)
N009	P002	O005	106.28(15)	N007	C00D	C00G	113.2(6)
P001	O005	P002	130.07(16)	N007	C00D	C1	108.3(5)
C00A	N006	P002	124.7(3)	C00G	C00D	C1	109.5(8)
C00D	N007	P001	127.8(3)				

Table A-14.6: Hydrogen Atom Coordinates ($\text{\AA} \times 10^4$) and Isotropic Displacement Parameters ($\text{\AA}^2 \times 10^3$) for O((iPrNH)₂PO)₂_1_b1.

Atom	x	y	z	U(eq)
H00A	8242	4119	4536	76
H00B	6000	5141	3173	76
H00C	5361	6087	6309	81
H00D	6919	4537	6641	89
H00E	5137	626	6408	207
H00F	4882	2789	6930	207
H00G	5635	2141	6889	207
H00H	7921	971	5375	209
H00I	8687	977	5277	209
H00J	8261	-1267	4936	209
H00K	7908	5894	6080	231
H00L	7994	5353	6881	231
H00M	7944	8273	6606	231
H1A	7112	9332	7367	232

H1B	6961	6547	7692	232
H1C	6405	8122	7305	232
H4A	8640	-15	3670	259
H4B	9134	1823	4070	259
H4C	8672	3018	3495	259
H0AA	6555	1615	2627	229
H0AB	5856	2016	2299	229
H0AC	5979	-300	2829	229
H3A	4831	5676	5222	223
H3B	4366	5152	5860	223
H3C	4643	2764	5427	223
H6A	5115	1394	3698	362
H6B	4942	3226	3063	362
H6C	5076	4475	3799	362
H008	5934(19)	2800(90)	5460(20)	39(11)
H006	7430(20)	630(90)	4080(20)	40(11)
H007	6710(30)	9620(120)	6020(30)	75(16)
H009	6230(20)	1310(110)	4150(30)	54(12)

Experimental

Single crystals of $C_{12}H_{32}N_4O_3P_2$ [**O((iPrNH)₂PO)₂_1_b1**] were [**Layering CHCl₃ solution with 30-40 petroleum ether**]. A suitable crystal was selected and [**Collected in oil and frozen**] on a **STOE STADIVARI** diffractometer. The crystal was kept at 293 K during data collection. Using Olex2 [1], the structure was solved with the ShelXT [2] structure solution program using Intrinsic Phasing and refined with the ShelXL [3] refinement package using Least Squares minimisation.

4. Dolomanov, O.V., Bourhis, L.J., Gildea, R.J., Howard, J.A.K. & Puschmann, H. (2009), *J. Appl. Cryst.* 42, 339-341.
5. Sheldrick, G.M. (2015). *Acta Cryst.* A71, 3-8.
6. Sheldrick, G.M. (2015). *Acta Cryst.* C71, 3-8.

Crystal structure determination of [**O((iPrNH)₂PO)₂_1_b1**]

Crystal Data for $C_{12}H_{32}N_4O_3P_2$ ($M = 342.35$ g/mol): orthorhombic, space group $Pca2_1$ (no. 29), $a = 20.3379(4)$ Å, $b = 5.04400(10)$ Å, $c = 19.1488(5)$ Å, $V = 1964.37(8)$ Å³, $Z = 4$, $T = 293$ K, $\mu(\text{CuK}\alpha) = 2.131$ mm⁻¹, $D_{\text{calc}} = 1.158$ g/cm³, 38282 reflections measured ($8.696^\circ \leq 2\theta \leq 136.94^\circ$), 3317 unique ($R_{\text{int}} = 0.0617$, $R_{\text{sigma}} = 0.0292$) which were used in all calculations. The final R_1 was 0.0411 ($I > 2\sigma(I)$) and wR_2 was 0.1092 (all data).

Refinement model description

Number of restraints - 1, number of constraints - unknown.

Details:

1. Fixed Uiso

At 1.2 times of:

All C(H) groups

At 1.5 times of:

All C(H,H,H) groups

2.a Ternary CH refined with riding coordinates:

C00A(H00A), C00B(H00B), C00C(H00C), C00D(H00D)

2.b Idealised Me refined as rotating group:

C00E(H00E,H00F,H00G), C00F(H00H,H00I,H00J), C00G(H00K,H00L,H00M),

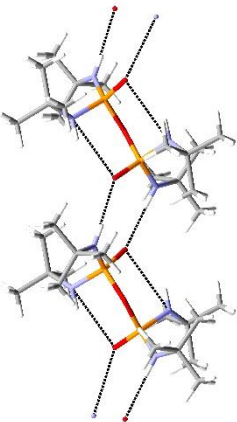
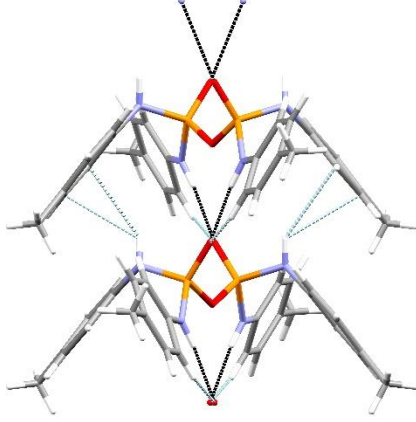
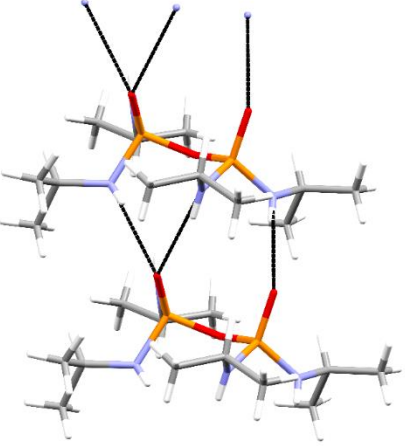
C1(H1A,H1B,H1C), C4(H4A,H4B,H4C), C0AA(H0AA,H0AB,H0AC),

C3(H3A,H3B,H3C), C6(H6A,H6B,H6C)

**APPENDIX 15: SUMMARY OF THE STRUCTURE COMPARISON OF KNOWN MONO-N-SUBSTITUTED
PYROPHOSPHORAMIDES.**

Spacegroups	$P2_1/c$	$Pccn$	$Pca2_1$
Compound	$O((t\text{BuNH})_2\text{PO})_2$ $O((2\text{-MePhNH})_2\text{PO})_2$	$O((4\text{-MePhNH})_2\text{PO})_2$	$O((i\text{PrNH})_2\text{PO})_2$
Data collection temperature	$t\text{Bu}$ - 150K 2-MePh (Poarayoubi) - 150K 2-MePh (Cameron) - 295K	90K	293K
Pyrophosphoramidate conformation (P–O–P oxygen in orange and direction of hydrogen bonding from H-donor to H-acceptor in red)			
Intramolecular bonding			
Hydrogen bonding	P=O---H-N (non-intermolecular bonding)	None	None
Non hydrogen bonding	$t\text{Bu}$ - None	None	None

	2-MePh - Ph---H-C(Me) (causing stacking)		
Intermolecular bonding			
Hydrogen bonding			
Non hydrogen bonding	<i>t</i> Bu - None 2-MePh (Poarayoubi) - Ph---H-C(Ph) (causing interlocking) 2-MePh (Cameron) - Ph---H-C(Me) (causing stacking)	Ph---H-C(Me) Ph---H-N P=O---H-C(Ph(C2))	None
Supramolecular bonding motif	Chain like structure with two molecules as components, growth in <i>c</i> -axis direction and perpendicular to <i>c</i> -axis direction.	Chain like structure with two molecules as components, growth in <i>c</i> -axis direction.	Chain like structure with one molecule as component, growth in <i>b</i> -axis direction.

Supramolecular bonding motif (diagram)			
Packing of neighbouring chains	<i>t</i> Bu - Parallel along <i>a</i> -axis direction (related by translation) Antiparallel along <i>b</i> -axis direction (related by 2_1 screw axis)	Antiparallel along <i>b</i> -axis direction (related by glide plane) Parallel along <i>a</i> -axis direction (related by translation)	Antiparallel along <i>a</i> -axis direction (related by 2_1 screw axis) Parallel along <i>b</i> -axis direction (related by glide plane)
	2-MePh (Poarayoubi) – Parallel in <i>a</i> -axis direction (related by translation) Antiparallel in <i>b</i> -axis direction (related by 2_1 screw axis)		

	2-MePh (Cameron) – Parallel in <i>a</i> -axis direction (related by glide plane) Antiparallel in <i>b</i> -axis direction (related by 2_1 screw axis)		
--	---------------------------------------------------------------------------------------------------------------------------------------------------------------------	--	--

APPENDIX 16: ORGANIC CO-FORMER PXRD ANALYSIS.

The three co-formers used in the current study were analysed using PXRD to determine their chemical and structural nature. In all three cases the crystalline phases used in this study were found to be the same as phases previously published in literature.

The biphenyl used proved to be the same polymorph described in most publications. In Figure A-16.1 it is compared to the most representative data, that is the structure published by Charbonneau and co-workers in 1977.⁴⁰³

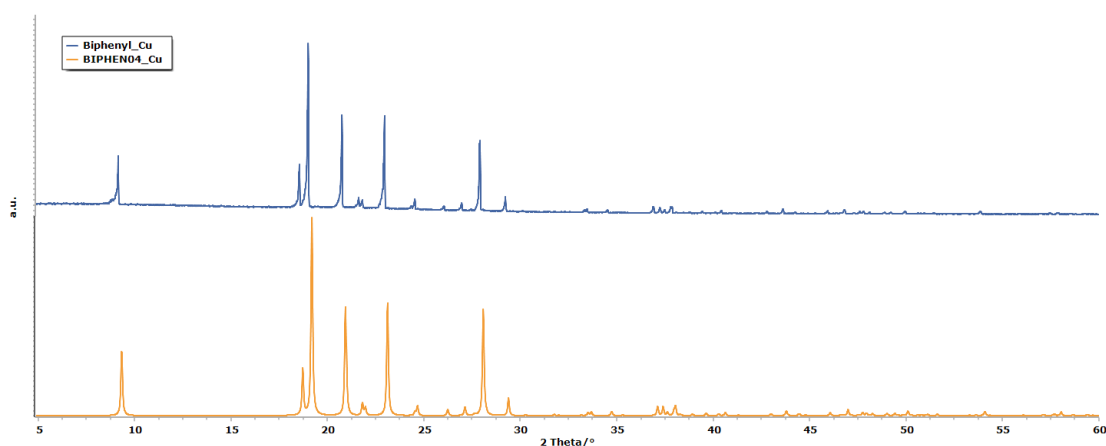


Figure A-16.1: Experimental PXRD patterns of biphenyl (blue) and calculated PXRD pattern of BIPHEN04 (orange).

Two crystal structures of 4,4'-bipyridine are known in literature, namely the anhydrous 4,4'-bipyridine (in *P*-1) published by Candana and co-workers and the di-hydrate (in *C*2) published by Huang and co-workers. Comparison with the calculated powder patterns of the two showed that the solid used in the current study was the anhydrous solid published by Candana and co-workers, as given in Figure A-16.2.

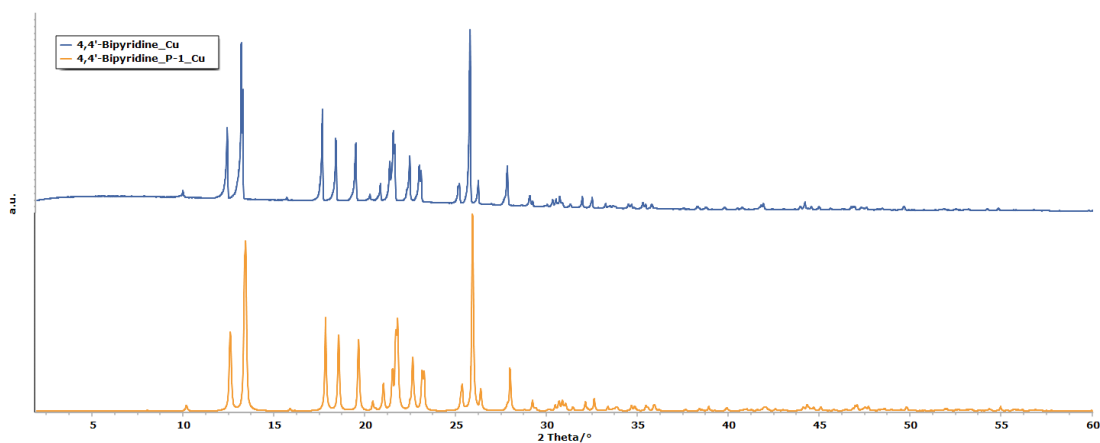


Figure A-16.2: Experimental PXRD patterns of 4,4'-bipyridine (blue) and calculated PXRD pattern of anhydrous 4,4'-bipyridine in a spacegroup $P-1$ (orange).

Two very structurally similar polymorphs of 4,4'-oxydianiline are known in literature, described by the refcodes SUCVER and SUCVER01 in the CSD.^{406,407} On comparison of the calculated powder patterns of both with that of the 4,4'-oxydianiline used in the current study it was observed that the solid used was the polymorph SUCVER as shown in Figure A-16.3.

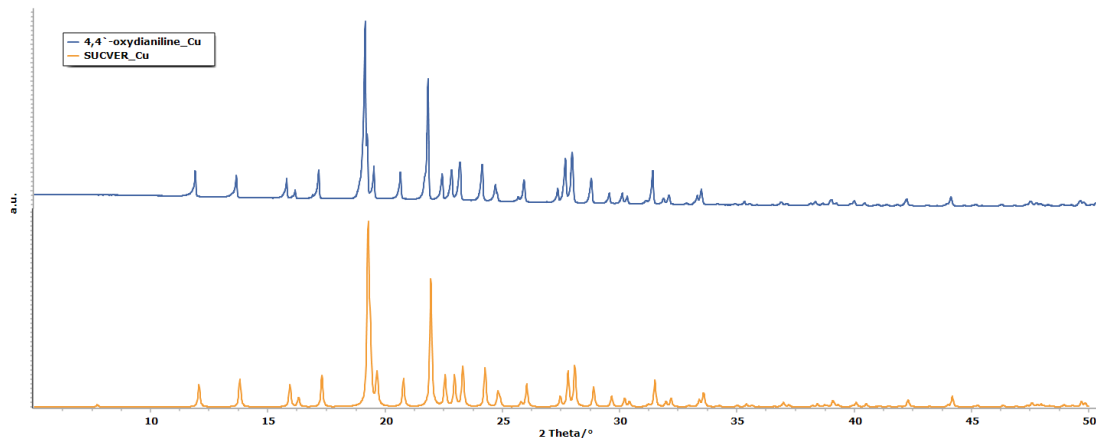


Figure A-16.3: Experimental PXRD patterns of 4,4'-oxydianiline (blue) and calculated PXRD pattern of SUCVER (orange).

APPENDIX 17: RAMAN SPECTROSCOPY OF CO-CRYSTALLISATION PRODUCTS.

Raman data was collected for all the organic co-formers used in this study and all three co-crystallisation products of $[\text{Sm}(\text{C}(\text{Ph}_2\text{PNSiMe}_3)_2)(\text{NCy}_2)(\text{THF})]_4$. Given that the data for the organic co-formers is not novel and the data for the co-crystallisation products yielded low quality spectra, a brief discussion is given in Section 4.3.1.3 while the spectra referred to in the text are presented hereunder.

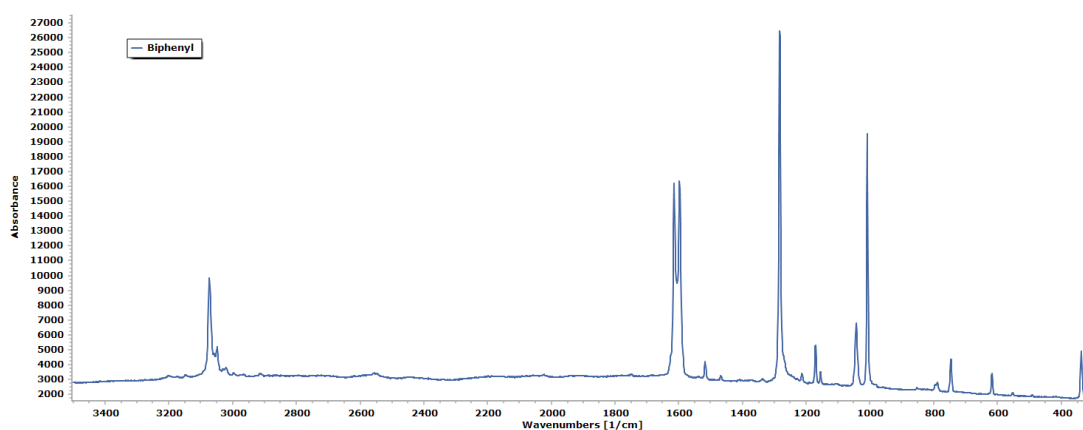


Figure A-17.1: Raman spectrum of biphenyl.

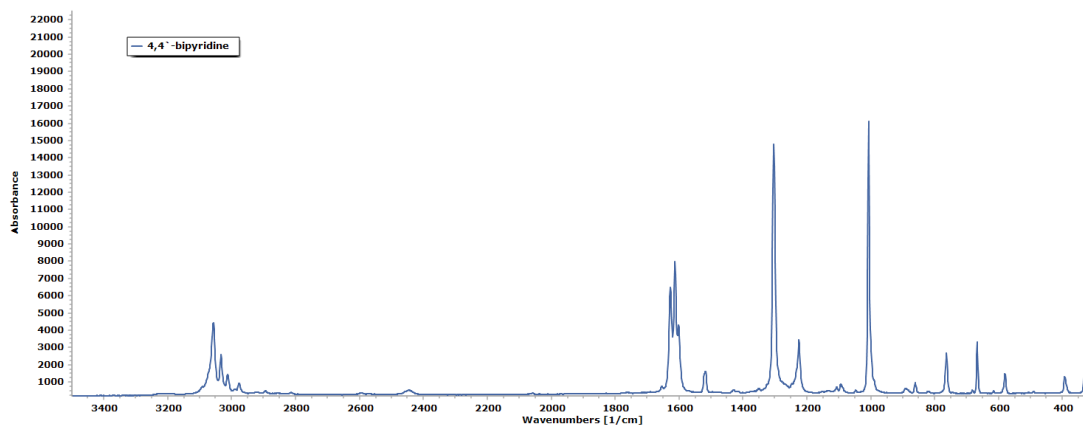


Figure A-17.2: Raman spectrum of 4,4'-bipyridine

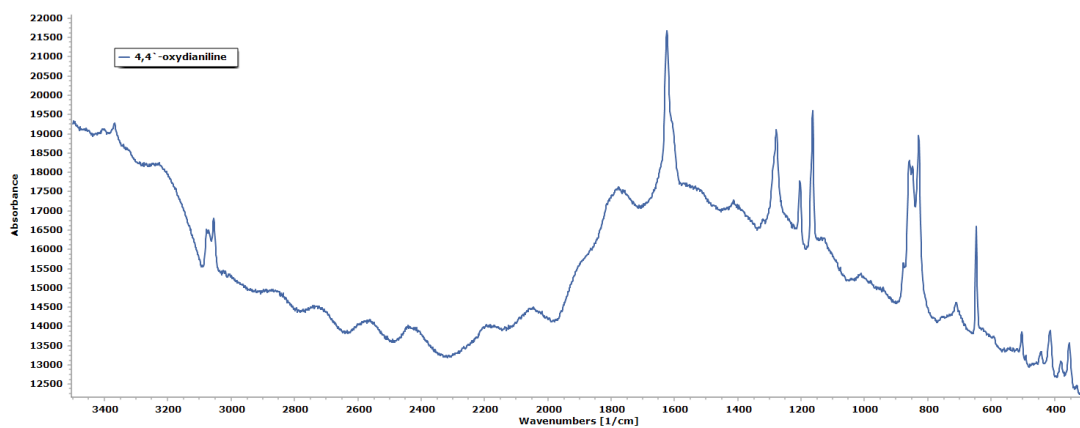


Figure A-17.3: Raman spectrum of 4,4'-Oxydianiline.

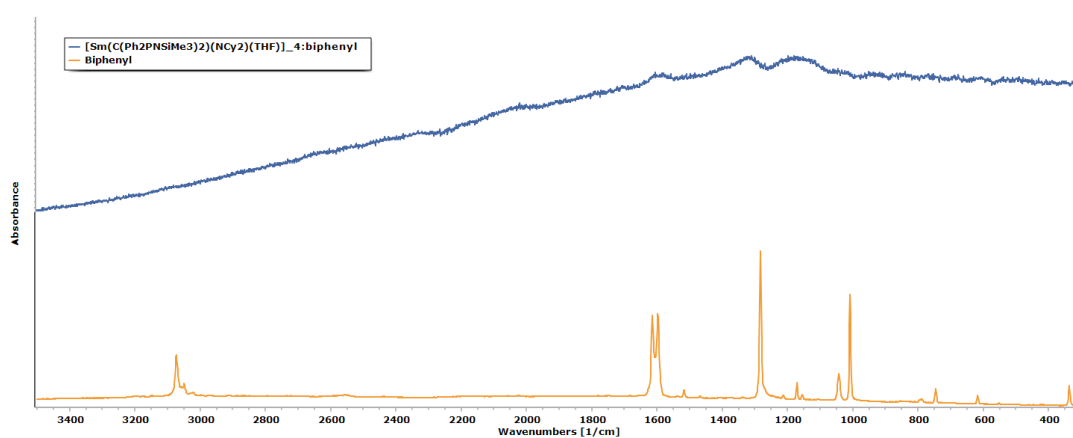


Figure A-17.4: Raman spectra of $[\text{Sm}(\text{C}(\text{Ph}_2\text{PNSiMe}_3)_2)(\text{NCy}_2)(\text{THF})]_4$:biphenyl (blue) and biphenyl (orange).

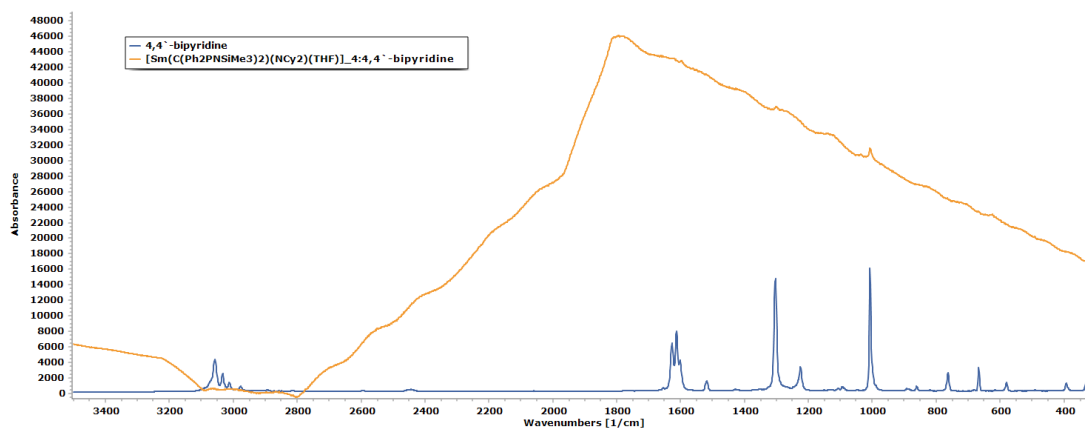


Figure A-17.5: Raman spectra of $[\text{Sm}(\text{C}(\text{Ph}_2\text{PNSiMe}_3)_2)(\text{NCy}_2)(\text{THF})]_4$:4,4'-bipyridine (orange) and 4,4'-bipyridine (blue).

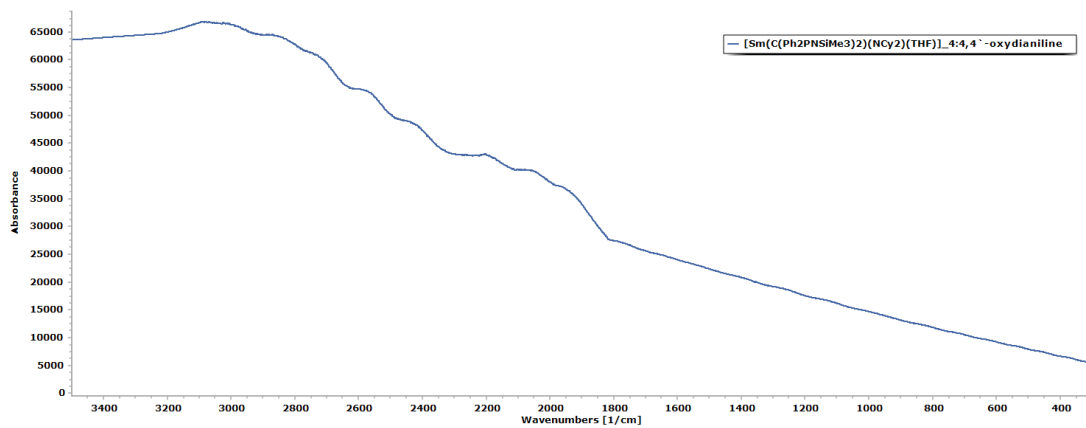


Figure A-17.6: Raman spectrum of [Sm(C(Ph₂PNSiMe₃)₂)(NCy₂)(THF)]₄:4,4'-oxydianiline.

APPENDIX 18: INITIAL CRYSTALLOGRAPHIC DATA FOR

[N(Ph₂PCH₃)(Ph₂PNH₂)] [Cl]·Ph₂P(O)NH₂.

Hereunder is the data regarding the crystal structure of the single crystal of [N(Ph₂PCH₃)(Ph₂PNH₂)] [Cl]·Ph₂P(O)NH₂ obtained from [Sm(C(Ph₂PNSiMe₃)₂)(NCy₂)(THF)]₄:4,4'-bipyridine. The data provided is provisional as structure solution is still ongoing.

Table A-18.1: Crystal data and structure refinement for [N(Ph₂PCH₃)(Ph₂PNH₂)] [Cl]·Ph₂P(O)NH₂.

Identification code	[N(Ph ₂ PCH ₃)(Ph ₂ PNH ₂)] [Cl]·Ph ₂ P(O)NH ₂
Empirical formula	C ₁₅ H ₁₉ N ₄ OP ₃ Cl
Formula weight	399.70
Temperature/K	293(2)
Crystal system	triclinic
Space group	<i>P</i> -1
<i>a</i> /Å	9.038(5)
<i>b</i> /Å	9.815(5)
<i>c</i> /Å	18.486(11)
<i>α</i> /°	93.92(5)
<i>β</i> /°	91.98(5)
<i>γ</i> /°	91.87(5)
Volume/Å ³	1634.0(16)
<i>Z</i>	2
ρ_{calc} /cm ³	0.812
μ /mm ⁻¹	0.270
F(000)	414.0
Crystal size/mm ³	? × ? × ?
Radiation	MoK α (λ = 0.71073)
2 Θ range for data collection/°	4.846 to 70.312
Index ranges	? ≤ <i>h</i> ≤ ?, ? ≤ <i>k</i> ≤ ?, ? ≤ <i>l</i> ≤ ?
Reflections collected	13173
Independent reflections	13173 [<i>R</i> _{int} = ?, <i>R</i> _{sigma} = 2.3050]
Data/restraints/parameters	13173/0/229
Goodness-of-fit on F ²	0.667
Final <i>R</i> indexes [<i>I</i> ≥ 2 σ (<i>I</i>)]	<i>R</i> ₁ = 0.1477, <i>wR</i> ₂ = 0.3299
Final <i>R</i> indexes [all data]	<i>R</i> ₁ = 0.6250, <i>wR</i> ₂ = 0.5199
Largest diff. peak/hole / e Å ⁻³	0.70/-0.70

Table A-18.2: Fractional Atomic Coordinates ($\times 10^4$) and Equivalent Isotropic Displacement Parameters ($\text{\AA}^2 \times 10^3$) for $[\text{N}(\text{Ph}_2\text{PCH}_3)(\text{Ph}_2\text{PNH}_2)][\text{Cl}]\cdot\text{Ph}_2\text{P}(\text{O})\text{NH}_2$. U_{eq} is defined as 1/3 of the trace of the orthogonalised U_{ij} tensor.

Atom	<i>x</i>	<i>y</i>	<i>z</i>	U_{eq}
Cl01	4958(5)	11087(4)	7446(2)	49.2(13)
P002	6535(5)	6991(4)	7249(2)	34.9(12)
P003	3876(5)	8075(4)	9653(3)	36.9(13)
P004	3508(5)	6613(4)	6666(2)	36.4(13)
O005	5203(12)	8442(10)	9261(5)	38(3)
N006	5066(13)	6170(12)	6938(6)	31(3)
N007	6390(13)	8329(13)	7820(7)	29(3)
N008	3829(15)	8535(11)	10526(7)	50(4)
C009	7559(15)	7660(14)	6556(7)	25(4)
C00A	852(17)	5315(16)	6350(8)	37(4)
C00B	811(16)	8467(14)	9492(8)	26(4)
C00C	8238(16)	7305(14)	5273(9)	31(4)
C00D	9017(17)	6184(15)	7992(8)	35(4)
C00E	2284(18)	5108(15)	6570(8)	33(4)
C00F	4015(16)	5527(14)	8985(8)	28(4)
C00G	7544(17)	5791(14)	7657(8)	31(4)
C00H	2395(18)	9795(14)	8749(8)	33(4)
C00I	1132(17)	10313(14)	8473(8)	30(4)
C00J	9415(18)	3926(15)	8300(8)	41(5)
C00K	3531(17)	6272(14)	9556(8)	30(4)
C00L	7127(18)	4405(14)	7686(8)	34(4)
C00M	279(19)	2930(16)	6534(8)	40(4)
C00N	7466(16)	6963(14)	5850(8)	27(4)
C00O	9819(19)	5283(15)	8324(9)	39(4)
C00P	-209(19)	9961(15)	8707(9)	40(4)
C00Q	3380(17)	8694(16)	5695(9)	40(4)
C00R	3736(18)	4084(16)	8863(9)	42(5)
C00S	8604(17)	8728(15)	6657(8)	32(4)
C00T	2891(17)	3529(16)	9399(8)	33(4)
C00U	2780(20)	3852(16)	6753(9)	48(5)
C00V	9530(20)	9030(17)	6068(9)	48(5)
C00W	2718(18)	5616(16)	10048(9)	40(4)
C00X	3853(18)	6886(16)	4481(9)	41(5)
C00Y	2714(18)	7844(15)	7243(9)	43(5)
C00Z	3495(17)	7294(15)	5778(8)	32(4)
C010	3673(19)	8243(17)	4419(10)	49(5)
C011	1759(18)	2748(16)	6735(8)	39(4)
C012	3434(17)	9140(16)	5003(9)	38(4)
C013	3697(17)	6402(16)	5167(8)	35(4)
C014	9401(19)	8282(15)	5378(9)	41(5)
C015	-167(19)	4151(16)	6315(9)	44(5)

C016	8034(18)	3450(16)	7986(8)	40(4)
C017	2427(17)	4188(15)	9980(9)	37(4)
C018	2249(18)	8867(15)	9287(9)	37(4)
C019	-405(19)	9081(15)	9205(9)	41(4)

Table A-18.3: Anisotropic Displacement Parameters ($\text{\AA}^2 \times 10^3$) for $[\text{N}(\text{Ph}_2\text{PCH}_3)(\text{Ph}_2\text{PNH}_2)][\text{Cl}] \cdot \text{Ph}_2\text{P}(\text{O})\text{NH}_2$. The Anisotropic displacement factor exponent takes the form: $-2\pi^2[\text{h}^2\text{a}^*2\text{U}_{11}+2\text{hka}^*\text{b}^*\text{U}_{12}+\dots]$.

Atom	U ₁₁	U ₂₂	U ₃₃	U ₂₃	U ₁₃	U ₁₂
P002	27(3)	36(3)	40(3)	7(2)	-20(2)	-11(2)
P003	38(3)	34(3)	37(3)	6(2)	-14(2)	-11(2)
P004	33(3)	33(3)	41(3)	2(2)	-23(2)	-8(2)
O005	38(7)	50(7)	24(7)	-22(5)	16(5)	-4(6)
N006	20(7)	55(8)	15(7)	-5(6)	-10(5)	-15(6)
N007	24(8)	41(8)	20(8)	-5(6)	-7(6)	-14(6)
N008	53(10)	19(7)	72(12)	-18(7)	-22(8)	-8(7)
C009	18(8)	38(9)	18(8)	7(7)	-15(6)	-21(7)

Table A-18.4: Bond Lengths for $[\text{N}(\text{Ph}_2\text{PCH}_3)(\text{Ph}_2\text{PNH}_2)][\text{Cl}] \cdot \text{Ph}_2\text{P}(\text{O})\text{NH}_2$.

Atom	Atom	Length/ \AA	Atom	Atom	Length/ \AA
P002	N006	1.598(11)	C00F	C00R	1.432(19)
P002	N007	1.639(13)	C00G	C00L	1.405(18)
P002	C009	1.757(15)	C00H	C00I	1.362(19)
P002	C00G	1.713(15)	C00H	C018	1.399(19)
P003	O005	1.470(11)	C00I	C00P	1.34(2)
P003	N008	1.648(14)	C00J	C00O	1.367(19)
P003	C00K	1.783(15)	C00J	C016	1.41(2)
P003	C018	1.817(16)	C00K	C00W	1.37(2)
P004	N006	1.564(12)	C00L	C016	1.395(19)
P004	C00E	1.812(16)	C00M	C011	1.40(2)
P004	C00Y	1.746(16)	C00M	C015	1.361(19)
P004	C00Z	1.813(15)	C00P	C019	1.317(19)
C009	C00N	1.430(18)	C00Q	C00Z	1.400(18)
C009	C00S	1.386(18)	C00Q	C012	1.38(2)
C00A	C00E	1.37(2)	C00R	C00T	1.40(2)
C00A	C015	1.44(2)	C00S	C00V	1.44(2)
C00B	C018	1.42(2)	C00T	C017	1.304(19)
C00B	C019	1.379(19)	C00U	C011	1.40(2)
C00C	C00N	1.350(19)	C00V	C014	1.43(2)
C00C	C014	1.40(2)	C00W	C017	1.414(19)
C00D	C00G	1.48(2)	C00X	C010	1.359(19)
C00D	C00O	1.330(18)	C00X	C013	1.39(2)
C00E	C00U	1.386(19)	C00Z	C013	1.40(2)
C00F	C00K	1.337(18)	C010	C012	1.37(2)

Table A-18.5: Bond Angles for [N(Ph₂PCH₃)(Ph₂PNH₂)]Cl·Ph₂P(O)NH₂.

Atom	Atom	Atom	Angle/°	Atom	Atom	Atom	Angle/°
N006	P002	N007	119.3(7)	C00P	C00I	C00H	121.7(15)
N006	P002	C009	112.1(6)	C00O	C00J	C016	120.5(15)
N006	P002	C00G	104.3(7)	C00F	C00K	P003	120.7(12)
N007	P002	C009	102.4(7)	C00F	C00K	C00W	118.1(14)
N007	P002	C00G	109.2(7)	C00W	C00K	P003	121.1(13)
C00G	P002	C009	109.4(7)	C016	C00L	C00G	123.4(15)
O005	P003	N008	118.6(7)	C015	C00M	C011	120.7(16)
O005	P003	C00K	109.9(7)	C00C	C00N	C009	125.8(15)
O005	P003	C018	111.1(7)	C00D	C00O	C00J	122.2(16)
N008	P003	C00K	106.9(7)	C019	C00P	C00I	123.0(17)
N008	P003	C018	102.4(7)	C012	C00Q	C00Z	118.1(16)
C00K	P003	C018	107.3(7)	C00T	C00R	C00F	113.3(16)
N006	P004	C00E	108.1(7)	C009	C00S	C00V	118.9(15)
N006	P004	C00Y	114.1(7)	C017	C00T	C00R	126.2(16)
N006	P004	C00Z	114.0(7)	C00E	C00U	C011	118.2(17)
C00Y	P004	C00E	108.7(8)	C014	C00V	C00S	122.4(17)
C00Y	P004	C00Z	106.0(7)	C00K	C00W	C017	122.0(16)
C00Z	P004	C00E	105.6(7)	C010	C00X	C013	117.1(16)
P004	N006	P002	133.8(8)	C00Q	C00Z	P004	121.6(12)
C00N	C009	P002	118.6(10)	C00Q	C00Z	C013	119.5(14)
C00S	C009	P002	124.8(11)	C013	C00Z	P004	118.9(11)
C00S	C009	C00N	116.0(13)	C00X	C010	C012	122.8(17)
C00E	C00A	C015	117.0(15)	C00M	C011	C00U	119.9(16)
C019	C00B	C018	119.5(14)	C010	C012	C00Q	120.8(16)
C00N	C00C	C014	118.9(16)	C00X	C013	C00Z	121.4(15)
C00O	C00D	C00G	121.0(14)	C00C	C014	C00V	117.0(16)
C00A	C00E	P004	115.9(12)	C00M	C015	C00A	120.4(16)
C00A	C00E	C00U	123.5(15)	C00L	C016	C00J	117.6(15)
C00U	C00E	P004	120.5(13)	C00T	C017	C00W	116.8(15)
C00K	C00F	C00R	123.5(14)	C00B	C018	P003	120.7(11)
C00D	C00G	P002	119.4(11)	C00H	C018	P003	120.1(13)
C00L	C00G	P002	125.8(12)	C00H	C018	C00B	119.0(14)
C00L	C00G	C00D	114.8(13)	C00P	C019	C00B	119.0(16)
C00I	C00H	C018	117.6(15)				

Table A-18.6: Hydrogen Atom Coordinates ($\text{\AA}\times 10^4$) and Isotropic Displacement Parameters ($\text{\AA}^2\times 10^3$) for $[\text{N}(\text{Ph}_2\text{PCH}_3)(\text{Ph}_2\text{PNH}_2)][\text{Cl}]\cdot\text{Ph}_2\text{P}(\text{O})\text{NH}_2$.

Atom	x	y	z	U(eq)
H00A	6490(150)	9220(130)	7570(70)	35
H00B	5600(140)	8440(120)	8420(70)	35
H00P	3904	9442	10592	60
H00I	4581	8173	10761	60
H00K	2978	8238	10698	60
H00C	551	6170	6228	44
H00R	689	7796	9819	31
H00D	8001	6898	4813	37
H00E	9389	7075	7970	42
H00T	4562	5971	8648	33
H00W	3320	10049	8587	39
H00Y	1201	10926	8112	36
H00J	10057	3311	8492	49
H00L	6197	4108	7496	41
H00M	-409	2208	6551	48
H00N	6816	6207	5782	33
H00O	10684	5587	8581	47
H00Z	-1037	10357	8508	48
H00Q	3271	9307	6095	48
H00	4081	3566	8468	50
H00S	8704	9241	7099	38
H0AA	2638	2601	9336	40
H00U	3774	3745	6883	57
H00V	10239	9739	6139	57
H1AA	2347	6126	10440	48
H00X	4070	6305	4083	49
H00F	2595	7493	7710	64
H00G	1763	8063	7043	64
H00H	3346	8653	7293	64
H010	3714	8578	3961	59
H011	2064	1895	6857	47
H012	3306	10058	4932	46
H013	3728	5468	5220	41
H014	10060	8437	5015	50
H015	-1135	4235	6141	53
H016	7738	2533	7979	48
H017	1929	3740	10331	44
H019	-1350	8877	9360	49